MOLECULAR MECHANISMS AND TARGETED THERAPIES FOR COLORECTAL CANCER

EDITED BY: Shilpa S. Dhar, Erika Ruiz-Garcia, Valeria Barresi and Oronzo Brunetti

PUBLISHED IN: Frontiers in Oncology and Frontiers in Cell and Developmental Biology

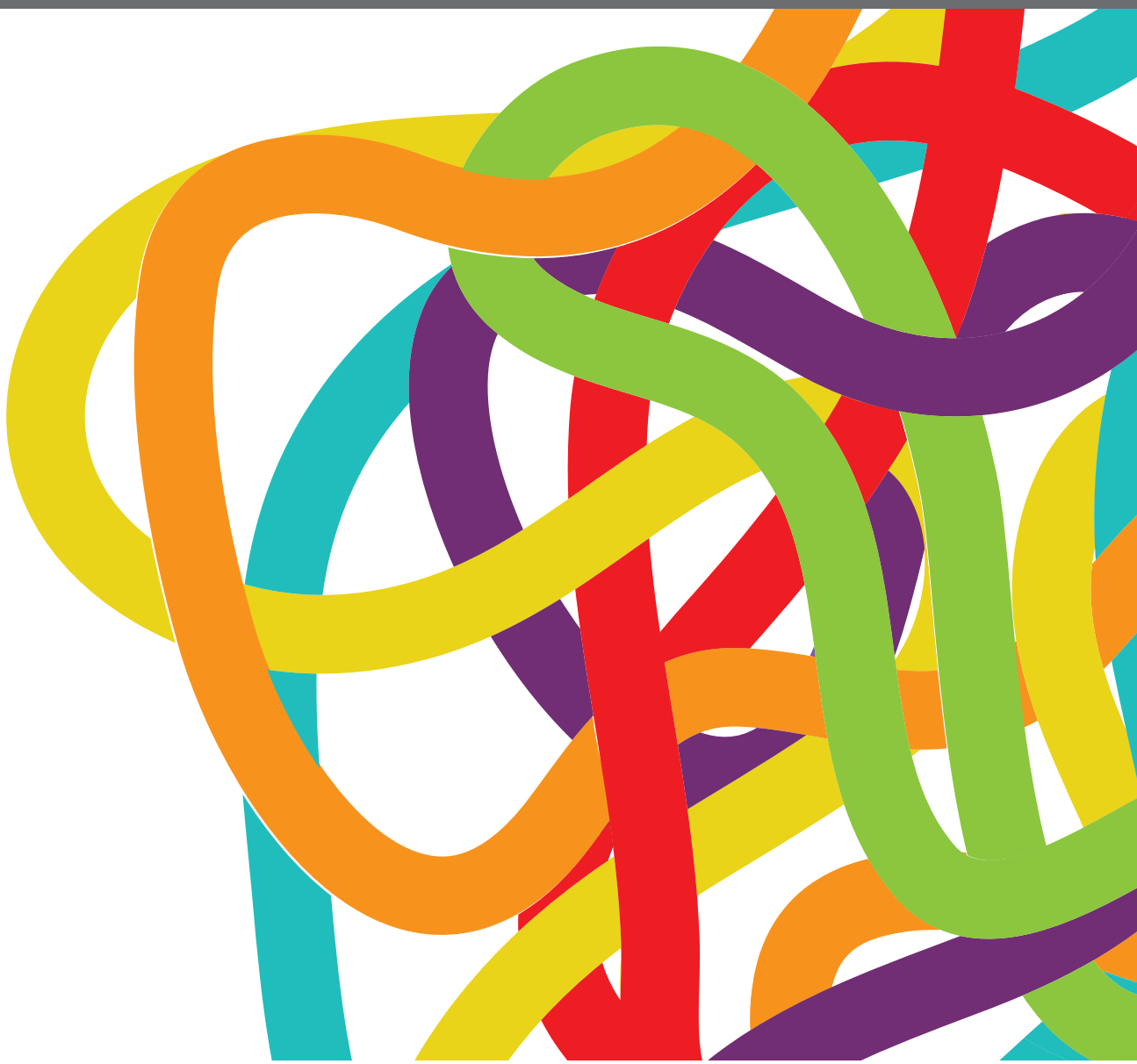

frontiers Research Topics

ISSN 1664-8714
ISBN 978-2-83250-641-7
DOI 10.3389/978-2-83250-641-7

About Frontiers

Frontiers is more than just an open-access publisher of scholarly articles: it is a pioneering approach to the world of academia, radically improving the way scholarly research is managed. The grand vision of Frontiers is a world where all people have an equal opportunity to seek, share and generate knowledge. Frontiers provides immediate and permanent online open access to all its publications, but this alone is not enough to realize our grand goals.

Frontiers Journal Series

The Frontiers Journal Series is a multi-tier and interdisciplinary set of open-access, online journals, promising a paradigm shift from the current review, selection and dissemination processes in academic publishing. All Frontiers journals are driven by researchers for researchers; therefore, they constitute a service to the scholarly community. At the same time, the Frontiers Journal Series operates on a revolutionary invention, the tiered publishing system, initially addressing specific communities of scholars, and gradually climbing up to broader public understanding, thus serving the interests of the lay society, too.

Dedication to Quality

Each Frontiers article is a landmark of the highest quality, thanks to genuinely collaborative interactions between authors and review editors, who include some of the world's best academicians. Research must be certified by peers before entering a stream of knowledge that may eventually reach the public - and shape society; therefore, Frontiers only applies the most rigorous and unbiased reviews.
Frontiers revolutionizes research publishing by freely delivering the most outstanding research, evaluated with no bias from both the academic and social point of view. By applying the most advanced information technologies, Frontiers is catapulting scholarly publishing into a new generation.

What are Frontiers Research Topics?

Frontiers Research Topics are very popular trademarks of the Frontiers Journals Series: they are collections of at least ten articles, all centered on a particular subject. With their unique mix of varied contributions from Original Research to Review Articles, Frontiers Research Topics unify the most influential researchers, the latest key findings and historical advances in a hot research area! Find out more on how to host your own Frontiers Research Topic or contribute to one as an author by contacting the Frontiers Editorial Office: frontiersin.org/about/contact

MOLECULAR MECHANISMS AND TARGETED THERAPIES FOR COLORECTAL CANCER

Topic Editors:
Shilpa S. Dhar, University of Texas MD Anderson Cancer Center, United States
Erika Ruiz-Garcia, National Institute of Cancerology (INCAN), Mexico
Valeria Barresi, University of Verona, Italy
Oronzo Brunetti, Bari John Paul II Cancer Institute, National Cancer Institute Foundation (IRCCS), Italy

Citation: Dhar, S. S., Ruiz-Garcia, E., Barresi, V., Brunetti, O., eds. (2022). Molecular Mechanisms and Targeted Therapies for Colorectal Cancer.
Lausanne: Frontiers Media SA. doi: 10.3389/978-2-83250-641-7

Table of Contents

frontiers in Oncology

CASE REPORT
published: 06 April 2021
doi: 10.3389/fonc.2021.612171

Case Report: Cetuximab in Combination With Chemotherapy for the Treatment of Multifocal Hepatic Metastases From Colorectal Cancer Guided by Genetic Tests

Chunhui Qiu[1†], Sidong Xie[2†], Na Cheng[3†], Qu Lin[4], Guanzhu Shen[5], Zhanwang Xiang[6], Tanxiao Huang[7], Xiaoni Zhang[7], Jingxian Duan[7], Li Wei[4*] and Zongheng Zheng[8*]*

[1] Department of Hepatic Surgery, The Third Affiliated Hospital of Sun Yat-sen University, Guangzhou, China, [2] Department of Radiology, The Third Affiliated Hospital of Sun Yat-sen University, Guangzhou, China, [3] Department of Pathology, The Third Affiliated Hospital of Sun Yat-sen University, Guangzhou, China, [4] Department of Medical Oncology, The Third Affiliated Hospital of Sun Yat-sen University, Guangzhou, China, [5] Department of Radiation Oncology, The Third Affiliated Hospital of Sun Yat-sen University, Guangzhou, China, [6] Department of Intenational Radiology, The Third Affiliated Hospital of Sun Yat-sen University, Guangzhou, China, [7] Department of Oncology, HaploX Biotechnology, Shenzhen, China, [8] Department of Gastrointestinal Surgery, The Third Affiliated Hospital of Sun Yat-sen University, Guangzhou, China

OPEN ACCESS

Edited by:
Erika Ruiz-Garcia, National Institute of Cancerology (INCAN), Mexico

Reviewed by:
Rui Manuel Reis, Barretos Cancer Hospital, Brazil
Ye Wei, Fudan University, China

***Correspondence:**
Jingxian Duan
duanjx@haplox.com
Zongheng Zheng
zhengzh@mail.sysu.edu.cn
Li Wei
weili6@mail.sysu.edu.cn

†These authors have contributed equally to this work

Specialty section:
This article was submitted to Molecular and Cellular Oncology, a section of the journal Frontiers in Oncology

Received: *30 September 2020*
Accepted: *16 March 2021*
Published: *06 April 2021*

Citation:
Qiu C, Xie S, Cheng N, Lin Q, Shen G, Xiang Z, Huang T, Zhang X, Duan J, Wei L and Zheng Z (2021) Case Report: Cetuximab in Combination With Chemotherapy for the Treatment of Multifocal Hepatic Metastases From Colorectal Cancer Guided by Genetic Tests. Front. Oncol. 11:612171. doi: 10.3389/fonc.2021.612171

Hepatic metastases were reported in up to 70% of colorectal cancer patients, among which multifocal hepatic metastasis represents one of the complications that lead to poor prognosis. The majority of the patients carrying multifocal hepatic metastases required pharmaceutical treatments to reduce the tumor size prior to surgical resection. However, the clinical responses to pharmaceutical agents were difficult to predict due to the heterogeneous nature of the multifocal tumors. Here, we report a case with multifocal hepatic metastases from colorectal cancer that was resistant to the primary chemotherapy and Bevacizumab plus chemotherapy, but responded to the combined therapy of Cetuximab and FOLFOX. Genetic tests had revealed that the tumor was highly metastatic due to the mutations of the WNT signaling pathway, and the metastatic tumors might be sensitive to Cetuximab. Consistent with the molecular characterizations, the metastatic tumors continue to emerge after chemotherapy, and rapidly relapsed in great numbers after liver resection. However, the combined therapy of Cetuximab and FOLFOX guided by the genetic tests significantly reduced the size and number of metastatic tumors. To conclude, deciphering the mutation profiles of multifocal metastatic tumors may guide the determination of treatment tactics, which may benefit the patients with non-resectable advanced carcinoma.

Keywords: colorectal cancer, hepatic metastases, multifocal tumors, Wnt signal pathway, APC and TP53 co-mutation

BACKGROUND

Colorectal cancer (CRC) represents the third most common cancer worldwide, causing over 500,000 deaths each year (1). Metastasis remains the key factor that shortens the survival of CRC patients. The 5-year survival of metastatic CRC was 35%-40% despite the fact that the diagnosis methods, treatment strategy, and best supportive care approaches had tremendously improved in

the past decades (2). Liver remains the most common site of CRC metastasis, approximately 50% of the CRC patients developed hepatic metastasis during the course of CRC (3). Hepatic resection was considered to be the standard treatment modality for hepatic metastases from CRC (4); however, only around 25% of the patients carrying hepatic metastases from CRC were eligible for hepatic resections considering the tumor size, location, and accessibility (5, 6). To extend the possibility of hepatic resection, neoadjuvant therapy was encouraged. Neoadjuvant chemotherapy was shown to significantly improve the 5-year survival of metastatic CRC patients to 38.9%-74% (7). The combination of chemotherapy and pharmaceutical agents achieved the objective response rate of 40.6%, converting 19/64 unresectable liver metastases from colorectal cancer to curative intent resection (8). Importantly, the resistance to certain pharmaceutical agents could be postulated based on the mutational states of gene markers.

The mutational landscape of CRC was fully revealed by whole-genome sequencing studies. Mutations in APC, KRAS, BRCA2, and TP53 were frequently observed in CRC and colorectal adenoma patients (9). In hepatic metastases of CRC, KRAS was reported to be a significantly mutated gene, and the mutation status of KRAS was believed to be the predictor of recurrence-free survival of the patients (10). Patients carrying KRAS mutation had significantly decreased progression-free survival following Cetuximab treatment (11). However, KRAS mutation was detected in around 27% of colorectal liver metastases (12), and not all KRAS wild-type patients would respond to Cetuximab (13). Therefore, it is crucial to investigate the predictive biomarkers for different treatment strategies of colorectal liver metastases. This case stands for a unique representation of rapid growing multifocal hepatic metastases that were resistant to chemotherapy and Bevacizumab plus chemotherapy, and relapsed quickly after liver resection with 18 metastatic tumors. Treatment guided by the mutational profiles of the tumors effectively reduced metastases and tumor growth.

CASE PRESENTATION

A 51-year-old male with no family history or chronic disease was admitted to the Third affiliated hospital of Sun Yat-sen University. Baseline examination showed that carcinoembryonic antigen (CEA) was 285.6 ug/L (**Supplementary Figure 1A**), and CA199 was within the normal range on Oct 30th, 2019. Colonoscopy showed a 1.3cm x 1.3cm disc-shaped bulging tumor in the splenic flexure of colon. Pathological examination, CT scan, MR scan, and PET-CT scan showed 1 primary tumor in the splenic flexure of colon (**Figures 1A–C**) and 9 liver metastases (**Figures 1D–F**, **Supplementary Table 1** and **Supplementary Figure 2**). 3 liver

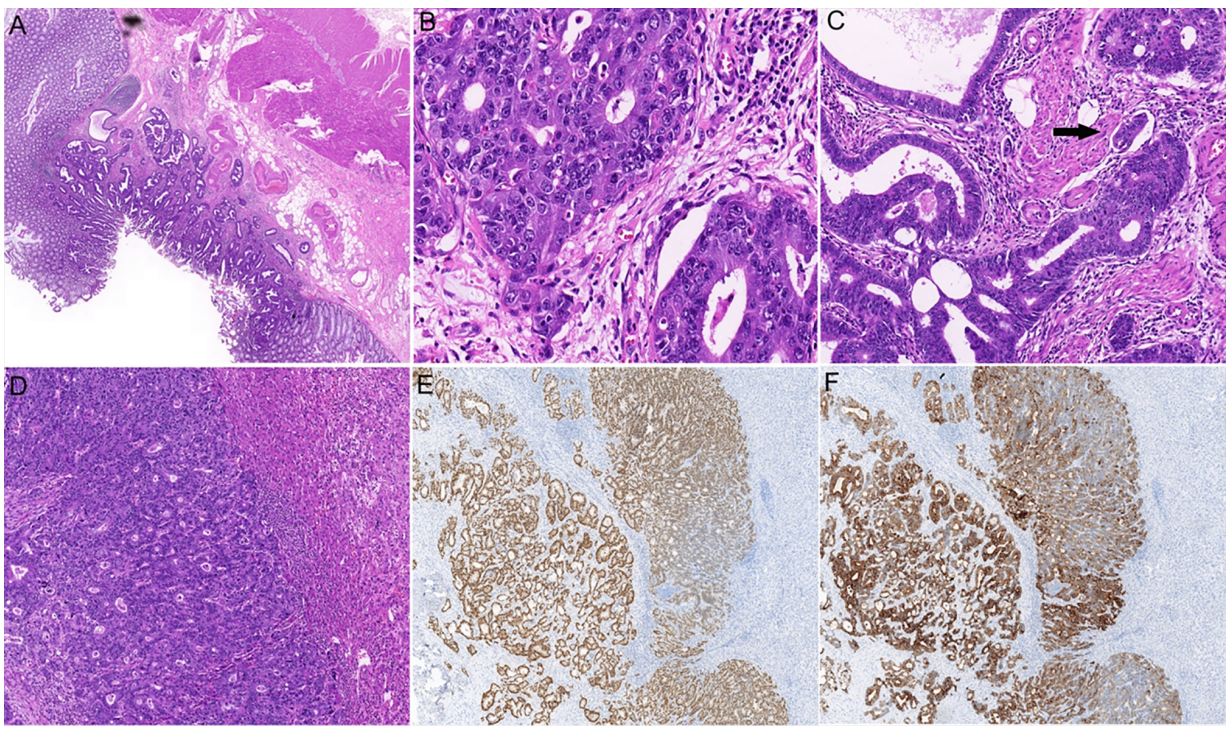

FIGURE 1 | Histopathological examination of the primary and metastatic tumors. **(A)** Hematoxylin and eosin (H&E) staining of colonic primary tumor shows glandular differentiation and invasion into the submucosa (×20). **(B)** High-power view shows the malignant epithelial cells arranging in a glandular or cribriform manner (×400). **(C)** The lymphovascular invasion of colonic adenocarcinoma is indicated by an arrow (×200). **(D)** H&E staining shows intrahepatic adenocarcinoma (×100). Immunostaining for CK20 **(E)**, ×50 and CDX2 **(F)**, ×50 confirmed the tumor originated in colon.

metastatic tumors were identified in the left lobe of the liver, whereas the other 6 tumors were in the right lobe. The mean size of the metastatic tumors was 13 ± 2.055mm, ranging from 4mm-22mm (**Supplementary Table 1** and **Supplementary Figure 1B**). Pathological examination showed moderately differentiated adenocarcinoma of the colon (**Figures 1A–C**) and liver metastasis (**Figures 1D–F**). Targeted sequencing showed that the tumors cells were KRAS, NRAS, and BRAF wild type with proficient MMR, and was negative for HER-2.

From the 30th of October to the 31st of December, 2019, 4 courses of mFolfox6 chemotherapy were performed. The dosage and durations were Oxaliplatin 85 mg/m2 IV day 1, Leucovorin 400 mg/m2 IV day 1, 5-FU 400 mg/m2 IV bolus on day 1, then 1200 mg/m2/day x 2 days (total 2400 mg/m2 over 46–48 hours) IV continuous infusion, repeated every 2 weeks. After chemotherapy, the sizes of 7/9 tumors were reduced, the average reduction was 2.778 ± 0.7027 mm (**Figure 2A**). However, the number of the liver metastasis increased, 10 more metastatic tumors emerged in segments II-VIII, and their sizes ranged from 4mm-12mm (5.82 mm on average, **Supplementary Table 1**, **Supplementary Figures 1B**, **2**). The changes in tumor sizes and numbers after different treatments are shown in **Figures 2A–D**, and the treatment records are shown in **Figure 3**. The CEA dropped to 105 ug/L, whereas CA199 remained normal (**Supplementary Figure 1A**). To further reduce the size and number of the tumors, enhanced treatment was recommended, and the combined treatment of EGFR inhibitor and chemotherapy was applied due to the fact that the patient harbored no RAS alteration according to the mutation profile of the patient.

Two cycles of Cetuximab (500 mg/m2 IV over 2 hours, day 1, every 2 weeks) in combination with FOLFOXIRI (Irinotecan 165 mg/m2 IV day 1, oxaliplatin 85 mg/m2 IV day 1,z Leucovorin 400aa mg/m2 day 1, fluorouracil 1200 mg/m2/day x 2 days, continuous infusion starting on day 1. Repeated every 2 weeks) were administered on January 3 and 17, 2020 respectively. The patient did not return to the hospital for treatment in February due to the

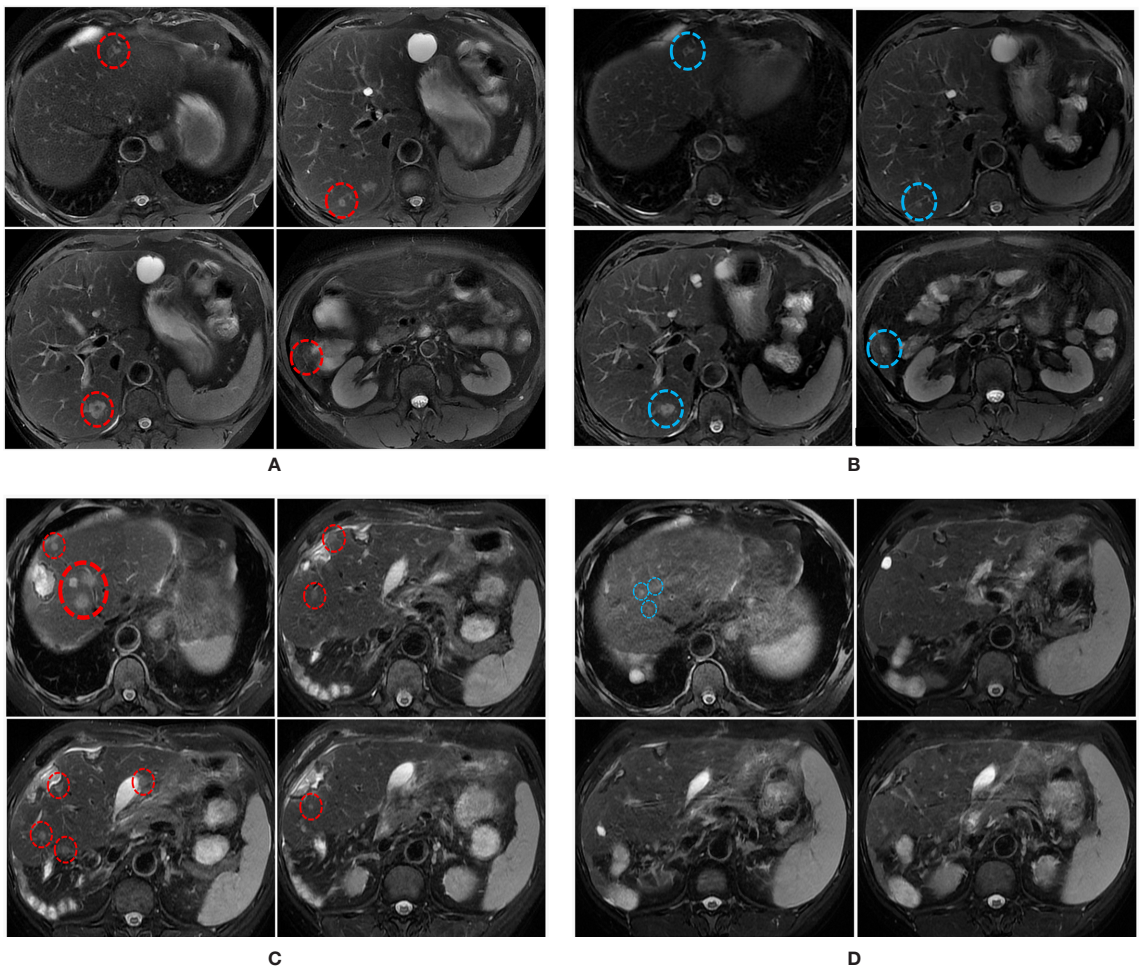

FIGURE 2 | MRI scans illustrating the changes in liver metastatic tumors over time. **(A)** MRI scans on the 30th of December 2019 shows multiple liver metastases (red circles). **(B)** MRI scans on the 7th of March 2020 shows the size of some liver metastases was reduced (blue circles) following the combination treatment. **(C)** MRI scans on the 16th of April 2020 shows multiple liver metastases (red circles). **(D)** MRI scans on the 28th of June 2020 shows the sizes and numbers of liver metastasis were significantly reduced following the combined treatment.

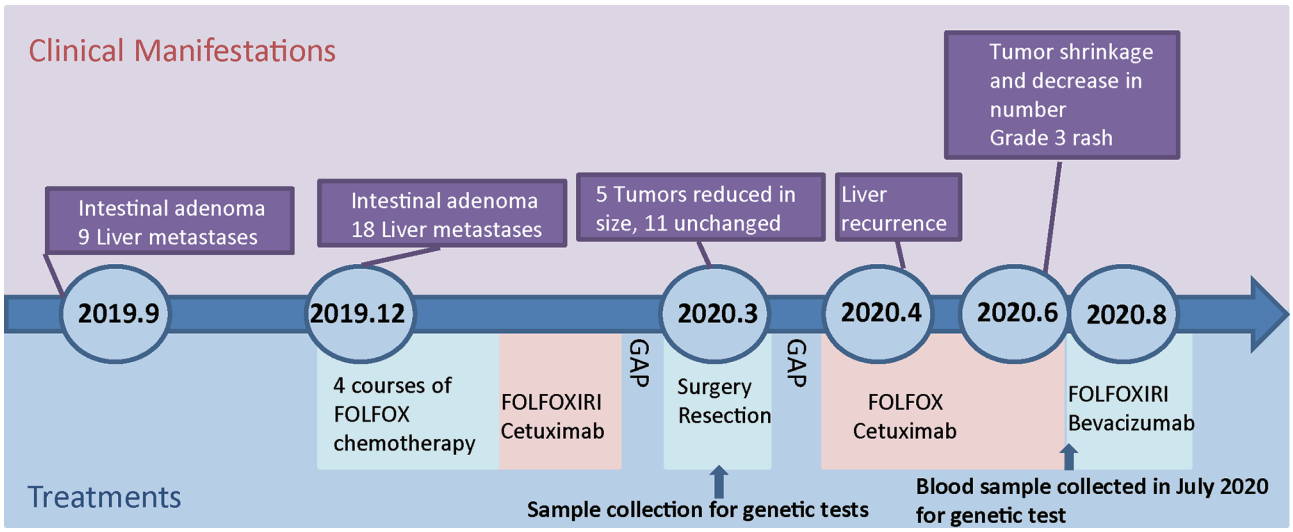

FIGURE 3 | Schematic diagram showing treatment record of the patient.

COVID-19 epidemic. He returned to our hospital in March 2020, his serum CEA dropped to 38.96 ug/L (**Supplementary Figure 1A**), and the CA199 remained normal. MRI scan on March 7th 2020 showed that 5 out of 18 liver metastatic tumors were reduced by 3 ± 0.55 mm (**Figure 2B**, **Supplementary Table 1** and **Supplementary Figure 2**), 11 tumors remained unchanged, and two tumors enlarged by 1mm. The average size of the metastatic tumors was 7.278 ± 0.885 mm, ranging from 4mm to 17 mm.

After MDT discussion, he received surgery on the 13th of March 2020. The intestinal lesion and all eighteen liver lesions were removed. Postoperative pathology examination reported middle grade adenocarcinoma of the colon with infiltration into the submucosa. Suspected vascular tumor thrombosis was also observed. T1-T7,T8-T10, T12, T13, T15-18 were identified as the metastases from the intestinal adenocarcinoma based on the immunohistochemistry staining results of CK20 and CDX2 (**Figures 1E, F**). T 11 and T14 No spare tissues were left in T11 and T14 for CK20 and CDX2 staining after DNA extraction, the H&E staining before DNA extraction confirmed that they were tumors. No metastatic cancer was found in 8 para-intestinal lymph nodes, 11 central lymph nodes, and 8 intermediate lymph nodes.

Whole-exome sequencing (WES) was performed on the intestinal adenocarcinoma sample collected during the surgery, and targeted sequencing with a panel of 680 cancer-related genes was performed on 13 hepatic tumors (T1-T7, T9-T12, T14, T15) that yielded sufficient amounts of tissues for the tests. The other 5 tumor samples did not reach the required tissue weight or tumor purity for DNA extraction, thus did not yield enough DNA for sequencing. The WES result revealed 18 somatic single-nucleotide variations and 3 insertion/deletion events (**Supplementary Table 2**). The top 5 genes with high variant allele fractions were LRRC14 (c.979C>T, 15.52%), P2RY10 (c.396del, 10.06%), GALNT2 (c.83G>A, 9.23%), CASS4 (c.719C>T, 9.18%), and PRAMEF1 (c.986A>T, 8.48%). Among the 21 mutation loci, FEM1C (c.983G>A, COSM6663046), UTRN (c.9299C>T, COSM6819331), LRRC14 (c.979C>T, COSM6703564), TP53 (c.733G>T, COSM11081), and ABCA7 (c.4513C>T, COSM2156640) were reported in the COSMIC (catalogue of somatic mutations in cancer) database; whereas the other sites of mutations were not documented in the database. The TMB of the sample was 0.53 Muts/Mb.

The targeted sequencing results of the hepatic tumors revealed substantial heterogeneity among these metastatic tumors. 13 mutation loci were reported, including FOXP2 c.A455T, IKZF1 c.G1143T, TP53 c.G733T, PLIN2 c.C1295T, EPHA5 c.A2303C, APC c.C847T and c.3927_3931del, SF3B1 c.G3890A, NTRK2 c.C1574G, CACNA1C c.G673A, FANCB c.G901C, VHL c.G430A, and AXIN2 c.17_20dup. Notably, only the mutations in TP53, PLIN2, and AXIN2 were shared by the hepatic metastases and the primary intestinal adenoma. As shown in the phylogenic tree of the tumors (**Figure 4A**), T9 was the metastatic tumor that is most closely related to the primary intestinal adenoma evolutionally, they displayed common mutational sites. T1 developed two more mutation sites FOXP2 and IKF1, which was followed by T2, T4, T5, T7, T12, and T14 who further developed 4 mutations. These tumors were located at the same branch of the phylogenic tree due to the fact that they exhibited the identical mutation profile, suggesting that they may be monoclonal and perhaps emerged at the same stage (**Figure 4B**). T10, T11 and T15 were evolutionally very close to T2, T4, T5, T7, T12, and T14, they further developed one or two mutations respectively. Co-mutation of TP53 and APC occurred in T2, T4 T5, T7, T10, T11, T12, T14, and T15, suggesting that these hepatic metastases may be sensitive to Cetuximab treatment (14). Further analysis showed that these tumor cells were KRAS wild-type and pMMR. The TMB was 3.76 ± 0.86Muts/Mb, indicating that the patient may not respond well to immunotherapy. Notably, the tumors harbored TP53 and

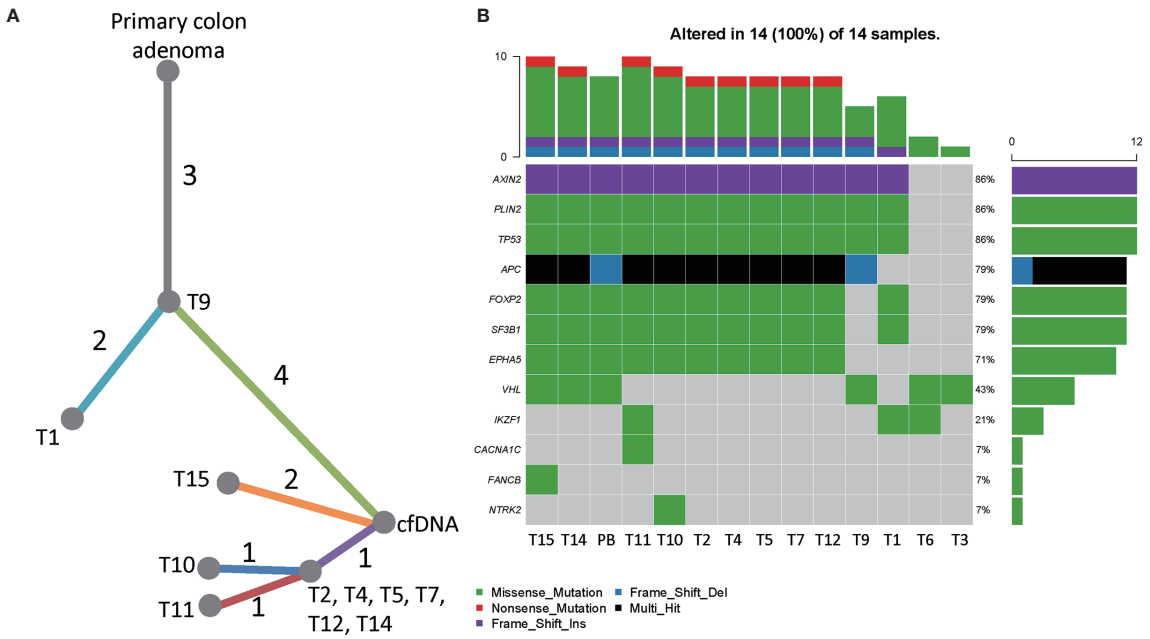

FIGURE 4 | The genetic heterogeneity of liver metastatic tumors. **(A)** A phylogenic tree showing the genomic similarity of the liver metastatic tumors and the primary intestinal adenoma. **(B)** Heatmap showing the frequencies and types of mutations of all mutated genes detected by targeted sequencing. T1-T15 were hepatic tumors and PB was the peripheral blood sample obtained in July 2020.

APC co-mutation had the mean TMB of 5.43 ± 0.69Muts/Mb, whereas all 4 tumors that did not contain the co-mutation had the TMB below the detection threshold.

The patient received no treatment after the surgery; however, the tumors relapsed in two months. The MRI review in April showed 18 metastases in the left lobe of the liver (segments II-VI), which possibly were recurrent tumors (**Figure 2C**). The average size of the tumors was 8.778 ± 0.712 mm, ranging from 4mm to 15mm (**Supplementary Table 3** and **Supplementary Figure 3**). The recurrent tumors were found in the liver but not the colon, suggesting that the liver metastasis harbored molecular alterations that facilitate rapid tumor growth. The sequencing results showed that key genes involved in the Wnt signaling had mutated, which favors transcription of epithelial-mesenchymal transition (EMT) supported metastasis. Although Cetuximab plus chemotherapy was not the optimal recommendation for the treatment of liver metastases, we still decided to continue with this plan as the mutation status of liver tumors and former treatment history both suggest that the tumors may respond to Cetuximab plus chemotherapy. The patient received six cycles of Cetuximab (Cetuximab 500 mg/m2 IV over 2 hours, day 1, every 2 weeks) combined with mFOLFOX6 (Oxaliplatin 85 mg/m2 IV day 1z Leucovorin 400 mg/m2 IV day 1aa 5-FU 400 mg/m2 IV bolus on day 1, then 1200 mg/m2/day x 2 days, total 2400 mg/m2 over 46–48 hours, IV continuous infusion, repeated every 2 weeks). After the treatment, 10 out of 18 tumors were eliminated, the rest 8 tumors were significantly reduced in size (10.38 ± 1.133 mm versus 6 ± 0.378 mm, p=0.008 (**Figure 2D**), **Supplementary Figure 1B**). Targeted sequencing of the cfDNAs captured from the peripheral blood sample on the 10th of July 2020 showed that the mutational profile of the patient remained unchanged (**Supplementary Table 2**), confirmed that the newly emerged tumors were recurrent tumors that shared the same mutations with the surgery-removed tumors. Despite the fact that the Cetuximab plus mFOLFOX6 regime gave rise to superior clinical responses as predicted by the genetic test, the patient developed a grade 3 rash after the therapy, which seriously affected the life-quality of the patient. As the result, the patient refused to continue the Cetuximab combination therapy. On August 24, 2020, the regimen was adjusted to Bevacizumab (Bevacizumab 5 mg/kg IV, day 1 Repeat every 2 weeks) combined with FOLFOXIRI (Irinotecan 180 mg/m2 IV over 30–90 minutes, day 1 Leucovorinaa 400 mg/m2 IV infusion to match duration of irinotecan infusion, day 1 5-FU 400 mg/m2 IV bolus day 1, then 1200 mg/m2/day x 2 days; total 2400 mg/m2 over 46–48 hours; continuous infusion repeated every 2 weeks). However, severe side effects in the gastrointestinal tract markedly impaired the life quality of the patient, and the CEA level increased to 494.8 ug/L. The patient chose to stop the treatment and never returned to the hospital after two courses of Bevacizumab plus FOLFOXIRI.

DISCUSSION

In this case of multifocal hepatic metastases from intestinal adenoma, we reported a large number of rapid growing hepatic metastases that harbored mutations of APC, AXIN2, TP53, PLIN2, and FOXP2. The sizes and numbers of the tumors

were markedly reduced by Cetuximab plus chemotherapy but not chemotherapy alone or Bevacizumab plus chemotherapy. The genomic landscape of colorectal cancers had been reported by multiple studies, APC and CTNNB1 were the hallmark mutations of CRC (15, 16). Mutations of *KRAS*, *BRAF*, *PIK3CA*, *AKT1*, *RNF43*, and *SMAD4* were observed more frequently in right-sided CRC, and alterations in the WNT signaling pathway were identified in approximately 96% of CRCs (15). The genomic landscape of liver cancer showed an overlap of prevalent mutations with CRC. TERT, TP53, and CTNNB1 were the frequently mutated genes observed in HCC patients, structural variations in CDKN2A, CCND1, APC, and TERT were also reported in virus-infected HCC (17). In hepatic metastases from CRC, COX-2 was shown to over-express (18), and KRAS mutation may predict the tumor recurrence patterns in patients who had hepatic resections of CRC metastases (10). Here, we report for the first time that TP53, PLIN2, and AXIN2 were the common mutations shared by the primary intestinal adenoma and multifocal hepatic metastases. The multifocal hepatic metastases displayed genetic heterogeneity which improves the understanding of the evolutionary and chronological relationships of the metastatic tumors.

Mutations of APC, CTNNBI or AXIN1 would lead to the accumulation of beta-catenin and interfere with the Wnt signaling pathway in HCC and CRC (19). We observed two mutation sites (in 9/13 tumors) in the exons of the APC gene, and both were loss-of-function mutation. It was shown that the inactivation of APC leads to the activation of Wnt signaling (20). Similarly, we reported the frame-shift mutation of AXIN2 in 11/13 liver metastatic tumors. This mutation results in a truncated form of protein with compromised protein function. It was known that AXIN2 was a negative regulator of the Wnt signaling pathway, hence, the observed mutation of AXIN2 may lead to the abnormal activation of the Wnt signaling pathway (21). Activation of the Wnt signaling pathway was shown to trigger the EMT-related genes including SNAIL1 (22); consequently, it would facilitate cell proliferation and the potency of invasiveness (23). In this case, it is highly likely that the Wnt signaling pathway was up-regulated due to the loss-of function mutations of APC and AXIN2, which increased the invasiveness of the tumors and caused multifocal metastases as well as recurrent metastasis in the liver. When first enrolled in the hospital, the patient developed 9 more hepatic tumors in 3 months, 8/9 of the tumors exhibiting TP53 and APC co-mutation also showed higher TMB level. After the resection, another 18 metastatic tumors emerged in the liver within two months. The rapid emerging of liver metastases may also be the result of the aberrant activation of the Wnt signaling. A population-based study reported that 45.8% liver metastases from colon cancer had 1-3 liver metastatic sites (24), the highly invasive metastases with 18 sites were rare in our clinical observation.

We also observed the co-mutation of TP53 and APC in 9/13 liver metastatic tumors. Studies had reported that the co-mutation of APC and TP53 was associated with sensitivity to Cetuximab therapy in Ras-normal metastatic CRC patients (14, 25). Indeed, FOLFIX chemotherapy alone caused an increased number of liver metastases, whereas the combined treatment of Cetuximab and chemotherapy significantly reduced the size and number of liver metastatic tumors between April 2020 and June 2020, which proved that the mutation profiles of tumors could guide the determination of clinical treatment strategy. In fact, these fast-growing metastatic tumors with loss-of function mutations of the negative regulator of the Wnt signaling pathway responded only to Cetuximab plus chemotherapy. When chemotherapy was applied alone, the number of metastatic tumors increased. The CEA level of the patient increased drastically when the treatment strategy was switched to Bevacizumab plus chemotherapy, and the sizes and number of the tumors were not reduced. Moreover, the surgery was accompanied by the rapid relapse of hepatic tumors. Despite the fact that surgical resection was considered to be the potentially curative treatment for colorectal liver metastases, our case showed that metastatic tumors with potentially Wnt signaling activating mutations may relapse very soon after the surgery, and Cetuximab plus chemotherapy was the optimal strategy for the treatment of tumors that has high potential to metastasize and multiply. Conducting genetic sequencing to check for Wnt signaling-activating mutations might be a good approach to identify such tumors. Notably, we showed that the tumors harbored loss-of function mutations of the negative regulator of the Wnt signaling pathway, which may lead to the aberrant activation of the pathway. However, we do not have spare samples to conduct immune-staining or functional tests. Whether the Wnt signaling pathway was up-regulated *in situ* requires additional experiments, and we could confirm the finding if similar samples are acquired in the future.

Systemic chemotherapy was applied as neoadjuvant therapy or adjuvant therapy in the treatment of CRC. First-line chemotherapy plans for metastatic CRC include FOLFOX (fluorouracil, leucovorin, oxaliplatin), FOLFIRI (fluorouracil, leucovorin, irinotecan), XELOX (capecitabine plus oxaliplatin), and FOLFOXFIRI (fluorouracil, leucovorin, oxaliplatin, irinotecan) (26). The combined use of Cetuximab, Bevacizumab, and chemotherapy in metastatic CRC was studied for decades; it was shown that patients carrying KRAS mutation had significantly decreased progression-free survival following Cetuximab treatment (11). A more recent study reported that the addition of Cetuximab to chemotherapy conferred disadvantages of survival in patients with operable disease (27). Collectively, these observations confirmed that the use of Cetuximab should be carefully considered, and should follow the guidance of the genetic test results. Despite the fact that the combined use of Cetuximab and chemotherapy reduced the hepatic metastases in this case, the severe adverse effect forced us to change the treatment plan to Bevacizumab plus chemotherapy, which further caused adverse effect in the gastrointestinal tract.

One limitation of the case is that we struggle to find an effective treatment strategy with less treatment-related adverse events. The disadvantage of the Cetuximab plus chemotherapy plan is that it was reported to induce skin rash in 16% of the patients, whereas in the control group (Chemotherapy alone)

only 1% of patients reported skin irritation (27). Alternatively, Bevacizumab was applied in combination with chemotherapy for the treatment of metastatic CRC, the treatment plan was shown to improve the progression-free survival of the patients, although grade 3 or 4 adverse events were more frequently observed too (28). It was reported that 19.7% patients receiving FOLFIRI plus Bevacizumab and 20.4% patients receiving FOLFOXIRI plus Bevacizumab experienced serious adverse events; 20.5%-50% of the patients reported neutropenia (28). Unfortunately, the patient could not endure the severe side effects caused by the treatments and did not return to the hospital since.

CONCLUSION

Next generation sequencing of the multifocal liver metastases from CRC revealed the genetic heterogeneity of the metastatic tumors. The mutations causing abnormal activation of the Wnt signaling pathway would possibly increase the invasiveness of the tumors and promote metastasis, which leads to rapid recurrence of the metastatic tumors in a short period of time after liver resection. Moreover, such tumors may respond well to Cetuximab plus chemotherapy but not chemotherapy alone or Bevacizumab plus chemotherapy. Treatment strategies should be selected based on the mutational profiles of the metastatic tumors.

DATA AVAILABILITY STATEMENT

The raw data supporting the conclusions of this article will be made available by the authors, without undue reservation.

ETHICS STATEMENT

Written informed consent was obtained from the patient for the publication of any potentially identifiable images or data included in this manuscript.

AUTHOR CONTRIBUTIONS

CQ, SX, and NC contributed equally to this work. All authors were involved in the drafting of the manuscript. ZZ and LW designed the clinical treatment for the patient. JD, TH, and XZ performed genetic tests and the data analysis. ZZ, SX, GS, NC, ZX, LW, QL, and CQ performed the clinical treatment for the patients. All authors contributed to the article and approved the submitted version.

FUNDING

This research was funded by the Science and Technology Planning Project of Guangdong Province, China (2015A020210044, 2014A020209022) and Shenzhen science, technology and innovation commission (JSGG20180508152646606).

SUPPLEMENTARY MATERIAL

The Supplementary Material for this article can be found online at: https://www.frontiersin.org/articles/10.3389/fonc.2021.612171/full#supplementary-material

REFERENCES

1. Bray F, Ferlay J, Soerjomataram I, Siegel RL, Torre LA, Jemal A. Global cancer statistics 2018: GLOBOCAN estimates of incidence and mortality worldwide for 36 cancers in 185 countries. *CA Cancer J Clin* (2018) 68:394–424. doi: 10.3322/caac.21492
2. Kopetz S, Chang GJ, Overman MJ, Eng C, Sargent DJ, Larson DW, et al. Improved survival in metastatic colorectal cancer is associated with adoption of hepatic resection and improved chemotherapy. *J Clin Oncol* (2009) 27:3677–83. doi: 10.1200/JCO.2008.20.5278
3. van der Pool AE, Damhuis RA, Ijzermans JN, de Wilt JH, Eggermont AM, Kranse R, et al. Trends in incidence, treatment and survival of patients with stage IV colorectal cancer: a population-based series. *Colorectal Dis* (2012) 14:56–61. doi: 10.1111/j.1463-1318.2010.02539.x
4. Baek HU, Kim SB, Cho EH, Jin SH, Yu HJ, Lee JI, et al. Hepatic resection for hepatic metastases from gastric adenocarcinoma. *J Gastric Cancer* (2013) 13:86–92. doi: 10.5230/jgc.2013.13.2.86
5. Bentrem DJ, Dematteo RP, Blumgart LH. Surgical therapy for metastatic disease to the liver. *Annu Rev Med* (2005) 56:139–56. doi: 10.1146/annurev.med.56.082103.104630
6. Hiraoka K, Kimura T, Logg CR, Tai CK, Haga K, Lawson GW, et al. Therapeutic efficacy of replication-competent retrovirus vector-mediated suicide gene therapy in a multifocal colorectal cancer metastasis model. *Cancer Res* (2007) 67:5345–53. doi: 10.1158/0008-5472.CAN-06-4673
7. Nigri G, Petrucciani N, Ferla F, La Torre M, Aurello P, Ramacciato G. Neoadjuvant chemotherapy for resectable colorectal liver metastases: what is the evidence? *Results Systematic Rev Comp Stud Surgeon* (2015) 13:83–90. doi: 10.1016/j.surge.2014.07.005
8. Levi FA, Boige V, Hebbar M, Smith D, Lepere C, Focan C, et al. Conversion to resection of liver metastases from colorectal cancer with hepatic artery infusion of combined chemotherapy and systemic cetuximab in multicenter trial OPTILIV. *Ann Oncol* (2016) 27:267–74. doi: 10.1093/annonc/mdv548
9. Borras E, San Lucas FA, Chang K, Zhou R, Masand G, Fowler J, et al. Genomic Landscape of Colorectal Mucosa and Adenomas. *Cancer Prev Res (Phila)* (2016) 9:417–27. doi: 10.1158/1940-6207.CAPR-16-0081
10. Kemeny NE, Chou JF, Capanu M, Gewirtz AN, Cercek A, Kingham TP, et al. KRAS mutation influences recurrence patterns in patients undergoing hepatic resection of colorectal metastases. *Cancer* (2014) 120:3965–71. doi: 10.1002/cncr.28954
11. Tol J, Koopman M, Cats A, Rodenburg CJ, Creemers GJ, Schrama JG, et al. Chemotherapy, bevacizumab, and cetuximab in metastatic colorectal cancer. *N Engl J Med* (2009) 360:563–72. doi: 10.1056/NEJMoa0808268
12. Nash GM, Gimbel M, Shia J, Nathanson DR, Ndubuisi MI, Zeng ZS, et al. KRAS mutation correlates with accelerated metastatic progression in patients with colorectal liver metastases. *Ann Surg Oncol* (2010) 17:572–8. doi: 10.1245/s10434-009-0605-3
13. Hsu HC, Thiam TK, Lu YJ, Yeh CY, Tsai WS, You JF, et al. Mutations of KRAS/NRAS/BRAF predict cetuximab resistance in metastatic colorectal cancer patients. *Oncotarget* (2016) 7:22257–70. doi: 10.18632/oncotarget.8076
14. Song K, Lu H, Jin L, Wang K, Guo W, Zheng H, et al. Qualitative Ras pathway signature for cetuximab therapy reveals resistant mechanism in colorectal cancer. *FEBS J* (2020) 287(23):5236–48. doi: 10.1111/febs.15306
15. Yaeger R, Chatila WK, Lipsyc MD, Hechtman JF, Cercek A, Sanchez-Vega F, et al. Clinical Sequencing Defines the Genomic Landscape of Metastatic

Colorectal Cancer. *Cancer Cell* (2018) 33:125–36.e3. doi: 10.1016/j.ccell.2017.12.004
16. Wood LD, Parsons DW, Jones S, Lin J, Sjoblom T, Leary RJ, et al. The genomic landscapes of human breast and colorectal cancers. *Science* (2007) 318:1108–13. doi: 10.1126/science.1145720.
17. Fujimoto A, Furuta M, Totoki Y, Tsunoda T, Kato M, Shiraishi Y, et al. Whole-genome mutational landscape and characterization of noncoding and structural mutations in liver cancer. *Nat Genet* (2016) 48:500–9. doi: 10.1038/ng.3547
18. Pantaleo MA, Astolfi A, Nannini M, Paterini P, Piazzi G, Ercolani G, et al. Gene expression profiling of liver metastases from colorectal cancer as potential basis for treatment choice. *Br J Cancer* (2008) 99:1729–34. doi: 10.1038/sj.bjc.6604681
19. Satoh S, Daigo Y, Furukawa Y, Kato T, Miwa N, Nishiwaki T, et al. AXIN1 mutations in hepatocellular carcinomas, and growth suppression in cancer cells by virus-mediated transfer of AXIN1. *Nat Genet* (2000) 24:245–50. doi: 10.1038/73448
20. Kim WK, Kwon Y, Jang M, Park M, Kim J, Cho S, et al. beta-catenin activation down-regulates cell-cell junction-related genes and induces epithelial-to-mesenchymal transition in colorectal cancers. *Sci Rep* (2019) 9:18440. doi: 10.1038/s41598-019-54890-9
21. Lustig B, Jerchow B, Sachs M, Weiler S, Pietsch T, Karsten U, et al. Negative feedback loop of Wnt signaling through upregulation of conductin/axin2 in colorectal and liver tumors. *Mol Cell Biol* (2002) 22:1184–93. doi: 10.1128/MCB.22.4.1184-1193.2002
22. Zhang J, Tian XJ, Xing J. Signal Transduction Pathways of EMT Induced by TGF-beta, SHH, and WNT and Their Crosstalks. *J Clin Med* (2016) 5(4):41. doi: 10.3390/jcm5040041
23. Jiang YG, Luo Y, He DL, Li X, Zhang LL, Peng T, et al. Role of Wnt/beta-catenin signaling pathway in epithelial-mesenchymal transition of human prostate cancer induced by hypoxia-inducible factor-1alpha. *Int J Urol* (2007) 14:1034–9. doi: 10.1111/j.1442-2042.2007.01866.x
24. Engstrand J, Nilsson H, Stromberg C, Jonas E, Freedman J. Colorectal cancer liver metastases - a population-based study on incidence, management and survival. *BMC Cancer* (2018) 18:78. doi: 10.1186/s12885-017-3925-x
25. Yang M, Schell MJ, Loboda A, Nebozhyn M, Li J, Teer JK, et al. Repurposing EGFR Inhibitor Utility in Colorectal Cancer in Mutant APC and TP53 Subpopulations. *Cancer Epidemiol Biomarkers Prev* (2019) 28:1141–52. doi: 10.1158/1055-9965.EPI-18-1383
26. Fakih MG. Metastatic colorectal cancer: current state and future directions. *J Clin Oncol* (2015) 33:1809–24. doi: 10.1200/JCO.2014.59.7633
27. Bridgewater JA, Pugh SA, Maishman T, Eminton Z, Mellor J, Whitehead A, et al. Systemic chemotherapy with or without cetuximab in patients with resectable colorectal liver metastasis (New EPOC): long-term results of a multicentre, randomised, controlled, phase 3 trial. *Lancet Oncol* (2020) 21:398–411. doi: 10.1016/S1470-2045(19)30798-3
28. Loupakis F, Cremolini C, Masi G, Lonardi S, Zagonel V, Salvatore L, et al. Initial therapy with FOLFOXIRI and bevacizumab for metastatic colorectal cancer. *N Engl J Med* (2014) 371:1609–18. doi: 10.1056/NEJMoa1403108

Conflict of Interest: JD, TH, and XZ were employed by the company, HaploX Biotechnology.

The remaining authors declare that the research was conducted in the absence of any commercial or financial relationships that could be construed as a potential conflict of interest.

frontiers in Oncology

ORIGINAL RESEARCH
published: 14 May 2021
doi: 10.3389/fonc.2021.627460

Cytoplasmic MSH2 Related to Genomic Deletions in the *MSH2/EPCAM* Genes in Colorectal Cancer Patients With Suspected Lynch Syndrome

Lin Dong[1], Shuangmei Zou[1], Xianglan Jin[2], Haizhen Lu[1], Ye Zhang[3], Lei Guo[1], Jianqiang Cai[4†] and Jianming Ying[1*†]*

[1] Department of Pathology, National Cancer Center/National Clinical Research Center for Cancer/Cancer Hospital, Chinese Academy of Medical Sciences and Peking Union Medical College, Beijing, China, [2] Department of Pathology, Peking University Shenzhen Hospital, Shenzhen, China, [3] Beijing Microread Genetics, Beijing, China, [4] Department of Hepatobiliary Surgery, National Cancer Center/National Clinical Research Center for Cancer/Cancer Hospital, Chinese Academy of Medical Sciences and Peking Union Medical College, Beijing, China

Background: A large proportion of patients with Lynch syndrome (LS) have MSH2 abnormalities, but genotype-phenotype studies of *MSH2* mutations in LS are still lacking. The aim of this study was to comprehensively analyze the clinicopathological characteristics and molecular basis of colorectal cancer (CRC) in patients with uncommon MSH2 cytoplasmic expression.

Methods: We retrospectively reviewed 4195 consecutive cases of CRC patients diagnosed between January 2015 and December 2017 at the Cancer Hospital Chinese Academy of Medical Sciences. Of the 4195 patients with CRC, 69 were indicated to have abnormal MSH2 expression through tumor immunohistochemical staining. Genetic tests, such as next-generation sequencing, large genomic rearrangement (LGR) analysis, microsatellite instability status analysis and genomic breakpoint analysis, were performed. Clinicopathological and molecular characteristics and clinical immunotherapy response were analyzed.

Results: Forty-five of 69 patients were identified to have LS with pathogenic germline mutations in *MSH2* and/or *EPCAM*. Of these LS patients, 26.7% were confirmed to harbor large genomic rearrangements (LGRs). Of note, three tumors from two unrelated family pedigrees exhibited a rare cytoplasmic MSH2 staining pattern that was found in LS patients with *EPCAM/MSH2* deletions. RNA analysis showed that two novel mRNA fusions of *EPCAM* and *MSH2* resulted in the predicted protein fusion with MSH2 cytoplasmic localization. Analyses of genomic breakpoints indicated that two novel deletions of *EPCAM* and *MSH2* originated from Alu repeat-mediated recombination events. Our study also provides clinical evidence for the beneficial effect of the PD-1 inhibitor pembrolizumab for CRC patients that exhibit cytoplasmic MSH2 staining.

OPEN ACCESS

Edited by:
Glaucia N M Hajj, International Center for Research, AC Camargo Cancer Center, Brazil

Reviewed by:
Giovana Tardin Torrezan, A.C.Camargo Cancer Center, Brazil
Haitao Luan, University of Nebraska Medical Center, United States
San Ming Wang, University of Macau, China

***Correspondence:**
Jianqiang Cai
caijianqiang188@sina.com
Jianming Ying
jmying@cicams.ac.cn

†These authors have contributed equally to this work and share senior authorship

Specialty section:
This article was submitted to Molecular and Cellular Oncology, a section of the journal Frontiers in Oncology

Received: *27 November 2020*
Accepted: *27 April 2021*
Published: *14 May 2021*

Citation:
Dong L, Zou S, Jin X, Lu H, Zhang Y, Guo L, Cai J and Ying J (2021) Cytoplasmic MSH2 Related to Genomic Deletions in the MSH2/EPCAM Genes in Colorectal Cancer Patients With Suspected Lynch Syndrome. Front. Oncol. 11:627460. doi: 10.3389/fonc.2021.627460

Conclusion: Our study demonstrates that the rare cytoplasmic MSH2 staining pattern should be fully recognized by pathologists and geneticists. Given the specific genotype-phenotype correlation in LS screening, we advocate that all CRC patients with cytoplasmic MSH2 staining in histology should be screened for LGRs of *EPCAM* and *MSH2*.

Keywords: DNA mismatch repair, Lynch syndrome, colorectal cancer, genetic testing, immunotherapy

INTRODUCTION

Lynch syndrome (LS), an autosomal dominant hereditary disorder, is the most common colorectal cancer (CRC) predisposition syndrome, accounting for 1%–3% of all newly diagnosed CRCs (1). LS is caused by pathogenic germline mutations in one of several dMMR genes (*MLH1*, *MSH2*, *MSH6* and *PMS2*) and deletions in *EPCAM* (2–4). Deficient DNA mismatch repair (dMMR) is defined as a lack of immunohistochemically detectable MMR protein expression in tumors and microsatellite instability (MSI), and it is the diagnostic hallmark of LS (5). Concurrent loss of MSH2 and MSH6 proteins, which can be revealed by a universal reflex testing program using immunohistochemistry (IHC), is a common dMMR expression pattern that generally indicates the presence of a germline *MSH2* mutation (6, 7). In addition, deletions of the 3' end of *EPCAM* are thought to lead to tissue-specific epigenetic silencing of *MSH2* through aberrant promoter methylation (2). *EPCAM* deletions account for approximately 20% of cases in which MSH2 and/or MSH6 are lost but there is no detectable *MSH2* germline mutation (8–10). These unique cases cannot be distinguished from those in which *MSH2* mutations are revealed by IHC analysis of MMR proteins (11). Multiplex ligation-dependent probe amplification (MLPA) analysis, which is used to detect large genomic rearrangements (LGRs), is a complementary diagnostic tool in comprehensive genetic testing strategies for LS (12, 13).

IHC analysis of MMR proteins is a cost-effective initial screening method for LS (14, 15). A previous study suggested that the protein expression pattern of MSH2 and MSH6 proteins can be categorized into three types: intact staining of both proteins, loss of both proteins, and isolated loss of MSH6 (16). Mutations in *MSH2* are generally thought to result in the loss of IHC-detectable MSH2 and MSH6. Some challenging cases present with loss of MSH2 and with patchy loss of MSH6, as reported by Dr. Pearlman (17). Cytoplasmic staining is commonly interpreted as having no known significance, with previous literature citing questionable IHC staining quality (14). Dr. Sekine delineated a cryptic nonfunctional in-frame EPCAM-MSH2 fusion protein resulting from a genomic rearrangement between *EPCAM* intron 5 and *MSH2* intron 2 in one LS patient with aberrant cytoplasmic MSH2 localization in colon cancer (18).

Mismatch repair status has been widely used as a positive predictive marker for clinical benefit of immune checkpoint blockade approved by US Food and Drug Administration in metastatic CRCs with dMMR or MSI-high (19). Immunotherapy treatment becomes a new and promising therapeutic option for advanced CRC patients. The importance of accurate interpretation of MMR protein IHC has been paid more attention by clinicians and pathologist (20, 21).

Unfortunately, no other studies are available that might shed light on whether this observation is simply an artifact or a valid finding in some *MSH2*-related LS cases. Due to this uncertainty, it is necessary to systematically assess rare cytoplasmic MSH2 abnormalities to avoid missing potential LS probands and to stratify CRC patients for immunotherapy. In this study, we investigated clinicopathological characteristics and performed molecular characterizations of MSH2 abnormalities in a large cohort of 4195 CRC patients with a particular focus on elucidating the association of cytoplasmic MSH2 staining with genotype in real-world LS patients.

MATERIALS AND METHODS

Selection of Cases

Among 4195 eligible patients from the **C**olo**r**ectal Cancer **I**nitiative **S**creening **P**rogram for **L**ynch **S**yndrome (**CRISPLS**) in the Cancer Hospital of the Chinese Academy of Medical Sciences between January 2015 and December 2017, we identified a cohort of 69 patients with loss of the MSH2 and/or MSH6 proteins who had been screened by IHC staining for tumor MMR proteins. Detailed information on the CRISPLS cohort was previously reported (22). Clinicopathological characteristics and information about cancer personal/family history were collected for patients from the CRISPLS cohort who had undergone surgical resection and for whom a sufficient DNA sample was available. The study was approved by the Ethics Committee of NCC/CICAMS (NCC1790). Individual informed consent was waived because of the retrospective nature of the study. Patients were informed if they were identified as having LS.

Immunohistochemistry Analysis

IHC analyses of MMR proteins, including MLH1, PMS2, MSH2, MSH6 and BRAF V600E, were routinely performed in CRC patients. One representative block of formalin-fixed, paraffin-embedded tumor tissue was selected per patient. Monoclonal antibodies against MLH1 (clone ES05), PMS2 (clone EPR3947), MSH2 (clone FE11), MSH6 (clone EP49) (Beijing Zhongshan Golden Bridge Biotechnology, China), and BRAF V600E (VE1) (Ventana Medical Systems, AZ, USA) were used. Briefly, after deparaffinization, rehydration and antigen-retrieval, 4-μm-thick sections were stained in a Ventana Benchmark IHC automated slide stainer and visualized using the OptiView DAB IHC detection kit (Ventana Medical Systems). The absence of nuclear

staining in tumor cells or very faint nuclear staining in focal tumor cells was defined as loss of protein expression (abnormal staining). Stromal/lymphoid cells and nearby normal glandular epithelium of the bowel served as positive internal controls.

PCR-Based Microsatellite Instability Analysis

Microsatellite instability (MSI) testing was performed on tumor and normal DNA using a fluorescence PCR-based assay (MSI-Reader MSI Analysis System; MICROREAD, Beijing, China) in which six mononucleotide repeat markers (NR-21, NR-24, NR-27, BAT-25, BAT-26 and MONO-27) and two pentanucleotide repeat loci (Penta-C and Penta-D) were amplified to confirm the identity of paired tumor and benign tissues. The PCR products were run on an Applied Biosystems 3500 Genetic Analyzer and analyzed using GeneMapper v5.0 software (Applied Biosystems, CA, USA). Tumors with shifts in two or more markers were classified as unstable MSI-high (23, 24).

Isolation of Genomic DNA

Formalin-fixed, paraffin-embedded tumors and adjacent normal tissue were collected from the cohort. Genomic DNA was extracted using a TGuide Genomic DNA One-Step Kit and a TGuide Automated Nucleic Acid Preparation Instrument (TIANGEN BIOTECH, Beijing, China) according to the manufacturer's instructions as previously described (22).

Germline Mutation Testing by Targeted Next-Generation Sequencing

Next-generation sequencing technology was performed with the Agilent SureSelect-XT Low Input Target Enrichment kit (Agilent Technologies, CA, USA) for germline mutation testing of *MMR* genes from genomic DNA extracted from normal FFPE samples according to the manufacturer's instructions. Molecular barcoded DNA libraries were hybridized with a commercial ClearSeq Inherited Disease multigene panel that covered total exons and intron boundaries within at least ±20 bases of the *EPCAM*, *MLH1*, *PMS2*, *MSH2* and *MSH6* genes (Agilent Technologies). A detailed protocol for variant annotation and classification was described previously (22, 25). Diagnosis of LS is dependent on identifying the pathogenic germline variants of MMR genes. Interpretations of germline variants are classified according to the database of the International Society of Gastrointestinal Hereditary Tumors (InSiGHT) and guideline of the American College of Medical Genetics and Genomics (ACMG). The carriers with likely pathogenic or pathogenic variants are defined as LS patients.

Multiplex Ligation-Dependent Probe Amplification (MLPA)

Large genomic rearrangements (LGRs) in *MSH2* and *EPCAM* genes among MSH2-deficient patients with no germline mutations identified by next-generation sequencing were assessed by MLPA using the SALSA MLPA P003 *MLH1/MSH2* kit (including the 3' end of *EPCAM*) and P072 *MSH6* kit (including the *EPCAM/MSH2* region) (MRC-Holland, Amsterdam, The Netherlands). Fragment analysis of amplified genomic DNA extracted from normal FFPE samples was performed on an ABI3500 capillary sequencer (Applied Biosystems). The MLPA data were quantitatively analyzed using Coffalyser.Net software (www.mlpa.com).

Reverse Transcription PCR and Amplification of *EPCAM-MSH2* Fusion Transcripts

Total RNA was extracted from the peripheral blood leukocytes of patients using TRIzol reagent (Agilent Technologies). cDNA was synthesized using a PrimeScript II 1st Strand cDNA Synthesis Kit (Takara, Japan) and analyzed for *EPCAM-MSH2* fusion transcripts. Polymerase chain reaction (PCR) products were loaded directly on 2% agarose gels and visualized under UV illumination. Selected PCR products were sequenced on an ABI 3500xl capillary DNA analyzer (Applied Biosystems, CA, USA). Details of the PCR primers used are provided in **Table S1**.

Analysis of Breakpoint Mapping

A series of long-range PCR experiments designed to span the putative deletion region were performed to characterize the exact breakpoints in the *EPCAM* and *MSH2* genes using a TaKaRa LA PCR Kit (Takara, Japan) according to the manufacturer's protocol. The PCR products were analyzed by electrophoresis on ethidium bromide-stained 1% agarose gels and then subjected to UV detection. The expected fragment was purified and sequenced on an ABI 3500xl capillary DNA analyzer (Applied Biosystems). Details of the PCR primers are provided in **Table S2**.

Statistical Analysis

A univariate analysis of categorical variables was performed by cross tabulation using a chi-square test to compute p-values. An unpaired t test was used for continuous variables. Statistical descriptions or analyses were conducted using SPSS (Version 22; SPSS Inc., Chicago, IL, USA) or Prism (Version 7; San Diego, CA, USA) software. All tests were 2-tailed, and p-values < 0.05 were considered statistically significant.

RESULTS

Clinicopathological Characteristics of the Study Cohort

We retrospectively enrolled a consecutive cohort of 4195 CRC patients. Among these patients, 345 were eligible, exhibiting dMMR, and 69 exhibited abnormal MSH2 protein expression (**Figure S1**). The frequency of MSH2 deficiency (dMSH2) among the dMMR group was 20% (69 of 345). The demographic and clinical characteristics of patients with MSH2-deficient CRC are summarized in **Table 1**. Briefly, the mean age was 50 years at diagnosis of CRC (standard deviation, 12.7), 94.2% was aged 70 years or younger, 65.2% was male, 47.8% occurred in the proximal colon, 46.4% was at tumor stage II, adenocarcinoma was most common histological type (91.3%). The differences in age of onset, personal history of cancer and family history of LS-related cancers between LS and dMSH2 were statistically significant.

TABLE 1 | Clinicopathological characteristics of patients with MSH2-deficient CRC.

	LS n = 45		Inconclusive dMSH2 n = 24		x^2/t	*P*-value
	No.	Percent	No.	Percent		
Age at diagnosis (years)						
Mean (SD)		48.3 (11.3)		53.3 (14.9)	–	0.120
≤70	45	100.0%	20	83.3%	-	0.012
>70		0.0%	4	16.7%		
Gender					3.757	0.053
Male	33	73.3%	12	50.0%		
Female	12	26.7%	12	50.0%		
Tumor location					3.202	0.362
Proximal colon	20	44.4%	13	54.2%		
Distal colon	9	20.0%	4	16.7%		
Rectum	11	24.4%	7	29.2%		
Other[a]	5	11.1%		0.0%		
Tumor stage					3.326	0.505
I	9	20.0%	4	16.7%		
II	20	44.4%	12	50.0%		
III	8	17.8%	6	25.0%		
IV	5	11.1%		0.0%		
NA	3	6.7%	2	8.3%		
Histological type					0.594	0.743
Adenocarcinoma	41	91.1%	22	91.7%		
Mucinous adenocarcinoma	3	6.7%	2	8.3%		
Other[b]	1	2.2%		0.0%		
Personal history of cancers					5.269	0.022
Yes	15	33.3%	2	8.3%		
No	30	66.7%	22	91.7%		
Family history of LSRC					11.829	0.003
Yes	30	66.7%	6	25.0%		
No	15	33.3%	17	70.8%		
Unknown		0.0%	1	4.2%		
Revised Bethesda guidelines					2.406	0.121
Met	40	88.9%	17	70.8%		
Not met	5	11.1%	7	29.2%		
Not available						
Amsterdam II criteria					7.134	0.028
Met	9	20.0%		0.0%		
Not met	36	80.0%	23	95.8%		
Not available		0.0%	1	4.2%		

dMSH2, deficient MSH2; LSRC, Lynch syndrome-related cancers; SD, standard deviation.

a. Ungrouped data, including 5 patients with 4 CRC tumors located in two sites among the proximal colon, distal colon or rectum, and 1 colon tumor with an unspecified location.

b. Indicates two synchronous cancers at the sigmoid colon and splenic flexure with mucinous carcinoma and adenocarcinoma histologic types, respectively.

Clinicopathological Characteristics of LS Patients With Genomic Rearrangement of *MSH2/EPCAM*

To estimate the frequency and specificity of *MSH2* germline mutations among patients with CRC in the real world, we systematically analyzed a consecutive CRC patient cohort that had been universally screened for LS in our previous study (22). Germline analyses were performed on samples from 69 patients with MSH2-deficient CRC. The frequencies of *MSH2/EPCAM* mutations among different categories of CRC subgroups are presented in detail in **Table S3**. Forty-five patients (1.1%) were identified as having LS with pathogenic germline mutations in *MSH2* and/or *EPCAM*. Of these, 12 (26.7%) were confirmed to carry LGRs in *MSH2/EPCAM* by MLPA, including six probands with *MSH2* genomic deletions, four with *MSH2-EPCAM* deletions (two cases from a family pedigree), and two with *EPCAM* deletions. The clinicopathological and molecular findings for these 12 patients with LGRs are presented in **Table 2**. All cases were identified as microsatellite instability-high (MSI-H) by PCR-MSI. Notably, all 12 of these patients were also ascertained to have a strong cancer family history. Patients with *MSH2/EPCAM* LGRs exhibited an earlier age of CRC onset (mean: 43.8 years) than those with LS with *MSH2* SNV/indel (mean: 49.9 years).

Aberrant Cytoplasmic Localization of the MSH2 Protein Among LS Patients

MSH2 abnormalities usually manifest as the absence of nuclear staining in tumor cells. Among the 69 patients with an MSH2 abnormality, we noted that three (4.3%) exhibited rare cytoplasmic MSH2 localization in tumor cells but showed patchy expression of the MSH6 protein that was somewhat weaker in tumor cells than in internal control cells (patient 164 and patient 271 from one family

TABLE 2 | Clinical, pathological and molecular findings in CRC tumors with *MSH2* LGR-associated LS.

CaseNo.	Age, y/Sex	MMR loss	MSI status	MSH2 abnormal location	Tumor location	Stage	Gene of LGR	NGS result	MLPA result	mRNA result	LS	Family history
49	61/M	MSH2-MSH6-	MSI-H	No	Proximal colon and rectum	II	*MSH2*	Neg	*MSH2* -16 del	ND	Yes	Yes
90	44/M	MSH2-MSH6-	MSI-H	No	Distal colon	I	*MSH2*	Neg	*MSH2* Exon 7 del	ND	Yes	Yes
100	54/M	MSH2-MSH6-	MSI-H	No	Proximal colon	IV	*MSH2* *EPCAM4*		*EPCAM* Exon 9 and *MSH2* Exon 1-14 del	ND	Yes	Yes
164#	17/F	MSH2-MSH6-	MSI-H	Cytoplasmic staining	Rectum	IV	*MSH2* *EPCAM*	Neg	*EPCAM* Exon 3-9 and *MSH2* Exon 1 del	*EPCAM-MSH2* fusion	Yes	Yes
165	53/M	MSH2-MSH6-	MSI-H	No	Proximal colon	III	*EPCAM*	Neg	EPCAM Exon 9 del	ND	Yes	Yes
168	37/M	MSH2-MSH6-	MSI-H	No	Distal colon	II	*MSH2* *EPCAM*	Neg	*EPCAM* Exon 9 and *MSH2* Exon 1-14 del	ND	Yes	Yes
205	48/F	MSH2-MSH6-	MSI-H	No	Rectum	II	*MSH2*	Neg	*MSH2* Exon 3-8 del	ND	Yes	Yes
212	60/M	MSH2-MSH6-	MSI-H	No	Rectum	I	*MSH2*	Neg	*MSH2* Exon 8-11 del	ND	Yes	Yes
234	28/M	MSH2-MSH6-	MSI-H	No	Rectum	I	*MSH2*	Neg	*MSH2* Exon 3 del	ND	Yes	Yes
271#	45/M	MSH2-MSH6-	MSI-H	Cytoplasmic staining	Distal colon	IV	*MSH2* *EPCAM*	Neg	*EPCAM* Exon 3-9 and *MSH2* Exon 1 del	*EPCAM-MSH2* fusion	Yes	Yes
318	49/M	MSH2-MSH6-	MSI-H	No	Rectum	I	*MSH2*	Neg	MSH2 Exon 1-3 del	ND	Yes	Yes
345	27/F	MSH2-MSH6-	MSI-H	Cytoplasmic staining	Proximal colon	III	*EPCAM*	Neg	*EPCAM* Exon 3-9 del	*EPCAM-MSH2* fusion	Yes	Yes

Del, deletion; F, female; IHC, immunohistochemistry; LGR, large genomic rearrangement; LS, Lynch syndrome; M, male; MLPA, multiplex ligation-dependent probe amplification; MMR, mismatch repair; MSI, microsatellite instability; Neg, negative; NGS, next-generation sequencing; No., number; ND, not done. # indicates that the patient is from a family pedigree shown in ***Figure 2A****.*

pedigree and patient 345) (**Figures 1** and **S2**). They presented a classical family history of LS cancer (**Figure 2**). PCR-MSI tests indicated a status of MSI-high in the tumors of these patients (**Figure S2**). MLPA tests identified combined deletions of *MSH2* and *EPCAM* in all three patients. Two patients had a heterozygous large genomic deletion in *EPCAM* (exons 3–9) and *MSH2* (exon 1). One patient harbored heterozygous deletion of exons 3–9 of *EPCAM* (**Figure S4**).

Alu-Mediated *EPCAM/MSH2* Cytoplasmic MSH2 Related to Genomic Deletions in the MSH2/EPCAM Genes in Colorectal Cancer Patients with Suspected Lynch Syndrome Rearrangement Is Responsible for Cytoplasmic Localization of MSH2 in LS Patients

To elucidate the molecular characteristics of cytoplasmic localization of MSH2 in tumors, we performed mapping analysis of gene fusions and gene breakpoints for two individual patients. Sanger sequencing of cDNA from the blood lymphocytes of the patients suggested that a fusion transcript of EPCAM and MSH2 was the source of aberrant MSH2 localization in tumors. Sequencing revealed a common fusion of exon 1 of EPCAM and exon 2 of MSH2 in patient 271 and patient 345. On the basis of this fusion transcript analysis, we performed a series of long-range PCR experiments on the region of interest between intron 1 of EPCAM and intron 1 of MSH2 to identify the precise breakpoint in the *MSH2/EPCAM* LGRs (**Figures S6** and **S7**). Ultimately, we mapped the breakpoint to intron 1 of EPCAM (hg38, chr2:47372970)/MSH2 upstream [hg38, chr2:47400492]) in patient 271 and to intron 1 of EPCAM (hg38, chr2:47370462)/intron 1 of MSH2 [hg38, chr2:47404894]) in patient 345. Both were novel mutations that were not reported in the International Society for Gastrointestinal Hereditary Tumours (InSiGHT) variant database (http://insight-database.org). Repeated Alu elements are implicated in the etiology of genomic rearrangement for many inherited cancers (26). Our analysis using RepeatMasker (http://www.repeatmasker.org) revealed that these breakpoints lay within Alu elements that share high sequence identities. A schematic diagram is shown in **Figure 3**.

Response to Treatment With a PD-1 Inhibitor in a Colon Cancer Patient With Cytoplasmic MSH2 Expression

Among patients with tumors showing abnormal MSH2 expression in our cohort, a 45-year-old male (patient 271) was diagnosed with retroperitoneal lymph node metastasis of stage IV colon cancer with rare MSH2 cytoplasmic localization. This patient underwent dissection of distal colon cancer at the age of 33. A cancer family history survey for this patient showed that nine members in three consecutive generations suffered from LS-related cancers (LSRC), including CRC in II6, III2, III5, III7, III11, III13, IV1; pancreatic cancer in II6; and endometrial cancer in III10 (**Figure 2A**). Patient IV1 (case 164) was retrospectively analyzed and identified as having the same MMR pattern as proband III5 (case 271). PCR-MSI confirmed that both patients showing a rare MSH2 cytoplasmic localization were MSI-high, which should be considered an uncommon dMMR pattern. Genetic testing identified this pedigree as LS harboring a novel pathogenic

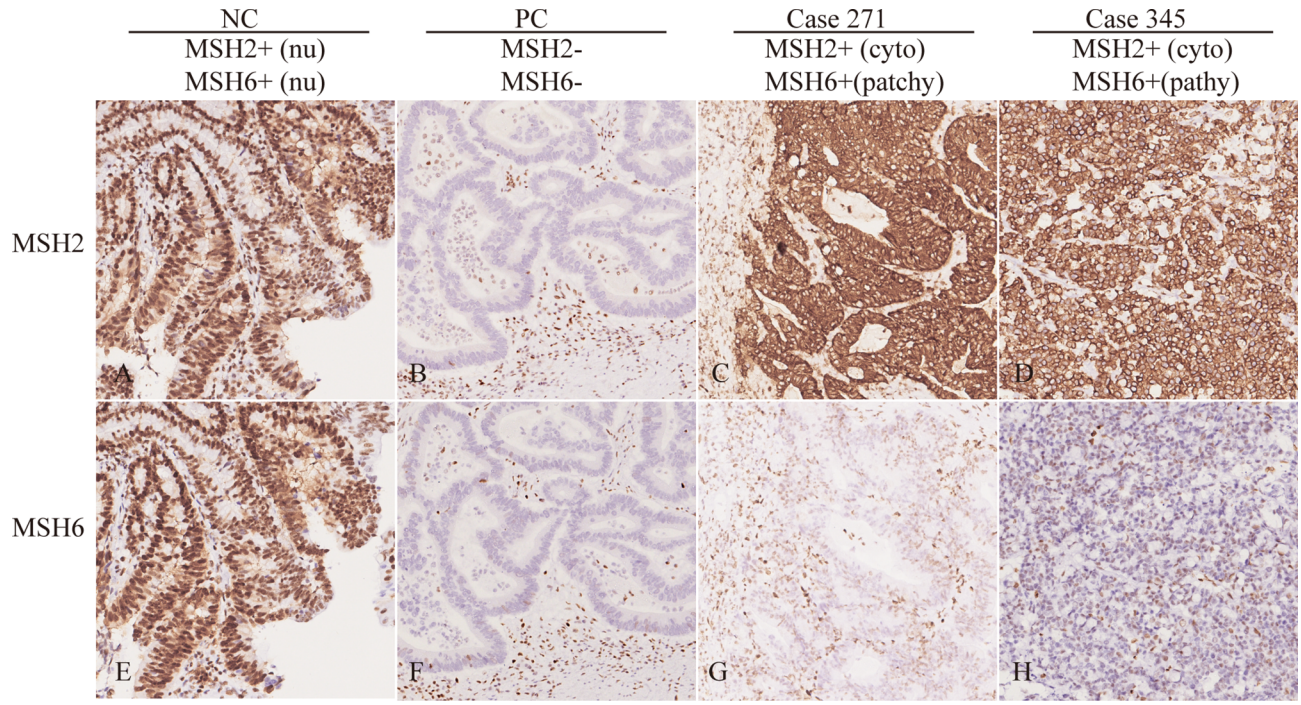

FIGURE 1 | Rare MSH2 cytoplasmic staining in CRC. IHC of MSH2 and MSH6 in selected patients showing protein expression in tumor cells. The NC (negative control with proficient MMR) showed nuclear staining of MSH2 and MSH6. The PC (positive control with deficient MMR) showed loss of nuclear staining of MSH2 and MSH6. However, patient 271 and 345 showed cytoplasmic MSH2 and patchy/weak MSH6 nuclear staining in tumor cells. Nu, nuclear; cyto, cytoplasmic.

genomic deletion of *EPCAM* and *MSH2* genes. Patient 271 was treated with the PD-1 inhibitor pembrolizumab in combination with capecitabine every 3 weeks for 19 cycles. The patient achieved a clinical partial response (PR) with a 56% reduction in the short axis diameter of the enlarged retroperitoneal lymph node, as revealed by computed tomography (CT) scans after a 19-month course of treatment (**Figure 4**).

DISCUSSION

In recent years, there has been increasing demand for immunotherapy and LS screening among CRC patients displaying MSI-high or dMMR (27–30). These developments highlight the importance of closely integrating pathologic diagnosis, clinical counseling, and molecular testing for precision medicine approaches to CRC therapy. The purpose of further emphasizing molecular pathology in CRC is to personalize patient treatment and screening of suspected LS patients. In our previous study, we found that a significant proportion of LS patients have LGRs in *MMR* genes in China, a finding that has often been missed by previous next-generation sequencing (22, 31). In the current study, we systematically investigated the diverse mutation patterns of *MSH2* and the clinicopathological characteristics of patients with MSH2 abnormalities in our cohort, especially LGRs, and the corresponding specific genotype-phenotype associations. We found that 12 of 45 (26.7%) LS patients were carriers of *MSH2* and/or *EPCAM* LGRs. Three of 12 (25%) probands with *MSH2*/*EPCAM* LGRs harbored a rare MSH2 chimeric fusion protein that was detectable in the cytoplasm of tumor cells by IHC. We also provided clinical evidence that a CRC patient harboring cytoplasmic MSH2 fusion proteins was responsive to treatment with immune checkpoint inhibitors.

MMR IHC profiles help discriminate which genes may be deficient in MMR function. Previous studies have indicated that genomic deletion of *MSH2* is a frequent causal event among LS patients (13, 32). One breakthrough study demonstrated that germline deletion of *EPCAM* also leads to inactivation of *MSH2* in families with LS (2). Diverse mutation patterns, especially large genomic deletions/duplications in the *MSH2* and/or *EPCAM* genes, increase the complexity of MSH2 IHC interpretation and molecular testing during LS screening (12, 18, 33–36). dMMR has emerged as a major predictive biomarker for the efficacy of immune checkpoint inhibitors in CRC (19). However, a *post hoc* analysis of clinical trials found that misinterpretation of IHC for MMR proteins was responsible for primary resistance to immune checkpoint inhibitors (21). One rare case of a patient with a *MSH2*/*EPCAM* LGR was reported to show distinct cytoplasmic localization of MSH2 (18). The study also revealed that there was an indication of EPCAM-MSH2 protein fusion rather than artificial nonspecific staining. The cases in this study and others demonstrate that there are still some challenges and pitfalls that pathologists need to avoid. However, because these atypical situations have not been well documented in the literature, they have not been effectively

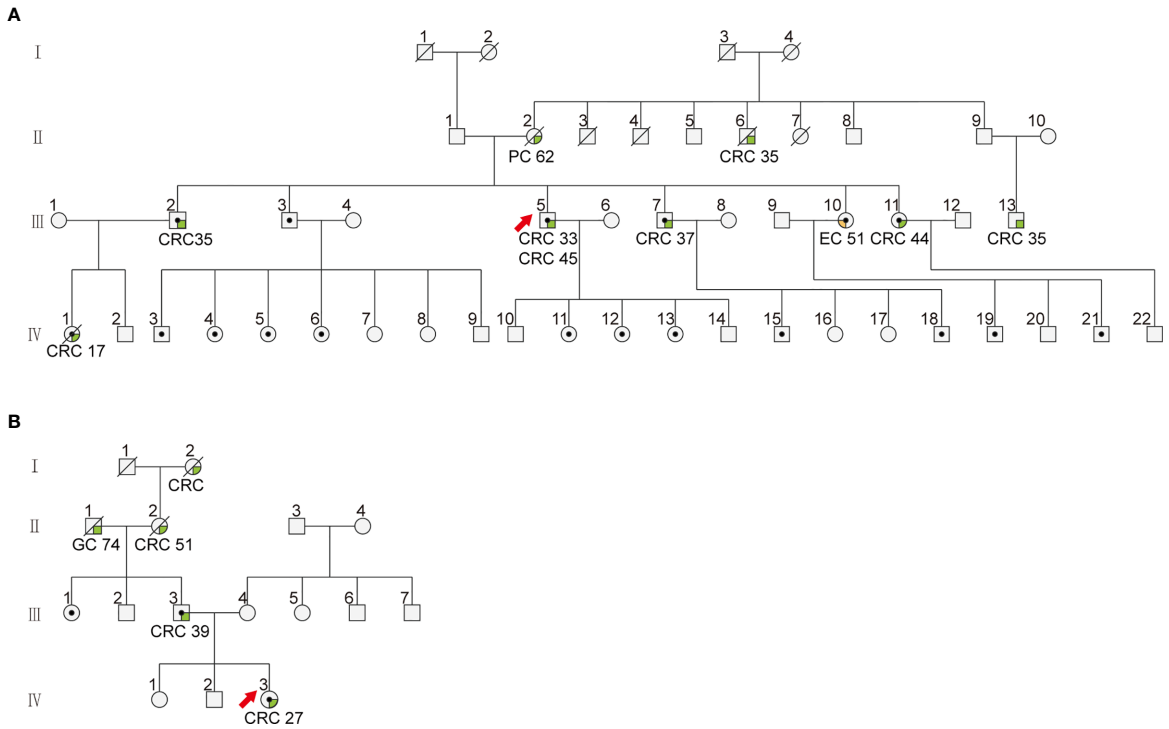

FIGURE 2 | The family pedigree of patients with cytoplasmic staining of MSH2 in colorectal cancer. The family pedigrees of **(A)** Patient 271 (III5) and 164 (IV1) and **(B)** patient 345 (IV3) investigated in this study. The proband is indicated by the red arrow. The black dots indicate mutation carriers confirmed by genetic testing. The cancer types and age of onset are listed beneath each affected family member.

translated into clinical practice guidelines and are easily misinterpreted by pathologists (37–39). In the current study, characterization of three probands with abnormal MSH2 localization by IHC revealed detectable and specific cytoplasmic staining of MSH2 and loss of nuclear MSH2 staining with patchy MSH6 expression in the nucleus. Complementary PCR-MSI tests confirmed an MSI-high pattern suggestive of dMMR in tumors with cytoplasmic MSH2 staining. All three patients were identified as having LS with combined deletion of *MSH2* and *EPCAM*, indicating an interestingly distinct phenotype-genotype association in LS screening. Together, the findings of our study based on a large consecutive CRC cohort demonstrate the pathologic characteristics of this novel MSH2 staining pattern and its possible association with germline mutations in *MMR* genes. Cases in which cytoplasmic MSH2 staining is combined with patchy or weak MSH6 staining in tumor cells are highly suspected to be LS.

IHC staining of MMR proteins should always be interpreted with caution. When interpreting staining as abnormal, pathologists should consider the localization, proportion, intensity and internal control of staining in tumor cells (40). Tumors carrying an *MSH2* germline mutation generally show a complete loss of MSH2 and MSH6 proteins, whereas other uncommon staining patterns, such as MSH2 loss and patchy MSH6 nuclear staining, as well as retained staining of MSH2 and MSH6, have drawn the attention of pathologists and genetic counselors during IHC analysis of MMR proteins (17, 41). The findings of this study highlight another uncommon staining pattern: MSH2 cytoplasmic staining and patchy MSH6 nuclear staining, rather than the absence of staining, in tumor cells. IHC staining of adjacent normal colorectal tissues showed possible MSH2 cytoplasmic expression and nuclear staining. This indicates that a "double hit" in *MSH2* causes inactivation of the normal allele, resulting in its absence in the nuclei of tumor cells. This study expands the pathologic interpretations of MSH2 IHC staining during LS prescreening and immunotherapy testing. The three patients with MSH2 abnormalities were all identified as having LS. The correlation between MSH2 cytoplasmic staining and large genomic deletions in *MSH2/EPCAM* is significant. Therefore, the dMMR pattern of cytoplasmic MSH2 staining and patchy/weak MSH6 nuclear staining should be helpful diagnostically in cases where LS is highly suspected by incorporating LGR analysis of *MSH2/EPCAM*. In addition, on the basis of these LS cases with ambiguous patchy/weak MSH6 staining, we also advocate for the use of four MMR proteins in IHC screens instead of the two-protein (MSH6 and PMS2) staining method (17, 42, 43).

EPCAM is an epithelial cell adhesion molecule located on the cell surface. The protein consists of a signal peptide, extracellular domain (N-terminal), transmembrane domain and cytoplasmic domain (C-terminal). Patients with cytoplasmic staining have a common feature of MSH2 C-terminal fusion with an EPCAM N-terminal fragment of 25 amino acids, including a complete signal peptide (44). The signal peptide is required for cytoplasmic

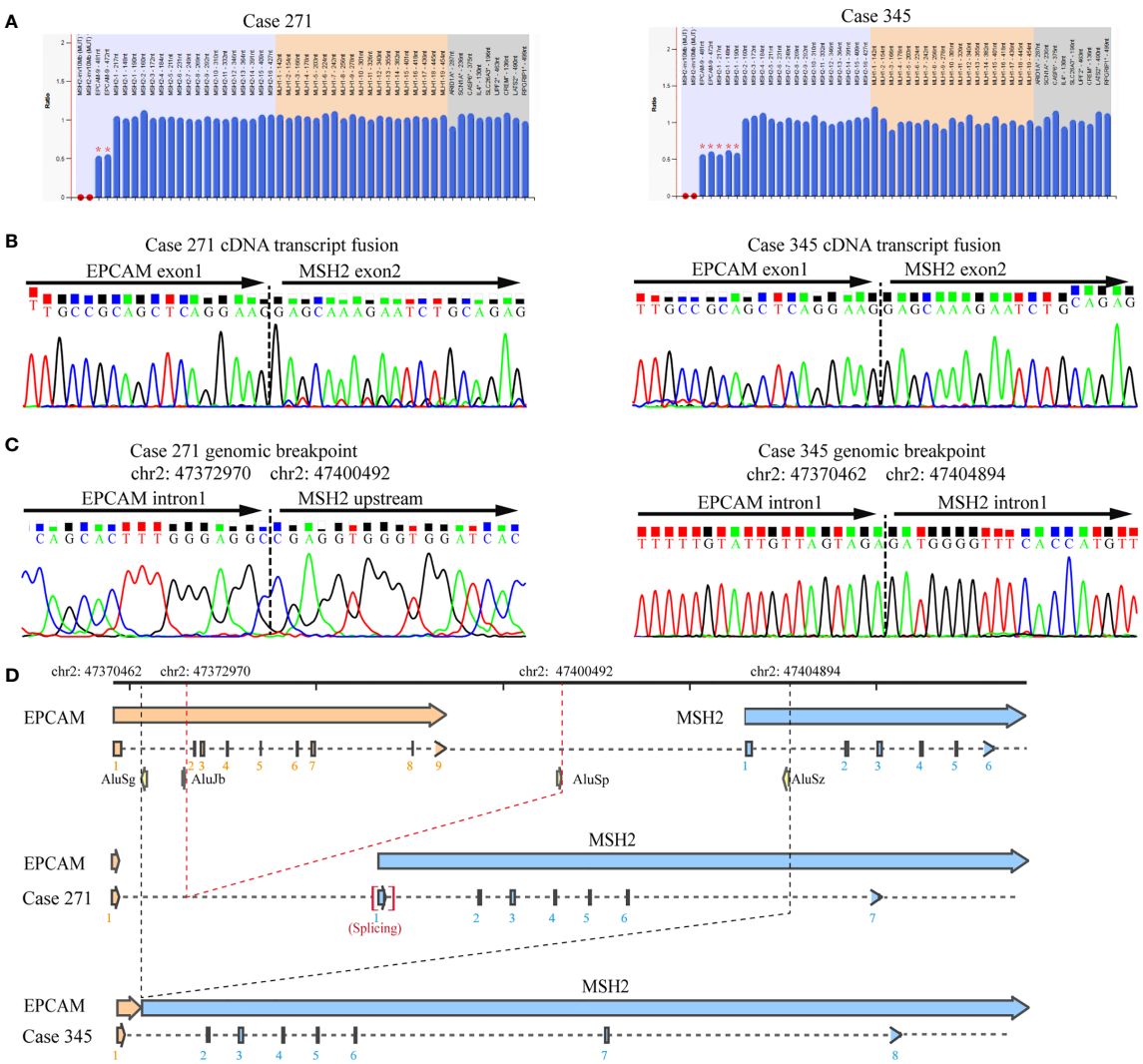

FIGURE 3 | Identification of the germline *EPCAM-MSH2* fusion in patients with suspected LS and cytoplasmic MSH2 staining. **(A)** MLPA testing identified the presence of a large genomic deletion in the *MSH2* and *EPCAM* genes in patients 271 and 345. **(B)** Sanger sequencing of *EPCAM* and *MSH2* transcripts amplified by the E1M23-1F and E1M23-2R primer pairs in the peripheral blood cDNA of the proband revealed a fusion between exon 1 of *EPCAM* and exon 2 of *MSH2*. **(C)** Sequencing analysis of long-range PCR products from genomic DNA defined the exact breakpoint, as indicated by the genomic locus. **(D)** Schematic representation showing the genomic deletions mediated by recombination between Alu elements.

membrane localization of the EPCAM protein. It is possible that the EPCAM signal peptide guides the cytoplasmic membrane translocation of EPCAM-MSH2 fusion proteins in this study. MSH2 and MSH6 in humans form an hMutSα heterodimer and are subsequently imported to the nucleus in a manner dependent on MSH6 nuclear localization sequences (45, 46). The EPCAM-MSH2 fusion proteins may interfere with binding and dimerization with MSH6. This defect in protein interaction in turn results in MSH6 protein instability without heterodimerization with MSH2, as indicated by weak or absent MSH6 staining in the nucleus (17).

In this study, 26.7% of LS CRC patients with MSH2 abnormalities carried pathogenic mutations in *MSH2*/*EPCAM* LGRs, consistent with previous studies (8, 11, 13). *EPCAM* deletions are generally considered to result in promoter hypermethylation and epigenetic silencing of the neighboring *MSH2* gene through transcriptional read-through (2). Our study indicates that nonfunctional chimeric proteins derived from fusion transcripts of *MSH2*/*EPCAM* LGRs were underestimated in LS screening. This was not accidental. Three out of 12 patients with *MSH2*/*EPCAM* LGRs exhibited a similar phenotype of cytoplasmic staining of MSH2. Although the three identified patients from two families harbored two different genomic aberrations, they were found to have the same *EPCAM-MSH2* transcript that involves the fusion of exon 1 of EPCAM and exon 2 of MSH2. A subsequent detailed analysis of breakpoint junctions indicated that the molecular mechanism underlying the novel

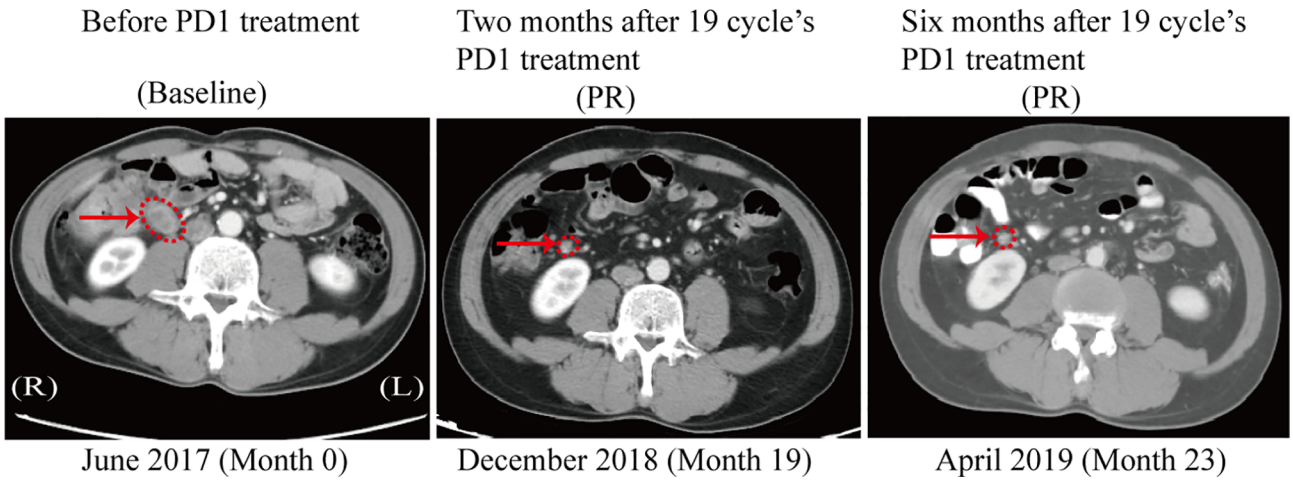

FIGURE 4 | CT scan after PD1 treatment in the patient with MSH2 cytoplasmic staining. A computed tomography (CT) scan revealed the clinical benefits of the PD-1 inhibitor pembrolizumab in the patient with cytoplasmic staining of MSH2. In June 2017, a baseline CT scan showed an enlarged retroperitoneal lymph node (1.8x2.0 cm) with a diagnosis of metastatic colon cancer (arrows). No disease progression was confirmed in this patient 6 months after completion of 19 cycles of immunotherapy, as demonstrated by a stable lymph node size of 0.8x0.8 cm between December 2018 and April 2019 (arrows).

rearrangements was intrachromosomal recombination mediated by Alu-Alu elements. They harbored different breakpoints in *EPCAM-MSH2* than those reported by Sekine et al. (18). Alu repeats are a family of short interspersed nuclear elements (SINEs) that are prevalent in the human genome. It has been shown that some genes, such as *MSH2* and *EPCAM*, are more prone to LGRs because of the presence of abundant homologous Alu elements (10, 47, 48). Therefore, molecular characterizations of uncommon cases from emerging clinical practice data definitely increase our understanding of LS etiology and contribute to refinements in corresponding genetic diagnostic approaches.

From a clinical standpoint, MMR-deficient CRC cases respond poorly to fluorouracil-based chemotherapeutics and are highly sensitive to immune checkpoint inhibitors (19, 30, 49–52). Misdiagnosis of dMMR and MSI status are the primary factors underlying resistance to immunotherapy among CRC patients (21). A lack of familiarity with the nuances of MMR IHC can lead to interpretive errors (15). Our findings suggest that CRCs with cytoplasmic localization of MSH2 should be considered dMMR and MSI-high. One case also demonstrated that anti-PD-1 immunotherapy shows a durable clinical benefit. Although this is only one example, we believe that, given their dMMR status, such patients should expect good efficacy with immune checkpoint inhibitor therapy. We suggest that PCR-MSI should be endorsed as a complementary test for abnormal patients that show equivocal immunostaining patterns to improve personalized targeted therapy.

In conclusion, our study demonstrates that the rare cytoplasmic MSH2 staining pattern in LS patients should be fully recognized by pathologists and geneticists. Given the specific genotype-phenotype correlation in LS screening, we advocate that all CRC patients with cytoplasmic MSH2 staining in histology should be screened for LGRs of *EPCAM* and *MSH2* in clinical practice.

DATA AVAILABILITY STATEMENT

The original contributions presented in the study are included in the article/**Supplementary Material**. Further inquiries can be directed to the corresponding authors.

ETHICS STATEMENT

The studies involving human participants were reviewed and approved by Cancer Hospital of the Chinese Academy of Medical Sciences. Written informed consent to participate in this study was provided by the participants' legal guardian/next of kin.

AUTHOR CONTRIBUTIONS

JC and JY designed and supervised the overall project. LD, SZ, and YZ compiled and analyzed the data and performed statistical analyses. LD, HL, and LG interpreted the data and drafted the manuscript. JY critically revised the manuscript for intellectual content. All authors contributed to the article and approved the submitted version.

FUNDING

This work was supported by grants from the Special Fund of the Chinese Central Government for Basic Scientific Research in Commonweal Research Institutes (2016ZX310024 and 2016ZX310176), Beijing Hope Run Special Fund of the Cancer Foundation of China (LC2017B14), the Non-Profit Central

Research Institute Fund of Chinese Academy of Medical Sciences (2019PT310026) and the National Key Research and Development Program (2017YFC1311005). The funders had no role in the study design, data acquisition, analysis, interpretation, writing or submission of the manuscript.

SUPPLEMENTARY MATERIAL

The Supplementary Material for this article can be found online at: https://www.frontiersin.org/articles/10.3389/fonc.2021.627460/full#supplementary-material

REFERENCES

1. Moreira L, Balaguer F, Lindor N, de la Chapelle A, Hampel H, Aaltonen LA, et al. Identification of Lynch Syndrome Among Patients With Colorectal Cancer. *JAMA* (2012) 308:1555–65. doi: 10.1001/jama.2012.13088
2. Ligtenberg MJ, Kuiper RP, Chan TL, Goossens M, Hebeda KM, Voorendt M, et al. Heritable Somatic Methylation and Inactivation of MSH2 in Families With Lynch Syndrome Due to Deletion of the 3' Exons of TACSTD1. *Nat Genet* (2009) 41:112–7. doi: 10.1038/ng.283
3. Li GM. Mechanisms and Functions of DNA Mismatch Repair. *Cell Res* (2008) 18:85–98. doi: 10.1038/cr.2007.115
4. Hampel H, Frankel WL, Martin E, Arnold M, Khanduja K, Kuebler P, et al. Screening for the Lynch Syndrome (Hereditary Nonpolyposis Colorectal Cancer). *N Engl J Med* (2005) 352:1851–60. doi: 10.1056/NEJMoa043146
5. Palter VN, Baker NA, Rabeneck L, Tinmouth J, Gagliardi AR, Kennedy ED, et al. A Framework to Build Capacity for a Reflex-Testing Program for Lynch Syndrome. *Genet Med* (2019) 21:1381–9. doi: 10.1038/s41436-018-0342-8
6. Pai RK, Pai RK. A Practical Approach to the Evaluation of Gastrointestinal Tract Carcinomas for Lynch Syndrome. *Am J Surg Pathol* (2016) 40:e17–34. doi: 10.1097/PAS.0000000000000620
7. Chen W, Swanson BJ, Frankel WL. Molecular Genetics of Microsatellite-Unstable Colorectal Cancer for Pathologists. *Diagn Pathol* (2017) 12:24. doi: 10.1186/s13000-017-0613-8
8. Rumilla K, Schowalter KV, Lindor NM, Thomas BC, Mensink KA, Gallinger S, et al. Frequency of Deletions of EPCAM (TACSTD1) in MSH2-Associated Lynch Syndrome Cases. *J Mol Diagn* (2011) 13:93–9. doi: 10.1016/j.jmoldx.2010.11.011
9. Cini G, Quaia M, Canzonieri V, Fornasarig M, Maestro R, Morabito A, et al. Toward a Better Definition of EPCAM Deletions in Lynch Syndrome: Report of New Variants in Italy and the Associated Molecular Phenotype. *Mol Genet Genomic Med* (2019) 7:e587. doi: 10.1002/mgg3.587
10. Perez-Cabornero L, Infante SM, Velasco SE, Lastra AE, Acedo BA, Miner PC, et al. Frequency of Rearrangements in Lynch Syndrome Cases Associated With MSH2: Characterization of a New Deletion Involving Both EPCAM and the 5' Part of MSH2. *Cancer Prev Res (Phila)* (2011) 4:1556–62. doi: 10.1158/1940-6207.CAPR-11-0080
11. Kloor M, Voigt AY, Schackert HK, Schirmacher P, von Knebel DM, Blaker H. Analysis of EPCAM Protein Expression in Diagnostics of Lynch Syndrome. *J Clin Oncol* (2011) 29:223–7. doi: 10.1200/JCO.2010.32.0820
12. Huth C, Kloor M, Voigt AY, Bozukova G, Evers C, Gaspar H, et al. The Molecular Basis of EPCAM Expression Loss in Lynch Syndrome-Associated Tumors. *Mod Pathol* (2012) 25:911–6. doi: 10.1038/modpathol.2012.30
13. Baudhuin LM, Ferber MJ, Winters JL, Steenblock KJ, Swanson RL, French AJ, et al. Characterization of Hmlh1 and Hmsh2 Gene Dosage Alterations in Lynch Syndrome Patients. *Gastroenterology* (2005) 129:846–54. doi: 10.1053/j.gastro.2005.06.026
14. Shia J. Immunohistochemistry Versus Microsatellite Instability Testing for Screening Colorectal Cancer Patients At Risk for Hereditary Nonpolyposis Colorectal Cancer Syndrome. Part I. the Utility of Immunohistochemistry. *J Mol Diagn* (2008) 10:293–300. doi: 10.2353/jmoldx.2008.080031
15. Hissong E, Crowe EP, Yantiss RK, Chen YT. Assessing Colorectal Cancer Mismatch Repair Status in the Modern Era: A Survey of Current Practices and Re-Evaluation of the Role of Microsatellite Instability Testing. *Mod Pathol* (2018) 31:1756–66. doi: 10.1038/s41379-018-0094-7
16. Kantelinen J, Kansikas M, Candelin S, Hampel H, Smith B, Holm L, et al. Mismatch Repair Analysis of Inherited MSH2 and/or MSH6 Variation Pairs Found in Cancer Patients. *Hum Mutat* (2012) 33:1294–301. doi: 10.1002/humu.22119
17. Pearlman R, Markow M, Knight D, Chen W, Arnold CA, Pritchard CC, et al. Two-Stain Immunohistochemical Screening for Lynch Syndrome in Colorectal Cancer May Fail to Detect Mismatch Repair Deficiency. *Mod Pathol* (2018) 31:1891–900. doi: 10.1038/s41379-018-0058-y
18. Sekine S, Ogawa R, Saito S, Ushiama M, Shida D, Nakajima T, et al. Cytoplasmic MSH2 Immunoreactivity in a Patient With Lynch Syndrome With an EPCAM-MSH2 Fusion. *Histopathology* (2017) 70:664–9. doi: 10.1111/his.13104
19. Le DT, Uram JN, Wang H, Bartlett BR, Kemberling H, Eyring AD, et al. PD-1 Blockade in Tumors With Mismatch-Repair Deficiency. *N Engl J Med* (2015) 372:2509–20. doi: 10.1056/NEJMoa1500596
20. Oliveira AF, Bretes L, Furtado I. Review of PD-1/PD-L1 Inhibitors in Metastatic Dmmr/MSI-H Colorectal Cancer. *Front Oncol* (2019) 9:396. doi: 10.3389/fonc.2019.00396
21. Cohen R, Hain E, Buhard O, Guilloux A, Bardier A, Kaci R, et al. Association of Primary Resistance to Immune Checkpoint Inhibitors in Metastatic Colorectal Cancer With Misdiagnosis of Microsatellite Instability or Mismatch Repair Deficiency Status. *JAMA Oncol* (2019) 5:551–5. doi: 10.1001/jamaoncol.2018.4942
22. Dong L, Jin X, Wang W, Ye Q, Li W, Shi S, et al. Distinct Clinical Phenotype and Genetic Testing Strategy for Lynch Syndrome in China Based on a Large Colorectal Cancer Cohort. *Int J Cancer* (2020) 146:3077–86. doi: 10.1002/ijc.32914
23. Suraweera N, Duval A, Reperant M, Vaury C, Furlan D, Leroy K, et al. Evaluation of Tumor Microsatellite Instability Using Five Quasimonomorphic Mononucleotide Repeats and Pentaplex PCR. *Gastroenterology* (2002) 123:1804–11. doi: 10.1053/gast.2002.37070
24. Rodriguez-Bigas MA, Boland CR, Hamilton SR, Henson DE, Jass JR, Khan PM, et al. A National Cancer Institute Workshop on Hereditary Nonpolyposis Colorectal Cancer Syndrome: Meeting Highlights and Bethesda Guidelines. *J Natl Cancer Inst* (1997) 89:1758–62. doi: 10.1093/jnci/89.23.1758
25. Richards S, Aziz N, Bale S, Bick D, Das S, Gastier-Foster J, et al. Standards and Guidelines for the Interpretation of Sequence Variants: A Joint Consensus Recommendation of the American College of Medical Genetics and Genomics and the Association for Molecular Pathology. *Genet Med* (2015) 17:405–24. doi: 10.1038/gim.2015.30
26. Elliott B, Richardson C, Jasin M. Chromosomal Translocation Mechanisms At Intronic Alu Elements in Mammalian Cells. *Mol Cell* (2005) 17:885–94. doi: 10.1016/j.molcel.2005.02.028
27. Nebot-Bral L, Brandao D, Verlingue L, Rouleau E, Caron O, Despras E, et al. Hypermutated Tumours in the Era of Immunotherapy: The Paradigm of Personalised Medicine. *Eur J Cancer* (2017) 84:290–303. doi: 10.1016/j.ejca.2017.07.026
28. Kloor M, von Knebel DM. The Immune Biology of Microsatellite-Unstable Cancer. *Trends Cancer* (2016) 2:121–33. doi: 10.1016/j.trecan.2016.02.004
29. Luchini C, Bibeau F, Ligtenberg M, Singh N, Nottegar A, Bosse T, et al. ESMO Recommendations on Microsatellite Instability Testing for Immunotherapy in Cancer, and Its Relationship With PD-1/PD-L1 Expression and Tumour Mutational Burden: A Systematic Review-Based Approach. *Ann Oncol* (2019) 30:1232–43. doi: 10.1093/annonc/mdz116
30. Overman MJ, McDermott R, Leach JL, Lonardi S, Lenz HJ, Morse MA, et al. Nivolumab in Patients With Metastatic DNA Mismatch Repair-Deficient or Microsatellite Instability-High Colorectal Cancer (Checkmate 142): An Open-Label, Multicentre, Phase 2 Study. *Lancet Oncol* (2017) 18:1182–91. doi: 10.1016/S1470-2045(17)30422-9
31. Zhang L, Bhaskaran SP, Huang T, Dong H, Chandratre K, Wu X, et al. Variants of DNA Mismatch Repair Genes Derived From 33,998 Chinese Individuals With and Without Cancer Reveal Their Highly Ethnic-Specific Nature. *Eur J Cancer* (2020) 125:12–21. doi: 10.1016/j.ejca.2019.11.004
32. Wijnen J, van der Klift H, Vasen H, Khan PM, Menko F, Tops C, et al. MSH2 Genomic Deletions are a Frequent Cause of HNPCC. *Nat Genet* (1998) 20:326–8. doi: 10.1038/3795

33. Kovacs ME, Papp J, Szentirmay Z, Otto S, Olah E. Deletions Removing the Last Exon of TACSTD1 Constitute a Distinct Class of Mutations Predisposing to Lynch Syndrome. *Hum Mutat* (2009) 30:197–203. doi: 10.1002/humu.20942
34. Liu Q, Hesson LB, Nunez AC, Packham D, Williams R, Ward RL, et al. A Cryptic Paracentric Inversion of MSH2 Exons 2-6 Causes Lynch Syndrome. *Carcinogenesis* (2016) 37:10–7. doi: 10.1093/carcin/bgv154
35. Kang SY, Park CK, Chang DK, Kim JW, Son HJ, Cho YB, et al. Lynch-Like Syndrome: Characterization and Comparison With EPCAM Deletion Carriers. *Int J Cancer* (2015) 136:1568–78. doi: 10.1002/ijc.29133
36. Martinez-Bouzas C, Ojembarrena E, Beristain E, Errasti J, Viguera N, Minguez MT. High Proportion of Large Genomic Rearrangements in Hmsh2 in Hereditary Nonpolyposis Colorectal Cancer (HNPCC) Families of the Basque Country. *Cancer Lett* (2007) 255:295–9. doi: 10.1016/j.canlet.2007.05.004
37. Sepulveda AR, Hamilton SR, Allegra CJ, Grody W, Cushman-Vokoun AM, Funkhouser WK, et al. Molecular Biomarkers for the Evaluation of Colorectal Cancer: Guideline From the American Society for Clinical Pathology, College of American Pathologists, Association for Molecular Pathology, and American Society of Clinical Oncology. *Arch Pathol Lab Med* (2017) 141:625–57. doi: 10.5858/arpa.2016-0554-CP
38. Gupta S, Provenzale D, Llor X, Halverson AL, Grady W, Chung DC, et al. Nccn Guidelines Insights: Genetic/Familial High-Risk Assessment: Colorectal, Version 2.2019. *J Natl Compr Canc Netw* (2019) 17:1032–41. doi: 10.6004/jnccn.2019.0044
39. Muller A, Giuffre G, Edmonston TB, Mathiak M, Roggendorf B, Heinmoller E, et al. Challenges and Pitfalls in HNPCC Screening by Microsatellite Analysis and Immunohistochemistry. *J Mol Diagn* (2004) 6:308–15. doi: 10.1016/S1525-1578(10)60526-0
40. Overbeek LI, Ligtenberg MJ, Willems RW, Hermens RP, Blokx WA, Dubois SV, et al. Interpretation of Immunohistochemistry for Mismatch Repair Proteins is Only Reliable in a Specialized Setting. *Am J Surg Pathol* (2008) 32:1246–51. doi: 10.1097/PAS.0b013e31816401bb
41. Ollila S, Sarantaus L, Kariola R, Chan P, Hampel H, Holinski-Feder E, et al. Pathogenicity of MSH2 Missense Mutations is Typically Associated With Impaired Repair Capability of the Mutated Protein. *Gastroenterology* (2006) 131:1408–17. doi: 10.1053/j.gastro.2006.08.044
42. Hall G, Clarkson A, Shi A, Langford E, Leung H, Eckstein RP, et al. Immunohistochemistry for PMS2 and MSH6 Alone Can Replace a Four Antibody Panel for Mismatch Repair Deficiency Screening in Colorectal Adenocarcinoma. *Pathology* (2010) 42:409–13. doi: 10.3109/00313025.2010.493871
43. Mojtahed A, Schrijver I, Ford JM, Longacre TA, Pai RK. A Two-Antibody Mismatch Repair Protein Immunohistochemistry Screening Approach for Colorectal Carcinomas, Skin Sebaceous Tumors, and Gynecologic Tract Carcinomas. *Mod Pathol* (2011) 24:1004–14. doi: 10.1038/modpathol.2011.55
44. Schnell U, Cirulli V, Giepmans BN. Epcam: Structure and Function in Health and Disease. *Biochim Biophys Acta* (2013) 1828:1989–2001. doi: 10.1016/j.bbamem.2013.04.018
45. Guerrette S, Wilson T, Gradia S, Fishel R. Interactions of Human Hmsh2 With Hmsh3 and Hmsh2 With Hmsh6: Examination of Mutations Found in Hereditary Nonpolyposis Colorectal Cancer. *Mol Cell Biol* (1998) 18:6616–23. doi: 10.1128/MCB.18.11.6616
46. Alani E, Sokolsky T, Studamire B, Miret JJ, Lahue RS. Genetic and Biochemical Analysis of Msh2p-Msh6p: Role of ATP Hydrolysis and Msh2p-Msh6p Subunit Interactions in Mismatch Base Pair Recognition. *Mol Cell Biol* (1997) 17:2436–47. doi: 10.1128/MCB.17.5.2436
47. Deininger P. Alu Elements: Know the Sines. *Genome Biol* (2011) 12:236. doi: 10.1186/gb-2011-12-12-236
48. Jiang Y, Zong W, Ju S, Jing R, Cui M. Promising Member of the Short Interspersed Nuclear Elements (Alu Elements): Mechanisms and Clinical Applications in Human Cancers. *J Med Genet* (2019) 56:639–45. doi: 10.1136/jmedgenet-2018-105761
49. Sargent DJ, Marsoni S, Monges G, Thibodeau SN, Labianca R, Hamilton SR, et al. Defective Mismatch Repair as a Predictive Marker for Lack of Efficacy of Fluorouracil-Based Adjuvant Therapy in Colon Cancer. *J Clin Oncol* (2010) 28:3219–26. doi: 10.1200/JCO.2009.27.1825
50. Ribic CM, Sargent DJ, Moore MJ, Thibodeau SN, French AJ, Goldberg RM, et al. Tumor Microsatellite-Instability Status as a Predictor of Benefit From Fluorouracil-Based Adjuvant Chemotherapy for Colon Cancer. *N Engl J Med* (2003) 349:247–57. doi: 10.1056/NEJMoa022289
51. Le DT, Durham JN, Smith KN, Wang H, Bartlett BR, Aulakh LK, et al. Mismatch Repair Deficiency Predicts Response of Solid Tumors to PD-1 Blockade. *Science* (2017) 357:409–13. doi: 10.1126/science.aan6733
52. Cohen R, Buhard O, Cervera P, Hain E, Dumont S, Bardier A, et al. Clinical and Molecular Characterisation of Hereditary and Sporadic Metastatic Colorectal Cancers Harbouring Microsatellite Instability/DNA Mismatch Repair Deficiency. *Eur J Cancer* (2017) 86:266–74. doi: 10.1016/j.ejca.2017.09.022

Conflict of Interest: Author YZ was employed by company Beijing Microread Genetics.

The remaining authors declare that the research was conducted in the absence of any commercial or financial relationships that could be construed as a potential conflict of interest.

frontiers in Oncology

ORIGINAL RESEARCH
published: 18 May 2021
doi: 10.3389/fonc.2021.651380

Predictive Efficacy of MiR-125b-5p, MiR-17-5p, and MiR-185-5p in Liver Metastasis and Chemotherapy Response Among Advanced Stage Colorectal Cancer Patients

Daniel Sur[1,2†], Loredana Balacescu[1,3†], Simona S. Cainap[4,5†], Simona Visan[3], Laura Pop[6], Claudia Burz[2,7], Andrei Havasi[2], Rares Buiga[8,9], Calin Cainap[1,2], Alexandru Irimie[10,11‡] and Ovidiu Balacescu[1,3‡]*

[1] 11th Department of Medical Oncology, University of Medicine and Pharmacy "Iuliu Hatieganu", Cluj-Napoca, Romania, [2] Department of Medical Oncology, The Oncology Institute "Prof. Dr. Ion Chiricuta", Cluj-Napoca, Romania, [3] Department of Genetics, Genomics and Experimental Pathology, The Oncology Institute "Prof. Dr. Ion Chiricuta", Cluj-Napoca, Romania, [4] Department of Pediatric Cardiology, Emergency County Hospital for Children, Pediatric Clinic no 2, Cluj-Napoca, Romania, [5] Department of Mother and Child, "Iuliu Hatieganu" University of Medicine and Pharmacy, Cluj-Napoca, Romania, [6] Research Center for Functional Genomics, Biomedicine and Translational Medicine, University of Medicine and Pharmacy "Iuliu Hatieganu", Cluj-Napoca, Romania, [7] Department of Immunology and Allergology, University of Medicine and Pharmacy "Iuliu Hatieganu", Cluj-Napoca, Romania, [8] Department of Pathology, The Oncology Institute "Prof. Dr. Ion Chiricuta", Cluj-Napoca, Romania, [9] Department of Pathology, "Iuliu Hatieganu", University of Medicine and Pharmacy, Cluj-Napoca, Romania, [10] 11th Department of Oncological Surgery and Gynecological Oncology, "Iuliu Hatieganu" University of Medicine and Pharmacy, Cluj-Napoca, Romania, [11] Department of Surgery, The Oncology Institute "Prof. Dr. Ion Chiricuta", Cluj-Napoca, Romania

MicroRNAs (miRNAs), a class of small non-coding RNAs represent potential biomarkers for colorectal cancer (CRC). The study hypothesized that miRNAs associated with liver metastases may also contribute to assessing treatment response when associated to plasma exosomes. In this study, we used two sets of biological samples, a collection of tumor tissues harvested from patients with CRC with and without liver metastases, and a collection of plasma from CRC patients with and without response to FOLFOX4/FOLFIRI regimens. We investigated 10 target miRNAs in the tissue of 28 CRC patients and identified miR-125b-5p, miR-17-5p, and miR-185-5p to be associated with liver metastasis. Further, we investigated the three miRNAs at the exosomal level in a plasma collection to test their association with chemotherapy response. Our data suggest that the elevated plasma levels of miR-17-5p and miR-185-5p could be predictive of treatment response. Overexpression of miR-17-5p and underexpression of miR-125b-5p and miR-185-5p in CRC tissue seem to be associated with metastatic potential. On the other hand, an increased expression of miR-125b-5p in plasma exosomes was potentially correlated with a more aggressive CRC phenotype.

Keywords: biomarkers, exosomes, colorectal cancer, liver metastases, miR-125b-5p, miR-17-5p, miR-185-5p, chemotherapy response

OPEN ACCESS

Edited by:
Alberto Danese, University of Ferrara, Italy

Reviewed by:
Vinay Randhawa, Panjab University, India
Omkar Suhas Vinchure, Hannover Medical School, Germany
Sandra Romero-Córdoba, National Autonomous University of Mexico, Mexico

***Correspondence:**
Ovidiu Balacescu
obalacescu@yahoo.com

†These authors have contributed equally to this work and share first authorship

‡These authors share last authorship

Specialty section:
This article was submitted to Molecular and Cellular Oncology, a section of the journal Frontiers in Oncology

Received: *09 January 2021*
Accepted: *21 April 2021*
Published: *18 May 2021*

Citation:
Sur D, Balacescu L, Cainap SS, Visan S, Pop L, Burz C, Havasi A, Buiga R, Cainap C, Irimie A and Balacescu O (2021) Predictive Efficacy of MiR-125b-5p, MiR-17-5p, and MiR-185-5p in Liver Metastasis and Chemotherapy Response Among Advanced Stage Colorectal Cancer Patients. Front. Oncol. 11:651380. doi: 10.3389/fonc.2021.651380

INTRODUCTION

Colorectal cancer (CRC) is a leading cause of cancer-related deaths worldwide (1). Poor prognosis and survival rates are mainly due to metastasis (2). Although the introduction of new cytotoxic and biologic therapies (anti-VEGF, anti-EGFR) has significantly improved patient prognosis, metastases to the liver and other distant organs impact clinical outcomes and quality of life (3).

MicroRNAs (miRNAs) are a class of small (19-24 nucleotides) non-coding RNA molecules that have the property of controlling gene expression post-transcriptionally (4). Due to their role in cancer progression and metastasis, miRNAs are considered an important class of molecules with the role of biomarkers. In CRC and other cancers, miRNAs are heavily dysregulated, affecting all cancer hallmarks (5).

MicroRNAs have also been associated with exosome trafficking from primary tumors to secondary metastatic sites (i.e., small extracellular vesicles associated with the metastatic process) (6, 7). Tumor-derived exosomes, through their cargo components, including miRNA and specific proteins, can alter the phenotype of the distant recipient cells by modulating their transcriptome in a Dicer-dependent manner (7). On this line, the exosomes released by CRC can transfer by organotropism, specific miRNAs to liver cells, sustaining the development of liver metastasis (8–10). Different miRNAs from tumor-related exosomes have been detected as biomarkers in the plasma of CRC patients (11, 12). A potential application of tissue or plasma miRNA detection would be to discriminate patients with or without metastases and stratification (or selection) of CRC patients for a given therapy. In a previous article, we pointed out the role of different miRNAs classes as candidates for CRC liver metastasis by modulating specific molecular pathways involved in liver metastasis of colorectal cancer (13). However, not all miRNAs altered in tumor tissue have the same correspondent alteration in the tumor-related exosomes. The level of miRNAs loaded into exosomes could be influenced by their mRNA-miRNA interaction in the donor cells (14). The mRNA-miRNA interactions inside a tumor cell can be affected by tumor progression and its response to the treatment. Thus, identifying tumor-exosomal miRNAs associated with both tumor invasion and metastasis and response to therapy is a major challenge in identifying new reliable markers.

Most studies investigating miRNAs as possible biomarkers are focused on either diagnosis, prognosis, or response to therapy. Identifying miRNA biomarkers to characterize a tumor phenotype better, predicting both metastasis and treatment response, represents a critical approach that we consider very challenging. Consequently, our study aims to identify miRNA biomarkers that could predict both liver metastasis and treatment response. In this regard, we have focused on identifying specific tissue miRNAs predicting CRC liver metastasis, which could also be associated with treatment response when evaluated in tumor-derived exosomes.

We focused on miR-17-5p (oncomiR) as a putative biomarker because previous studies indicated it as tissue and exosomal biomarker for liver metastasis. However, to our knowledge, there are no studies investigating the role of exosomal miR-17-5p as a treatment predictor for CRC liver metastasis treated with FOLFOX or FOLFIRI regimens. Nevertheless, recent data pointed out the association of high levels of miR-17-5p in primary tissue of CRC and its liver metastasis (15), an increased level of miR-17-5p in exosomes released by CRC with liver metastases (16, 17), and CRC-associated fibroblasts (18). Albeit the association of mir-17-5p with metastatic CRC resistance to therapy was previously investigated on cell lines, no study presents data on patients with CRC treated with FOLFOX or FOLFIRI (19).

Other miRNAs of interest that we focused on included two tumor suppressor miRNAs, miR-185-5p and miR-125b-5p. MiR-185-5p published data revealed its downregulation in CRC progression and metastasis (20), mediating metastasis and stemness when it is sponged by circRNAs (21) or inhibited by lncRNA (22). However, no studies present data about the association of exosomal-mir-185 with CRC liver metastasis, while only one study associated miR-185 expression of radiosensitivity in CRC (23). Downregulation of miR-125b-5p is associated with CRC proliferation (24) and prognosis (25). There is no data concerning exosomal miR-125b-5p role as a predictor for CRC liver metastasis. Nevertheless, aberrant downregulation of miR-125b-5p was recently associated with drug resistance in CRC (26) and liver metastasis (27).

The standard of care for advanced CRC is FOLFOX (i.e., leucovorin, 5-fluorouracil, and oxaliplatin) or FOLFIRI (i.e., leucovorin, 5-fluorouracil, and irinotecan) in conjunction with targeted therapies. Irinotecan and oxaliplatin are extensively used with 5-fluorouracil and leucovorin as the first-line and second-line treatments for metastatic CRC patients (28). The results of previous studies demonstrated that FOLFOX and FOLFIRI are standard regimens for novel clinical trials and can be used for most metastatic CRC patients (28, 29).

Our study aims to investigate if the miR-17-5p, and miR-185-5p and miR-125b-5p associated with liver metastases, may also contribute to the assessment of treatment response (using FOLFOX or FOLFIRI) when evaluated in plasma-derived exosomes.

METHODOLOGY

Patients and Samples

The present study was conducted on two CRC sample collections, including 28 FFPE tissues and 35 plasma samples, harvested from 63 patients with CRC, treated in The Oncology Institute Prof. Dr. Ion Chiricuta, Cluj-Napoca, Romania. The inclusion criteria were: 1) stages II-IV CRC diagnosis with radiological clinical progression in terms of liver metastasis, 2) availability of tumor tissue biopsies or surgical specimens, 3) availability of patients for blood sample collection, 4) HP confirmation of diagnosis by a pathologist, 5) measurability of the tumor according to the Response Evaluation Criteria in Solid Tumors criteria (version 1.1), 6) follow-up of at least 60 months from the first therapy for metastatic disease, 7) disease measurability at the baseline with

demonstrated disease progression or response based on radiologic or clinical assessment.

The study was carried out based on the approval of the Ethics Committees of the Oncology Institute Prof. Dr. Ion Chiricuta and the University of Medicine and Pharmacy Iuliu Hatieganu, Cluj-Napoca, Romania. All patients gave their consent in accordance with the Declaration of Helsinki.

Study Design

This study aims to identify miRNAs with a dual role in predicting liver metastasis and treatment response to FOLFOX4/FOLFIRI regimens in CRC. Because we have not a matching collection of tissue-plasma for the same patients, we proposed a study design based on retrospective and prospective approaches. The retrospective study included a group of FFPE samples harvested from CRC patients with and without liver metastasis at follow-up, while the prospective study included plasma harvested from CRC patients with different responses to FOLFOX4/FOLFIRI regimens. The clinical and demographic features were recorded for each patient.

Tissue Study

Our first aim was to identify specific miRNAs associated with CRC liver metastasis. In this part of the study, we included tissue samples from 28 patients with stage II or III CRC, with a very rigorous clinical follow-up. The patients were assigned into two groups: those who developed liver metastasis (M+) and those with no liver metastases (M-).

Plasma Study

The second aim was to investigate if specific tissue miRNAs, associated with CRC liver metastasis, could predict CRC treatment response when they are evaluated in plasma exosomes. To this aim, a total of 35 patients with stage II-IV CRC were included in the study. Peripheral blood was collected before starting a FOLFOX4/FOLFIRI-based systemic therapy. The patients were divided into partial treatment responders (PR; n=16) and non-responders (NR; n=19).

Treatment Schedule

None of the patients from the tissue group have been treated with radiotherapy or chemotherapy before surgery. The CRC tissue samples were obtained after CRC surgery. Subsequently, the patients received standard adjuvant chemotherapy based on fluoropyrimidine plus oxaliplatin.

All patients from the plasma group received systemic FOLFOX4/FOLFIRI chemotherapy. In the current study, 18 (51.42%) patients received the FOLFIRI treatment, and 17 (48.57%) subjects received FOLFOX4+/-Avastin, Cetuximab, or no targeted therapy, depending on their clinical features and mutational status, with 71.42% of the patients in this group undergoing surgery.

Tissue Processing and RNA Extraction From FFPE Samples

From each FFPE tumor sample, five sections of 10 μm each were provided in similar conditions by macrodissection by a specialized pathologist. The RNA was isolated using a *miRNeasy FFPE kit (Qiagen*) according to the manufacture's instructions. Shortly, the sections were deparaffinized and treated with Proteinase K as mentioned in the protocol. The recovered supernatant was further used for RNA extraction using silica gel columns, including DNase treatment. Finally, the total RNA was eluted with RNase-free water and stored at -80°C until its further use. The RNA quantification was evaluated by NanoDrop ND-1000 spectrophotometer (*Thermo Fisher Scientific*).

Plasma Collection and RNA Extraction from Exosomes

Peripheral blood from CRC patients was collected at baseline by venipuncture in EDTA collection tubes. The plasma was separated by double centrifugation of blood at 4,000 and 12,000 rpm for 10 min at 4°C. Provided plasma was aliquoted (400 ul) and stored at -80°C until its further use. According to the producer's instructions, about 400 ul of 0.8-μm-filtered plasma for each sample has been used for exosomes isolation with the Total Exosome Isolation Kit from plasma (Thermo Fisher). Shortly, the filtered plasma was treated with 0.05 volume of Proteinase K and incubated at 37°C for 10 minutes. About 120 ul of precipitation reagent was added to the sample, following a 30 minutes incubation at 4°C and a 10.000xg centrifugation. The resulting pellets (exosomes) were resuspended in 200 ul PBS and used for RNA extraction, with the *Total Exosome RNA and Protein Isolation Kit* (Thermo Fisher). In the extraction steps, before adding the Acid-Phenol-Chloroform as is mentioned in the protocol, we used a volume of 2.5 ul of exogenous cel-miR-39 spike-in ($2x10^8$ transcripts), to be further used for normalization of miRNA expression.

Selection of miRNAs of Interest

Our first thought to identify putative miRNA biomarkers that could have a double role in CRC liver metastasis and treatment response was to conduct an R&D study on a set of 84 miRNAs involved in modulating cancer stem cells status (data not presented). We performed a miScript miRNA PCR Array Human Cancer Stem Cells analysis (MIHS-118Z-Qiagen), considering that tumor stem cells are responsible for the invasive phenotype and treatment resistance (30). Our preliminary data indicated that miR-150-5p, miR-125b-5p, and miR-185-5p were statistically differentially expressed between CRC patients with and without liver metastasis. As a consequence, these three miRNAs were first considered for more extensive validation in FFPE tissue samples.

Further, based on the literature review, we selected several functionally relevant miRNAs based on two criteria: i) miRNAs associated with CRC liver metastases and ii) miRNAs mediating invasion and metastasis through exosomes (**Table 1**).

In brief, we selected 3 miRNAs significantly expressed between CRC patients with and without liver metastasis in the pilot study (miR-150-5p, miR-125b-5p, and miR-185-5p) and other seven miRNAs of interest considering their role in cancer metastasis, exosomal presence, and treatment response. These miRNAs of interest, including oncomiRs [miR-17-5p (19), miR-21-5p (38),

TABLE 1 | MicroRNAs related to colorectal cancer liver metastasis.

No.	miRNAs	miRBase unique identifier	miRNA role	Ref
1	hsa-miR-17-5p	MIMAT0000070	oncomiR	(17)
2	hsa-miR-21-5p	MIMAT0000076	oncomiR	(31)
3	hsa-miR-92a-3p	MIMAT0000092	oncomiR	(17)
4	hsa-miR-31-5p	MIMAT0000089	oncomiR	(32)
5	hsa-miR-192-5p	MIMAT0000222	TS miR	(33)
6	hsa-miR-26a-5p	MIMAT0000082	TS miR	(34)
7	hsa-miR-150-5p	MIMAT0000451	TS miR	(35)
8	hsa-miR-125b-5p	MIMAT0000423	TS miR	(36)
9	hsa-miR-185-5p	MIMAT0000455	TS miR	(20)
10	hsa-miR-193a-3p	MIMAT0000459	TS miR	(37)
11	hsa-miR-16-5p	MIMAT0000069	TS miR (endogen normalizer for FFPE)	
12	cel-miR-39	MIMAT0000010	(Spike-in exogen normalization for exosomes)TS miR (endogen normalizer for FFPE)	

hsa-miR, homo sapiens microRNA; oncomiR, oncogenic microRNA; TS miR, tumor suppressor microRNA.

and miR-31-5p (39)] modulating the invasive phenotype of CRC, TS miRs [miR-125b-5p (40), miR-185-5p (41), and miR-193a-3p (42)] modulating tumor microenvironment, oncomiR [miR-92a-3p (17)], and TS miR [miR-192-5p (43), miR-26a-5p (44), and miR-150-5p (45)] mediating invasion and metastasis through exosomes. In addition, exogenous (cel-miR-39) and endogenous (miR-16-5p) controls were used for miRNA investigation. Only the miRNAs relevant in the tissue samples were further evaluated in plasma exosomes to identify putative tumor exosomal-miRNAs that may be associated with both tumor metastasis and treatment response.

Assessment of microRNA Expression

To evaluate the level of miRNA expression, we used the one-step advanced miRNA system, through which we can simultaneously assess a large number of miRNAs using the same pre-amplified cDNA. In this line, we generated cDNAs from 10 ng of total RNAs extracted from each FFPE sample and 4 µl of exosomal RNAs extracted from each plasma sample, using *TaqMan® Advanced miRNA cDNA Synthesis Kit* following the manufacturer's protocol. Considering the low quantity of exosomal-miRNA in the plasma and the input limits for the cDNA synthesis kit, we maximized the volume of input RNA used for cDNA synthesis, using 4 µl of exosomal RNA of each sample. Finally, the cDNA was pre-amplified using universal RT miRNA primers.

A volume of 2 µl of diluted cDNA (1:10 v/v) was used to investigate miRNA expression with *TaqMan® Fast Advanced Master Mix (2X)* and specific miRNA advanced assays, in a final volume of 10 µl, using the LC480 device (Roche) under specific miR-advanced PCR settings: 1) a step of removing RNA contaminants by activating the enzyme UNG (uracil-n glycosylase) at 55°C for 2 minutes; 2) amplifying the enzyme (Taq polymerase) at 95°C for 20 sec; 3) PCR amplification through a set of 40 PCR cycles including 2 reaction steps, at 95°C for 3 sec and at 60°C for 30 sec. The expression level of the miRNA of interest was calculated using the ΔΔCt relative quantification method. Considering its stable expression in a large number of biological samples, miR-16-5p was used to normalize the expression level of the investigated miRNAs in FFPE samples while cel-miR-39 was used to normalize the expression of exosomal miRNAs. MicroRNA expression was calculated using the ΔΔCt relative quantification method.

Statistical Analysis

According to data distribution, the correlation between clinicopathological characteristics and tissue or plasma miRNAs expression was evaluated with Mann-Whitney U test or unpaired sample *t*-test for two categorical variables or Kruskall-Wallis test, followed by Dunn's multiple comparison *post hoc* test in case of three categorical variables. The DFS was defined as the time from diagnosis until the appearance of the liver metastasis, censoring patients with no metastasis at their last follow-up. In order to evaluate the association between DFS and miRNAs, each miRNA expression was classified according to its median value, based on which the patients were allocated into high- or low-expression group. The survival curves were estimated using the Kaplan-Meier method, and log-rank test was used to compare the survival distributions. Multivariate Cox proportional hazards regression models were used to adjust for age, gender and tumor grade.

RESULTS

Patients and Tumor Characteristics

The baseline characteristics of the patients enrolled in the study are detailed in **Table 2**. There were no significant differences between the tissue and plasma datasets in terms of the distribution of pathological and other characteristics, except for tumor size. In this regard, more patients with T3 tumors were included in the tissue study, while those with T3 and T4 tumors were evenly distributed in the plasma study. Considering the lymph nodes status, N1 and N2 were more frequently observed in both tissue and plasma investigations. The G2 (moderate differentiated) status was more frequent in both study groups. Regarding tumor location, for the tissue samples, we included 17 left-sided CRC samples and 11 right-sided CRC tumors, while plasma samples were collected from 24 patients that had left-sided CRC tumors and 11 patients who presented right-sided CRC tumors. All the samples evaluated in the study were adenocarcinomas (Adk).

TABLE 2 | Clinical and pathological data of the patients enrolled in tissue and plasma study.

Variable	Tissue study (n=28)	Plasma study (n=35)	P-value	Statistical test
	Median (range)	*Median (range)*		
Age (years)	55.5 (36-84)	60 (19-82)	0.598	Mann-Whitney U test
Body mass index	25.6 (17.3-36.5)	25.7 (18.4-40.4)	0.682	Mann-Whitney U test
	n (%)	*n (%)*		
Gender				
F	12 (42.9%)	13 (37.1%)	0.796	Fischer's exact test
M	16 (57.1%)	22 (62.9%)		
Tumor size				
T2	1 (3.6%)	1 (2.9%)	**0.0174***	Fischer's exact test
T3	22 (78.6%)	16 (45.7%)		
T4	5 (17.9%)	16 (45.7%)		
NA	–	2 (5.7%)		
Lymph nodes				
N0	3 (10.7%)	6 (17.1%)	0.566	Fischer's exact test
N1	14 (50.0%)	12 (34.3%)		
N2	11 (39.3%)	13 (37.1%)		
Nx	–	4 (11.4%)		
Metastasis	***In evolution***	***Baseline***		
M-/M0	16 (57.1%)	11 (31.4%)	–	–
M+/M1	12 (42.9%)	22 (62.9%)		
Mx	–	2 (5.7%)		
Lymphatic invasion				
L0	8 (28.6%)	7 (20.0%)	0.999	Fischer's exact test
L1	18 (64.3%)	15 (42.9%)		
Lx	2 (7.1%)	13 (37.1%)		
Perineural invasion				
P0	16 (57.1%)	11 (31.4%)	0.524	Fischer's exact test
P1	7 (25.0%)	8 (22.9%)		
Px	5 (17.9%)	16 (45.7%)		
Grade				
G1	5 (17.9%)	4 (11.4%)	0.926	Fischer's exact test
G2	18 (64.3%)	19 (54.3%)		
G3	5 (17.9%)	5 (14.3%)		
NA	–	7 (20.0%)		
Stage				
S2	3 (10.7%)	4 (11.4%)	0.168	Fischer's exact test
S3	25 (89.3%)	8 (22.9%)		
S4	–	23 (65.7%)		

*$p \leq 0.05$.

Investigation of MicroRNA in Colorectal Cancer Tissue

Liver metastasis is the leading cause of death among CRC patients. Based on the evidence, approximately 50% of CRC patients develop liver metastases (46). MicroRNAs are involved in the post-transcriptional regulation of mRNAs and are abnormally expressed in cancer with an essential role in tumorigenesis. As a comprehensive analysis of the combined effects of altered activities of miRNAs in CRC has not been carried out, there are still many questions why miRNAs might affect tumor progression or patient outcomes (11).

In order to identify specific miRNA associated with liver CRC metastasis, we investigated the expression of 10 target miRNAs in the FFPE tissue of the primary tumors of CRC patients with and without liver metastases. Our results indicated an increased level of miR-17-5p (Fold change (FC)=1.83, p=0.042) in the liver metastases group (M+) as compared to that in non-metastatic (M-). Furthermore, a down-regulation of miR-125b-5p (FC=0.73, p=0.035) and miR-185-5p (FC=0.70, p=0.025) was observed in M+ patients compared to M- patients (**Figure 1**).

We performed the analysis of the studied microRNAs in the following publicly available colorectal cancer datasets: GSE35834, GSE147603, GSE81581, GSE98406, GSE56350, GSE53159, GSE51429 and GSE46622. In GSE56350 dataset we found a decreased expression of hsa-miR-185-5p (FR=-1.87, p=0.0004, FDR 2%) in CRC liver metastases (n=15) compared to primary tumors (n=46). Analysis of 14 matched CRC liver metastases and primary tumors (GSE98406 dataset) showed downregulation of hsa-miR-125-5p (FR=-2.07, p=0.034, FDR 79%) while expression profiling by RT-PCR in the GSE51429 training set highlighted a slight under-expression (FR=-1.11, p=0.011, FDR 12%) in CRC liver metastasis (n=12) vs. primary tumors (n=20). Making use of GSE81581 data, we evaluated hsa-miR-17-5p expression in 19 CRC liver metastases versus 23 primary tumors. The results pointed out a 1.3-fold increase in expression of has-miR-17-5p in liver metastases tissues (FR=1.32, p=0.049, FDR 23%).

We also analyzed the correlations among the three miRNAs expression and the clinicopathological data (**Table 3**). Our data revealed that high miR-17-5p expression was significantly correlated with tumor size (FC T4 *vs.* T3 = 2.01, p=0.027) and perineural invasion (FC P1 *vs.* P0 = 1.67, p=0.01). However, miR-125b-5p and miR-185-5p showed no significant correlation with the clinicopathological data except being correlated to metastases.

We further evaluated the association of miRNAs expression with disease-free survival (DFS) of 28 FOLFOX4/FOLFIRI CRC treated patients. At the time of evaluation, the median follow-up was 26.5 months. In the univariate survival analysis, miR-125b-5p (HR=3.7, 95% CI=1.162-11.81, p=0.027) and miR-185-5p (HR=3.59, 95% CI=1.127-11.41, p=0.031) were significantly associated with DFS, the log-rank tests pointed out that CRC patients with low tissue levels of miR-125-5p and miR-185-5p had significantly shorter DFS than those with high tissue levels of these miRNAs (**Figures 2A, B**). In the multivariate survival analysis, miR-125b-5p was an independent prognostic factor for DFS (HR=4.971, 95% CI=1.12-22.067, p=0.035, **Table 4**, Section A) but miR-185-5p did not reach the significance threshold, although it had a low p-value (HR=3.834, 95% CI=0.976-15.062, p=0.054, **Table 4**, Section B). MiR-17-5p had no prognostic value either in univariate (**Figure 2C**) or multivariate analysis (**Table 4**, Section C). Further, we tested if there is a combined effect of these 3 microRNAs. We found that the patients with high tissue expression of miR-17-5p and low tissue expression of miR-125b-5p and miR-185-5p, assigned to group Panel 3, had shorter DFS than patients with any other combination (HR=19.43, 95% CI= 3.772-100.1, p= 0.0004) as resulted from log-rank univariate analysis (**Figure 2D**) and multivariate survival analysis (HR=6.116, 95% CI=1.714-21.827, p=0.005, **Table 4**, Section D). When we considered combined effect of these microRNAs regardless of the observed pattern in tissue, none of them had a prognostic value. (**Table 4**, Section E).

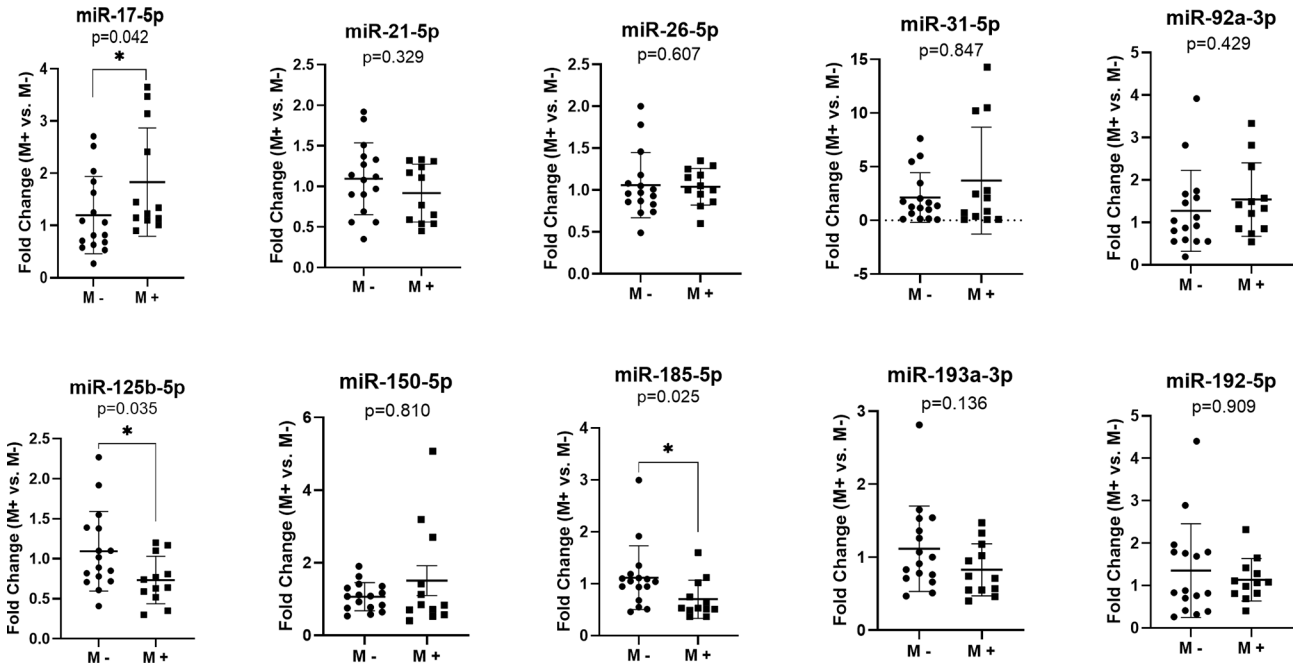

FIGURE 1 | MicroRNAs expression in the primary tumor tissues of colorectal patients with liver metastases (M+) (n=12) *versus* patients without metastases (M-) (n=16); according to data distribution, differential expression was tested using the non-parametric Mann-Whitney U test (miR-17-5p; miR-21-5p; miR-26-5p; miR-31-5p; miR-92a-3p; miR-150-5p; miR-185-5p; miR-193a-3p; miR-192-5p) or parametric unpaired sample t-test (miR-125b-5p). Fold change for each sample was calculated relative to M- group. *p≤0.05.

TABLE 3 | Relation of clinicopathological data and miRNA expression while comparing patients with and without metastases in the tissue study.

Variable	miR-17-5p P-value	miR-125b-5p P-value	miR-185-5p P-value	Statistical test
Age <50 *vs.* >50	0.718	0.631	0.362	Mann Whitney
Gender M *vs.* F	0.099	0.296	0.331	Mann Whitney
Tumor size T3 *vs.* T4	**0.027***	0.595	0.973	Mann Whitney
Lymph nodes N0 *vs.* N1 *vs.* N2	0.064	0.931	0.268	Kruskal-Wallis
Metastasis (in evolution) M- *vs.* M+	**0.042***	**0.035***	**0.025***	Mann Whitney
Lymphatic invasion L0 *vs.* L1	0.304	0.597	0.907	Mann Whithey
Perineural invasion P0 *vs.* P1	**0.010***	0.547	0.508	Mann Whitney
Grade G1 *vs.* G2 *vs.* G3	0.986	0.981	0.646	Kruskal-Wallis
Stage S2 *vs.* S3	0.710	0.766	0.188	Mann Whitney

*$p \leq 0.05$.

Investigation of MicroRNA in Plasma Exosomes

Exosomes are being involved in the metastatic process of a primary tumor transferring microRNA cancer-specific cargo. Based on the evidence, they can be identified in the plasma of patients (47). In line with this, we investigated if the liver metastasis-associated exosomal miRNAs could predict the treatment response in CRC patients. The miRNAs that were differentially expressed in liver metastases group *vs.* non-metastatic one (i.e., miR-17-5p, miR-125b-5p, miR-185-5p) and had a prognostic value (i.e., miR-125b-5p and miR-185-5p) in tissue study were evaluated in the plasma exosomes of CRC patients with partial treatment responses (PR) or non-responses (NR) including progressive and stationary disease.

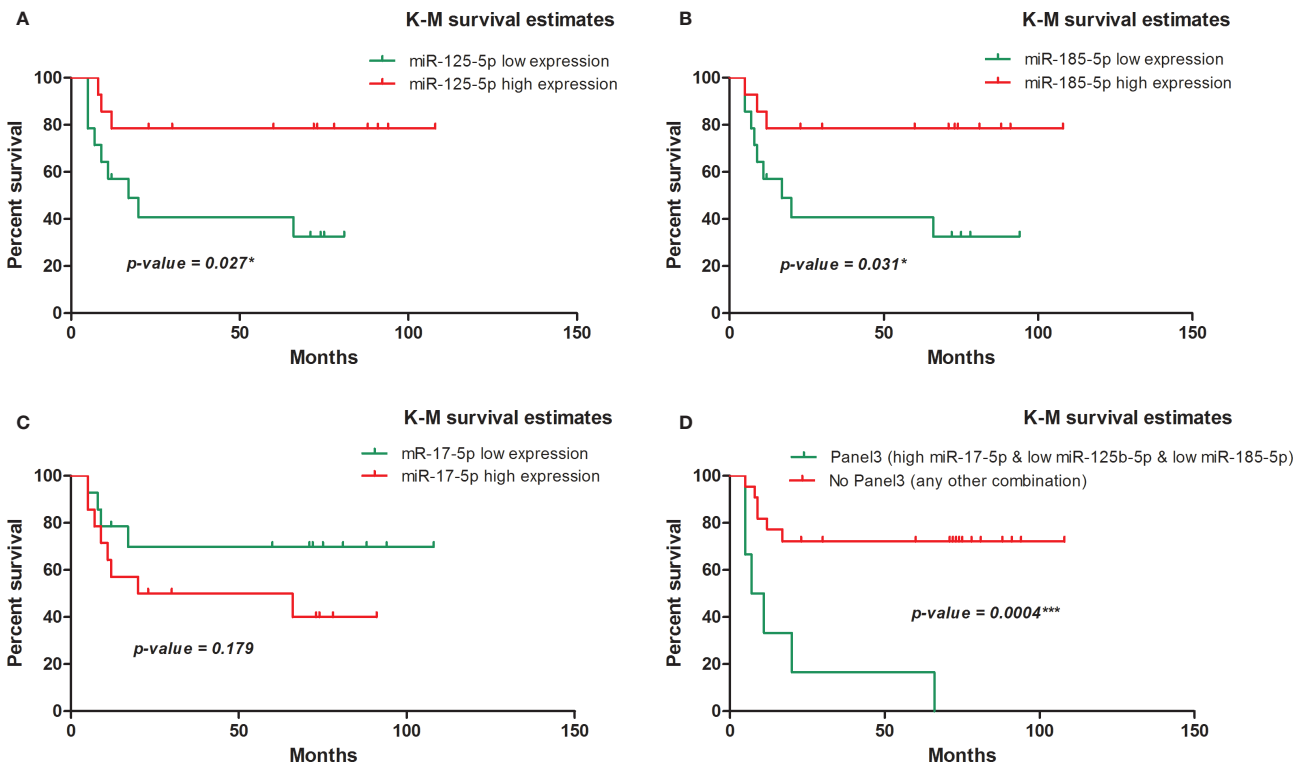

FIGURE 2 | Kaplan-Meier survival curve for disease-free survival in 28 patients with colorectal cancer involved in the tissue study. **(A)** According to dichotomized miR-125-5p expression, (HR=3.7, 95% CI=1.162-11.81, p=0.027* [log-rank test]). **(B)** According to dichotomized miR-185-5p expression, (HR=3.59, 95% CI=1.127-11.41, p=0.031* [log-rank test]). **(C)** According to dichotomized miR-17-5p expression, (HR=0.45, 95% CI=0.144-1.435, p=0.179 [log-rank test]). **(D)** According to dichotomized expression pattern of miR-17-5p, miR-125b-5p and miR-185-5p observed in CRC tissue (HR=19.43, 95% CI= 3.772 - 100.1, p= 0.0004*** [log-rank test]).

Treatment response included CT/PET-CT assessment according to clinical evaluation protocols.

The exosomal miR-17-5p (FC NR vs. PR=1.92, p=0.005) and miR-185-5p (FC=2.12, p=0.030) expression were significantly upregulated in nonresponder patients compared to patients with complete or partial response to therapy, regardless of the treatment received (**Figure 3**).

The expression of miR-17-5p was significantly increased in non-responders versus responders when considering both FOLFOX4 (FC NR *vs.* PR=1.99, p=0.034) or FOLFIRI (FC NR *vs.* PR=1.76, p=0.0099) treatment. On the other hand, high expression of miR-185-5p (FC NR *vs.* PR=2.22, p=0.034) was statistically correlated with a lack of response only for FOLFIRI therapy (**Figure 4**).

The results revealed no statistical significance for miR-125b-5p exosomal expression in terms of treatment response. However, analyses between miR-125b-5p plasma exosomes and clinicopathological data revealed an increased expression of miR-125b-5p in the plasma of patients with high tumor grade (FC G3 *vs.* G2 = 1.73, p=0.016) and stage (FC S4 *vs.* S3 = 2.04, p=0.046; (**Table 5**).

The summary of the two studies is presented in **Table 6**. Our data suggest that the elevated plasma levels of miR-17-5p and miR-185-5p could be predictive of treatment response. Overexpression of miR-17-5p and underexpression of miR-125b-5p and miR-185-5p in CRC tissue seem to be associated with metastatic potential. On the other hand, an increased expression of miR-125b-5p in plasma exosomes was potentially correlated with a more aggressive CRC phenotype.

DISCUSSION

The results of our study revealed that tissue expression of miR-17-5p, miR-125b-5p, and miR-185-5p is correlated with CRC liver metastasis. Also, in the plasma samples, exosomal miR-17-5p and miR-185-5p were predictive for treatment response. Accordingly, these miRNAs could act as a starting point for identifying new predictive biomarkers. MicroRNAs play essential roles in tumorigenesis and metastasis processes; thus, they could be used as prognostic and therapy predictive measures in various cancers (48, 49).

MiR-17-5p plays the role of oncomiR in CRC cases (50), while miR-125b-5p and miR-185-5p act as tumor suppressors (51, 52). First, our results from the tissue study indicated that

TABLE 4 | Multivariate survival analysis of (Section A) miR-125b-5p; (Section B) miR-185-5p; (Section C) miR-17-5p; (Section D) Panel3 expression pattern (high tissue miR-17-5p expression & low tissue miR-125b-5p expression & low tissue miR-185-5p expression); (Section E) combined effect of miR-17-5p, miR-125b-5p and miR-185-5p adjusted for age, gender and tumor grade.

Section A			
Variable	**HR**	**95% CI for HR**	**p-value**
Gender (M *vs.* F)	0.766	0.21-2.794	0.686
Age	0.988	0.933-1.046	0.671
Tumor grade (G3 *vs.* G2 *vs.* G1)	3.04	0.737-12.542	0.124
miR-125b-5p (low *vs.* high)	4.971	1.12-22.067	**0.035***
Section B			
Variable	**HR**	**95% CI for HR**	**p-value**
Gender (M *vs.* F)	0.575	0.142-2.336	0.439
Age	1.02	0.956-1.088	0.551
Tumor grade (G3 *vs.* G2 *vs.* G1)	1.886	0.699-5.093	0.21
miR-185-5p (low *vs.* high)	3.834	0.976-15.062	0.054
Section C			
Variable	**HR**	**95% CI for HR**	**p-value**
Gender (M *vs.* F)	0.634	0.137-2.927	0.56
Age	1.003	0.938-1.072	0.932
Tumor grade (G3 *vs.* G2 *vs.* G1)	2.041	0.739-5.632	0.168
miR-17-5p (low *vs.* high)	0.423	0.121-1.474	0.177
Section D			
Variable	**HR**	**95% CI for HR**	**p-value**
Gender (M *vs.* F)	1.037	0.225-4.772	0.963
Age	0.992	0.929-1.06	0.818
Tumor grade (G3 *vs.* G2 *vs.* G1)	2.461	0.691-8.767	0.165
Panel3 (Panel3 *vs.* No Panel3)	6.116	1.714-21.827	**0.005****
Section E			
Variable	**HR**	**95% CI for HR**	**p-value**
Gender (M *vs.* F)	0.999	0.227-4.407	0.999
Age	0.994	0.93-1.062	0.85
Tumor grade (G3 *vs.* G2 *vs.* G1)	3.414	0.819-14.234	0.092
miR-17-5p (low *vs.* high)	0.364	0.096-1.387	0.139
miR-125b-5p (low *vs.* high)	3.518	0.604-20.488	0.162
miR-185-5p (low *vs.* high)	2.133	0.415-10.953	0.364

Hazard ratio (HR) were obtained from Cox proportional hazards regression models, HR>1 indicating that the low expression of miRNAs or Panel3 expression pattern is associated with short DFS.
**p≤0.05;*
***p≤0.01.*

high levels of miR-17-5p in primary CRC could be associated with metastatic potential and serve as a predictive biomarker. Furthermore, miR-17-5p appeared over-expressed in the group of patients with liver metastases, suggesting a possible involvement in the metastasis process. On this line, several studies confirmed the overexpression of miR-17-5p in CRC tissue specimens (53–55). However, the overexpression of miR-17-5p could be due to the interaction with the tumor microenvironment or due to liver metastasis in CRC. Therefore, the perception of miR-17-5p pathways could help in explaining the mechanisms of principal liver metastases in CRC (15).

On the other hand, miR-185-5p and miR-125b-5p appear down-regulated in CRC tissue compared to normal mucosa in other existing studies (52, 56). These results are similar to ours, implying that miR-185-5p and miR-125b-5p could bring new information for discriminating and stratifying CRC patients. Our results also showed that patients with low tissue expression of miR-125b-5p and miR-185-5p has a shorter DFS compared to patients with elevated tissue levels of these miRNAs. The univariate/multivariate analysis showed that miR-17-5p had no prognostic feature. Unfortunately, there aren't any large-scale studies focusing on these two miRNAs in the literature concerning CRC for further underlying this position.

Second, our prospective study, including plasma samples from a cohort of 35 patients with advanced CRC, showed that overexpressed exosomal miR-17-5p and miR-185-5p were associated with treatment response. Exosomal miR-125b-5p had no statistical significance concerning treatment response. There are scarce data about the association of exosomal miRNAs with prognosis and treatment response in CRC cases, although recent studies have suggested that miRNA from the tumor or plasma exosomes could serve as cancer biomarkers to assist in prognosis and prediction of treatment responses (57, 58). Previous studies have demonstrated the potentiality of

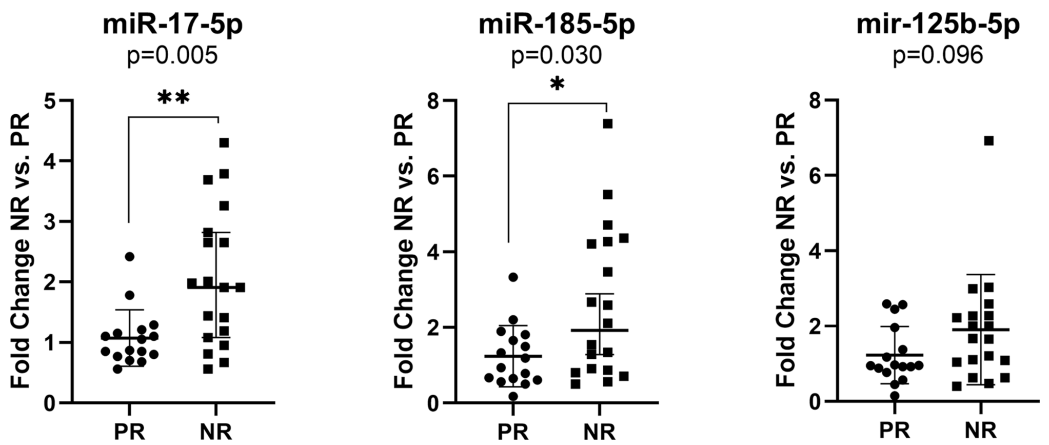

FIGURE 3 | Expression of miR-17-5p, miR-185-5p, and miR-125b-5p in the plasma exosomes of non-responders *versus* responder (n=19/16) colorectal cancer patients regardless of the treatment received. According to data distribution, differential expression was tested using the non-parametric Mann-Whitney U test. Fold change for each sample was calculated relative to PR group. *p≤0.05; **p≤0.01.

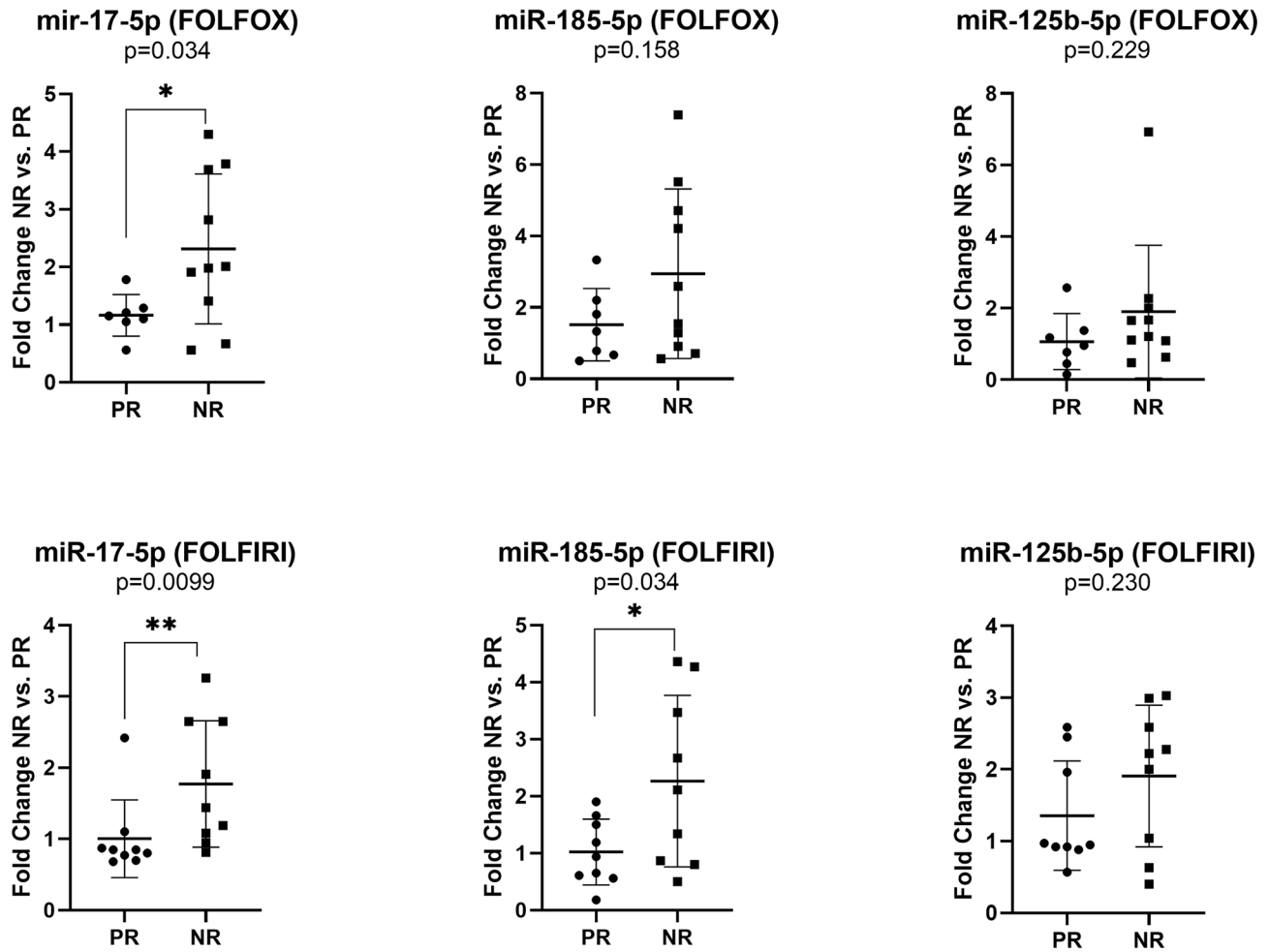

FIGURE 4 | Expression of miR-17-5p, miR-185-5p, and miR-125b-5p in the plasma exosomes of non-responders *versus* responder colorectal cancer patients for FOLFOX4 (n=10/7) and FOLFIRI (n=9/9) therapy. According to data distribution, differential expression was tested using the non-parametric Mann-Whitney U test (miR-17-5p and miR-125b-5p) or parametric unpaired t-test (miR-185-5p). Fold change for each sample was calculated relative to PR group *p≤0.05; **p≤0.01.

TABLE 5 | Significant differences between miRNAs with clinical data in the studied plasma samples.

Variable	miR-17-5p P-value	miR-125b-5p P-value	miR-185-5p P-value	Statistical test
Age <50 vs. >50	0.418	0.324	0.809	Mann Whitney
Gender M *vs.* F	0.891	0.707	0.932	Mann Whitney
Tumor size T3 *vs.* T4	0.157	0.146	0.317	Mann Whitney
Lymph nodes N0 *vs.* N1 *vs.*N2	0.329	0.367	0.371	Kruskal-Wallis
Metastasis (baseline) M0 *vs.* M1	0.339	0.163	0.479	Mann Whitney
Lymphatic invasion L0 *vs.* L1	0.778	0.481	0.887	Mann Whitney
Perineural invasion P0 *vs.* P1	0.772	0.265	0.710	Mann Whitney
Grade G1 *vs.* G2 *vs.* G3	0.500	**0.016*** **(G2 *vs.*G3)**	0.393	Kruskal-Wallis
Stage S2 *vs.* S3 *vs.* S4	0.396	**0.046*** **(S3 *vs.* S4)**	0.950	Kruskal-Wallis

*$p \leq 0.05$.

TABLE 6 | Summary of the tissue and plasma studies.

	miR-17-5p expression	miR-125b-5p expression	miR-185-5p expression
Tissue study			
M+ vs. M-	↑	↓	↓
T3 vs. T2	↑		
P1 vs. P0	↑		
Univariate Survival Analysis		↓ - short DFS	↓ - short DFS
Multivariate Survival Analysis		↓ - short DFS	
Plasma study			
NR vs. PR (FOLFOX4 & FOLFIRI)	↑		↑
NR vs. PR (FOLFOX4)	↑		
NR vs. PR (FOLFIRI)	↑		↑
G3 *vs.* G2		↑	
S4 *vs.* S3		↑	

exosomal miR-17-5p as a non-invasive biomarker for both diagnosis and predicting tumor grade and stage in CRC (17, 59). Moreover, exosomal miR-17-5p and miR-185-5p are significantly upregulated in non-responsive patients treated with FOLFOX4/FOLFIRI (60, 61).

In patients with metastatic CRC, two miRNAs (i.e., miR-107 and miR-99a-3p) were found to predict response to traditional chemotherapy treatment (62). In addition, miR-224 and miR-143 were associated with treatment response to fluoropyrimidine-based chemotherapy (63). Serum miR-19a appears upregulated in advanced CRC cases that manifest resistance to FOLFOX, suggesting its potential to evaluate the treatment response (64). In another study, high expression of miR-625-3p was linked to poor response to FOLFOX/XELOX (Oxaliplatin and capecitabine) regimen in patients with metastatic CRC (65). Plasma exosomal miR-125b can be used as an indicator of resistance to mFOLFOX6 chemotherapy in patients with advanced or recurrent CRC (66). On the other hand, exosomal miR-128-3p can be used as a biomarker and also a therapeutic tool to improve the response to oxaliplatin in advanced CRC patients with acquired resistance to this drug (67). In rectal cancer, the profiling signature of miR-17/92 cluster can provide a reliable biomarker source for treatment response (68).

Our results showed that miR-17-5p was highly expressed in the plasma exosomes of non-responsive CRC patients regardless of the received treatment schedule (69). Although, the lack of association of miR-17-5p with DFS is surprising in the context of its differential expression in liver metastases versus non-metastatic patients, this result could be related to the size of the study group. In an *in-vitro* study, chemotherapy seemed to increase the expression of miR-17-5p in CRC cells and induce chemoresistance by repressing the PTEN factor (19). A panel of six miRNAs, which included miR-17-5p, proved to have biomarker potential in predicting response to 5-FU-based chemotherapy in metastatic first-line CRC patients (70).

Based on the evidence, miR-125a and miR-125b are underexpressed in the tumoral tissues of CRC, compared with adjacent nontumoral tissue (71). A more recent study on CRC cell lines showed that miR-125 targets and inhibits vascular endothelial growth factor (VEGF) expression and can be used as a therapeutic target (72). In our study, the prognostic role of miR-125b-5p and miR-185-5p was correlated with a significantly shorter DFS. It is also known that miR-185 acts as a tumor suppressor in other gastrointestinal tumors like gastric cancers (73) and hepatocellular carcinomas (74).

In an experimental study, Dong-xu W (20). showed that miR-185 overexpression acts as a tumor suppressor in CRC cells by suppressing the Wnt/β-catenin signal. High expression of miR-185 and low expression of miR-133b are correlated with poor survival and metastasis in CRC cases (41). A previous study demonstrated the role of STIM1 in the metastasis of CRC and that miR-185 directly targets the STIM1 pathway, making it a potential biomarker (75).

The small number of used samples gives the limitation of our study. However, considering our study's design with a statistical power limited for clinical application, our data can be regarded as hypothesis-generating for future studies.

CONCLUSION

The results of the current study revealed that the investigated miRNAs (i.e., miR-17-5p, mir-125b-5p, and miR-185-5p) significantly correlated with metastasis and treatment response of advanced CRC patients. These miRNAs can act as great non-invasive biomarkers for the prediction of CRC patients at high risk of liver metastasis and treatment evaluation for CRC subjects. However, our data should be validated on larger cohorts of patients to ensure the efficacy of these miRNAs in predicting both metastasis and treatment failure in advanced CRC.

DATA AVAILABILITY STATEMENT

The raw data supporting the conclusions of this article will be made available by the authors, without undue reservation.

ETHICS STATEMENT

The studies involving human participants were reviewed and approved by Ethics Committees of the Oncology Institute Prof. Dr. Ion Chiricuta and the University of Medicine and Pharmacy Iuliu Hatieganu, Cluj-Napoca, Romania. The patients/participants provided their written informed consent to participate in this study.

AUTHOR CONTRIBUTIONS

Conceptualization: OB, DS and LB. Methodology: OB, LB and DS. Software: OB and LB. Validation: SV, LP, LB, and OB. Formal analysis: OB, LB, SC. Investigation: DS, CB, SC, SV, LP, and RB.

Resources: OB, CC, SC, and RB. Data curation: SV, LP, CB, and AH, Writing (original draft preparation): DS, OB, and LB, Writing (review and editing): OB, LB, DS and CC. Visualization: CB, RB, and AH. Supervision: AI and OB. Project administration: AI and OB. Funding acquisition: CC, CB, and AI. All authors contributed to the article and approved the submitted version.

FUNDING

This research was funded by the grant Partnership for the transfer of knowledge in biogenomics applications in oncology and related fields-BIOGENONCO, Project co-financed by FEDR through Competitiveness Operational Programme 2014–2020 (contract No. 10/01.09.2016).

ACKNOWLEDGMENTS

The authors- LB, DS, OB, and CC- were supported by the BIOGENONCO grant, 10/01.09.2016 (MySMIS-Code:105774). We want to acknowledge the payment of this article APC by the Romanian National Medical Oncology Society (SNOMR).

REFERENCES

1. Bray F, Ferlay J, Soerjomataram I, Siegel RL, Torre LA, Jemal A. Global Cancer Statistics 2018: GLOBOCAN Estimates of Incidence and Mortality Worldwide for 36 Cancers in 185 Countries. *CA Cancer J Clin* (2018) 68:394–424. doi: 10.3322/caac.21492
2. Dekker E, Tanis PJ, Vleugels JLA, Kasi PM, Wallace MB. Colorectal Cancer. *Lancet* (2019) 394:1467–80. doi: 10.1016/S0140-6736(19)32319-0
3. Adam R, Kitano Y. Multidisciplinary Approach of Liver Metastases From Colorectal Cancer. *Ann Gastroenterol Surg* (2019) 3:50–6. doi: 10.1002/ags3.12227
4. Peng Y, Croce CM. The Role of microRNAs in Human Cancer. *Signal Transduct Target Ther* (2016) 1:15004. doi: 10.1038/sigtrans.2015.4
5. Kim J, Yao F, Xiao Z, Sun Y, Ma L. MicroRNAs and Metastasis: Small RNAs Play Big Roles. *Cancer Metastasis Rev* (2018) 37:5–15. doi: 10.1007/s10555-017-9712-y
6. Maas SLN, Breakefield XO, Weaver AM. Extracellular Vesicles: Unique Intercellular Delivery Vehicles. *Trends Cell Biol* (2017) 27:172–88. doi: 10.1016/j.tcb.2016.11.003
7. Melo SA, Sugimoto H, O'Connell JT, Kato N, Villanueva A, Vidal A, et al. Cancer Exosomes Perform Cell-Independent Microrna Biogenesis and Promote Tumorigenesis. *Cancer Cell* (2014) 26:707–21. doi: 10.1016/j.ccell.2014.09.005
8. Bebelman MP, Smit MJ, Pegtel DM, Baglio SR. Biogenesis and Function of Extracellular Vesicles in Cancer. *Pharmacol Ther* (2018) 188:1–11. doi: 10.1016/j.pharmthera.2018.02.013
9. Hoshino A, Costa-Silva B, Shen T, Rodrigues G, Hashimoto A, Mark MT, et al. Tumour Exosome Integrins Determine Organotropic Metastasis. *Nature* (2015) 527:329–35. doi: 10.1038/nature15756
10. Qiu M, Hu J, Yang D, Cosgrove DP, Xu R. Pattern of Distant Metastases in Colorectal Cancer: A SEER Based Study. *Oncotarget* (2015) 6(36):38658–66. doi: 10.18632/oncotarget.6130
11. Mousavi S, Moallem R, Hassanian SM, Sadeghzade M, Mardani R, Ferns GA, et al. Tumor-Derived Exosomes: Potential Biomarkers and Therapeutic Target in the Treatment of Colorectal Cancer. *J Cell Physiol* (2019) 234:12422–32. doi: 10.1002/jcp.28080
12. Ogata-Kawata H, Izumiya M, Kurioka D, Honma Y, Yamada Y, Furuta K, et al. Circulating Exosomal microRNAs as Biomarkers of Colon Cancer. *PloS One* (2014) 9:1–9. doi: 10.1371/journal.pone.0092921
13. Balacescu O, Sur D, Cainap C, Visan S. The Impact of miRNA in Colorectal Cancer Progression and Its Liver Metastases. *Int J Mol Sci* (2018) 19(12 ():3711. doi: 10.3390/ijms19123711
14. Squadrito ML, Baer C, Burdet F, Maderna C, Gilfillan GD, Lyle R, et al. Endogenous RNAs Modulate MicroRNA Sorting to Exosomes and Transfer to Acceptor Cells. *Cell Rep* (2014) 8:1432–46. doi: 10.1016/j.celrep.2014.07.035
15. Lai H, Zhang J, Zuo H, Liu H, Xu J, Feng Y, et al. Overexpression of miR-17 is Correlated With Liver Metastasis in Colorectal Cancer. *Med (United States)* (2020) 99:1–7. doi: 10.1097/MD.0000000000019265
16. Han K, Wang FW, Cao CH, Ling H, Chen JW, Chen RX, et al. CircLONP2 Enhances Colorectal Carcinoma Invasion and Metastasis Through Modulating the Maturation and Exosomal Dissemination of Microrna-17. *Mol Cancer* (2020) 19:1–18. doi: 10.1186/s12943-020-01184-8
17. Fu F, Jiang W, Zhou L, Zhi C. Circulating Exosomal miR-17-5p and Mir-92a-3p Predict Pathologic Stage and Grade of Colorectal Cancer. *Transl Oncol* (2018) 11:221–32. doi: 10.1016/j.tranon.2017.12.012
18. Zhang Y, Wang S, Lai Q, Fang Y, Wu C, Liu Y, et al. Cancer-Associated Fibroblasts-Derived Exosomal miR-17-5p Promotes Colorectal Cancer Aggressive Phenotype by Initiating a RUNX3/MYC/TGF-β1 Positive Feedback Loop. *Cancer Lett* (2020) 491:22–35. doi: 10.1016/j.canlet.2020.07.023
19. Fang L, Li H, Wang L, Hu J, Jin T, Wang J, et al. MicroRNA-17-5p Promotes Chemotherapeutic Drug Resistance and Tumour Metastasis of Colorectal Cancer by Repressing PTEN Expression. *Oncotarget* (2014) 5:2974–87. doi: 10.18632/oncotarget.1614
20. Dong-xu W, Jia L, Su-juan Z. MicroRNA-185 is a Novel Tumor Suppressor by Negatively Modulating the Wnt/β-Catenin Pathway in Human Colorectal Cancer. *Indian J Cancer* (2016) 52:182. doi: 10.4103/0019-509x.186576
21. Zhang L, Dong X, Yan B, Yu W, Shan L. CircAGFG1 Drives Metastasis and Stemness in Colorectal Cancer by Modulating YY1/CTNNB1. *Cell Death Dis* (2020) 11(7):542. doi: 10.1038/s41419-020-2707-6
22. Lu W, Huang Z, Wang J LH. Long non-Coding RNA DANCR Accelerates Colorectal Cancer Progression Via Regulating the miR-185-5p/HMGA2 Axis. *J Biochem* (2021) mva:1–24. doi: 10.1093/jb/mvab011
23. Afshar S, Najafi R, Sedighi Pashaki A, Sharifi M, Nikzad S, Gholami MH, et al. MiR-185 Enhances Radiosensitivity of Colorectal Cancer Cells by Targeting IGF1R and IGF2. *BioMed Pharmacother* (2018) 106:763–9. doi: 10.1016/j.biopha.2018.07.002
24. Yang M, Tang X, Wang Z, Wu X, Tang D, Wang D. MiR-125 Inhibits Colorectal Cancer Proliferation and Invasion by Targeting TAZ. *Biosci Rep* (2019) 39:1–10. doi: 10.1042/BSR20190193
25. Zhou Xg, Huang Xl, Liang Sy, Tang Sm, Wu Sk, Huang Tt, et al. Identifying miRNA and Gene Modules of Colon Cancer Associated With Pathological Stage by Weighted Gene Co-Expression Network Analysis. *Onco Targets Ther* (2018) 11:2815–30. doi: 10.2147/OTT.S163891
26. Park GB, Jeong JY KD. GLUT5 Regulation by AKT1/3-miR-125b-5p Downregulation Induces Migratory Activity and Drug Resistance in TLR-modified Colorectal Cancer Cells. *Carcinogenesis* (2020) 41:1329–40. doi: 10.1093/carcin/bgaa074
27. Pecqueux M, Liebetrau I, Werft W, Dienemann H, Muley T, Pfannschmidt J, et al. A Comprehensive microRNA Expression Profile of Liver and Lung Metastases of Colorectal Cancer With Their Corresponding Host Tissue and its Prognostic Impact on Survival. *Int J Mol Sci* (2016) 17(10):1755. doi: 10.3390/ijms17101755
28. Kang BW, Kim TW, Lee JL, Ryu MH, Chang HM, Yu CS, et al. Bevacizumab Plus FOLFIRI or FOLFOX as Third-Line or Later Treatment in Patients With Metastatic Colorectal Cancer After Failure of 5-Fluorouracil, Irinotecan, and Oxaliplatin: A Retrospective Analysis. *Med Oncol* (2009) 26:32–7. doi: 10.1007/s12032-008-9077-8
29. Van Cutsem E, Cervantes A, Adam R, Sobrero A, Van Krieken JH, Aderka D, et al. ESMO Consensus Guidelines for the Management of Patients With Metastatic Colorectal Cancer. *Ann Oncol* (2016) 27:1386–422. doi: 10.1093/annonc/mdw235
30. Liao WT, Ye YP, Deng YJ, Bian XW, Ding YQ. Metastatic Cancer Stem Cells: From the Concept to Therapeutics. *Am J Stem Cells* (2014) 3:46–62.
31. Shao Y, Chen T, Zheng X, Yang S, Xu K, Chen X, et al. Colorectal Cancer-derived Small Extracellular Vesicles Establish an Inflammatory Pre-Metastatic Niche in Liver Metastasis. *Carcinogenesis* (2018) 39:1368–79. doi: 10.1016/j.apcata.2013.01.023

32. Xu XM, Qian JC, Deng ZL, Cai Z, Tang T, Wang P, et al. Expression of miR-21, miR-31, miR-96 and miR-135b is Correlated With the Clinical Parameters of Colorectal Cancer. *Oncol Lett* (2012) 4:339–45. doi: 10.3892/ol.2012.714
33. Liying G, Anathbandhu C, Geoffrey T, Wisecarver JL, Are C, Michael Brattain JW. Microrna-192 Suppresses Liver Metastasis of Colon Cancer. *Oncogene* (2014) 33:5332–40. doi: 10.1038/onc.2013.478
34. Fan D, Lin X, Zhang F, Zhong W, Hu J, Chen Y, et al. MicroRNA 26b Promotes Colorectal Cancer Metastasis by Downregulating Phosphatase and Tensin Homolog and Wingless-Type MMTV Integration Site Family Member 5A. *Cancer Sci* (2018) 109:354–62. doi: 10.1111/cas.13451
35. Guo YH, Wang LQ, Li B, Xu H, Yang JH, Zheng LS, et al. Wnt/β-Catenin Pathway Transactivates microRNA-150 That Promotes EMT of Colorectal Cancer Cells by Suppressing CREB Signaling. *Oncotarget* (2016) 7:42513–26. doi: 10.18632/oncotarget.9893
36. Nishida N, Yokobori T, Mimori K, Sudo T, Tanaka F, Shibata K, et al. MicroRNA miR-125b is a Prognostic Marker in Human Colorectal Cancer. *Int J Oncol* (2011) 38:1437–43. doi: 10.3892/ijo.2011.969
37. Teng Y, Ren Y, Hu X, Mu J, Samykutty A, Zhuang X, et al. MVP-Mediated Exosomal Sorting of miR-193a Promotes Colon Cancer Progression. *Nat Commun* (2017) 8:1–16. doi: 10.1038/ncomms14448
38. Yu W, Zhu K, Wang Y, Yu H, Guo J. Overexpression of miR-21-5p Promotes Proliferation and Invasion of Colon Adenocarcinoma Cells Through Targeting CHL1. *Mol Med* (2018) 24:1–12. doi: 10.1186/s10020-018-0034-5
39. Peng H, Wang L, Su Q, Yi K, Du J, Wang Z. MiR-31-5p Promotes the Cell Growth, Migration and Invasion of Colorectal Cancer Cells by Targeting NUMB. *BioMed Pharmacother* (2019) 109:208–16. doi: 10.1016/j.biopha.2018.10.048
40. Park GB, Jeong JY, Kim D. Modified TLR-mediated Downregulation of miR-125b-5p Enhances CD248 (Endosialin)-Induced Metastasis and Drug Resistance in Colorectal Cancer Cells. *Mol Carcinog* (2019) 59:154–67. doi: 10.1002/mc.23137
41. Akçakaya P, Ekelund S, Kolosenko I, Caramuta S, Özata D, Xie H, et al. miR-185 and miR-133b Deregulation is Associated With Overall Survival and Metastasis in Colorectal Cancer. *Int J Oncol* (2011) 39:311–8. doi: 10.3892/ijo.2011.1043
42. Lin M, Duan B, Hu J, Yu H, Sheng H, Gao H, et al. Decreased Expression of miR-193a-3p is Associated With Poor Prognosis in Colorectal Cancer. *Oncol Lett* (2017) 14:1061–7. doi: 10.3892/ol.2017.6266
43. Yan S, Han B, Gao S, Wang X, Wang Z, Wang F, et al. Exosome-Encapsulated microRNAs as Circulating Biomarkers for Colorectal Cancer. *Oncotarget* (2017) 8:60149–58. doi: 10.18632/oncotarget.18557
44. Ghanbari R, Mosakhani N, Asadi J, Nouraee N, Mowla SJ, Yazdani Y, et al. Downregulation of Plasma MiR-142-3p and MiR-26a-5p in Patients With Colorectal Carcinoma. *Iran J Cancer Prev* (2015) 8(3):e2329. doi: 10.17795/ijcp2329
45. Zou SL, Chen YL, Ge ZZ, Qu YY, Cao Y, Kang ZX. Downregulation of Serum Exosomal miR-150-5p is Associated With Poor Prognosis in Patients With Colorectal Cancer. *Cancer Biomarkers* (2019) 26:69–77. doi: 10.3233/CBM-190156
46. Tomlinson JS, Jarnagin WR, DeMatteo RP, Fong Y, Kornprat P, Gonen M, et al. Actual 10-Year Survival After Resection of Colorectal Liver Metastases Defines Cure. *J Clin Oncol* (2007) 25:4575–80. doi: 10.1200/JCO.2007.11.0833
47. Thind A, Wilson C. Exosomal miRNAs as Cancer Biomarkers and Therapeutic Targets. *J Extracell Vesicles* (2016) 5:1–11. doi: 10.3402/jev.v5.31292
48. Guo Y, Bao Y, Yang W. Regulatory miRNAs in Colorectal Carcinogenesis and Metastasis. *Int J Mol Sci* (2017) 18(4):890. doi: 10.3390/ijms18040890
49. Thomas J, Ohtsuka M, Pichler M, Ling H. Microrna: Clinical Relevance in Colorectal Cancer. *Int J Mol Sci* (2015) 16:28063–76. doi: 10.3390/ijms161226080
50. Kong W, Cheng Y, Liang H, Chen Q, Kun X, Huang Z, et al. Prognostic Value of mir-17-5p in Cancers: A Meta-Analysis. *Onco Targets Ther* (2018) 11–3541–9. doi: 10.2147/OTT.S150340
51. Wang Y, Zeng G, Jiang Y. The Emerging Roles of MiR-125b in Cancers. *Cancer Manag Res* (2020) 12:1079–88. doi: 10.2147/CMAR.S232388
52. Sun W, Nie W, Wang Z, Zhang H, Li Y, Fang X. Lnc Haglr Promotes Colon Cancer Progression Through Sponging mir-185-5p and Activating Cdk4 and Cdk6 In Vitro and In Vivo. *Onco Targets Ther* (2020) 13:5913–25. doi: 10.2147/OTT.S246092
53. Chen XJ, Shi KQ, Wang YQ, Song M, Zhou W, Tu HX, et al. Clinical Value of Integrated-Signature miRNAs in Colorectal Cancer: miRNA Expression Profiling Analysis and Experimental Validation. *Oncotarget* (2015) 6:37544–56. doi: 10.18632/oncotarget.6065
54. Kara M, Yumrutas O, Ozcan O, Celik OI, Bozgeyik E, Bozgeyik I, et al. Differential Expressions of Cancer-Associated Genes and Their Regulatory miRNAs in Colorectal Carcinoma. *Gene* (2015) 567:81–6. doi: 10.1016/j.gene.2015.04.065
55. Monzo M, Navarro A, Bandres E, Artells R, Moreno I, Gel B, et al. Overlapping Expression of microRNAs in Human Embryonic Colon and Colorectal Cancer. *Cell Res* (2008) 18:823–33. doi: 10.1038/cr.2008.81
56. Wang X, Chen L, Jin H, Wang S, Zhang Y, Tang X, et al. Screening miRNAs for Early Diagnosis of Colorectal Cancer by Small RNA Deep Sequencing and Evaluation in a Chinese Patient Population. *Onco Targets Ther* (2016) 9:1159–66. doi: 10.2147/OTT.S100427
57. Sur D, Coza O, Havasi A, Cainap C, Burz C, Cainap SS, et al. Exosomal miRNAs in Colorectal Cancer: The Carriers of Useful News. *J BUON* (2020) 25:23–34.
58. Baassiri A, Nassar F, Mukherji D, Shamseddine A, Nasr R, Temraz S. Exosomal non Coding RNA in LIQUID Biopsies as a Promising Biomarker for Colorectal Cancer. *Int J Mol Sci* (2020) 21(4):1398. doi: 10.3390/ijms21041398
59. Zhang H, Zhu M, Shan X, Zhou X, Wang T, Zhang J, et al. A Panel of seven-miRNA Signature in Plasma as Potential Biomarker for Colorectal Cancer Diagnosis. *Gene* (2019) 687:246–54. doi: 10.1016/j.gene.2018.11.055
60. Gustavsson B, Carlsson G, MacHover D, Petrelli N, Roth A, Schmoll HJ, et al. A Review of the Evolution of Systemic Chemotherapy in the Management of Colorectal Cancer. *Clin Colorectal Cancer* (2015) 14:1–10. doi: 10.1016/j.clcc.2014.11.002
61. Neugut AI, Lin A, Raab GT, Hillyer GC, Keller D, O'Neil DS, et al. FOLFOX and FOLFIRI Use in Stage Iv Colon Cancer: Analysis of SEER-Medicare Data. *Clin Color Cancer* (2019) 18:133–40. doi: 10.1016/j.clcc.2019.01.005
62. Molina-Pinelo S, Carnero A, Rivera F, Estevez-Garcia P, Bozada JM, Limon ML, et al. MiR-107 and miR-99a-3p Predict Chemotherapy Response in Patients With Advanced Colorectal Cancer. *BMC Cancer* (2014) 14:1–10. doi: 10.1186/1471-2407-14-656
63. Amankwatia EB, Chakravarty P, Carey FA, Weidlich S, Steele RJC, Munro AJ, et al. MicroRNA-224 is Associated With Colorectal Cancer Progression and Response to 5-Fluorouracil-Based Chemotherapy by KRAS-dependent and-Independent Mechanisms. *Br J Cancer* (2015) 112:1480–90. doi: 10.1038/bjc.2015.125
64. Chen Q, Xia HW, Ge XJ, Zhang YC, Tang QL, Bi F. Serum miR-19a Predicts Resistance to FOLFOX Chemotherapy in Advanced Colorectal Cancer Cases. *Asian Pacific J Cancer Prev* (2013) 14:7421–6. doi: 10.7314/APJCP.2013.14.12.7421
65. Rasmussen MH, Jensen NF, Tarpgaard LS, Qvortrup C, Rømer MU, Stenvang J, et al. High Expression of microRNA-625-3p is Associated With Poor Response to First-Line Oxaliplatin Based Treatment of Metastatic Colorectal Cancer. *Mol Oncol* (2013) 7:1–10. doi: 10.1016/j.molonc.2013.02.016
66. Yagi T, Iinuma H, Hayama T, Matsuda K, Nozawa K, Tsukamoto M, et al. Plasma Exosomal microRNA-125b as a Monitoring Biomarker of Resistance to mFOLFOX6-based Chemotherapy in Advanced and Recurrent Colorectal Cancer Patients. *Mol Clin Oncol* (2019) 11:416–24. doi: 10.3892/mco.2019.1911
67. Liu T, Zhang X, Du L, Wang Y, Liu X, Tian H, et al. Exosome-Transmitted miR-128-3p Increase Chemosensitivity of Oxaliplatin-Resistant Colorectal Cancer. *Mol Cancer* (2019) 18:43. doi: 10.1186/s12943-019-0981-7
68. Kral J, Korenkova V, Novosadova V, Langerova L, Schneiderova M, Liska V, et al. Expression Profile of miR-17/92 Cluster is Predictive of Treatment Response in Rectal Cancer. *Carcinogenesis* (2018) 39:1359–67. doi: 10.1093/carcin/bgy100
69. Ma Y, Zhang P, Wang F, Zhang H, Yang Y, Shi C, et al. Elevated Oncofoetal miR-17-5p Expression Regulates Colorectal Cancer Progression by Repressing its Target Gene P130. *Nat Commun* (2012) 3:1291. doi: 10.1038/ncomms2276
70. Neerincx M, Poel D, Sie DLS, van Grieken NCT, Shankaraiah RC, Van Der Wolf-De Lijster FSW, et al. Combination of a Six microRNA Expression

Profile With Four Clinicopathological Factors for Response Prediction of Systemic Treatment in Patients With Advanced Colorectal Cancer. *PloS One* (2018) 13:1–20. doi: 10.1371/journal.pone.0201809

71. Chen H, Xu Z. Hypermethylation-Associated Silencing of miR-125a and Mir-125b: A Potential Marker in Colorectal Cancer. *Dis Markers* (2015) 2015:1–7. doi: 10.1155/2015/345080
72. Wu QB, Chen J, Zhu JW, Yin X, You HY, Lin YR, et al. MicroRNA-125 Inhibits RKO Colorectal Cancer Cell Growth by Targeting VEGF. *Int J Mol Med* (2018) 42:665–73. doi: 10.3892/ijmm.2018.3632
73. Tan B, Li Y, Zhao Q, Fan L, Wang D. ZNF139 Increases Multidrug Resistance in Gastric Cancer Cells by Inhibiting Mir-185. *Biosci Rep* (2018) 38: BSR20181023. doi: 10.1042/bsr20181023
74. Qadir XV, Han C, Lu D, Zhang J, Wu T. MiR-185 Inhibits Hepatocellular Carcinoma Growth by Targeting the DNMT1/PTEN/Akt Pathway. *Am J Pathol* (2014) 184:2355–64. doi: 10.1016/j.ajpath.2014.05.004
75. Zhang Z, Liu X, Feng B, Liu N, Wu Q, Han Y, et al. STIM1, a Direct Target of microRNA-185, Promotes Tumor Metastasis and is Associated With Poor Prognosis in Colorectal Cancer. *Oncogene* (2015) 34:4808–20. doi: 10.1038/onc.2014.404

Conflict of Interest: The authors declare that the research was conducted in the absence of any commercial or financial relationships that could be construed as a potential conflict of interest.

frontiers in Oncology

ORIGINAL RESEARCH
published: 20 May 2021
doi: 10.3389/fonc.2021.621346

Scaphium affine Ethanol Extract Induces Anoikis by Regulating the EGFR/Akt Pathway in HCT116 Colorectal Cancer Cells

Hye Won Kawk[1], *Gun-He Nam*[1], *Myeong Jin Kim*[1], *Sang-Yong Kim*[2] *and Young-Min Kim*[1]*

[1] Department of Biological Science and Biotechnology, College of Life Science and Nano Technology, Hannam University, Daejeon, South Korea, [2] Department of Food Science and Bio Technology, Shinansan University, Ansan, South Korea

Scaphium affine ethanol extracts (SAE) is a species that has been shown to contain various physiological effects; however, its anticancer effects have yet to be revealed. We qualitatively evaluated β-sitosterol in SAE through high-performance liquid chromatography (HPLC). The cytotoxicity in HCT116 and HT29 colorectal cancer cells and CCD841 normal colon cells was confirmed through WST-1 assays. Selective cytotoxicity was observed in colorectal cancer cells, with greater cytotoxicity demonstrated in the HCT116 cell line. As such, the HCT116 colorectal cell line was selected for subsequent experiments. After HCT116 cells were treated with SAE, it was confirmed that the apoptosis rate was increased in a SAE dose-dependent manner through Annexin V assay. SAE further showed dose-dependent suppression of invasion through invasion assays. Anoikis induction through the EGFR/Akt pathway in HCT116 colorectal cancer cells was confirmed by Western blotting. The tumor suppressive effects of SAE was assessed *in vivo* using a xenograft model of human HCT116 colorectal cancer cells. As a result, we confirmed that SAE decreased tumor size in a dose-dependent manner and that p-EGFR and cleaved-caspase 3 in tumors were also regulated in a dose-dependent manner. This study showed that SAE, by containing β-sitosterol with proven anticancer effects, induces anoikis through the EGFR/Akt pathway in HCT116 colorectal cancer cells both *in vitro* and *in vivo*.

Keywords: *Scaphium affine*, HCT116 colorectal cancer cells, anoikis, EGFR/Akt pathway, xenograft model

OPEN ACCESS

Edited by:
Shilpa S. Dhar, University of Texas MD Anderson Cancer Center, United States

Reviewed by:
Keith R. Laderoute, Consultant, Redwood City, CA, United States
Luyong Zhang, China Pharmaceutical University, China

***Correspondence:**
Young-Min Kim
ym1938@naver.com

Specialty section:
This article was submitted to Molecular and Cellular Oncology, a section of the journal Frontiers in Oncology

Received: *26 October 2020*
Accepted: *30 March 2021*
Published: *20 May 2021*

Citation:
Kawk HW, Nam G-H, Kim MJ, Kim S-Y and Kim Y-M (2021) Scaphium affine Ethanol Extract Induces Anoikis by Regulating the EGFR/Akt Pathway in HCT116 Colorectal Cancer Cells. Front. Oncol. 11:621346. doi: 10.3389/fonc.2021.621346

INTRODUCTION

Cancer is a disease caused by the random proliferation and metastasis of cells. Its incidence is high, and it is considered to be the leading cause of death in developed countries (1). The incidence of colorectal cancer, one of the most prevalent malignant tumors worldwide, is rapidly increasing due to industrialization and urbanization (2). The main risk factors for colorectal cancer include abnormal diets, such as substantial consumption of foods containing high animal fats and sugars, and excessive alcohol consumption. Smoking, long-term use of nonsteroidal anti-inflammatory

drugs, colorectal diseases, metabolic syndrome, and heredity (only 5% of cases) are also potential causes of colorectal cancer (3, 4). Symptoms of colorectal cancer include alternating diarrhea and constipation as well as the appearance of mucus and blood in the feces. These symptoms can be accompanied by colon infarction, anemia, weight loss, and abdominal lumps (5, 6).

The treatment of colorectal cancer mainly involves surgical resection of the tumor, combined with anticancer drugs or radiation therapy (7). However, these interventions lead to adverse effects such as reduced immunity, normal cells toxicity, genetic damage, and hair loss (8). Accordingly, various studies have been conducted on new bioactive substances with anticancer effects that have been developed by considering the efficacy of harmless natural substances to reduce the adverse effects of chemotherapy and to selectively suppress the growth and proliferation of cancer cells through various mechanisms (9, 10).

Scaphium affine, used in this study, is the seed of *S. affine*, belonging to the family Sterculiaceae. *S. affine* has been proven to possess various effects such as ulcer-protective, antioxidant, and anti-inflammatory effects, but no anticancer effects have yet been proven (11–14). β-sitosterol, which has been found to be a physiologically active ingredient in many natural products, has been proven to have anticancer effects. Therefore, β-sitosterol-containing natural substances may have anticancer effects on colorectal cancer (15–17).

Adherent cells sometimes acquire migration, adhesion, and proliferation properties in an unsuitable environment. Most cells perceive this as an abnormal phenomenon, resulting in the loss in normal cell-matrix interactions, cessation in cell cycle progression, and eventually the induction of a specific type of apoptosis known as anoikis. However, when anoikis resistance occurs, cancer cells gain the ability to metastasize and invade (18–20).

Epidermal growth factor receptor (EGFR) belongs to the ErbB receptor family of tyrosine kinases. EGFR expression is associated with tumor differentiation, apoptosis, metastasis, and angiogenesis. It also plays a key role in the induction of anoikis (21, 22). EGFR functionally modulates caveolin-1, which is a major component of lipid rafts and caveolae, and regulates cellular behaviors such as cholesterol homeostasis, including anoikis. Src, a non-receptor tyrosine kinase, is an activating factor of EGFR and regulates cell proliferation and growth by promoting downstream signaling (23). Akt is directly involved in cell proliferation and growth through the influence of Src signaling. When EGFR, a key factor in anoikis induction, is suppressed, caveolin-1, src, and Akt are suppressed. Inactivation of Akt inhibits cell proliferation and growth, which consequently leads to anoikis induction *via* the intrinsic apoptosis pathway (24–28).

Herein, we performed a qualitative evaluation of β-sitosterol in *S. affine* ethanol extracts (SAE). We aimed to verify the EGFR/Akt pathway-mediated anoikis-inducing effects of SAE *in vitro* in HCT116 colorectal cancer cells. In addition, we investigated the effects of SAE on tumor suppression *in vivo* using an HCT116 human colorectal cancer xenograft model in Balb/c-nu mice, which are ideal hosts for rapid growth of tumor cell lines due to their lack of immunity.

MATERIALS AND METHODS

Reagents

The SAE (CA01-060) used in this study was obtained from the Korea Plant Extract Bank at the Korea Research Institute of Bioscience and Biotechnology (Daejeon, Korea). A voucher specimen (PBC-131AS) was kept in the herbarium of the Korea Research Institute of Bioscience and Biotechnology. The plant (70 g) was dried in the shade and powdered and was added to 1L of ethyl alcohol 95.0% (GR grade, Daejung Chemical & Metals Co., Ltd), and extracted through 30 cycles (40KHz, 1500W, 15 min ultrasonication-120 min standing per cycle) at room temperature using an ultrasonic extractor (SDN-900H, SD-ultrasonic Co., Ltd). After filtration (Qualitative Filter No.2, Hyundai Micro Co., Ltd.), SAE (1.62 g) was obtained. Various concentrations of SAE were prepared by dissolving in dimethyl sulfoxide (DMSO; Samchun Co., Ltd., Korea) and were refrigerated at -4°C for use. β-sitosterol, an indicator component, was purchased from Sigma-Aldrich (Danvers, MA, USA) and was dissolved in methyl alcohol (Samchun Co., Ltd., Korea). Gefitinib (20 mM) was purchased from Abcam (Cambridge, UK), and LY294002 (20 mM) was purchased from Calbiochem (San Diego, CA, USA). Both inhibitors were diluted with DMSO. WST-1 solution was purchased from Dogen Bio (Seoul, Korea). Primary antibodies against t-EGFR (cat #2232), p-EGFR (cat #2234), t-Akt (cat #9272), p-Akt (cat #9271), p-Src (cat #2101), t-caveolin-1 (cat #3267), p-caveolin-1 (cat #3251), p53 (cat #9282), Bcl-2 (cat #2876), Bak (cat #6947), PARP (cat #9542), and β-actin (cat #4967) were purchased from Cell Signaling Technology (Danvers, MA, USA), whereas t-Src (cat #sc-8056) antibody was purchased from Santa Cruz Biotechnology (Dallas, TX, USA). Caspase 3 (cat #ab2302) antibodies were purchased from Abcam (Cambridge, UK). Among the secondary antibodies, anti-mouse IgG and HRP-linked antibody were purchased from Cell Signaling Technology, while goat anti-human IgG H&L (HRP) was purchased from Abcam. The Muse™ Annexin V and Dead Cell Assay kit was purchased from Luminx (Austin, TX, USA).

Identification of Active Compounds of SAE With High-Performance Liquid Chromatography (HPLC)

SAE was diluted to 1 mg/mL using methyl alcohol and filtered. β-sitosterol was diluted to 0.01 mg/ml in the same manner and used for qualitative analysis. All materials were analyzed by injection into HPLC 2694 separation modules (Waters, USA) with separation flow rate of 1 mL/min through a SunFire™ C-18 column (4.6 × 250 mm, 5 μm, SunFire, Germany). In addition, the mobile phase of all materials was detected using the Dual Absorbance Detector 2487 (Waters) at 205 nm for 1 h with 5:95 water to acetonitrile.

Cell Culture

HCT116 and HT29 colorectal cancer cells and CCD841 normal colon cells were obtained from the American Type Culture Collection (ATCC, Manassas, VA, USA). HCT116 and HT29 colorectal cancer cells were grown in RPMI medium (HyClone, UT, USA) containing 1% antibiotics (100 U/mL penicillin and 100 mg streptomycin/mL) and 10% fetal bovine serum (HyClone) at 37°C in a 5% CO_2 atmosphere. CCD841 normal colon cells were grown in DMEM (HyClone) containing 1% antibiotics (100 U/mL penicillin and 100 mg/mL streptomycin) and 10% fetal bovine serum (HyClone) at 37°C in a 5% CO_2 atmosphere. After washing in PBS (HyClone), the cells were suspended in trypsin-EDTA (HyClone) every 2 days.

WST-1 Assay

Cells were seeded at 4.0×10^5 cells/ml in a 24-well plate for 24 h and were incubated with SAE (50, 75, 100, 125 and 150 μg/mL) for 24 h. The inhibitors, gefitinib and LY294002, were pretreated for 60 – 120 min prior to treatment with SAE (100 μg/mL). The cells were incubated with 100 μl/mL WST-1 solution for 60 min. The optical densities of the solutions were then quantified at a 450 nm wavelength using a FLUOstar Omega system (BMG Labtech, Germany).

Determination of Apoptosis by Annexin V Staining

Cells were seeded at 1.0×10^6 cells/mL in a 6-well plate. After 24 h incubation, the cells were treated with various concentrations of SAE (75 and 125 μg/mL) for 24 h. The cells were resuspended in PBS. Then, 100 μL of Muse™ Annexin V and Dead cell reagent was added to 100 μL of the resuspended cells. After incubation for 20 min at room temperature, the dyed cells were analyzed in a Muse™ Cell Analyzer (EMD Millipore).

Cell Invasion Assay

An SPL insert hanging 24-well plate (SPL Life Sciences, Korea) with a pore size of 8 μm was used. Corning Matrix (Corning, NY, USA) was applied to the insert. Cells were seeded at 4.0×10^5 cells/mL with serum-free RPMI media in the insert. The bottom of the 24-well plate included RPMI media containing 1% antibiotics (100 U/mL penicillin and 100 mg streptomycin/mL) and 10% fetal bovine serum. SAE (75 and 125 μg/mL) was then added to the insert and incubated for 24 h, followed by 10% trichloroacetic acid for 1 h, and 0.25% crystal violet (Sigma-Aldrich) for 2 h. The dyed HCT116 colorectal cancer cells were observed using an inverted microscope (×100 magnification, Axiovert 100, Zeiss, Germany).

Western Blotting

Cells were seeded at 1.0×10^6 cells/mL in a 6-well plate. After 24 h incubation, the cells were treated with various concentrations of SAE (75 and 125 μg/mL) for 24 h. Inhibitors, gefitinib and LY294002, were pretreated for 60 – 120 min prior to treatment with SAE (100 μg/mL). After 24 h, the cells were rinsed with precooled PBS, and proteins were extracted using RIPA buffer (Radioimmunoprecipitation assay buffer; 50 mM Tris-HCl, pH 7.6, 150 mM NaCl, 1% Triton X-100, 1% sodium deoxycholate, 0.1% SDS, 2 mM EDTA; ForBioKorea, Korea) containing 1X Halt Protease and Phosphatase Inhibitor cocktail (Thermo Fisher, USA). The extracted protein was quantified to 20 μg by Bradford analysis using a Bio-Rad protein assay dye reagent concentrate (Bio-Rad, CA, USA). Proteins were separated by size using 8% or 12% acrylamide gels and then transferred to a nitrocellulose membrane (GE Healthcare Life Sciences, MA, USA). Blocking was performed using 5% bovine serum albumin (BSA; MP Biomedicals, CA, USA). Primary antibodies (t-EGFR, p-EGFR, t-caveolin, p-caveolin, t-Src, p-Src, t-Akt, p-Akt, p53, Bcl-2, Bak, caspase 3, PARP, and β-actin) reacted overnight at 4°C, while secondary antibodies (anti-mouse IgG, HRP-linked Antibody and Goat Anti-Human IgG H&L (HRP) Antibody) reacted for 120 min at 4°C. Western blotting was repeated at least 3 times for each experiment. SuperSignal™ West Femto Maximum Sensitivity Substrate (ThermoFisher, MA, USA) was used to react with the bound antibody substrate. Protein expression was confirmed using a UVITEC gel imaging system (Philekorea, Seoul, Korea). All western blotting images were quantitatively represented using ImageJ (National Institutes of Health, Washington, D.C., USA).

In Vivo Xenograft Model

Male, 4-week-old Balb/c nu/nu mice were obtained from Envigo (Indiana, USA) and were housed in sterile, filter-topped cages. A total of 18 mice were randomly and equally divided into 3 group. The experiments were conducted in 3 groups [the negative control (N), SAE 75 mg/kg/day, and SAE 100 mg/kg/day group). The animals were provided with the appropriate accommodation, environment, food, water, and care for their health and to minimize distress. The mice were maintained under specifically controlled conditions (ambient temperature 23 ± 2°C, humidity 50 ± 5%, 12 h light/dark cycle). Body weight was measured once per week. For tumor induction, HCT116 human colorectal cancer cells (2.5×10^5 cells/0.25 mL) were subcutaneously injected into the left flank of mice of all 3 groups (negative control, SAE 75 mg/kg/day, and SAE 100 mg/kg/day). Seven days after the injection of cells, the presence of tumor was confirmed. The animals were treated with SAE at 75 mg/kg/day or 100 mg/kg/day for another 14 days. The tumor size was measured using a digital caliper (Asimeto, Germany) at 7-day intervals, and the tumor volume was calculated using the following formula: $V = 0.5 \times (\text{length} \times \text{width} \times \text{height})$. The animals were euthanized by CO_2 asphyxiation followed by cervical dislocation, and the tumors were collected for histological analysis. The animal study was reviewed and approved by the Hannam University Animal Experimental Ethics Approval Committee (NHU2020-6; Daejeon, Korea).

Immunohistochemistry

The tumors were fixed in 3.7% formaldehyde (10% neutral buffered formalin, Samchun Chemicals, Pyeongtaek, Korea) for 48 h, embedded in paraffin (Leica 39601006, Leica, Hessen, Germany) using a Tissue Processor (ASP300s, Leica), and sectioned into 3 μM thick slices using a rotary microtome (Leica RM2255, Leica). Tumor tissue sections were

pre-warmed for 40 min at 60°C oven and were deparaffinized in ultraclear xylene (AvantiK, NJ, USA) for 3 rounds of 7 min each, 99.9% ethanol (GD Trade, Korea) for 2 rounds of 3 min each, 95% ethanol (GD Trade) for 2 rounds of 3 min each, 80% ethanol for 3 min, and 70% ethanol for 3 min using automatic H&E staining (Tissue-TeK, Prisma E2, Sakura, Japan). The tumor sections were treated with 3% H_2O_2 for 15 min, and non-specific binding blocking was performed using 5% BSA. The sections were then treated with a primary antibody (p-EGFR, cleaved-caspase 3) for 60 min at 4°C, and subsequently with a secondary antibody (HRP-conjugated anti-rabbit Ig) for 30 min. The sections were added to the DAB solution, incubated for 7 min, and rinsed with tap water for 10 min for DAB development. The sections were incubated with hematoxylin for 3 min, rinsed with tap water for 10 min, and dehydrated using an automated system (70%, 80%, 95%, 100% ethanol, xylene). All images were quantitatively represented using ImageJ.

TUNEL Assay

Apoptosis was assessed using the TdT-mediated dUTP nick-end labeling (TUNEL) method. The tumors were fixed in 3.7% formaldehyde (10% neutral buffered formalin) for 48 h, embedded in paraffin, and sectioned into 3 μM thick slices. The paraffin was removed at 60°C for 40 min, and the tumor tissue sections were deparaffinized in ultraclear xylene for 3 rounds of 7 min each, 99.9% ethanol for 2 rounds of 3 min each, 95% ethanol for 2 rounds of 3 min each, 80% ethanol for 3 min, and 70% ethanol for 3 min using automatic H&E staining. Tumor tissue sections were processed using the ApopTag Peroxidase *in situ* Apoptosis Detection Kit (Vector Laboratories, USA). DAB solution was added and incubated for 7 min, and rinsed with tap water for 10 min for DAB development. Tumor tissue sections were incubated with Mayer hematoxylin for 3 min, rinsed with tap water for 10 min, and dehydrated using an automated system (70%, 80%, 95%, 100% ethanol, Xylene). All images were quantitatively represented using ImageJ.

Statistical Analysis

All experiments were repeated at least 3 times. Statistical analyses were performed using the t-test (SPSS, Inc., Chicago, IL, USA). $p < 0.05$, $p < 0.01$, and $p < 0.001$ were considered to indicate a statistically significant difference. Error bars represent standard error.

RESULTS

Qualitative Analysis of Bioactive Compounds (β-sitosterol) in SAE

β-sitosterol, a bioactive compound with proven anticancer effects, was qualitatively evaluated through HPLC of SAE. To identify β-sitosterol in SAE, we compared the retention time of the compound analyzed in SAE to that of β-sitosterol (**Figures 1A, B**). HPLC analysis of β-sitosterol in SAE and standard compound analysis showed a retention time of 2.039 min, confirming that β-sitosterol is present in SAE. By setting β-sitosterol as an indicator component, it (i.e. β-sitosterol) may act as a surrogate marker for anticancer effects of SAE.

Cytotoxicity of SAE in HCT116 and HT29 Colorectal Cancer Cells by WST-1 Assays

To verify the cytotoxicity of SAE in HCT116 and HT29 colorectal cancer cells, both cell lines were treated with different concentrations of SAE(50, 75, 100, 125, and 150 μg/mL) for 24 h. Cytotoxicity was measured using WST-1 assays. HCT116 colorectal cancer cells showed % cell viability of 97.5%, 86.6%, 69.3%, 55.2%, and 41.2% at 50, 75, 100, 125, and 150 μg/mL, respectively (**Figure 2A**), whereas HT29 colorectal cancer cells showed % cell viability of 100.3%, 93.5%, 82.2%, 69.8%, and 55.4%, respectively (**Figure 2B**). These results indicated the dose-dependent cytotoxicity of SAE on HCT116 and HT29 colorectal cancer cells and that cytotoxicity was more effective on HCT116 colorectal cancer cells. In addition, when CCD841 normal colon cells were treated with SAE under the same conditions, no cytotoxicity was observed as % cell viability remained at 90% or more at all concentrations (**Figure 2C**). Therefore, the cytotoxicity of SAE was shown to be specific to HCT116 and HT29 colorectal cancer cells. Due to the greater cytotoxicity shown in HCT116 colorectal cancer cells, subsequent experiments were conducted on this cell line.

Effect of SAE on Apoptosis Induction, and Invasion Inhibition in HCT116 Colorectal Cancer Cells

Anoikis are a form of apoptosis caused by lack of intercellular interaction or loss of adhesion. To confirm that apoptosis was induced, we treated HCT116 colorectal cancer cells with 75 and 125 μg/mL SAE for 24 h, and phosphatidylserine (PS) expressed during apoptosis was stained with Annexin V. The staining ratio of PS was identified at each concentration of SAE using a flow cytometer to determine the ratio of apoptosis. The results showed that apoptosis was induced at 1.50% in the N group, 11.35% with 75 μg/mL SAE, and 45.60% with 125 μg/mL SAE. In addition, 75 ug/mL of low toxicity also involved apoptosis in induction by stimulation, but no significance was observed (**Figure 3A**). These results indicated that SAE induced apoptosis in HCT116 colorectal cancer cells in a dose-dependent manner. Anoikis resistance is a prerequisite for metastasis and invasion in cancer cells, and the induction of anoikis in an abnormal environment inhibits this behavior of cancer cells. A cell invasion assay was used to assess the inhibitory effects of SAE on HCT116 colorectal cancer cell invasion, and SAE was shown to suppress invasion in a dose-dependent manner (**Figure 3B**). These results highlighted that the anoikis-inducing effects of SAE associated with the invasion-inhibitory effect of SAE.

Effects of SAE on Anoikis Signaling Protein Expression in HCT116 Colorectal Cancer Cells

When anoikis occurs, the cell membrane receptor p-EGFR, a key factor in anoikis, is inhibited, thereby deactivating p-

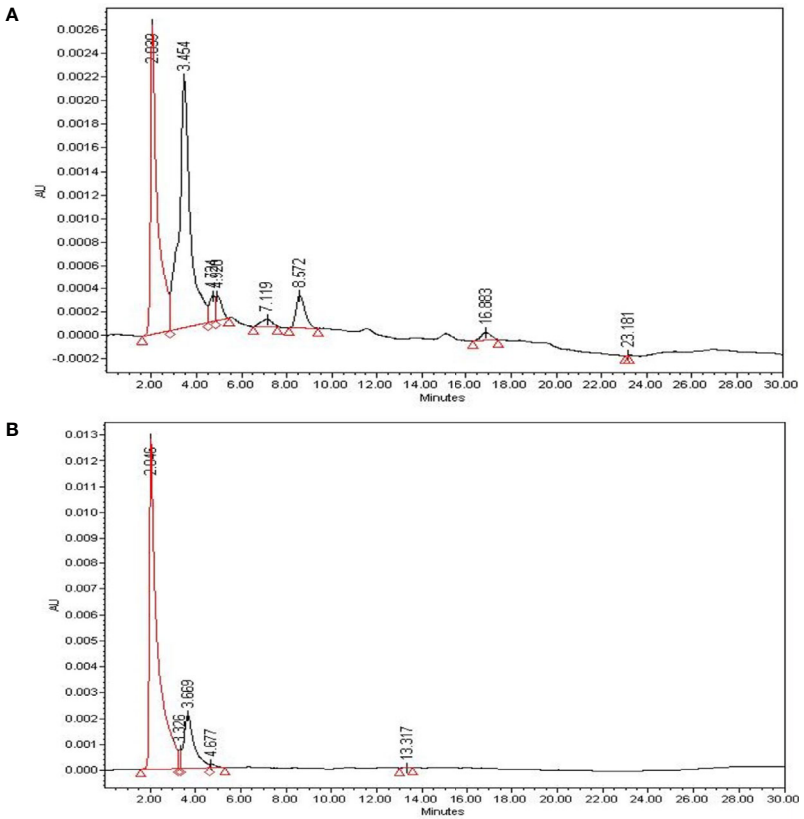

FIGURE 1 | The identification of bioactive compounds in SAE. **(A)** HPLC profiles of SAE at 1 mg/mL (total extract). **(B)** HPLC profiles of standard β-sitosterol at 0.01 mg/mL (2.046 min). The X-axis represents retention time (min), and the Y-axis represents absorption units (AU). The detector was set at 205 nm.

caveolin and p-Src. Accordingly, p-Akt, which regulates cell growth and proliferation, is deactivated, and tumor suppressor p53 is activated to induce the intrinsic apoptotic pathway. In this experiment, the trend of anoikis-inducing signaling proteins in HCT116 cells following 75 and 125 μg/mL SAE exposure for 24 h was examined. The results showed that SAE dose-dependently decreased p-EGFR and p-caveolin-1, which decreased p-Src. p-Akt showed a tendency to decrease, while p53 increased. Furthermore, SAE decreased Bcl-2, which maintains mitochondrial membrane potential, and increased Bak, which loss of mitochondrial membrane potential. Caspase 3 fragments PARP, which repairs DNA. And cleaved-caspase 3, an activated form of caspase 3, showed a tendency to increase, while pro-caspase 3 decreased in a dose-dependent manner. As the activity of caspase 3 increased, cleaved-PARP, the deactivated form of PARP, increased. The above changes were also observed at 75 ug/mL of low toxicity by stimulation. Overall, these results demonstrated that the concentration-dependent anoikis-inducing effects of SAE in HCT116 colorectal cancer cells proceeds by inducing the intrinsic apoptotic pathway through the regulation of anoikis-related signaling proteins such as EGFR, caveolin-1, Src, and Akt (**Figure 4**).

Effects of EGFR/Akt Inhibitors on the Survival Rates of HCT116 Colorectal Cancer Cells the Expression of Anoikis Signaling Proteins

To determine how EGFR and Akt affect the induction of anoikis in HCT116 colorectal cancer cells by SAE, we treated the cells with 20 μM EGFR inhibitor and 20 μM Akt inhibitor (gefitinib and LY294002) with or without SAE (100 μg/mL) for 24 h. WST-1 assays were subsequently performed. The cell viability were observed to be 64.8% with SAE treatment, 77.9% with gefitinib treatment, 73.6% with LY294002 treatment, 48.8% with the combined treatment of SAE and gefitinib, and 49.1% with the combined treatment of SAE and LY294002. EGFR and Akt were found to affect the growth and proliferation of HCT116 colorectal cancer cells, and SAE was also found to exhibit inhibitory effects on proliferation, similar to the inhibitors (**Figure 5A**). To investigate the tendency of anoikis induction by EGFR and Akt regulation, Western blotting was performed by treating HCT116 colorectal cancer cells with SAE, gefitinib, and LY294002 under the same conditions as the above experiment. Briefly, inhibition of EGFT and Akt would lead to decrease in p-EGFR, p-caveolin-1, p-Src, and p-Akt decreased; and as p53 increases, Bcl-2 would decrease and

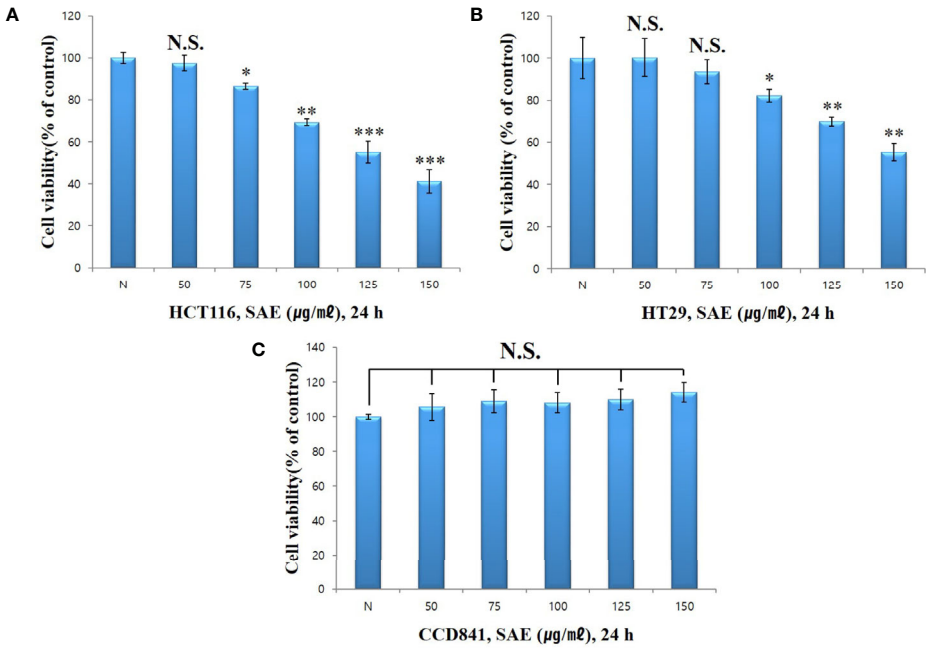

FIGURE 2 | The effect of SAE on the viability of HCT116, HT29, and CCD841 cells. Cell viability was measured by WST-1 assays. **(A)** HCT116 cells were pretreated with SAE for 24 h. **(B)** HT29 cells were pretreated with SAE for 24 h. **(C)** CCD841 cells were pretreated with SAE for 24 h. Statistical analysis was performed using t-tests. *p < 0.05, **p < 0.01 and ***p < 0.001 compared to the controls. N.S., not significant (each experiment, n = 3). N., Negative control; 50., SAE 50 μg/mL; 75., SAE 75 μg/mL; 100., SAE 100 μg/mL; 125., SAE 125 μg/mL; 150., SAE 150 μg/mL.

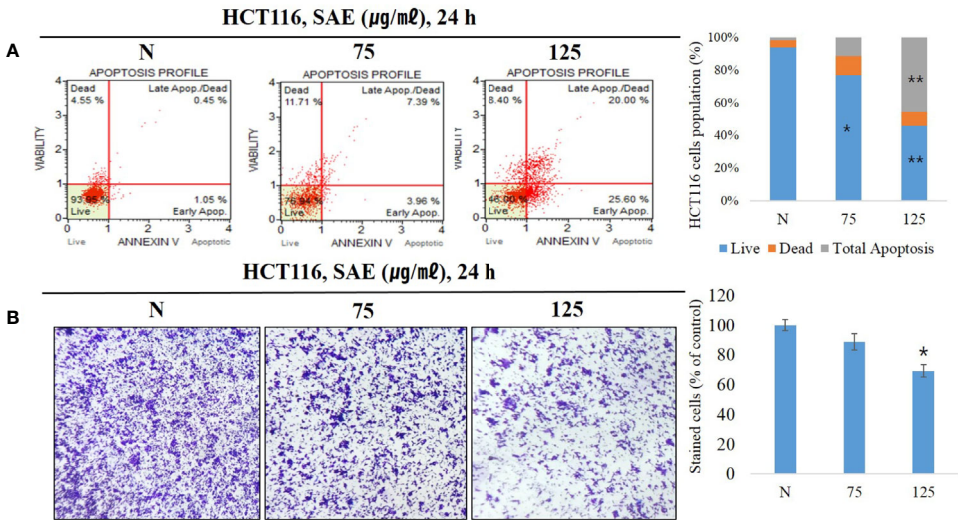

FIGURE 3 | HCT116 cells were treated with SAE at different concentrations (75 and 125 μg/mL) for 24 h. **(A)** The apoptotic effects of SAE were evaluated using the Muse™ Annexin V assay. Data were analyzed by flow cytometry. **(B)** Cell invasion was measured using invasion assays. Statistical analyses were performed using t-tests; *P < 0.05, **P < 0.01 compared to N groups (each experiment, n= 3). N., Negative control; 75., SAE 75 μg/mL; 100., SAE 100 μg/mL.

Bak would increase, while activation of caspase 3 would decrease pro-caspase 3 and increase cleaved-caspase 3, which would deactivate PARP, and cause an increase in cleaved-PARP. Our results showed that such expression level of each of these proteins were more prominent when treated in combination with SAE and each of the inhibitors than when

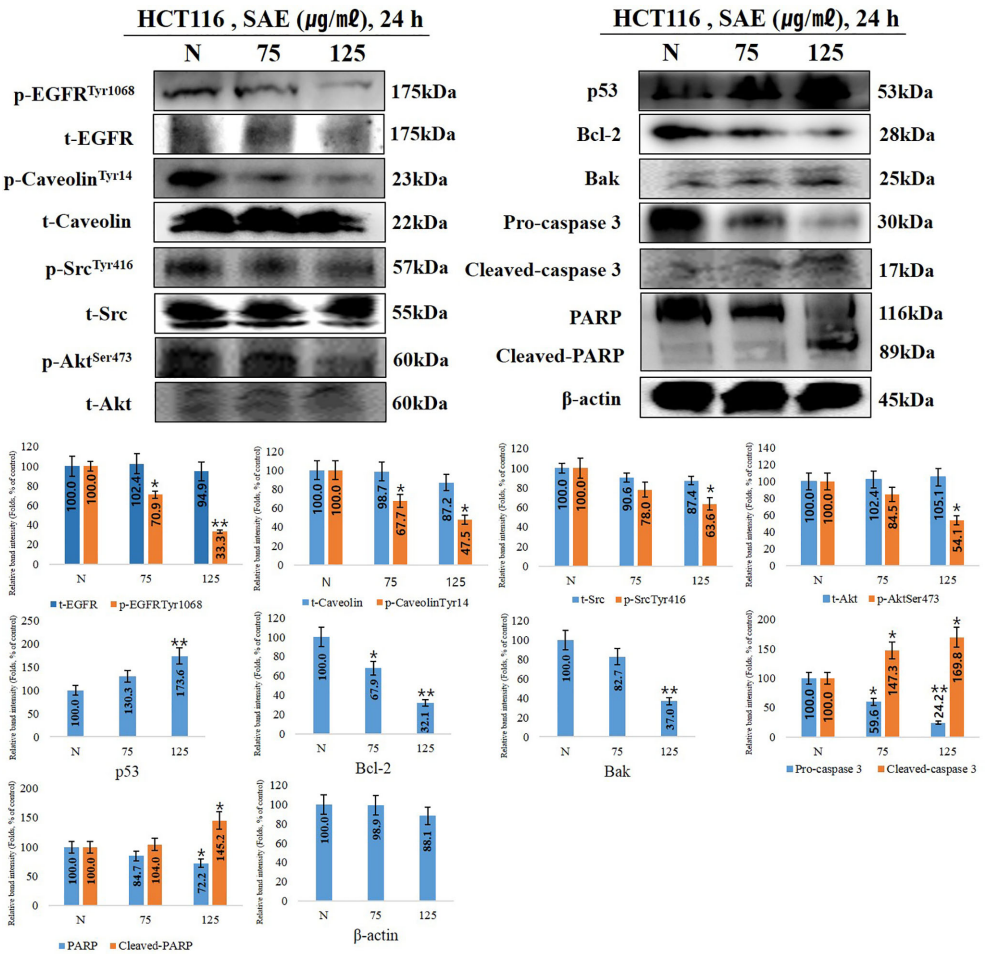

FIGURE 4 | The effects of SAE on the expression of anoikis regulatory proteins. HCT116 cells were treated with the indicated concentrations of SAE for 24 h. The expressions of p-EGFR, p-caveolin, t-caveolin, p-Src, t-Src, p-Akt, p53, Bcl-2, Bak, PARP, and cleaved-PARP. Pro-caspase 3, cleaved-caspase 3, and β-actin were analyzed by Western blotting (each experiment, n = 3). All Western blotting images were quantitatively represented using ImageJ (National Institutes of Health). Statistical analyses were performed using t-tests; *P < 0.05, **P < 0.01 compared to N groups (each experiment, n= 3). The error bars represent the standard error. N., Negative control; 75., SAE 75 μg/mL; 100., SAE 100 μg/mL.

treated with a single substance. Thus, it was confirmed that anoikis were induced through the regulation of the EGFR/Akt pathway of SAE by further inhibiting the EGFR/Akt pathway, which was not inhibited by the inhibitor (**Figure 5B**).

In Vivo Inhibition of Tumor Growth by SAE

When anoikis, apoptosis due to loss of cell adhesion, occurs normally, it can partially inhibit tumor cell invasion, metastasis, and angiogenesis, and it is also involved in the inhibition of tumor proliferation (29). To investigate tumor suppression by SAE *in vivo*, we established a HCT116 colorectal cancer xenograft model by transplanting human HCT116 cells into 4-week-old male Balb/c-nu mice. We found no changes in body weight in both the control group and the SAE groups (75 mg/kg/day and 100 mg/kg/day in PBS) (**Figure 6A**); however, tumor size was reduced to a greater extent in the SAE groups than in the control group. In addition, tumor size decreased effectively as the concentration of SAE increased (**Figure 6B**). The number of TUNEL-positive cells represents a marker of apoptosis, as indicated by DNA degradation. To analyze apoptosis in all groups of tumor tissues, we performed a TUNEL assay and observed that TUNEL-positive cells increased in all SAE concentration groups compared with the control group, and a dose-dependent increase was confirmed (**Figure 6C**). p-EGFR and cleaved-caspase 3 expressions were further evaluated by immunohistochemistry. Compared with the control group, lower p-EGFR and higher cleaved-caspase 3 expression levels were demonstrated in all SAE concentration groups, which indicated a concentration-dependent effect of SAE on both factors (**Figure 6C**). These results demonstrated the tumor suppression effects of SAE and confirmed that SAE regulates the activity of EGFR and caspase 3 in tumor cells.

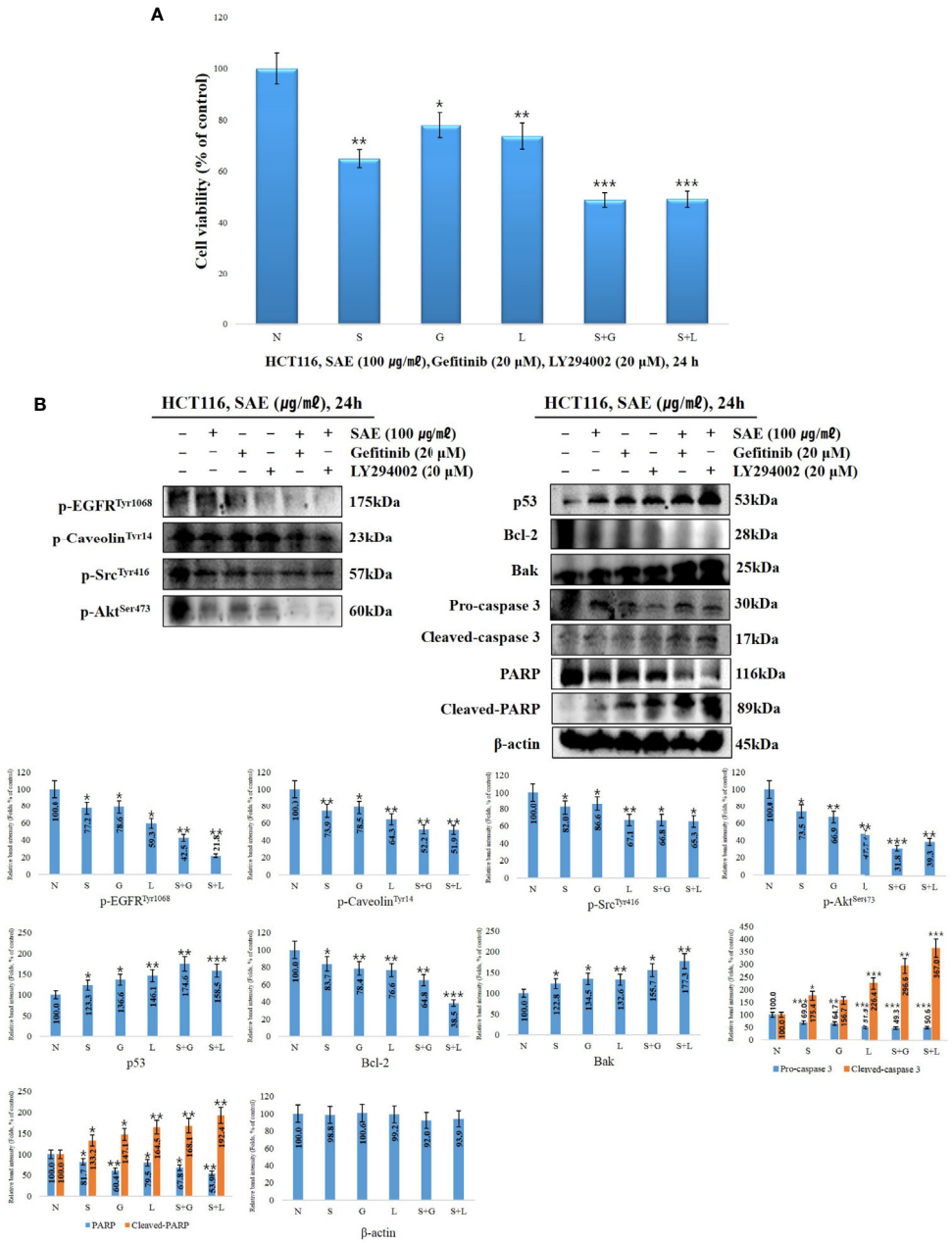

FIGURE 5 | The effects EGFR/Akt inhibition on cell proliferation and signaling protein expression. HCT116 cells were treated with 20 μM gefitinib, 20 μM LY294002, and 100 μg/mL SAE for 24 h. **(A)** Cell viability was measured by WST-1 assays. Statistical analyses were performed using t-tests; *p < 0.05, **p < 0.01, ***p < 0.001. (each experiment, n = 3). N., Negative control; S., SAE; G., Gefitinib; L., LY294002. **(B)** The cells were treated with 20 μM gefitinib, 20 μM LY294002, and 100 μg/mL SAE for 24 h. The expressions of p-EGFR, p-caveolin, P-Src, p-Akt, p53, Bcl-2, Bak, PARP, and cleaved PARP. Pro-caspase 3, cleaved-caspase 3, and β-actin were analyzed by Western blotting (each experiment, n=3). All western blotting images were quantitatively represented using ImageJ (National Institutes of Health). Statistical analyses were performed using t-tests; *P < 0.05, **P < 0.01, ***p < 0.001 compared to N groups (each experiment, n= 3). The error bars represent the standard error. N., Negative control; S., SAE; G., Gefitinib; L., LY294002.

DISCUSSION

Recently, many cancer-related studies have been conducted on traditional medicinal plants, with the focus of identifying new compounds with physiological effects and investigating their potential value as anticancer drugs (30). These studies provide the basis for developing anticancer drugs that have fewer side effects and that can serve as an alternative to mitigate commercial anticancer drug resistance (31, 32). Since the characteristics of many cancer cells, such as invasiveness and metastasis, are mediated by anoikis

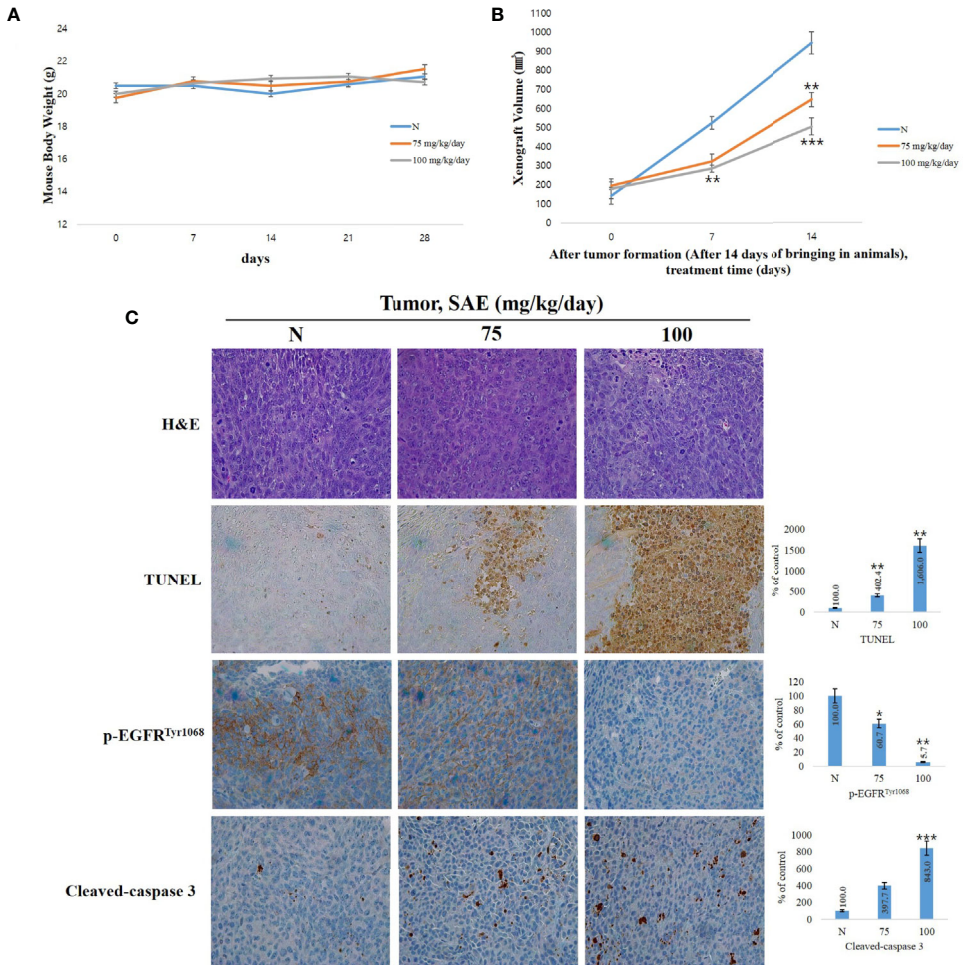

FIGURE 6 | SAE suppresses tumor growth *in vivo*. **(A)** Measurement of body weight. **(B)** Measurement of tumor size. SAE treated groups (75 or 100) were compared against untreated groups (N). Statistical analyses were performed using t-tests; *p < 0.05, **p < 0.01, ***p < 0.001. N.S., not significant. **(C)** H&E staining, TUNEL assay and immunohistochemistry (IHC) of specific proteins (p-EGFR, cleaved-caspase 3). Tumor sections were observed using an optical microscope at ×400. All images were quantitatively represented using ImageJ (National Institutes of Health). Statistical analyses were performed using t-tests; *P<0.05, **P<0.01, ***p < 0.001 compared to N groups (each experiment, n= 3). The error bars represent the standard error. N, Negative control; 75, SAE 75 mg/kg/day; 100, SAE 100 mg/kg/day.

resistance, targeting and treating cancer cells are often difficult. This thereby suggests that direct induction of anoikis that would cause a loss of adhesion in cancer cells can partially inhibit cancer cell proliferation, invasion, and metastasis (33). This study therefore investigated the mechanisms of anoikis induction and tumor suppression in HCT116 colorectal cancer cells following exposure to SAE, an extract of traditional medicinal plants.

Scaphium affine is also known as S. lychnophora. β-sitosterol is also found in seeds of S. lychnophora (Scaphium affine) which was discovered by Wang et al. (34). The anticancer effects of β-sitosterol has been shown in colorectal cancer cells (35, 36). Therefore, β-sitosterol was established as an indicator component in this study, and qualitative evaluation through HPLC was performed to determine whether the indicator component was extracted when extracting the SAE used in the study (37, 38). With the assumption that SAE contains other apoptosis-inducing components besides β-sitosterol, we are investigating the qualitative evaluation of other components that induce apoptosis in HCT116 colorectal cancer cells. Additionally, a quantitative evaluation is being conducted to confirm the effect of β-sitosterol.

The WST-1 assay showed that cytotoxicity was induced in HCT116 and HT29 colorectal cancer cells upon exposure to SAE. Dose-dependent cytotoxicity was observed in both cell lines, and greater cytotoxicity was observed in the HCT116 cell line. When the same method was applied to CCD841 normal colon epithelial cells, cytotoxicity was not observed at all concentrations. These results indicated that SAE cytotoxicity is specific to colorectal cancer cells.

Anoikis refers to apoptosis induced by abnormal adhesion and loss of adhesion. Anoikis are intrinsic apoptosis induced by blocking specific signals that regulate the interaction between cells and the extracellular matrix (ECM). Therefore, in order to

confirm normal anoikis induction, it is necessary whether or not apoptosis is induced. Therefore, it was confirmed by Annexin V that SAE induces apoptosis in a dose-dependent manner in HCT116 colorectal cancer cells. Additionally, given that the normal functioning of anoikis inhibits the invasion and metastasis of cancer cells, a cell invasion assay was performed to investigate the inhibitory effects of SAE on cell invasion. Our findings confirmed that SAE dose-dependently inhibits the invasiveness of HCT116 colorectal cancer cells, and that these results are associated with the anoikis-inducing effects of SAE.

EGFR plays a key role in the induction of anoikis (39, 40). When EGFR is activated, caveolin-1, which inhibits anoikis and promotes tumor metastasis, is also activated, and Src, a signaling transducer, subsequently activates Akt to promote cancer cell and tumor proliferation (41). Activation of this cascade increases anoikis resistance; therefore, inhibition of both EGFR and Akt are required to induce anoikis. To examine whether anoikis is induced by SAE, we assessed factors associated with anoikis induction using Western blotting. It was observed that EGFR, caveolin-1, and Src were inhibited by SAE, which led to the loss of adhesion and the disruption of signal transduction, resulting in inactivation of Akts that are directly involved in cell growth and proliferation. Furthermore, the tumor suppressor p53 was observed to be increased, while Bcl-2, which maintains mitochondrial membrane potential, was found to be suppressed, and Bak, which increases mitochondrial membrane permeability, was increased. In addition, increased cleaved-caspase 3, an activated form of caspase 3, and decreased pro-caspase 3, an inactivated form, and fragmented PARP, which repairs DNA, were observed, which resulted in an increase in cleaved-PARP (26, 42–45). Accordingly, expression of the identified anoikis-inducing factors showed a tendency to increase or decrease with SAE in a dose-dependent manner.

To demonstrate anoikis induction through the EGFR/Akt signalling pathway, cell viability and changes in the trends of associating factors were assessed through treatment with gefitinib (EGFR inhibitor) and LY294002 (Akt inhibitor). Greater cytotoxicity was observed when cells were treated with a combination of SAE and EGFR/Akt inhibitors than with SAE or EGFR/Akt inhibitors alone in the WST-1 assay. The Western blot assay also showed that anoikis-related factors tend to show stronger effects when treated in combination than when treated with SAE or inhibitor alone. Due to the similar effects observed between SAE and EGFR/Akt inhibitors and stronger effects observed by treated in combination, we confirmed that SAE induces anoikis through the EGFR/Akt pathway.

To confirm the tumor suppressing effects of SAE, a xenograft model of HCT116 colorectal cancer cells was established, and we found no changes in body weight of the experimental animals in the SAE group, alongside reduced tumor size when compared to the control group. In addition, the TUNEL assay confirmed that SAE increased apoptosis rates in tumor cells and decreased p-EGFR and increased cleaved-caspase 3 in a dose-dependent manner.

In conclusion, this study showed that SAE containing physiological compounds such as β-sitosterol, which have been shown to have anticancer effects in colorectal cancer cells, induces anoikis through the EGFR/Akt pathway. This study is the first to report the *in vitro* and *in vivo* anticancer effects of SAE on HCT116 colorectal cancer cells. This study provides a basis for the potential use of SAE as an alternative anticancer drug for anoikis resistant-related invasion and metastasis. In addition, this study may facilitate separation and screening of compounds with anti-cancer potential for substitution of colorectal cancer chemotherapeutic drugs.

DATA AVAILABILITY STATEMENT

The original contributions presented in the study are included in the article/supplementary material. Further inquiries can be directed to the corresponding author.

ETHICS STATEMENT

The animal study was reviewed and approved by Hannam University Animal Experimental Ethics Approval Committee.

AUTHOR CONTRIBUTIONS

HK, G-HN, MK, and S-YK carried out the WST-1 assays, flow cytometry (cell cycle arrest and Annexin V staining), and Western blotting, established the tumor xenograft model, and performed the H&E staining, TUNEL assay, and immunohistochemistry. HK and G-HN performed the HPLC analyses. HK and Y-MK wrote the manuscript. All authors contributed to the article and approved the submitted version.

FUNDING

The authors declare that this study received funding from the Forbio Ltd. The funder was not involved in the study design, collection, analysis, interpretation of data, the writing of this article or the decision to submit it for publication.

REFERENCES

1. Jemal A, Bray F, Center MM, Ferlay J, Ward E, Forman D. Global Cancer Statistics. *CA: Cancer J Clin* (2011) 61(2):69–90. doi: 10.3892/ijo.23.6.1657
2. Razali FN, Sinniah SK, Hussin H, Abidin NZ, Shuib AS. Tumor Suppression Effect of Solanum Nigrum Polysaccharide Fraction on Breast Cancer via Immunomodulation. *Int J Biol Macromolecules* (2016) 92:185–93. doi: 10.1016/j.ijbiomac.2016.06.079
3. McCleary NJ, Niedzwiecki D, Hollis D, Saltz LB, Schaefer P, Whittom R, et al. Impact of Smoking on Patients With Stage III Colon Cancer: Results From Cancer and Leukemia Group B 89803. *Cancer: Interdiscip Int J Am Cancer Soc* (2010) 116(4):957–66. doi: 10.1002/cncr.24866

4. Kwak EL, Chung DC. Hereditary Colorectal Cancer Syndromes: an Overview. *Clin Colorectal Cancer* (2007) 6(5):340–4. doi: 10.3816/CCC.2007.n.002
5. Byar KL, Berger AM, Bakken SL, Cetak MA. Impact of Adjuvant Breast Cancer Chemotherapy on Fatigue, Other Symptoms, and Quality of Life. *Oncol Nurs Forum* (2006) 33(1):E18. Oncology Nursing Society. doi: 10.1188/06.ONF.E18-E26
6. Rasmussen S, Larsen PV, Søndergaard J, Elnegaard S, Svendsen RP, Jarbøl DE. Specific and Non-Specific Symptoms of Colorectal Cancer And Contact to General Practice. *Family Pract* (2015) 32(4):387–94. doi: 10.1093/fampra/cmv032
7. Van Emburgh BO, Sartore-Bianchi A, Di Nicolantonio F, Siena S, Bardelli A. Acquired Resistance to EGFR-Targeted Therapies in Colorectal Cancer. *Mol Oncol* (2014) 8(6):1084–94. doi: 10.1016/j.molonc.2014.05.003
8. Fan Y, Wang W, Song W, Chen H, Teng A, Liu A. Partial Characterization and Anti-Tumor Activity of an Acidic Polysaccharide from Gracilaria Lemaneiformis. *Carbohydr Polymers* (2012) 88(4):1313–8. doi: 10.1016/j.carbpol.2012.02.014
9. Nam GH, Jo KJ, Park YS, Kawk HW, Kim SY, Kim YM. In vitro and in vivo Induction of p53-Dependent Apoptosis by Extract of Euryale ferox Salisb in A549 Human Caucasian Lung Carcinoma Cancer Cells Is Mediated Through Akt Signaling Pathway. *Front Oncol* (2019) 9:406. doi: 10.3389/fonc.2019.00406
10. Tragulpakseerojn J, Yamaguchi N, Pamonsinlapatham P, Wetwitayaklung P, Yoneyama T, Ishikawa N, et al. Anti-Proliferative Effect of Moringa Oleifera Lam (Moringaceae) Leaf Extract on Human Colon Cancer HCT116 Cell Line. *Trop J Pharm Res* (2017) 16(2):371–8. doi: 10.4314/tjpr.v16i2.16
11. Oppong MB, Yang LI, Banahene PO, Shi-Ming FANG, Feng QIU. Ethnopharmacology, Phytochemistry, and Pharmacology of Sterculia Lychnophora Hance (Pangdahai). *Chin J Natural Medicines* (2018) 16(10):721–31. doi: 10.1016/S1875-5364(18)30112-2
12. Ogale SC, Kasture SB, Kasture VS, Tiwari R, Temrikar Z. Screening of Methanolic Extract of Sterculia Scaphigera Wall Seeds for Ulcerprotective & Antioxidant Activity. *World J Pharm Pharm Sci* (2014) 4:1332–46.
13. Palve A, Shetty P, Pimpliskar M, Jadhav RN. Study on Antibacterial and Antifungal Activities of Sterculia Lychnophora Extracts [J]. *Int J Curr Microbiol Appl Sci* (2015) 4(11):336–41.
14. Dhage P, Kasture SB, Mohan M. Analgesic, Anti-Inflammatory, Antioxidant and Antiulcer Activity of Ethanolic Extract of Sterculia Scaphigera Hance (sterculiaceae) Seeds in Mice and Rats. *IJBPR* (2013) 4:35–45.
15. Awad AB, Chen YC, Fink CS, Hennessey T. beta-Sitosterol Inhibits HT-29 Human Colon Cancer Cell Growth and Alters Membrane Lipids. *Anticancer Res* (1996) 16(5A):2797–804.
16. Alvarez-Sala A, Attanzio A, Tesoriere L, Garcia-Llatas G, Barberá R, Cilla A. Apoptotic Effect of a Phytosterol-Ingredient and its Main Phytosterol (β-sitosterol) in Human Cancer Cell Lines. *Int J Food Sci Nutr* (2019) 70(3):323–34. doi: 10.1080/09637486.2018.1511689
17. Malek SNA, Shin SK, Wahab NA, Yaacob H. Cytotoxic Components of Pereskia bleo (Kunth) DC.(Cactaceae) Leaves. *Molecules* (2009) 14(5):1713–24. doi: 10.3390/molecules14051713
18. Frisch SM, Ruoslahti E. Integrins and anoikis. *Curr Opin Cell Biol* (1997) 9(5):701–6. doi: 10.1016/S0955-0674(97)80124-X
19. Simpson CD, Anyiwe K, Schimmer AD. Anoikis Resistance and Tumor Metastasis. *Cancer Lett* (2008) 272(2):177–85. doi: 10.1016/j.canlet.2008.05.029
20. Kim YN, Koo KH, Sung JY, Yun UJ, Kim H. Anoikis Resistance: an Essential Prerequisite For Tumor Metastasis. *Int J Cell Biol* (2012) 2012:11. doi: 10.1155/2012/306879
21. Kim H, Sung JY, Park EK, Kho S, Koo KH, Park SY, et al. Regulation of Anoikis Resistance by NADPH Oxidase 4 and Epidermal Growth Factor Receptor. *Br J Cancer* (2017) 116(3):370–81. doi: 10.1038/bjc.2016.440
22. Kim E, Khuri F, Herbst R. Epidermal Growth Factor Receptor Biology (IMC-C225). *Curr Opin Oncol* (2001) 13(6):506–13. doi: 10.1097/00001622-200111000-00014
23. Tai YL, Chu PY, Lai IR, Wang MY, Tseng HY, Guan JL, et al. An EGFR/Src-Dependent β4 Integrin/FAK Complex Contributes to Malignancy of Breast Cancer. *Sci Rep* (2015) 5:16408. doi: 10.1038/srep16408
24. Wang S, Yu S, Shi W, Ge L, Yu X, Fan J, et al. Curcumin Inhibits the Migration and Invasion of Mouse Hepatoma Hca-F Cells Through Down-regulating Caveolin-1 Expression and Epidermal Growth Factor Receptor Signaling. *IUBMB Life* (2011) 63(9):775–82. doi: 10.1002/iub.507|
25. Zhang B, Peng F, Wu D, Ingram AJ, Gao B, Krepinsky JC. Caveolin-1 Phosphorylation is Required for Stretch-Induced EGFR and Akt Activation in Mesangial Cells. *Cell Signalling* (2007) 19(8):1690–700. doi: 10.1016/j.cellsig.2007.03.005
26. Paoli P, Giannoni E, Chiarugi P. Anoikis Molecular Pathways and its Role in Cancer Progression. *Biochim Biophys Acta (BBA)-Mol Cell Res* (2013) 1833(12):3481–98. doi: 10.1016/j.bbamcr.2013.06.026
27. Sotgia F, Martinez-Outschoorn UE, Howell A, Pestell RG, Pavlides S, Lisanti MP. Caveolin-1 and Cancer Metabolism in the Tumor Microenvironment: Markers, Models, and Mechanisms. *Annu Rev Pathol: Mech Dis* (2012) 7:423–67. doi: 10.1146/annurev-pathol-011811-120856
28. Li S, Chen Y, Zhang Y, Jiang X, Jiang Y, Qin X, et al. Shear Stress Promotes Anoikis Resistance of Cancer Cells via Caveolin-1-Dependent Extrinsic and Intrinsic Apoptotic Pathways. *J Cell Physiol* (2019) 234(4):3730–43. doi: 10.1002/jcp.27149|
29. Guadamillas MC, Cerezo A, del Pozo MA. Overcoming Anoikis–Pathways to Anchorage-Independent Growth In Cancer. *J Cell Sci* (2011) 124(19):3189–97. doi: 10.1242/jcs.072165
30. Jung IL. Soluble Extract from Moringa Oleifera Leaves with a New Anticancer Activity. *PloS One* (2014) 9(4):e95492. doi: 10.1371/journal.pone.0095492
31. Gordaliza M. Natural Products as Leads to Anticancer Drugs. *Clin Trans Oncol* (2007) 9(12):767–76. doi: 10.1007/s12094-007-0138-9
32. Nam GH, Lee SJ, Kim GY, Jeon MJ, Jo KJ, Park YS, et al. The Extracts from Allium Hookeri Induces p53-Independent Apoptosis Through Mitochondrial Intrinsic Pathways in AGS Human Gastric Carcinoma Cells. *J Cancer Sci Ther* (2018) 10:198–204. doi: 10.4172/1948-5956.1000544
33. Rennebeck G, Martelli M, Kyprianou N. Anoikis and Survival Connections in the Tumor Microenvironment: is there a Role in Prostate Cancer Metastasis? *Cancer Res* (2005) 65(24):11230–5. doi: 10.1158/0008-5472
34. Wang RF, Yang XW, Ma CM, Shang MY, Liang JY, Wang X, et al. Alkaloids from the Seeds of Sterculia Lychnophora (Pangdahai). *Phytochemistry* (2003) 63(4):475–8. doi: 10.1016/S0031-9422(03)00182-1
35. Bin Sayeed MS, Ameen SS. Beta-Sitosterol: a Promising but Orphan Nutraceutical to Fight Against Cancer. *Nutr Cancer* (2015) 67(8):1216–22. doi: 10.1080/01635581.2015.1087042
36. Novotny L, Mahmoud F, Abdel-Hamid ME, Hunakova L. Anticancer Potential of β-sitosterol. *Int J Clin Pharmacol Pharmacother* (2017) 2:129. doi: 10.15344/2456-3501/2017/129
37. Baskar AA, Ignacimuthu S, Paulraj GM, Al Numair KS. Chemopreventive Potential of β-Sitosterol in Experimental Colon Cancer Model-an in vitro and in vivo Study. *BMC Complement Altern Med* (2010) 10(1):24. doi: 10.1186/1472-6882-10-24
38. Choi YH, Kong KR, Kim Y, Jung KO, Kil JH, Rhee SH, et al. Induction of Bax and Activation of Caspases During β-Sitosterol-Mediated Apoptosis in Human Colon Cancer Cells. *Int J Oncol* (2003) 23(6):1657–62. doi: 10.3892/ijo.23.6.1657
39. Wang K, Zhu X, Mei D, Ding Z. Caveolin-1 Contributes to Anoikis Resistance in Human Gastric Cancer SGC-7901 Cells via Regulating Src-Dependent EGFR-ITGB1 Signaling. *J Biochem Mol Toxicol* (2018) 32(10):e22202. doi: 10.1002/jbt.22202|
40. Tencer L, Burgermeister E, Ebert MP, Liscovitch M. Rosiglitazone Induces Caveolin-1 by PPARγ-Dependent and PPRE-Independent Mechanisms: the Role of EGF Receptor Signaling and its Effect on Cancer Cell Drug Resistance. *Anticancer Res* (2008) 28(2A):895–906.
41. Yang J, Zhu T, Zhao R, Gao D, Cui Y, Wang K, et al. Caveolin-1 Inhibits Proliferation, Migration, and Invasion of Human Colorectal Cancer Cells by Suppressing Phosphorylation of Epidermal Growth Factor Receptor. *Med Sci Monitor Int Med J Exp Clin Res* (2018) 24:332–41. doi: 10.12659/msm.907782
42. Green DR, Kroemer G. The Pathophysiology of Mitochondrial Cell Death. *Science* (2004) 305(5684):626–9. doi: 10.1126/science.1099320
43. Nam GH, Jo KJ, Park YS, Kawk HW, Yoo JG, Jang JD, et al. Bacillus/Trapa japonica Fruit Extract Ferment Filtrate Enhances Human Hair Follicle Dermal Papilla Cell Proliferation via the Akt/ERK/GSK-3β Signaling Pathway. *BMC Complement Altern Med* (2019) 19(1):1–11. doi: 10.1186/s12906-019-2514-8
44. Nam GH, Jo KJ, Park YS, Kawk HW, Yoo JG, Jang JD, et al. The Peptide AC 2 Isolated from Bacillus-Treated Trapa Japonica Fruit Extract Rescues DHT (dihydrotestosterone)-Treated Human Dermal Papilla Cells and Mediates mTORC1 Signaling for Autophagy and Apoptosis Suppression. *Sci Rep* (2019) 9(1):1–11. doi: 10.1038/s41598-019-53347-3

45. Weber GF. Time and Circumstances: Cancer Cell Metabolism at Various Stages of Disease Progression. *Front Oncol* (2016) 6:257. doi: 10.3389/fonc.2016.00257

Conflict of Interest: The authors declare that the research was conducted in the absence of any commercial or financial relationships that could be construed as a potential conflict of interest.

frontiers in Oncology

ORIGINAL RESEARCH
published: 25 May 2021
doi: 10.3389/fonc.2021.640276

LncRNA DLEU1 Contributes to the Growth and Invasion of Colorectal Cancer *via* Targeting miR-320b/PRPS1

Dong Xu[1†], Fei Yang[2†], Yongchao Fan[3], Wanling Jing[3], Jianfei Wen[4], Wen Miao[3], Xiaoyan Ding[3] and Hongbao Yang[3]*

[1] Department of General Surgery, Gaochun People's Hospital, Nanjing, China, [2] Department of Internal Medicine, Gaochun People's Hospital, Nanjing, China, [3] Center for New Drug Safety Evaluation and Research, Institute of Pharmaceutical Science, China Pharmaceutical University, Nanjing, China, [4] Department of General Surgery, The First Affiliated Hospital of Nanjing Medical University, Nanjing, China

OPEN ACCESS

Edited by:
Massimo Bonora, University of Ferrara, Italy

Reviewed by:
Chunyan Gu, Nanjing University of Chinese Medicine, China
Ye Yang, Nanjing University of Chinese Medicine, China

***Correspondence:**
Hongbao Yang
yhb@cpu.edu.cn

[†]These authors have contributed equally to this work

Specialty section:
This article was submitted to Molecular and Cellular Oncology, a section of the journal Frontiers in Oncology

Received: *11 December 2020*
Accepted: *06 May 2021*
Published: *25 May 2021*

Citation:
Xu D, Yang F, Fan Y, Jing W, Wen J, Miao W, Ding X and Yang H (2021) LncRNA DLEU1 Contributes to the Growth and Invasion of Colorectal Cancer via Targeting miR-320b/PRPS1. Front. Oncol. 11:640276. doi: 10.3389/fonc.2021.640276

Growing evidences suggest that long non-coding RNAs (lncRNAs) are closely correlated to the development of human cancer, such as colorectal cancer (CRC). A previous report suggested that DLEU1 accelerated CRC development. However, DLEU1's underlying mechanism in CRC remains unclear. In our study, the level of DLEU1 in CRC tissues is investigated by qRT-PCR. Our data exhibited that DLEU1 level was observably increased in CRC tissues and CRC cell lines and was closely associated with bad prognosis of CRC patients. CRC cell proliferation was repressed by sh-LncRNA DLEU1, whereas cell apoptosis was markedly stimulated. Moreover, knockdown of DLEU1 inhibited cell migration and invasion. Mechanistically, through interacting with miR-320b in CRC, DLEU1 promoted the level of PRPS1 which was a target of miR-320b. The rescue experiment confirmed that knockdown of DLEU1 repressed cell proliferation, migration and invasion while stimulated cell apoptosis via miR-320b/phosphoribosyl pyrophosphate synthetase 1 (PRPS1) axis. Meanwhile, the data of xenograft model exhibited that inhibition of DLEU1 suppressed tumor growth *in vivo*. In summary, DLEU1 knockdown may repress PRPS1 expression via miR-320b, and then repress cell proliferation, migration and invasion while stimulate cell apoptosis. Our research may provide a novel target for the treatment of CRC.

Keywords: colorectal cancer, lncRNA, DLEU1, miR-320b, PRPS1

INTRODUCTION

Colorectal cancer (CRC) is the third most common malignant tumor globally (1). In China, CRC has the fourth highest malignancies incidence and accounts for 9.2% of the total cancer death (2). Genetic variation and cellular environment are the main causes affecting tumor occurrence, development and metastasis (3). Despite the development of surgery, chemotherapy, radiotherapy and immunotherapy, the recurrence and metastasis rate is still high in 70% of

patients with stage 2 and 3 of CRC (4). However, the understanding of molecular mechanisms of proliferation, apoptosis, migration and invasion is extremely limited. A deep understanding of the invasion and development of CRC is critical to accelerate the development of its diagnosis and treatment.

Emerging evidences suggest that long non-coding RNAs (lncRNAs) are closely related to the development of human cancer and regulate several cell functions (5). A lot of lncRNAs have been found to inhibit or promote the development of CRC. For evidence, lncRNA ZNF667-AS1 and lncRNA XIST can suppress the invasion, development and migration of CRC (6, 7). Nevertheless, lncRNA SNHG16, LINC00460 and IncARSR may act essential roles in promoting the development of CRC (8–10).

The lncRNA deleted in lymphocytic leukemia 1 (DLEU1) located on chromosome 13q14.3 has been reported to be abnormally expressed in many cancers (11). DLEU1 is obviously overexpressed in breast cancer and accelerates migration, invasion of breast cancer cells (12). Besides, DLEU1 is also found to be highly expressed in osteosarcoma (13), glioblastoma multiforme (14) and hepatocellular carcinoma (15), and aggravates cancer progression.

Recent studies reported that lncRNAs play an important role in tumor occurrence and development by sponging miRNA to modulate the expression of protein-coding genes (16). DLEU1 accelerates cell proliferation and invasion in bladder cancer via miR-99b/HS3ST3B1 Axis (17). A study conducted by Liu et al. (18) found that through sponging miR-381 and elevating HOXA13 level in cervical cancer, DLEU1 stimulates cell proliferation and invasion. However, the significant role of DLEU1 in the development of CRC remains unclear.

In this study, we investigated the effect of DLEU1 on the development of CRC and established a competitive endogenous RNA (ceRNA) network, namely DLEU1/miR-320b/phosphoribose pyrophosphate synthase 1 (PRPS1) axis. This possible mechanism has been confirmed by bioinformatics and biological experiments. Our findings may provide a new diagnostic biomarker and a potential therapeutic target for CRC.

MATERIALS AND METHODS

Patients and Specimens

Tumor tissues and paired non-tumor tissues were obtained from CRC patients (n=30) by surgery. Patients received no chemotherapy or radiotherapy before surgery. All the participants signed informed consent form. All samples used in this study were approved by the Ethics Committee of Southeast University Affiliated Zhongda Hospital (No. 2017ZDKYSB165).

qRT-PCR

Total RNAs were obtained from tissues and cells using TRIzol (Applygen, Beijing, China). qRT-PCR was carried by employing Reverse Transcription Kit (Haigene, Harbin, China) for miR-320b and Kit (Haigene, Harbin, China) for DLEU1 and PRPS1. qRT-PCR was performed as previously described (19). The primers were listed in **Table 1**. U6 and β-actin acted as endogenous controls.

Cell Culture and Transfection

CRC cell lines (LoVo, SW620, HCT116 and SW480) and normal cells HIEC were obtained from Cobioer (Nanjing, China) and followed their instructions to culture at 37°C. Sh-LncRNA DLEU1 (sequence: CAACGGAAUGUAUCAAUGATT), sh-PRPS1 (sequence: GCAGCTCCCACCAGGACTTAT), sh-NC(sequence: TTCTCCGAACGTGTCACGT), miR-320b mimics (sequence: AAAAGCUGGGUUGAGAGGGCAA), NC mimics (sequence: UUCUCCGAACGUGUCACGUTT), miR-320b inhibitors(sequence: UUGCCCUCUCAACCCAGCUUUU) and NC inhibitors(sequence: CAGUACUUUUGUGUAGUACAA) were obtained from RIBOBIO (Guangzhou, China). Cell transfection was conducted following the instruction of Lipofectamine 2000 (Invitrogen, CA, USA). Stably DLEU1-knockdown cell lines were screened out as previously reported (20). In brief, oligonucleotide for small hairpin RNA (shRNA) targeting DLEU1 was synthesized and inserted into the shRNA vector pGPH1/Neo (GenePharma, Shanghai, China). The DLEU1 shRNA vector was transfected into LoVo and SW480 cells with Lipofectamine 3000 (Invitrogen, CA, USA) and selected for 4 weeks with neomycin (1000 μg/ml). Scrambled shRNA (sh-NC) was applied as control. After culturing for 48 h, cells were utilized for follow-up study.

CCK-8 Assay

Cell viability was assessed using CCK8 kit (MedChemExpress, Shanghai, China). Cells (3000/well) were cultured for 48 h in 96-well plates. Followed by incubating with 10 μL CCK8 for 3-4 h, the absorbance was assessed using GloMax<sp>® System (Promega, WI, USA) at 450 nm (21).

EdU Assay

The EdU Kit (Beyotime Biotechnology, Nanjing, China) was employed in this study. In brief, after incubation with 10 μM EdU for 2 h, Cells were incubated with 4% formaldehyde, followed by 0.3% Triton X-100 for 10 min. After that, cells were incubated for 30 min with Click Additive Solution in

TABLE 1 | Primer sequences for qRT-PCR.

Primer name	(5'-3') Primer sequences
miR-320b-Forward	5′-GATGCTGAAAAGCTGGGTTG-3'
miR-320b-Reverse	5′- TATGGTTGTTCTGCTCTCTGTCTC-3′
U6-Forward	5′- GCTTCGGCAGCACATATACTAAAAT-3′
U6-Reverse	5′- CGCTTCACGAATTTGCGTGTCAT-3′
DLEU1-Forward	5′- TGCATTTAAAACCGCCCTGC-3′
DLEU1-Reverse	5′- TTGAAGAAGGAGACCACGCC-3′
PRPS1-Forward	5′- GGAAATTGGTGAAAGTGTA-3′
PRPS1-Reverse	5′-CCACAAGCACCATGCGGTCC-3′
β-actin-Forward	5′- GACCTGACTGACTACCTCATGAAGAT-3′
β-actin-Reverse	5′- GTCACACTTCATGATGGAGTTGAAGG-3′

darkness. Finally, 1X Hoechst 33342 was employed for nucleus staining (22).

Western Blot

Cell lysates were isolated using cell lysis buffer (Cell Signaling Technology, Shanghai, China). The membranes were transferred and blocked at RT for 1 h, followed by primary antibodies incubation: rabbit anti-PCNA (1:1000, ab92552), anti-Ki-67 (1:5000, ab92742), anti-BAX (1:5000, ab32503), anti-Bcl-2 (1:1000, ab59348), anti-Cleaved-caspase3 (1:1000, ab49822), anti-Cleaved-caspase9 (1:1000, ab2324), anti-Cox-2 (1:1000, ab179800), anti-MMP-2 (1:5000, ab92536), anti-MMP-9 (1:10000, ab76003), anti-PRPS1 (1:3000, ab137577) and rabbit anti-β-actin (1:2000, ab8227), and then re-probed with immunoglobulin G (IgG) (1:2000, ab6721) antibody. The chemiluminescence kit (Millipore, Germany) was applied to evaluate the immune response zone and Image J software (ImageJ Software Inc., USA) was used to quantify the integrated density of each band. Antibodies mentioned before were supplied by Abcam (Cambridge, UK).

Flow Cytometry Assay

The apoptotic rate of CRC cancer cells was evaluated by Annexin V-FITC/PI Apoptosis Detection Kit (Yeasen, Shanghai, China) via flow cytometry. After cultured for 48 h, cells were harvested, following by staining with 10 μL of Annexin V-FITC and PI. Then cells were analyzed by flow cytometer (BD, New Jersey, USA) (23).

Wound Healing Assay

Cells were cultured in a six-well plate for 24 h. A total of 100 μL pipette tips were used for wounds scratched of each group. Wound was recorded at 0 or 48 h. The distance was assessed by ImageJ software (ImageJ Software Inc., MD, USA). Wound healing rate = (scratch width at 0 h - 48 h)/scratch width at 0 h × 100% (24).

Transwell Assay

The 24-well transwell chamber (CORNING, New York, USA) was employed for cell invasion following the manufacturer. CRC cells in medium without serum were added to the Matrigel-coated upper chamber. After culturing at 37°C for 24 h, non-invasive cells were eliminated. And invasive cells were counted with Phase-Contrast Microscope (Olympus, Tokyo, Japan). Migration assay was conducted in the same manner with upper chamber without Matrigel (25).

Subcellular Fractionation

The nuclear and cytoplasm fractions were separated with PARIS Kit (Life Technologies). RNAs in each fraction were extracted. The level of DLEU1 was examined using qRT-PCR. GAPDH and U6 acted as fractionation indicators (26).

Dual Luciferase Reporter Assay

To confirm that DLEU1 and PRPS1 were targets of miR-320b, LncRNA DLEU1-WT (containing the binding sites of miR-320b at DLEU1), LncRNA DLEU1-Mut (mutation of binding sites), PRPS1-WT (containing the binding sites of miR-320b at PRPS1 3'UTR) and PRPS1-MUT (mutation of binding sites) were cloned into Luciferase Reporter Vector (Invitrogen, CA, USA). LncRNA DLEU1-WT, LncRNA DLEU1-Mut, PFKL-WT or PFKL-MUT were co-transfected with miR-320b mimics into LoVo and SW480 cells. After 48-h transfection, LoVo and SW480 were explored using a Reporter Vector System (Invitrogen, CA, USA) using a Glomax20/20 luminometer (Promega, WI, USA) (27).

RNA Immunoprecipitation (RIP) Assay

Cells were lysed by RIP lysis buffer (Millipore, USA) and then incubated with magnetic beads conjugated with IgG (1:100, ab109489, Abcam, UK) or Ago2 (1:100, ab32381, Abcam, UK) antibody. Then RNA was purified and investigated using qRT-PCR (28).

Animal Study

All animal experiments were conducted with the approval of the Institutional Animal Care & Use Committee of China Pharmaceutical University (JN2018035). The nude mice were kept under specific pathogen-free conditions. Water and a basal diet were given ad libitum. Subcutaneously injected 100 μL cell suspension (1 × 107 cells/ml) of stably DLEU1-knockdown or control SW480 cells into the left hind leg of every mouse (n=3 per group). The tumor volume was determined every 5 days using the formula: 0.5 × length × width2. Twenty-five days after the injection, the mice were sacrificed. Tumors were separated and weighted at the same time (28).

Histology

Tumor tissues were embedded in paraffin, sectioned, dewaxed and rehydrated. Antigens retrieval was conducted using citrate (10 mmol/L, pH 6.0) solution at 100°C for 10 min, followed by immersing the section in 3% hydrogen peroxide for 10 min and incubating overnight with antibody Ki-67 (1:50, ab15580) at 4° C. Incubated the section with IgG (1:2000, ab205718) at room temperature for 2 h. Lastly, 3, 3′-diaminobenzidine tetrahydrochloride was used for visualization, and hematoxylin was used for counter-staining. The nuclei of the tumor cells were calculated by randomly counting 3 fields. The percentage of apoptotic bodies was calculated as: apoptotic/total nuclei × 100 (29).

Statistical Analysis

Data are shown as mean ± SD. SPSS 21.0 (IBM Corp., NY, USA) was applied for statistical analysis of all data. T-test was used for comparison between two groups, and one-way ANOVA and Tukey's post-tests were used for multiple groups. The level of significance was set at $P < 0.05$.

RESULTS

DLEU1 Is Highly Expressed in CRC Tissues and Cells

To evaluate the effect of DLEU1 in CRC, the level of DLEU1 in CRC was obtained from GEPIA. The expression profile

exhibited that DLEU1 level was observably increased in CRC tissues compared to non-tumor tissues (**Figure 1A**). In the meantime, the level of DLEU1 in CRC tissues was investigated by qRT-PCR, and our data indicated that DLEU1 level was upregulated with the development of CRC. As shown in **Figure 1B**, DLEU1 level was higher in stage III + IV than I + II. Moreover, the prognosis data demonstrated that the DLEU1 was positively related to the development of CRC patients (**Figure 1C**). Furthermore, the level of DLEU1 in CRC cell lines was investigated by qRT-PCR, which showed that DLEU1 level was higher in CRC cell lines than normal cells HIEC, CRC cell lines LoVo and SW480 were chosen for subsequent experiments (**Figure 1D**).

Knockdown of DLEU1 Inhibits Proliferation and Stimulates Apoptosis of CRC Cells

To further assess the effect of DLEU1 on CRC cell proliferation, sh-LncRNA DLEU1 was used in LoVo and SW480 cells to knock down DLEU1 stably. The qRT-PCR results confirmed that DLEU1 level was observably repressed by sh-LncRNA DLEU1 (**Figure 2A**). We conducted CCK-8 assay and observed that cell viability was diminished by sh-LncRNA DLEU1 (**Figure 2B**). In addition, the results of EdU assay indicated that cell proliferation was diminished by sh-LncRNA DLEU1 (**Figure 2C**). Moreover, proliferation-related protein levels were investigated by western blot. The data demonstrated that PCNA and Ki-67 were markedly suppressed by sh-LncRNA DLEU1 (**Figure 2D**).

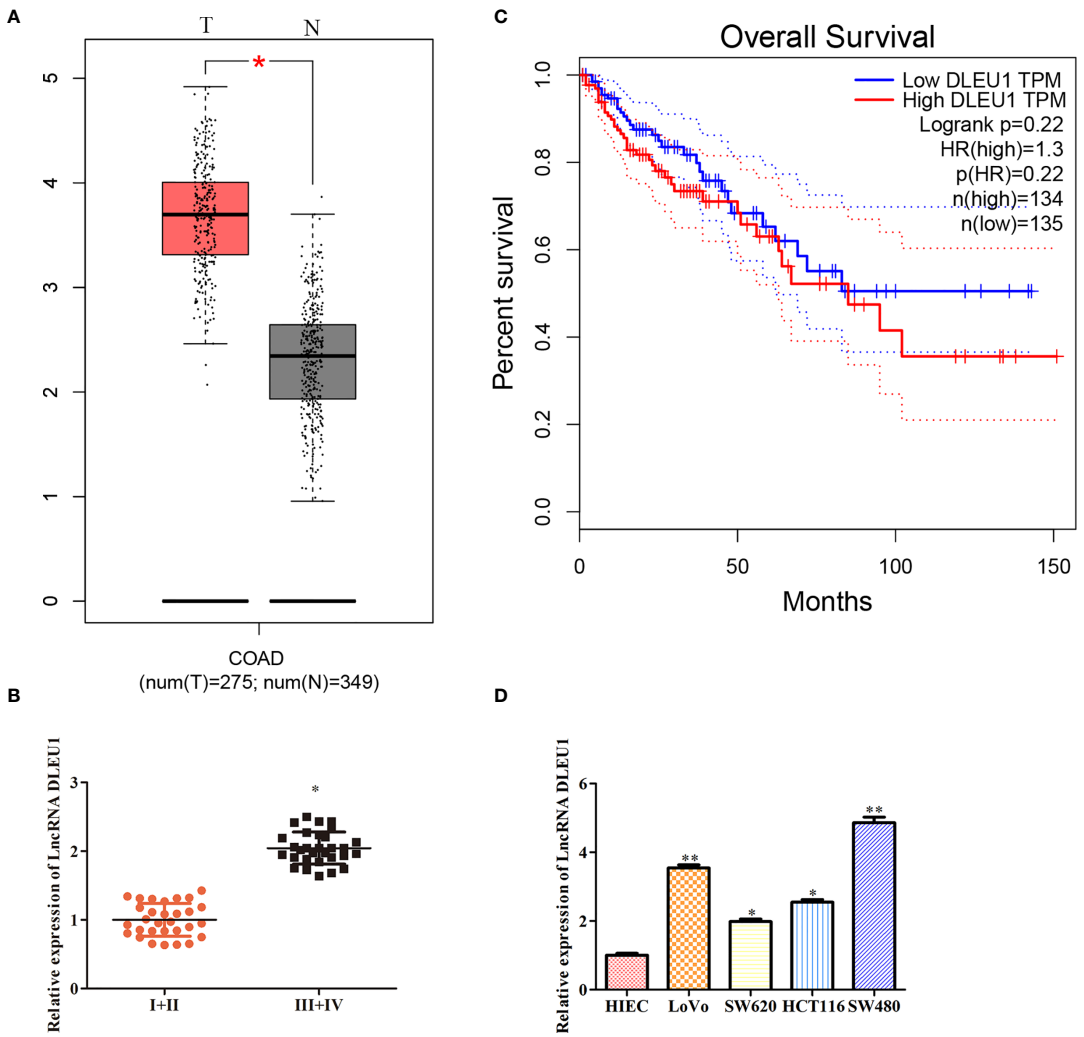

FIGURE 1 | DLEU1 is highly expressed in CRC tissues and cancer cells. **(A)** The expression profile of DLEU1 was obtained from GEPIA (http://gepia.cancer-pku.cn/index.html), *$P < 0.05$ *vs*. non-tumor tissues. **(B)** The relative expression of DLEU1 was determined by qRT-PCR in CRC tissues of different clinical stage, *$P < 0.05$ *vs*. stage I + II tissues. **(C)** Overall survival curves showed the association between the DLEU1 level and overall survival of CRC patients were obtained from GEPIA (http://gepia.cancer-pku.cn/index.html). **(D)** The relative expression of DLEU1 was determined by qRT-PCR in CRC cell lines, *$P < 0.05$, **$P < 0.01$ *vs*. normal intestinal epithelial cells HIEC.

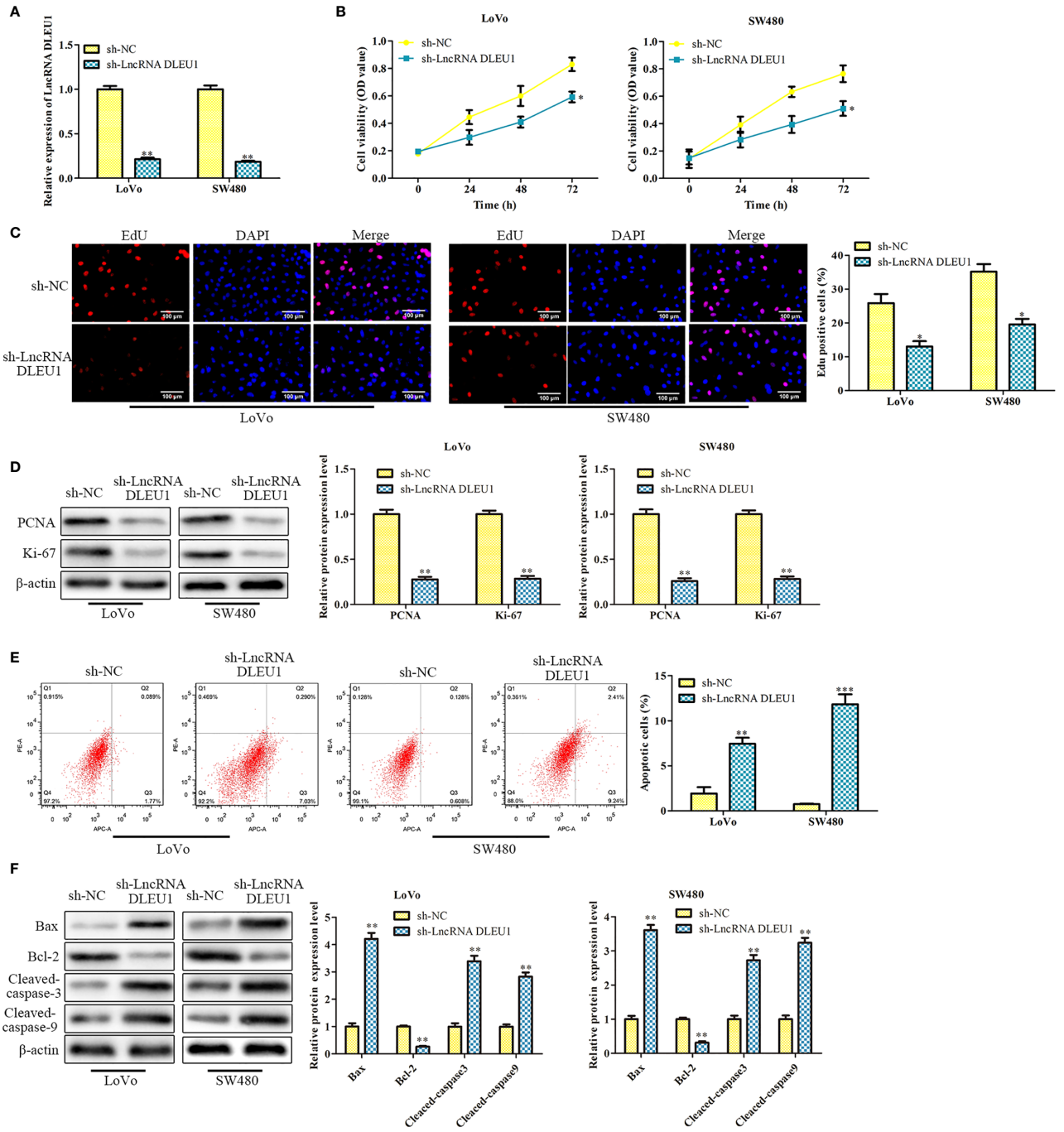

FIGURE 2 | Knockdown of DLEU1 inhibits proliferation and stimulates apoptosis of CRC cells. **(A)** The relative expression of DLEU1 was determined by qRT-PCR in LoVo and SW480 cells. **(B)** The cell viability was determined using CCK-8 assay in LoVo and SW480 cells. **(C)** The cell proliferation was determined using EdU assay in LoVo and SW480. **(D)** The proliferation-related protein levels of PCNA and Ki-67 were investigated by western blot in LoVo and SW480 cells. **(E)** The cell apoptosis was determined using low cytometry assay in LoVo and SW480 cells. **(F)** The apoptosis-related protein levels of Bcl-2, Bax, Cleaved-caspase3 and Cleaved-caspase9 were investigated by western blot in LoVo and SW480 cells. $^{*}P < 0.05$, $^{**}P < 0.01$, $^{***}P < 0.001$ *vs*. sh-NC.

In addition, the effect of DLEU1 on CRC cell apoptosis was assessed by flow cytometry. The cell apoptosis was markedly stimulated by sh-LncRNA DLEU1 (**Figure 2E**). Western blot was performed to evaluate the apoptosis-related protein levels, and we observed that Bcl-2 was suppressed, whereas Bax, Cleaved-caspase3 and 9 were remarkably promoted by sh-LncRNA

DLEU1 (**Figure 2F**). Taken together, inhibition of DLEU1 repressed CRC cell proliferation and stimulates apoptosis.

Knockdown of DLEU1 Represses Cell Migration and Invasion

After knockdown of DLEU1 using sh-LncRNA DLEU1 in LoVo and SW480 cells, wound-healing assay was performed to evaluate cell migration. The data indicated that cell migration was markedly suppressed by sh-LncRNA DLEU1 (**Figure 3A**).What's more, the finding of transwell assay suggested that cell invasion was suppressed by sh-LncRNA DLEU1 (**Figure 3B**). Moreover, invasion-related protein levels were investigated by western blot. The data demonstrated that Cox-2, MMP-2 and MMP-9 were markedly suppressed by sh-LncRNA DLEU1 (**Figure 3C**). Collectively, these results demonstrated that inhibition of DLEU1 repressed cell migration and invasion.

DLEU1 Interacts With miR-320b in CRC

After subcellular fractionation assay, the levels of DLEU1 in the nuclear and cytoplasm of both LoVo and SW480 cells were determined using qRT-PCR. The data indicated that DLEU1 was mainly in the cytoplasm (**Figure 4A**). Bioinformatics analysis indicated that DLEU1 interacted with miR-320b (**Figure 4B**), which was confirmed by dual luciferase reporter assay. As shown in **Figure 4C**, miR-320b mimics markedly repressed the luciferase activity of LncRNA DLEU1-WT in LoVo and SW480 cells, whereas it had no significant effect on the luciferase activity of LncRNA DLEU1-MUT.We conducted qRT-PCR analysis after DLEU1 knockdown in LoVo and SW480 cells and observed that miR-320b was promoted by sh-LncRNA DLEU1 (**Figure 4D**). Results of RIP assay indicated that both DLEU1 and miR-320b were enriched in Ago2 group (**Figure 4E**), which further demonstrated the interaction between DLEU1 and miR-320b.

Next, the expression of miR-320b in CRC tissues and cell lines was evaluated using qRT-PCR. The finding exhibited that miR-320b level was observably suppressed in CRC tissues and cell lines compared to non-tumor tissues and HIEC (**Figures 4F, G**). Pearson's correlation analysis results indicated that DLEU1 was negatively correlated with miR-320b in CRC tissues (**Figure 4H**).

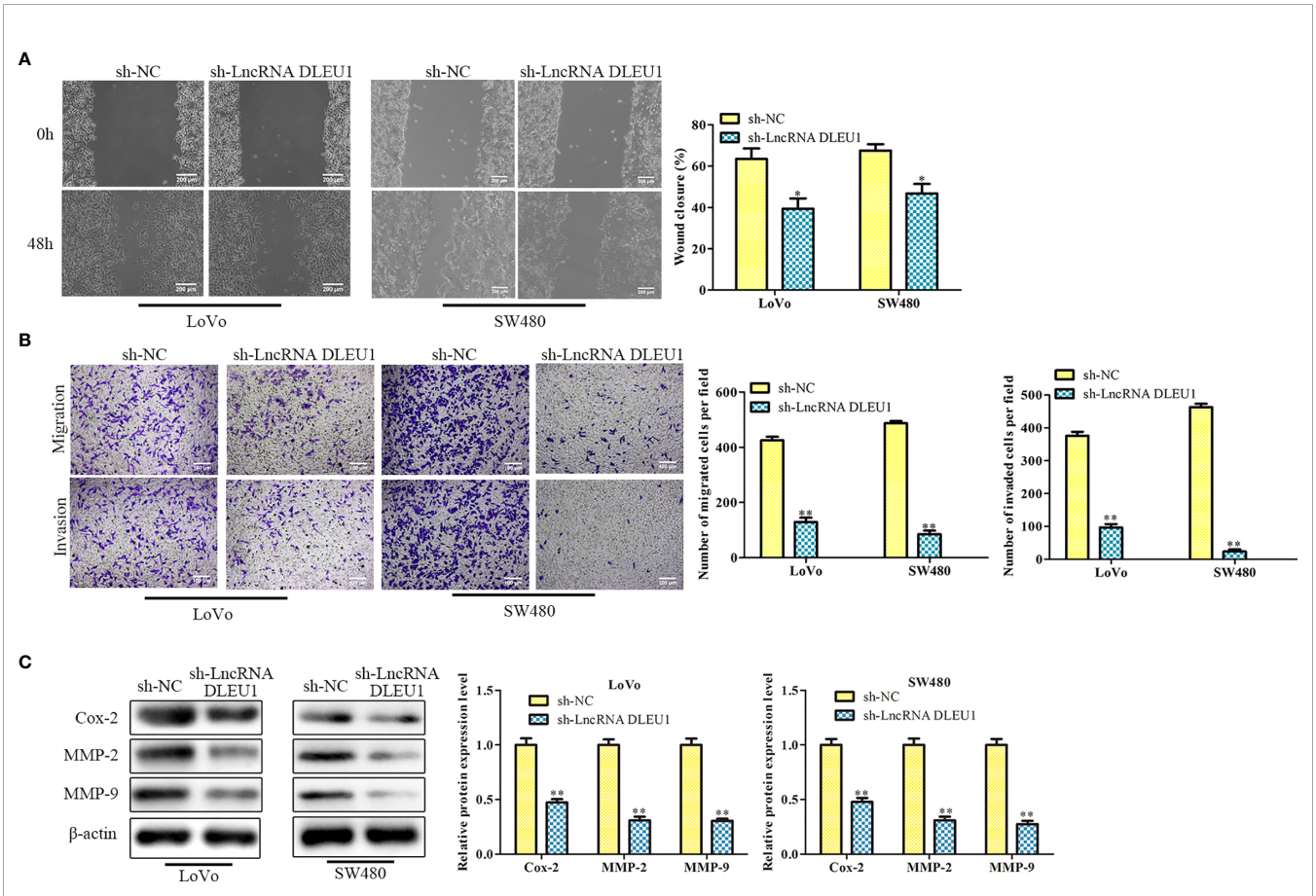

FIGURE 3 | Knockdown of DLEU1 represses cell migration and invasion. **(A)** The cell migration was determined by wound-healing assay in LoVo and SW480 cells. **(B)** The cell invasion was determined using transwell assay in LoVo and SW480 cells. **(C)** The invasion-related protein levels of Cox-2, MMP-2 and MMP-9 were investigated by western blot in LoVo and SW480 cells. *$P < 0.05$, **$P < 0.01$ *vs*. sh-NC.

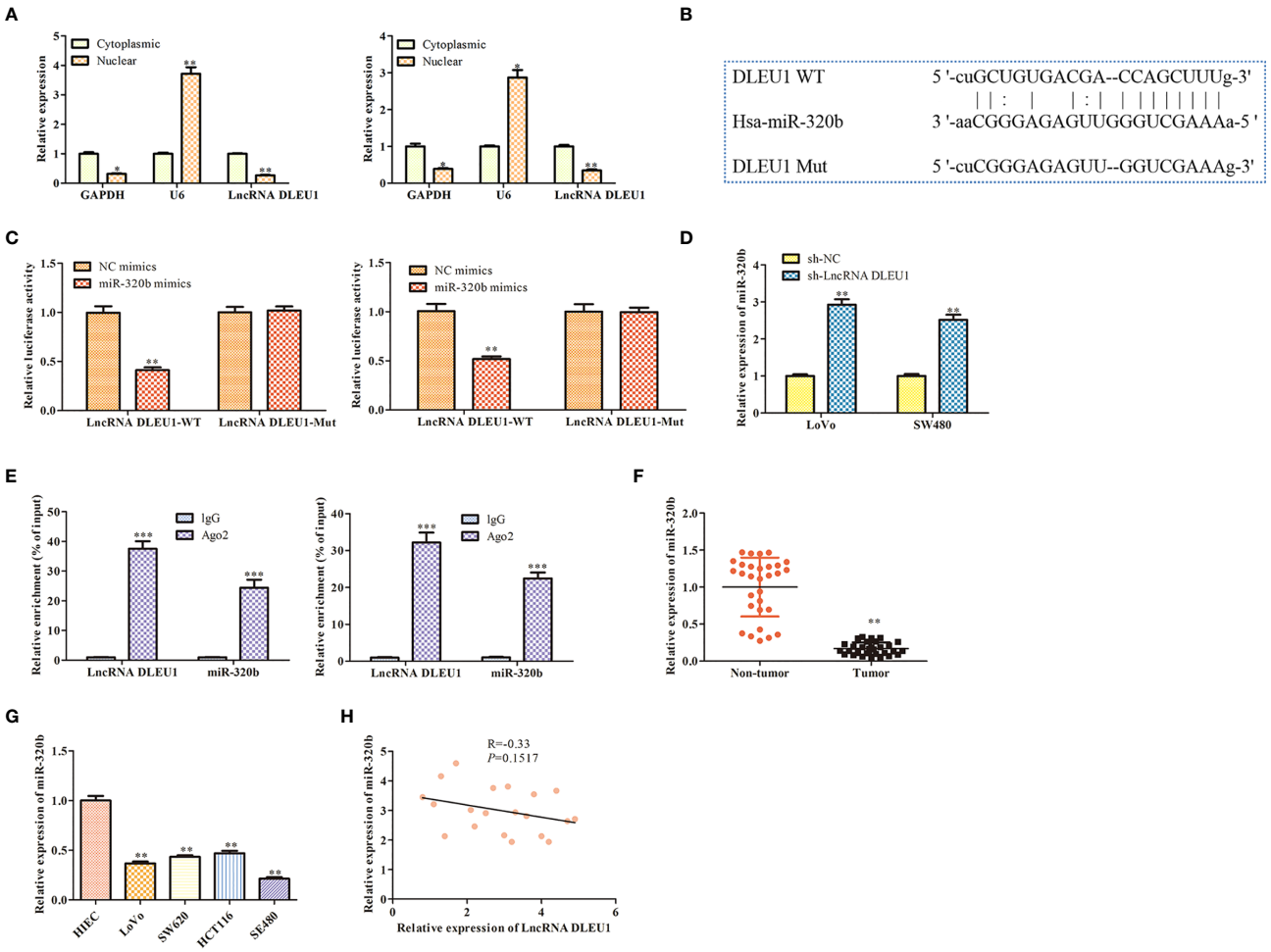

FIGURE 4 | DLEU1 interacts with miR-320b in CRC. **(A)** The levels of DLEU1 in the nuclear and cytoplasm of both LoVo and SW480 cells were determined using qRT-PCR after subcellular fractionation assay, $^{*}P < 0.05$, $^{**}P < 0.01$ *vs*. cytoplasmic. **(B)** DLEU1 interacted with miR-320b via bioinformatics analysis. **(C)** DLEU1 interacted with miR-320b using dual luciferase reporter assay, $^{**}P < 0.01$ *vs*. NC mimic. **(D)** The levels of miR-320b was determined using qRT-PCR, $^{**}P < 0.01$ *vs*. sh-NC. **(E)** Relative enrichment of DLEU1 and miR-320b in LoVo and SW480 cells was determined using RIP assay, $^{***}P < 0.001$ *vs*. IgG. **(F)** The relative expression of miR-320b was determined by qRT-PCR in non-tumor and CRC tissues, $^{**}P < 0.01$ *vs*. non-tumor tissues. **(G)** The relative expression of miR-320b was determined by qRT-PCR in CRC cell lines, $^{*}P < 0.05$, $^{**}P < 0.01$ *vs*. HIEC. **(H)** The correlation between DLEU1 and miR-320b was assessed using Pearson's correlation analysis.

MiR-320b Represses Proliferation and Promotes Apoptosis of CRC Cells

To further assess the effect of miR-320b on CRC cell proliferation, miR-320b mimics was used in LoVo and SW480 cells to upregulate miR-320b. The qRT-PCR results confirmed that miR-320b level was observably elevated by miR-320b mimics (**Figure 5A**). We conducted CCK-8 assay and observed that cell viability was diminished by miR-320b mimics (**Figure 5B**). The results of EdU assay indicated that cell proliferation was suppressed by miR-320b mimics (**Figure 5C**). What's more, we conducted flow cytometry assay and observed that cell apoptosis was markedly stimulated by miR-320b mimics (**Figure 5D**). Afterwards, we conducted transwell assay and observed that cell migration and invasion were suppressed by miR-320b mimics (**Figure 5E**). Taken together, miR-320b repressed CRC cell proliferation, migration and invasion, while stimulated apoptosis.

PRPS1 Is a Target Gene of miR-320b

Our bioinformatics analysis result confirmed that PRPS1 was a target gene of miR-320b (**Figure 6A**). Results of dual luciferase reporter assay indicated that miR-320b mimics markedly suppressed the luciferase activity of PRPS1 WT, whereas it had no significant effect when the putative binding sites were mutated (**Figure 6B**). Besides, qRT-PCR and western blot results indicated that both mRNA and protein level of PRPS1 were suppressed by miR-320b mimics. These results verified that PRPS1 was a target gene of miR-320b (**Figures 6C, D**). Next, the expression of PRPS1 in CRC tissues and cell lines was

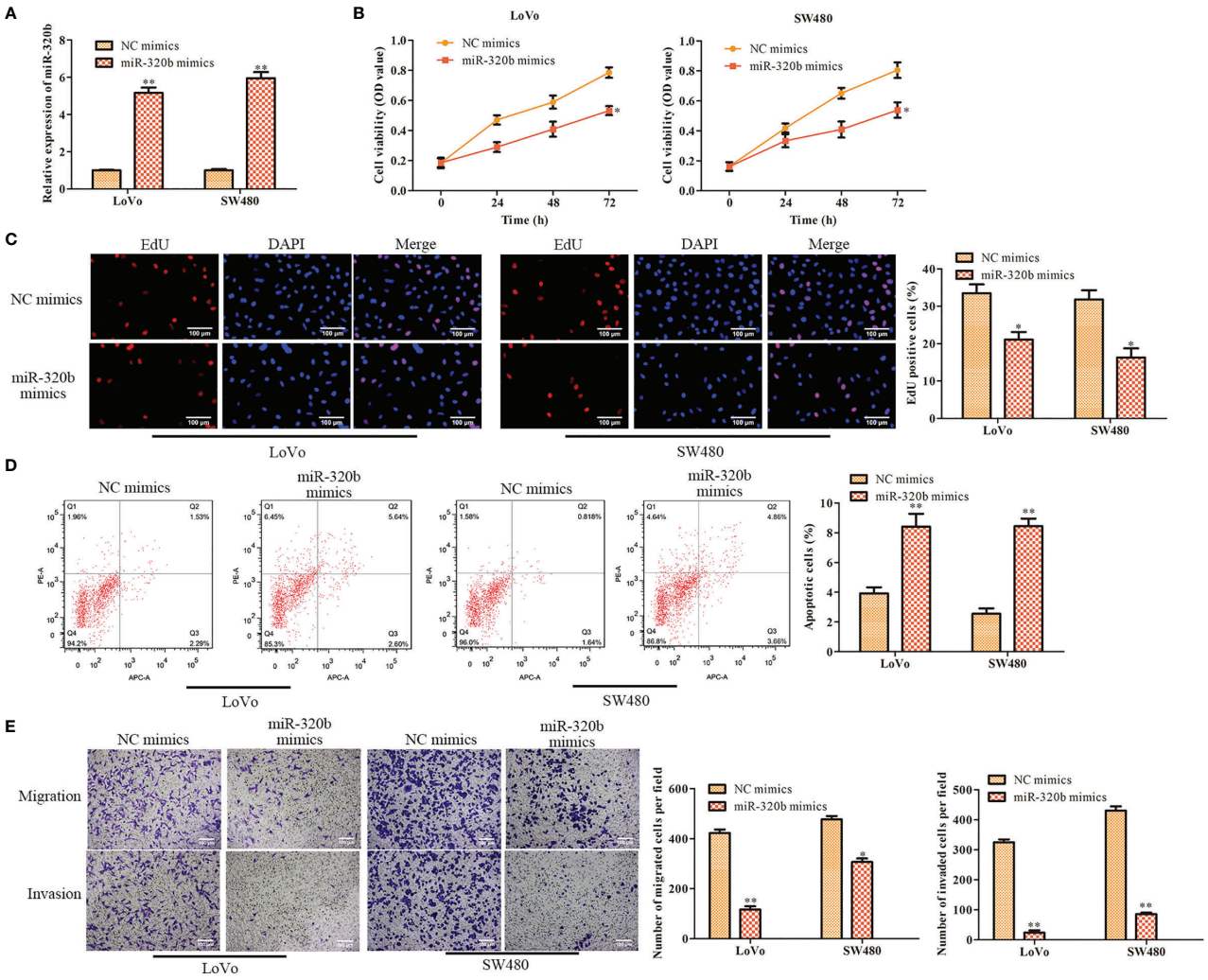

FIGURE 5 | MiR-320b represses proliferation and stimulates apoptosis of CRC cells. **(A)** The relative expression of miR-320b was determined by qRT-PCR in LoVo and SW480 cells. **(B)** The cell viability was determined using CCK-8 assay in LoVo and SW480 cells. **(C)** The cell proliferation was determined using EdU assay in LoVo and SW480. **(D)** The cell apoptosis was determined using flow cytometry assay in LoVo and SW480 cells. **(E)** The cell migration and invasion were determined using transwell assay in LoVo and SW480 cells. $^{*}P < 0.05$, $^{**}P < 0.01$ *vs*. NC mimics.

evaluated using qRT-PCR. The finding exhibited that PRPS1 level was observably elevated in CRC tissues and cell lines, compared to non-tumor tissues and HIEC (**Figures 6E, F**).

Knockdown of DLEU1 Represses Cell Proliferation, Migration and Invasion While Stimulates Cell Apoptosis *via* miR-320b/PRPS1 Axis

MiR-320b inhibitors was used in LoVo and SW480 cells in which DLEU1 was knocked down stably. qRT-PCR was carried out to detect miR-320b expression and the data exhibited that miR-320b was suppressed by miR-320b inhibitors (**Figure 7A**). In the meantime, sh-PRPS1 was used in LoVo and SW480 cells in which DLEU1 was knocked down stably. The data of qRT-PCR exhibited that PRPS1 was suppressed by sh-PRPS1 (**Figure 7A**).

In order to evaluate the functions of DLEU1/miR-320b/PRPS1 axis, we transfected both miR-320b inhibitors and sh-PRPS1 into LoVo and SW480 cells in which DLEU1 was knocked down stably, followed by CCK-8 and EdU assay. The data of CCK-8 and EdU assay exhibited that cell proliferation was stimulated by miR-320b inhibitors, which was attenuated by sh-PRPS1 (**Figures 7B, C**). The data of flow cytometry assay exhibited that cell apoptosis was suppressed by miR-320b inhibitors, which was reversed by sh-PRPS1 (**Figure 7D**). We conducted transwell assay and observed that cell migration and invasion were stimulated by miR-320b inhibitors, which were attenuated by sh-PRPS1 (**Figure 7E**). Taken together, knockdown of DLEU1 repressed cell proliferation, migration and invasion while stimulated cell apoptosis via miR-320b/PRPS1 axis.

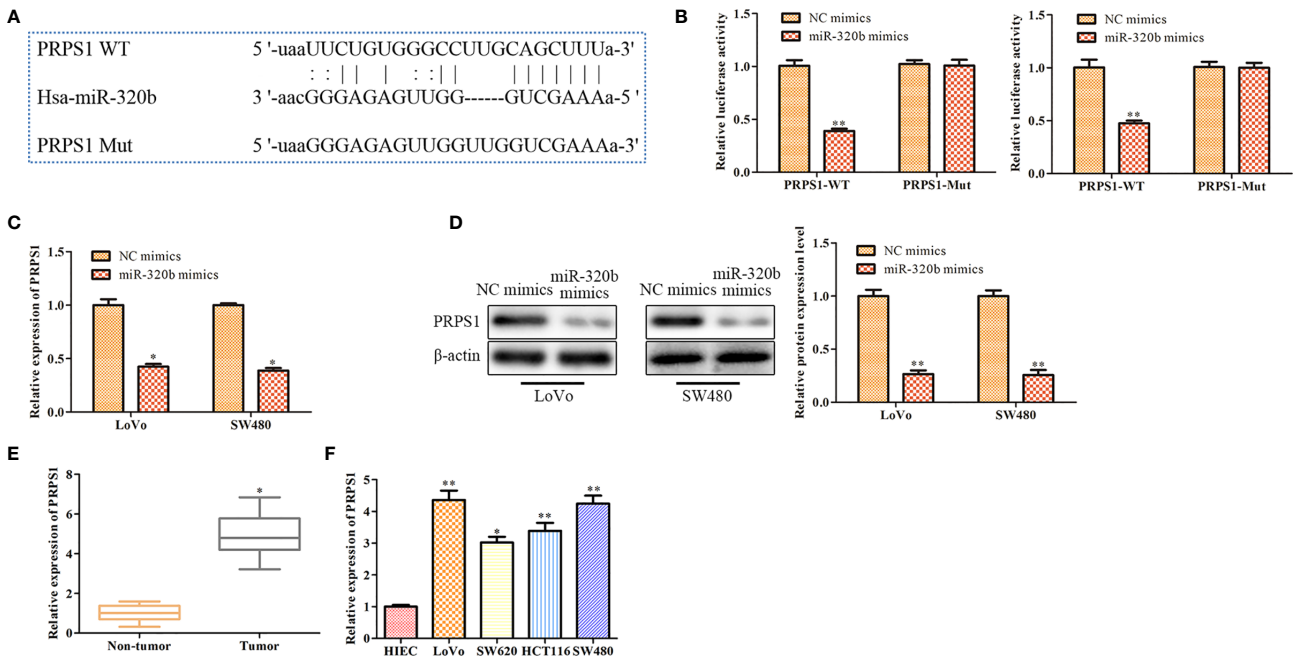

FIGURE 6 | PRPS1 is a target gene of miR-320b. **(A)** PRPS1 was predicted as a target of miR-320b via bioinformatics analysis. **(B)** miR-320b was bound to 3'UTR of PRPS1 using dual luciferase reporter assay, $^{**}P < 0.01$ *vs*. NC mimics. **(C)** The level of PRPS1 was determined by qRT-PCR, $^{*}P < 0.05$ *vs*. NC mimics. **(D)** The level of PRPS1 was determined by Western blot, $^{**}P < 0.01$ *vs*. NC mimics. **(E)** The relative expression of PRPS1 was determined by qRT-PCR in non-tumor and CRC tissues, $^{*}P < 0.05$ *vs*. non-tumor tissues. **(F)** The relative expression of PRPS1 was determined by qRT-PCR in CRC cell lines, $^{*}P < 0.05$, $^{**}P < 0.01$ *vs*. HIEC.

Inhibition of DLEU1 Suppresses Tumor Growth *In Vivo*

To evaluate the function of DLEU1 *in vivo*, a xenograft model of CRC was established by subcutaneous injection of stably DLEU1-knockdown SW480 cells. As shown in **Figures 8A–C**, DLEU1 inhibition markedly repressed tumour size, growth and weight compared to sh-NC group. HE staining was performed and the results revealed that cell necrosis was significantly elevated by sh-LncRNA DLEU1 (**Figure 8D**). IHC and TUNEL assay were carried out to assess the Ki-67 expression and cell apoptosis in tumor tissues, respectively. Our data revealed that Ki-67 positive cells was alleviated by sh-LncRNA DLEU1, whereas the percentage of apoptotic bodies was elevated by sh-LncRNA DLEU1 (**Figure 8D**). Lastly, the expression of DLEU1, miR-320b and PRPS1 were determined by qRT-PCR. The data revealed that the expression of DLEU1 and PRPS1 were repressed by sh-LncRNA DLEU1, whereas miR-320b was stimulated by sh-LncRNA DLEU1 (**Figure 8E**). The above results confirmed that inhibition of DLEU1 suppressed tumor growth *in vivo*.

DISCUSSION

Globally, CRC is the third major reason of death caused by cancer (30). Cancer development and metastasis are the major reasons of CRC death, peculiarly for patients in advanced stage (31). Tumor metastasis was often characterized by accelerated invasion and migration. It's vital to clarify the underlying mechanisms of CRC development.

In recent years, studies have shown that lncRNA DLEU1 is involved in the development of CRC. In the absence of a comprehensive molecular mechanism, no targeted therapeutic drugs have been developed to date. DLEU1 acts as an oncogene in various types of cancers. A study conducted by Zhang et al (32) reveals that DLEU1 plays a tumorigenic role in non-small cell lung cancer. Similarly, DLEU1 is found to stimulate endometrial cancer development (33). Moreover, carcinogenic effect of DLEU1 is found in gastric cancer (34). In this study, our data demonstrated that DLEU1 was highly expressed in CRC tissues and cell lines. We also revealed that knockdown of DLEU1 repressed proliferation, migration and invasion while stimulated apoptosis of CRC cells. These results were consistent with the previous study conducted by Liu et al. (20).

DLEU1 has been reported to interact with miRNAs to regulate gene expression in various cancers. For examples, DLEU1 accelerates the development of pancreatic ductal adenocarcinoma carcinogenesis through the miR-381/CXCR4 axis (35). While in endometrial cancer, DLEU1 regulates SP1 expression *via* sponging miR-490 and aggravates the cancer development (36). In addition, DLEU1 aggravates the progression of ovarian cancer through interacting with miR-490-3p to modulate CDK1 expression (37). To further verify the regulatory mechanism of DLEU1 in CRC, an interaction between

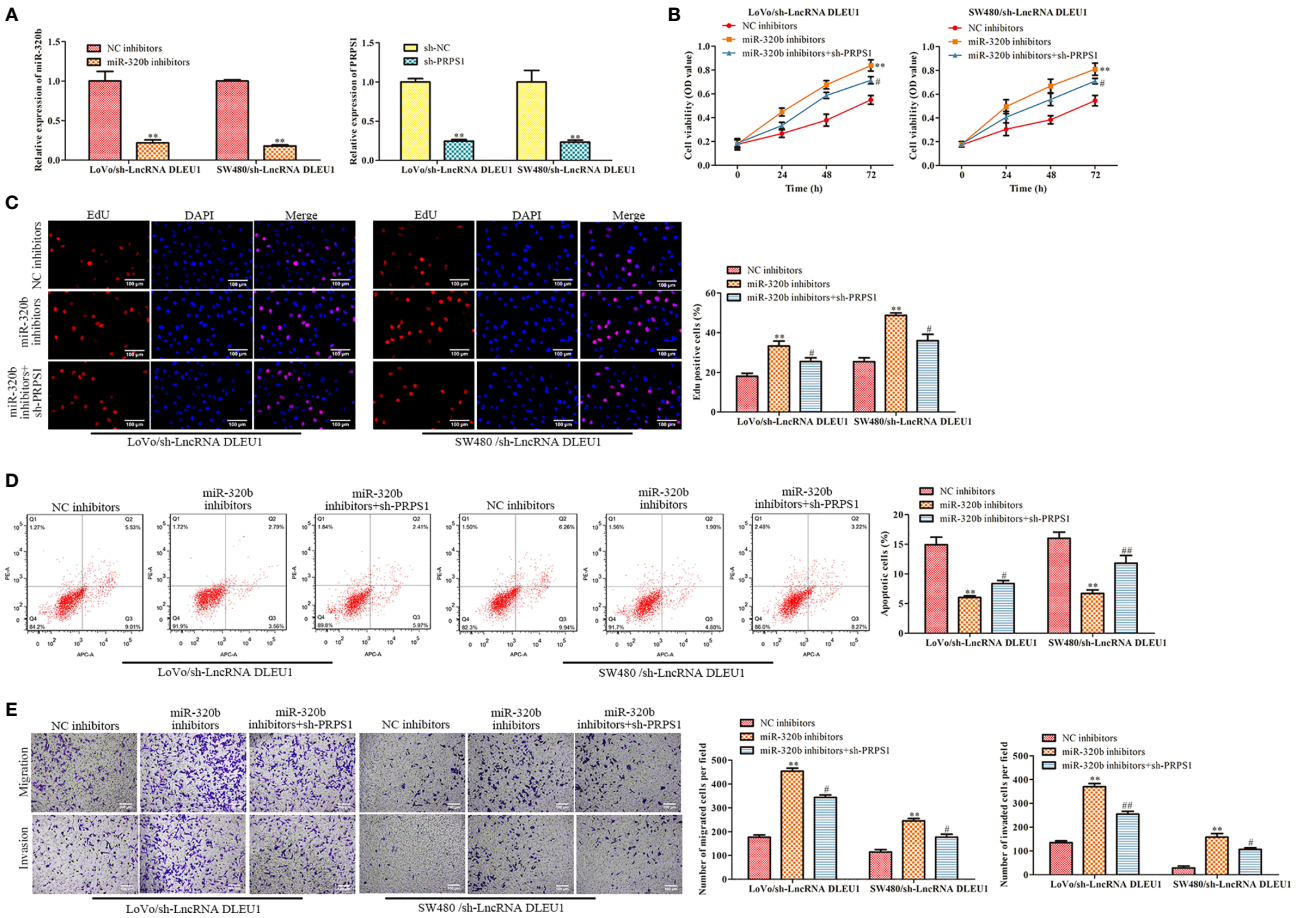

FIGURE 7 | Knockdown of DLEU1 represses cell proliferation, migration and invasion while stimulates cell apoptosis *via* miR-320b/PRPS1 axis. **(A)** The relative expression of miR-320b and PRPS1 were determined by qRT-PCR in LoVo and SW480 cells, $^{**}P < 0.01$ *vs*. NC inhibitors or sh-NC. **(B)** The cell viability was determined using CCK-8 assay in LoVo and SW480 cells, $^{**}P < 0.01$ *vs*. NC inhibitors, $^{\#}P < 0.05$ *vs*. miR-320b inhibitors. **(C)** The cell proliferation was determined using EdU assay in LoVo and SW480, $^{**}P < 0.01$ *vs*. NC inhibitors, $^{\#}P < 0.05$ *vs*. miR-320b inhibitors. **(D)** The cell apoptosis was determined using flow cytometry assay in LoVo and SW480 cells, $^{**}P < 0.01$ *vs*. NC inhibitors, $^{\#}P < 0.05$, $^{\#\#}P < 0.01$ *vs*. miR-320b inhibitors. **(E)** The cell migration and invasion were determined using transwell assay in LoVo and SW480 cells, $^{**}P < 0.01$ *vs*. NC inhibitors, $^{\#}P < 0.05$, $^{\#\#}P < 0.01$ *vs*. miR-320b inhibitors.

DLEU1 and miR-320b was revealed, and that interaction was confirmed by dual luciferase reporter assay and RIP assay in this study.

In plenty of studies, miRNAs, like miR-140 (38), miR-211-5p (39) and miR-29a (40), have been verified to repress proliferation, migration and invasion of tumor cells. As a member of the miR-320 family, miR-320b is found to serve as a tumor suppressor in various cancers (41). A study conducted by Lv et al. (42) reveals that upregulation of miR-320b markedly enhances cell apoptosis and suppresses cell proliferation, migration and invasion in glioma. Besides, through targeting c-Myc, miR-320b attenuates cell proliferation in CRC cells (43). This study exhibited that miR-320b level was observably suppressed in CRC tissues and cell lines. *In vitro* functional studies revealed that miR-320b repressed cell proliferation and stimulated cell apoptosis.

The further mechanism research showed that PRPS1 was a target gene of miR-320b, and its level was observably elevated in CRC tissues and cell lines. PRPS1 is a key enzyme to producing the consensus precursor of nucleotide synthesis (44). Abnormally elevated level of PRPS1 is closely associated with poor prognosis in neuroblastoma, whereas suppression of PRPS1 alleviates cell proliferation and tumor growth (45). Moreover, silence of PRPS1 diminishes cell viability and promotes cell apoptosis in human breast cancer cells (46).

CONCLUSION

In summary, our findings elucidated that DLEU1 and PRPS1 were elevated while miR-320b was alleviated in CRC tissues and cell lines. Knockdown of DLEU1 repressed cell proliferation,

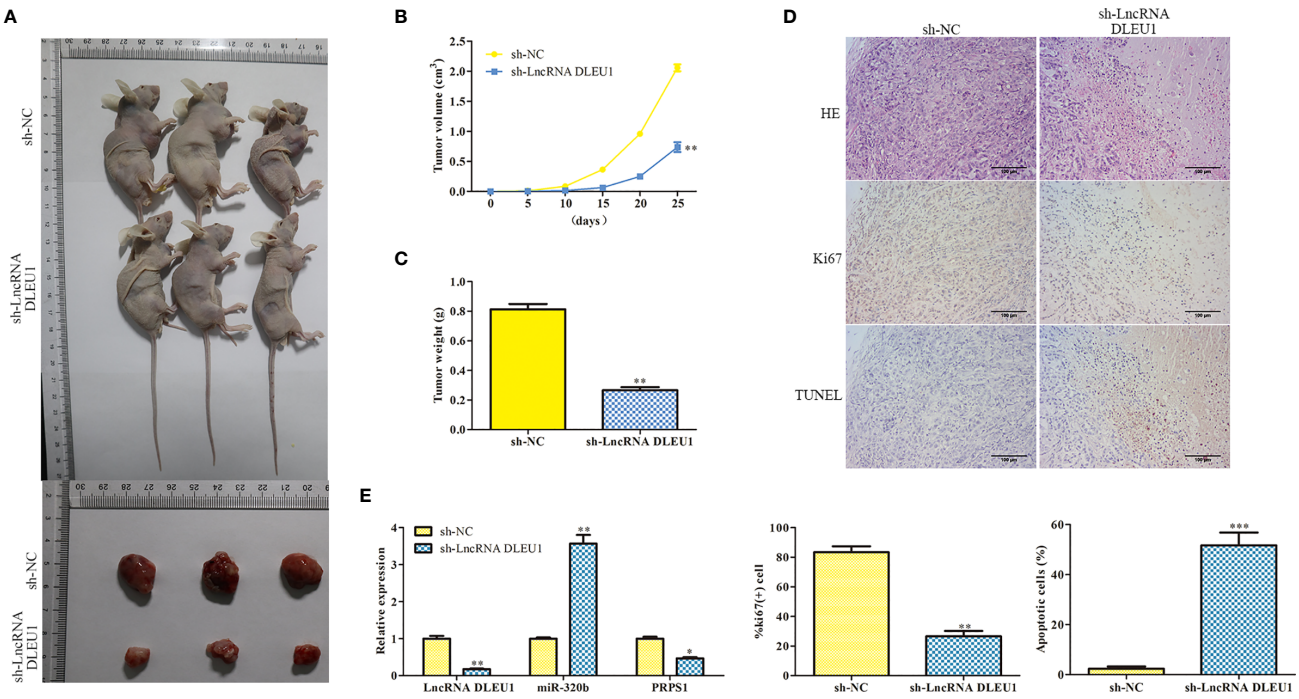

FIGURE 8 | Inhibition of DLEU1 suppresses tumor growth *in vivo*. **(A)** Representative images of xenograft tumors. **(B)** Tumor growth curve. **(C)** Tumor weight. **(D)** Cell necrosis, the Ki-67 expression and cell apoptosis were determined using HE, IHC and TUNEL assay, respectively. **(E)** The expression of DLEU1, miR-320b and PRPS1 were determined by qRT-PCR. $^{*}P < 0.05$, $^{**}P < 0.01$, $^{***}P < 0.001$ *vs*. sh-NC.

migration and invasion while stimulated cell apoptosis via miR-320b/PRPS1 axis. Therefore, the DLEU1/miR-320b/PRPS1 axis served as a potential mechanism for CRC development, and our finding provides an exploitable therapeutic target for CRC.

DATA AVAILABILITY STATEMENT

The raw data supporting the conclusions of this article will be made available by the authors, without undue reservation.

ETHICS STATEMENT

The studies involving human participants were reviewed and approved by The Ethics Committee of Southeast University Affiliated Zhongda Hospital. The patients/participants provided their written informed consent to participate in this study. The animal study was reviewed and approved by China Pharmaceutical University.

AUTHOR CONTRIBUTIONS

DX and HY conceived the project and designed the experiments. DX performed the study, analyzed the data, and wrote the paper. YF, WJ, JW, WM, and XD performed the study. DX and YF analyzed the data. HY analyzed the data and critically revised the manuscript. All authors contributed to the article and approved the submitted version.

FUNDING

This study was supported in part by grants from the Health and Family Planning Commission of Jiangsu Province (#H201409, Z2020069), the Health and Family Planning Commission of Nanjing, Jiangsu Province (#YKK16231).

REFERENCES

1. Arnold M, Sierra MS, Laversanne M, Soerjomataram I, Jemal ABray F. Global Patterns and Trends in Colorectal Cancer Incidence and Mortality. *Gut* (2017) 66:683–91. doi: 10.1136/gutjnl-2015-310912
2. Gu MJ, Huang QC, Bao CZ, Li YJ, Li XQ, Ye D, et al. Attributable Causes of Colorectal Cancer in China. *BMC Cancer* (2018) 18:38. doi: 10.1186/s12885-017-3968-z
3. Aran V, Victorino AP, Thuler LCFerreira CG. Colorectal Cancer: Epidemiology, Disease Mechanisms and Interventions to Reduce Onset and

Mortality. *Clin Colorectal Cancer* (2016) 15:195–203. doi: 10.1016/j.clcc.2016.02.008
4. Stewart Coats AJ, Ho GF, Prabhash K, von Haehling S, Tilson J, Brown R, et al. Espindolol for the Treatment and Prevention of Cachexia in Patients With Stage III/IV non-Small Cell Lung Cancer or Colorectal Cancer: A Randomized, Double-Blind, Placebo-Controlled, International Multicentre Phase II Study (the ACT-ONE Trial). *J Cachexia Sarcopenia Muscle* (2016) 7:355–65. doi: 10.1002/jcsm.12126
5. Zhang Z, Yang W, Li N, Chen X, Ma F, Yang J, et al. LncRNA MCF2L-AS1 Aggravates Proliferation, Invasion and Glycolysis of Colorectal Cancer Cells Via the Crosstalk With miR-874-3p/FOXM1 Signaling Axis. *Carcinogenesis* (2021) 42:263–71. doi: 10.1093/carcin/bgaa093
6. Zhuang L, Ding W, Ding W, Zhang Q, Xu X, Xi D. LncRNA ZNF667-AS1 (Nr_036521.1) Inhibits the Progression of Colorectal Cancer Via Regulating ANK2/JAK2 Expression. *J Cell Physiol* (2021) 236:2178–93. doi: 10.1002/jcp.30004
7. Li W, He Y, Cheng Z. Long Noncoding RNA XIST Knockdown Suppresses the Growth of Colorectal Cancer Cells Via Regulating microRNA-338-3p/PAX5 Axis. *Eur J Cancer Prev* (2021) 30:132–42. doi: 10.1097/CEJ.0000000000000596
8. Chen ZY, Wang XY, Yang YM, Wu MH, Yang L, Jiang DT, et al. LncRNA SNHG16 Promotes Colorectal Cancer Cell Proliferation, Migration, and Epithelial-Mesenchymal Transition Through Mir-124-3p/MCP-1. *Gene Ther* (2020) 13:7555–69. doi: 10.1038/s41434-020-0176-2
9. Wang L, Chen X, Sun X, Suo J. Long Noncoding RNA LINC00460 Facilitates Colorectal Cancer Progression by Negatively Regulating Mir-613. *Onco Targets Ther* (2020) 13:7555–69. doi: 10.2147/OTT.S254489
10. Li S, Zhu K, Liu L, Gu J, Niu H, Guo J. lncARSR Sponges miR-34a-5p to Promote Colorectal Cancer Invasion and Metastasis Via hexokinase-1-mediated Glycolysis. *Cancer Sci* (2020) 111:3938–52. doi: 10.1111/cas.14617
11. Garding A, Bhattacharya N, Claus R, Ruppel M, Tschuch C, Filarsky K, et al. Epigenetic Upregulation of LncRNAs At 13q14.3 in Leukemia is Linked to the In Cis Downregulation of a Gene Cluster That Targets NF-Kb. *PloS Genet* (2013) 9:e1003373. doi: 10.1371/journal.pgen.1003373
12. Wang C, Xie XX, Li WJ, Jiang DQ. LncRNA DLEU1/microRNA-300/RAB22A Axis Regulates Migration and Invasion of Breast Cancer Cells. *Eur Rev Med Pharmacol Sci* (2019) 23:10410–21. doi: 10.26355/eurrev_201912_19680
13. Chen X, Zhang C, Wang X. Long Noncoding RNA DLEU1 Aggravates Osteosarcoma Carcinogenesis Via Regulating the miR-671-5p/DDX5 Axis. *Artif cells Nanomed Biotechnol* (2019) 47:3322–8. doi: 10.1080/21691401.2019.1648285
14. Wang J, Quan X, Peng DHu G. Long non–Coding RNA DLEU1 Promotes Cell Proliferation of Glioblastoma Multiforme. *Mol Med Rep* (2019) 20:1873–82. doi: 10.3892/mmr.2019.10428
15. Zhang W, Liu S, Liu K, Liu Y. Long non-Coding RNA Deleted in Lymphocytic Leukaemia 1 Promotes Hepatocellular Carcinoma Progression by Sponging miR-133a to Regulate IGF-1R Expression. *J Cell Mol Med* (2019) 23:5154–64. doi: 10.1111/jcmm.14384
16. Liu B, Liu Y, Zhou M, Yao S, Bian Z, Liu D, et al. Comprehensive ceRNA Network Analysis and Experimental Studies Identify an IGF2-AS/miR-150/IGF2 Regulatory Axis in Colorectal Cancer. *Pathol Res Pract* (2020) 216:153104. doi: 10.1016/j.prp.2020.153104
17. Li Y, Shi B, Dong F, Zhu X, Liu B, Liu Y. Long Non-coding RNA DLEU1 Promotes Cell Proliferation, Invasion, and Confers Cisplatin Resistance in Bladder Cancer by Regulating the miR-99b/HS3ST3B1 Axis. *Front Genet* (2019) 10:280. doi: 10.3389/fgene.2019.00280
18. Liu C, Tian X, Zhang J, Jiang L. Long Non-coding RNA DLEU1 Promotes Proliferation and Invasion by Interacting With miR-381 and Enhancing Hoxa13 Expression in Cervical Cancer. *Front Genet* (2018) 9:629. doi: 10.3389/fgene.2018.00629
19. Zhao TF, Jia HZ, Zhang ZZ, Zhao XS, Zou YF, Zhang W, et al. LncRNA H19 Regulates ID2 Expression Through Competitive Binding to hsa-miR-19a/b in Acute Myelocytic Leukemia. *Mol Med Rep* (2017) 16:3687–93. doi: 10.3892/mmr.2017.7029
20. Liu T, Han Z, Li H, Zhu Y, Sun Z, Zhu A. LncRNA DLEU1 Contributes to Colorectal Cancer Progression Via Activation of KPNA3. *Mol Cancer* (2018) 17:118. doi: 10.1186/s12943-018-0873-2
21. Chen C, Liu WR, Zhang B, Zhang LM, Li CG, Liu C, et al. LncRNA H19 Downregulation Confers Erlotinib Resistance Through Upregulation of PKM2 and Phosphorylation of AKT in EGFR-mutant Lung Cancers. *Cancer Lett* (2020) 486:58–70. doi: 10.1016/j.canlet.2020.05.009
22. Liu C, Jiang YH, Zhao ZL, Wu HW, Zhang L, Yang Z, et al. Knockdown of Histone Methyltransferase WHSC1 Induces Apoptosis and Inhibits Cell Proliferation and Tumorigenesis in Salivary Adenoid Cystic Carcinoma. *Anticancer Res* (2019) 39:2729–37. doi: 10.21873/anticanres.13399
23. Wang X, Gao X, Tian J, Zhang R, Qiao Y, Hua X, et al. LINC00261 Inhibits Progression of Pancreatic Cancer by Down-Regulating Mir-23a-3p. *Arch Biochem Biophys* (2020) 689:108469. doi: 10.1016/j.abb.2020.108469
24. Cui LH, Xu HR, Yang W, Yu LJ. LncRNA PCAT6 Promotes non-Small Cell Lung Cancer Cell Proliferation, Migration and Invasion Through Regulating Mir-330-5p. *OncoTargets Ther* (2018) 11:7715–24. doi: 10.2147/ott.s178597
25. Wu W, Guo L, Liang Z, Liu Y, Yao Z. Lnc-SNHG16/miR-128 Axis Modulates Malignant Phenotype Through WNT/β-Catenin Pathway in Cervical Cancer Cells. *J Cancer* (2020) 11:2201–12. doi: 10.7150/jca.40319
26. Zhang L, Niu H, Ma J, Yuan BY, Chen YH, Zhuang Y, et al. The Molecular Mechanism of LncRNA34a-mediated Regulation of Bone Metastasis in Hepatocellular Carcinoma. *Mol Cancer* (2019) 18:120. doi: 10.1186/s12943-019-1044-9
27. Zhang RL, Aimudula A, Dai JH, Bao YX. RASA1 Inhibits the Progression of Renal Cell Carcinoma by Decreasing the Expression of miR-223-3p and Promoting the Expression of FBXW7. *Biosci Rep* (2020) 40:1–12. doi: 10.1042/bsr20194143
28. Li Z, Wu X, Gu L, Shen Q, Luo W, Deng C, et al. Long non-Coding RNA ATB Promotes Malignancy of Esophageal Squamous Cell Carcinoma by Regulating miR-200b/Kindlin-2 Axis. *Cell Death Dis* (2017) 8:e2888. doi: 10.1038/cddis.2017.245
29. Li Y, Chen F, Chen J, Chan S, He Y, Liu W, et al. Disulfiram/Copper Induces Antitumor Activity Against Both Nasopharyngeal Cancer Cells and Cancer-Associated Fibroblasts Through ROS/MAPK and Ferroptosis Pathways. *Cancers* (2020) 12:1–20. doi: 10.3390/cancers12010138
30. Torre LA, Bray F, Siegel RL, Ferlay J, Lortet-Tieulent J, Jemal A. Global Cancer Statistics, 2012. *CA: Cancer J Clin* (2015) 65:87–108. doi: 10.3322/caac.21262
31. Tomida C, Aibara K, Yamagishi N, Yano C, Nagano H, Abe T, et al. The Malignant Progression Effects of Regorafenib in Human Colon Cancer Cells. *J Med Invest JMI* (2015) 62:195–8. doi: 10.2152/jmi.62.195
32. Zhang S, Guan Y, Liu X, Ju M, Zhang Q. Long non-Coding RNA DLEU1 Exerts an Oncogenic Function in non-Small Cell Lung Cancer. *Biomed Pharmacother = Biomed Pharmacother* (2019) 109:985–90. doi: 10.1016/j.biopha.2018.10.175
33. Du Y, Wang L, Chen S, Liu Y, Zhao Y. LncRNA DLEU1 Contributes to Tumorigenesis and Development of Endometrial Carcinoma by Targeting Mtor. *Mol Carcinog* (2018) 57:1191–200. doi: 10.1002/mc.22835
34. Li X, Li Z, Liu Z, Xiao J, Yu S, Song Y. Long non-Coding RNA DLEU1 Predicts Poor Prognosis of Gastric Cancer and Contributes to Cell Proliferation by Epigenetically Suppressing KLF2. *Cancer Gene Ther* (2018) 25:58–67. doi: 10.1038/s41417-017-0007-9
35. Gao S, Cai Y, Zhang H, Hu F, Hou L, Xu Q. Long Noncoding RNA DLEU1 Aggravates Pancreatic Ductal Adenocarcinoma Carcinogenesis Via the miR-381/CXCR4 Axis. *J Cell Physiol* (2019) 234:6746–57. doi: 10.1002/jcp.27421
36. Shao W, Li Y, Chen F, Jia H, Jia J, Fu Y. Long non-Coding RNA DLEU1 Contributes to the Development of Endometrial Cancer by Sponging miR-490 to Regulate SP1 Expression. *Die Pharmazie* (2018) 73:379–85. doi: 10.1691/ph.2018.8352
37. Wang LL, Sun KX, Wu DD, Xiu YL, Chen X, Chen S, et al. DLEU1 Contributes to Ovarian Carcinoma Tumourigenesis and Development by Interacting With miR-490-3p and Altering CDK1 Expression. *J Cell Mol Med* (2017) 21:3055–65. doi: 10.1111/jcmm.13217
38. Yang S, Li X, Shen W, Hu H, Li C, Han G. Mir-140 Represses Esophageal Cancer Progression Via Targeting ZEB2 to Regulate Wnt/β-Catenin Pathway. *J Surg Res* (2020) 257:267–77. doi: 10.1016/j.jss.2020.07.074
39. Qin X, Zhang J, Lin Y, Sun XM, Zhang JN, Cheng ZQ. Identification of MiR-211-5p as a Tumor Suppressor by Targeting ACSL4 in Hepatocellular Carcinoma. *J Trans Med* (2020) 18:326. doi: 10.1186/s12967-020-02494-7
40. Liu YB, Wang Y, Zhang MD, Yue W, Sun CN. MicroRNA-29a Functions as a Tumor Suppressor Through Targeting STAT3 in Laryngeal Squamous Cell Carcinoma. *Exp Mol Pathol* (2020) 116:104521. doi: 10.1016/j.yexmp.2020.104521
41. Tadano T, Kakuta Y, Hamada S, Shimodaira Y, Kuroha M, Kawakami Y, et al. MicroRNA-320 Family is Downregulated in Colorectal Adenoma and Affects

Tumor Proliferation by Targeting CDK6. *World J Gastrointest Oncol* (2016) 8:532–42. doi: 10.4251/wjgo.v8.i7.532
42. Lv QL, Du H, Liu YL, Huang YT, Wang GH, Zhang X, et al. Low Expression of microRNA-320b Correlates With Tumorigenesis and Unfavorable Prognosis in Glioma. *Oncol Rep* (2017) 38:959–66. doi: 10.3892/or.2017.5762
43. Wang H, Cao F, Li X, Miao H, E J, Xing J, et al. miR-320b Suppresses Cell Proliferation by Targeting c-Myc in Human Colorectal Cancer Cells. *BMC Cancer* (2015) 15:748. doi: 10.1186/s12885-015-1728-5
44. Jing X, Wang XJ, Zhang T, Zhu W, Fang Y, Wu H, et al. Cell-Cycle-Dependent Phosphorylation of PRPS1 Fuels Nucleotide Synthesis and Promotes Tumorigenesis. *Cancer Res* (2019) 79:4650–64. doi: 10.1158/0008-5472.can-18-2486
45. Li J, Ye J, Zhu S, Cui H. Down-Regulation of Phosphoribosyl Pyrophosphate Synthetase 1 Inhibits Neuroblastoma Cell Proliferation. *Cells* (2019) 8:1–19. doi: 10.3390/cells8090955
46. He M, Chao L, You YP. PRPS1 Silencing Reverses Cisplatin Resistance in Human Breast Cancer Cells. *Biochem Cell Biol = Biochim Biol Cell* (2017) 95:385–93. doi: 10.1139/bcb-2016-0106

Conflict of Interest: The authors declare that the research was conducted in the absence of any commercial or financial relationships that could be construed as a potential conflict of interest.

frontiers in Oncology

ORIGINAL RESEARCH
published: 10 June 2021
doi: 10.3389/fonc.2021.681579

Competing Endogenous RNA in Colorectal Cancer: An Analysis for Colon, Rectum, and Rectosigmoid Junction

Lucas Maciel Vieira[1,2*], *Natasha Andressa Nogueira Jorge*[2], *João Batista de Sousa*[3], *João Carlos Setubal*[4], *Peter F. Stadler*[2,5,6,7,8] *and Maria Emília Machado Telles Walter*[1]

[1] Departamento de Ciência da Computação, Instituto de Ciência Exatas, University of Brasília, Brasília, Brazil, [2] Bioinformatics Group, Department of Computer Science, and Interdisciplinary Center for Bioinformatics, Leipzig, Germany, [3] Division of Coloproctology, Department of Surgery, University of Brasília School of Medicine, Brasília, Brazil, [4] Department of Biochemistry, Institute of Chemistry, University of São Paulo, São Paulo, Brazil, [5] Max Planck Institute for Mathematics in the Science, Leipzig, Germany, [6] Institute for Theoretical Chemistry, University of Vienna, Wien, Austria, [7] Facultad de Ciencias, Universidad National de Colombia, Sede Bogotá, Colombia, [8] Santa Fe Institute, Santa Fe, CA, United States

OPEN ACCESS

Edited by:
Peti Thuwajit,
Mahidol University, Thailand

Reviewed by:
Nicolò Musso,
University of Catania, Italy
Ali M. Ardekani,
Avicenna Research Institute (ARI), Iran

***Correspondence:**
Lucas Maciel Vieira
lucas.maciel.vieira@gmail.com

Specialty section:
This article was submitted to Molecular and Cellular Oncology, a section of the journal Frontiers in Oncology

Received: *16 March 2021*
Accepted: *22 April 2021*
Published: *10 June 2021*

Citation:
Vieira LM, Jorge NAN, de Sousa JB, Setubal JC, Stadler PF and Walter MEMT (2021) Competing Endogenous RNA in Colorectal Cancer: An Analysis for Colon, Rectum, and Rectosigmoid Junction. Front. Oncol. 11:681579. doi: 10.3389/fonc.2021.681579

Background: Colorectal cancer (CRC) is a heterogeneous cancer. Its treatment depends on its anatomical site and distinguishes between colon, rectum, and rectosigmoid junction cancer. This study aimed to identify diagnostic and prognostic biomarkers using networks of CRC-associated transcripts that can be built based on competing endogenous RNAs (ceRNA).

Methods: RNA expression and clinical information data of patients with colon, rectum, and rectosigmoid junction cancer were obtained from The Cancer Genome Atlas (TCGA). The RNA expression profiles were assessed through bioinformatics analysis, and a ceRNA was constructed for each CRC site. A functional enrichment analysis was performed to assess the functional roles of the ceRNA networks in the prognosis of colon, rectum, and rectosigmoid junction cancer. Finally, to verify the ceRNA impact on prognosis, an overall survival analysis was performed.

Results: The study identified various CRC site-specific prognosis biomarkers: hsa-miR-1271-5p, *NRG1*, hsa-miR-130a-3p, *SNHG16*, and hsa-miR-495-3p in the colon; *E2F8* in the rectum and *DMD* and hsa-miR-130b-3p in the rectosigmoid junction. We also identified different biological pathways that highlight differences in CRC behavior at different anatomical sites, thus reinforcing the importance of correctly identifying the tumor site.

Conclusions: Several potential prognostic markers for colon, rectum, and rectosigmoid junction cancer were found. CeRNA networks could provide better understanding of the differences between, and common factors in, prognosis of colon, rectum, and rectosigmoid junction cancer.

Keywords: colorectal cancer, competing endogenous RNA, TCGA, long non-coding RNA, miRNA, mRNA

INTRODUCTION

Colorectal cancer (CRC) is one of the most common and lethal cancers in the world (1). The most common histopathological type of CRC is adenocarcinoma (2). CRC can be classified according to its three major affected sites: colon, rectum, and rectosigmoid junction. Together these make up the large bowel. The colon corresponds to the largest portion, the rectum is located at the end, and the rectosigmoid junction is the transition between colon sigmoid and rectum. A tumor site is classified as belonging to the rectosigmoid junction when differentiation between rectum and sigmoid is not possible (3). CRC tumor site identification is important, due to different treatment strategies: for the colon, radical resection, depending on the stage, combined with chemotherapy is used; for rectum, only radical surgery or neoadjuvant chemorradiation followed or not by radical resection (4); while for the rectosigmoid junction, the best treatment still remains unknown (5). Because erroneous diagnosis of the CRC site can lead to overtreatment with chemotherapy, the identification of the CRC tumor site is a process that should be carefully analyzed, especially in the rectosigmoid junction (4). Better understanding of the biological characteristics of CRC at each site may provide insight into its development and progression.

Many studies have highlighted the importance of long non-coding RNAs (lncRNAs) in understanding the biological mechanisms of CRC and other types of cancer. LncRNAs are molecules greater than 200 nucleotides that do not encode for proteins and act mainly as transcriptional regulators by interacting with other molecules, such as miRNAs and mRNAs (6). These interaction mechanisms between lncRNAs and other molecules are explained by the competing endogenous RNA (ceRNA) hypothesis, which describes the interactions and their influence on altered protein expression levels (7). CeRNA network analyses have reported differentially expressed lncRNAs involved in breast, gastric, and many other types of cancer (8–10). Specifically for CRC, many studies also analyzed the ceRNAs networks and indicated potential diagnosis and prognosis biomarkers for colon, rectal, and colorectal cancer in general (1, 11–16). Most of these studies investigated the ceRNAs of CRC without differentiating the anatomical sites; however, different CRC sites present unique characteristics and treatment responses. Therefore, the identification of exclusive biomarkers for colon, rectum, or rectosigmoid junction could aid in understanding differences in the disease prognosis and progress. To the best of our knowledge, our study is the first to establish specific ceRNA networks for (i) colon; (ii) rectum; and (iii) rectosigmoid junction, and to associate them with specific biological mechanisms in order to clarify the differences and common factors between these sites.

In this study, we analyzed the functional and prognostic roles of lncRNAs, miRNAs, and mRNAs in colon, rectum, and rectosigmoid junction cancer, based on specific ceRNA networks constructed by using data from The Cancer Genome Atlas (TCGA) rectal adenocarcinoma (READ) and colon adenocarcinoma (COAD) projects.

MATERIALS AND METHODS

Data

The RNA expression value raw count and clinical information data of patients with colon, rectum, and rectosigmoid junction CRC sites were downloaded from TCGA (17). The selection criteria was: (1) open access to information; (2) sample types from primary tumor or solid normal tissue; (3) patients with adenocarcinomas.

Analysis of Differentially Expressed RNAs

We used the GDCRNATools v1.6 (18) R package and implemented the limma (19) method to obtain differentially expressed (DE) lncRNAs, miRNAs, and protein coding genes (*PCGs*) for cancer and normal tissue. The expression profiles were normalized by the voom method implemented in the GDCRNATools. The RNAs presenting FDR ≤ 0.05 and $|\log FC| \geq 2$ were considered statistically significant.

CeRNA Network Construction

The ceRNA networks, for each CRC site, were constructed using the GDCRNATools v1.6 package of R, and the DE lncRNAs, miRNAs, and mRNAs. The network is based on the mRNA-miRNA-lncRNA interactions predicted by the spongeScan (20) algorithm and the starBase v2.0 (21) database. In the ceRNA networks, positively correlated mRNAs and lncRNAs act as sponges by sharing a significant number of miRNA binding sites and suppressing their functioning. The ceRNA networks generated show the possible molecule interactions related to each CRC site.

Functional Analysis

The functional analysis to assess the biological processes in the ceRNAs was done with the enrichment module of GDCRNATools. The gene list used for Gene Ontology (GO) (22), Kyoto Encyclopedia of Genes and Genomes (KEGG) (23), and Disease Ontology (DO) (24) came from the org.Hs.eg.db database v3.11.4, and all the human pathways from KEGG were considered. The adjusted p-value ≤ 0.05 was set as the threshold for statistical significance for GO, KEGG, and DO. Although some pathways present FDR > 0.05, they were still included as they represent good discussion points for the CRC functional analysis.

Survival Analysis

The Cox Proportional-Hazards (CoxPH) model from GDCRNATools was used to calculate the hazard ratio (HR) of the ceRNA molecules. An outlier removal was performed and only molecules with $|\text{higherLimit} - \text{HR}| \leq 6$ and $|\text{lowerLimit} - \text{HR}| \leq 6$ were considered. The survival curve was constructed by using the Kaplan Meier (KM) analysis from GDCRNATools. CoxPH and KM were used $p < 0.05$ as the threshold for statistical significance.

RESULTS

Differentially Expressed RNAs

We obtained a total RNA expression raw count of 541 cancer and 48 non-tumor samples from 539 patients with CRC from the

TCGA-COAD and TCGA-READ projects. A differential expression analysis was performed for each type of CRC. In the colon analysis, we found 140 upregulated and 75 downregulated lncRNAs, 213 upregulated and 136 downregulated miRNAs, and 1,179 upregulated and 1,906 downregulated *PCGs* (**Figure 1A**). In the rectum, we found 46 upregulated and 37 downregulated lncRNAs, 119 upregulated and 99 downregulated miRNAs, and 535 upregulated and 1,532 downregulated *PCGs* (**Figure 1B**). In the rectosigmoid junction, we found 149 upregulated and 59 downregulated lncRNAs, 181 upregulated and 108 downregulated miRNAs, and 1,005 upregulated and 1,880 downregulated *PCGs* (**Figure 1C**).

CeRNA Networks

A ceRNA network, represented by a graph with its vertex (nodes) representing the molecules and the lines connecting them representing the interactions between the molecules, was established for each of the CRC sites. For colon, a ceRNA network consisting of 239 nodes and 506 interactions was established. For rectum, a ceRNA network consisting of 79 nodes and 136 interactions was established. For rectosigmoid junction, a ceRNA network consisting of 131 nodes and 210 interactions was established. We also analyzed the intersection between the ceRNA networks and found that: colon and rectum share 2 nodes and 2 interactions; colon and rectosigmoid junction share 48 nodes and 77 interactions; rectum and rectosigmoid junction share 12 nodes and 23 interactions; and all three sites share 47 nodes and 76 interactions. Furthermore, we performed an analysis to find individual nodes and interactions for each CRC site, finding that: colon has 142 nodes and 351 unique interactions; rectum has 18 nodes and 35 unique interactions; and rectosigmoid junction has 24 nodes and 34 unique interactions. **Figure 2** shows all the described networks.

The intersection between each of the three site-specific ceRNA networks is regulated by the lncRNAs: *MAGI2-AS3*, *HAGLR-AS3*, *SNHG1*, and *SNHG15* (**Figure 3**). *HAGLR-AS3*, *SNHG1*, and *SNHG15* compose three different small ceRNA networks by sponging hsa-miR-125a-3p, hsa-miR-377-3p, and hsa-miR-24-3p, respectively. In the *MAGI2-AS3* network, we see the ceRNA mechanism affecting a great number of *PCGs via* hsa-miR-374b-5p and hsa-miR-374a-5p, suggesting that this lncRNA has a great impact on the main CRC mechanism, which occurs at all sites.

Functional and Survival Analysis

A functional enrichment analysis was performed with GO, KEGG, and DO, to indicate the potential biological roles of the ceRNAs, lncRNAs, and *PCGs* (**Figure 4**). Each of the sites presented a different main functional characteristic: colon pathways are mainly related to endothelial differentiation; rectum pathways are mainly related to apoptosis; and rectosigmoid junction pathways are mainly related to signal transduction.

To better understand the impact of ceRNA networks, we also performed a functional enrichment analysis for the *MAGI2-HAGLR-AS3-SNHG1-SNHG15* intersection ceRNA network (**Figure 3**), and for each site-specific ceRNA network. The molecules present in the ceRNA network common in all CRC sites are mainly related to cell morphogenesis pathways (**Figure 5A**), such as regulation of Wnt signaling and cell morphogenesis and the process of insulin resistance. In the colon-specific (**Figure 5B**) ceRNA network, the most significant pathways are involved in tissue differentiation and

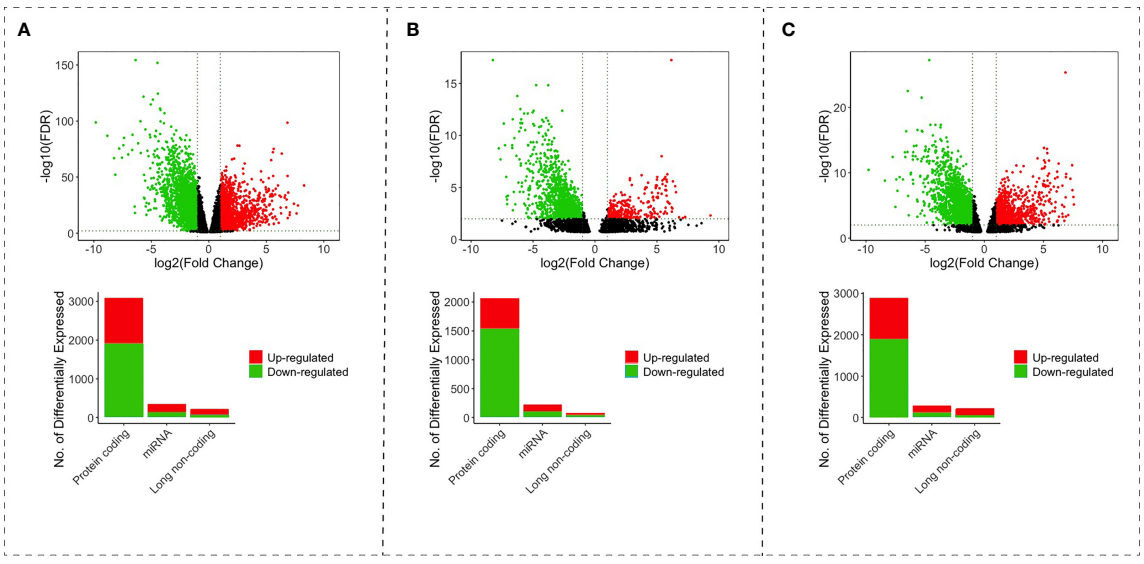

FIGURE 1 | Volcano and bar plot with differentially expressed lncRNAs, miRNAs and mRNAs of colon **(A)**, rectum **(B)**, and rectosigmoid junction **(C)** sites. The red points and bars represent upregulated RNAs. The green points and bars represent downregulated RNAs.

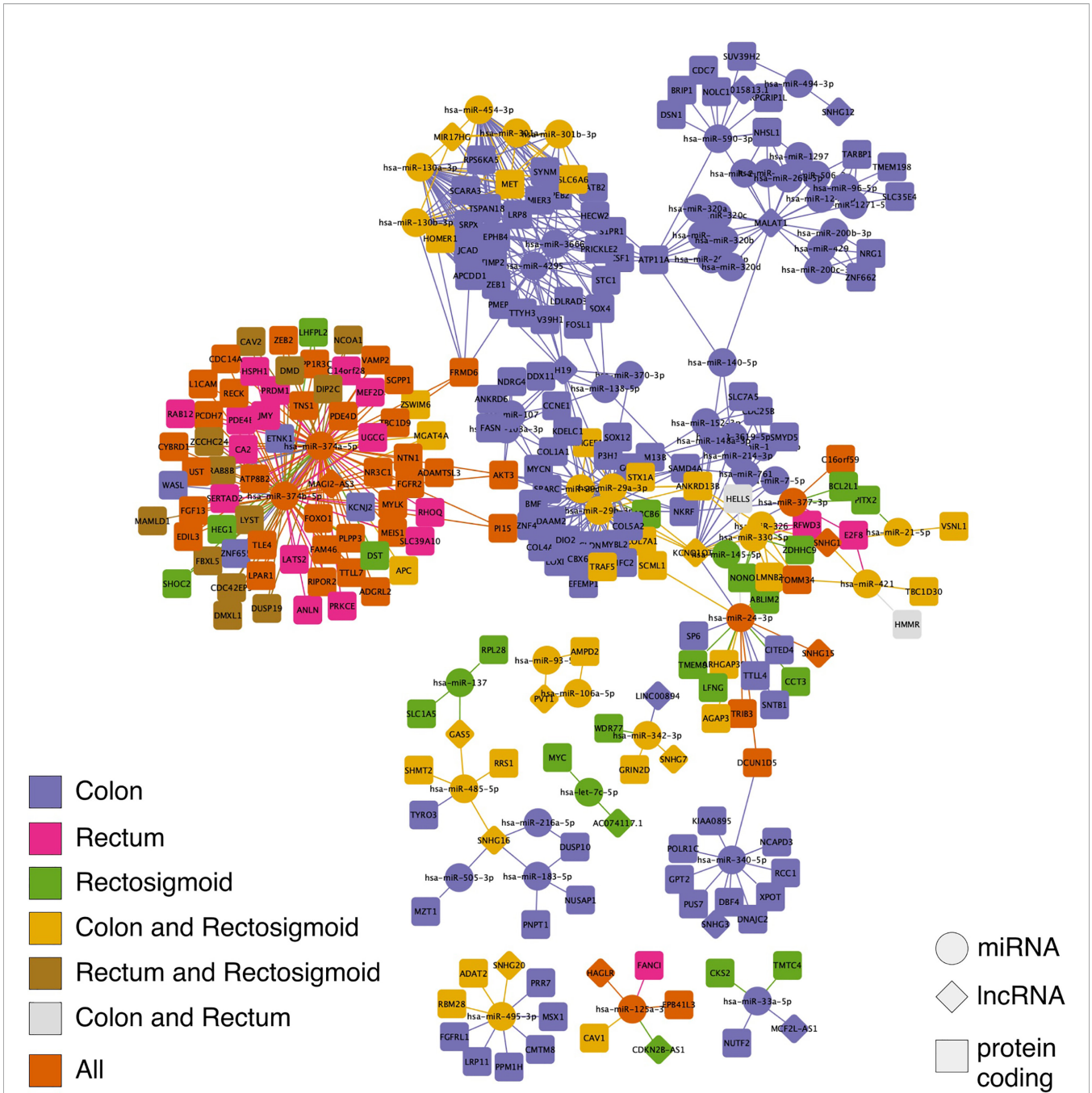

FIGURE 2 | Competing endogenous RNA (ceRNA) network in colon, rectum and rectosigmoid junction sites. The diamonds represent lncRNAs, the circles represent miRNAs, and the squares represent *PCGs*. The molecules and interactions of each CRC site can be identified by color.

development, such as endothelial cell differentiation and connective tissue development, while the rectum-specific (**Figure 5C**) ceRNA network is related to cell differentiation. No pathways were significant for the rectosigmoid junction site (**Figure 5D**).

Clinical data from CRC patients was used to obtain the HR and to build the overall survival time curve. For each CRC site, we had data from 391 colon, 84 rectum, and 66 rectosigmoid junction patients. Using CoxPH, we identified 20 molecules from the previous ceRNA networks with relevant HR, being 14 in colon, 3 in rectum, and 4 in rectosigmoid junction molecules (**Figure 6**). The *DMD* gene was the only molecule with high HR, present in more than one CRC site.

Clinical data and the expression profile of the HR relevant genes were used for overall survival analysis. These analyses were divided into two sets: the molecules with lowest pValue

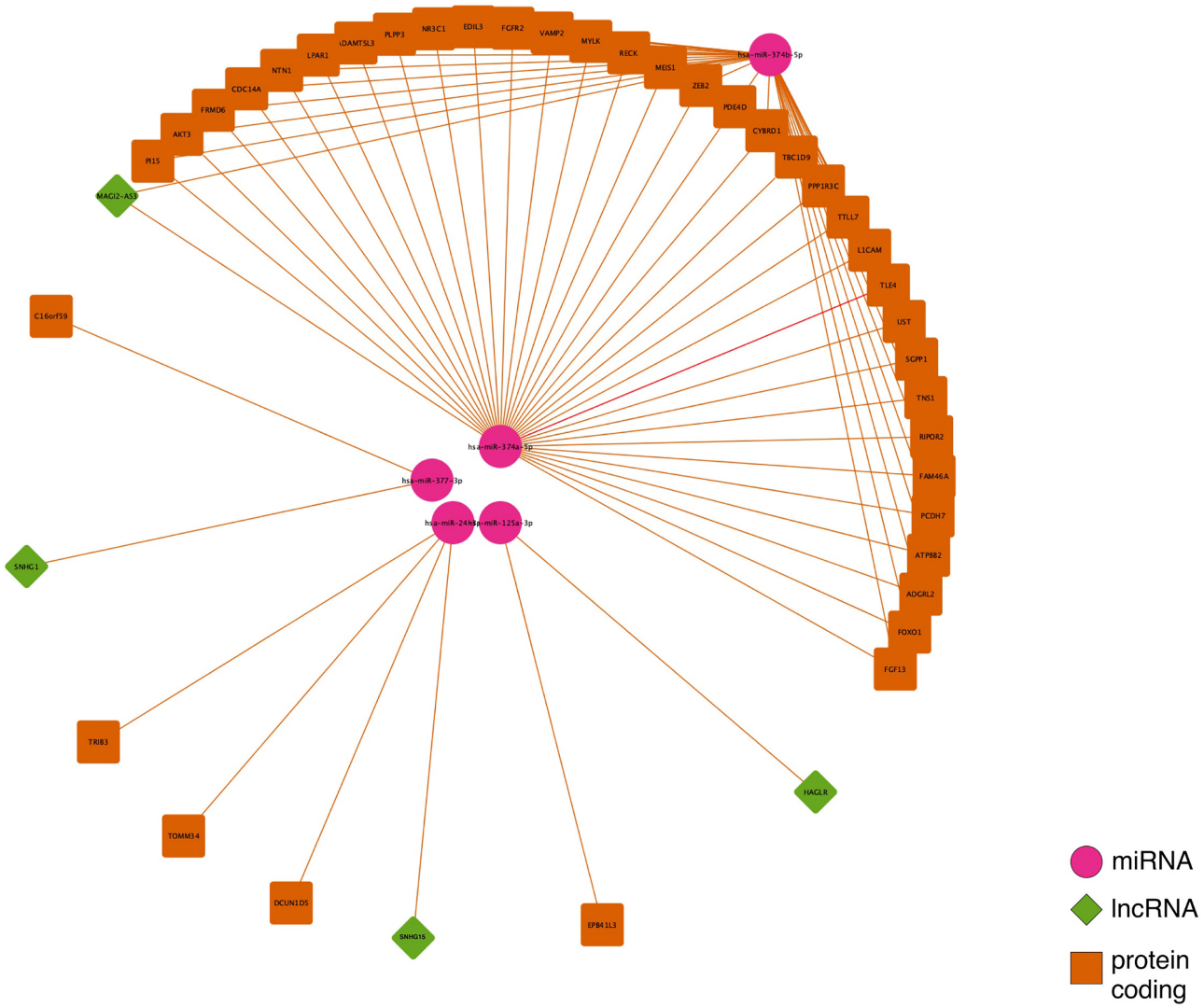

FIGURE 3 | Competing endogenous RNA (ceRNA) network intersection for colon, rectum and rectosigmoid junction sites.

according to the KM method (**Figure 7**) and the molecules with lowest pValue according to the KM and COxPh methods (**Figure 8**).

Regarding the KM method (**Figure 7**), we found some *PCGs* that were not in the group of 20 molecules found with CoxPH (**Figure 6**), but are relevant for overall patient survival, such as *RPS6KA5* for colon, *DMXL1* for rectum, and *AGAP3* for rectosigmoid junction.

Regarding the CoxPH method (**Figure 7**), we identified molecules that can be considered potential biomarkers for patient prognosis. The CoxPH methodology also revealed several molecules to be significant for overall survival in each anatomical site (**Figure 8**), many of which are concurrent with KM method results, such as has-miR-1271-5p, *E2F8*, and hsa-miR-130-3p.

Most of the relevant molecules for colon cancer patient survival (**Figures 7** and **8**) are present in distinct regions of the ceRNA network, with the exception of miR-1275-5p and *NRG1*. These two molecules are connected by MALAT1 ceRNA (**Figure 9**).

DISCUSSION

CRC is one of the most common and lethal cancers worldwide. The treatment therapy is directly related to tumor location. Due to heterogeneous characteristics, tumors located in the rectosigmoid junction are treated as either colon or rectum tumors. Therefore, obtaining molecular markers that could help identify tumor site and molecular characteristics is

FIGURE 4 | Functional enrichment analysis of *PCGs* and lncRNAs included in the ceRNA network of colon **(A)**, rectum **(B)**, and rectosigmoid junction **(C)** sites. The top 5 enrichment results for GO biological processes, cellular component, molecular function, DO and KEGG are shown in different colors. Asterisks (*) indicate pathways presenting FDR > 0.05.

necessary. In this sense, ceRNA networks allow us to evaluate differentially expressed molecules as well as miRNA-lncRNA-PCG interactions and control mechanisms.

In this study, we used differentially expressed lncRNAs, *PCGs*, and miRNAs to build specific ceRNA networks for the anatomical sites most affected by CRC and identify different and common factors involved in the progression of CRC. Moreover, we further accessed the relevance of each of these molecules in the ceRNA in regard to their impact on prognosis and their functional implications.

Previous works (11, 15, 16) have reported a protagonist role for the lncRNA *H19* as protagonist in regulating various cancer-

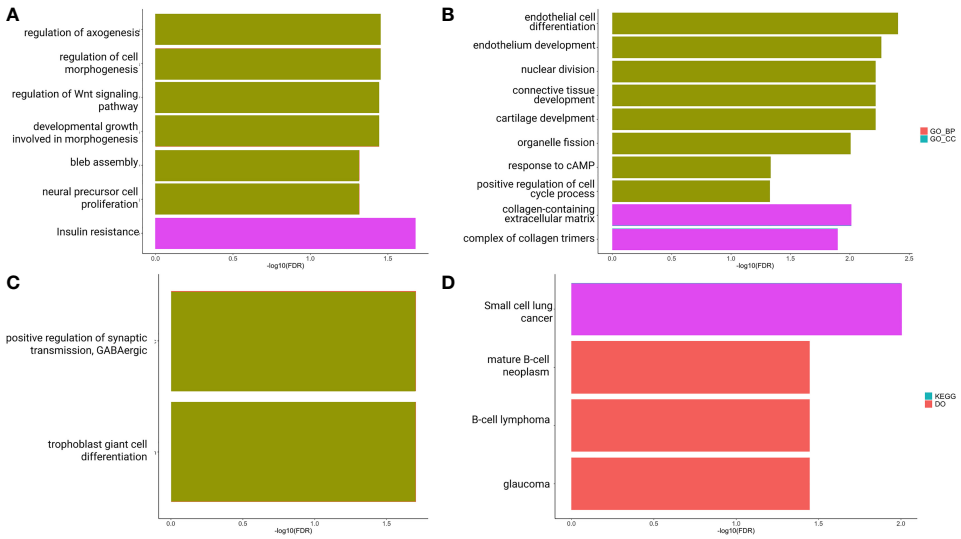

FIGURE 5 | Functional enrichment analysis of *PCGs* and lncRNAs included in the ceRNA network: common to colon, rectum and rectosigmoid junction **(A)**; specific to colon **(B)**; specific to rectum and **(C)**; specific to rectosigmoid junction **(D)** sites.

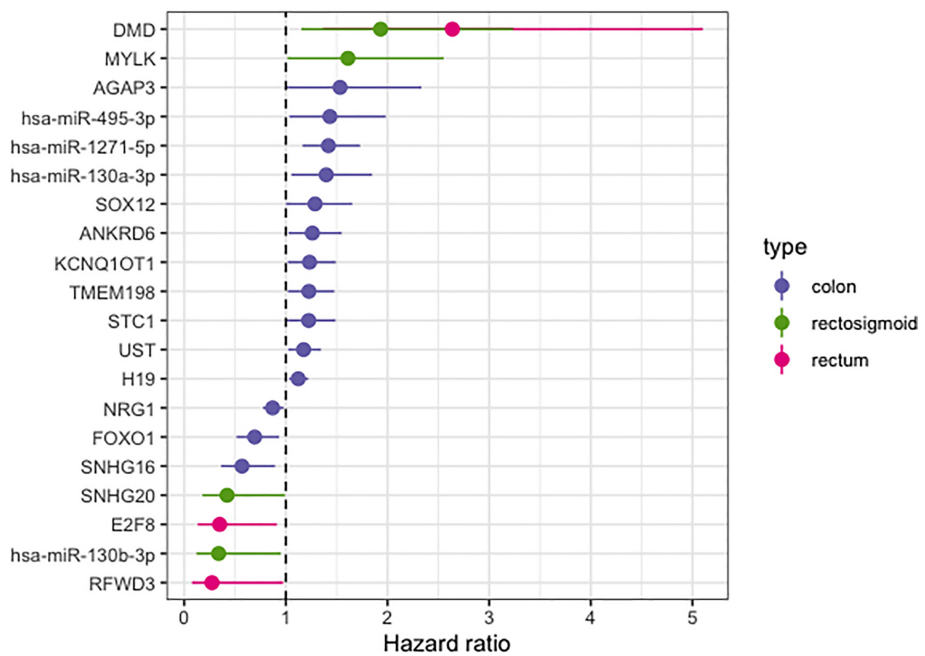

FIGURE 6 | Hazard ratio forest plot of survival associated RNAs in the ceRNA network for colon, rectum and rectosigmoid junction sites. The molecules with hazard ratio < 1 indicate risk factors, and those with hazard ratio > 1 indicate protective factors.

related mRNAs in colon cancer and in CRC in general. However, in our analysis, *H19* is only present in the colon exclusive network and not in that of the rectum, also described by Zhiyuan et al. (14). In this network, *H19* presents itself as a risk factor and acts as ceRNA for *SOX12*, *ANKRD6*, *STC1*, and hsa-miR-130a-3p, all of which are present as putative risk factors.

Colon, rectum and rectosigmoid junction presented common ceRNA networks regulated by the lncRNAs *MAGI2-AS3*, *HAGLR-AS3*, *SNHG1*, and *SNHG15*, suggesting some

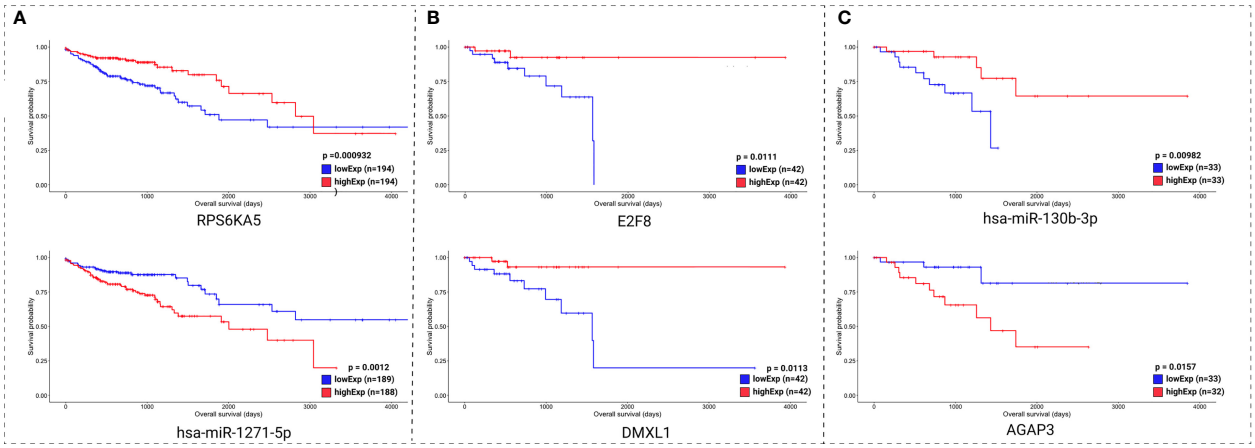

FIGURE 7 | Kaplan-Meier survival curves for the two best scored molecules for colon **(A)**, rectum **(B)**, and rectosigmoid junction **(C)** sites. Horizontal axis: overall survival time (in days). Vertical axis: survival probability.

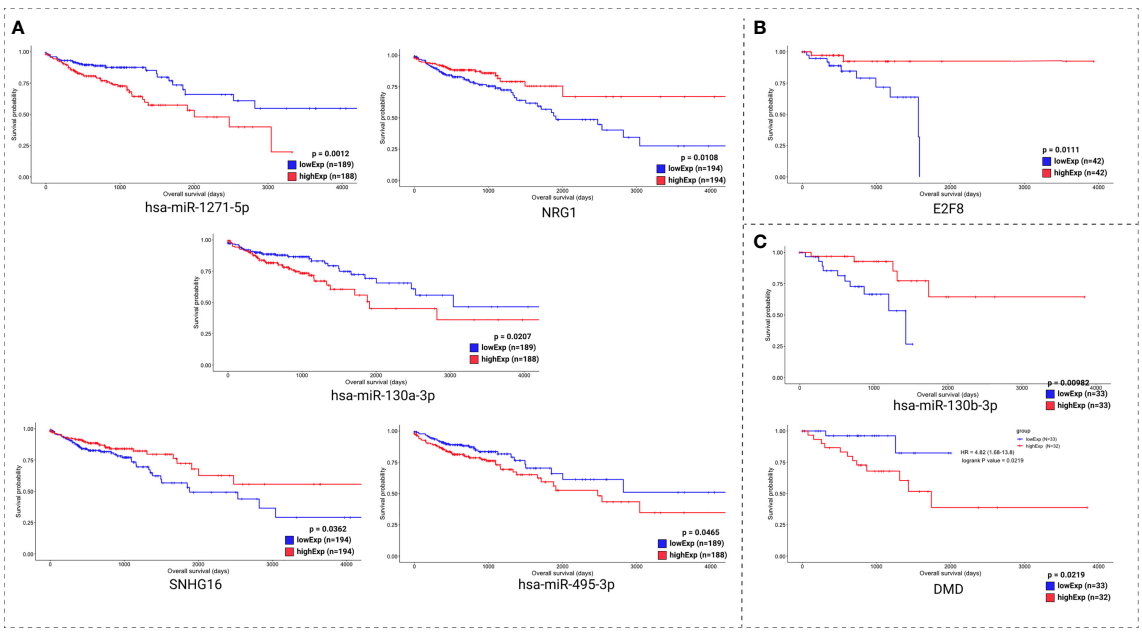

FIGURE 8 | Kaplan-Meier survival curves for the best scored molecules with top HR from CoxPH for colon **(A)**, rectum **(B)**, and rectosigmoid junction **(C)** sites.

similarities in CRC development independent of the anatomical site (**Figure 3**). These common mechanisms are related to the regulation of Wnt signaling, cell morphogenesis, and proliferation (**Figure 5A**), which are known to be present in cancer. The lncRNAs regulating common ceRNA networks were already correlated with known cancer pathways, such as: MAGI2-AS3 with cell apoptosis and proliferation in CRC (25); *HAGLR-AS3* with cell proliferation, invasion, and apoptosis (26); *SNHG1* with cell growth and promotion of CRC through the Wnt/β-catenin signaling pathway (27, 28); and SNHG15 with cell proliferation, apoptosis, and activation of the Wnt/β-catenin signal in CRC (29, 30). These studies indicate *MAGI2-AS3*, *HAGLR-AS3*, *SNHG1*, and *SNHG15* as potential biomarkers involved in regulation of Wnt signaling, cell morphogenesis, and proliferation. Our study is the first to bring together all of these molecules and related ceRNA networks as common factors in all CRC sites and to indicate their joint use as potential biomarkers for colon, rectum, and rectosigmoid junction cancer

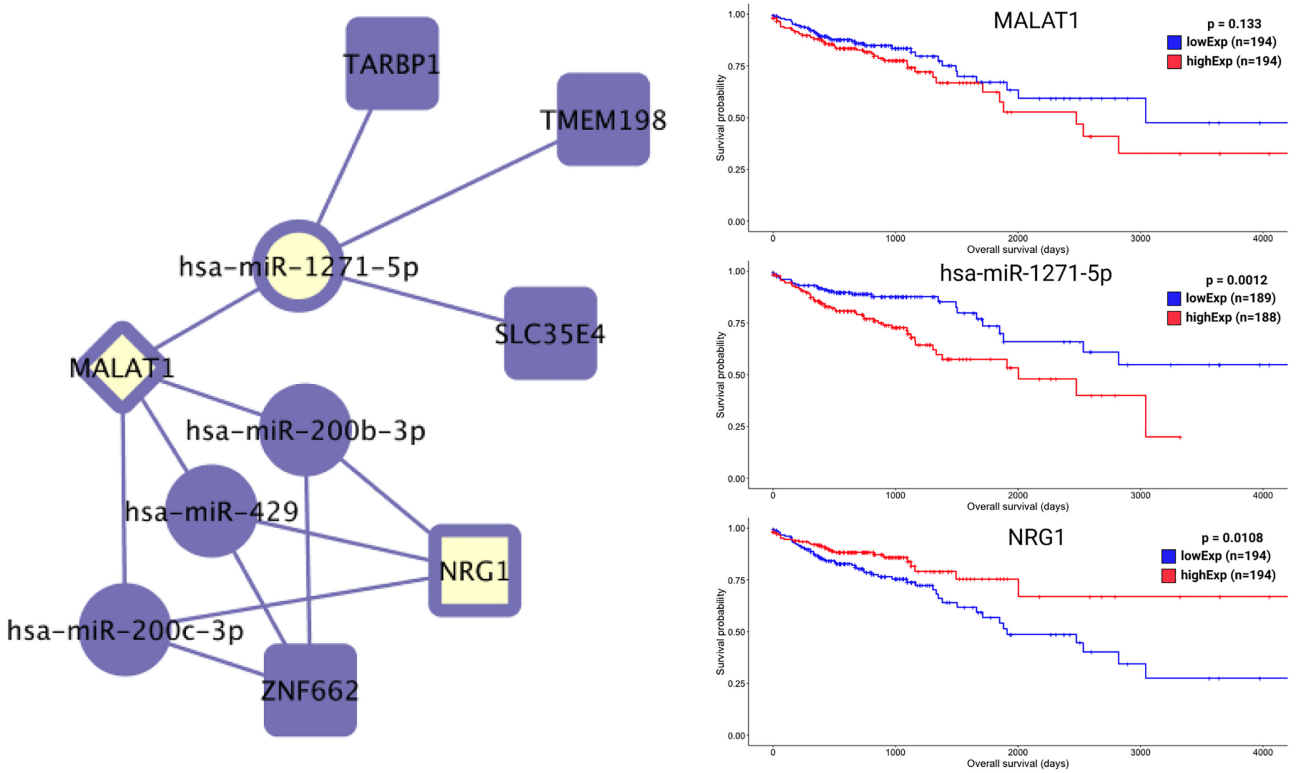

FIGURE 9 | Colon-specific ceRNA network and overall survival for hsa-mir-1271-5p, *NRG1* and MALAT1. Here, we can see the opposing putative roles of hsa-mir-1271-5p and *NRG1* on overall survival time. MALAT1 is shown as a link that relates hsa-mir-1271-5p and *NRG1* regulation, as well as behaving like hsa-mir-1271-5p on patient overall survival time.

common behavior. Within the *MAGI2-AS3* network, we found the dystrophin gene (*DMD*). *DMD* plays a special role in muscle fiber integrity (31), and it was the only gene identified as a potentially significant risk factor in both rectum and rectosigmoid junction sites. Duchenne muscular dystrophy is a disease known to be associated with *DMD*, and our functional analysis relates the biological disease's pathways from DO to the rectum ceRNA (**Figure 4B**). This gene is part of a network where it is regulated by miRNAs hsa-miR-374a-5p and hsa-miR-374b-5p, and the lncRNA *MAGI2-AS3*. These three ncRNAs connected to DMD are also 'sponged' by the PCG FOXO1, which is critical to tumor suppression and apoptosis (32) and presented a putative protective role in colon CRC tumors. Although Zhong et al. (11) previously reported their interaction, the authors did not mention the *DMD* and FOXO1 genes, nor did they evaluate their putative role as biomarkers or as survival factors. Therefore, to the best of our knowledge, this is the first time that *DMD* is reported as a potential biomarker for poor prognosis in CRC. In the case of the rectosigmoid junction, we found *DMD* and hsa-miR-130b-3p to be relevant to patient prognosis. Some studies have reported the importance of hsa-miR-130b-3p in poor prognosis of CRC (33, 34). It is worth noting that hsa-miR-130b-3p, which is relevant to the rectosigmoid junction is in the same ceRNA network as hsa-miR-130a, which is relevant to colon prognosis. Both molecules are regulated by the lncRNA MIR17HG, which may indicate that this ceRNA network is relevant to both colon and rectosigmoid junction. However, the miRNA responsible for poor patient prognosis is different for each site.

The specific networks for colon and rectum present distinct enriched biological pathways, with more specific endothelial development in the colon and cell morphology in the rectum. Due to the low number of samples for the rectosigmoid junction, we were unable to find a statistically significant pathway for this network. However, the pathways found are related to phosphorylation and signal transduction. These different biological pathways highlight differences in CRC behavior between distinct anatomical sites, thus reinforcing the importance of correctly identifying the tumor site.

E2F8 and *RFWD3* presented putative protective roles for rectum CRC tumors. *E2F8* encodes transcription factors that regulate development by the cell cycle (35), and *RFWD3* is known to be essential in the process of repairing DNA interstrand cross-links (36). Both genes are connected with the lncRNA *SNHG1* but are regulated by different miRNA. The *SNHG1* ceRNA network is common for all CRC sites, but only interacts with *RFWD3* and *E2F8* in the rectum, indicating a potential role for this network in rectum cancer. The *E2F8* gene

has been reported as relevant to CRC as well as in regulating cancer progression (35, 37) and our survival analysis indicates better survival for high *E2F8* expression levels. Previous studies (35, 37) have identified *E2F8* as a biomarker for colon cancer, but they did not evaluate the potential role of *SNHG1-RFWD3-E2F8* ceRNA network interaction in rectum cancer.

The *RPS6KA5* gene encodes for a tyrosine kinase and has been indicated as a biomarker for colon cancer (38) through interaction with hsa-miR-130a (39). In our colon-specific network, the lncRNA MIR17HG sponges hsa-miR-130a and interacts with *RPS6KA5*. Hsa-miR-1271-5p, hsa-miR-130a, *SOX12*, *ANKRD6*, *TMEM198*, *STC1*, *H19*, and *NRG1* all presented potential risk factors for colon cancer. Most of these molecules are present in distinct regions of the ceRNA network, with the exception of miR-1275-5p and *NRG1*. Both of these molecules are connected to the lncRNA MALAT1 and present opposing putative roles (**Figure 9**). Some studies (11, 15, 16) have previously reported the effects of *H19* ceRNA on CRC, but both our network and survival analyses suggest its influence only in the case of tumors located in the colon. No enrichment pathway of the rectosigmoid junction presented an exclusive HR relevant molecule.

In further consideration of the overall survival evidence, we reaffirm the potential role as prognosis biomarkers for hsa-miR-1271-5p, *NRG1*, hsa-miR-130a-3p, *SNHG16*, and hsa-miR-495-3p, in the colon; *E2F8*, in the rectum; and of *DMD* and hsa-miR-130b-3p, in the rectosigmoid junction.

This study had some limitations. Firstly, although several novel lncRNAs, *PCGs*, and miRNAs with clinical significance for CRC were found, the study was performed with TCGA data and no further experimental validation was carried out. Secondly, less information was analyzed for rectum and rectosigmoid junction tissue than for that of colon, which could influence site-specific results. Research on ceRNAs in CRC is still in development and requires further experimental studies and greater amount of data from colon, rectum, and rectosigmoid cancer in order to improve our understanding of the biomarkers found.

In conclusion, this study constructed a ceRNA network for colon, rectum, and rectosigmoid that provides clinical significance and functional implications for cancer at each of these sites. The results indicate several potential prognostic markers for colon, rectum, and rectosigmoid cancer, and also suggest that the ceRNAs found can help explain the differences between, and common factors on, prognosis for these CRC sites.

DATA AVAILABILITY STATEMENT

The raw data supporting the conclusions of this article will be made available by the authors, without undue reservation.

AUTHOR CONTRIBUTIONS

LV contributed to conception and design of the study, wrote the manuscript, and performed the analysis. NJ collaborated and reviewed the study on the bioinformatics methods and biology assumptions. JCS, MW, and PS reviewed and collaborated to key points at the discussion and methodology on a bioinformatics perspective. JBS reviewed and collaborated to key points at the discussion and methodology on a medical perspective. All authors contributed to the article and approved the submitted version.

ACKNOWLEDGMENTS

The results shown here are in whole or part based upon data generated by the TCGA Research Network: https://www.cancer.gov/tcgahttps://www.cancer.gov/tcga. This study was financed in part by the Coordenação de Aperfeiçoamento de Pessoal de Nível Superior – Brasil (CAPES) – Finance Code 001 and the Free State of Saxony (EraPerMed proj. no. 100371715). We acknowledge support from Leipzig University for Open Access Publishing.

REFERENCES

1. Qiaowei F, Bingrong L. Comprehensive Analysis of a Long Noncoding RNA-Associated Competing Endogenous RNA Network in Colorectal Cancer. *OncoTargets Ther* (2018) 11:2453. doi: 10.2147/OTT.S158309
2. Ulrich N, Anina Z, Christoph S, Tara M, Matthias M, Tibor S, et al. Mucinous and Signet-Ring Cell Colorectal Cancers Differ From Classical Adenocarcinomas in Tumor Biology and Prognosis. *Ann Surg* (2013) 258:775. doi: 10.1097/SLA.0b013e3182a69f7e
3. Christian W, James B, Anne L, Elisabeth E. *TNM Supplement: A Commentary on Uniform Use*. Hoboken, New Jersey: John Wiley & Sons (2019).
4. Ruud L, Marcel F, Gerwin F, Frank B, Aart B. The Localisation of Cancer in the Sigmoid, Rectum or Rectosigmoid Junction Using Endoscopy or Radiology—What Is the Most Accurate Method? *J Gastrointest Oncol* (2014) 5:469. doi: 10.3978/j.issn.2078-6891.2014.087
5. Xu G, Zheng J, Tianyi M, Zheng L, Hanqing H, Zhixun Z, et al. Radiotherapy Dose Led to a Substantial Prolongation of Survival in Patients With Locally Advanced Rectosigmoid Junction Cancer: A Large Population Based Study. *Oncotarget* (2016) 7:28408. doi: 10.18632/oncotarget.8630
6. Pieter-Jan V, Kenneth V, Gerben M, Klaas V, Lennart M, Jo V, et al. An Update on Lncipedia: A Database for Annotated Human lncRNA Sequences. *Nucleic Acids Res* (2015) 43:D174–80. doi: 10.1093/nar/gku1060
7. Leonardo S, Laura P, Yvonne T, Lev K, Paolo PP. A Cerna Hypothesis: The Rosetta Stone of a Hidden RNA Language? *Cell* (2011) 146:353–8. doi: 10.1016/j.cell.2011.07.014
8. Tayier T, Linlin L, Zumureti A, Shumei F. Comprehensive Analysis of the Aberrantly Expressed Lncrna-Associated Cerna Network in Breast Cancer. *Mol Med Rep* (2019) 19:4697–710. doi: 10.3892/mmr.2019.10165
9. Gang Z, Shuwei L, Jiafei L, Yuqiu G, Qiaoyan W, Gaoxiang M, et al. Lncrna MT1JP Functions as a Cerna in Regulating FBXW7 Through Competitively Binding to Mir-92a-3p in Gastric Cancer. *Mol Cancer* (2018) 17:1–11. doi: 10.1186/s12943-018-0829-6
10. Yunpeng Z, Yanjun X, Li F, Feng L, Zeguo S, Tan W, et al. Comprehensive Characterization of Lncrna-Mrna Related Cerna Network Across 12 Major Cancers. *Oncotarget* (2019) 7:64148. doi: 10.18632/oncotarget.11637
11. Min-Er Z, Yanyu C, Guannan Z. Lncrna H19 Regulates PI3K–Akt Signal Pathway by Functioning as a Cerna and Predicts Poor Prognosis in Colorectal Cancer: Integrative Analysis of Dysregulated ncRNA-Associated Cerna Network. *Springer* (2019) 19:148. doi: 10.1186/s12935-019-0866-2
12. Jun-Hao L, Shun L, Hui Z, Liang-Hu Q, Jian-Hua Y. Lncrna CACS15 Contributes to Oxaliplatin Resistance in Colorectal Cancer by Positively Regulating ABCC1 Through Sponging Mir-145. *Arch Biochem Biophys* (2019) 663:183–91. doi: 10.1016/j.abb.2019.01.005

13. Qian-Rong H, Pan XB. Prognostic lncRNAs, miRNAs, and mRNAs Form a Competing Endogenous RNA Network in Colon Cancer. *Frontiers* (2019) 9:712. doi: 10.3389/fonc.2019.00712
14. Zhiyuan Z, Sen W, Dongjian J, Wenwei Q, Qingyuan W, Jie L, et al. Construction of a Cerna Network Reveals Potential lncRNA Biomarkers in Rectal Adenocarcinoma. *Oncol Rep* (2018) 39:2101–13. doi: 10.3892/or.2018.6296
15. Hongda P, Jingxin P, Shibo S, Lei J, Hong L, Zhangru Y. Identification and Development of Long non-Coding RNA-Associated Regulatory Network in Colorectal Cancer. *J Cell Mol Med* (2019) 23:5200–10. doi: 10.1111/jcmm.14395
16. Hui Z, Zhuo W, Jianzhong W, Rong M, Jifeng F. Long Noncoding Rnas Predict the Survival of Patients With Colorectal Cancer as Revealed by Constructing an Endogenous RNA Network Using Bioinformation Analysis. *Cancer Med* (2019) 8:863–73. doi: 10.1002/cam4.1813
17. Katarzyna T, Patrycja C, Maciej W. The Cancer Genome Atlas (TCGA): An Immeasurable Source of Knowledge. *Contemp Oncol* (2015) 19:A68. doi: 10.5114/wo.2014.47136
18. Ruidong L, Han Q, Shibo W, Julong W. Gdcrnatools: An R/Bioconductor Package for Integrative Analysis of lncRNA, Mirna and Mrna Data in GDC. *Bioinformatics* (2018) 34:2515–7. doi: 10.1093/bioinformatics/bty124
19. Matthew R, Belinda P DIW, Yifang H, Charity L, Wei S, et al. Limma Powers Differential Expression Analyses for Rna-Sequencing and Microarray Studies. *Nucleic Acids Res* (2015) 43:e47–7. doi: 10.1093/nar/gkv007
20. Pedro F, Sonia T, Toni G, Anton E, Ana C. Spongescan: A Web for Detecting Microrna Binding Elements in lncRNA Sequences. *Nucleic Acids Res* (2016) 44:W176–80. doi: 10.1093/nar/gkw443
21. Jun-Hao L, Shun L, Hui Z, Liang-Hu Q, Jian-Hua Y. Starbase V2. 0: Decoding Mirna-Cerna, Mirna-Ncrna and Protein–RNA Interaction Networks From Large-Scale CLIP-Seq Data. *Nucleic Acids Res* (2014) 42:D92–7. doi: 10.1093/nar/gkt1248
22. Michael A, Catherine B, Judith B, David B, Heather B, Michael CJ, et al. Gene Ontology: Tool for the Unification of Biology. *Nat Genet* (2000) 25:25–9. doi: 10.1038/75556
23. Minoru K, Susumu G. KEGG: Kyoto Encyclopedia of Genes and Genomes. *Nucleic Acids Res* (2000) 28:27–30. doi: 10.1093/nar/28.1.27
24. Lynn S, Elvira M, James M, Becky T, Mike S, Lance N, et al. Human Disease Ontology 2018 Update: Classification, Content and Workflow Expansion. *Nucleic Acids Res* (2019) 47:D955–62. doi: 10.1093/nar/gky1032
25. Yuping Z, Bo L, Zhuo L, Lai J, Gang W, Min L, et al. Long Noncoding MAGI2-AS3 Promotes Colorectal Cancer Progression Through Regulating Mir-3163/Tmem106b Axis. *J Cell Physiol* (2019) 235:4824–33. doi: 10.1002/jcp.29360
26. Weixuan S, Wenting N, Zhaoyi W, Haolong Z, Yezhou L, Xuedong F. Lnc HAGLR Promotes Colon Cancer Progression Through Sponging Mir-185-5p and Activating CDK4 and CDK6 In Vitro and In Vivo. *OncoTargets Ther* (2020) 13:5913. doi: 10.2147/OTT.S246092
27. Mu X, Xiaoxiang C, Kang L, Kaixuan Z, Xiangxiang L, Bei P, et al. The Long Noncoding RNA SNHG1 Regulates Colorectal Cancer Cell Growth Through Interactions With EZH2 and Mir-154-5p. *Mol Cancer* (2019) 17:1–16. doi: 10.1186/s12943-018-0894-x
28. Yuping Z, Bo L, Zhuo L, Lai J, Gang W, Min L, et al. Up-Regulation of lncRNA Snhg1 Indicates Poor Prognosis and Promotes Cell Proliferation and Metastasis of Colorectal Cancer by Activation of the Wnt/β-Catenin Signaling Pathway. *Oncotarget* (2017) 8:111715. doi: 10.18632/oncotarget.22903
29. Min L, Zehua B, Guoying J, Jia Z, Surui Y, Yuyang F, et al. Lnc RNA-SNHG 15 Enhances Cell Proliferation in Colorectal Cancer by Inhibiting Mir-338-3p. *Cancer Med* (2019) 8:2404–13. doi: 10.1002/cam4.2105
30. Min L, Zehua B, Guoying J, Jia Z, Surui Y, Yuyang F, et al. Long Noncoding RNA SNHG15 Enhances the Development of Colorectal Carcinoma Via Functioning as a Cerna Through Mir-141/Sirt1/Wnt/β-Catenin Axis. *Artif Cells Nanomed Biotechnol* (2019) 47:2536–44. doi: 10.1080/21691401.2019.1621328
31. Sylvie TG, Julie M, Michel K, Mireille C. Normal and Altered Pre-Mrna Processing in the DMD Gene. *Hum Genet* (2017) 136:1155–72. doi: 10.1007/s00439-017-1820-9
32. Yun-Cheol C, Ji-Young K, Woo PJ, Kee-Beom K, Hyein O, Kyung-Hwa L, et al. Foxo1 Degradation Via G9a-Mediated Methylation Promotes Cell Proliferation in Colon Cancer. *Nucleic Acids Res* (2019) 47:1692–705. doi: 10.1093/nar/gky1230
33. Tommaso C, Alessandra F, Carolina V, Lina S, Massimo P, Carmelo L, et al. Microrna-130b Promotes Tumor Development and is Associated With Poor Prognosis in Colorectal Cancer. *Neoplasia* (2013) 15:1086–99. doi: 10.1593/neo.13998
34. Yanyang Z, Gang M, Yao L, Tomoya I, Jianguo G, Jian L, et al. Microrna 130b Suppresses Migration and Invasion of Colorectal Cancer Cells Through Downregulation of Integrin β1. *PloS One* (2014) 9:e87938. doi: 10.1371/journal.pone.0087938
35. Zhiyuan Z, Jie L, Huang Y, Wen P, Wenwei Q, Jiou G, et al. Upregulated Mir-1258 Regulates Cell Cycle and Inhibits Cell Proliferation by Directly Targeting E2F8 in CRC. *Cell Prolif* (2018) 51:e12505. doi: 10.1111/cpr.12505
36. Yo-Chuen L, Yating W, Rosaline H, Sumanprava G, Susan W, K AM, et al. PCNA-Mediated Stabilization of E3 Ligase RFWD3 At the Replication Fork is Essential for Dna Replication. *Proc Natl Acad Sci* (2018) 115:13282–7. doi: 10.1073/pnas.1814521115
37. Peng-yu Y, Xin-an Z. Knockdown of E2F8 Suppresses Cell Proliferation in Colon Cancer Cells by Modulating the Nf-κb Pathway. *Ann Clin Lab Sci* (2019) 49:474–80.
38. Peng S, Jianping W, Yao T, Chunxia X, Xingguo Z. Gene Pair Based Prognostic Signature for Colorectal Colon Cancer. *Medicine* (2018) 97:2–3. doi: 10.1097/MD.0000000000012788
39. Jian X, Jian Z, Rui Z. Four Micrornas Signature for Survival Prognosis in Colon Cancer Using TCGA Data. *Sci Rep* (2016) 6:6–7. doi: 10.1038/srep38306

Conflict of Interest: The authors declare that the research was conducted in the absence of any commercial or financial relationships that could be construed as a potential conflict of interest.

frontiers in Cell and Developmental Biology

ORIGINAL RESEARCH
published: 03 January 2022
doi: 10.3389/fcell.2021.795133

SCG2 is a Prognostic Biomarker Associated With Immune Infiltration and Macrophage Polarization in Colorectal Cancer

Hao Wang[1,2†], *Jinwen Yin*[2,3†], *Yuntian Hong*[2,4], *Anli Ren*[2,3], *Haizhou Wang*[2,3], *Mengting Li*[2,3], *Qiu Zhao*[2,3*], *Congqing Jiang*[2,4*] *and Lan Liu*[2,3*]

[1]*Department of Oncology, Shanghai East Hospital, Tongji University School of Medicine, Shanghai, China,* [2]*Hubei Clinical Center and Key Lab of Intestinal and Colorectal Diseases, Wuhan, China,* [3]*Department of Gastroenterology, Zhongnan Hospital of Wuhan University, Wuhan, China,* [4]*Department of Colorectal and Anal Surgery, Zhongnan Hospital of Wuhan University, Wuhan, China*

OPEN ACCESS

Edited by:
Oronzo Brunetti, Istituto Nazionale dei Tumori (IRCCS), Italy

Reviewed by:
Gianandrea Pasquinelli, University of Bologna, Italy
Ariz Mohammad, Washington University in St. Louis, United States

***Correspondence:**
Qiu Zhao
qiuzhao@whu.edu.cn
Congqing Jiang
wb002554@whu.edu.cn
Lan Liu
lliugi@whu.edu.cn

†*These authors share first authorship*

Specialty section:
This article was submitted to Molecular and Cellular Oncology, a section of the journal Frontiers in Cell and Developmental Biology

Received: *14 October 2021*
Accepted: *01 December 2021*
Published: *03 January 2022*

Citation:
Wang H, Yin J, Hong Y, Ren A, Wang H, Li M, Zhao Q, Jiang C and Liu L (2022) SCG2 is a Prognostic Biomarker Associated With Immune Infiltration and Macrophage Polarization in Colorectal Cancer. Front. Cell Dev. Biol. 9:795133. doi: 10.3389/fcell.2021.795133

Colorectal cancer (CRC) is the second most lethal malignancy around the world. Limited efficacy of immunotherapy creates an urgent need for development of novel treatment targets. Secretogranin II (SCG2) is a member of the chromogranin family of acidic secretory proteins, has a role in tumor microenvironment (TME) of lung adenocarcinoma and bladder cancer. Besides, SCG2 is a stroma-related gene in CRC, its potential function in regulating tumor immune infiltration of CRC needs to be fully elucidated. In this study, we used western blot, real-time PCR, immunofluorescence and public databases to evaluate SCG2 expression levels and distribution. Survival analysis and functional enrichment analysis were performed. We examined TME and tumor infiltrating immune cells using ESTIMATE and CIBERSORT algorithm. The results showed that SCG2 expression was significantly decreased in CRC tumor tissues, and differentially distributed between tumor and adjacent normal tissues. SCG2 was an independent prognostic predictor in CRC. High expression of SCG2 correlated with poor survival and advanced clinical stage in CRC patients. SCG2 might regulate multiple tumor- and immune-related pathways in CRC, influence tumor immunity by regulating infiltration of immune cells and macrophage polarization in CRC.

Keywords: colorectal cancer, SCG2, prognosis, tumor immunology, macrophage polarization

INTRODUCTION

Colorectal cancer (CRC) is the fourth most commonly diagnosed cancer, causing more than ninety thousand deaths worldwide every year (Bray et al., 2018; Siegel et al., 2020). Although diagnosis and treatment have been improved substantially, the prognosis of patients remains poor, especially in those with higher TNM stage (Luebeck et al., 2013; Miller et al., 20162016). Abnormal expression of multiple genes is usually associated with the occurrence of CRC (Meyerson et al., 2010). However, the molecular mechanisms underlying CRC remain unclear. It is urgent to identify novel diagnostic biomarkers and prognostic predictors for this disease.

New treatment modalities have been proposed for CRC, such as immunotherapy (Overman et al., 2018). Recently, studies have shown that the tumor microenvironment (TME) significantly affects CRC progression and therapeutic efficacy (Halama et al., 2011). Monoclonal antibodies against programmed cell death 1 (PD-1), programmed death ligand-1 (PD-L1) and cytotoxic T-lymphocyte–associated antigen 4 (CTLA4) have been proven effective in clinical trials (Rotte, 2019).

However, anti-PD-1/PD-L1 therapy is unsatisfactory in metastatic CRC (Le et al., 2015), whereas anti-CTLA-4 treatment showed a limited response rate in advanced CRC (Chung et al., 2010). Therefore, it is of paramount importance to find novel immunotherapy targets of CRC.

Secretogranin II (SCG2) is a member of the tyrosine-sulphated granin family expressed in endocrine, neuroendocrine and neuronal tissues (Troger et al., 2017). It is relevant to secretory vesicle formation and packaging peptide hormones into vesicles (Beuret et al., 2004). SCG2 has an important role in enhancing endothelial cell proliferation, migration, and angiogenesis (Albrecht-Schgoer et al., 2012; Hannon et al., 2018). Studies have revealed that the derived peptides of SCG2, such as secretoneurin (SN) and EM66, are useful markers of neuroendocrine tumors (Guillemot et al., 2012). Besides, SCG2 could predict prognosis in Non-small cell lung cancer as a potentially secreted biomarker (Cury et al., 2019), reflect the TME of lung adenocarcinoma (Wang and Chen, 2020) and bladder cancer (Luo et al., 2020). Recently, Liu et al. (2020) identified SCG2 was a stroma-related gene and predicted poor outcomes in CRC patients. However, the relationship between SCG2 and tumor immunity of CRC is largely unknown, and the mechanisms underlying it remain to be intensively investigated.

This study analyzed SCG2 expression profiles and described its potential prognostic value, multiple biological functions, related signal pathways in CRC. This report's findings revealed the potential role SCG2 played in regulating tumor immunity and provided a possible mechanism based on bioinformatic analysis.

MATERIALS AND METHODS

Specimen Collection

We obtained 61 pairs of CRC primary tumor tissues and adjacent tissues from patients who underwent surgery at Zhongnan Hospital of Wuhan University (Wuhan, China) between June 2019 and September 2019. None of the patients received any preoperative therapy such as adjuvant chemotherapy or radiotherapy. Samples of the collected tissues were preserved in RNAlater Stabilization solution (Invitrogen, United States) and stored in the department of Biological Repositories (Zhongnan Hospital of Wuhan University). Our study was approved by Zhongnan Hospital Ethics Committee (ethics code 2018025), and every patient signed informed consent.

RNA Extraction and qRT-PCR

Total RNA was extracted using Trizol reagent (Invitrogen, United States), and cDNA was reverse transcribed from 1ug of purified RNA using PrimeScriptTM RT reagent kit (Toyobo, Osaka). The quantification of mRNA was examined using quantitative real-time polymerase chain reaction (qRT-PCR) on Biorad CFX (Biorad, United States), and gene expression was normalized by GAPDH. The primer sequences were obtained from PrimerBank and synthesized by TSINGKE (Wuhan, China) as follows: GAPDHF-5′CTGGGCTACACTGAGCACC3′, R-5′AAGTGGTCGTTGAGGGCAATG3′, SCG2F-5′ACCAGACCTCAGGTTGGAAAA3′, R-5′ACCAGACCTCAGGTTGGAAAA3′. We used the comparative CT (2-ΔΔCT) to calculate the gene mRNA expression levels, and the experiment was repeated three times with three biological replicates for each treatment.

Protein Extraction and Western Blotting

According to the reagent instructions, total protein in tissues was extracted with RIPA lysis buffer (Boyotime, China), including a protease inhibitor cocktail (Thermo Scientific, United States). We performed western blot using standard methods with the specific antibody, SCG2 (1:1,000, Absin, abs117155), GAPDH (1:10000, Proteintech, 60004-1-Ig).

Immunofluorescence

Tumor samples were immediately fixed with 4% Paraformaldehyde (PFA) for 1 h and dehydrated overnight at 4°C. We used the following primary antibodies for immunofluorescence: mouse anti-SCG2 (1:100, Absin, abs117155) and rat anti-CD68 (1:100, Novusbio, 100–683). Fluorescent secondary antibodies CY3-conjugated anti-mouse SCG2 (1:1,000) and FITC-conjugated anti-rat CD68 antibody (1:1,000) were incubated for 30 min at 25°C. Nuclei were counter stained with DAPI for 10 min. We randomly chose at least five optical fields (20× or 40× magnification) per tumor section for morphometric evaluation.

Data Acquisition

RNA-sequencing expression data and clinicopathological information of 469 CRC patients were downloaded from The Cancer Genome Atlas (TCGA) database. GSE39582 cohort containing microarray gene expression profiles and clinical data was downloaded from the Gene Expression Omnibus (GEO) database. The proteome data of CRC patients was obtained from the Clinical Proteomic Tumor Analysis Consortium (CPTAC) Assay Portal (Whiteaker et al., 2014).

SCG2 Expression Analysis

We identified SCG2 mRNA expression levels in multiple human cancers from the Tumor Immune Estimation Resource (TIMER) database (Li et al., 2017). In TCGA and GEO cohorts, the mRNA expression profiles of SCG2 were visualized, respectively. In the CPTAC cohort, the protein expression levels of SCG2 in 91 pairs of tumor and adjacent tissues were examined. qRT-PCR and WB were utilized to detect RNA and protein levels of SCG2. Finally, immunofluorescence assay was used to detect the expression and distribution of SCG2 protein in tumor and adjacent tissues of CRC patients.

Survival Analysis and Significant Prognostic Marker Analysis

Patients were divided into high-SCG2 expression group and low-SCG2 expression group according to the median expression value of SCG2. We used R packages "survival" and "survminer" to analyze the correlation between SCG2 expression and overall

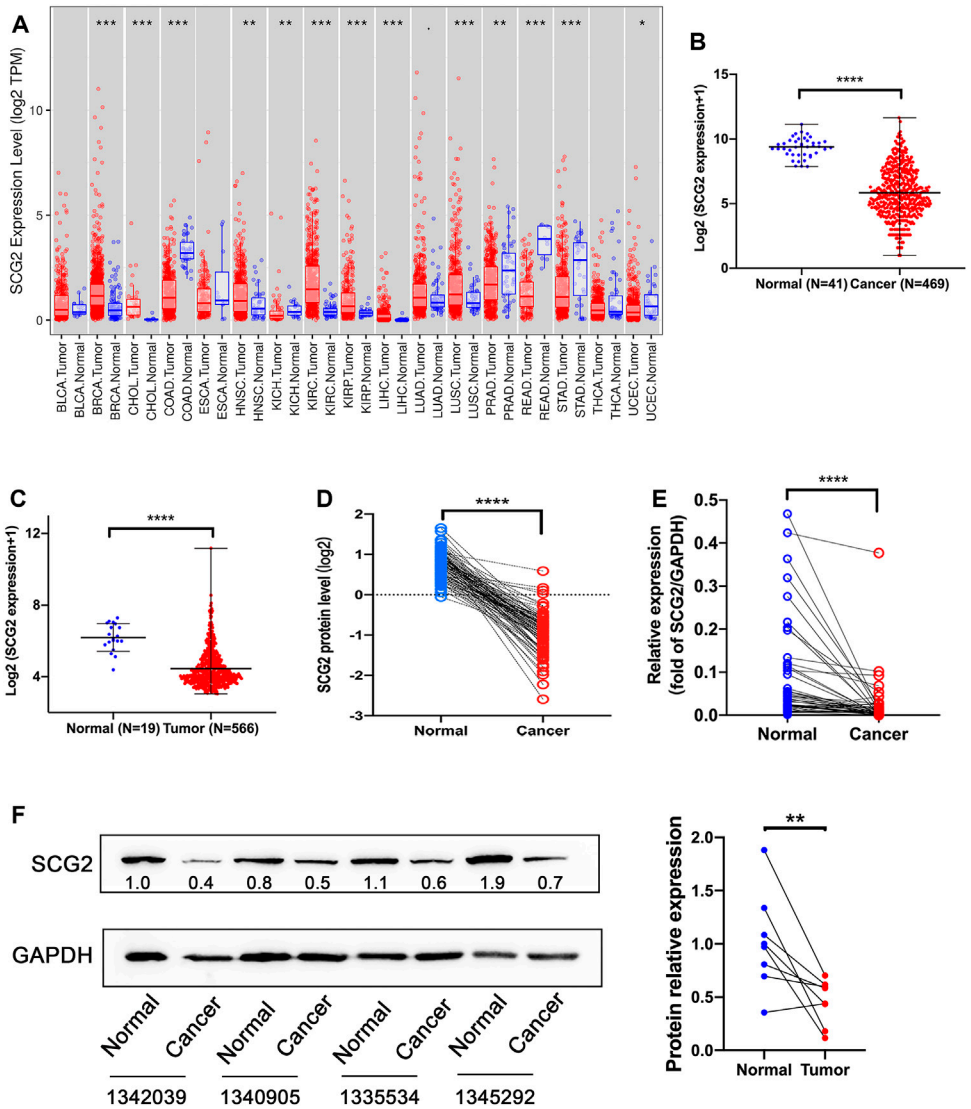

FIGURE 1 | Expression analysis of SCG2. **(A)** The SCG2 expression level in multiple cancer types from TCGA database. **(B,C)** SCG2 mRNA expression levels in normal and tumor tissues of CRC from TCGA and GEO database. **(D)** SCG2 protein levels in 96 paired CRC tissues from CPTAC. **(E)** SCG2 mRNA expression level in tumor and adjacent samples. **(F)** Quantification of SCG2 protein expression in tumor and adjacent samples. **(A–C)** Examined by Mann-Whitney U test; **(D–F)** Examined by Wilcoxon signed rank test; $^{*}p < 0.05$, $^{**}p < 0.01$, $^{***}p < 0.001$, $^{****}p < 0.0001$.

survival (OS) time, disease-free survival (DFS) time. Besides, univariate and multivariate survival analyses were applied to examine the independent prognostic factors in CRC, using the "coxph" function in the "survival" package.

SCG2 Related Genes and Functional Enrichment Analysis

To further study the SCG2-related molecular mechanisms, we performed differential expression genes (DEGs) analysis based on the medium value of SCG2 expression using the package "DESeq2." Genes were ranked with positive correlation coefficients with SCG2 (Log2FoldChange ≥ 1, $p < 0.01$). Then Gene Ontology (GO) and Kyoto Encyclopedia of Genes and Genomes (KEGG) enrichment analysis were conducted using "enrichGo" and "enrichKEGG" functions in the "clusterprofiler" package. We conducted a PPI network based on DEGs by Cytoscape software, and its plug-in "ClueGO" was applied for further function enrichment analysis.

Gene Set Enrichment Analysis

We performed Gene Set Enrichment Analysis (GSEA) to further understand the upregulated pathways in the high SCG2 expression group by GSEA 4.1 software. The number permutations for each gene were set to 1,000, false discovery rate (FDR) < 0.5 and normalized enrichment score (NES) > 1 were set at the cut-off criteria.

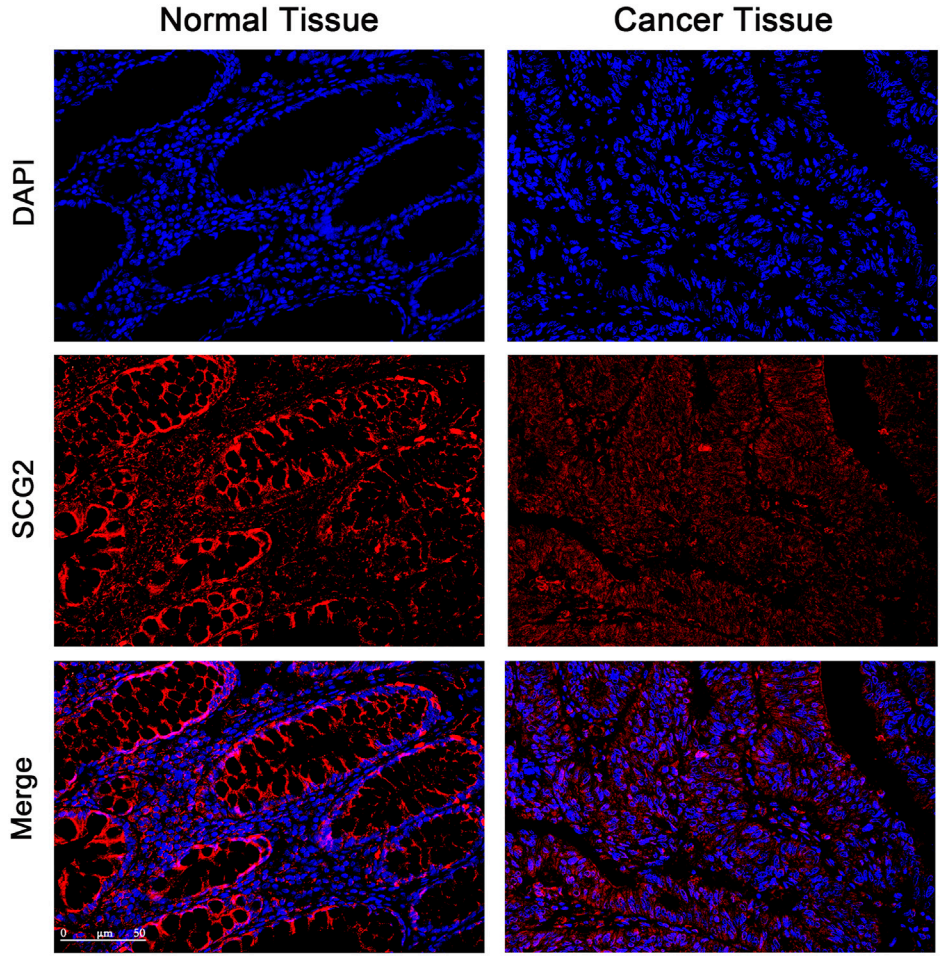

FIGURE 2 | Immunofluorescence images of SCG2 (red) and DAPI (blue) in tumor and adjacent tissues of CRC patients. Seven pairs of tumors and adjacent tissues were examined, six of the tumor tissues showed deceased SCG2 expression compared to adjacent normal tissues.

TABLE 1 | Univariate Cox regression of prognostic factors in CRC patients.

Parameters	TCGA	Univariate cox regression		GSE39582	Univariate cox regression	
	HR (95%CI)	z-score	*p*-value	HR (95%CI)	z-score	*p*-value
Sex (female vs. male)	0.809 (0.469–1.395)	-0.761	0.446	1.127 (0.823–1.542)	0.744	0.457
Age (≥60 vs. <60)	1.781 (0.918–3.456)	1.707	0.088	1.318 (0.9675–1.796)	1.751	0.080
TNM stage (III-IV vs. I-II)	2.739 (1.575–4.764)	3.568	3.6e-04	2.337 (1.871–2.918)	0.113	7e-14
Invasion depth (T3/T4 vs. T1/T2)	4.748 (1.152–19.57)	2.155	0.031	1.948 (1.478–2.567)	4.372	2.23e-06
Lymph node metastasis (N1/N2/N3 vs. N0)	2.308 (1.345–3.962)	3.036	0.002	1.479 (1.239–1.764)	4.339	1.43e-05
Distant metastasis (M1 vs. M0)	4.379 (2.462–7.788)	5.028	4.96e-07	7.779 (5.360–11.29)	10.79	2e-16
SCG2 expression (High vs. low)	2.111 (1.127–3.659)	2.661	0.008	1.510 (1.111–2.053)	2.629	0.009

HR: hazard ratio; CI: confidence interval.

Characterization of the TME

Tumor infiltrating immune cells (TIICs) in tumor samples and normal samples of the TCGA cohort were calculated using the CIBERSORT algorithm based on RNA-seq (Newman et al., 2015). The signature TIICs matrix "LM22" was set to 1,000 permutations. Tumor immune single-cell analysis was investigated with the "Dataset" module in Tumor Immune Single Cell Hub (TISCH, http://tisch.comp-genomics.org), which built a Single-cell RNA sequencing (scRNA-seq) atlas of 76 high-quality tumor datasets across 27 cancer types from

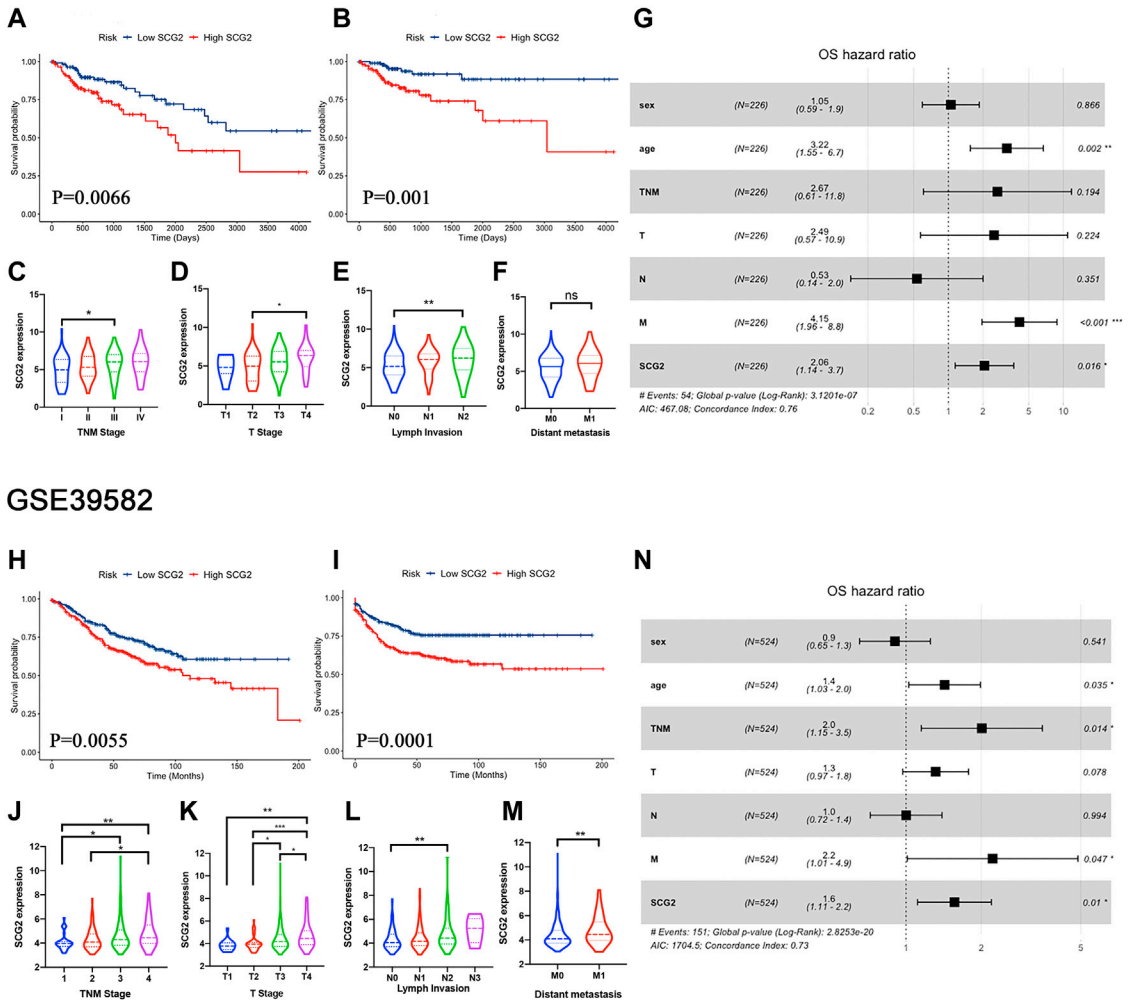

FIGURE 3 | High SCG2 expression is associated with worse survival and advanced clinical stage in CRC patients. **(A,B)** OS, DFS in the TCGA CRC cohort. **(C–F)** SCG2 expression was higher in patients of advanced T, N, M, TNM stage in the TCGA CRC cohort. **(G)** Multivariate Cox analysis of patients in the TCGA CRC cohort showing the HRs of different factors. **(H,I)** OS, DFS in the GSE39582 CRC cohort. **(J–M)** SCG2 expression was higher in patients of advanced T, N, M, TNM stage in the GSE39582 CRC cohort. **(N)** Multivariate Cox analysis of patients in the GSE39582 CRC cohort showing the HRs of different factors. HRs, hazard ratios. **(C–E,J–L)** Examined by Kruskal-Wallis H test; **(F,M)** Examined by Mann-Whitney U test; $^{*}p < 0.05$, $^{**}p < 0.01$, $^{***}p < 0.001$.

GEO and ArrayExpress (Sun et al., 2021). Thirteen kinds of major lineage immune cells from GSE146771 cohort were analyzed.

Correlation Analysis of SCG2 and TIICs

We applied the Estimation of STromal and Immune cells in MAlignant Tumours using Expression data (ESTIMATE) algorithm to calculate stromal and immune scores that predicted the levels of infiltrating stromal and immune cells in each patient (Yoshihara et al., 2013) and analyzed the correlations between SCG2 expression and the two scores. We further compared the proportions of twenty-two immune cell phenotypes in SCG2 high or low expression group using CIBERSORT algorithm. The correlations between SCG2 and tumor-associated macrophages (TAMs), M2 gene markers were analyzed to identify the relevance of SCG2 and macrophage polarization. The correlations between SCG2 expression and gene markers of various immune cells including CRC immune checkpoint genes were analyzed by TIMER (Li et al., 2017).

Statistical Analysis

SPSS Statistics 26, GraphPad prism 8, R 4.0.2 were used for statistical analyses. The measurement data were presented as mean ± standard deviation. Statistical differences between two groups were examined by Wilcoxon signed rank test or Mann-Whitney U test. Statistical differences across three or more groups were examined by Kruskal-Wallis H test. Correlations were

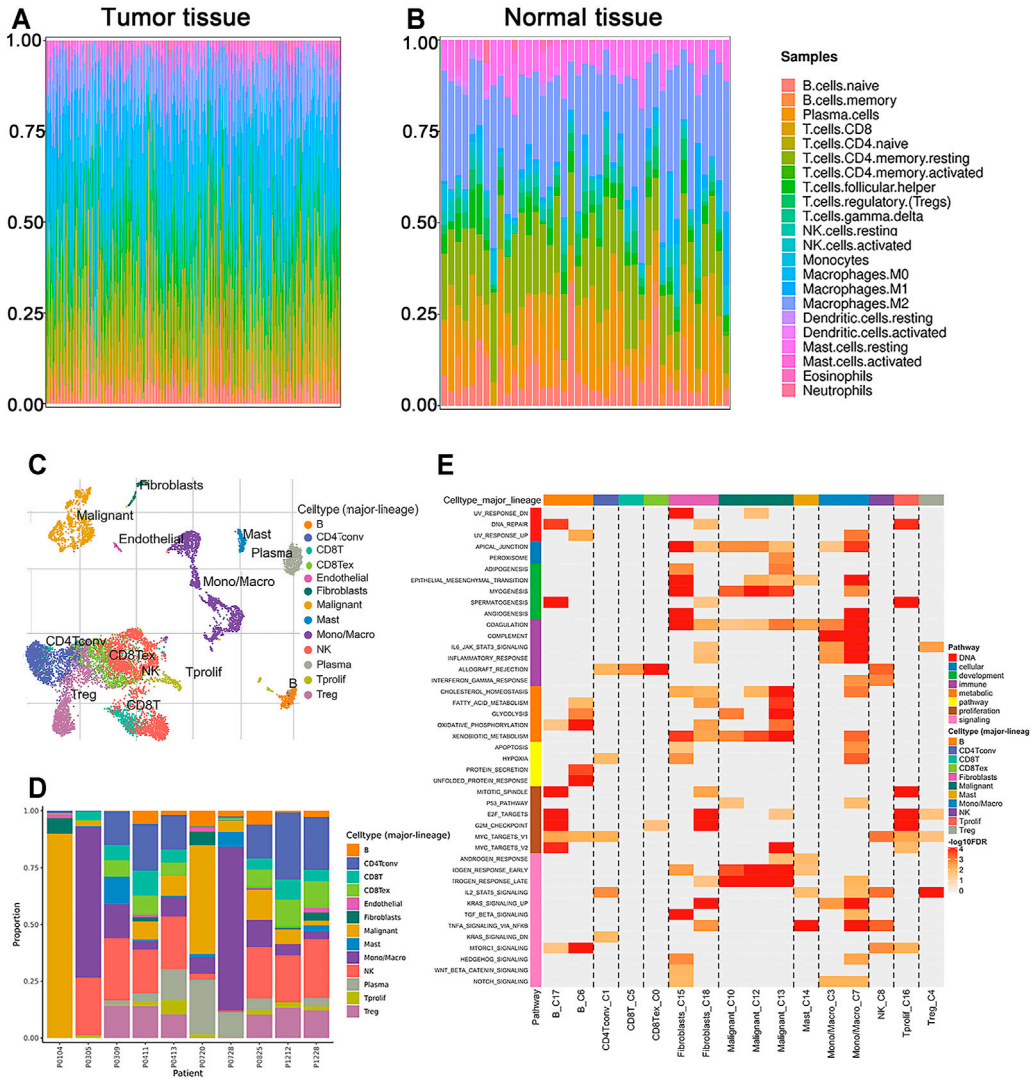

FIGURE 4 | The proportions of TIICs in TME and enrichment analysis by GSEA. **(A,B)** Composition of 22 immune cells in the tumor and normal tissues of CRC patients in TCGA cohort. **(C,D)** Components of TME at the single-cell resolution of CRC patients in GSE146771 cohort. **(E)** Enriched upregulated hallmark pathways in different immune cells.

examined with the Spearman rank correlation test (weakly correlation when R > 0.1, moderate correlation when R > 0.3, strong correlation when R > 0.5). Statistically significant differences were considered when $p < 0.05$.

RESULTS

Expression Profiles of SCG2 in Human Cancers

To evaluate SCG2 expression in various human cancers, we analyzed TCGA RNA-seq using TIMER database. The SCG2 expression levels were higher in breast invasive carcinoma (BRCA), cholangiocarcinoma (CHOL), head and neck cancer (HNSC), kidney renal clear cell carcinoma (KIRC), kidney renal papillary cell carcinoma (KIRP), liver hepatocellular carcinoma (LIHC), lung squamous cell carcinoma (LUSC) compared with adjacent normal tissues. However, SCG2 expression was significantly lower in colon adenocarcinoma (COAD), kidney chromophobe (KICH), prostate adenocarcinoma (PRAD), rectum adenocarcinoma (READ), stomach adenocarcinoma (STAD), uterine corpus endometrial carcinoma (UCEC) compared with adjacent normal tissues (**Figure 1A**). These results suggested SCG2 expressed abnormally in various tumor types.

We then assessed SCG2 mRNA expression levels in TCGA and GEO cohorts and found significantly lower SCG2 expression levels in cancer tissues than normal tissues (**Figures 1B,C**). SCG2 protein expression was also lower in cancer tissues than adjacent tissues in CPTAC database (**Figure 1D**). To confirm the

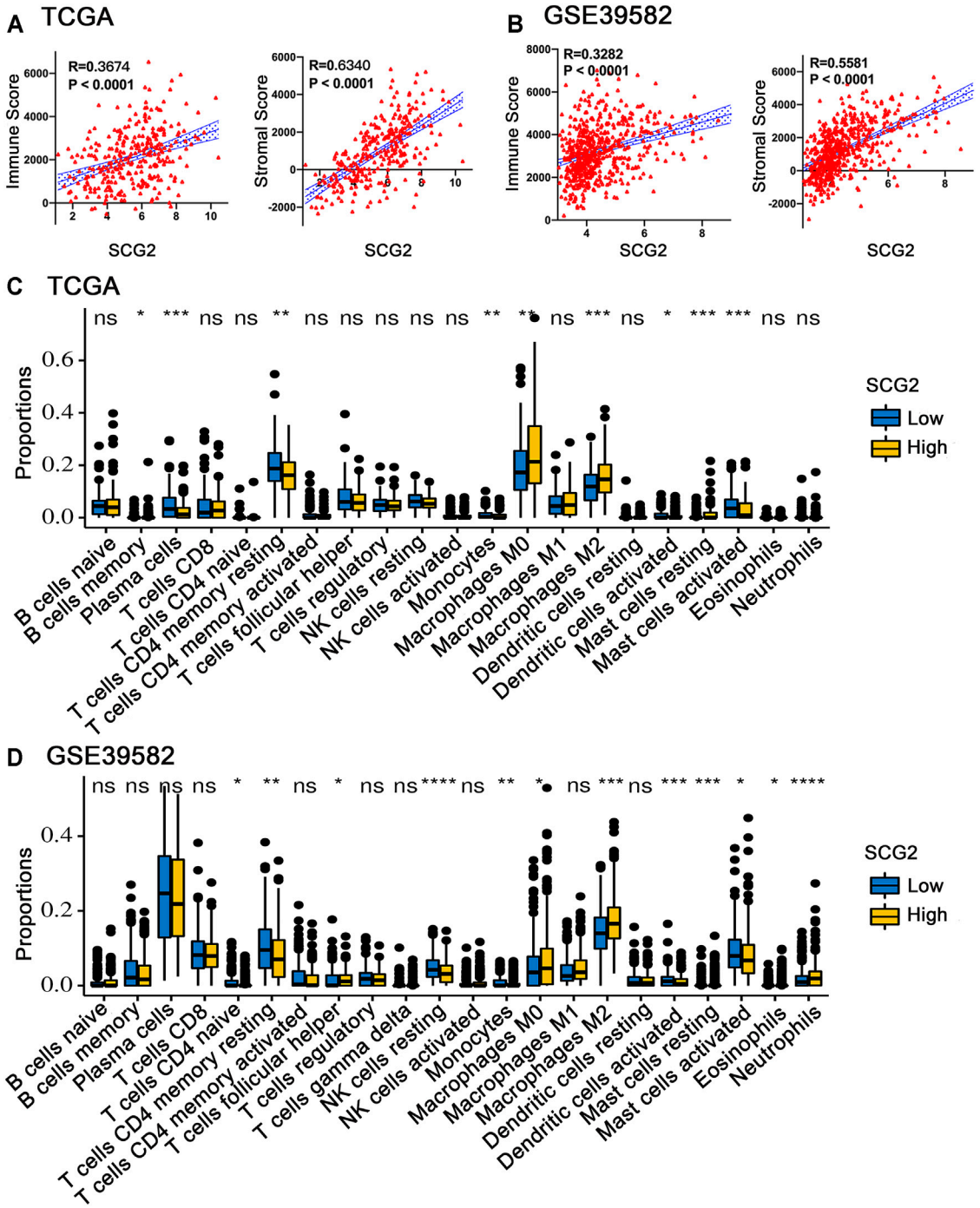

FIGURE 5 | Correlation between SCG2 expression and TIICs. **(A)** The correlation analysis between SCG2 expression and immune score, stromal score in TCGA cohort. **(B)** The correlation analysis between SCG2 expression and immune score, stromal score in GSE39582 cohort. **(C,D)** Twenty-two kinds of tumor-infiltrating immune cells are plotted according to the SCG2 expression level in TCGA and GSE39582 cohort. **(A,B)** Examined by Spearman's correlation analysis; **(C,D)** Examined by Mann-Whitney U test; $^{*}p < 0.05$, $^{**}p < 0.01$, $^{***}p < 0.001$, $^{****}p < 0.0001$.

expression profile data, we examined mRNA and protein levels in tumor and normal tissues of CRC patients using qRT-PCR and Western blot (**Figures 1E,F**).

The expression and distribution of SCG2 protein in tumor and adjacent tissues were monitored by immunofluorescence microscopy (**Figure 2**). In normal tissues, SCG2 was mainly

TABLE 2 | Correlation analysis between SCG2 and markers of immune cells.

Terms	Markers	None		Purity	
		Cor	*p*	Cor	*p*
T cell exhaustion	PDCD1 (PD-1)	0.226	***	0.244	***
	CTLA4	0.265	***	0.277	***
	CD274 (PD-L1)	0.280	***	0.289	***
	PDCD1LG2 (PD-L2)	0.379	***	0.376	***
	HAVCR2	0.435	***	0.36	***
	TIGIT	0.338	***	0.351	***
	BTLA	0.253	***	0.253	***
	CD244	0.091	0.052	0.104	0.036
	CD96	0.245	***	0.254	***
	IDO1	0.208	***	0.221	***
	KDR	0.509	***	0.521	***
	TGFBR1	0.554	***	0.545	***
	GZMB	0.045	0.341	0.062	0.215
	LAG3	0.206	***	0.232	***
Monocyte	CD86 (B7-2)	0.438	***	0.435	***
	CSF1R	0.426	***	0.418	***
TAM	CCL2	0.510	***	0.495	***
	CD68	0.340	***	0.348	***
	IL10	0.295	***	0.312	***
M1 Macrophage	IRF5	0.251	***	0.258	***
	INOS (NOS2)	0.222	***	0.189	**
	COX2 (PTGS2)	0.176	**	0.172	**
M2 Macrophage	CD163	0.467	***	0.465	***
	VSIG4	0.432	***	0.419	***
	MS4A4A	0.415	***	0.498	***
CD8+T	CD8A	0.227	***	0.240	***
	CD8B	0.135	*	0.139	*
CD4+T	CD4	0.398	***	0.396	***
	CD40LG (CD40L)	0.147	*	0.154	*
	CXCR4	0.432	***	0.436	***
T cell (general)	CD3D	0.124	*	0.133	*
	CD3E	0.230	***	0.252	***
	CD2	0.219	***	0.232	***
	CD28	0.350	***	0.356	***
Th1	TBX21	0.239	***	0.270	***
	STAT4	0.228	***	0.228	***
	STAT1	0.305	***	0.325	***
	IFNG	0.074	0.114	0.082	0.100
Th2	STAT6	0.141	*	0.142	*
	STAT5A	0.131	*	0.151	*
Th17	STAT3	0.278	***	0.293	***
	IL17A	0.238	***	0.239	***
Treg	FOXP3	0.311	***	0.321	***
	STAT5B	0.341	***	0.365	***
	TGFB1	0.473	***	0.472	***
	CD25 (IL2RA)	0.289	***	0.290	***
B cell	CD19	0.207	***	0.221	***
	CD79A	0.272	***	0.284	***
Neutrophils	CD66b (CEACAM8)	–0.271	***	–0.283	***
	CD11b (ITGAM)	0.423	***	0.427	***
	CCR7	0.243	***	0.264	***
Natural Killer cell	CD16 (FCGR3A)	0.476	***	0.473	***
	CD56 (NCAM1)	0.448	***	0.447	***
	KIR2DL1	0.052	0.266	0.063	0.206
	KIR2DL3	0.076	0.106	0.094	0.058
	KIR2DL4	0.069	0.139	0.084	0.090
	KIR3DL1	0.109	0.020	0.125	0.012
	KIR3DL2	0.111	0.018	0.131	*
Dendritic cell	HLA-DRA	0.267	***	0.266	***
	HLA-DPA1	0.328	***	0.324	***
	BOCA-1 (CD1C)	0.306	***	0.298	***
	BOCA-4 (NRP1)	0.605	***	0.612	***
	CD11c (ITGAX)	0.431	***	0.438	***

TAM, tumor-associated macrophage; Th, T helper cell; Treg, regulatory T cell.
None, correlation without adjustment; Purity, correlation adjusted by tumor purity.
Cor, R value of Spearman's correlation. *p < *0.01*, **p < *0.001*, ***p < *0.0001*.

distributed in colonic glands, possibly related to intestinal fluid secretion, whereas in tumor tissues, the intestinal mucosal tissues were destroyed and SCG2 expression decreased.

Prognostic Significance of SCG2 Expression in CRC

A univariate Cox survival analysis based on TCGA database indicated that TNM stage (p = 3.6e-04), Invasion depth (p = 0.031), Lymph node metastasis (p = 0.002), distant metastasis (p = 4.96e-07), and SCG2 expression (p = 0.008) were significant risk factors for overall survival (**Table 1**). Survival analysis using the Kaplan-Meier method showed that higher SCG2 expression was significantly correlated with shorter OS (p = 0.009) and DFS (p < 0.001) in TCGA cohorts (**Figures 3A,B**). SCG2 mRNA expression was associated with advanced TNM stage, T stage, and lymph invasion (**Figures 3C–F**). The forest plot based on multivariate Cox regression analysis showed that age (p = 0.002), M stage (p = 2.07e-04), and SCG2 expression (p = 0.016) were independent prognosis factors of CRC patients (**Figure 3G**). The above results were verified in independent cohort GSE39582 (**Table 1**; **Figures 3H–N**). Besides, we used the patients from our hospital to analyze the correlation between SCG2 expression and tumor histological grading, there was no significant difference (**Supplementary Figure S1A**). Overall, elevated SCG2 mRNA expression was significantly associated with poor prognosis and advanced clinicopathological parameters in CRC patients.

Analysis of SCG2 Co-expressed Genes

Genes in co-expression modules are always involved in same biological pathways (Stuart et al., 2003) and have disease predictive value (Yang et al., 2014). We performed genetic difference analysis based on SCG2 medium expression level. The heat map displayed differential expressed genes according to the Pearson correlation (**Supplementary Figure S1B**). We verified the correlations between SCG2 and MYH11, SYNPO2, DDR2, FABP4, TNS1 in TIMER (all R > 0.5, p < 0.0001, shown in **Supplementary Figures S1C–G**). Furthermore, high expressions of FABP4, DDR2, and TNS1 were associated with worse overall survival in CRC patients (**Supplementary Figures S1H–J**), MYH11 and TNS1 were associated with advanced clinical stage (**Supplementary Figures S1K,L**). It was possible that abnormal expression of SCG2 and these genes involved in CRC progression contributing to a worse prognosis.

To explore the potential molecular function of SCG2 in CRC, we performed KEGG pathway enrichment and GO analyses with the SCG2 co-expressed genes. KEGG enrichment analysis showed that these genes were associated with many signaling pathways (**Supplementary Table S1**), including known cancer-related pathways such as the PI3K-Akt signaling pathway and ECM-receptor interaction pathway. GO annotations further suggested these genes were associated with many biological processes (**Supplementary Table S2**)

We then performed PPI network analysis based on SCG2 co-expressed genes in TCGA and GSE39582 cohort (**Supplementary Figure S2A**). 56 seed and cluster genes in the network were

selected for further enrichment analysis (**Supplementary Figure S2B**). The result indicated that SCG2 and its co-expressed genes could directly or indirectly regulate various immune-related processes, including macrophage polarization (**Supplementary Figure S2C**).

GSEA Validates SCG2-Related Pathways

To further study the SCG2-associated signaling pathways in CRC, GSEA was performed between samples in low and high SCG2 expression groups. GSEA identified a total of 20 considerably upregulated hallmark pathways in the high SCG2 expression group (**Supplementary Table S3**). The tumor related pathways involved in tumorigenesis, tumor invasion, and metastasis included "Kras signaling up," "Hedgehog signaling," "Notch signaling," "Wnt beta catenin signaling," "TGF beta signaling," "Epithelial mesenchymal transition," and "Angiogenesis." The inflammatory and immune related pathways included "Complement," "IL2 STAT5 signaling," "Inflammatory response," "IL6 JAK STAT3 signaling," and "Allograft rejection." A summary of the enrichment results is shown in **Supplementary Figure S3**.

Evaluation of TIICs in CRC

TIIC is an integral part of tumor immune microenvironment (Deschoolmeester et al., 2010). In the current study, we estimated the proportion of twenty-two immune cells in the tumor and normal samples of TCGA using the CIBERSORT algorithm (**Figures 4A,B**). The composition of immune cells in TME varied significantly between both intragroup and intergroup. Additionally, the components of TME at single-cell resolution were investigated using TISCH database. TIICs of GSE146771 cohort and each patient's cell type proportion were displayed (**Figures 4C,D**). GSEA showed the enriched upregulated hallmark pathways in different cells (**Figure 4E**). Interestingly, the pathways enriched in monocyte-macrophages, "Epithelial mesenchymal transition," "Angiogenesis," "Complement," "Inflammatory response" and "IL6 JAK STAT3 signaling," were also significantly enriched in high SCG2 expression group (**Supplementary Figure S3**).

SCG2 Expression Significantly Correlate With TIICs in CRC

We conducted ESTIMATE analysis to explore the relationship between SCG2 and TME. The results suggested that high SCG2 expression was significantly associated with higher immune score and stromal store in CRC (**Figures 5A,B**). CIBERSORT analysis showed that the proportions of resting memory CD4 cells, monocytes, activated dendritic cells, and activated mast cells were downregulated in the high SCG2 expression group, whereas M0 macrophages, M2 macrophages, and resting mast cells were significantly upregulated in the high SCG2 group (**Figures 5C,D**). We further performed correlation analysis between SCG2 expression and various TIICs gene markers (**Table 2**). Significant correlations were observed between SCG2 expression and T cell exhaustion (immune checkpoint genes), general T cells, CD8 + T cells, CD4 + T cells, Th1, Tfh, Th17, Monocyte, M1 macrophages, M2 macrophages, natural killer (NK) cell, dendritic cells, neutrophils in CRC. The results demonstrated that SCG2 expression was correlated with TME and TIICs in CRC.

SCG2 Expression Associated With M2 Macrophage Polarization

The expressions of TAM and M2 macrophage marker genes were higher in monocyte-macrophage cells from tumor samples than from normal samples or peripheral blood mononuclear cell (PBMC) (**Supplementary Figure S4**). It indicated that, in the TME, macrophages tend to polarize towards M2 phenotype and differentiate into TAMs thus performed pro-tumoral functions. CIBERSORT analysis suggested the proportion of M2 macrophages increased in the SCG2 high expression group, but the proportion of M1 macrophages not significantly changed (**Figures 5C,D**). Additionally, clear correlations existed between SCG2 expression and the marker genes of M2 macrophages and TAMs (**Figures 6A–F**). The aforementioned results prompted us to hypothesize that SCG2 could promote the polarization of M2 macrophages. To validate this conjecture, we performed confocal immunofluorescence microscopy to confirm the colocalization between SCG2 and macrophage. As shown in **Figure 7**, SCG2 was colocalized with macrophages in tumor tissues, whereas there was no apparent colocalization in normal tissues. Altogether, the above results suggested that SCG2 might promote tumor infiltrating macrophages polarization toward M2 phenotype and play a pro-tumoral role in CRC.

DISCUSSION

CRC is a common health problem and one of the leading causes of cancer death worldwide (Ferlay et al., 2015). Despite numerous studies effort to improve our surgical treatment, radiotherapy, chemotherapy, and immunotherapy over the years, the prognosis of patients with advanced CRC remains poor (Seymour et al., 2007). In the present study, we explored the role of SCG2 in colorectal cancer, revealed its prognostic value, biological functions, associated pathways, and regulation of tumor immunity by analyzing open-access databases comprehensively.

SCG2 expression was remarkably decreased in tumor tissues compared with normal tissues of CRC. In normal tissues, our results showed that SCG2 was mainly distributed in colonic glands, which possibly related to intestinal fluid secretion. In contrast, in tumor tissues, the intestinal mucosal tissues were destroyed and total SCG2 expression was decreased. Additionally, SCG2 expression was associated with T, N, M, and TNM stages in CRC patients. Higher expression of SCG2 was significantly correlated to worse OS and DFS. Multivariate cox analysis also showed that SCG2 expression level was an independent prognostic marker in CRC.

To investigate the biological roles of SCG2, we carried out a gene differential expression analysis based on SCG2 median expression level. Then functional enrichment analyses were performed using the genes positively correlated with SCG2.

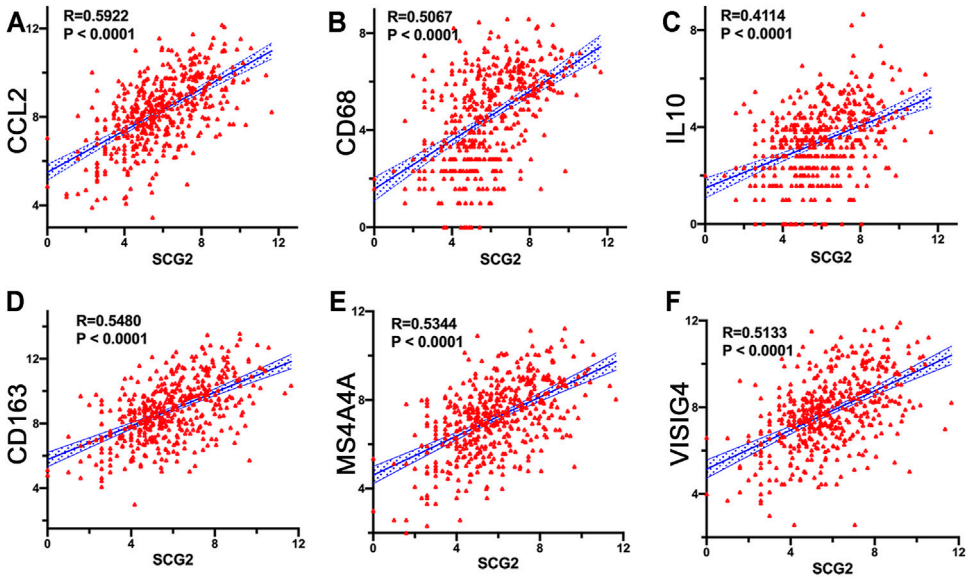

FIGURE 6 | Correlation of SCG2 expression with macrophage polarization. **(A–C)** Correlation analysis between SCG2 expression and TAM markers genes (CCL2, CD68, IL10). **(D–F)** Correlation analysis between SCG2 expression and M2 Macrophage markers genes (CD163, MS4A4A, VSIG4). Examined by Spearman's correlation analysis.

The results suggested that SCG2 was strongly correlated with MYH11, SYNPO2, DDR2, FABP4, and TNS1, which were all involved in tumorigenesis and inflammatory immune response (Gan et al., 2019; Gao et al., 2020; Liu et al., 2020; Matrai et al., 2020; Sun et al., 2020; Tian et al., 2020). Higher expression of these genes might associate with worse survival and higher clinical stage of CRC patients.

Functional enrichment analysis revealed that SCG2 was correlated with several tumorigenesis related pathways such as "PI3K-Akt," "Wnt," and "TGF-beta pathways" (Schatoff et al., 2017; Koveitypour et al., 2019). A few pathways related to tumor metastasis included "ECM-receptor interaction" and "focal adhesion" (Gu et al., 2018; Machackova et al., 2020). Furthermore, numerous genes were involved in immune-related processes. "Regulation of actin cytoskeleton" plays a vital role in immune response, tumor migration, and invasion (Schmitz et al., 2000; C. Wickramarachchi et al., 2010); "B cell receptor" is initiated via interaction between B cell receptor and specific antigens and plays a crucial role in immune system (Li et al., 2019); "leukocyte transendothelial migration" tightly regulates inflammation and is associated with the transient crossing of leukocytes through the blood vessel wall (Schimmel et al., 2017). These results indicated that SCG2 might have regulatory roles in tumor progression and immune moderation.

The result of GSEA suggested high SCG2 expression might activate the IL6 JAK STAT3 signaling pathway and IL2–STAT5 signaling pathway in CRC patients. Previous studies have shown that STAT3 was activated in TIICs, including TAMs, amplifying immune suppression, and targeting IL-6 to regulate STAT3 signaling pathway was considered a potential immunotherapy for CRC (Wang and Sun, 2014; Verdeil et al., 2019). STAT5 also played a critical role in tumor immunity, regulated Treg cell's function and development. Consistent activation of STAT5 was associated with suppressing antitumor immunity and increased tumor proliferation and invasion (Rani and Murphy, 2016). These findings indicated SCG2 might relate to the efficiency of immunotherapy in CRC patients.

The TIICs in TME are critical players in tumor progression, modulate tumor inflammation and metastasis variously (Gonzalez et al., 2018). We quantified each CRC sample's immune and stromal cell infiltration levels using immune and stromal scores evaluated by ESTIMATE algorithm, respectively. Our results showed the two scores were significantly correlated with SCG2 expression in CRC patients. Some studies have demonstrated that both immune and stromal scores were associated with poor prognosis in CRC patients (Liu et al., 2020; Yuan et al., 2020).

CIBERSORT analysis showed that multiple immune cells had significantly different proportions between SCG2 high and low expression groups. Notably, the proportions of M0 and M2 macrophages in the SCG2 high expression group were considerably higher than those in the SCG2 low expression group, whereas M1 macrophages showed no significant change. Besides, SCG2 expression was moderately or strongly correlated with M2 macrophage marker genes and TAM marker genes but was slightly correlated with M1 macrophage marker genes. Similarly, confocal immunofluorescence microscopy showed SCG2 had an apparent colocalization with macrophages in tumor tissues. The previous study has demonstrated that SN, SCG2 derived peptide, could induce macrophage accumulation and angiogenesis (Liu et al., 2018). These results indicated that high expression of SCG2 might promote M0 macrophages polarize to M2 and eventually

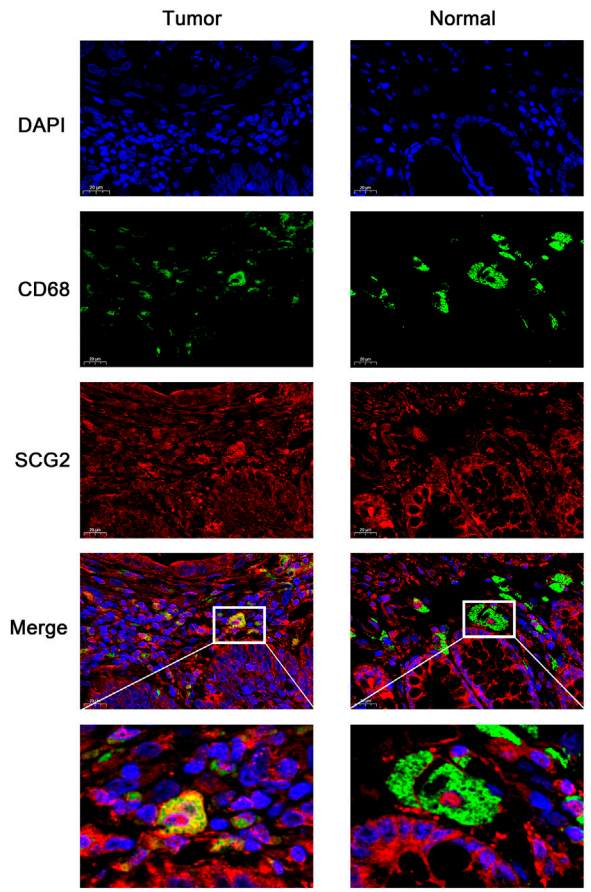

FIGURE 7 | Immunofluorescence images of DAPI (blue), CD68 (green), SCG2 (red), and the merge photos in normal tissues and cancer tissues of CRC patients.

differentiate into TAMs, enhancing tumor cell invasion, metastasis, angiogenesis, and inhibiting the anti-tumoral immune surveillance (Kim and Bae, 2016), predict a worse prognosis of CRC patients (Waniczek et al., 2017).

We also found a positive correlation between SCG2 expression and immune checkpoint markers PD-1, PD-L1/2, CTLA-4, TIM-3, TIGIT in CRC patients. The binding of PD-L1/2 to the PD-1 receptor leads to T-cell function's deactivation, allowing tumor cells to evade immune attacks (Chen and Han, 2015). Upregulation of PD-1 and Tim-3 was associated with the poor prognosis of CRC patients in stage I-III (Kuai et al., 2020), and high expression of TIGIT was associated with advanced TNM stage and poor DFS in CRC patients with mismatch repair deficiency (Zhou et al., 2020). The correlations between SCG2 expression and immune checkpoint genes indicated a potential mechanism of SCG2 regulation on T cell exhaustion and provided a new target for tumor immunotherapy.

However, our study had some limitations. First, we conducted analysis mainly based on samples from TCGA and GEO cohorts, it would be better to confirm the findings in a larger sample size. Second, genetic difference analysis based on RNA-seq might not be precise. Additionally, the mechanisms of SCG2 regulating the infiltration of immune cells and macrophage polarization require further experimental investigation, which would be a future direction for our research.

In conclusion, our study revealed that overexpression of SCG2 predicted poor prognosis and advanced clinical stage in CRC patients. SCG2 was associated with tumor immune cells infiltration, promoted M2 macrophage polarization, and correlated with immune checkpoint expression in CRC. In summary, SCG2 played a critical role in the regulation of tumor immunity and made it a potential biomarker and therapeutic target in CRC.

DATA AVAILABILITY STATEMENT

The datasets presented in this study can be found in online repositories. The names of the repository/repositories and accession number(s) can be found in the article/Supplementary Material.

ETHICS STATEMENT

The studies involving human participants were reviewed and approved by the Zhongnan Hospital Ethics Committee. The patients/participants provided their written informed consent to participate in this study.

AUTHOR CONTRIBUTIONS

HoW: Data acquisition, Methodology, Writing -original draft. JY: Software, Writing–review, and editing. YH: Resources. AR: Softwares. HzW: Visualization. ML: Softwares.

FUNDING

This work was supported by the Hubei Provincial National Natural Science Foundation of China (Project 2018CFB446) and the Health Commission of Hubei Province Scientific Research (Project WJ 2019H025).

ACKNOWLEDGMENTS

We acknowledge the public database TIMER, TCGA, GEO, CPTAC, TISCH for free use.

SUPPLEMENTARY MATERIAL

The Supplementary Material for this article can be found online at: https://www.frontiersin.org/articles/10.3389/fcell.2021.795133/full#supplementary-material

REFERENCES

Albrecht-Schgoer, K., Schgoer, W., Holfeld, J., Theurl, M., Wiedemann, D., Steger, C., et al. (2012). The Angiogenic Factor Secretoneurin Induces Coronary Angiogenesis in a Model of Myocardial Infarction by Stimulation of Vascular Endothelial Growth Factor Signaling in Endothelial Cells. *Circulation* 126 (21), 2491–2501. doi:10.1161/circulationaha.111.076950

Beuret, N., Stettler, H., Renold, A., Rutishauser, J., and Spiess, M. (2004). Expression of Regulated Secretory Proteins Is Sufficient to Generate Granule-like Structures in Constitutively Secreting Cells. *J. Biol. Chem.* 279 (19), 20242–20249. doi:10.1074/jbc.m310613200

Bray, F., Ferlay, J., Soerjomataram, I., Siegel, R. L., Torre, L. A., and Jemal, A. (2018). Global Cancer Statistics 2018: GLOBOCAN Estimates of Incidence and Mortality Worldwide for 36 Cancers in 185 Countries. *CA: A Cancer J. Clinicians* 68 (6), 394–424. doi:10.3322/caac.21492

Chen, L., and Han, X. (2015). Anti-PD-1/PD-L1 Therapy of Human Cancer: Past, Present, and Future. *J. Clin. Invest.* 125 (9), 3384–3391. doi:10.1172/jci80011

Chung, K. Y., Gore, I., Fong, L., Venook, A., Beck, S. B., Dorazio, P., et al. (2010). Phase II Study of the Anti-cytotoxic T-Lymphocyte-Associated Antigen 4 Monoclonal Antibody, Tremelimumab, in Patients with Refractory Metastatic Colorectal Cancer. *Jco* 28 (21), 3485–3490. doi:10.1200/jco.2010.28.3994

Cury, S. S., de Moraes, D., Freire, P. P., de Oliveira, G., Marques, D. V. P., Fernandez, G. J., et al. (2019). Tumor Transcriptome Reveals High Expression of IL-8 in Non-small Cell Lung Cancer Patients with Low Pectoralis Muscle Area and Reduced Survival. *Cancers (Basel)* 11 (9), 1251. doi:10.3390/cancers11091251

C. Wickramarachchi, D., Theofilopoulos, A. N., and Kono, D. H. (2010). Immune Pathology Associated with Altered Actin Cytoskeleton Regulation. *Autoimmunity* 43 (1), 64–75. doi:10.3109/08916930903374634

Deschoolmeester, V., Baay, M., Van Marck, E., Weyler, J., Vermeulen, P., Lardon, F., et al. (2010). Tumor Infiltrating Lymphocytes: an Intriguing Player in the Survival of Colorectal Cancer Patients. *BMC Immunol.* 11, 19. doi:10.1186/1471-2172-11-19

Ferlay, J., Soerjomataram, I., Dikshit, R., Eser, S., Mathers, C., Rebelo, M., et al. (2015). Cancer Incidence and Mortality Worldwide: Sources, Methods and Major Patterns in GLOBOCAN 2012. *Int. J. Cancer* 136 (5), E359–E386. doi:10.1002/ijc.29210

Gan, L., Camarena, V., Mustafi, S., and Wang, G. (2019). Vitamin C Inhibits Triple-Negative Breast Cancer Metastasis by Affecting the Expression of YAP1 and Synaptopodin 2. *Nutrients* 11 (12), 2997. doi:10.3390/nu11122997

Gao, J., Zhang, H.-P., Sun, Y.-H., Guo, W.-Z., Li, J., Tang, H.-W., et al. (2020). Synaptopodin-2 Promotes Hepatocellular Carcinoma Metastasis via Calcineurin-Induced Nuclear-Cytoplasmic Translocation. *Cancer Lett.* 482, 8–18. doi:10.1016/j.canlet.2020.04.005

Gonzalez, H., Hagerling, C., and Werb, Z. (2018). Roles of the Immune System in Cancer: from Tumor Initiation to Metastatic Progression. *Genes Dev.* 32 (19-20), 1267–1284. doi:10.1101/gad.314617.118

Gu, C., Wang, X., Long, T., Wang, X., Zhong, Y., Ma, Y., et al. (2018). FSTL1 Interacts with VIM and Promotes Colorectal Cancer Metastasis via Activating the Focal Adhesion Signalling Pathway. *Cell Death Dis.* 9 (6), 654. doi:10.1038/s41419-018-0695-6

Guillemot, J., Thouënnon, E., Guérin, M., Vallet-Erdtmann, V., Ravni, A., Montéro-Hadjadje, M., et al. (2012). Differential Expression and Processing of Secretogranin II in Relation to the Status of Pheochromocytoma: Implications for the Production of the Tumoral Marker EM66. *J. Mol. Endocrinol.* 48 (2), 115–127. doi:10.1530/jme-11-0077

Halama, N., Michel, S., Kloor, M., Zoernig, I., Benner, A., Spille, A., et al. (2011). Localization and Density of Immune Cells in the Invasive Margin of Human Colorectal Cancer Liver Metastases Are Prognostic for Response to Chemotherapy. *Cancer Res.* 71 (17), 5670–5677. doi:10.1158/0008-5472.can-11-0268

Hannon, P. R., Duffy, D. M., Rosewell, K. L., Brännström, M., Akin, J. W., and Curry, T. E. (2018). Ovulatory Induction of SCG2 in Human, Nonhuman Primate, and Rodent Granulosa Cells Stimulates Ovarian Angiogenesis. *Endocrinology* 159 (6), 2447–2458. doi:10.1210/en.2018-00020

Kim, J., and Bae, J.-S. (2016). Tumor-Associated Macrophages and Neutrophils in Tumor Microenvironment. *Mediators Inflamm.* 2016, 6058147. doi:10.1155/2016/6058147

Koveitypour, Z., Panahi, F., Vakilian, M., Peymani, M., Seyed Forootan, F., Nasr Esfahani, M. H., et al. (2019). Signaling Pathways Involved in Colorectal Cancer Progression. *Cell Biosci.* 9, 97. doi:10.1186/s13578-019-0361-4

Kuai, W., Xu, X., Yan, J., Zhao, W., Li, Y., Wang, B., et al. (2020). Prognostic Impact of PD-1 and Tim-3 Expression in Tumor Tissue in Stage I-III Colorectal Cancer. *Biomed. Res. Int.* 2020, 5294043. doi:10.1155/2020/5294043

Le, D. T., Uram, J. N., Wang, H., Bartlett, B. R., Kemberling, H., Eyring, A. D., et al. (2015). PD-1 Blockade in Tumors with Mismatch-Repair Deficiency. *N. Engl. J. Med.* 372 (26), 2509–2520. doi:10.1056/NEJMoa1500596

Li, J., Yin, W., Jing, Y., Kang, D., Yang, L., Cheng, J., et al. (2019). The Coordination between B Cell Receptor Signaling and the Actin Cytoskeleton during B Cell Activation. *Front. Immunol.* 9, 3096. doi:10.3389/fimmu.2018.03096

Li, T., Fan, J., Wang, B., Traugh, N., Chen, Q., Liu, J. S., et al. (2017). TIMER: A Web Server for Comprehensive Analysis of Tumor-Infiltrating Immune Cells. *Cancer Res.* 77 (21), e108–e110. doi:10.1158/0008-5472.can-17-0307

Liu, J. W., Yu, F., Tan, Y.-F., Huo, J.-P., Liu, Z., Wang, X.-J., et al. (2020). Profiling of Tumor Microenvironment Components Identifies Five Stroma-Related Genes with Prognostic Implications in Colorectal Cancer. *Cancer Biother. Radiopharm.* doi:10.1089/cbr.2020.4118

Liu, W., Wang, F., Zhao, M., Fan, Y., Cai, W., and Luo, M. (2018). The Neuropeptide Secretoneurin Exerts a Direct Effect on Arteriogenesis *In Vivo* and *In Vitro*. *Anat. Rec.* 301 (11), 1917–1927. doi:10.1002/ar.23929

Luebeck, E. G., Curtius, K., Jeon, J., and Hazelton, W. D. (2013). Impact of Tumor Progression on Cancer Incidence Curves. *Cancer Res.* 73 (3), 1086–1096. doi:10.1158/0008-5472.can-12-2198

Luo, Y., Chen, L., Zhou, Q., Xiong, Y., Wang, G., Liu, X., et al. (2020). Identification of a Prognostic Gene Signature Based on an Immunogenomic Landscape Analysis of Bladder Cancer. *J. Cel Mol Med.* 24 (22), 13370–13382. doi:10.1111/jcmm.15960

Machackova, T., Vychytilova-Faltejskova, P., Souckova, K., Trachtova, K., Brchnelova, D., Svoboda, M., et al. (2020). MiR-215-5p Reduces Liver Metastasis in an Experimental Model of Colorectal Cancer through Regulation of ECM-Receptor Interactions and Focal Adhesion. *Cancers (Basel)* 12 (12), 3518. doi:10.3390/cancers12123518

Matrai, C., Motanagh, S., Mirabelli, S., Ma, L., He, B., Chapman-Davis, E., et al. (2020). Molecular Profiles of Mixed Endometrial Carcinoma. *Am. J. Surg. Pathol.* 44 (8), 1104–1111. doi:10.1097/PAS.0000000000001519

Meyerson, M., Gabriel, S., and Getz, G. (2010). Advances in Understanding Cancer Genomes through Second-Generation Sequencing. *Nat. Rev. Genet.* 11 (10), 685–696. doi:10.1038/nrg2841

Miller, K. D., Siegel, R. L., Lin, C. C., Mariotto, A. B., Kramer, J. L., Rowland, J. H., et al. (20162016). Cancer Treatment and Survivorship Statistics, 2016. *CA: A Cancer J. Clinicians* 66 (4), 271–289. doi:10.3322/caac.21349

Newman, A. M., Liu, C. L., Green, M. R., Gentles, A. J., Feng, W., Xu, Y., et al. (2015). Robust Enumeration of Cell Subsets from Tissue Expression Profiles. *Nat. Methods* 12 (5), 453–457. doi:10.1038/nmeth.3337

Overman, M. J., Lonardi, S., Wong, K. Y. M., Lenz, H.-J., Gelsomino, F., Aglietta, M., et al. (2018). Durable Clinical Benefit with Nivolumab Plus Ipilimumab in DNA Mismatch Repair-Deficient/Microsatellite Instability-High Metastatic Colorectal Cancer. *Jco* 36 (8), 773–779. doi:10.1200/jco.2017.76.9901

Rani, A., and Murphy, J. J. (2016). STAT5 in Cancer and Immunity. *J. Interferon Cytokine Res.* 36 (4), 226–237. doi:10.1089/jir.2015.0054

Rotte, A. (2019). Combination of CTLA-4 and PD-1 Blockers for Treatment of Cancer. *J. Exp. Clin. Cancer Res.* 38 (1), 255. doi:10.1186/s13046-019-1259-z

Schatoff, E. M., Leach, B. I., and Dow, L. E. (2017). Wnt Signaling and Colorectal Cancer. *Curr. Colorectal Cancer Rep.* 13 (2), 101–110. doi:10.1007/s11888-017-0354-9

Schimmel, L., Heemskerk, N., and van Buul, J. D. (2017). Leukocyte Transendothelial Migration: A Local Affair. *Small GTPases* 8 (1), 1–15. doi:10.1080/21541248.2016.1197872

Schmitz, A. A. P., Govek, E.-E., Böttner, B., and Van Aelst, L. (2000). Rho GTPases: Signaling, Migration, and Invasion. *Exp. Cel Res.* 261 (1), 1–12. doi:10.1006/excr.2000.5049

Seymour, M. T., Maughan, T. S., Ledermann, J. A., Topham, C., James, R., Gwyther, S. J., et al. (2007). Different Strategies of Sequential and Combination

Chemotherapy for Patients with Poor Prognosis Advanced Colorectal Cancer (MRC FOCUS): a Randomised Controlled Trial. *The Lancet* 370 (9582), 143–152. doi:10.1016/s0140-6736(07)61087-3

Siegel, R. L., Miller, K. D., Goding Sauer, A., Fedewa, S. A., Butterly, L. F., Anderson, J. C., et al. (2020). Colorectal Cancer Statistics, 2020. *CA A. Cancer J. Clin.* 70 (3), 145–164. doi:10.3322/caac.21601

Stuart, J. M., Segal, E., Koller, D., and Kim, S. K. (2003). A Gene-Coexpression Network for Global Discovery of Conserved Genetic Modules. *Science* 302 (5643), 249–255. doi:10.1126/science.1087447

Sun, D., Wang, J., Han, Y., Dong, X., Ge, J., Zheng, R., et al. (2021). TISCH: a Comprehensive Web Resource Enabling Interactive Single-Cell Transcriptome Visualization of Tumor Microenvironment. *Nucleic Acids Res.* 49 (D1), D1420–D1430. doi:10.1093/nar/gkaa1020

Sun, Y. L., Zhang, Y., Guo, Y. C., Yang, Z. H., and Xu, Y. C. (2020). A Prognostic Model Based on Six Metabolism-Related Genes in Colorectal Cancer. *Biomed. Res. Int.* 2020, 5974350. doi:10.1155/2020/5974350

Tian, W., Zhang, W., Zhang, Y., Zhu, T., Hua, Y., Li, H., et al. (2020). FABP4 Promotes Invasion and Metastasis of colon Cancer by Regulating Fatty Acid Transport. *Cancer Cel Int.* 20, 512. doi:10.1186/s12935-020-01582-4

Troger, J., Theurl, M., Kirchmair, R., Pasqua, T., Tota, B., Angelone, T., et al. (2017). Granin-derived Peptides. *Prog. Neurobiol.* 154, 37–61. doi:10.1016/j.pneurobio.2017.04.003

Verdeil, G., Lawrence, T., Schmitt-Verhulst, A. M., and Auphan-Anezin, N. (2019). Targeting STAT3 and STAT5 in Tumor-Associated Immune Cells to Improve Immunotherapy. *Cancers (Basel)* 11 (12), 1832. doi:10.3390/cancers11121832

Wang, S.-W., and Sun, Y.-M. (2014). The IL-6/JAK/STAT3 Pathway: Potential Therapeutic Strategies in Treating Colorectal Cancer. *Int. J. Oncol.* 44 (4), 1032–1040. doi:10.3892/ijo.2014.2259

Wang, Z., and Chen, X. (2020). Establishment and Validation of an Immune-Associated Signature in Lung Adenocarcinoma. *Int. Immunopharmacology* 88, 106867. doi:10.1016/j.intimp.2020.106867

Waniczek, D., Lorenc, Z., Śnietura, M., Wesecki, M., Kopec, A., and Muc-Wierzgoń, M. (2017). Tumor-Associated Macrophages and Regulatory T Cells Infiltration and the Clinical Outcome in Colorectal Cancer. *Arch. Immunol. Ther. Exp.* 65 (5), 445–454. doi:10.1007/s00005-017-0463-9

Whiteaker, J. R., au, fnm., Halusa, G. N., Hoofnagle, A. N., Sharma, V., MacLean, B., et al. (2014). CPTAC Assay Portal: a Repository of Targeted Proteomic Assays. *Nat. Methods* 11 (7), 703–704. doi:10.1038/nmeth.3002

Yang, Y., Han, L., Yuan, Y., Li, J., Hei, N., and Liang, H. (2014). Gene Co-expression Network Analysis Reveals Common System-Level Properties of Prognostic Genes across Cancer Types. *Nat. Commun.* 5, 3231. doi:10.1038/ncomms4231

Yoshihara, K., Shahmoradgoli, M., Martínez, E., Vegesna, R., Kim, H., Torres-Garcia, W., et al. (2013). Inferring Tumour Purity and Stromal and Immune Cell Admixture from Expression Data. *Nat. Commun.* 4, 2612. doi:10.1038/ncomms3612

Yuan, W., Cai, W., Huang, X., and Peng, S. (2020). Prognostic Value of Immune Scores in the Microenvironment of Colorectal Cancer. *Oncol. Lett.* 20 (5), 1. doi:10.3892/ol.2020.12119

Zhou, X., Ding, X., Li, H., Yang, C., Ma, Z., Xu, G., et al. (2020). Upregulation of TIGIT and PD-1 in Colorectal Cancer with Mismatch-Repair Deficiency. *Immunological Invest.* 50, 338–355. doi:10.1080/08820139.2020.1758130

Conflict of Interest: The authors declare that the research was conducted in the absence of any commercial or financial relationships that could be construed as a potential conflict of interest.

Publisher's Note: All claims expressed in this article are solely those of the authors and do not necessarily represent those of their affiliated organizations, or those of the publisher, the editors and the reviewers. Any product that may be evaluated in this article, or claim that may be made by its manufacturer, is not guaranteed or endorsed by the publisher.

frontiers in Cell and Developmental Biology

ORIGINAL RESEARCH
published: 20 January 2022
doi: 10.3389/fcell.2021.783527

Identification of Tumor Antigens and Design of mRNA Vaccine for Colorectal Cancer Based on the Immune Subtype

*Cong Liu[1], Dimitri Papukashvili[1], Yu Dong[2], Xingyun Wang[1], Xing Hu[1], Nuo Yang[1], Jie Cai[1], Fengfei Xie[1], Nino Rcheulishvili[1] and Peng George Wang[1]**

[1]School of Medicine, Southern University of Science and Technology, Shenzhen, China, [2]Department of Biomedical Engineering, Southern University of Science and Technology, Shenzhen, China

mRNA vaccines have become a promising alternative to conventional cancer immunotherapy approaches. However, its application on colorectal cancer (CRC) remains poorly understood. We herein identified potential antigens for designing an effective mRNA vaccine, further to build an immune landscape for the accurate selection of patients for mRNA vaccine therapy. Raw transcriptome data from The Cancer Genome Atlas (TCGA) and Gene Expression Omnibus (GEO) databases were retrieved. Consensus clustering algorithm was applied to divide the CRC samples into four immune subtypes. Immunogenomics analysis was further integrated to characterize the immune microenvironment of each immune subtype. Six tumor antigens were found to be associated with poor prognosis and infiltration of antigen-presenting cells (APCs) in CRC patients. Furthermore, each of the immune subtypes showed differential cellular and molecular features. The IS2 and IS4 exhibited significantly improved survival and higher immune cell infiltration compared with IS1 and IS3. Immune checkpoint molecules and human leukocyte antigen also showed significant differential expression in four immune subtypes. Moreover, we performed graph structure learning-based dimensionality reduction to visualize the immune landscape of CRC. Our results revealed a complex immune landscape that may provide directions for mRNA vaccine treatment of CRC and define appropriate vaccination patients.

Keywords: mRNA vaccine, colorectal cancer, tumor immune microenvironment, tumor antigens, immune subtype, immune landscape

OPEN ACCESS

Edited by:
Shilpa S. Dhar, University of Texas MD Anderson Cancer Center, United States

Reviewed by:
Marcio Chaim Bajgelman, National Center for Research in Energy and Materials, Brazil
Xin Wang, The Chinese University of Hong Kong, China

****Correspondence:***
Peng George Wang
wangp6@sustech.edu.cn

Specialty section:
This article was submitted to Molecular and Cellular Oncology, a section of the journal Frontiers in Cell and Developmental Biology

Received: *26 September 2021*
Accepted: *31 December 2021*
Published: *20 January 2022*

Citation:
Liu C, Papukashvili D, Dong Y, Wang X, Hu X, Yang N, Cai J, Xie F, Rcheulishvili N and Wang PG (2022) Identification of Tumor Antigens and Design of mRNA Vaccine for Colorectal Cancer Based on the Immune Subtype. Front. Cell Dev. Biol. 9:783527. doi: 10.3389/fcell.2021.783527

INTRODUCTION

Colorectal cancer (CRC) is the third most frequently diagnosed tumor, with the second highest mortality rate worldwide (Sung et al., 2021). Currently, effective treatments for CRC mainly include surgical resection, chemotherapy, and radiotherapy (van der Stok et al., 2017). However, morbidity and mortality remain high as approximately 80% of CRC patients show recurrence during the first 3 years (Augestad et al., 2017). Thus, new therapeutic strategies are needed to enhance the survival rate of patients with CRC.

To date, cancer immunotherapies, such as immune checkpoint blockade (ICB) and chimeric antigen receptor T (CAR-T) cell therapy have gained tremendous success (Hargadon et al., 2018;

Pantin and Battiwalla, 2020). Messenger RNA (mRNA) vaccine has recently represented a promising alternative to conventional immunotherapy for anti-cancer treatments. *In vitro* transcribed (IVT) mRNA-based gene therapy was initially considered to be an unsuitable approach due to its high immunogenicity and instability. In recent years, along with the development of mRNA synthesis, chemical modification of mRNA and advancing the technology of delivery systems have greatly improved mRNA stability and translation efficacy. IVT mRNA can be designed to express proteins transiently by ensuring that its structure resembles the natural mRNA (Sahin et al., 2014; Kowalzik et al., 2021). Moreover, immunogenicity has gradually become controllable that is of great application prospect in tumor immunotherapy and other biological treatments (Kallen et al., 2013). Compared with the currently available drugs, the mRNA-based approach has a number of advantages: 1) mRNA is produced and purified *in vitro*, without any need of the complex process of protein drug and viral vector preparation; 2) IVT mRNA production process is highly versatile. The production of different target proteins is feasible, hence, time-saving for drug development and efficiency improvement; 3) mRNA only needs to enter the cytoplasm to be translated into protein without entering the nucleus, so no gene insertion and integration take place that improves the safety of the drug (De Keersmaecker et al., 2020); 4) The half-life can be changed by modulating the sequence and the delivery vector (Pardi et al., 2018). mRNA encoding tumor antigens transported via lipid nanoparticle enters into the antigen presenting cells (APCs) and is expressed into the targeted antigen. The expressed tumor antigens can be presented on the surface of APCs by major histocompatibility complexes (MHC) to evoke an anti-tumor response (Miao et al., 2021). Clinical trials have demonstrated that although the protein expression of mRNA is transient, it is effective for tumor immunotherapy applications. In the clinical trials, mRNA vaccines have been applied to treat solid tumors, including non-small cell lung cancers, melanoma, prostate cancer, and glioblastoma (Sebastian et al., 2014; Kubler et al., 2015; Papachristofilou et al., 2019; Batich et al., 2020). mRNA cancer vaccines are combined with ICB to further improve antitumor efficacy (Miao et al., 2021). A great deal of clinical trials has been started and consistently verified the feasibility and suitability of mRNA vaccines for cancer treatment.

Due to the high heterogeneity of CRC at the genetic and molecular level, which affects the efficacy of immunotherapy, there is no mRNA vaccine developed against CRC to date. The effectiveness of mRNA vaccines critically depends on making the antigen(s) of interest available to professional APCs.

The present study aims to predict the potential tumor antigen of CRC for designing an mRNA vaccine. Furthermore, the anti-CRC mRNA cancer vaccine is designed and the immune subtype for identifying suitable CRC patients for vaccination is also explored. Each of the four immune subtypes was correlated with different molecular, cellular features, and clinical outcomes. Our results might provide the theoretical basis of developing an mRNA cancer vaccine and facilitate the selection of optimal CRC patients for vaccination.

MATERIALS AND METHODS

Patients and Datasets

The RNA sequencing (RNA-seq) gene expression data of 612 CRC samples and their clinicopathologic information were downloaded from TCGA database (https://gdc-portal.nci.nih.gov/) as our discovery cohort. RNA-seq data of 598 CRC samples (GSE39582) and the clinical information were downloaded from the Gene Expression Omnibus (GEO) database (https://www.ncbi.nlm.nih.gov/geo/). An independent cohort GSE39582 was used for further validation. Building on TCGA datasets, gene mutation information was obtained via secondary databases like cBioportal (http://www.cbioportal.org/). To discover unbiased immune subtypes, we identified 1,989 IRGs in five different categories including single-cell RNA-seq data, the gene of co-stimulatory and co-inhibitory molecules, the gene of cytokine and cytokine receptors, genes involved in antigen processing and presentation, and other immune-related genes (Chen et al., 2019; Li et al., 2019).

cBioPortal Database Analysis

The cBioPortal (http://www.cbioportal.org/) was used to analyze and visualize cancer genomics data sets including copy number variation and mutation (Cerami et al., 2012). The genetic alterations of potential tumor antigens against tumors were obtained from cBioPortal based on 612 CRC samples in TCGA.

GEPIA Database Analysis

The online database Gene Expression Profiling Interactive Analysis (GEPIA2) (http://gepia2.cancer-pku.cn/) which is based on samples from the TCGA and the GTEx (Genotype-Tissue Expression) databases was used for gene expression analysis to further clarify the relationship between tumor antigen gene expression and CRC prognosis (Tang et al., 2017). ANOVA was used for differential expression analysis to compare the tumor to paired normal samples. The chromosomal distribution of over- or under-expressed genes were plotted in differential genes with $|Log2FC| > 1$ and q-value < 0.01. Kaplan–Meier estimates of OS and RFS were performed to evaluate the prognostic value of identified tumor antigens.

TIMER Database Analysis

To assess the correlation between the infiltration level of APCs and the expression of the identified tumor antigens TIMER database was used. (https://cistrome.shinyapps.io/timer/). TIMER includes 10,897 samples across 32 cancer types from TCGA to estimate the abundance of immune infiltrates. Prognostic gene expression data was used to calculate the

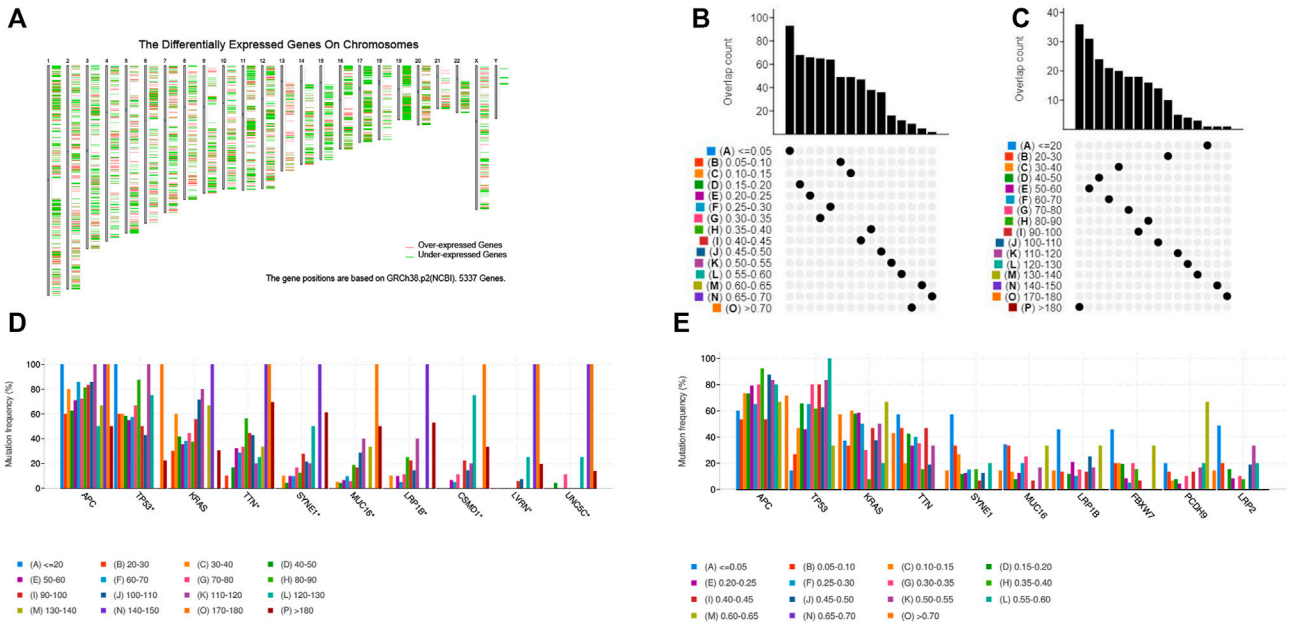

FIGURE 1 | Identification of potential tumor-associated antigens of CRC. **(A)** Chromosomal distribution of up-regulated and down-regulated genes in CRC. **(B)** Overlapping samples in altered genome fraction group. **(C)** Overlapping samples in mutation count group. **(D)** Highest frequency genes in mutation count group. **(E)** Highest frequency genes in altered genome fraction group.

abundance of six immune cell types (B cells, CD4+T cells, CD8+T cells, neutrophils, macrophages, and dendritic cells) in CRC patients using the TIMER (Li et al., 2017).

Discovery and Validation of the Immune Subtypes

Based on the expression of 1,989 IRGs, the 201 IRGs impacting prognosis of CRC patients by univariate Cox regression analysis was performed in subsequent analysis. Consensus clustering analysis was used to identify the four immune subtypes by using the R package "Consensus Cluster Plus" with parameters defined as a maximum of nine clusters. To assess the robustness of the identified immune subtypes, we further conducted the same algorithm in the validation cohort (GEO). In-group-proportion statistic was calculated to validate the similarity of immune subtypes across the discovery and validation cohorts.

Assessing the Clinicopathological, Cellular and Molecular Characteristics Associated With the Immune Subtypes

The correlation between immune subtypes and clinicopathological characteristics was evaluated by the Chi-square test. The prognostic value of the immune subtypes with OS as the endpoint was analyzed by the log-rank test and multivariable Cox proportional hazards regression model. The ANOVA algorithm was performed to assess the correlation between immune subtypes and different immune-related molecular and cellular characteristics. Finally, we employed the ssGSEA algorithm via R packages "GSVA" to comprehensively calculate the enrichment score of CRC samples on each immune-related term.

Defining the Immune Landscape

Considering the dynamic nature of the immune system, the dimensionality reduction analysis using the graph learning-based method was performed to reveal the intrinsic structure and visualize the distribution of individual patients (Trapnell et al., 2014). The discriminative dimensionality reduction with trees (DDRTree) was performed for dimension reduction (Qiu et al., 2017). Finally, the immune landscape was visualized with the function plot cell trajectory (Monocle) with the color corresponding to the immune subtype identified above (Qi et al., 2017; Wang and Mao, 2019).

Statistical Analysis

All statistical analyses and data visualization were performed in R version 4.0.5, and GraphPad Prism 8.0. $p < 0.05$ was considered statistically significant.

RESULTS

Identification of Potential Tumor Antigens in CRC

To identify potential tumor antigens of CRC, 2658 over-expressed genes that could potentially encode tumor-associated antigens (TAA) were detected by screening for aberrantly expressed genes (**Figure 1A**). In addition, 14,751 mutated

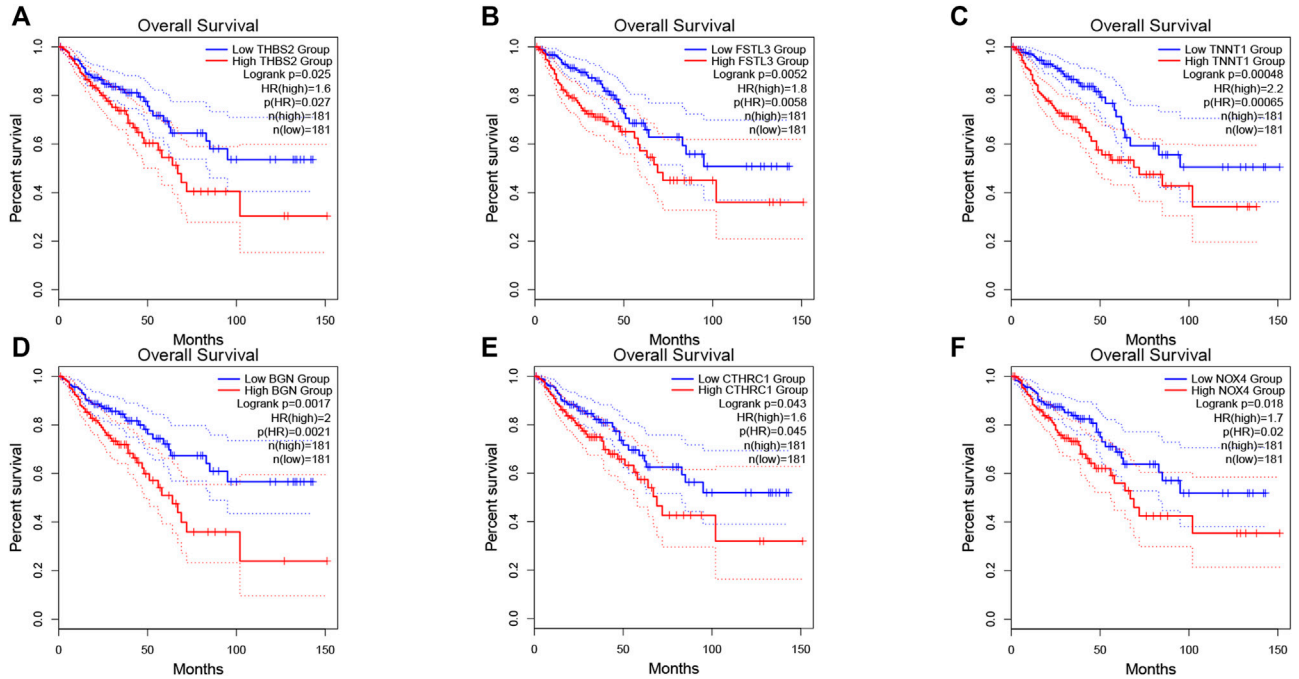

FIGURE 2 | Correlation of tumor antigens with CRC prognosis. **(A–F)** The association of THBS2 **(A)**, FSTL3 **(B)**, TNNT1 **(C)**, BGN **(D)**, CTHRC1 **(E)**, and NOX4 **(F)** expression levels with the OS of CRC patients. The red line represents the samples with highly expressed genes and the blue line indicates the samples with lowly expressed genes.

genes encoding TAA were filtered by analyzing fraction of genome altered and tumor mutational count in CRC patients (**Figures 1B,C**). Mutational analysis showed that the adenomatous polyposis coli (APC), tumor suppressor P53 (TP53), KRAS proto-oncogene GTPase (KARS), titin (TTN), spectrin repeat containing nuclear envelope protein 1 (SYNE1), mucin 16 (MUC16), and low-density lipoprotein receptor-related protein 1B (LRP1B) were the most frequently mutated genes in the fraction genome alteration and tumor mutational count group (**Figures 1D,E**). Collectively, we identified 2052 over-expressed and mutated genes.

Correlation of Tumor Antigens with CRC Prognosis and APCs for mRNA Vaccine Design

The prognosis-associated tumor antigens were selected from the above-mentioned genes as promising candidates for designing the mRNA vaccine. Fifty-one genes were strongly correlated with the overall survival (OS) of CRC. Only six genes were closely related to the disease-free survival (RFS) (**Supplementary Figure S1**). The survival analysis revealed that elevated expression of thrombospondin 2 (THBS2), follistatin like 3 (FSTL3), troponin T1 (TNNT1), biglycan (BGN), collagen triple helix repeat containing 1 (CTHRC1), and NADPH oxidase 4 (NOX4) were associated with poor OS in CRC (**Figures 2A–F**). In addition, we found a shorter RFS time in patients with higher expression levels of THBS2, FSTL3, TNNT1, BGN, CTHRC1, and NOX4 (**Supplementary Figure S2**). The effectiveness of mRNA vaccines strongly relies on the availability of the target antigen(s) to professional APCs, especially dendritic cells (DCs), macrophages, and B cells. Therefore, we investigated whether the expression of THBS2, FSTL3, TNNT1, BGN, CTHRC1, and NOX4 was correlated with immune cell infiltration levels in CRC via the Tumor Immune Estimation Resource (TIMER) database. The results demonstrated that elevated expression of THBS2, FSTL3, BGN, CTHRC1, and NOX4 was exhibited in increased infiltration of macrophages, DCs and B cells in CRC, although it was insignificant in B cells. Additionally, TNNT1 expression has the same tendency of increased infiltration of macrophages, DCs, and B cells (**Figures 3A–F**). Taken together, we designed mRNA encoding the antigen of interest flanked by 5′ and 3′ untranslated regions (UTRs). As shown in **Figure 4**, six tumor antigens (THBS2, FSTL3, TNNT1, BGN, CTHRC1, and NOX4) were identified as potential therapeutic candidates for the anti-CRC mRNA vaccine that can be processed and presented by APCs to activate a robust immune response.

Immune Subtypes of CRC

Immunophenotyping can be used to reflect the immune status of the tumor microenvironment, thus, allow the selection of patients for mRNA vaccine treatment. Therefore, consensus clustering was performed in 568 CRC samples based on the immune-related genes (IRGs). The results were visualized using a cumulative distribution function (CDF) plot and a delta area plot, in which k represents the number of immune subtypes. Four robust immune subtypes (IS1-IS4) were identified and the IRGs appeared to be stably clustered when $K = 4$ (**Figures 5A–C**). Significantly prognostic impact of the immune subtypes in TCGA cohort

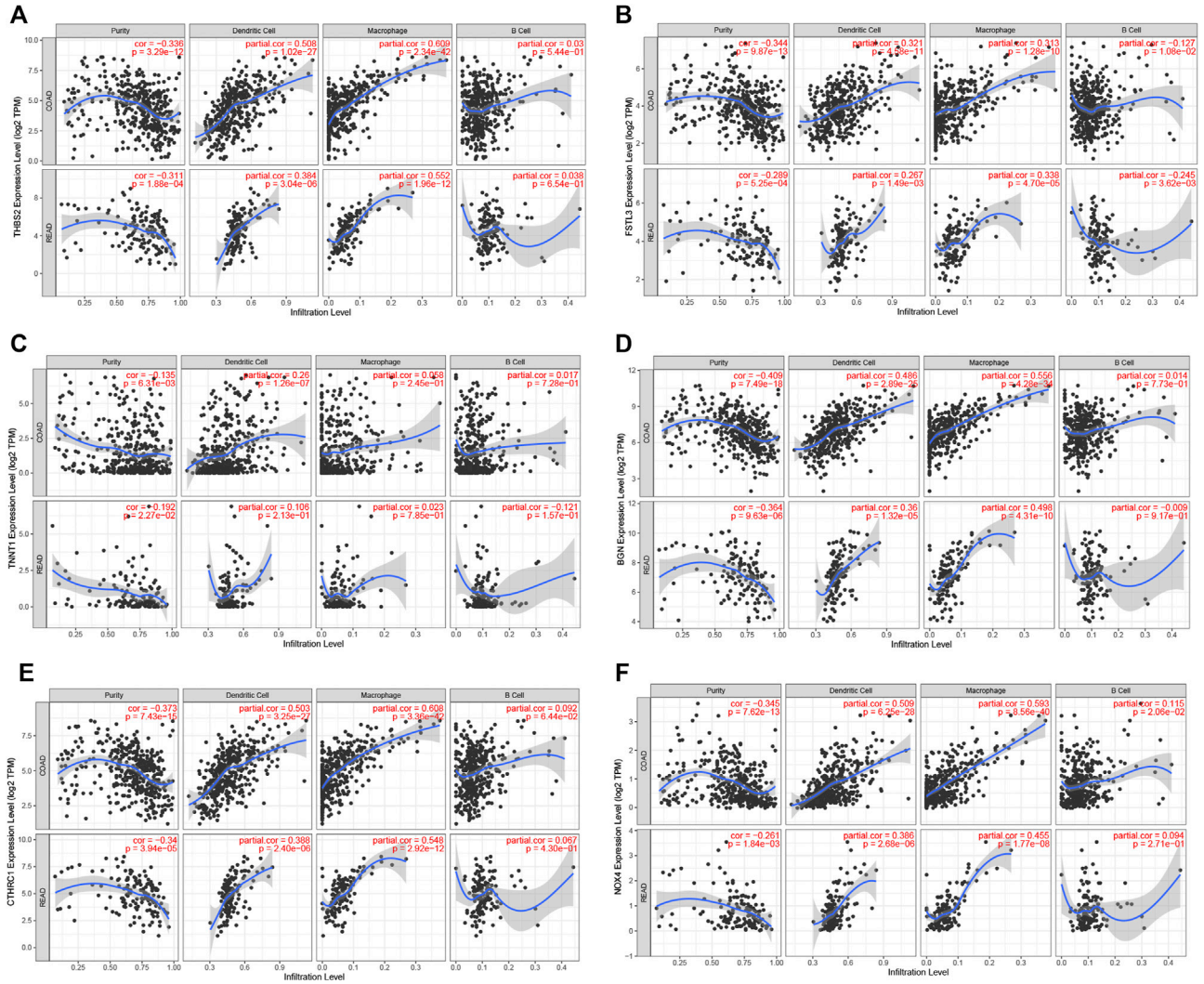

FIGURE 3 | Correlation of tumor antigens expression with antigen-presenting cells level in CRC. **(A–F)** Correlation between THBS2 **(A)**, FSTL3 **(B)**, TNNT1 **(C)**, BGN **(D)**, CTHRC1 **(E)**, and NOX4 **(F)** expression and the level of infiltrating immune cells dendritic cells, macrophages, and B cells in CRC.

was observed. Immune subtypes IS2 and IS4 were associated with a better prognosis for OS. Conversely, patients in IS1 and IS3 displayed the poorer survival probability in the TCGA cohort (**Figure 5D**). Consistent with our results obtained from the TCGA cohort, each of the immune subtypes was related to prognosis in the GEO cohort as well (**Figure 5E**). Among all immune subtypes, IS2 and IS4 were associated with the lower stage (**Figures 5F,G**) compared with IS1 and IS3. Taken together, immunophenotyping could be a robust prognostic indicator and its accuracy is superior to conventional stage of the tumor in CRC.

Correlation of Immune Subtypes with Tumor Mutational Burden

High tumor mutational burden (TMB) can increase the tumor immunogenicity, allow the immune system to recognize and attack the cancer cells by T cell-mediated antitumor immunity. Therefore, TMB for each patient can be detected and calculated using the VarScan method in the TCGA cohort. Subtypes IS2 and IS4 had significantly higher TMB than subtypes IS1 and IS3 (**Figure 6A**). Furthermore, somatic mutation profiling revealed a high frequency of mutations in APC (78%), TP53 (59%), TTN (50%), KRAS (43%), SYNE1 (29%), and MUC16 (28%) across immune subtype (**Figure 6B**). These findings suggest that the immune subtype is a promising tool to predict TMB in CRC patients and clinical response to mRNA vaccine. Therefore, patients belong to IS2 and IS4 may respond positively to the mRNA vaccine.

Correlation of Immune Subtypes with Immune Checkpoint Molecules and HLA

Immune checkpoint molecules and human leukocyte antigen (HLA) are essential for immune function and have diverse

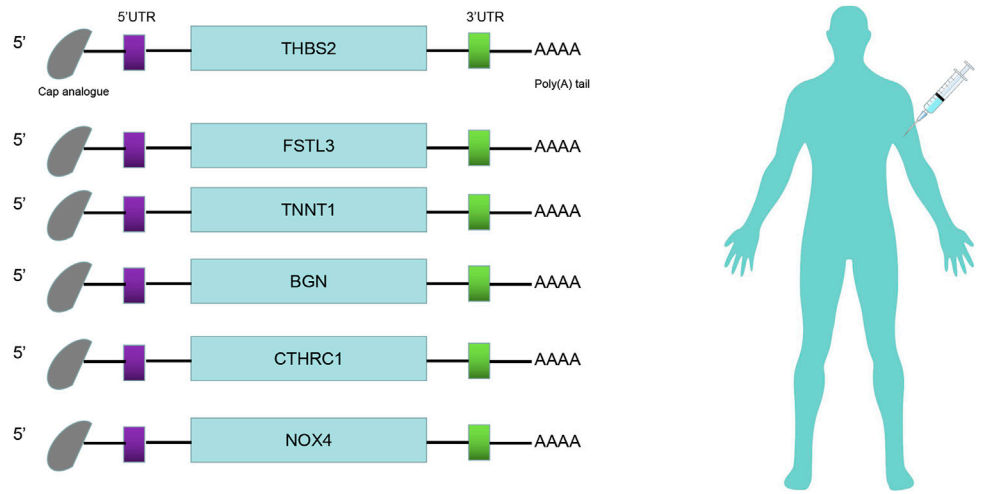

FIGURE 4 | mRNA-vaccine design. Structure of the anti-CRC mRNA vaccine. The 5′-cap analog, 5′- and 3′-untranslated regions (UTRs), and poly(A) tail were optimized for stability and translational efficiency.

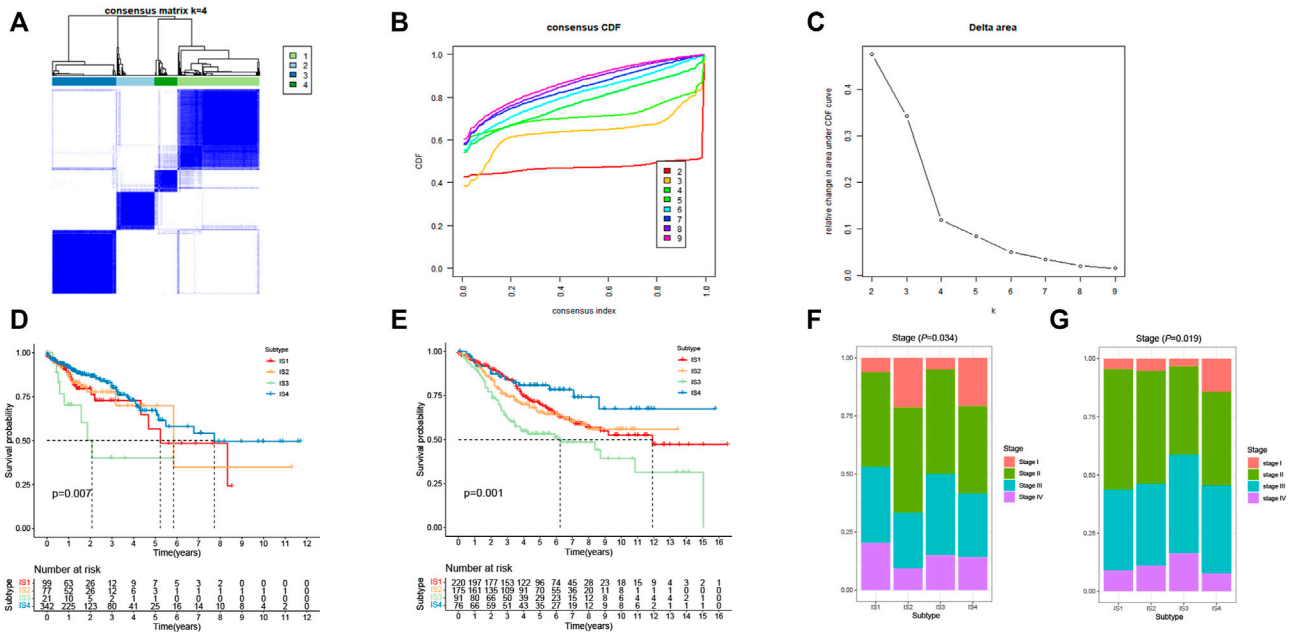

FIGURE 5 | Identification of immune subtypes of CRC. **(A)** Consensus clustering matrix of CRC samples for $k = 4$. **(B)** Cumulative distribution function (CDF) curve of the consistency score for different immune subtype numbers ($k = 2$–9). **(C)** Delta area plot showing the relative change in area under the CDF curve from $k = 2$ to $k = 9$, which assisted in determining the optimal immune subtype numbers. **(D)** Kaplan-Meier survival curves of CRC immune subtypes in TCGA cohort. **(E)** Kaplan-Meier survival curves of CRC immune subtypes in GEO cohort. **(F)** Stages of CRC patients among the IS1-IS4 immune subtypes in TCGA cohort. **(G)** Stages of CRC patients among the IS1-IS4 immune subtypes in GEO cohort.

clinical implications in cancer immunotherapy. Therefore, we next analyzed the relationship between the CRC immune subtypes and the expression level of immune checkpoint molecule genes and HLA. We found that 30 immune checkpoint-related genes were significantly differentially expressed among the immune subtypes. For example, TNFSF4, TNFRSF9, TNFRSF4, TNFRSF18, LAG3, JAK2, PTPRC, IL12B, IFNG, ICOS, HAVCR2, CTLA4, CD8A, CD86, CD80, CD40, CD28, and CD274 were significantly downregulated in IS3 tumors, while TNFSF9, TNFSF4 TNFRSF9, TNFRSF4, TNFRSF18, PTPRC, CTLA4, CD8A, CD86, CD80, CD40, CD28, and CD274 were strongly elevated in IS2 tumors

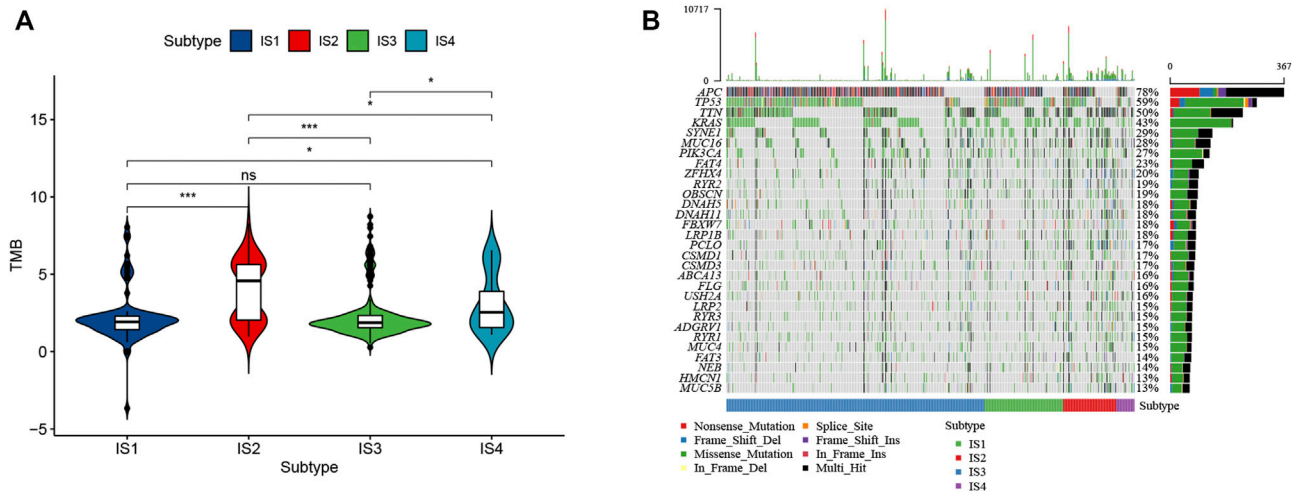

FIGURE 6 | Correlation of immune subtypes with TMB in CRC. **(A)** The TMB of CRC samples from four immune subtypes. **(B)** The alteration landscape of CRC across four immune subtypes.

(**Figures 7A,B**). Next, we assessed the expression level of HLA genes in the four immune subtypes and determined that the expression levels were significantly elevated in IS2 and IS4 than in IS1 and IS3 (**Figures 7C,D**). HLA plays important role in the activation of anti-tumor immunity through interactions with T cell receptors. Thus, the response of patients with IS2 and IS4 on mRNA vaccine treatment might be more promising.

Cellular and Molecular Features of CRC Immune Subtypes

The tumor immune microenvironment (TIME) plays a crucial role in CRC progression, thus influences the effectiveness of the mRNA vaccine. We assessed the relationship between the immune subtypes and 29 immune-related molecular features in the TCGA and GEO cohorts by the single-sample gene set enrichment analysis (ssGSEA) algorithm (**Figures 8A,B**). The results showed that IS2 and IS4 have significantly higher levels of B cells, CD+8 T cells, Th1 cells, and macrophages compared with IS1 and IS3. Moreover, we calculated stromal and immune scores to quantify the abundances of infiltrating stromal and immune cells for each sample in TCGA and GEO. These results also demonstrated that IS2 and IS4 have higher Immune Score than IS1 and IS3 (**Figure 8C**). Thus, IS2 and IS4 are immune-hot phenotypes, while IS1 and IS3 are immune-cold phenotypes. Similar results were also validated in patients in the GEO cohort (**Figure 8D**).

To better understand the association of CRC immune subtypes with six pan-cancer immunotypes we extracted 11 immune-related molecular features from a previous study and demonstrated that the expression of 11 molecular signatures was significantly different among the four immune subtypes (**Figure 8E**). Antigen-specific T cell receptor (TCR) and B cell receptor (BCR) repertoires play a significant role in the immune system for the recognition of malignant cells. We observed that IS2 and IS4 had higher scores in TCR richness and BCR richness. Higher TCR richness may enhance anticancer immunity. Therefore, immunotype can be used to reflect CRC immune status and to select suitable patients for mRNA vaccine treatment.

Immune Landscape of CRC

The immune landscape is increasingly recognized to be important in cancer development, progression, and response to therapy. Subsequently, we sought to visualize the immune landscape by the graph learning-based dimensionality reduction technique. We observed that the immune-hot subtype IS2 and immune-cold subtype IS3 were distributed at the opposite end of the horizontal axis in the immune landscape (**Figure 9A**). The horizontal axis in the immune landscape may represent the overall immune infiltration. As shown in **Figure 9B**, the horizontal axis was associated with various immune cells, of which activated CD8+ T cells, activated CD4+ T cells, and type 1 T helper cells showed the positive correlation.

The immune landscape further revealed significant intra-cluster heterogeneity within each subtype. IS3 could be further divided into four subgroups based on the distribution location in the immune landscape (**Figure 9C**). The further prognostic analysis demonstrated that IS3D has the best prognosis among IS3A, IS3B, and IS3C (**Figure 9D**). Collectively, the immune landscape based on immune subtypes can precisely recognize immune components of each CRC patient as well as predict their prognoses that are beneficial for selecting personalized therapeutics for mRNA vaccine.

DISCUSSION

Therapy of CRC has been improved over the years with advanced surgical and chemotherapeutic procedures but challenges in terms of efficiency and adverse effects still

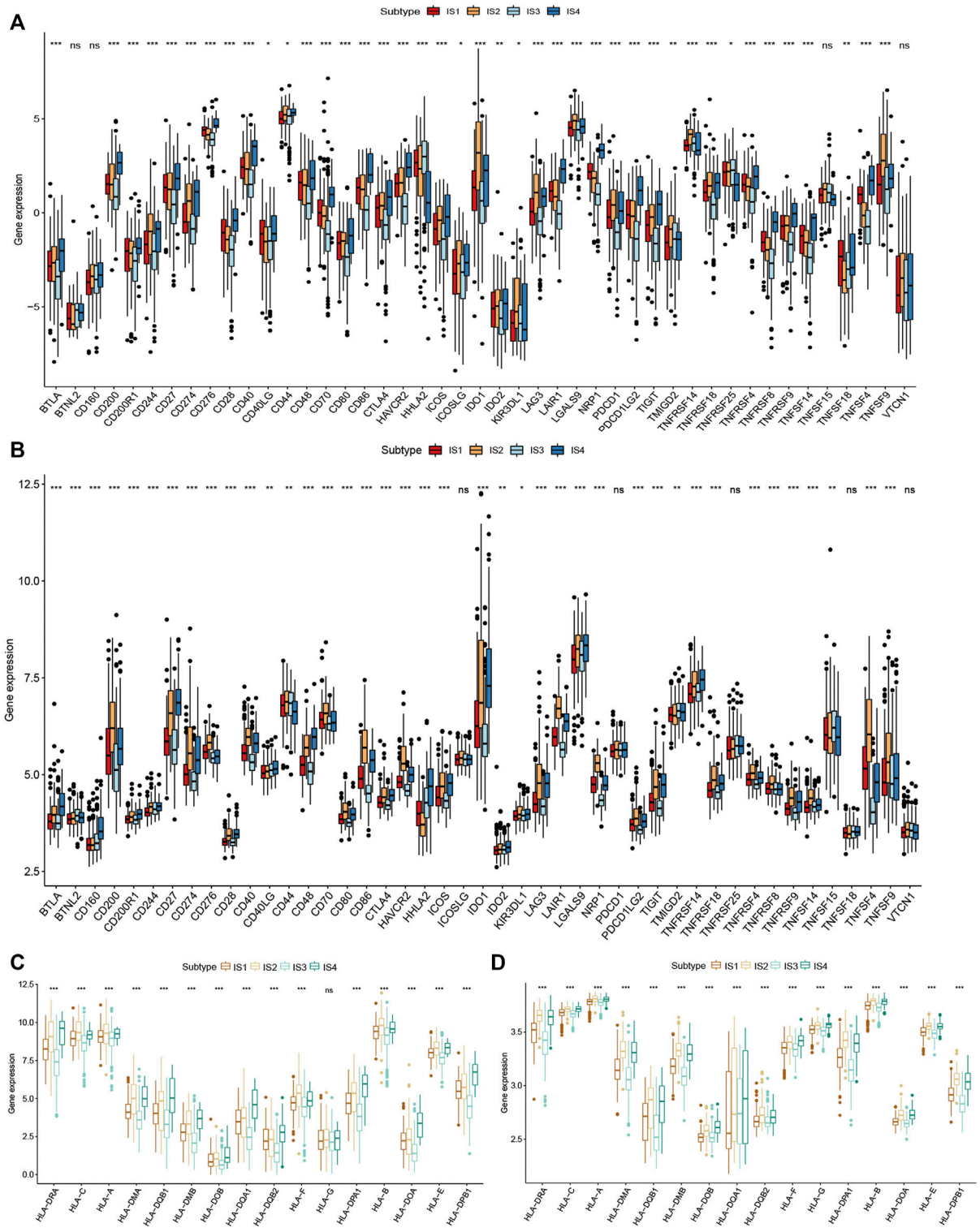

FIGURE 7 | Correlation of immune subtypes with immune checkpoint molecules and HLA genes expression in CRC. **(A)** The expression of immune checkpoint molecules among CRC immune subtypes in TCGA cohort. **(B)** The expression of immune checkpoint molecules among CRC immune subtypes in GEO cohort. **(C)** The expression of HLA genes among the CRC immune subtypes in TCGA cohort. **(D)** The expression of HLA genes among the CRC immune subtypes in GEO cohort. *$p < 0.05$, **$p < 0.01$, and ***$p < 0.001$.

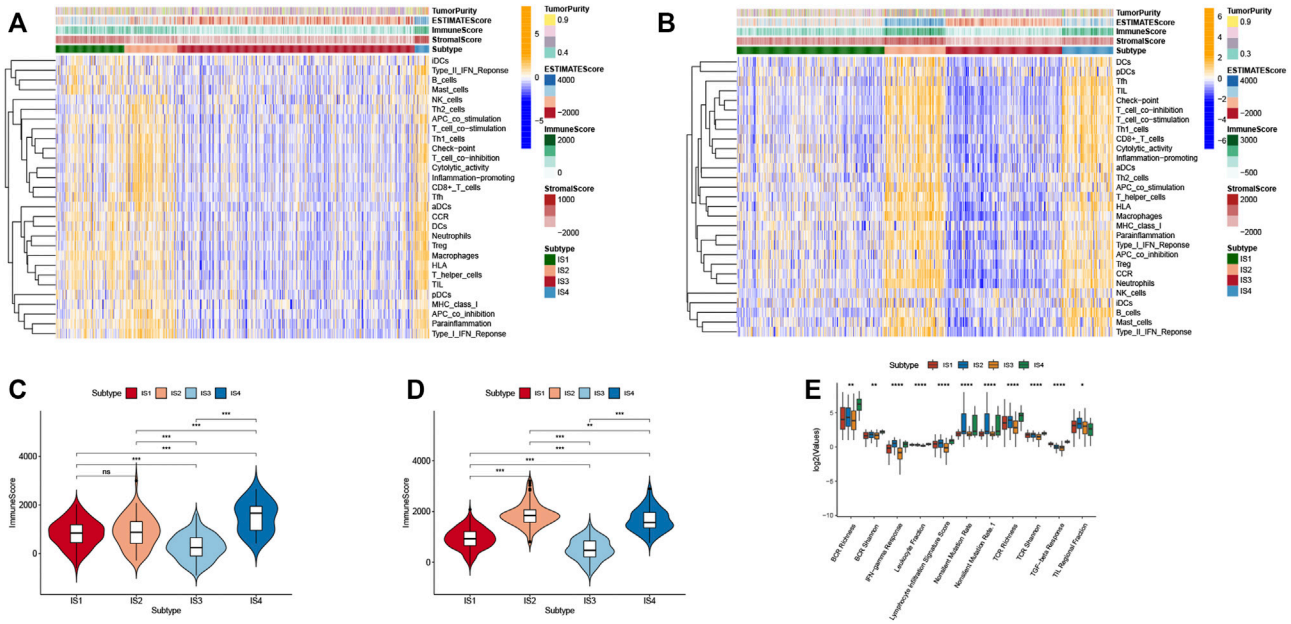

FIGURE 8 | Cellular and molecular features of immune subtypes. **(A)** The enrichment levels of 29 immune-related gene sets among CRC immune subtypes in TCGA cohort. **(B)** The difference in Immune Scores between four immune subtypes in TCGA cohort. **(C)** The enrichment levels of 29 immune-related gene sets among CRC immune subtypes in GEO cohort. **(D)** The difference in Immune Scores between four immune subtypes in GEO cohort. **(E)** The enrichment levels of 11 immune-related gene sets among CRC immune subtypes.

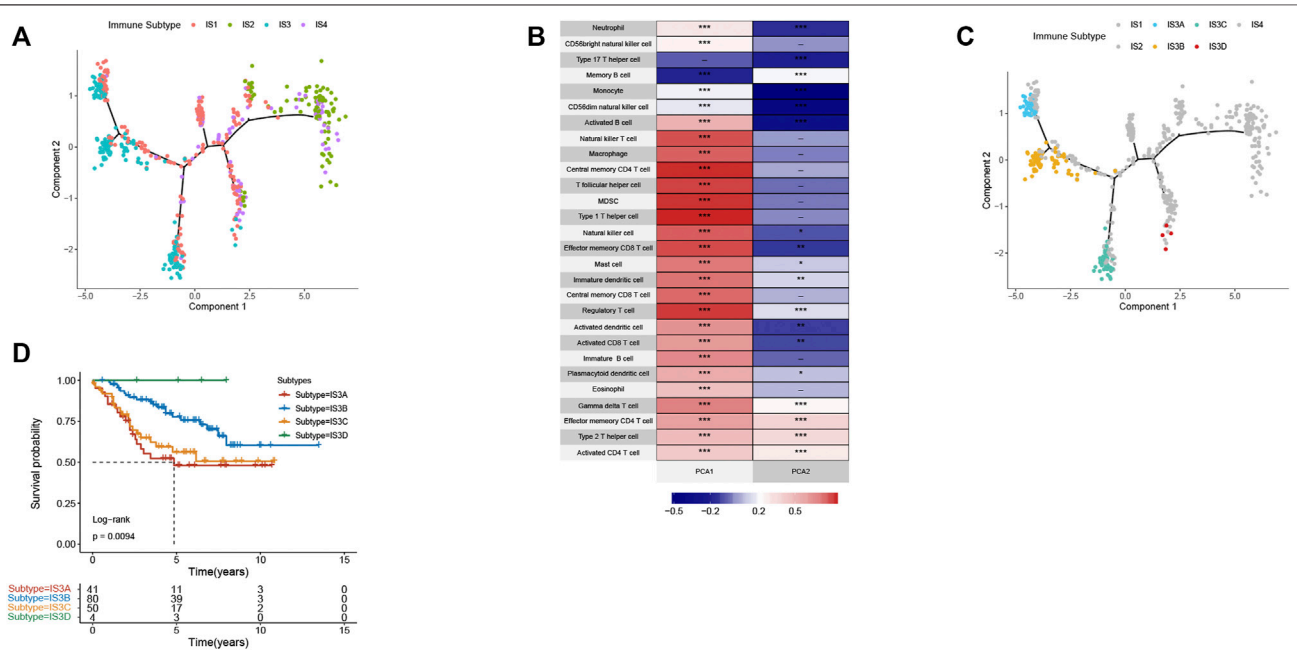

FIGURE 9 | The immune landscape of CRC. **(A)** The immune landscape of CRC. Each point represents a patient with colors corresponding to the immune subtype defined previously. **(B)** Correlation between PCA1/2 and immune cell signatures. **(C)** Immune landscape of the subsets of CRC IS3 based on their location in the immune landscape. **(D)** Different subtypes in IS3 associated with different prognoses.

need to be accomplished. Especially late-stage CRC patients still have a relatively poor prognosis (Hammond et al., 2016; Russo et al., 2019). mRNA vaccines have become a promising platform for cancer treatment. Nevertheless, tumor heterogeneity is one of the biggest setbacks in implementing mRNA vaccine-based therapy. In this study, the abnormal

gene expression patterns and mutational landscape of CRC were constructed and a range of targeted antigens, including THBS2, FSTL3, TNNT1, BGN, CTHRC1, and NOX4 were identified as promising mRNA vaccine candidates. The overexpression of these antigens was associated with poor prognosis and high infiltration of APCs in CRC. Thus, these antigens play important roles in CRC development and progression. According to the abovementioned, the sequence of tumor antigens can be modified and cloned into appropriate plasmids for synthesizing mRNA. IVT mRNA will be encapsulated with lipid nanoparticles. Optimized mRNA encoding CRC antigens will be injected into CRC patients to induce an immune response against tumor cells to eradicate the tumor. mRNA vaccines encoding these tumor antigens (THBS2, FSTL3, TNNT1, BGN, CTHRC1, and NOX4) induce a cell-mediated immune response and humoral immune response that are beneficial for efficient clearance of cancer cells. Although further clinical evaluation of the candidates is required, their potential for anti-CRC mRNA vaccine development is consolidated by previous studies. For instance, THBS2 is a biomarker for clinical stages and a strong prognostic indicator in CRC. Increased THBS2 expression was significantly associated with clinical stages (TNM). Furthermore, THBS2 has been reported to regulate apoptosis, cell proliferation, and adhesion (Wang et al., 2016; Tian et al., 2018). FSTL3 is an oncogene and may be involved in CRC progression via the promotion of bone morphogenetic protein (BMP) signaling pathway (Karagiannis et al., 2013). Similarly, TNNT1 expression was closely correlated with the clinical stage, facilitated the proliferation, migration, and invasion of CRC cells (Chen Y. et al., 2020). BGN has been reported to be implicated in CRC liver metastasis (Ma et al., 2018). BGN activity influences CRC progression via its participation in other pathways (Chen D. et al., 2020). Previous studies have reported that knockout of BGN can inhibit the proliferation and migration of CRC cells (Xing et al., 2015a). In addition, BGN can promote angiogenesis through upregulating vascular endothelial growth factor (VEGF) expression in CRC patients (Xing et al., 2015b; Suhovskih et al., 2015). Moreover, BGN can also serve as a prognostic biomarker in CRC patients (You et al., 2015). CTHRC1 promotes human CRC cell proliferation and invasiveness by activating Wnt/planar cell polarity (PCP) signaling pathway (Yang et al., 2015). Upregulated CTHRC1 predicts poor prognosis and promotes epithelial-mesenchymal transition in CRC (Ni et al., 2018). NOX4 plays an important role in CRC progression and metastasis (Shen et al., 2020). High NOX4 expression was significantly correlated with clinicopathologic classifications and poor survival of CRC patients. NOX4 promoted CRC cells proliferation, migration, and invasion by regulating relevant pathway (Lin et al., 2017). To our knowledge, this is the first study that screened the CRC antigens for the development of mRNA vaccine for cancer.

Given that tumor heterogeneity restricts the widespread application of mRNA vaccine in CRC patients, a comprehensive understanding of the immune landscape of CRC is therefore essential for the design of efficient immunotherapy strategies. Four reproducible immune subtypes of CRC were identified based on IRGs expression profile to provide new insights for designing advanced mRNA vaccine strategies for CRC treatment. We observed that each of the four immune subtypes was correlated with distinct clinical characteristics, and accordingly revealed different patterns in molecular and cellular features. IS2 and IS4 tumors displayed a better prognosis than other subtypes in TCGA and GEO datasets. TMB is a critical intrinsic factor that affects tumor response to immunotherapy. High TMB can be used as an independent biomarker for the selection of patients for mRNA vaccine therapy (Havel et al., 2019). Patients with IS2 and IS4 tumors showed higher TMB, which may have a greater response to mRNA vaccine treatment. Moreover, we found that the IS2 and IS4 tumors had higher expression of HLA and immune checkpoint molecules and showed a more prominent Th1/IFNγ gene signature. HLA expression contributes to the activation of anti-tumor immunity through interactions with T cell receptors. Moreover, the complex immune landscape of CRC revealed substantial heterogeneity between individual patients and the same immune subtype, which provided complementary information for personalized mRNA-based cancer vaccines.

TIME plays a vital role for mRNA vaccine to elicit tumor immune response, it is critical to further understand diverse immune cell components of different immune subtypes. We found that each of the four immune subtypes was related to distinct cellular and molecular features. Among all immune subtypes, IS2 and IS4 have high immune scores compared with IS1 and IS3, which indicated that IS2 and IS4 are immunologically "hot" tumors while IS1 and IS3 are immunologically "cold" tumors. High immune scores subtype (IS2 and IS4) showed better survival outcomes. Previous studies proposed the "hot" tumor displayed higher tumor sensitivity to immunotherapy (Galon et al., 2006; Galon and Bruni, 2019). These findings further showed that patients in the immune-cold subtype have the lowest degree of B cells and CD4+T cells infiltration, while the immune-hot subtype exhibited high levels of infiltrating immune cells. IS2 and IS4 displayed abundant tumor-infiltrating lymphocytes (TILs), cytotoxic T cells, natural killer cells, and macrophages, the high level of TILs recognize ample tumor antigens with their diverse receptors. IS2 and IS4 had higher scores in TCR richness and BCR richness. Higher TCR richness may enhance anticancer immunity (Thorsson et al., 2018). Moreover, IS2 and IS4 exhibited higher inflammation-promoting, IFN-γ response, and TGF-β response gene expression compared with IS1 and IS3. Thus, patients with IS2 and IS4 tumors are more suitable for mRNA vaccine therapy, IS1 and IS3 may respond to mRNA vaccine combined with ICB therapy. However, our study was limited because it was retrospective, and identified mRNA vaccine antigens of the current investigation demand validation by prospective studies. The findings should be interpreted with this limitation in mind. Additionally, we

will attempt to validate the accuracy of the identified six antigens in our following work.

In summary, our findings depicted the immune landscape of CRC and eventually identified four immune subtypes. THBS2, FSTL3, TNNT1, BGN, CTHRC1, and NOX4 are the potential targets of the CRC mRNA vaccine. Patients with IS2 and IS4 are suitable candidates for vaccination. In addition, we design an anti-CRC mRNA vaccine. Hence, this study may guide a personalized approach for mRNA vaccine development against CRC.

DATA AVAILABILITY STATEMENT

Publicly available datasets were analyzed in this study. This data can be found here: TCGA database (https://gdc-portal.nci.nih.gov/), GEO database (https://www.ncbi.nlm.nih.gov/geo/), cBioPortal (http://www.cbioportal.org/), GEPIA2 (http://gepia2.cancer-pku.cn/), and TIMER database https://cistrome.shinyapps.io/timer/.

AUTHOR CONTRIBUTIONS

CL and PW designed the study. CL performed the bioinformatic analyses and wrote the manuscript. YD, XW, XH, NY, JC, NR, and FX participated in data collection. DP and PW revised the manuscript. All authors reviewed and approved the final manuscript.

FUNDING

This work is supported by grant from Department of Education of Guangdong Province Research Project (2020KZDZX1181).

SUPPLEMENTARY MATERIAL

The Supplementary Material for this article can be found online at: https://www.frontiersin.org/articles/10.3389/fcell.2021.783527/full#supplementary-material

REFERENCES

Augestad, K. M., Merok, M. A., and Ignatovic, D. (2017). Tailored Treatment of Colorectal Cancer: Surgical, Molecular, and Genetic Considerations. *Clin. Med. Insights Oncol.* 11, 117955491769076. doi:10.1177/1179554917690766

Batich, K. A., Mitchell, D. A., Healy, P., Herndon, J. E., Sampson, J. H., and Sampson, J. H. (2020). Once, Twice, Three Times a Finding: Reproducibility of Dendritic Cell Vaccine Trials Targeting Cytomegalovirus in Glioblastoma. *Clin. Cancer Res.* 26 (20), 5297–5303. doi:10.1158/1078-0432.CCR-20-1082

Cerami, E., Gao, J., Dogrusoz, U., Gross, B. E., Sumer, S. O., Aksoy, B. A., et al. (2012). The cBio Cancer Genomics Portal: An Open Platform for Exploring Multidimensional Cancer Genomics Data: Figure 1. *Cancer Discov.* 2 (5), 401–404. doi:10.1158/2159-8290.CD-12-0095

Chen, D., Qin, Y., Dai, M., Li, L., Liu, H., Zhou, Y., et al. (2020). BGN and COL11A1 Regulatory Network Analysis in Colorectal Cancer (CRC) Reveals that BGN Influences CRC Cell Biological Functions and Interacts with miR-6828-5p. *Cmar* Vol. 12, 13051–13069. doi:10.2147/CMAR.S277261

Chen, Y.-P., Wang, Y.-Q., Lv, J.-W., Li, Y.-Q., Chua, M. L. K., Le, Q.-T., et al. (2019). Identification and Validation of Novel Microenvironment-Based Immune Molecular Subgroups of Head and Neck Squamous Cell Carcinoma: Implications for Immunotherapy. *Ann. Oncol.* 30 (1), 68–75. doi:10.1093/annonc/mdy470

Chen, Y., Wang, J., Wang, D., Kang, T., Du, J., Yan, Z., et al. (2020). TNNT1, Negatively Regulated by miR-873, Promotes the Progression of Colorectal Cancer. *J. Gene Med.* 22 (2), e3152. doi:10.1002/jgm.3152

De Keersmaecker, B., Claerhout, S., Carrasco, J., Bar, I., Corthals, J., Wilgenhof, S., et al. (2020). TriMix and Tumor Antigen mRNA Electroporated Dendritic Cell Vaccination Plus Ipilimumab: Link between T-Cell Activation and Clinical Responses in Advanced Melanoma. *J. Immunother. Cancer* 8 (1), e000329. doi:10.1136/jitc-2019-000329

Galon, J., and Bruni, D. (2019). Approaches to Treat Immune Hot, Altered and Cold Tumours with Combination Immunotherapies. *Nat. Rev. Drug Discov.* 18 (3), 197–218. doi:10.1038/s41573-018-0007-y

Galon, J., Costes, A., Sanchez-Cabo, F., Kirilovsky, A., Mlecnik, B., Lagorce-Pagès, C., et al. (2006). Type, Density, and Location of Immune Cells within Human Colorectal Tumors Predict Clinical Outcome. *Science* 313 (5795), 1960–1964. doi:10.1126/science.1129139

Hammond, W. A., Swaika, A., and Mody, K. (2016). Pharmacologic Resistance in Colorectal Cancer: a Review. *Ther. Adv. Med. Oncol.* 8 (1), 57–84. doi:10.1177/1758834015614530

Hargadon, K. M., Johnson, C. E., and Williams, C. J. (2018). Immune Checkpoint Blockade Therapy for Cancer: An Overview of FDA-Approved Immune Checkpoint Inhibitors. *Int. Immunopharmacology* 62, 29–39. doi:10.1016/j.intimp.2018.06.001

Havel, J. J., Chowell, D., and Chan, T. A. (2019). The Evolving Landscape of Biomarkers for Checkpoint Inhibitor Immunotherapy. *Nat. Rev. Cancer* 19 (3), 133–150. doi:10.1038/s41568-019-0116-x

Kallen, K.-J., Heidenreich, R., Schnee, M., Petsch, B., Schlake, T., Thess, A., et al. (2013). A Novel, Disruptive Vaccination Technology. *Hum. Vaccin. Immunother.* 9 (10), 2263–2276. doi:10.4161/hv.25181

Karagiannis, G. S., Berk, A., Dimitromanolakis, A., and Diamandis, E. P. (2013). Enrichment Map Profiling of the Cancer Invasion Front Suggests Regulation of Colorectal Cancer Progression by the Bone Morphogenetic Protein Antagonist, Gremlin-1. *Mol. Oncol.* 7 (4), 826–839. doi:10.1016/j.molonc.2013.04.002

Kowalzik, F., Schreiner, D., Jensen, C., Teschner, D., Gehring, S., and Zepp, F. (2021). mRNA-Based Vaccines. *Vaccines* 9 (4), 390. doi:10.3390/vaccines9040390

Kübler, H., Scheel, B., Gnad-Vogt, U., Miller, K., Schultze-Seemann, W., Vom Dorp, F., et al. (2015). Self-adjuvanted mRNA Vaccination in Advanced Prostate Cancer Patients: a First-In-Man Phase I/IIa Study. *J. Immunotherapy Cancer* 3, 26. doi:10.1186/s40425-015-0068-y

Li, B., Cui, Y., Nambiar, D. K., Sunwoo, J. B., and Li, R. (2019). The Immune Subtypes and Landscape of Squamous Cell Carcinoma. *Clin. Cancer Res.* 25 (12), 3537. doi:10.1158/1078-0432.CCR-18-4085

Li, T., Fan, J., Wang, B., Traugh, N., Chen, Q., Liu, J. S., et al. (2017). TIMER: A Web Server for Comprehensive Analysis of Tumor-Infiltrating Immune Cells. *Cancer Res.* 77 (21), e108–e110. doi:10.1158/0008-5472.CAN-17-0307

Lin, X.-L., Yang, L., Fu, S.-W., Lin, W.-F., Gao, Y.-J., Chen, H.-Y., et al. (2017). Overexpression of NOX4 Predicts Poor Prognosis and Promotes Tumor Progression in Human Colorectal Cancer. *Oncotarget* 8 (20), 33586–33600. doi:10.18632/oncotarget.16829

Ma, Y.-S., Huang, T., Zhong, X.-M., Zhang, H.-W., Cong, X.-L., Xu, H., et al. (2018). Proteogenomic Characterization and Comprehensive Integrative Genomic Analysis of Human Colorectal Cancer Liver Metastasis. *Mol. Cancer* 17 (1), 139. doi:10.1186/s12943-018-0890-1

Mao, Q., Wang, L., Tsang, I. W., and Sun, Y. (2017). Principal Graph and Structure Learning Based on Reversed Graph Embedding. *IEEE Trans. Pattern Anal. Mach. Intell.* 39 (11), 2227–2241. doi:10.1109/TPAMI.2016.2635657

Miao, L., Zhang, Y., and Huang, L. (2021). mRNA Vaccine for Cancer Immunotherapy. *Mol. Cancer* 20 (1), 41. doi:10.1186/s12943-021-01335-5

Ni, S., Ren, F., Xu, M., Tan, C., Weng, W., Huang, Z., et al. (2018). CTHRC1 Overexpression Predicts Poor Survival and Enhances Epithelial-Mesenchymal

Transition in Colorectal Cancer. *Cancer Med.* 7 (11), 5643–5654. doi:10.1002/cam4.1807

Pantin, J., and Battiwalla, M. (2020). Upsetting the Apple CAR-T (Chimeric Antigen Receptor T-cell Therapy) - Sustainability Mandates USA Innovation. *Br. J. Haematol.* 190 (6), 851–853. doi:10.1111/bjh.16685

Papachristofilou, A., Hipp, M. M., Klinkhardt, U., Früh, M., Sebastian, M., Weiss, C., et al. (2019). Phase Ib Evaluation of a Self-Adjuvanted Protamine Formulated mRNA-Based Active Cancer Immunotherapy, BI1361849 (CV9202), Combined with Local Radiation Treatment in Patients with Stage IV Non-small Cell Lung Cancer. *J. Immunotherapy Cancer* 7 (1), 38. doi:10.1186/s40425-019-0520-5

Pardi, N., Hogan, M. J., Porter, F. W., and Weissman, D. (2018). mRNA Vaccines - a new era in Vaccinology. *Nat. Rev. Drug Discov.* 17 (4), 261–279. doi:10.1038/nrd.2017.243

Qiu, X., Mao, Q., Tang, Y., Wang, L., Chawla, R., Pliner, H. A., et al. (2017). Reversed Graph Embedding Resolves Complex Single-Cell Trajectories. *Nat. Methods* 14 (10), 979–982. doi:10.1038/nmeth.4402

Russo, M., Crisafulli, G., Sogari, A., Reilly, N. M., Arena, S., Lamba, S., et al. (2019). Adaptive Mutability of Colorectal Cancers in Response to Targeted Therapies. *Science* 366 (6472), 1473–1480. doi:10.1126/science.aav4474

Sahin, U., Karikó, K., and Türeci, Ö. (2014). mRNA-based Therapeutics - Developing a New Class of Drugs. *Nat. Rev. Drug Discov.* 13 (10), 759–780. doi:10.1038/nrd4278

Sebastian, M., Papachristofilou, A., Weiss, C., Früh, M., Cathomas, R., Hilbe, W., et al. (2014). Phase Ib Study Evaluating a Self-Adjuvanted mRNA Cancer Vaccine (RNActive) Combined with Local Radiation as Consolidation and Maintenance Treatment for Patients with Stage IV Non-small Cell Lung Cancer. *BMC Cancer* 14, 748. doi:10.1186/1471-2407-14-748

Shen, C.-J., Chang, K.-Y., Lin, B.-W., Lin, W.-T., Su, C.-M., Tsai, J.-P., et al. (2020). Oleic Acid-Induced NOX4 Is Dependent on ANGPTL4 Expression to Promote Human Colorectal Cancer Metastasis. *Theranostics* 10 (16), 7083–7099. doi:10.7150/thno.44744

Suhovskih, A. V., Aidagulova, S. V., Kashuba, V. I., and Grigorieva, E. V. (2015). Proteoglycans as Potential Microenvironmental Biomarkers for colon Cancer. *Cell Tissue Res* 361 (3), 833–844. doi:10.1007/s00441-015-2141-8

Sung, H., Ferlay, J., Siegel, R. L., Laversanne, M., Soerjomataram, I., Jemal, A., et al. (2021). Global Cancer Statistics 2020: GLOBOCAN Estimates of Incidence and Mortality Worldwide for 36 Cancers in 185 Countries. *CA A. Cancer J. Clin.* 71 (3), 209–249. doi:10.3322/caac.21660

Tang, Z., Li, C., Kang, B., Gao, G., Li, C., and Zhang, Z. (2017). GEPIA: a Web Server for Cancer and normal Gene Expression Profiling and Interactive Analyses. *Nucleic Acids Res.* 45 (W1), W98–W102. doi:10.1093/nar/gkx247

Thorsson, V., Gibbs, D. L., Brown, S. D., Wolf, D., Bortone, D. S., Ou Yang, T. H., et al. (2018). The Immune Landscape of Cancer. *Immunity* 48 (4), 812–e14. doi:10.1016/j.immuni.2018.03.023

Tian, Q., Liu, Y., Zhang, Y., Song, Z., Yang, J., Zhang, J., et al. (2018). THBS2 Is a Biomarker for AJCC Stages and a strong Prognostic Indicator in Colorectal Cancer. *J. BUON* 23 (5), 1331–1336.

Trapnell, C., Cacchiarelli, D., Grimsby, J., Pokharel, P., Li, S., Morse, M., et al. (2014). The Dynamics and Regulators of Cell Fate Decisions Are Revealed by Pseudotemporal Ordering of Single Cells. *Nat. Biotechnol.* 32 (4), 381–386. doi:10.1038/nbt.2859

van der Stok, E. P., Spaander, M. C. W., Grünhagen, D. J., Verhoef, C., and Kuipers, E. J. (2017). Surveillance after Curative Treatment for Colorectal Cancer. *Nat. Rev. Clin. Oncol.* 14 (5), 297–315. doi:10.1038/nrclinonc.2016.199

Wang, L., and Mao, Q. (2019). Probabilistic Dimensionality Reduction via Structure Learning. *IEEE Trans. Pattern Anal. Mach. Intell.* 41 (1), 205–219. doi:10.1109/TPAMI.2017.2785402

Wang, X., Zhang, L., Li, H., Sun, W., Zhang, H., and Lai, M. (2016). THBS2 Is a Potential Prognostic Biomarker in Colorectal Cancer. *Sci. Rep.* 6, 33366. doi:10.1038/srep33366

Xing, X., Gu, X., and Ma, T. (2015a). Knockdown of Biglycan Expression by RNA Interference Inhibits the Proliferation and Invasion of, and Induces Apoptosis in, the HCT116 colon Cancer Cell Line. *Mol. Med. Rep.* 12 (5), 7538–7544. doi:10.3892/mmr.2015.4383

Xing, X., Gu, X., Ma, T., and Ye, H. (2015b). Biglycan Up-Regulated Vascular Endothelial Growth Factor (VEGF) Expression and Promoted Angiogenesis in colon Cancer. *Tumor Biol.* 36 (3), 1773–1780. doi:10.1007/s13277-014-2779-y

Yang, X. M., You, H. Y., Li, Q., Ma, H., Wang, Y. H., Zhang, Y. L., et al. (2015). CTHRC1 Promotes Human Colorectal Cancer Cell Proliferation and Invasiveness by Activating Wnt/PCP Signaling. *Int. J. Clin. Exp. Pathol.* 8 (10), 12793–12801.

You, Y. N., Rustin, R. B., and Sullivan, J. D. (2015). Oncotype DX colon Cancer Assay for Prediction of Recurrence Risk in Patients with Stage II and III colon Cancer: A Review of the Evidence. *Surg. Oncol.* 24 (2), 61–66. doi:10.1016/j.suronc.2015.02.001

Conflict of Interest: The authors declare that the research was conducted in the absence of any commercial or financial relationships that could be construed as a potential conflict of interest.

Publisher's Note: All claims expressed in this article are solely those of the authors and do not necessarily represent those of their affiliated organizations, or those of the publisher, the editors, and the reviewers. Any product that may be evaluated in this article, or claim that may be made by its manufacturer, is not guaranteed or endorsed by the publisher.

frontiers in Cell and Developmental Biology

ORIGINAL RESEARCH
published: 31 January 2022
doi: 10.3389/fcell.2022.812271

Identification of Key Genes Related With Aspartic Acid Metabolism and Corresponding Protein Expression in Human Colon Cancer With Postoperative Prognosis and the Underlying Molecular Pathways Prediction

Weixuan Sun[1], *Chaoran Jia*[2], *Xiaojun Zhang*[2], *Zhaoyi Wang*[1]*, *Yaping Li*[3]* and *Xuedong Fang*[1]*

[1]China-Japan Union Hospital of Jilin University, Changchun, China, [2]Northeast Normal University, Changchun, China, [3]The Second Hospital of Jilin University, Changchun, China

Objective: Colon cancer is one of the most frequent and lethal neoplasias. Altered metabolic activity is a well-known hallmark for cancer. The present study is aiming to screen key genes associated with tumor metabolism and construct a prognostic signature of colon cancer patients.

Methods: Glutamine- and UC- metabolism related genes were downloaded from GSEA MsigDB. Three key genes were screened by Cox regression analysis with data samples downloaded from TCGA and GSE29623 database. Consistent clustering based on the prognostic genes identified was employed to divide the colon cancer samples into two clusters with significant OS differences. The mRNA and protein expression of the key genes in colon tissues and matched adjacent noncancerous tissues of 16 patients were detected by IHC, qPCR, and Western blot to validate the constructed clustering model. GO, GSVA, and IPA were used to predict the relevant metabolic pathways.

Results: According to the three key genes identified, i.e., ASNS, CEBPA, and CAD, the cohort can be divided into two clusters with prognosis differences. Clinical specimen results confirmed that the risk model established was effective, and the different

OPEN ACCESS

Edited by:
Oronzo Brunetti,
Bari John Paul II Cancer Institute, National Cancer Institute Foundation (IRCCS), Italy

Reviewed by:
Eric Stephen Goetzman, University of Pittsburgh, United States
Josep Centelles, University of Barcelona, Spain
Ovidio Bussolati, University of Parma, Italy

***Correspondence:**
Zhaoyi Wang
wangzhaoyi@jlu.edu.cn
Yaping Li
yaping@jlu.edu.cn
Xuedong Fang
fangxd@jlu.edu.cn

Specialty section:
This article was submitted to Molecular and Cellular Oncology, a section of the journal Frontiers in Cell and Developmental Biology

Received: *10 November 2021*
Accepted: *17 January 2022*
Published: *31 January 2022*

Citation:
Sun W, Jia C, Zhang X, Wang Z, Li Y and Fang X (2022) Identification of Key Genes Related With Aspartic Acid Metabolism and Corresponding Protein Expression in Human Colon Cancer With Postoperative Prognosis and the Underlying Molecular Pathways Prediction. Front. Cell Dev. Biol. 10:812271. doi: 10.3389/fcell.2022.812271

Abbreviations: ASNS, asparagine synthetase; BP, biological process; CAD, carbamoyl-phosphate synthetase 2, aspartate transcarbamylase, and dihydroorotase; CC, cellular components; CDF, cumulative distribution function; CEBPA, CCAAT/enhancer binding protein alpha; CLP, common lympoid progenitors; CRC, colorectal cancer; CRE, cAMP response element; CREB, cAMP response element-binding protein; CXCR4, CXC chemokine receptor 4; FDR, false discovery rate; GEO, gene expression omnibus; GO, gene ontology; GSVA, gene set variation analysis; HRP, horseradish peroxidase; IHC, immunohistochemistry; IPA, ingenuity pathway analysis; KEGG, Kyoto Encyclopedia of genes and genomes; NER, nucleotide excision repair; OS, overall survival; PD-1, programmed cell death protein 1; PD-L1, programmed death ligand 1; PPAR, peroxisome proliferators-activated receptors; RNA pol II, RNA polymerase II; ssGSEA, single sample gene set enrichment Analysis; TCGA, The cancer genome Atlas; Th2 cells, T-helper 2 cells; TIDE, tumor immune dysfunction and exclusion; TME, tumor microenvironment; TNM staging, Tumor-Node-Metastasis staging; t-SNE, t-distributed stochastic neighbor embedding; UC, urea cycle.

expression pattern of ASNS and CEBPA was correlated with TNM stage and lymph node metastasis, whilst that of CAD was correlated with post-operative tumor metastasis and recurrence. Molecular mechanism prediction indicated that CREB, insulin, and RNA Pol II were the key nodes affecting CEBPA and ASNS expression. Moreover, TIDE algorithm reflected the better immune response of the cluster with shorter OS. Further immune infiltration and checkpoints analyses provided important reference for clinicians to perform individualized immunotherapy.

Conclusion: Differential expression profile of three aspartic acid metabolic-associated genes, ASNS, CEBPA, and CAD, can be considered as a risk model with a good evaluation effect on the prognosis of colon cancer patients.

Keywords: consensus clustering, colon cancer, immune infiltration, prognostic signature, aspartic acid metabolism

INTRODUCTION

After dismissing the revelation of the "Warburg effect" for almost a century, the study of metabolic reprogramming has been revived as the understanding of cancer occurrence, development, and metastasis mechanism deepened (Ward and Thompson, 2012). Aside from the fact that tumor cells rely on aerobic glycolysis rather than the mitochondrial oxidative phosphorylation to survive (Vander et al., 2009), other metabolic alterations on malignant tumors have been gradually discovered, including both the lipid and amino acid metabolisms. Lipid uptake and storage are elevated in malignant tumors, while lipogenesis is strongly up-regulated to accommodate increased membrane biogenesis (Röhrig and Schulze, 2016; Pascual et al., 2017). Regarding the reprogramming of amino acid metabolism, glutamine, the most abundant circulating amino acid, is one of the hubs linking the metabolic processes (Altman et al., 2016). The high glutamine level in the blood provides carbon and nitrogen for cells. The glutamine-derived carbon can be used to synthesize amino acids and fatty acids, while the nitrogen from glutamine directly affects the biosynthesis of purines and pyrimidines (Rubin, 1990; Lane and Fan, 2015). Abnormal changes in glutamine related metabolic processes are considered to be hallmarks of tumorigenesis. Under glutamine deficiency condition, asparagine can complement glutamine as an important nitrogen source to support tumor cell proliferation (Zhang et al., 2014). Since glutamine is often found to be limited in the tumor microenvironment (TME), asparagine can even support epithelial breast cancer cells to proliferate in the absence of exogenous glutamine. In this context, asparagine supports *de novo* biosynthesis of glutamine through enhancing the expression of glutamine syntheses (Pavlova et al., 2018). And asparagine restriction reduces the expression of genes involved in the epithelial-mesenchymal transition, a key step for metastasis to initiate (Knott et al., 2018). While glutamine metabolism is crucial for ammonium assimilation, UC is the main pathway converting excess nitrogen into disposable form, which is an important process for ammonium alienation. UC dysregulation is considered to be a general tumor metabolic hallmark based on recent discoveries, for instance, UC rewiring toward pyrimidine synthesis promotes carcinogenesis (Krebs, 1970; Spinelli et al., 2017).

It is noteworthy to mention that other than tumor cells, the immune cells located in the surrounding TME also undergo amino acid metabolic reprogramming. For example, glutamine levels alteration can activate the tumor-infiltrating T cells and influence tumor growth by directly contacting or stimulating other cells in the TME (Keshet et al., 2018).

As one of the most prevalent and high-incidence cancers, CRC is a very heterogeneous disease that develops through a gradual accumulation of genetic and epigenetic changes (Simon, 2016). Although inexhaustive, some initial attempts have been made to uncover the mechanism of metabolic reprogramming in CRC (Renner et al., 2017). Typically, metabolomics analysis of serum/plasma samples from patients revealed the six most affected metabolic pathways in CRC, including protein biosynthesis, glutamine metabolism, ammonia cycle, alanine metabolism, aspartic acid metabolism and citric acid cycle (Wilkinson et al., 2010).

Indeed, CRC comprises both colon cancer and rectal cancer because they share many physiological features. Compared with that of rectal cancer, the early diagnosis and treatment of colon cancer patients shows much better prognosis (Freeman, 2013). However, in many patients with colon cancer, TNM staging-the existing "gold standard" prediction model-does not accurately predict tumor recurrence, metastasis, or survival. TNM staging is suboptimal as seen by the variation in target-therapy outcomes that exists amongst patients of the same stage. Thus, we employed bioinformatics techniques to obtain critical nitrogen metabolism-related genes and explored their survival predictive potential by classifying the colon cancer patients into two clusters. We further compared the underlying molecular mechanism and the immune behavior of the two clusters, and indicated their benefits for individualized target- and immuno-therapy.

MATERIALS AND METHODS

Data Collection

The transcripts and complete clinical data of 415 patients were downloaded from the Cancer Genome Atlas (TCGA) database.

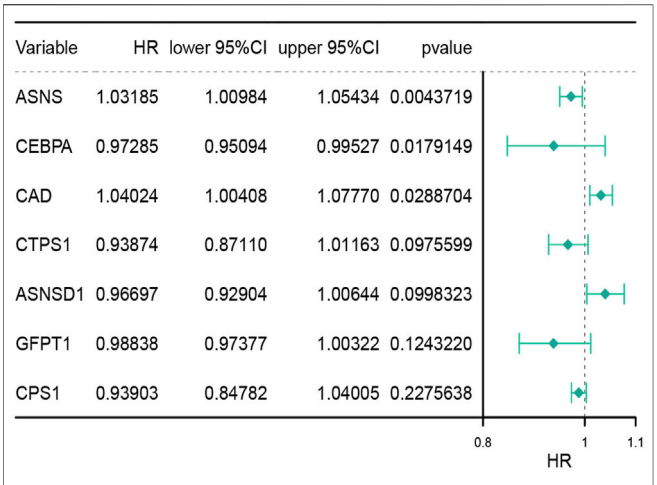

FIGURE 1 | Multivariate analysis of genes associated with glutamine metabolism and the urea cycle to identify key genes. HR stands for risk ratio, the lower/Upper 95% CI was the 95% confidence interval of the risk value. $n = 415$.

Gene Expression Omnibus (GEO) data source: GSE29623, 67 cases of colon cancer samples with complete clinical data were selected to verify the results of TCGA data analysis. The gene sets of UC metabolism and glutamine metabolism were downloaded from GSEA MsigDB. Gene set of UC metabolism: GO_ UREA_ CYCLE, GO_ UREA_ METABOLIC_ Process, including 13 genes. Glutamine metabolism gene set: GO_ GLUTAMINE_ METABOLIC_ Process, including 23 genes.

Cox Regression Analysis

Univariate Cox regression analysis was employed to select the genes with p-value < 0.2 by the proportional hazards model. The selected genes were incorporated into the multivariate Cox regression analysis, and genes with p-value < 0.05 were selected as prognostic genes. Cox regression analysis was used to determine the independent clinical risk factors, including patient age, gender, tumor TNM staging, etc.

Consistent Clustering

Consistent clustering of the TCGA and GEO databases were based on the prognostic genes obtained previously. The software package "ConsensusClusterPlus" was used for consistent clustering, and the optimal number of subgroups was evaluated using cumulative distribution function and consensus matrices (Li et al., 2014). Moreover, t-distributed Stochastic Neighbor Embedding (t-SNE) clustering algorithm was conducted to verify the clustering results.

Gene Ontology, Gene Set Variation Analysis, and Ingenuity Pathway Analysis Enrichment Analysis

Using the limma package, the differential expression of 415 different TCGA samples was analyzed, and the cutoff criteria set as log2FoldChange <0.5 and false discovery rate (FDR) < 0.05. The GO system comprised three sections: biological process, molecular functions, and cellular components. To further explore the functions of the differential genes, GO function enrichment analysis was performed using the cluster profiler software. The screening condition was |t-value| > 2 and p-value < 0.05 (Hänzelmann et al., 2013). The GSVA is a non-parametric unsupervised analysis method, mainly used to evaluate the gene set enrichment of chips and transcriptomes. GSVA transforms a matrix of "sample × gene" into a matrix of "sample × pathway", which directly reflects the connection between the sample and the reaction pathway. Similarly, using the limma package to do the same analysis on the results of GSVA (still a matrix) can find pathways with significant differences between samples. A more comprehensive functional enrichment analysis was conducted using the IPA software to elucidate the affected genes and signal pathways.

XCell Immune Infiltration Analysis

XCell (http://XCell.ucsf.edu/) is a single sample Gene Set Enrichment Analysis (ssGSEA) based approach. The abundance scores of 64 immune cell types were enriched by XCell (Aran et al., 2017). TIDE (tumor immune dysfunction and exclusion) (http://tide.dfci.harvard.edu) algorithm was used to predict the immunotherapy response of each patient.The statistical model of TIDE was trained on clinical tumor profiles without immune checkpoint blockade treatments since the immune evasion mechanisms in treatment-naïve tumors are influence patient response to immunotherapies (Jiang et al., 2018).

Patients Specimens and Clinical Data Collection

The primary colon cancer tissues and corresponding adjacent nontumor samples were retrieved from the China-Japan Union Hospital of Jilin University between January 2016 and January 2017. The eligibility criteria for the specimens are as follows: 1) patients aged 55–70 who received radical colon cancer surgery without any chemotherapy, radiotherapy or other intervention within 3 years; 2) no history of serious basal metabolic disease; 3) patients with follow-up information for more than 3 years available to determine whether other organ metastasis or recurrence occurred. A total of 16 colon cancer patients meeting the above conditions were screened. Specimens from these patients satisfied these criteria were immediately stockpiled at −80 after surgery and progressed for analysis. All patients were confirmed as colon cancer by postoperative histopathological examination, and the type identification and TNM staging were carried out by the pathology department of the China-Japan Union Hospital of Jilin University. Besides, the clinical data of patients were acquired from the electronic medical record of the department of gastrointestinal colorectal and anal surgery of China-Japan Union Hospital of Jilin University.

Immunohistochemistry

The slides were incubated at 65°C for 45 min and then dewaxed. Subsequently, we retrieved the antigen using citrate buffer and

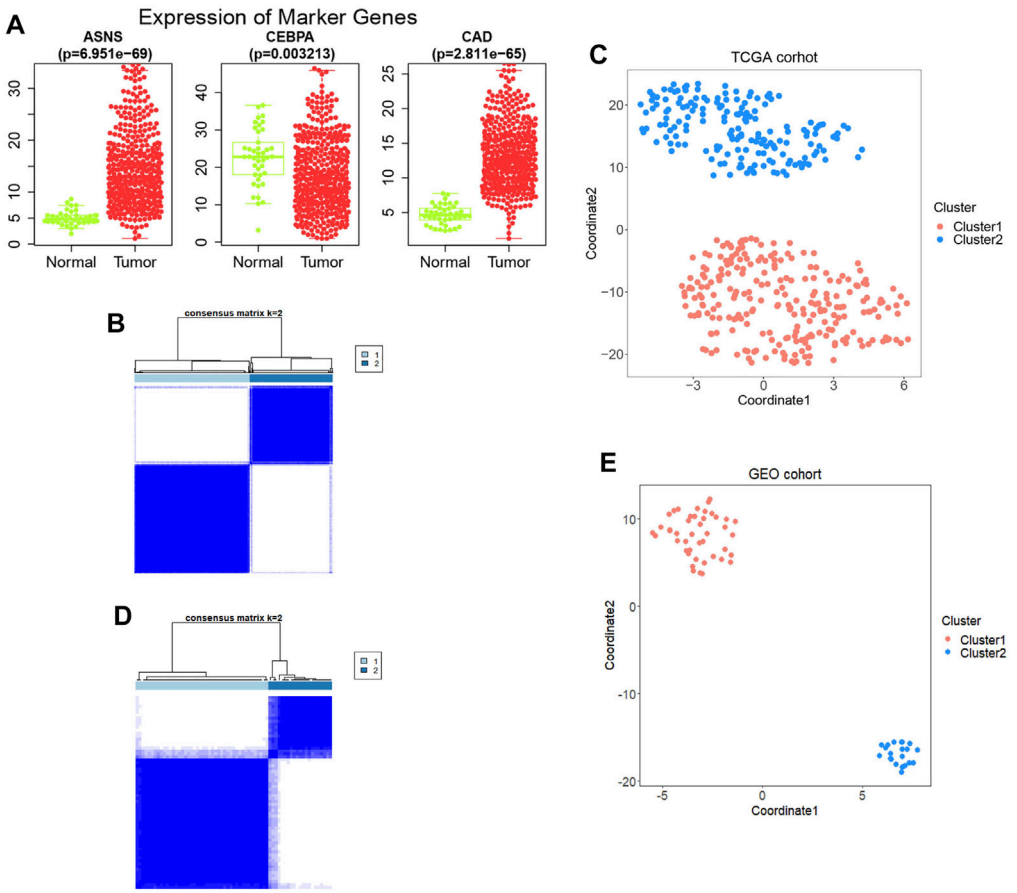

FIGURE 2 | (A) The expression levels of the three genes obtained between tumor samples and normal control samples. **(B)** Construction of the prognostic signature based on TCGA cohort and consensus clustering. The cohort was divided into two distinct clusters when $k = 2$. **(C)** The tSNE clustering algorithm divides colon cancer samples from TCGA into two clusters. **(D)** Construction of the prognostic signature based on GSE29623 cohort and consensus clustering. The cohort was divided into two distinct clusters when $k = 2$. **(E)** The tSNE clustering algorithm divides colon cancer samples from GSE29623 into two clusters.

blocking endogenous peroxidase with 3% H_2O_2. After nonspecific antigen blocking, the slides were incubated with antibodies at 4°C overnight. The antibodies against ASNS (dilution 1:200) and CEBPA (dilution 1:200) were purchased from Cellsignal (92479S; 8178S), and the antibody against CAD (dilution 1: 200) was purchased from Proteintech (16617-1-AP). The next day, slides were incubated with secondary antibody labeled with Horseradish Peroxidase (HRP) at room temperature for 1 h. Finally, the reaction was visualized using Diaminobezidin and the slides were counter stained with hematoxylin. The digital scanner of tissue section was used to collect the image on the immunohistochemical section. The Seville image analysis system was used to automatically read the tissue measurement area, as well as the number of weak, medium, and strong positive cells in the measurement area (negative without coloring, 0 point; weak positive light yellow, 1 point; medium positive brown yellow, 2 points; strong positive brown, 3 points). The total number of cells were analyzed and calculated respectively. The positive cell rate reflecting the protein expression on the section was also calculated.

qRT-PCR

Primers used for qPCR were designed using the Primer 5.0 gene primer design software. All primers were synthesized by Comate Bioscience Company Limited (Jilin, China) (ASNS-F: CTTTTA TCAGGGGGCTTGGAC, ASNS-R: CAGTAAATCGGGGCT GTCTTC; CEBPA-F: CACACCAGAAAGCTAGGTCGTG, CEBPA-R: AATGCTGAAGGCATACAGTACAAAC; CAD-F: CCAGACGTTGCTGATCAACCC, CAD-R: CCACACCAC AGTTCAGAGCAGTC). The mRNA expression levels were detected in triplicate using the SYBR Green I dye method. The β-actin was used as a reference gene. The RT-PCR reaction mixture consisted of cDNA (1 μl), PCR-Master Mix (5 μl), PCR-F-Primer (0.5 μl), PCR-R-Primer (0.5 μl), and RNase-free H_2O (3 μl) in a total volume of 10 μl. The RT-PCR reaction conditions were as follows: denaturation at 95°C for 1 min, followed by 40 cycles of denaturation at 95°C for 15 s, annealing at 60°C for 15 s, and extension at 72°C for 15 s. At the end of the reaction, the melting curve was recorded for the 60–95°C temperature range, and the reaction products were stored at 4°C. Data from the Eppendorf real-time PCR

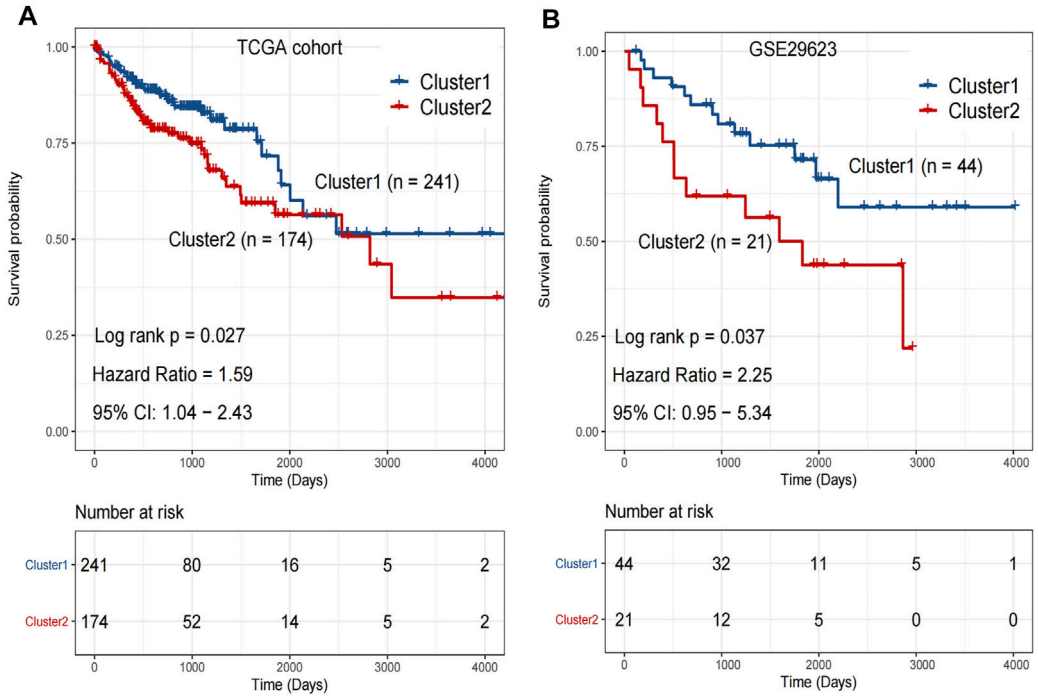

FIGURE 3 | (A) The overall survival rate of Cluster 1 was significantly longer than that of Cluster 2 in TCGA. $p < 0.05$. **(B)** The overall survival rate of Cluster 1 was significantly longer than that of Cluster 2 in GSE29623. $p < 0.05$. Analyzed using unpaired *t*-test.

instrument (Hamburg, Germany). We obtained the mRNA CT value of the target gene through qPCR, and then calculated it with the mRNA CT value of the GAPDH, and finally obtained the relative expression of the mRNA of the target gene. The specific formula is as follows:

△CT = CT target gene -Ct GAPDH; △△CT = △CT experimental-△CT control; Relative expression = $2^{-\triangle\triangle CT}$

Western Blotting

Total protein from tissue samples or cells was extracted and protein concentrations were quantified using a BCA assay kit (Beyotime Biotechnology, China). Then protein samples were electrophoresed on 12% sodium dodecyl sulfate-polyacrylamide (SDS-PAGE) gels and subsequently transferred to polyvinylidene difluoride (PVDF) membranes, which were blocked with 5% skimmed milk and incubated at 4°C overnight with targeted primary antibodies on a rotating wheel. The membranes were washed three times and immediately following the incubation with corresponding HRP-conjugated secondary antibodies for 1 h and then imaging. The gray value was calculated by the AlphaEase FC software. The ratio of the gray value of the target band to the corresponding internal reference β-Actin reflected the relative expressions.

The antibodies against ASNS (dilution 1:500) and CEBPA (dilution 1:500) was purchased from Cellsignal (92479S; 8178S), the antibody against the CAD (dilution 1:500) was purchased from Proteintech (16617-1-AP), and the antibody against β-Actin (dilution 1:500) was purchased from Servicebio (GB12001).

RESULTS

Construction of a Cluster Model Using Three Key Genes Identified, i.e., ASNS, CEBPA, and CAD, for Colon Cancer.

Thirty-six genes related to glutamine metabolism and UC metabolism were obtained from GSEA MsigDB database. These genes were analyzed by univariate Cox regression analysis in 415 colon cancer samples from TCGA database. 11 genes with $p < 0.2$ related to OS were screened (**Supplementary Figure S1**). Then the 11 genes were analyzed by multivariate Cox regression analysis. Three genes with p value <0.05 related to OS were screened (**Figure 1**; **Supplementary Figure S2**), i.e., ASNS, CEBPA, and CAD, as the key genes to differentiate the cohort. Their expression was significantly different in colon cancer and normal colon samples in TCGA (**Figure 2A**).

Based on the expression profiles of ASNS, CEBPA, and CAD, 415 TCGA colon cancer samples were analyzed by consistent clustering (**Figure 2B**) and tSNE algorithm (**Figure 2C**), and the samples were divided into two clusters, Cluster 1 and Cluster 2, with longer and shorter survival time, respectively. In order to verify our clustering results, we applied the three genes obtained for consistent clustering and tSNE algorithm analysis in 67 colon cancer samples from GSE29623, and stratified the cohort into two clusters successfully (**Figures 2D,E**). However, the specific expression of ASNS, CEBPA, and CAD in the two clusters remains unclear.

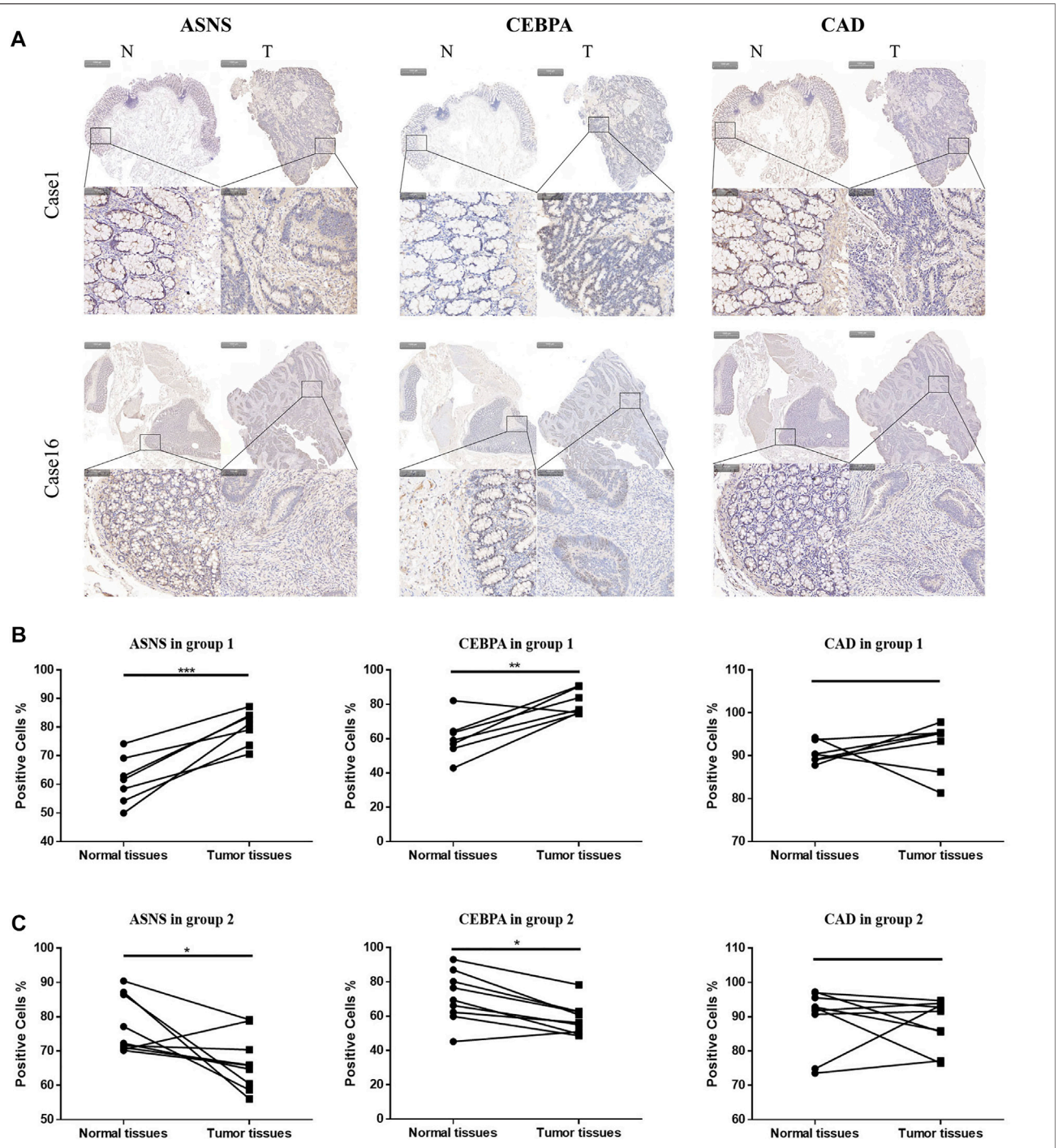

FIGURE 4 | (A) Typical images of IHC in 16 pairs of colon cancer tissues showing the protein expression of ASNS, CEBPA and CAD in colon cancer tissues and adjacent nontumor tissues. Up panel, scale bar 1000 μm; down panel, scale bar 100 μm. **(B)** Immunohistochemical positive cell rates of ASNs, CEBPA, and CAD in 7 colon cancer tissues and adjacent nontumor tissues in group 1. **(C)** Immunohistochemical positive cell rates of ASNS, CEBPA and CAD in 9 colon cancer tissues and adjacent nontumor tissues in group 2. *$p < 0.05$, **$p < 0.01$ and ***$p < 0.001$, analyzed using unpaired *t*-test. Group 1, n = 7; Group 2, $n = 9$.

TABLE 1 | Clinical information on selected colon cancer patients for validation, which were divided into two groups, i.e., Group 1 and Group 2, according to different N stages.

Sample ID	Case 1	Case 2	Case 3	Case 4	Case 5	Case 6	Case 7
Gender	M	M	M	F	M	M	M
Age	69	65	64	67	63	61	59
Tumor size (cm)	20	12	24	31.5	5.25	11.76	2.4
TNM stage	T3N0Mx	T3N0Mx	T3N0Mx	T3N0Mx	T3N0Mx	T3N0Mx	T3N0Mx
Date of surgery	2016.5	2016.5	2016.6	2016.7	2016.9	2016.11	2017.1
Metastasis or recurrence within 3 years	Occurrence	Not occurrence	Occurrence	Not occurrence	Occurrence	Not occurrence	Occurrence
Group 1							

Sample ID	Case 8	Case 9	Case 10	Case 11	Case 12	Case 13	Case 14	Case 15	Case 16
Gender	M	F	F	M	F	F	F	M	M
Age	69	69	68	59	67	66	61	69	67
Tumor size (cm)	9	13.13	21	14	6.75	202.5	24	40.5	7.5
TNM stage	T3N1Mx	T3N1Mx	T3N1Mx	T3N2Mx	T4N1Mx	T3N1Mx	T3N1Mx	T3N1Mx	T3N1Mx
Date of surgery	2016.4	2016.5	2016.5	2016.7	2016.7	2016.8	2016.9	2016.11	2017.1
Metastasis or recurrence within 3 years	Not occurrence	Not occurrence	Occurrence	Not occurrence	Occurrence	Occurrence	Not occurrence	Occurrence	Occurrence
Group 2									

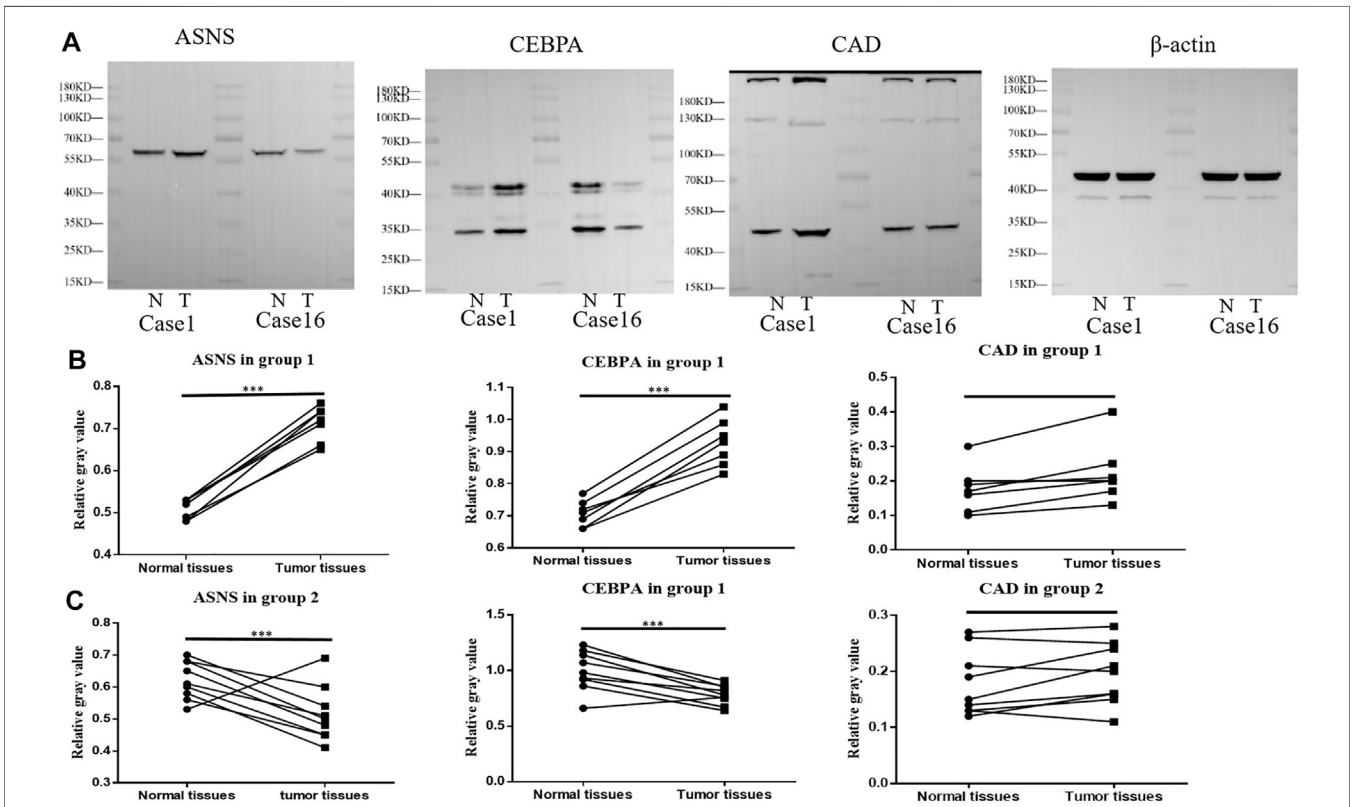

FIGURE 5 | (A) ASNS, CEBPA, and CAD expression levels in Case 1 and Case 16 of tumor specimens and adjacent normal specimens. **(B)** The relative gray values of western blot, which represent the relative protein expression level, of ASNS, CEBPA, and CAD in 7 Colon cancer tissues and adjacent nontumor tissues in **(B)** Group 1 and **(C)** Group 2.*$p < 0.05$, **$p < 0.01$ and ***$p < 0.001$, analyzed using unpaired *t*-test. Group 1, $n = 7$; Group 2, $n = 9$.

TABLE 2 | mRNA relative expression of ASNS, CEBPA, and CAD in Group 1 and Group 2.

Group 1	ASNS		CEBPA		CAD	
	N	T	N	T	N	T
Case 1	1.00	1.67	1.00	1.85	1.00	1.86
Case 2	0.69	1.61	1.52	2.24	0.66	1.06
Case 3	0.97	1.45	0.94	1.72	1.51	0.88
Case 4	0.86	1.98	0.60	2.30	1.78	0.42
Case 5	1.62	1.84	1.77	2.14	1.34	1.55
Case 6	0.66	1.65	0.79	1.92	1.64	0.46
Case 7	1.49	1.63	3.41	2.46	1.07	1.56
Group 2	**ASNS**		**CEBPA**		**CAD**	
	N	T	N	T	N	T
Case 8	1.81	1.54	2.42	1.43	1.17	1.61
Case 9	1.53	1.57	2.04	1.38	1.06	1.61
Case 10	2.07	0.78	2.99	0.59	0.35	2.42
Case 11	1.93	1.62	2.44	1.99	1.65	1.19
Case 12	1.76	0.62	2.17	0.81	1.12	0.58
Case 13	2.19	0.96	2.33	0.84	2.06	0.56
Case 14	1.70	1.41	2.54	2.17	0.92	2.52
Case 15	1.30	1.17	2.33	1.13	1.65	0.73
Case 16	1.81	1.36	2.10	1.31	0.95	1.01

Comparision of OS Differences and Clinical Risk Scores Between Each Two Clusters Obtained From TCGA and GSE29623 Databases.

Kaplan-Meier analysis was performed on the clusters of colon cancer samples from TCGA (Cluster 1: n = 241 v.s. Cluster 2: n = 174) and GSE29623 databases (Cluster 1: n = 44 v.s. Cluster 2: n = 21). The OS of Cluster 2 was significantly lower than that of Cluster 1 in both databases (**Figures 3A,B**).

The clinical risk features for each colon cancer patient included age, gender, tumor grade, stage, etc. The colon cancer samples in TCGA were analyzed by Cox regression. Univariate cox regression analysis showed that tumor stage, T stage, N stage, M stage, and our clustering were risk factors associated with clinical prognosis (**Supplementary Figure S3**).

Validation of the Constructed Cluster Models With Clinical Samples.

We further examined the expression of ASNS, CEBPA, and CAD in tumor tissues and adjacent normal tissues from different colon cancer patients. It was verified that our clustering model could divide colon cancer patients into two clusters with different clinical characteristics.

More specifically, 16 pairs of primary colon cancer tissues from the Department of Gastrointestinal Colorectal Surgery in China-Japan Union Hospital of Jilin University were analyzed by IHC staining (**Figure 4A**). Among them, patients 1–7 (Group 1) had no lymph node metastasis (N0 stage), and patients 8–16 (Group 2) had lymph node metastasis (N1 or N2 stage) (**Table 1**). Results showed that in Group 1, the protein level of ASNS and CEBPA was higher in tumor tissues than in adjacent normal colon tissues, while in Group 2, the results were opposite. As for the CAD expression, the level in the tumor and non-tumor normal tissues was similiar in both Group 1 and Group 2 (**Figures 4B,C**).

Further Western blotting and blot gray value analysis were performed to verify the protein expression in 16 pairs of samples (**Figure 5A**; **Supplementary Figure S4**). The results were consistent with IHC staining. The expression of ASNS and CEBPA in tumor tissues of Group 1 was higher than that in non-tumor normal tissues, while the expression of ASNS and CEBPA in tumor tissues of Group 2 was lower than that in non-tumor normal tissues. There was no significant difference in the expression of CAD in tumor tissues and non-tumor tissues in different groups (**Figures 5B,C**). The low expression of ASNS and CEBPA in colon cancer tissues was closely related to the occurrence of lymph node metastasis, which had an impact on prognosis and shortened OS (Freeman., 2013).

The mRNA expressions of ASNS,CEBPA, and CAD in 16 pairs of specimens were detected by qPCR (**Table 2**), and the correlation analysis was conducted with the clinical characteristics and prognosis of patients. The results showed that the expression of ASNS was correlated with the size of tumor growth,that of CEBPA was correlated with the gender of patients and TNM stage of tumor, and that of CAD was highly correlated with recurrence and metastasis (**Table 3**).

The above experiments have preliminary verified the clustering model. According to the different expressions of ASNS, CEBPA, and CAD, colon cancer patients could be divided into two clusters with different postoperative outcomes.

Different Expressions of Pathways Related to Biological Function and Substance Metabolism in the Two Clusters

In TCGA database, we describe differences in gene expression between two clusters. Differential expression analysis demonstrated 157 significantly differentially expressed genes, of Cluster 2 relative to Cluster 1, including 26 up-regulated genes and 131 down-regulated genes (**Figure 6A**). Then GO annotation was performed to understand the influence of these different genes on various functions in the cell. GO BP analysis revealed that these genes were markedly enriched in lipid transport, lipid localization, and alcohol metabolic process. For GO CC analysis, the top three significantly enriched terms were apical part of cell, apical plasma membrane, and cell projection membrane (**Figure 6B**). We associated the first 11 cell function items obtained by GO analysis with the enriched differential genes (**Figure 6C**). It is worth mentioning that we enriched the biological process of reduced glutathione. Since reduced glutathione is closely related to glutamine metabolism (glutamine is the precursor of reduced glutathione), we further analyzed the differential genes in the biological process of reduced glutathione, SLC7A11, CHAC1, and GGT6. Correlations between them and the three key genes previously screened were determined (**Figure 6D**). The results showed that ASNS was positively correlated with CHAC1, while CEBPA was

TABLE 3 | Relationship between ASNS, CEBPA, and CAD expression level and clinicopathological variables in 16 colon cancer patients.

Pathological characteristics	n	Low expression (n)	High expression (n)	*p* value
Age(years)				0.547
≥65	10	3	7	
<65	6	4	2	
Gender				0.174
M	10	3	7	
F	6	4	2	
Tumor size (cm)				0.043
≥20	7	5	2	
<20	9	2	7	
TNM stage				0.674
T3N0Mx	7	3	4	
T3N1Mx	7	3	4	
T3N2Mx	1	0	1	
T4N1Mx	1	1	0	
Metastasis or recurrence within 3 years				0.953
Occurrence	9	4	5	
Not occurrence	7	3	4	
Pathological characteristics	**n**	**Low expression (n)**	**High expression (n)**	***p* value**
Age(years)				0.156
≥65	10	3	7	
<65	6	0	6	
Gender				0.01
M	10	0	10	
F	6	3	3	
Tumor size (cm)				0.409
≥20	7	2	5	
<20	9	1	8	
TNM stage				0.034
T3N0Mx	7	0	7	
T3N1Mx	7	2	5	
T3N2Mx	1	0	1	
T4N1Mx	1	1	0	
Metastasis or recurrence within 3 years				0.102
Occurrence	9	3	6	
Not occurrence	7	0	7	
Pathological characteristics	**n**	**Low expression (n)**	**High expression (n)**	***p* value**
Age(years)				0.547
≥65	10	5	5	
<65	6	2	4	
Gender				0.174
M	10	3	7	
F	6	4	2	
Tumor size (cm)				0.053
≥20	7	5	2	
<20	9	2	7	
TNM stage				0.674
T3N0Mx	7	3	4	
T3N1Mx	7	3	4	
T3N2Mx	1	0	1	
T4N1Mx	1	1	0	
Metastasis or recurrence within 3 years				0.001
Occurrence	9	1	8	
Not occurrence	7	6	1	

negatively correlated with SLC7A11. This provided the explaination of the correlation between ASNS, CEBPA, and glutathione metabolism.

In the TCGA colon cancer sample, GSVA analysis was performed to correlate the differential gene set with the KEGG pathway. It was found that 81 pathways were active in Cluster 1 (T < 2), such as metabolic pathway, cellular signal transduction pathway, and tumor pathway, while 19 pathways were active in Cluster 2 (T > 2), such as glycine, nitrogen and tetrahydrofolate metabolism pathway (**Figure 7A**). Among the 25 pathways with

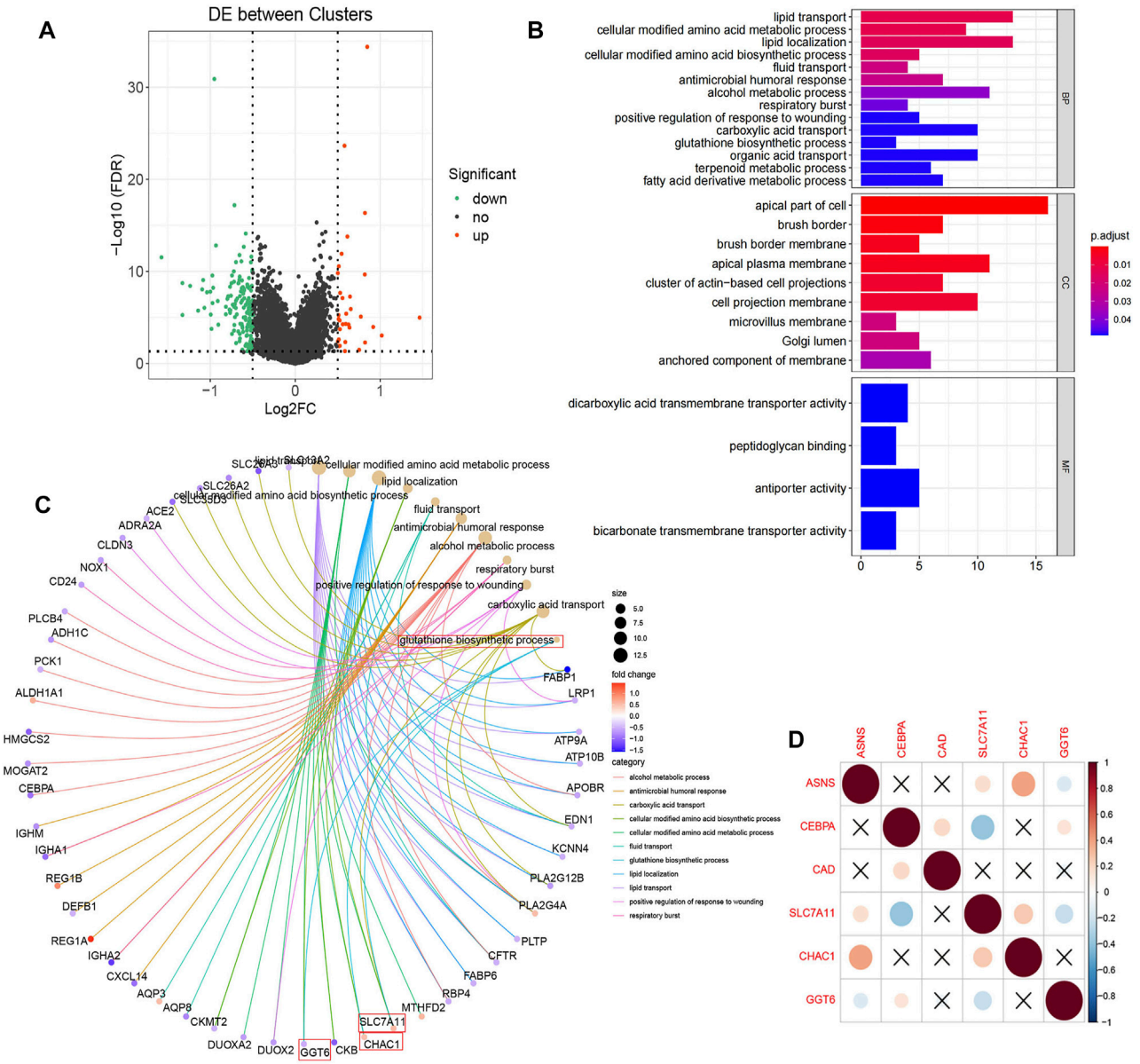

FIGURE 6 | (A) Volcano plot displayed the 157 differentially expressed genes of Cluster 2 screened relative to Cluster 1 with 26 up-regulated (red dots) and 131 down-regulated (green dots).The black dots indicate genes that are not significantly different. **(B)** The enriched GO BP, CC, and MF terms of the differential genes. **(C)** The GO entry network diagram, showing the top 11 network relationships of GO enrichment. The process of glutathione synthesis and the genes it contains are indicated with red boxes. **(D)** Correlation diagram of the prognostic genes and glutathione synthesis process enriched genes.

the largest absolute t value, 20 pathways were activated in Cluster 1 samples, including renin-angiotensin system, PPAR signaling pathway, WNT signaling pathway, etc.; while five pathways were activated in Cluster 2 samples, including protein export, folate carbon pool, nuclear maneuver repair, etc. (**Figures 7B,C**).

IPA Gene Interaction Network Prediction of Key Genes ASNS and CEBPA

The differential gene interaction network between Cluster 1 and Cluster 2 was constructed by IPA software. Based on IPA data of the identified molecular interactions reported in the literature, a gene pathway network containing ASNS and CEBPA emerged (**Figure 8A**). In our results, CREB, insulin, and RNA Pol II are critical nodes in the CEBPA- related pathway (**Figure 8B**). CREB, insulin, and RNA Pol II are the upstream of CEBPA, and their overexpression may down-regulate CEBPA. We further obtained all downstream differential genes of CEBPA, among which it is noteworthy that CEBPA, as an upstream gene of ASNS, upregulates the expression of ASNS (**Figure 8C**).

We clustered colon cancer samples in TCGA by the differential expression of ASNS, CEBPA, and CAD, and the

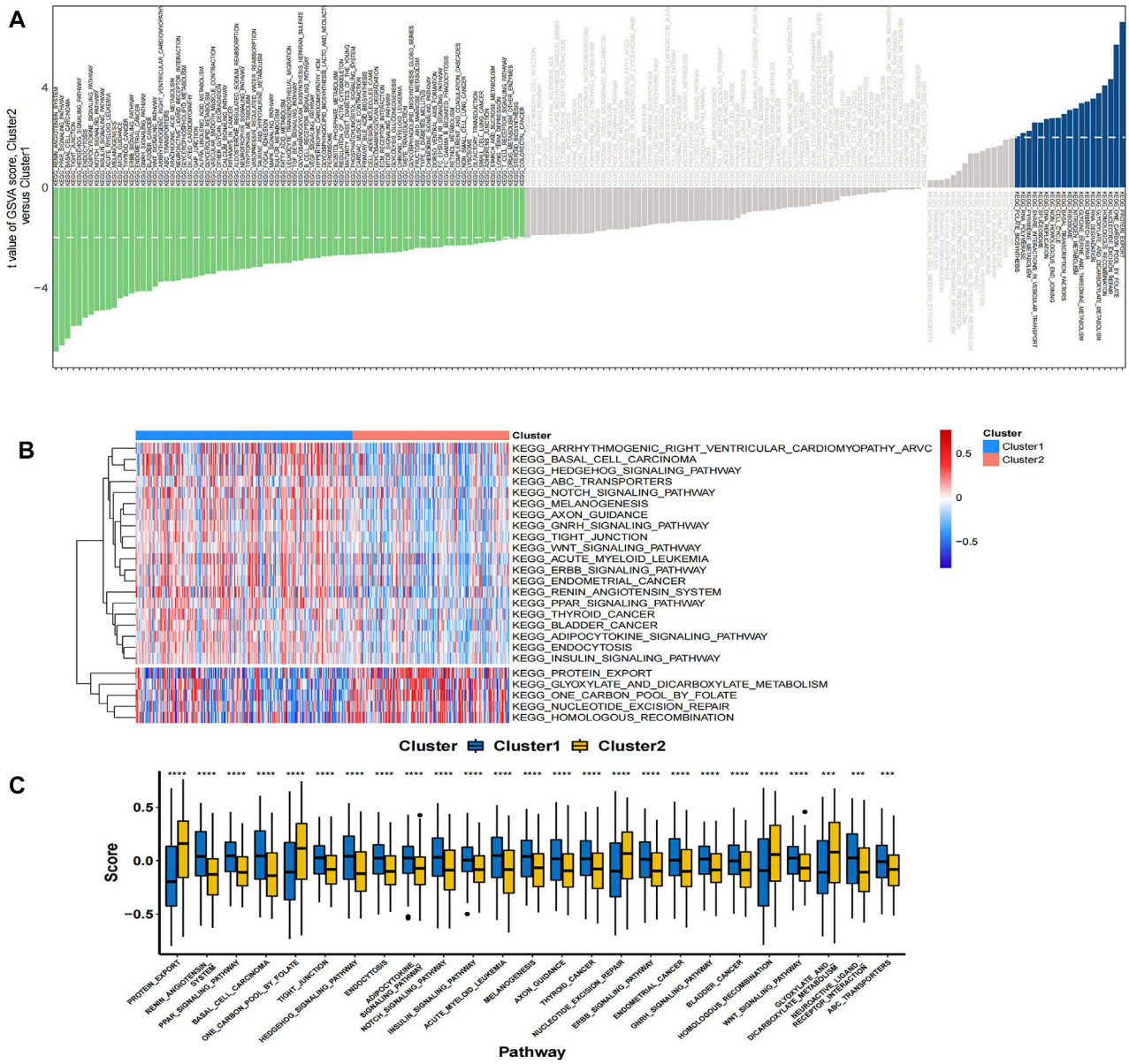

FIGURE 7 | (A) The bar plots show the results of GSVA in the TCGA cohort. A negative t-value means that the pathway is enriched in Cluster 1, and a positive t-value means that it is enriched in Cluster 2. **(B)** The cluster heat map of the top 25 enriched KEGG pathways. **(C)** The boxplot showed different activation levels of GSVA-enriched KEGG pathways in Clusters 1 and 2. ***$p < 0.001$, and ****$p < 0.0001$. Analyzed using unpaired *t*-test.

results showed that the interaction between ASNS and CEBPA and their upstream and downstream genes was responsible for the differences in cell functional status and substance metabolism levels between Cluster 1 and Cluster 2.

Preliminary Survey of the Difference in the Immune Microenvironment of the Two Clusters Stratified.

We have already confirmed that ASNS and CEBPA expression were associated with lymph node metastasis in colon cancer patients. To further assist the individual immunotherapy, we investigated the immune infiltrating and immune checkpoint genes in Cluster 1 and Cluster 2 samples. The differential immune infiltration features and the associated potential immunotherapeutic responses of the two clusters were explored by XCell and TIDE algorithm. The XCell software was employed to analyze the difference of the infiltrated immune cells between Cluster 1 and Cluster 2 in colon cancer samples from TCGA database. Th2 cells, CLP cells, and $CD4^+$ memory T cells showed higher cell infiltration in Cluster 2; while $CD4^+$ Tcm cells, $CD4^+$ Tem cells, eosinophiles, monocytes, and Tgd cells were found to have the similar exhibition between the two

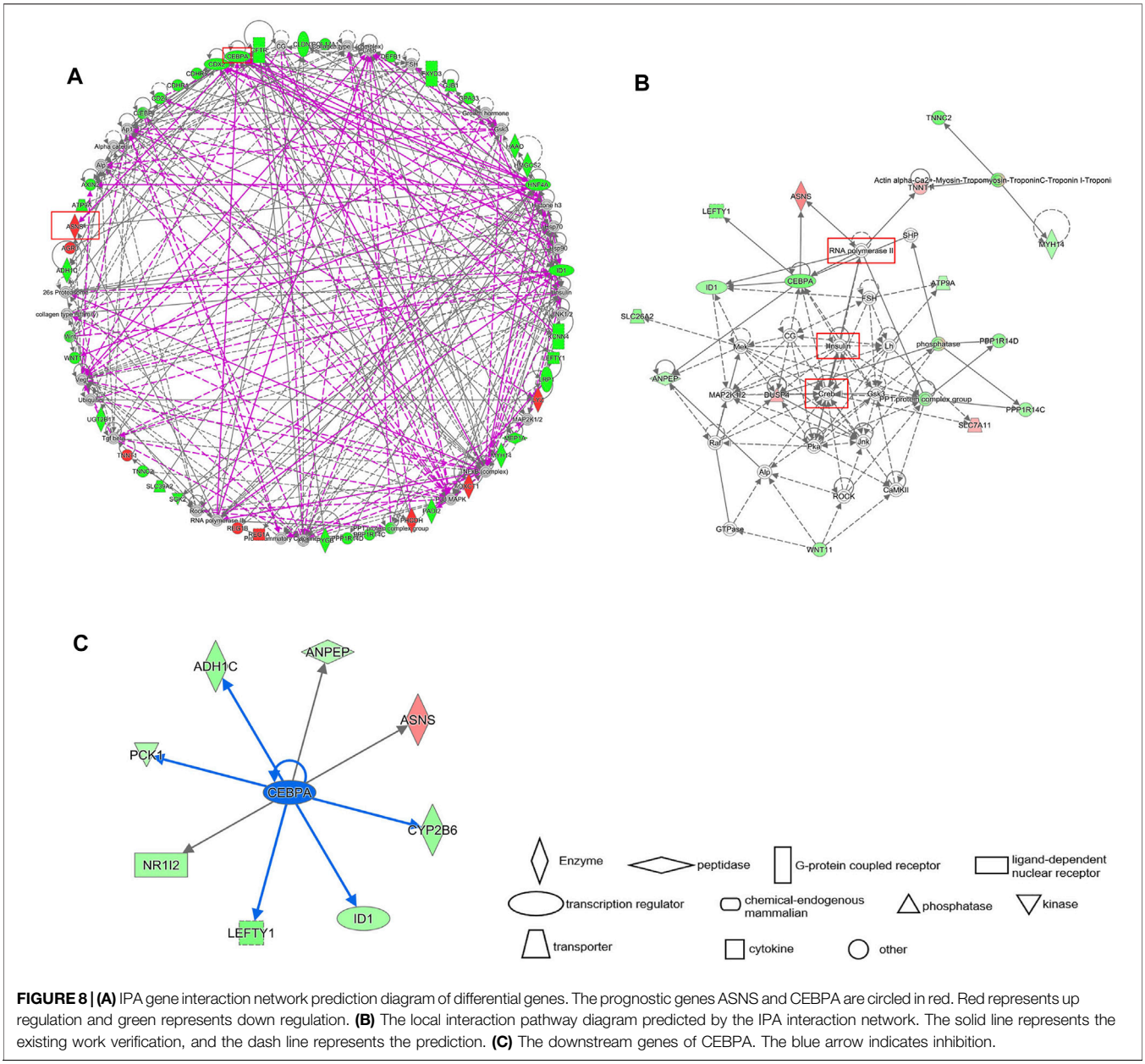

FIGURE 8 | (A) IPA gene interaction network prediction diagram of differential genes. The prognostic genes ASNS and CEBPA are circled in red. Red represents up regulation and green represents down regulation. **(B)** The local interaction pathway diagram predicted by the IPA interaction network. The solid line represents the existing work verification, and the dash line represents the prediction. **(C)** The downstream genes of CEBPA. The blue arrow indicates inhibition.

clusters (**Figures 9A,B**). To link individual responses to immunotherapeutic responses, the TIDE algorithm was used. The lower TIDE score of Cluster 2 samples indicated that they may respond better to immunotherapy (**Figure 9C**). The expression levels of common immune checkpoints in Cluster 1 and Cluster 2 were also checked. CEACAM1, LGALS9, and CD40LG were highly expressed in Cluster 1, while CD274 (PD-L1) and CXCR4 were highly expressed in Cluster 2 (**Figure 9D**).

DISCUSSION

It has become evident that CRC is a highly heterogeneous disease with complex molecular pathogenesis. The classical TNM staging system benefits the clinical management of CRC for years. Consider the disappointing outcome of targeted drugs and immune checkpoint therapies on CRC patients; it is imperative to develop new biomarkers that enable the stratification of patients with CRC, which can guide the more-precise use of innovative therapies (Punt et al., 2017). Various central metabolic pathways, which intimately entwined with cell signaling and epigenetic networks, dysregulated in CRC cells. Moreover, the metabolic machineries and nutrient-sensing mechanisms orchestrated the behavior of immune cells located in the TME (Li et al., 2019).

In this study, three key genes, ASNS, CEBPA, and CAD, were screened by Cox regression analysis in colon cancer. ASNS consumes ATP to catalyze the conversion of aspartic acid and

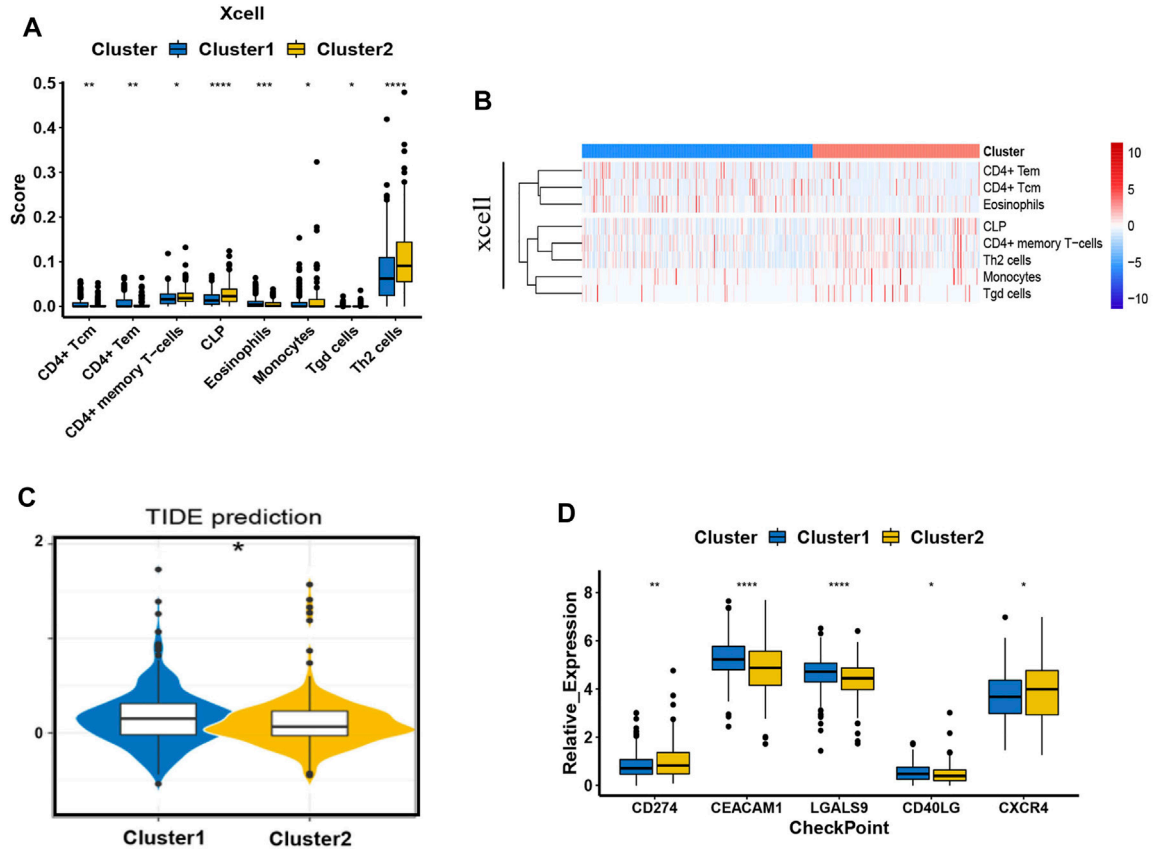

FIGURE 9 | Immune behavior comparison between the two clusters. **(A)** The boxplots show the XCell scores for the enriched immunocytes. Within each group, the scattered dots represent values for cellular expression; whereas the thick line represents the median value. The statistical difference of the two clusters was compared using the Kruskal-Wallis test, and the asterisk above the box plot represents the degree of significance. **(B)** The heat map of the XCell immune infiltration analysis. **(C)** The boxplot representation of TIDE scores in Cluster 1 versus Cluster 2. **(D)** The expression pattern of five common types of immune checkpoints. *$p < 0.05$, **$p < 0.01$, ***$p < 0.001$, and ****$p < 0.0001$. Analyzed using unpaired *t*-test.

glutamine to asparagine and glutamate (Lomelino et al., 2017). Pyrimidines synthesis in cancerous proliferation can be regulated by enhancing aspartate availability for the enzymatic complex CAD. (Rabinovich et al., 2015). CEBPA, as a transcription factor, is a key regulator of many metabolic processes, such as lipid metabolism and amino acid metabolism (Diehl, 1998). Moreover, C/EBP homology protein negatively regulates the stress-dependent induction of the asparagine synthetase gene (Su and Kilberg, 2008).

TCGA data analysis and IHC staining of clinical tumor samples showed that ASNS and CEBPA tended to be underexpressed in the Cluster 2 with poor prognosis. Subsequently, we identified CEBPA as the upstream gene of ASNS, and showed a positive correlation between CEBPA and ASNS. To further reveal the underlying mechanism, we identified the upstream factors, i.e., CREB, Insulin, and RNA Pol II in the predicted signal network. CREB levels are generally positively correlated with tumor grade, stage, metastasis, increased recurrence rate, and poor prognosis (Steven et al., 2020). It has also been reported that CEBPA binds to CRE in the liver and antagonizes CREB (Roesler, 2000). And CREB often antagonizes insulin *in vivo* (Altarejos and Montminy, 2011). Insulin resistance is one of the factors that induce colon cancer and other tumors (McNabney and Henagan, 2017). Insulin can also activate CEBPA expression (Marques-Oliveira et al., 2018). Therefore, it can be speculated that CREB antagonizes the effect of insulin in colon cancer, reduces the activation and expression of CEBPA, and play a carcinogenic role. Furthermore, we found that CREB directly upregulated SLC7A11 expression, and CEBPA negatively correlated with SLC7A11. Studies have shown that SLC7A11 can promote cysteine absorption and glutathione biosynthesis, prevent oxidative stress, thus, significantly increase glutamine metabolism, and promote the growth of cancer cells (Koppula et al., 2018). It is possible that CREB up-regulation of SLC7A11 also play a carcinogenic role in colon cancer. Moreover, RNA Pol II was predicted to be an upstream factor associated with both CEBPA and ASNS. Rapid proliferation of tumor cells increases the expression of RNA Pol II. Transcription-

coupled subpathway of nucleotide excision repair (NER) is activated by the stalling of RNA Pol II during transcriptional elongation (Marteijn et al., 2014). Our prediction model suggested that overexpression of RNA pol II down-regulated CEBPA and ASNS in Cluster 2.

The immune infiltration results showed that compared with the Cluster 1 patients, the degree of Th2 cell infiltration was much higher in Cluster 2 patients with a shorter survival time. In addition, the TIDE score of Cluster 2 patients was lower, indicating a better response to immunotherapy. It was also found that the expression of both CXCR4 and CD274 (PD-L1) in Cluster 2 were higher through the immune checkpoint analysis. Recent *PNAS* study reported that CXCR4 inhibition in combination with blockade of the PD-1/PD-L1 induced T cell infiltration and anticancer responses in human pancreatic and colorectal cancers (Biasci et al., 2020). Therefore, due to the high expression of CXCR4 and PD-L1 in Cluster 2, the synergistic treatment of anti-PD-1 and blocking CXCR4 targeting Cluster 2 patients may produce better therapeutic effects.

It was found that in our cluster model, ASNS and CEBPA play an important role in the prognosis of colon cancer patients, and patients with low ASNS and CEBPA expression had a worse prognosis, i.e., more prone to lymph node metastasis. Additionally, the expression profile of CAD was also associated with prognosis, i.e., patients with high CAD expression were more likely to metastasis and recurrence. CEBPA was the upstream gene of ASNS, and the expression of CEBPA and ASNS is positively correlated.We predict that upstream factors such as CREB, insulin, and RNA Pol II can regulate downstream genes, such as ASNS and SLC7A11, by affecting the expression of CEBPA, ultimately changing the cellular function and metabolism in colon cancer tissues. It even affects the infiltration of immune cells in TME, which may further affect the immunotherapy response of patients. Besides, these results suggested that aspartic acid metabolism play an important role in colon cancer and deserve further exploration.

CONCLUSION

In summary, three genes associated with metabolic processes were selected as the key genes for risk clustering model establishment of colon cancer patients. The model was verified by molecular biological experiments performed on clinical specimens. The GO annotation and GSVA analysis were carried out to distinguish the pathway activities between the two clusters with OS differences. The signaling networks were predicted by IPA, and hub nodes were identified. These findings suggest that the key genes may serve as new prognostic markers for colon cancer. Moreover, the immune response comparison between the two clusters was also conducted to provide references for individualized immunotherapy.

DATA AVAILABILITY STATEMENT

Publicly available datasets were analyzed in this study. This data can be found here: TCGA database: https://tcga-data.nci.nih.gov/tcga/, GEO database(GSE29623), https://www.ncbi.nlm.nih.gov/geo/.

ETHICS STATEMENT

The studies involving human participants were reviewed and approved by the Ethics Committee of China-Japan Union Hospital of Jilin University. The patients/participants provided their written informed consent to participate in this study. Written informed consent was obtained from the individual(s) for the publication of any potentially identifiable images or data included in this article.

AUTHOR CONTRIBUTIONS

XF and ZW conceived and designed the study. WS, XZ, and CJ performed all biological tests and bioinformatics analysis. YL and ZW drafted the manuscript. All authors discussed the results and commented on the manuscript. All authors contributed to the article and approved the submitted version.

FUNDING

This work was supported by the Natural Science Foundation of Jilin Province (20190201008JC; 20200201622JC), the Health Science and Technology Capacity Improvement project fund Jilin Province Health Commission (2021JC021), the Department of science and technology of Jilin Province project fund (20200404102YY) and the Scientific and Technological Research Project of Jilin Education Department (JJKH20211174KJ).

ACKNOWLEDGMENTS

We thank the Natural Science Foundation of Jilin Province (20190201008JC; 20200201622JC), the Health Science and Technology Capacity Improvement project fund of Jilin Province (2021JC021), and the Department of science and technology of Jilin Province (20200404102YY), the Scientific and Technological Research Project of Jilin Educational Committee (JJKH20211174KJ).

SUPPLEMENTARY MATERIAL

The Supplementary Material for this article can be found online at: https://www.frontiersin.org/articles/10.3389/fcell.2022.812271/full#supplementary-material

REFERENCES

Altarejos, J. Y., and Montminy, M. (2011). CREB and The CRTC Co-Activators: Sensors For Hormonal and Metabolic Signals. *Nat. Rev. Mol. Cel Biol* 12 (3), 141–151. doi:10.1038/nrm3072

Altman, B. J., Stine, Z. E., and Dang, C. V. (2016). From Krebs to Clinic: Glutamine Metabolism to Cancer Therapy. *Nat. Rev. Cancer* 16 (10), 619–634. doi:10.1038/nrc.2016.71

Aran, D., Hu, Z., and Butte, A. J. (2017). xCell: Digitally Portraying the Tissue Cellular Heterogeneity Landscape. *Genome Biol.* 18 (1), 220. doi:10.1186/s13059-017-1349-1

Biasci, D., Smoragiewicz, M., Connell, C. M., Wang, Z., Gao, Y., Thaventhiran, J. E. D., et al. (2020). CXCR4 Inhibition in Human Pancreatic and Colorectal Cancers Induces an Integrated Immune Response. *Proc. Natl. Acad. Sci. U S A.* 117, 28960–28970. doi:10.1073/pnas.2013644117

Diehl, A. M. (1998). Roles of CCAAT/enhancer-Binding Proteins in Regulation of Liver Regenerative Growth. *J. Biol. Chem.* 273 (47), 30843–30846. doi:10.1074/jbc.273.47.30843

Freeman, H. J. (2013). Early Stage Colon Cancer. *World J. Gastroenterol.* 19 (46), 8468–8473. doi:10.3748/wjg.v19.i46.8468

Hänzelmann, S., Castelo, R., and Guinney, J. (2013). GSVA: Gene Set Variation Analysis for Microarray and RNA-Seq Data. *BMC Bioinformatics* 14, 7. doi:10.1186/1471-2105-14-7

Jiang, P., Gu, S., Pan, D., Fu, J., Sahu, A., Hu, X., et al. (2018). Signatures of T Cell Dysfunction and Exclusion Predict Cancer Immunotherapy Response. *Nat. Med.* 24 (10), 1550–1558. doi:10.1038/s41591-018-0136-1

Keshet, R., Szlosarek, P., Carracedo, A., and Erez, A. (2018). Rewiring Urea Cycle Metabolism in Cancer to Support Anabolism. *Nat. Rev. Cancer* 18 (10), 634–645. doi:10.1038/s41568-018-0054-z

Knott, S. R. V., Wagenblast, E., Khan, S., Kim, S. Y., Soto, M., Wagner, M., et al. (2018). Asparagine Bioavailability Governs Metastasis in a Model of Breast Cancer. *Nature* 554 (7692), 378–381. doi:10.1038/nature25465

Koppula, P., Zhang, Y., Zhuang, L., and Gan, B. (2018). Amino Acid Transporter SLC7A11/xCT at the Crossroads of Regulating Redox Homeostasis and Nutrient Dependency of Cancer. *Cancer Commun.* 38 (1), 12. doi:10.1186/s40880-018-0288-x

Krebs, H. A. (1970). The History of the Tricarboxylic Acid Cycle. *Perspect. Biol. Med.* 14 (1), 154–172. doi:10.1353/pbm.1970.0001

Lane, A. N., and Fan, T. W.-M. (2015). Regulation of Mammalian Nucleotide Metabolism and Biosynthesis. *Nucleic Acids Res.* 43 (4), 2466–2485. doi:10.1093/nar/gkv047

Li, R., Qian, J., Wang, Y.-Y., Zhang, J.-X., and You, Y.-P. (2014). Long Noncoding RNA Profiles Reveal Three Molecular Subtypes in Glioma. *CNS Neurosci. Ther.* 20 (4), 339–343. doi:10.1111/cns.12220

Li, X., Wenes, M., Romero, P., Huang, S. C.-C., Fendt, S.-M., and Ho, P.-C. (2019). Navigating Metabolic Pathways to Enhance Antitumour Immunity and Immunotherapy. *Nat. Rev. Clin. Oncol.* 16 (7), 425–441. doi:10.1038/s41571-019-0203-7

Lomelino, C. L., Andring, J. T., McKenna, R., and Kilberg, M. S. (2017). Asparagine Synthetase: Function, Structure, and Role in Disease. *J. Biol. Chem.* 292 (49), 19952–19958. doi:10.1074/jbc.R117.819060

Marques-Oliveira, G. H., Silva, T. M., Lima, W. G., Valadares, H. M. S., and Chaves, V. E. (2018). Insulin As A Hormone Regulator Of The Synthesis And Release Of Leptin By White Adipose Tissue. *Peptides* 106, 49–58. doi:10.1016/j.peptides.2018.06.007

Marteijn, J. A., Lans, H., Vermeulen, W., and Hoeijmakers, J. H. J. (2014). Understanding Nucleotide Excision Repair and its Roles in Cancer and Ageing. *Nat. Rev. Mol. Cel Biol* 15 (7), 465–481. doi:10.1038/nrm3822

McNabney, S., and Henagan, T. (2017). Short Chain Fatty Acids in the Colon and Peripheral Tissues: A Focus On Butyrate, Colon Cancer, Obesity and Insulin Resistance. *Nutrients* 9 (12), 1348. doi:10.3390/nu9121348

Pascual, G., Avgustinova, A., Mejetta, S., Martín, M., Castellanos, A., Attolini, C. S.-O., et al. (2017). Targeting Metastasis-Initiating Cells through the Fatty Acid Receptor CD36. *Nature* 541 (7635), 41–45. doi:10.1038/nature20791

Pavlova, N. N., Hui, S., Ghergurovich, J. M., Fan, J., Intlekofer, A. M., White, R. M., et al. (2018). As Extracellular Glutamine Levels Decline, Asparagine Becomes an Essential Amino Acid. *Cel Metab.* 27 (2), 428–438. doi:10.1016/j.cmet.2017.12.006

Punt, C. J. A., Koopman, M., and Vermeulen, L. (2017). From Tumour Heterogeneity to Advances in Precision Treatment of Colorectal Cancer. *Nat. Rev. Clin. Oncol.* 14 (4), 235–246. doi:10.1038/nrclinonc.2016.171

Rabinovich, S., Adler, L., Yizhak, K., Sarver, A., Silberman, A., Agron, S., et al. (2015). Diversion of Aspartate in ASS1-Deficient Tumours Fosters De Novo Pyrimidine Synthesis. *Nature* 527 (7578), 379–383. doi:10.1038/nature15529

Renner, K., Singer, K., Koehl, G. E., Geissler, E. K., Peter, K., Siska, P. J., et al. (2017). Metabolic Hallmarks of Tumor and Immune Cells in the Tumor Microenvironment. *Front. Immunol.* 8, 248. doi:10.3389/fimmu.2017.00248

Roesler, W. J. (2000). What Is a cAMP Response Unit? *Mol. Cel Endocrinol* 162 (1-2), 1–7. doi:10.1016/s0303-7207(00)00198-2

Röhrig, F., and Schulze, A. (2016). The Multifaceted Roles of Fatty Acid Synthesis in Cancer. *Nat. Rev. Cancer* 16 (11), 732–749. doi:10.1038/nrc.2016.89

Rubin, A. L. (1990). Suppression of Transformation by and Growth Adaptation to Low Concentrations of Glutamine in NIH-3T3 Cells. *Cancer Res.* 50 (9), 2832–2839.

Simon, K. (2016). Colorectal Cancer Development and Advances in Screening. *Clin. Interv. Aging* 11, 967–976. doi:10.2147/CIA.S109285

Spinelli, J. B., Yoon, H., Ringel, A. E., Jeanfavre, S., Clish, C. B., and Haigis, M. C. (2017). Metabolic Recycling of Ammonia via Glutamate Dehydrogenase Supports Breast Cancer Biomass. *Science* 358 (6365), 941–946. doi:10.1126/science.aam9305

Steven, A., Friedrich, M., Jank, P., Heimer, N., Budczies, J., Denkert, C., et al. (2020). What Turns CREB on? And off? And Why Does it Matter? *Cell. Mol. Life Sci.* 77 (20), 4049–4067. doi:10.1007/s00018-020-03525-8

Su, N., and Kilberg, M. S. (2008). C/EBP Homology Protein (CHOP) Interacts with Activating Transcription Factor 4 (ATF4) and Negatively Regulates the Stress-dependent Induction of the Asparagine Synthetase Gene. *J. Biol. Chem.* 283 (50), 35106–35117. doi:10.1074/jbc.M806874200

Vander Heiden, M. G., Cantley, L. C., and Thompson, C. B. (2009). Understanding the Warburg Effect: The Metabolic Requirements of Cell Proliferation. *Science* 324 (5930), 1029–1033. doi:10.1126/science.1160809

Ward, P. S., and Thompson, C. B. (2012). Metabolic Reprogramming: A Cancer Hallmark Even Warburg Did Not Anticipate. *Cancer Cell* 21 (3), 297–308. doi:10.1016/j.ccr.2012.02.014

Wilkinson, N. W., Yothers, G., Lopa, S., Costantino, J. P., Petrelli, N. J., and Wolmark, N. (2010). Long-Term Survival Results of Surgery Alone Versus Surgery Plus 5-Fluorouracil and Leucovorin For Stage II and Stage III Colon Cancer: Pooled Analysis of NSABP C-01 through C-05. A Baseline from Which to Compare Modern Adjuvant Trials. *Ann. Surg. Oncol.* 17 (4), 959–966. doi:10.1245/s10434-009-0881-y

Zhang, J., Fan, J., Venneti, S., Cross, J. R., Takagi, T., Bhinder, B., et al. (2014). Asparagine Plays a Critical Role in Regulating Cellular Adaptation to Glutamine Depletion. *Mol. Cel* 56 (2), 205–218. doi:10.1016/j.molcel.2014.08.018

Conflict of Interest: The authors declare that the research was conducted in the absence of any commercial or financial relationships that could be construed as a potential conflict of interest.

frontiers in Cell and Developmental Biology

ORIGINAL RESEARCH
published: 21 February 2022
doi: 10.3389/fcell.2022.796703

Multi-Platform-Based Analysis Characterizes Molecular Alterations of the Nucleus in Human Colorectal Cancer

Wei Zhang[1,2†], Minmin Wu[3†], Xucan Gao[1], Chiyu Ma[1], Huixuan Xu[1], Liewen Lin[1], Jingquan He[1], Wanxia Cai[1], Yafang Zhong[1], Donge Tang[1], Min Tang[3]* and Yong Dai[1]**

[1]Department of Clinical Medical Research Center, The Second Clinical Medical College, Jinan University (Shenzhen People's Hospital), Shenzhen, China, [2]South China Hospital, Health Science Center, Shenzhen University, Shenzhen, China, [3]Key Laboratory of Clinical Laboratory Diagnostics of Ministry of Education, Chongqing Medical University, Chongqing, China

OPEN ACCESS

Edited by:
Erika Ruiz-Garcia,
National Institute of Cancerology (INCAN), Mexico

Reviewed by:
Yoshikatsu Koga,
National Cancer Center, Japan
Emenike K. Onyido,
Swansea University Medical School, United Kingdom

***Correspondence:**
Donge Tang
donge66@126.com
Min Tang
catom@126.com
Yong Dai
daiyong22@aliyun.com

†These authors have contributed equally to this work

Specialty section:
This article was submitted to Molecular and Cellular Oncology, a section of the journal Frontiers in Cell and Developmental Biology

Received: 17 October 2021
Accepted: 31 January 2022
Published: 21 February 2022

Citation:
Zhang W, Wu M, Gao X, Ma C, Xu H, Lin L, He J, Cai W, Zhong Y, Tang D, Tang M and Dai Y (2022) Multi-Platform-Based Analysis Characterizes Molecular Alterations of the Nucleus in Human Colorectal Cancer. Front. Cell Dev. Biol. 10:796703. doi: 10.3389/fcell.2022.796703

Background: The disturbed molecular alterations of nucleus may promote the development of colorectal cancer (CRC). A multi-platform-based analysis of nucleus of CRC patients helps us to better understand the underlying mechanism of CRC and screen out the potential drug targets for clinical treatment. However, such studies on nucleus in human CRC are still lacking.

Methods: We collected the cancerous and para-cancerous tissues from eight CRC patients and performed a multiplex analysis of the molecular changes of the nucleus, including structural variations (SVs), DNA methylation, chromatin accessibility, proteome and phosphorproteome.

Results: In our study, we revealed a significant molecular change of nucleus of CRC patients using our original proteomic and phosphorylomic datasets. Subsequently, we characterized the molecular alterations of nucleus of CRC patients at multiple dimensionalities, including DNA, mRNA, protein and epigenetic modification. Next, we found that the great molecular changes of nucleus might affect the biological processes named endocytosis and ubiquitin-mediated proteolysis. Besides, we identified DYNC1LI2 and TPR as the potentially hub proteins within the network of nuclear genes in CRC cells. Furthermore, we identified 1905 CRC-specific SVs, and proclaimed 17 CRC-specific SVs were probably associated with the disturbance of immune microenvironment of CRC patients. We also revealed that the SVs of CXCL5, CXCL10 and CXCL11 might be the core SVs among all the immune-relevant SVs. Finally, we identified seven genes as the upstream transcriptional factors potentially regulating the expression of nuclear genes, such as YY1 and JUN, using a multi-omics approach.

Conclusion: Here, we characterized the molecular changes of nucleus of CRC patients, disclosed the potentially core nuclear genes within the network, and identified the probable upstream regulator of nucleus. The findings of this study are helpful to understand the pathogenic molecular changes of nucleus in CRC patients and provide a functional context for drug development in future.

Keywords: nucleus, colorectal cancer, structural variations, immune microenvironment, multiomics

INTRODUCTION

Colorectal cancer (CRC) is one of the most common tumors in the world, ranking the third among all malignant tumors (Bray et al., 2018). With the improvements of surgery and novel targeted and immune drugs, the 5-year survival rate of CRC patients has been increased in recent years (Siegel et al., 2020). However, there still are 149,500 new cases and 52,980 deaths caused by CRC in the United States a year in 2020 (Siegel et al., 2020). Therefore, it is of great significance to understand the molecular changes and functional genes of human CRC.

Frequently, tumors may be induced by the changes of several genes at multiple molecular levels. Nowadays, omics studies are emerging as an effective way to study tumorigenesis, which one-time access to most intracellular information in cells or tissues (Rusk, 2019), such as genomic and epigenomic studies. At present, mono-omics techniques have already been widely used in detection of molecular defects of tumors, but it is not sufficient to elucidate the complex mechanism of carcinogenesis (Rusk, 2019). Therefore, we need the method of multi-omics cross-analysis to study the same patients at distinct molecular levels to understand the functional context of tumors. In the previous studies, we performed a multi-omics investigation of cancerous and para-cancerous tissues of CRC patients, revealing the dysfunctions of mitochondria in CRC patients [(Zhang et al., 2021a; Zhang et al., 2021b)].

It is well known that genetic mutations, chromatin instability and some other "nuclear anomalous events" play core roles in the initiation and progression of CRC (Choong and Tsafnat, 2012; Okugawa et al., 2015). Until now, our knowledge towards the nucleus is more in the view of genome, but the changes of nucleus at other molecular dimensionalities are barely known. In this study, we disclosed the global molecular changes of nucleus in CRC patients in the view of structural variations (SVs), DNA methylation, chromatin accessibility, and proteome and phosphoproteome using our original datasets. Besides, we analyzed the network of the nuclear genes in CRC patients and searched for the hub genes within the network. Furthermore, we identified the probable upstream transcription factors (TFs) that regulated the activity of nucleus. Finally, we analyzed the global chromatin SVs of CRC patients and uncovered the probable pathogenic SVs.

MATERIALS AND METHODS

Patients

The primary CRC samples were acquired from Shenzhen People's Hospital, and this project was approved by the Ethics Committee of Shenzhen People's Hospital (LL-KY-2019213). All the participants were voluntary and signed the informed consent forms. Eight patients with colorectal adenocarcinoma were eligible for inclusion in this study who had undergone surgical resection without prior radiotherapy or chemotherapy. Also, the hereditary colon cancer was excluded. The clinical information of CRC patients were described in **Supplementary Table S1**.

Protein Extraction and Digestion

Sample collection was performed as described in our previous articles (Sato et al., 2011; Zhang et al., 2021a; Zhang et al., 2021b). Both tumor and normal adjacent tissues were obtained from the colon segment, and normal adjacent colorectal mucosa was collected from 5 cm away from the tumors. Then, the samples were stored in liquid nitrogen for at least 3 hours. Next, the frozen samples were ground to powder and uniformly mixed at 1:4 by volume with the lysis buffer containing 8 M urea (Sigma) and 1% protease inhibitor cocktail (156535140, Millipore). The resulting mixture was ultrasonic treated for three times on ice with a high-intensity ultrasonic processor (Scientology, China) and then centrifuged at 12,000 × *g* for 10 min at 4 °C to remove the fragments. Finally, the BCA kit (P0011-1, Beyotime) was used to determine the protein concentration of the supernatant. The protein-containing samples were incubated with 5 mM dithiothreitol (Sigma) at 56°C for 30 min, then mixed with 11 mM iodoacetamide (Sigma) and incubated at 37°C for 15 min in dark. Next, 100 mM triethylammonium bicarbonate (Sigma) were added to dilute the urea concentration to 2 M. Finally, the mixture was digested with trypsin (V9012, Promega) in two rounds. That is, the ratio of mixture and trypsin was 1:50 and 1:100, digested for12 h and 4 h respectively.

LC-MS/MS Analyses

LC-MS/MS was performed as described in previous study (Sun et al., 2019). The trypsin digested polypeptide samples were dissolved in liquid chromatographic mobile phase A (0.1% formic acid solution, Fluka) and separated using an ultra-high phase system. After separation, the mixture was injected into NSI ion source for ionization and then analyzed by timsTOF Pro mass spectrometer (Bruker Daltonics, MA, United States). The second-order mass spectrometry scanning range was 100–1700m/z, and the fragmentation of precursors with charge states 0 to five was performed. Dynamic exclusion was set to 30 s in secondary MS. Secondary MS data were retrieved using Maxquant (V1.6.6.0) as Homo sapiens 9606 SP 20191115 (sequence 20,380).

Whole Genome Bisulfite Sequencing (WGBS)

The genomic DNA was extracted with SMRTbell Express Template Prep Kit 2.0 (100–938-900, Pacific Bioscience) and tested for quality and concentration. DNA samples were segmayed by ultrasound for bisulfite transformation, and the DNA methylation sequencing library construction Kit EZDNA methylation-Gold ™ Kit (D5005, ZYMO Research) was used to connect single strand DNA fragments for PCR amplification. The amplified products were purified and tested for their integrity using a 2,100 Bioanalyzer (Agilent). Finally, the HiSeq X10 sequencing platform (Illumina) was used for the double-terminal sequencing of the library, and the results were compared with each methylation regions.

Long-Read Whole Genome Sequencing

The high quality genomic DNA was obtained using the same method as WGBS. The DNA fragments with a growth of about

20 kb were fragmented using the g-GUBETM (520,079, Covaris) and enriched by the magnetic beads (100-317-100, Pacific Bioscience). The DNA fragments were added with stem rings to synthesize the sequences using DNA polymerase (101-731-100, Pacific Bioscience). The DNA quality was assessed and sequenced using the HiSeq X10 sequencing platform (Illumina), which produced paired 150 bp readings of the terminal.

Assay to detect transposase-accessible chromatin based on high throughput sequencing (ATAC-Seq)

The ATAC-seq was performed as reported in previous study (Buenrostro et al., 2015). In brief, the suspension conteining 50,000 single-cell was processed for transposition and purification. After the cell lysis, 2.5 μL Tn5 transpoase and 1× TD buffer were added to the remaining cell precipitate, 50 μL in total, and incubated at 37°C for 30 min. The DNA sample was then processed using the MinElute reaction Clearance Kit (51,306, QIAGEN), and the DNA libraries were generated using the TruePrep DNA Library preparation Kit V2 (TD501/TD502/TD503, Vazyme Biotecho) based on the Illumina sequencing platform. Subsequently, the StepOnePlus real-time PCR system was used to verify the quality of the library.The high-quality libraries were then sequenced using the HiSeq X Ten sequencing platform (Illumina) based on 150 bp paired-end reading.

Databases and Software

The RNA-Seq datasets were acquired from The Cancer Genome Atlas (TCGA), including 51 healthy people and 647 CRC patients (colonic or rectal intestinal mucosa were examined using the RNA-Sequencing). The patients with incomplete survival time were excluded, and 538 patients were ultimately included in this study. The resulting expression matrix of the TCGA data sets has been uploaded as the Supplementary Information. The datasets of immune cell infiltration were obtained from Xcell database. Gene Ontology (GO) and Kyoto Encyclopedia of Genes and Genomes (KEGG) analysis were performed through DAVID database (https://david.ncifcrf.gov/). The subcellular enrichment was performed using WoLFPSOR v.0.2 software. The protein-protein interaction (PPI) network was constructed using Cytoscape and Metascape.

Data Available

The datasets of proteome and phosphoproteome have been uploaded to the ProteomeXchange Consortium with the accessing number PXD021314 and PXD021318. The datasets of ATAC-seq, WGBS and LWGS have been stored in Sequence Read Archive (SRA) with the accessing number PRJNA693028.

Statistical Analyses

t-test was utilized to calculate the significance of differentially expressed genes. Fisher's exact test was used to analyze the significance of enrichment. p value <0.05 was considered statistically significant.

RESULTS

Integrated proteome and phosphoproteome revealed a tremendous molecular alteration of the nucleus of CRC patients.

To uncover the molecular changes of nucleus of CRC cells, we first collected the cancerous tissues and the normal adjacent tissues from CRC patients (n = 6–8). Samples of two patients at each stage were pooled into a single one for the following test (**Supplementary Table S1**). We then performed a multiplex analysis of the CRC cells and normal cells using the data sets of our own, comparing the global SVs, DNA methylation, chromatin accessibility, proteome and phosphoproteome between these two groups (**Figure 1A**).

Since proteins are the fundamental units for cellular biological functions, we primarily analyzed the proteome and phosphoproteome of the CRC cells compared to the normal adjacent cells. As a result, we found 496 proteins were up-regulated and 597 proteins were down-regulated in CRC cells versus the normal cells using the proteomic analysis (fold changes >1.5, $p < 0.05$, **Supplementary Table S1**). Meanwhile, we identified 587 differentially expressed phosphorylation in CRC cells versus the normal cells using the phosphoproteomic analysis (fold changes >1.5, $p < 0.05$, **Supplementary Table S1**). Next, we performed enrichment investigations of the above differentially expressed proteins and phosphorylation using GO analysis and subcellular analysis. The results exhibited that many nuclear proteins were enriched in the expression-increased proteins (29% of all the up-regulated proteins) (**Figure 1B**). Similarly, a great number of nuclear proteins were also enriched in the altered phosphorylation (53% of all the differentially expressed phosphorylation) (**Figure 1C**). On the other hand, GO analysis also confirmed these results. Many expression-elevated proteins located in nucleoplasm and spindle pole (**Figure 1D**), and many differentially-expressed phosphorylation located in nucleolus, nucleoplasm, nucleus, membrane, and condensed chromosome. These results indicated that the nucleus were greatly changed during the initiation and development of human CRC. In addition, the abnormal alterations of phosphorylation of nuclear proteins might be closely related to the carcinogenesis of CRC.

The proteogenomic characterization of the nucleus of CRC patients.

A comprehensive study of the molecular changes of the nucleus of CRC cells at distinct levels is helpful to enhance our understanding of the dysfunctional contributions of nucleus in carcinogenesis. Therefore, we investigated the SVs (n = 6), DNA methylation (n = 6), chromatin accessibility (n = 6), proteins (n = 8), and phospholation (n = 8) of all the nuclear genes (proteins having a nucleus location) in CRC cells versus normal cells. Moreover, we also analyzed the mRNA expression of all the nuclear genes using the RNA-seq datasets of 538 CRC patients and 51 healthy individuals downloaded from the TCGA. The results showed that 1852 nuclear genes had CRC-specific SVs at non-exon sites and 53 nuclear genes had CRC-specific SVs at exon sites (**Figure 2A**). 825 nuclear genes were hyper-methylated and 1320 nuclear genes were hypo-methylated in CRC cells compared to normal cells (**Figure 2B**). 5,001 nuclear genes

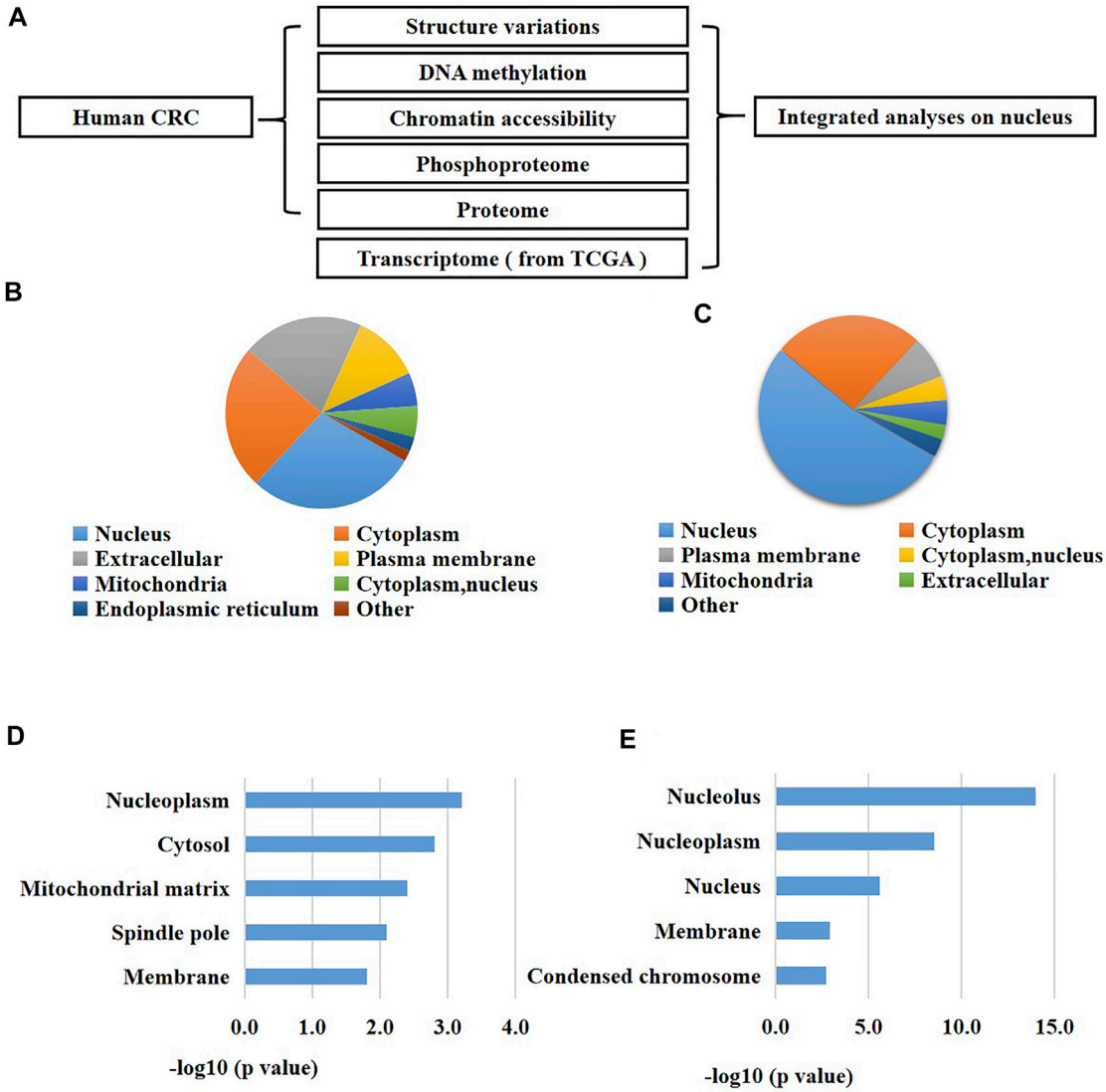

FIGURE 1 | An integrated analysis revealed a significant change of nucleus in CRC patients. **(A)** A schematic overview of the study. **(B)** Subcellular enrichment analysis of the up-regulated proteins of CRC cells versus normal cells. **(C)** Subcellular enrichment analysis of all differentially expressed phosphorylation of CRC cells versus normal cells. **(D)** GO enrichment analysis of the up-regulated proteins of CRC cells versus normal cells. **(E)** GO enrichment analysis of all differentially expressed phosphorylation of CRC cells versus normal cells.

had increased chromatin accessibility and 691 nuclear genes had decreased chromatin accessibility in CRC cells compared to normal cells (**Figure 2C**). The mRNA expression of 2,989 nuclear genes were up-regulated and the mRNA expression of 1390 nuclear genes were down-regulated in CRC cells compared to normal cells (**Figure 2D**). The protein expression of 142 nuclear genes were up-regulated and the protein expression of 73 nuclear genes were down-regulated in CRC cells compared to normal cells (**Figure 2E**). 80 nucleoproteins had more phosphorylation and 158 nucleoproteins had less phosphorylation in CRC cells compared to normal cells (**Figure 2F**).

It is well known that the genes transcription are influenced by SVs, DNA methylation, and chromatin accessibility. Therefore, we further explored the probable reasons for the altered mRNA expression of the nuclear genes in CRC cells. As a result, 596 expression-changed nuclear genes had SVs (60% of all expressed-changed nuclear genes) (**Figure 2G**). Among 2,145 nuclear genes with altered DNA methylation, the mRNA expression of 770 genes were altered in CRC cells (35.9% of all expressed-changed nuclear genes) (**Figure 2H**). Among 5,230 nuclear genes with altered chromatin accessibility, the mRNA expression of 3,039 genes were altered in CRC cells (58.1% of all expressed-changed nuclear genes) (**Figure 2I**). These results suggested that SVs might have a bigger influence on the transcription of the nuclear genes in CRC patients.

Proteogenomic changes of functional genes may affect tumor progression. Consequently, we searched for the molecular

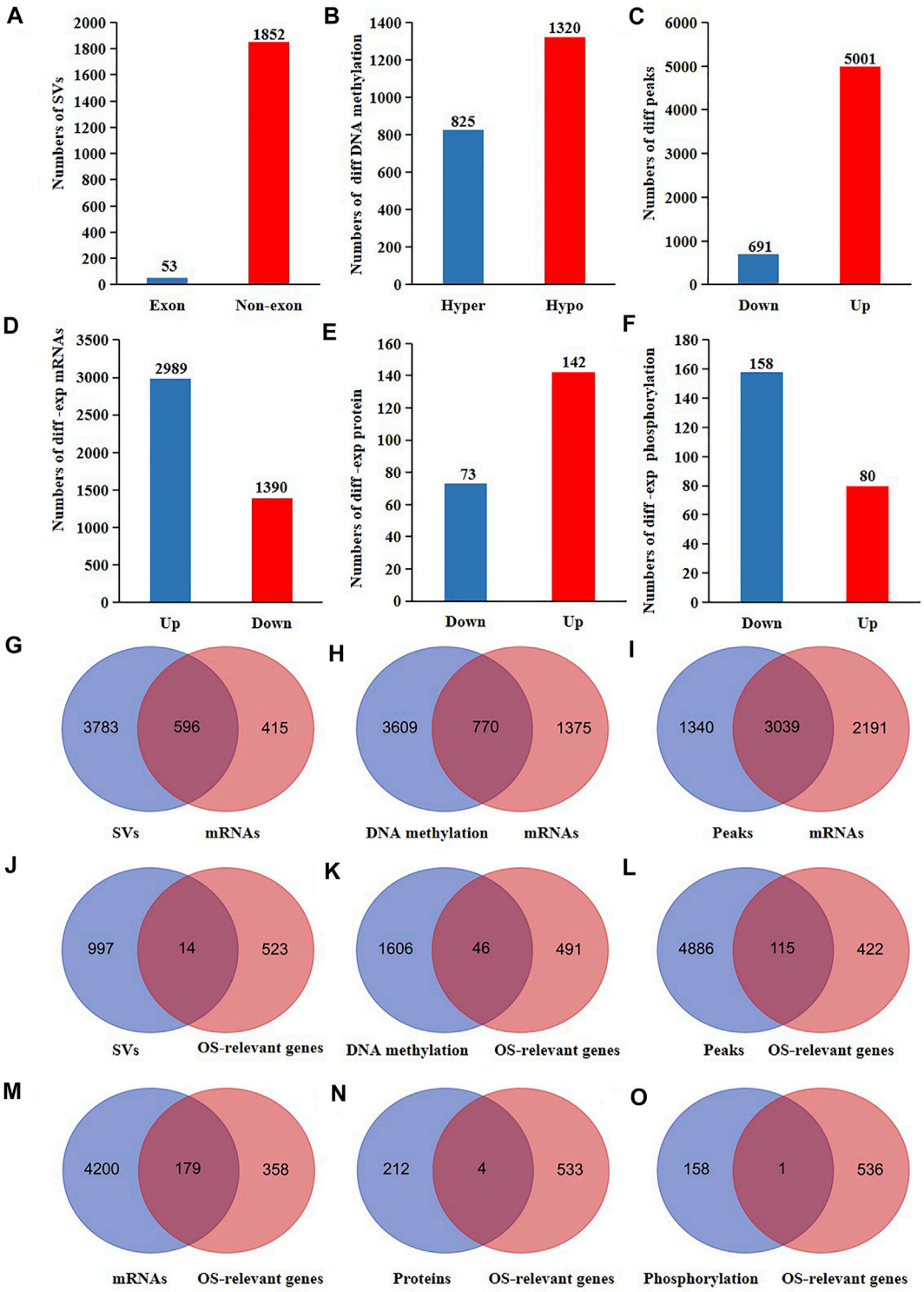

FIGURE 2 | The proteogenomic alterations of nucleus of CRC patients. The different **(A)** SVs **(B)** DNA methylation **(C)** accessible chromatin peaks **(D)** mRNAs **(E)** proteins, and **(F)** phosphorylation of nuclear genes of CRC cells compared to normal cells. Venn analyses of the different **(G)** SVs **(H)** DNA methylation **(I)** accessible chromatin peaks and the differentially expressed mRNAs of nuclear genes of CRC cells compared to normal cells. Venn analyses of the different **(J)** SVs, **(K)** DNA methylation, **(L)** accessible chromatin peaks, **(M)** mRNA, **(N)** proteins, **(O)** phosphorylations, and the OS-relevant nuclear genes of CRC patients.

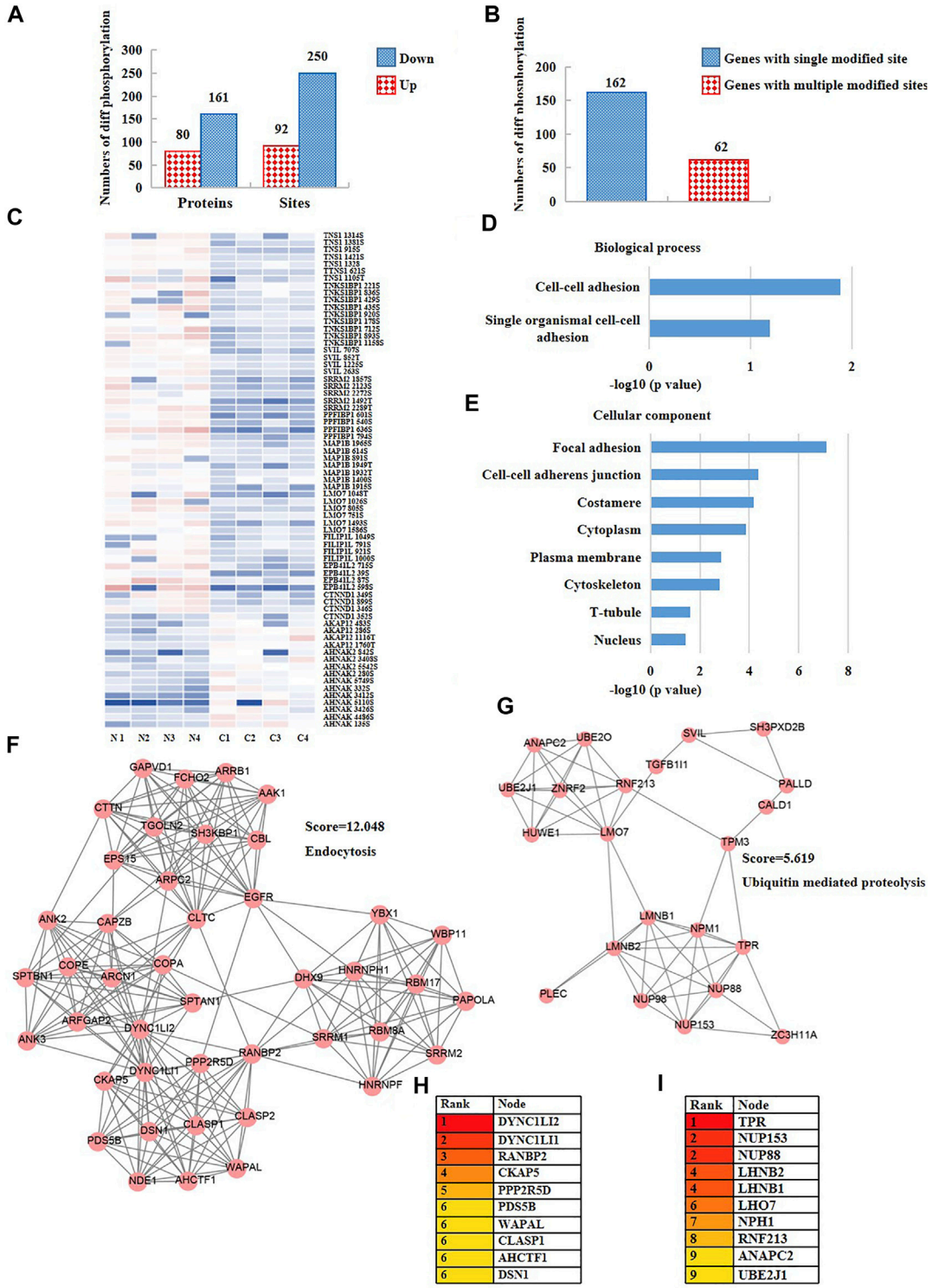

FIGURE 3 | The phosphoproteomic analysis of nuclear proteins disclosed DYNC1LI2 and TPR potentially as the hub genes in CRC. **(A)** The numbers of differentially expressed phosphorylation of CRC cells versus normal cells. **(B)** The numbers of differentially expressed phosphorylation having one-site changes or having more than two sites of changes. **(C)** The heat map showing the phosphorylation content of nucleoproteins of CRC cells versus normal cells. **(D)** Biological process, and **(E)** cellular component enrichment analysis of all differentially expressed phosphorylation of CRC cells versus normal cells. **(F,G)** Two closely-tied groups within the network of all differentially phosphorylated nuclear proteins. **(H,I)** Hub proteins within the two closely-tied groups.

changes of the survival-relevant nuclear genes in CRC patients using the data sets from TCGA. We primarily performed a survival analysis of all mRNAs detected in colonic cells. The results showed that 537 genes were associated with the overall survival rates (OS) of CRC patients (**Supplementary Table S1**). Subsequently, we overlapped the 537 OS-relevant genes with all the different SVs, DNA methylation, chromatin accessibility, mRNAs, proteins, and phosphorylation of CRC cells. As a result, we found that 14 OS-relevant nuclear genes had CRC-specific SVs, 46 OS-relevant nuclear genes had hyper or hypo DNA methylation, 115 OS-relevant nuclear genes had different chromatin accessibility, 179 nuclear OS-relevant genes had differentially expressed mRNAs, four OS-relevant nuclear genes had differentially expressed proteins, and one OS-relevant nuclear genes had altered phosphorylation (**Figures 2J–O**). These results showed that both the genomic and post-translational modifications of nuclear genes were potentially related to the outcomes of CRC patients.

The phosphoproteomic analysis uncovered significant changes of phosphorylation of nuclear proteins of CRC patients and identified DYNC1LI2 and TPR as the potential hub genes within the nucleus network.

It is well known that phosphorylation is a type of post-translational modification that switches protein activity and regulates intracellular signal transmission. Altered phosphorylation contents in cells may cause tumors. According to the above results, the phosphoproteome of nuclear in CRC patients was significantly changed. To explore the cellular functions of the altered phosphorylation, we first calculated the numbers and sites of the different phosphorylation of nuclear genes of CRC cells versus the normal cells. As a result, the phosphorylation of 80 nuclear proteins were up-regulated and 161 proteins were down-regulated in CRC cells versus the normal cells. 92 phosphorylation sites were up-regulated and 250 sites were down-regulated in CRC cells versus the normal cells (**Figure 3A**, **Supplementary Table S1**). Among all the proteins with differentially expressed phosphorylation, 162 proteins only had one single differentially expressed phosphorylation site, and 62 proteins had two or more than two differentially expressed phosphorylation sites (**Figure 3B**, **Supplementary Table S1**). Subsequently, to understand the functions of the proteins with more than two differentially expressed phosphorylation, we analyzed the phosphorylation expression of 13 highly phosphorylated ($n \geq 4$) nuclear proteins. The results showed that most of these phosphorylation were reduced in CRC cells versus the normal cells (**Figure 3C**). The KEGG and GO analysis revealed that the functions of these proteins were mainly about cell-cell adhesion and cytoskeletal proteins (**Figures 3D,E**, **Supplementary Table S1**). Furthermore, we constructed the network of the nuclear proteins with differentially expressed phosphorylation using Cytoscape and analyzed the closely connected protein groups using MCODE. As a result, the groups with the highest scores were relevant to the processes including endocytosis (score = 12.048) (**Figure 3F**) and ubiquitin-mediated proteolysis (score = 5.619) (**Figure 3G**). In addition, we analyzed the hub proteins within the two groups using Cytohubba. The results revealed that DYNC1LI2 (**Figure 3H**) and TPR (**Figure 3I**) were probably the most important genes within the network. Next, we investigated the phosphorylation of DYNC1LI2 and TPR in CRC cells compared to the normal cells using our original phosphoproteomic datasets. The results revealed that DYNC1LI2 (**Figure 3H**) and TPR (**Figure 3I**) were probably the most important genes within the network. Next, we investigated the phosphorylation of DYNC1LI2 and TPR in CRC cells compared to the normal cells using our original phosphoproteomic datasets. As a result, the phosphorylation of DYNC1LI2 at Ser196 was up-regulated and TPR at Ser2155 was down-regulated in CRC cells versus normal cells (**Supplementary Figure S1**).

The alterations of content and phosphorylation may affect the activity of proteins. To explore the network of nuclear proteins, we performed PPI analysis and function enrichment analysis of all the differentially expressed proteins and phosphorylation using Metascape. As shown in **Figure 4A**, the biological functions of all the expression- or phosphorylation-altered proteins were mainly involved in actin cytoskeleton organization, nucleocytoplasmic transport, ribosomal large subunit biogenesis, RNA splicing, and regulation of cellular component organization. Besides, five closely-tied protein group were enriched, whose functions were relevant to mRNA processing, mRNA transport, PID MET pathway, and SUMOylation (**Figures 4B,C**). It has been reported that SUMOylation are closely related to cancer initiation and progression (Xie et al., 2020). There is a crosstalk between ubiquitination and SUMOylation in cells (Chelbi-Alix and Thibault, 2021), and SUMOylation plays a significant role in maintaining genomic stability via SUMO-targeted ubiquitin ligase (STUbL) (Nie and Boddy, 2016). Interestingly, we also found a significant change of ubiquitination pathway when we performed KEGG enrichment analysis of all down-regulated phosphorylation in CRC cells versus the normal cells (**Supplementary Figure S2**). Consequently, we conjectured that there may be a crosstalk between SUMOylation and ubiquitination in CRC cells as well, which synergistically promotes the development of CRC (**Figure 3G**).

The multi-platform-based investigation uncovered the TFs potentially regulating the activity of nucleus of CRC patients.

The transcription of genes is regulated by their upstream TFs. In our above results, the mRNA expression of a large number of nuclear genes were altered in CRC cells versus normal cells, which prompted us to investigate whether their upstream TFs had abnormal molecular changes. We inquired all the nuclear genes which had different expression at both mRNA and protein levels through hTFtarget database. Subsequently, we obtained 144 experimentally confirmed TFs which were identified in colonic cells (**Supplementary Table S1**). TFs bind unique sequences (motif) of promoter to launch gene transcription. Consequently, we first analyzed the highly opened motifs in CRC cells and para-cancerous cells through comparing the global chromatin accessibility. The results showed that the binding motifs of TFs SP1, SP2, KLF5, ZBTB7B, GLIS1, and ESRRA were highly opened only in para-cancerous cells and potentially regulated 94.7, 78.9, 21.1, 5.3, 5.3, and 5.3% of all

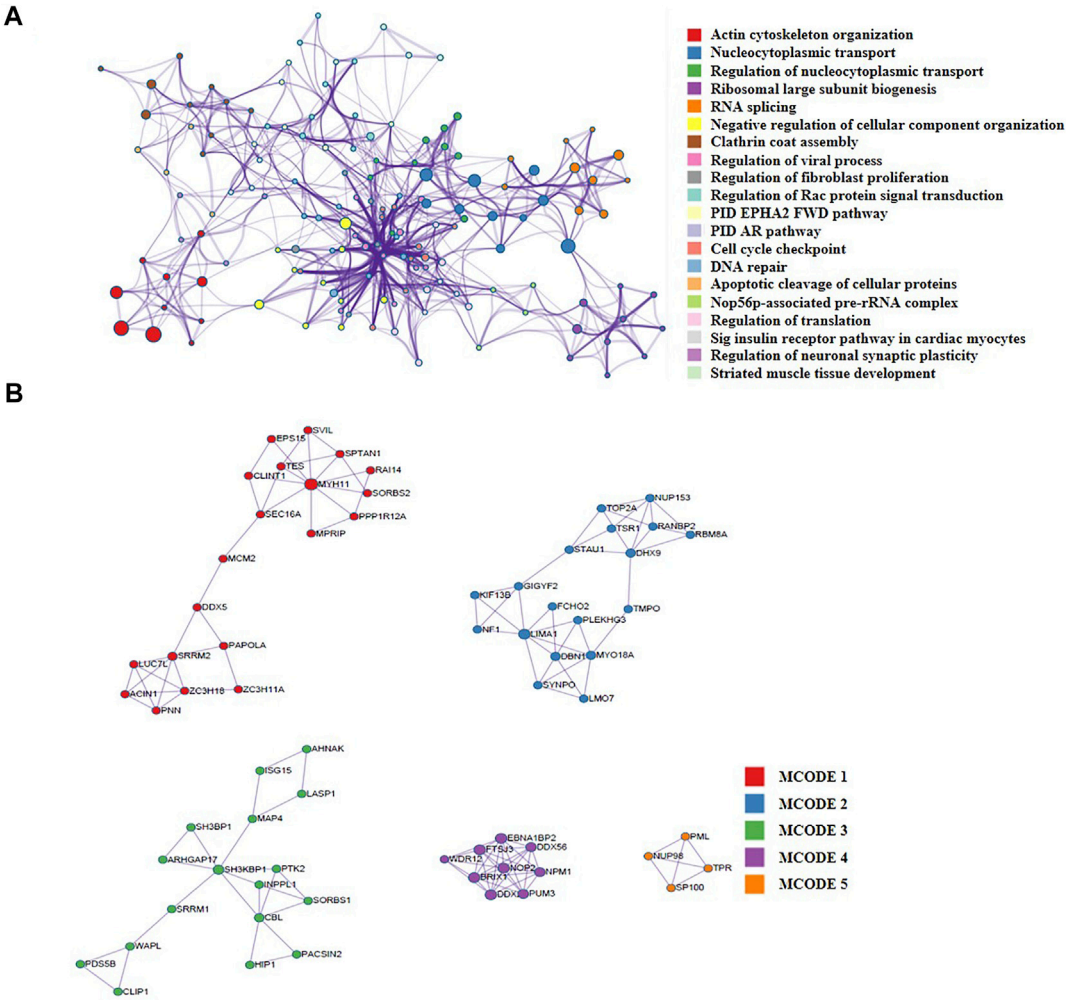

C

MCODE_1	GO:0006397	mRNA processing	-7.1
MCODE_1	GO:0008380	RNA splicing	-6.1
MCODE_1	GO:0014706	striated muscle tissue development	-5.2
MCODE_2	GO:0006405	RNA export from nucleus	-5.7
MCODE_2	GO:0006913	nucleocytoplasmic transport	-5.6
MCODE_2	GO:0051028	mRNA transport	-5.6
MCODE_3	GO:0030036	actin cytoskeleton organization	-7.0
MCODE_3	GO:0097435	supramolecular fiber organization	-7.0
MCODE_3	M48	PID MET PATHWAY	-6.9
MCODE_4	GO:0042273	ribosomal large subunit biogenesis	-13.6
MCODE_4	GO:0042254	ribosome biogenesis	-12.2
MCODE_4	GO:0022613	ribonucleoprotein complex biogenesis	-10.6
MCODE_5	R-HSA-3108214	SUMOylation of DNA damage response and repair proteins	-10.3
MCODE_5	R-HSA-3108232	SUMO E3 ligases SUMOylate target proteins	-8.8
MCODE_5	R-HSA-2990846	SUMOylation	-8.7

FIGURE 4 | The proteomic and phosphoproteomic investigations uncovered the network of nuclear proteins in CRC patients and identified the functional modules within the network. **(A)** A functional network characterized by altered nuclear proteins and phosphorylation of CRC cells versus normal cells. **(B,C)** Five closely-tied groups within the network.

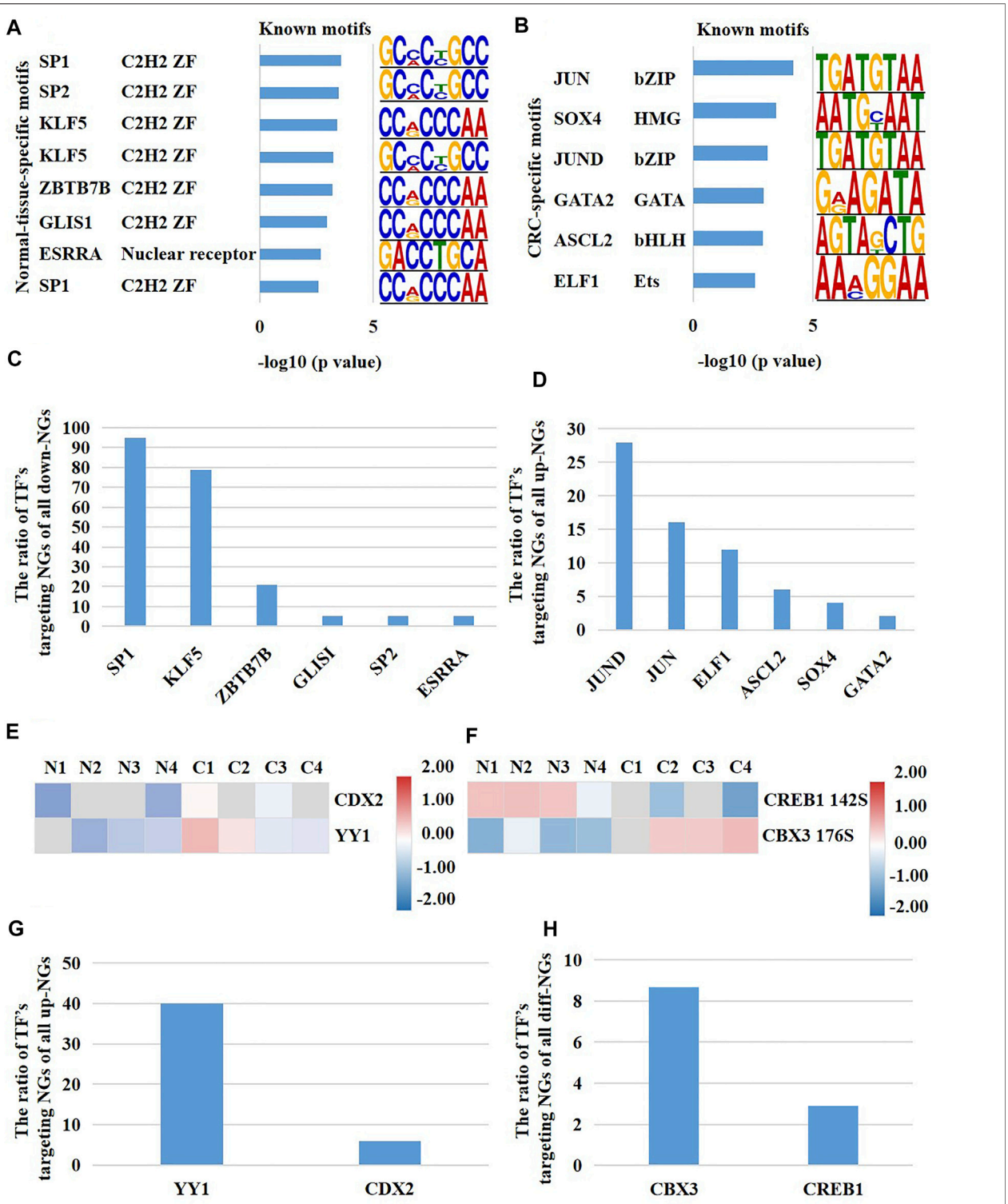

FIGURE 5 | A multi-platform-based analysis disclosed the upstream TFs potentially regulating the activity of nucleus in CRC patients. **(A)** The normal-cell-specific TFs, and **(B)** the CRC-cell-specific TFs reflected by binding motifs. The proportion of TF's potentially targeting nuclear genes of all **(C)** down-regulated nuclear genes and **(D)** up-regulated nuclear genes of CRC cells versus normal cells. Potential TFs which targeted the differentially expressed nuclear genes of CRC cells versus normal cells were altered on **(E)** the protein expression and **(F)** phosphorylation. The proportion of TF's potentially targeting nuclear genes of **(G)** the up-regulated nuclear genes and **(H)** all differentially expressed nuclear genes. NGs represented nuclear genes.

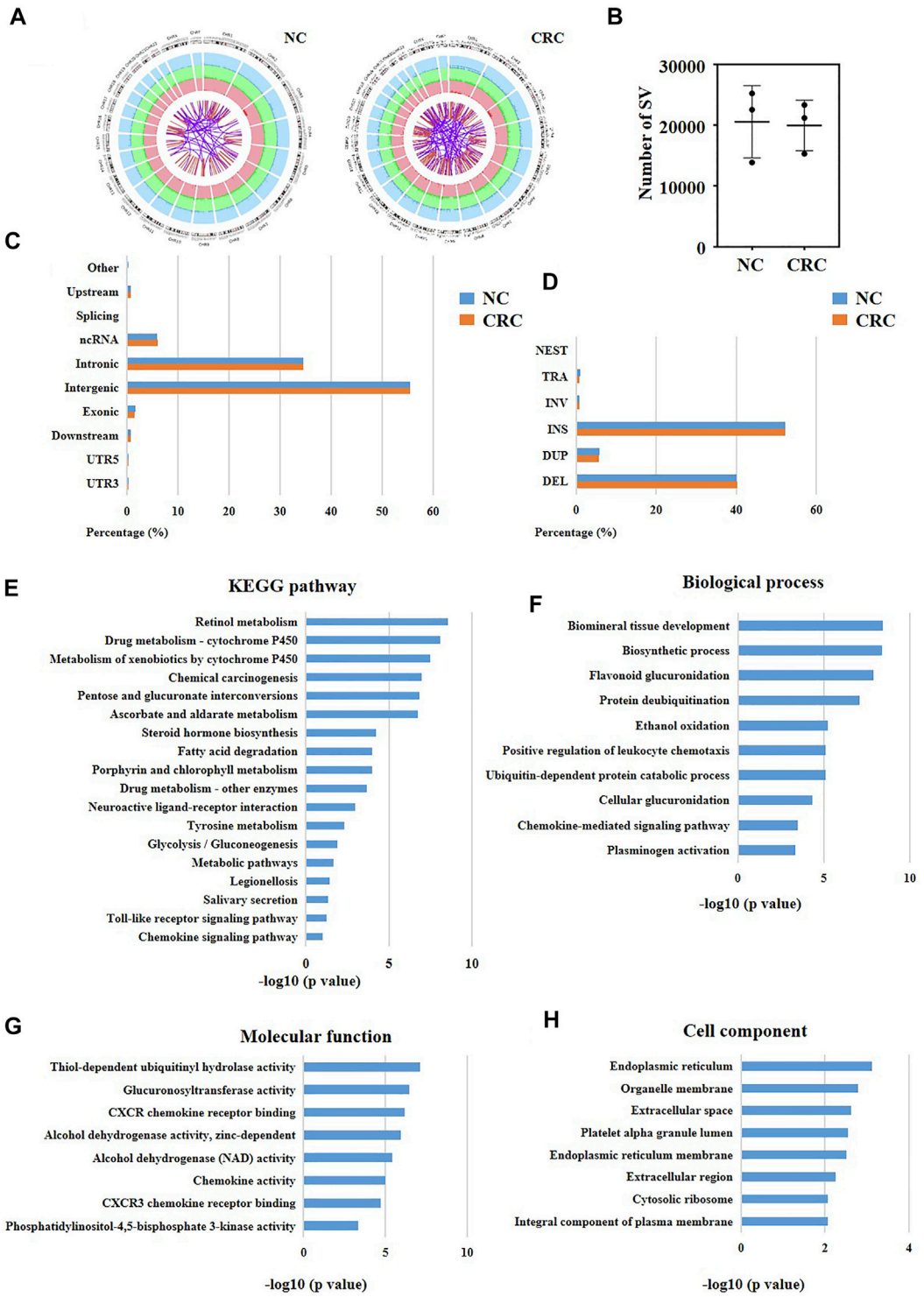

FIGURE 6 | Identification of potential pathogenic SVs in CRC patients. **(A)** Circos plot showing the whole picture of SVs of normal cells and CRC cells. The outermost circle records different chromosomes. The second and third circles record different types of SVs. In the second circle, dark green represents insertion, dark blue represents deletion, and dark red represents amplification (light green, light blue, and light red are the corresponding background colors). In the third circle, red represents inversion, and purple represents interchromosomal translocations. NC represented normal cells. **(B)** The numbers of SVs of normal cells and CRC cells. **(C)** The located sites and **(D)** types of SVs of normal cells and CRC cells. **(E–H)** KEGG and GO analysis of the nuclear genes with CRC-specific SVs at exons.

down-regulated nuclear genes, respectively (**Figures 5A,C**). On the other hand, the binding motifs of TFs JUN, SOX4, JUND, GATA2, ASCL2, and ELF1 were only opened in CRC cells and potentially regulated 28, 16, 12, 6, 4, and 2% of up-regulated nuclear genes in CRC cells, respectively (**Figures 5B,D**). Next, we evaluated the protein content and phosphorylation of the 144 TFs in CRC cells and normal cells. As a result, CDX2 and YY1 showed an increased protein expression in CRC cells versus normal cells (**Figure 5E**), and CDX2 and YY1 probably targeted 6 and 40% of all up-regulated differentially expressed nuclear genes, respectively (**Figure 5G**). Meanwhile, the phosphorylation of CBX3 at Ser176 and CRBE1 at Ser142 were down-regulated and up-regulated in CRC cells versus normal cells, respectively (**Figure 5F**), and CBX3 and CREB1 probably targeted 8.7 and 2.9% of all differentially expressed nuclear genes (**Figure 5H**). In summary, these results identified the potentially functional TFs of nuclear genes in CRC cells, including SP1, KLF5, JUND, JUN, ELF1, YY1, and CBX3.

The SVs of nuclear genes were potentially associated with the disorder of immune microenvironment in CRC patients.

SVs are a type of chromosome variation, characterized by large fragments (>50bp) of deletion, duplication, inversion, and translocation (Escaramís et al., 2015). Chromosome instability and specific SVs may cause tumors (Li et al., 2020). Consequently, we compared all SVs of CRC cells (**Figure 6A**) with SVs of normal adjacent cells using our original LWGS datasets (**Figure 6B**). Next, we calculated the numbers of SVs in CRC cells and normal cells, and found that there was no significant difference between these two groups (**Figure 6C**). Also, we analyzed the loci and types of SVs of CRC cells and normal cells, and the results showed that there was no significant difference between these two groups either (**Figures 6D,E**). We observed that the SVs located at introns and intergenes the most (**Figure 6D**), and insertion and deletion were the most common SVs types (**Figure 6E**). Since there was no significant difference in the overall number, type, and site of SVs between CRC cells and normal cells, we speculated that the specific SVs of CRC cells might be associated with the development of CRC. Hence, we screened out the CRC-specific SVs and obtained 1905 SVs ultimately (**Supplementary Table S1**). It was well known that exons contributed to protein translation in eukaryotes, which reminded us that SVs at exons might be associated with the initiation of CRC. Therefore, we classified CRC-specific SVs which located at exons into four categories. The SVs recorded in the Copy Number Variations and Related Diseases (CNVD) (a database recording malignant SVs) (Qiu et al., 2012) but not in the Genomic Variants database (DGV) (a database recording benign SVs) (MacDonald et al., 2014) were regarded as high-risk SVs. The SVs recorded in both CNVD and DGV databases were regarded as moderate-risk SVs. The SVs recorded only in DGV were regarded as low-risk SVs. The SVs with no records in any databases were regarded as possibly-deleterious SVs. Consequently, we identified one high-risk, nine moderate-risk, 29 probable-risk and 31 unknown-risk SVs in total (**Supplementary Table S1**).

To determine the functions of these high-risk and moderate-risk SVs, we further performed KEGG (**Figure 6E**) and GO (**Figures 6F–H**) analyses. The KEGG result showed that these SVs were mainly enriched in immune-related pathways, including toll-like receptor signaling pathway and chemokine signaling pathway (**Figure 6E**). Similarly, we also discovered that some immune pathways were enriched using GO analysis, such as positive regulation of leukocyte chemotaxis and chemokine-mediated signaling pathway. These results suggested that the CRC-specific SVs might be relevant to the dysfunctions of immune microenvironment in CRC patients.

In recent years, immunotherapy has achieved great curative effects in CRC treatment [(Becht et al., 2016; Kather et al., 2018; Ganesh et al., 2019)]. However, more reliable theoretical guidance is still needed for the selection of patents treated with immune drugs. In the above results, we observed that high-risk and moderate-risk SVs of CRC were highly enriched in immune-related pathways. Consequently, we further studied these immune-related genes which harbored CRC-specific SVs. Shown in **Figures 7A,B**, we found that 17 of the 20 immune-related genes had a changed mRNA expression based on the data sets from TCGA. We then investigated the network of the 17 immune-related genes using Cytoscape (**Figure 7C**). Subsequently, we searched for the hub genes within the network using Cytohubba. Shown in **Figures 7D,E**, the top eight genes were CXCL5, CXCL10, CXCL11, CXCL6, CXCL1, CXCL2, CXCL3, and CXCL13. We observed that these genes were all chemokine ligands. We further analyzed the association between the expression of the top three hub genes and immune microenvironment using the datasets from Xcell database. The results showed that CXCL5 expression was significantly correlated with microenvironment score, immune score, and the infiltration of regulatory T cells (tregs), gamma delta T cells, natural killer (NK) T cells, $CD4^+$ memory T cells, T helper two cells (Th2), T helper one cells (Th1), neutrophils, and a total of 19 immune cells (**Figure 7F**). CXCL10 expression was associated with stroma score, microenvironment score, immune score, and the infiltration of tregs, T cell gamma delta, NK T cells, $CD8^+$ naive T cells, $CD8^+$ effector memory T cells, $CD8^+$ central memory T cells, $CD8^+$ T cells, $CD4^+$ naive T cells, $CD4^+$ memory T cells, and a total of 30 immune cells (**Figure 7F**). CXCL11 expression was associated with microenvironment score, immune score and the infiltration of tregs, gamma delta T cells, NK T cells, $CD8^+$ naive T cells, $CD8^+$ effector memory T cells, $CD8^+$ central memory T cells, $CD8^+$ T cells, $CD4^+$ T cells, and a total of 27 immune cells (**Figure 7F**). Furthermore, we validated the protein expression of the highlighted genes CXCL11, CXCL10, and CXCL5 using the immunohistochemical results from the Human Protein Atlas, and found that the staining intensity of CXCL11 was higher expressed in CRC tissues versus normal colon tissues (**Figure 7G**), which was consistent with the mRNA result. However, CXCL5 was not detected in both normal colon tissues or cancer tissues, and there was no immunohistochemical results of CXCL10 in the database. The above results indicated that the SVs of CXCL5, CXCL10, and CXCL11 might be associated with the disturbance of immune microenvironment of CRC patients.

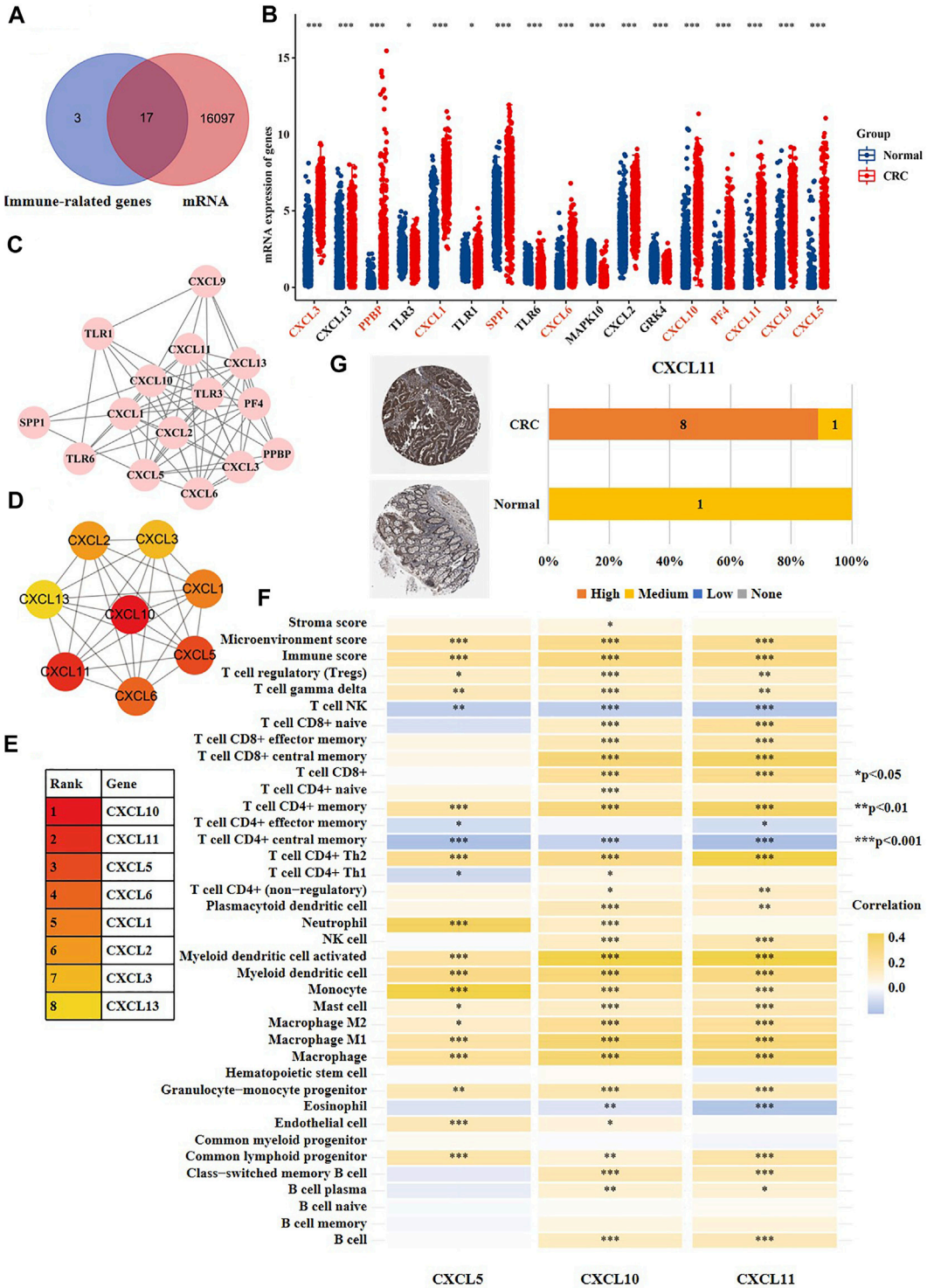

FIGURE 7 | The CRC-specific SVs might affect immune microenvironment of CRC patients. **(A)** The overlapping analysis of 20 immune-related genes (purple) that developed SVs at exons and all differentially expressed genes of CRC cells versus normal cells (red). **(B)** The mRNA expression of 17 genes screened out from **Figure 7A** in CRC cells versus normal cells. The red color indicated that the labeled gene was up-regulated in CRC cells versus normal cells, and the black color indicated that the labeled gene was down-regulated in CRC cells versus normal cells. **(C)** The network of the 17 genes. **(D,E)** The top eight hub genes among the 17 genes. **(F)** The correlation between gene expression of CXCL5, CXCL10, CXCL11 and stroma score, microenvironment score, immune score and immune infiltration. **(G)** The immunohistochemical result of CXCL11 in human normal colon tissues and CRC tissues.

DISCUSSION

Fully understanding of the pathogenesis of cancer is helpful to screen therapeutic targets for clinic. As one of the most active organelles, the nucleus regulates genetic storage, replication, and transcription in eukaryotic cells. In our study, we examined the global SVs, DNA methylation, chromatin accessibility, proteome and phosphoproteome of CRC cells versus normal cells. As a result, we observed that several nuclear genes were altered at multiple molecular layers in CRC patients, such as UTP18, ANKS4B, KBTBD11, and PKP2. Frequently, genes with multiplex-level molecular changes may play a more important role in tumorigenesis. It is noteworthy that UTP18 has molecular changes at four levels, including protein expression, phosphorylation, DNA methylation, and chromatin accessibility. Studies have demonstrated that UTP18 is associated with preribosomal RNA splicing, ribosomal biogenesis, and translation maintaining. The over-expression of UTP18 in neuroblastoma promotes the expression of VEGF, Bcl-2, HIF1α, and c-MYC, improves the adaptability of tumor cells to environmental stress, and reduces the death of neuroblastoma cells after exposure to hydrogen peroxide, hypoxia or glucose deprivation (Yang et al., 2015). Additionally, a comprehensive bioinformatics study have also revealed that high expression of UTP18 promotes the growth of CRC cells (Hu et al., 2019).

Our study proclaimed an tandem and multi-layer crosstalk between phosphorylation and ubiquitination in CRC cells. It is well known that post-translational modification is crucial for regulating biological functions and dynamic activities of proteins. Our phosphoproteomic results showed that the phosphoric-acid-modified nuclear proteins involved in a series of ubiquitination-relevant processes, including DNA damage response and repair protein ubiquitination and E3 ligase target protein ubiquitination. Ubiquitination exists in almost all eukaryotic cells and is associated with the maintenance of genomic integrity, cell cycle, immune response, and intracellular signal transduction (Han et al., 2018). Meanwhile, we also observed a crosstalk between ubiquitination and SUMOylation in CRC cells. Many studies have demonstrated that the disorder of SUMOylation may lead to the development of diseases [(Eifler and Vertegaal, 2015; Rabellino et al., 2017; Seeler and Dejean, 2017)]. Our study disclosed the interaction between phosphorylation, ubiquitination and SUMOylation, and highlighted their collaborative work in the development of CRC.

Furthermore, we revealed the TFs that potentially regulated the activity of nucleus in CRC cells, including SP1, SOX4, KLF5, JUND, JUN, YY1, CDX2, CBX3, CREB1. Among them, SP1 has been well studied in tumors [(Vizcaíno et al., 2015; Bajpai and Nagaraju, 2017; Chen et al., 2018)]. Interestingly, the previous study has uncovered that SP1 mediates the bidirectional communication between mitochondria and nucleus. The functional changes of mitochondria can activate SP1, and then affect the transcription of a series of downstream genes (Soledad et al., 2019). This suggests an interaction between mitochondria and nucleus in CRC cells via SP1. YY1 is also a well-known oncogene. YY1 can maintain the survival of tumor cells and promote adaptation of cells to tumor microenvironment by regulating numerous genes related to cell proliferation, cell cycle, and inflammatory response [(Meliala et al., 2020)].

Besides, we disclosed that the CRC-specific immune-relevant SVs were mainly enriched in toll-like receptor pathway and chemokine pathways. Many reports have demonstrated the toll-like receptor signaling is associated with the activation of both innate and adaptive immune responses, and has an core role in the initiation and development of CRC [(Yang et al., 2017; Tintelnot and Stein, 2019; Rezasoltani et al., 2020)]. Currently, several drugs against toll-like receptor ligands (TRLs) have been approved by Food and Drug Administration (FDA) for cancer treatments, such as Bacillus calmette, monophosphoryl lipid A, and imiquimod [(Moradi-Marjaneh et al., 2018; Le Naour et al., 2020)]. Our results reveal new potential therapeutic targets of toll-like receptor pathway for CRC treatments.

The immunohistochemical results showed that CXCL5 was not detected in both normal colon tissues or cancer tissues, while its mRNA expression was up-regulated in CRC cells versus normal adjacent cells. As we know, gene expression is divided into two dimensions, including the mRNA level and protein level. According to a large number of studies, the protein abundance in cells is obviously different from mRNA in terms of half-life, synthesis rate and quantity [(Schwanhäusser et al., 2011; Rodriguez et al., 2019)]. Besides, there is frequently complex post-transcription processing after transcription, such as non-coding RNA and mRNA modification.

In conclusion, we characterized the molecular changes of nucleus of CRC cells at distinct levels, and uncovered the potential hub genes and drug targets using a multi-omics approach. To our best knowledge, this is the first that the panoramic description of the multi-level molecular changes of nucleus of CRC cells is provided. The findings of our study may improve the understanding of pathogenesis of CRC and provide novel biomarkers and drug targets for clinic.

DATA AVAILABILITY STATEMENT

The datasets presented in this study can be found in online repositories. The names of the repository/repositories and accession number(s) can be found below: http://www.proteomexchange.org/, PXD021314. http://www.proteomexchange.org/, PXD021318. https://www.ncbi.nlm.nih.gov/, PRJNA693028.

ETHICS STATEMENT

The studies involving human participants were reviewed and approved by the Ethics Committee of Shenzhen People's Hospital. The patients/participants provided their written informed consent to participate in this study.

AUTHOR CONTRIBUTIONS

WZ, MT, YD, and DT designed and supervised this study; WZ and MW analyzed the data and wrote manuscript; WC collected the

specimen; XG, CM, and HX interpreted the data; LL and JH revised the manuscript; YZ analyzed the data; all authors read and approved the final manuscript.

FUNDING

This study was supported by the National Natural Science Foundation of China (No. 82003172), Shenzhen Fund for Guangdong Provincial High-level Clinical Key Specialties (No. SZGSP001), the Postdoctoral Science Foundation of China (No. 2020M673065), the Guangdong Basic and Applied Basic Research Foundation (No. 2019A1515111138), the science and technology plan of Shenzhen (No. JCYJ20180306140810282).

SUPPLEMENTARY MATERIAL

The Supplementary Material for this article can be found online at: https://www.frontiersin.org/articles/10.3389/fcell.2022.796703/full#supplementary-material

REFERENCES

Bajpai, R., and Nagaraju, G. P. (2017). Specificity Protein 1: Its Role in Colorectal Cancer Progression and Metastasis. *Crit. Rev. Oncology/Hematology* 113, 1–7. doi:10.1016/j.critrevonc.2017.02.024

Becht, E., de Reyniès, A., Giraldo, N. A., Pilati, C., Buttard, B., Lacroix, L., et al. (2016). Immune and Stromal Classification of Colorectal Cancer Is Associated with Molecular Subtypes and Relevant for Precision Immunotherapy. *Clin. Cancer Res.* 22 (16), 4057–4066. doi:10.1158/1078-0432.CCR-15-2879

Bray, F., Ferlay, J., Soerjomataram, I., Siegel, R. L., Torre, L. A., and Jemal, A. (2018). Global Cancer Statistics 2018: GLOBOCAN Estimates of Incidence and Mortality Worldwide for 36 Cancers in 185 Countries. *CA: A Cancer J. Clinicians* 68 (6), 394–424. doi:10.3322/caac.21492

Buenrostro, J. D., Wu, B., Chang, H. Y., and Greenleaf, W. J. (2015). ATAC-seq: A Method for Assaying Chromatin Accessibility Genome-Wide. *Curr. Protoc. Mol. Biol.* 109, 21291–21299. doi:10.1002/0471142727.mb2129s109

Chelbi-Alix, M. K., and Thibault, P. (2021). Crosstalk between SUMO and Ubiquitin-like Proteins: Implication for Antiviral Defense. *Front. Cel Dev. Biol.* 9, 671067. doi:10.3389/fcell.2021.671067

Chen, X., Zeng, K., Xu, M., Hu, X., Liu, X., Xu, T., et al. (2018). SP1-induced lncRNA-ZFAS1 Contributes to Colorectal Cancer Progression via the miR-150-5p/VEGFA axis. *Cell Death Dis* 9 (10), 982. doi:10.1038/s41419-018-0962-6

Choong, M. K., and Tsafnat, G. (2012). Genetic and Epigenetic Biomarkers of Colorectal Cancer. *Clin. Gastroenterol. Hepatol.* 10 (1), 9–15. doi:10.1016/j.cgh.2011.04.020

Eifler, K., and Vertegaal, A. C. O. (2015). SUMOylation-Mediated Regulation of Cell Cycle Progression and Cancer. *Trends Biochem. Sci.* 40 (12), 779–793. doi:10.1016/j.tibs.2015.09.006

Escaramís, G., Docampo, E., and Rabionet, R. (2015). A Decade of Structural Variants: Description, History and Methods to Detect Structural Variation. *Brief. Funct. Genomics* 14 (5), 305–314. doi:10.1093/bfgp/elv014

Ganesh, K., Stadler, Z. K., Cercek, A., Mendelsohn, R. B., Shia, J., Segal, N. H., et al. (2019). Immunotherapy in Colorectal Cancer: Rationale, Challenges and Potential. *Nat. Rev. Gastroenterol. Hepatol.* 16 (6), 361–375. doi:10.1038/s41575-019-0126-x

Han, Z.-J., Feng, Y.-H., Gu, B.-H., Li, Y.-M., and Chen, H. (2018). The post-translational Modification, SUMOylation, and Cancer (Review). *Int. J. Oncol.* 52 (4), 1081–1094. doi:10.3892/ijo.2018.4280

Hu, M., Fu, X., Si, Z., Li, C., Sun, J., Du, X., et al. (2019). Identification of Differently Expressed Genes Associated with Prognosis and Growth in Colon Adenocarcinoma Based on Integrated Bioinformatics Analysis. *Front. Genet.* 10, 1245. doi:10.3389/fgene.2019.01245

Kather, J. N., Halama, N., and Jaeger, D. (2018). Genomics and Emerging Biomarkers for Immunotherapy of Colorectal Cancer. *Semin. Cancer Biol.* 52 (Pt 2), 189–197. doi:10.1016/j.semcancer.2018.02.010

Le Naour, J., Galluzzi, L., Zitvogel, L., Kroemer, G., and Vacchelli, E. (2020). Trial Watch: TLR3 Agonists in Cancer Therapy. *Oncoimmunology* 9 (1), 1771143. doi:10.1080/2162402X.2020.1771143

Li, Y., Roberts, N. D., Roberts, N. D., Wala, J. A., Shapira, O., Schumacher, S. E., et al. (2020). Patterns of Somatic Structural Variation in Human Cancer Genomes. *Nature* 578 (7793), 112–121. doi:10.1038/s41586-019-1913-9

MacDonald, J. R., Ziman, R., Yuen, R. K. C., Feuk, L., and Scherer, S. W. (2014). The Database of Genomic Variants: a Curated Collection of Structural Variation in the Human Genome. *Nucl. Acids Res.* 42 (Database issue), D986–D992. doi:10.1093/nar/gkt958

Meliala, I. T. S., Hosea, R., Kasim, V., and Wu, S. (2020). The Biological Implications of Yin Yang 1 in the Hallmarks of Cancer. *Theranostics* 10 (9), 4183–4200. doi:10.7150/thno.43481

Moradi-Marjaneh, R., Hassanian, S. M., Fiuji, H., Soleimanpour, S., Ferns, G. A., Avan, A., et al. (2018). Toll like Receptor Signaling Pathway as a Potential Therapeutic Target in Colorectal Cancer. *J. Cel Physiol* 233 (8), 5613–5622. doi:10.1002/jcp.26273

Nie, M., and Boddy, M. (2016). Cooperativity of the SUMO and Ubiquitin Pathways in Genome Stability. *Biomolecules* 6 (1), 14. doi:10.3390/biom6010014

Okugawa, Y., Grady, W. M., and Goel, A. (2015). Epigenetic Alterations in Colorectal Cancer: Emerging Biomarkers. *Gastroenterology* 149 (5), 1204–1225. e12. doi:10.1053/j.gastro.2015.07.011

Qiu, F., Xu, Y., Li, K., Li, Z., Liu, Y., DuanMu, H., et al. (2012). CNVD: Text Mining-Based Copy Number Variation in Disease Database. *Hum. Mutat.* 33 (11), E2375–E2381. doi:10.1002/humu.22163

Rabellino, A., Andreani, C., and Scaglioni, P. P. (2017). The Role of PIAS SUMO E3-Ligases in Cancer. *Cancer Res.* 77 (7), 1542–1547. doi:10.1158/0008-5472.CAN-16-2958

Rezasoltani, S., Ghanbari, R., Looha, M. A., Mojarad, E. N., Yadegar, A., Stewart, D., et al. (2020). Expression of Main Toll-like Receptors in Patients with Different Types of Colorectal Polyps and Their Relationship with Gut Microbiota. *Ijms* 21 (23), 8968. doi:10.3390/ijms21238968

Rodriguez, J., Ren, G., Day, C. R., Zhao, K., Chow, C. C., and Larson, D. R. (2019). Intrinsic Dynamics of a Human Gene Reveal the Basis of Expression Heterogeneity. *Cell* 176 (1-2), 213–226. doi:10.1016/j.cell.2018.11.026

Rusk, N. (2019). Multi-omics Single-Cell Analysis. *Nat. Methods* 16 (8), 679. doi:10.1038/s41592-019-0519-3

Sato, T., Stange, D. E., Ferrante, M., Vries, R. G. J., Van Es, J. H., Van den Brink, S., et al. (2011). Long-term Expansion of Epithelial Organoids from Human colon, Adenoma, Adenocarcinoma, and Barrett's Epithelium. *Gastroenterology* 141 (5), 1762–1772. doi:10.1053/j.gastro.2011.07.050

Schwanhäusser, B., Busse, D., Li, N., Dittmar, G., Schuchhardt, J., Wolf, J., et al. (2011). Global Quantification of Mammalian Gene Expression Control. *Nature* 473 (7347), 337–342. doi:10.1038/nature10098

Seeler, J.-S., and Dejean, A. (2017). SUMO and the Robustness of Cancer. *Nat. Rev. Cancer* 17 (3), 184–197. doi:10.1038/nrc.2016.143

Siegel, R. L., Miller, K. D., Goding Sauer, A., Fedewa, S. A., Butterly, L. F., Anderson, J. C., et al. (2020). Colorectal Cancer Statistics, 2020. *CA A. Cancer J. Clin.* 70 (3), 145–164. doi:10.3322/caac.21601

Soledad, R. B., Charles, S., and Samarjit, D. (2019). The Secret Messages between Mitochondria and Nucleus in Muscle Cell Biology. *Arch. Biochem. Biophys.* 666, 52–62. doi:10.1016/j.abb.2019.03.019

Sun, H., Ou, B., Zhao, S., Liu, X., Song, L., Liu, X., et al. (2019). USP11 Promotes Growth and Metastasis of Colorectal Cancer via PPP1CA-mediated Activation of ERK/MAPK Signaling Pathway. *EBioMedicine* 48, 236–247. doi:10.1016/j.ebiom.2019.08.061

Tintelnot, J., and Stein, A. (2019). Immunotherapy in Colorectal Cancer: Available Clinical Evidence, Challenges and Novel Approaches. *Wjg* 25 (29), 3920–3928. doi:10.3748/wjg.v25.i29.3920

Vizcaíno, C., Mansilla, S., and Portugal, J. (2015). Sp1 Transcription Factor: A Long-Standing Target in Cancer Chemotherapy. *Pharmacol. Ther.* 152, 111–124. doi:10.1016/j.pharmthera.2015.05.008

Xie, M., Yu, J., Ge, S., Huang, J., and Fan, X. (2020). SUMOylation Homeostasis in Tumorigenesis. *Cancer Lett.* 469, 301–309. doi:10.1016/j.canlet.2019.11.004

Yang, H. W., Kim, T.-M., Song, S. S., Menon, L., Jiang, X., Huang, W., et al. (2015). A Small Subunit Processome Protein Promotes Cancer by Altering Translation. *Oncogene* 34 (34), 4471–4481. doi:10.1038/onc.2014.376

Yang, Y., Weng, W., Peng, J., Hong, L., Yang, L., Toiyama, Y., et al. (2017). Fusobacterium Nucleatum Increases Proliferation of Colorectal Cancer Cells and Tumor Development in Mice by Activating Toll-like Receptor 4 Signaling to Nuclear Factor−κB, and Up-Regulating Expression of MicroRNA-21. *Gastroenterology* 152 (4), 851–866. e24. doi:10.1053/j.gastro.2016.11.018

Zhang, W., Tang, D., Lin, L., Fan, T., Xia, L., Cai, W., et al. (2021). Integrative Multiplatform-Based Molecular Profiling of Human Colorectal Cancer Reveals Proteogenomic Alterations Underlying Mitochondrial Inactivation. *Am. J. Cancer Res.* 11 (6), 2893–2910.

Zhang, W., Lin, L., Xia, L., Cai, W., Dai, W., Zou, C., et al. (2021). Multi-omics Analyses of Human Colorectal Cancer Revealed Three Mitochondrial Genes Potentially Associated with Poor Outcomes of Patients. *J. Transl Med.* 19 (1), 273. doi:10.1186/s12967-021-02939-7

Conflict of Interest: The authors declare that the research was conducted in the absence of any commercial or financial relationships that could be construed as a potential conflict of interest.

Publisher's Note: All claims expressed in this article are solely those of the authors and do not necessarily represent those of their affiliated organizations, or those of the publisher, the editors and the reviewers. Any product that may be evaluated in this article, or claim that may be made by its manufacturer, is not guaranteed or endorsed by the publisher.

frontiers in Oncology

ORIGINAL RESEARCH
published: 31 March 2022
doi: 10.3389/fonc.2022.849338

In Vitro Characterization of ^{177}Lu-DOTA-M5A Anti-Carcinoembryonic Antigen Humanized Antibody and HSP90 Inhibition for Potentiated Radioimmunotherapy of Colorectal Cancer

Tabassom Mohajershojai[1], *Preeti Jha*[1,2], *Anna Boström*[3], *Fredrik Y. Frejd*[1], *Paul J. Yazaki*[4] *and Marika Nestor*[1]*

[1] Department of Immunology, Genetics and Pathology, Uppsala University, Uppsala, Sweden, [2] Department of Medicinal Chemistry, Uppsala University, Uppsala, Sweden, [3] Ridgeview Instruments AB, Uppsala, Sweden, [4] Department of Immunology and Theranostics, Beckman Research Institute, City of Hope, Duarte, CA, United States

OPEN ACCESS

Edited by:
Shilpa S. Dhar,
University of Texas MD Anderson Cancer Center, United States

Reviewed by:
Gabriele Multhoff,
Technical University of Munich, Germany
Deuk-Su Kim,
KT&G R&D Center, South Korea

***Correspondence:**
Marika Nestor
marika.nestor@igp.uu.se

Specialty section:
This article was submitted to Molecular and Cellular Oncology, a section of the journal Frontiers in Oncology

Received: 05 January 2022
Accepted: 22 February 2022
Published: 31 March 2022

Citation:
Mohajershojai T, Jha P, Boström A, Frejd FY, Yazaki PJ and Nestor M (2022) In Vitro Characterization of ^{177}Lu-DOTA-M5A Anti-Carcinoembryonic Antigen Humanized Antibody and HSP90 Inhibition for Potentiated Radioimmunotherapy of Colorectal Cancer. Front. Oncol. 12:849338. doi: 10.3389/fonc.2022.849338

Carcinoembryonic antigen (CEA) is an antigen that is highly expressed in colorectal cancers and widely used as a tumor marker. ^{131}I and ^{90}Y-radiolabeled anti-CEA monoclonal antibodies (mAbs) have previously been assessed for radioimmunotherapy in early clinical trials with promising results. Moreover, the heat shock protein 90 inhibitor onalespib has previously demonstrated radiotherapy potentiation effects *in vivo*. In the present study, a ^{177}Lu-radiolabeled anti-CEA hT84.66-M5A mAb (M5A) conjugate was developed and the potential therapeutic effects of ^{177}Lu-DOTA-M5A and/or onalespib were investigated. The ^{177}Lu radiolabeling of M5A was first optimized and characterized. Binding specificity and affinity of the conjugate were then evaluated in a panel of gastrointestinal cancer cell lines. The effects on spheroid growth and cell viability, as well as molecular effects from treatments, were then assessed in several three-dimensional (3D) multicellular colorectal cancer spheroid models. Stable and reproducible radiolabeling was obtained, with labeling yields above 92%, and stability was retained at least 48 h post-radiolabeling. Antigen-specific binding of the radiolabeled conjugate was demonstrated on all CEA-positive cell lines. Dose-dependent therapeutic effects of both ^{177}Lu-DOTA-M5A and onalespib were demonstrated in the spheroid models. Moreover, effects were potentiated in several dose combinations, where spheroid sizes and viabilities were significantly decreased compared to the corresponding monotherapies. For example, the combination treatment with 350 nM onalespib and 20 kBq ^{177}Lu-DOTA-M5A resulted in 2.5 and 2.3 times smaller spheroids at the experimental endpoint than the corresponding monotreatments in the SNU1544 spheroid model. Synergistic effects were demonstrated in several of the more effective combinations. Molecular assessments validated the therapy results and displayed increased apoptosis in

several combination treatments. In conclusion, the combination therapy of anti-CEA ^{177}Lu-DOTA-M5A and onalespib showed enhanced therapeutic effects over the individual monotherapies for the potential treatment of colorectal cancer. Further *in vitro* and *in vivo* studies are warranted to confirm the current study findings.

Keywords: carcinoembryonic antigen (CEA), 177Lu-DOTA-M5A mAb, combination (combined) therapy, multicellular 3D spheroids, colorectal cancer, molecular radiotherapy, HSP90 (heat shock protein 90), onalespib (AT13387)

INTRODUCTION

Gastrointestinal (GI) cancers are a collective term describing cancers that affect the digestive system. The most common diagnosed GI cancers are colorectal cancer, gastric cancer, and liver cancer (1). Colorectal cancer is the third most commonly diagnosed cancer and the second cause of cancer death worldwide (2). Carcinoembryonic antigen (CEA) is a well-known cancer-associated biomarker, which has been found in several solid tumors including GI and breast cancers (3–5). Consequently, CEA has been used as a target for cancer diagnosis, research, and targeted therapy (6–8).

High expression of CEA on the basolateral surface of colorectal cancer cells has made it a suitable target for colorectal cancer-targeted therapies, including antibody–drug conjugates and radionuclide therapies (7, 9–14). Despite a large number of *in vivo*, preclinical, and clinical studies on targeting CEA, the underlying cellular and molecular mechanisms involved in tumor suppression and metastasis inhibition by targeting CEA are not fully clear. CEA is a glycosylphosphatidylinositol (GPI) membrane-bound protein with a very slow rate of internalization (15) with no direct downstream signaling pathway but can influence other pathways indirectly such as the transforming growth factor (TGF)-β pathway (16).

Radioimmunotherapy (RIT) is a promising approach for the treatment of many cancers. Targeting an antigen that is specifically and highly expressed on cancer cells can be a suitable way to preferentially deliver therapeutic radionuclides to tumors. The efficiency of RIT requires a specific and long enough interaction between antigen and radiolabeled conjugate (antibody) in order to deliver an optimal tumoricidal radiation dose. RIT has been demonstrated as an effective therapy for hematological malignancies, whereas the effects on solid tumors have been more limited due to characteristics such as antigen heterogenicity, drug penetration limitations, tumor location, limited vascularization of the tumor, and rapid cell proliferation. Despite these factors, RIT has still shown promise for some solid tumors such as colorectal cancers (17–19).

Several CEA-targeting antibodies have previously been labeled with various radionuclides and explored *in vitro*, *in vivo*, and in clinical trials, demonstrating promising results (10–12, 20, 21). T84.66 is a well-characterized anti-CEA murine IgG_1 monoclonal antibody (mAb) that does not cross-react with other members of the *CEA* gene family and has successfully been used for ^{111}In imaging of patients with primary colorectal adenocarcinomas (22, 23). To avoid human immune responses, the T84.66 mAb was reconstituted to a chimeric version (cT84.66), where it was conjugated with the bifunctional chelates Diethylenetriamine Pentaacetate (DTPA) and Dodecane Tetraacetic Acid (DOTA) and radiolabeled with ^{111}In and ^{90}Y. The cT84.66 hT84.66, M5A was evaluated in extensive RIT clinical studies (21 trials with over 250 patients) as a single agent or in combination with standard of care chemotherapy agents (24). The clinical studies demonstrated that the antibody was well tolerated and feasible to use clinically in combination with chemotherapy agents (7, 24–29). Recently, a humanized version of T84.66 (hT84.66, M5A) was developed to lower potential immunogenicity (30). A Phase I ^{90}Y-DOTA-M5A RIT study was conducted in patients with advanced CEA-expressing tumors, and some therapeutic effects were observed, suggesting a therapeutic potential of this agent (11).

In recent years, ^{177}Lu has been established as a promising radionuclide for targeted radionuclide therapies, of which cost-effectiveness, availability, well-suited physical and biological half-life, and desired energy in order to minimize off-target effects are some of the contributing factors (31). However, the anti-CEA humanized mAb M5A has not previously been assessed with ^{177}Lu and subsequent use for RIT. Therefore, the first aim of this study was to optimize ^{177}Lu labeling of M5A and characterize the conjugate *in vitro*.

Other interesting targets for cancer therapy are the heat shock proteins (HSPs), which are involved in many oncogenic pathways. HSPs are a large family of molecular chaperones involved in protein folding, maturation, and degradation. Under stress conditions such as heat shock, oxidative stress, and any other stress events leading to protein damages, HSP responses are critical (32). HSP90 is a known cellular protein acting on numerous hallmarks of cancer, such as cell proliferation, apoptosis, and invasiveness. Particularly, HSP90 plays a key role in regulatory protein folding pathways, transcription factors, and cellular kinases (33). On a molecular level, HSP90 influences, e.g., Receptor Tyrosine Kinases (RTKs), Phosphoinositide 3-Kinase (PI3K)/AKT, and Mitogen-Activated Protein Kinase (MAPK)/Extracellular-Signal-Regulated Kinase (ERK) pathways. It can partially regulate Wnt and TGF-β signaling pathways as well. RTK blockade, e.g., toward epidermal growth factor receptor (EGFR) or vascular endothelial growth factor receptor (VEGFR), combined with HSP90 inhibitors demonstrated therapeutic potential in preclinical and clinical colorectal studies (34–36). High HSP90 expression is associated with invasion, metastasis, and poor prognosis of colorectal cancers and gastric cancers (37,

38). Therefore, inhibition of HSP90 may be a feasible strategy to increase cytotoxicity and suppress protection mechanisms of cancer cells influencing different pathways simultaneously (39). Though there are plenty of HSP90 inhibitors in clinical trials, none is approved for cancer monotherapy due to toxicity and difficult formulation of the first-generation of inhibitors (40). Onalespib (AT13387) is a second-generation HSP90 inhibitor indicated to have better solubility and minimal hepatotoxicity as compared to the first-generation HSP90 inhibitors (e.g., 17-AAG and 17-DMAG) in both preclinical and clinical trials (41). Onalespib has been used alone and in combination with chemotherapy drugs and radiation for solid tumors in preclinical and clinical studies (42–44). Radiosensitizing features have been demonstrated *in vivo* when onalespib was combined with external beam radiation in e.g., colorectal cancer models (45) and with targeted radionuclide therapy using ^{177}Lu-DOTATATE in neuroendocrine cancer models (46). Thus, the radiosensitizing property of onalespib in addition to its aforementioned inhibition on cellular pathways makes it a highly interesting candidate to combine with ^{177}Lu-DOTA-M5A in colorectal cancer treatment. Thus, the second aim of this study was to evaluate the effects of HSP90 inhibition in colorectal cancer models *in vitro* and to assess the radiosensitizing potential in combination with ^{177}Lu-DOTA-M5A.

To conclude, the aim of the present study was to develop and characterize a ^{177}Lu-DOTA-M5A conjugate and assess if therapeutic effects could be further potentiated through HSP90 inhibition. Therapeutic and molecular effects of both monotreatments and the combination treatments were assessed in a panel of colorectal cancer cell lines using two-dimensional (2D) models, and three-dimensional (3D) multicellular spheroid models.

MATERIALS AND METHODS

Cell Culture and Maintenance

The human GI CEA-positive cell line SNU1544 [colon adenocarcinoma, doubling time 42 h (47)] obtained from Korean Cell Line Bank (KCLB) was cultured in RPMI [Biowest, MO, USA, containing 25 nM N-2-Hydroxyethylpiperazine-N'-2-Ethanesulfonic Acid (HEPES)] supplemented with 10% (v/v) fetal bovine serum (FBS; Sigma Aldrich, MO, USA) that was heat inactivated at 56°C for 30 min. MKN45 cell line [gastric adenocarcinoma, doubling time 60 h (48)] obtained from German Collection of Microorganisms and Cell Culture (DSMZ) was cultured in RPMI supplemented with 20% FBS. HT55 cell line [colon carcinoma, doubling time 28 h (49)] obtained from European Collection of Authenticated Cell Culture (ECACC) was cultured in Minimum Essential Medium (MEM) (Biowest, MO, USA) supplemented with 20% FBS. LS174T cell line [colon adenocarcinoma, doubling time 26 h (50)] obtained from ECACC was cultured in the same media as HT55 cell line except supplemented with 10% FBS. The human colon adenocarcinoma HT29 [doubling time 24 h (51)] obtained from American Type Culture Collection (ATCC) was cultured in McCoy's (Biowest, MO, USA) supplemented with 10% FBS. All media were supplemented with L-glutamine (Biochrom GmbH, 2 mM) and antibiotics (100 IU penicillin and 100 µg/ml streptomycin, Biochrom GmbH, Germany). Monolayer cultures were grown in tissue culture flasks (VWR, PA, USA) and incubated in an atmosphere containing 5% CO_2 at 37°C. After reaching 70%–80% confluency, cell passaging was performed using Trypsin-EDTA (Biochrom GmbH, Germany). Differences in cell culture media and supplements may to some extent impact cellular processes. In the present study, all studied cell lines were grown in the culture conditions recommended by the suppliers.

Anti-Carcinoembryonic Antigen M5A Monoclonal Antibody and Onalespib

The hT84.66-M5A (M5A) mAb is a humanized IgG_1 mAb derived from the murine T84.66 mAb by Complementary Determining Region (CDR) grafting based on structure design (30). The M5A mAb was conjugated with NHS-DOTA as previously described (52). Briefly, diafiltration was used for buffer exchange, conjugation, and concentration of DOTA-M5A mAb using an Amicon ultrafiltration stirred cell 8300 under vacuum (MilliporeSigma, Burlington, MA, USA). The M5A mAb (5 mg, 5 mg/ml) was equilibrated in 10 diavolumes of conjugation buffer (100 mM sodium bicarbonate buffer, 5 mM DTPA, pH 8.5). A 10-M excess of DOTA-NHS ester dissolved in the conjugation buffer (0.282 mg, 10 mg/ml, Macrocylics, Plano, TX, USA) was added to the M5A mAb in a total volume of 1 ml and allowed to stir for 1 h at room temperature. The reaction was buffer exchanged with 18 diavolumes of post-conjugation buffer (250 mM ammonium acetate, pH 7.0) and filtered under sterile condition (0.2 µm, Thermo Fisher Scientific, Waltham, MA, USA). All buffers were prepared using Ultra Trace water (Thermo Fisher Scientific) and sterile filtered prior to use. The resulting DOTA-M5A conjugate was characterized by measurement of protein concentration ($A_{280\ nm}$), Isoelectric Focusing (IEF) analysis (Criterion IEF pre-cast gel, pH 3-10, Bio-Rad Laboratories, Hercules, CA, USA), High Performance Liquid Chromatography (HPLC)-size exclusion chromatography (HPLC-SEC, Superdex-200 10/300 column, Cytiva, Marlborough, MA, USA), and the quadrupole time-of-flight (QTOF) mass spectrometry (model 6520, Agilent Technologies, Santa Clara, CA, USA; **Supplementary Figure S1**).

For immunoreactivity, DOTA-M5A mAb was radiolabeled with ^{64}Cu with 97.5% radiolabeling yield as confirmed by instant thin-layer chromatography (ITLC, mAb stays at origin, ^{64}Cu-DTPA migrates to front). The purity of ^{64}Cu-DOTA-M5A (r_t = 40.55 min) was analyzed by HPLC-SEC (Superdex 200 10/300 column, with an in-line OD_{280} UV detector and radiodetector, 0.5 ml/min, PBS-1% HSA, isocratic; **Supplementary Figure S2**). The radioconjugate ^{64}Cu-DOTA-M5A (200,000 cpms) was incubated with 20× molar excess of soluble CEA for 30 min at room temperature. The reaction mixture was then analyzed on HPLC-SEC Superdex 200, monitoring for a molecular size shift of the radioactive mAb to an increased molecular size (**Supplementary Figure S2**).

The lyophilized onalespib (AT13387) (Selleckchem, TX, USA) was dissolved in Dimethyl Sulfoxide (DMSO) to a stock concentration of 61.0471 mM and stored at -20°C until required for the experiments. Onalespib was thawed and diluted further in cell media for cellular treatments.

^{177}Lu Radiolabeling and Purification

Prior to ^{177}Lu labeling, DOTA-M5A mAb was buffer exchanged to either sodium acetate (0.2 M, pH 5.5) or ammonium acetate (0.1 M, pH 5.5) using spin column (Amicon Ultra-0.5 ml, Merck, Germany). The nominal molecular weight cutoff (NMWCO) of the spin column was 3 kDa. Spin column was rinsed once with NaOH (0.1 M, 500 µl, 14,000 rpm, 10 min, 22°C) followed by subsequent rinsing with the sodium acetate or ammonium acetate buffer under similar conditions. The desired amount of DOTA-M5A was loaded on a rinsed column, its volume was made up to 500 µl with buffer, and the sample was rinsed as mentioned before. The concentrated antibody was dissolved in the desired buffer volume and collected in a new tube. The concentration of final DOTA-M5A was measured using Nanodrop (Denovix DS-11 Spectrophotometer, DE, USA). Molecular mass of conjugate was approximated to 150 kDa (**Supplementary Figure S1**).

^{177}Lu radiolabeling was optimized (**Supplementary Figures S3, S4**), and the optimized conditions were then applied for ^{177}Lu labeling of DOTA-M5A. Briefly, mixture of ^{177}Lu (15 MBq, in 0.04 M HCl, ITG GmbH) and DOTA-M5A (50 µg) dissolved in sodium acetate (0.2 M, pH 5.5) or ammonium acetate (0.1 M, pH 5.5) was stirred on the thermoshaker (TS-100C Smart, Biosan, Lativa) at 42°C for 1 h (350 rpm), yielding the final specificity activity of 300 kBq/µg (≥90% radiochemical yield). The extent of radiolabeling was assessed with ITLC (Biodex Medical Systems) using citric acid (0.2 M, pH 5.5) as a mobile phase, and the radiolabeling yield was quantified using phosphoimager (BAS-1800II, Fujifilm). Radiolabeling purity (≥99.9%) of ^{177}Lu-DOTA-M5A was assessed using HPLC-SEC (in-line OD_{280} UV-detector and radiodetector: Chromater Alpha; Phenomenex, BioSep-SEC-s3000, LC Column 300 × 7.8 mm, 1.0 ml/min, 0.1 M phosphate buffer, pH 6.8, isocratic; **Supplementary Figure S4**: UV-detection, r_t = 8.65 min, radio-detector, r_t = 8.75 min). The ^{177}Lu-DOTA-M5A was purified as and when required using spin column (Amicon Ultra-0.5 ml, Merck, Germany, 3 kDa NMWCO).

Stability Assays

The stability of ^{177}Lu-DOTA-M5A was assessed in mouse serum and in EDTA condition, respectively. Briefly, for stability in serum, ^{177}Lu-DOTA-M5A (10 µg) was added to individual Eppendorf tubes containing either PBS (80 µl) or mixture of mouse serum and PBS (1/1, v/v, total volume of 80 µl). For the EDTA challenge test, 500-M excess of EDTA (dissolved in metal-free water) was added to ^{177}Lu-DOTA-M5A. Metal-free water was added to ^{177}Lu-DOTA-M5A in a separate tube, as control. Samples were stirred well and placed on thermoblock for 48 h at 37°C. Stability was analyzed for the overall radiolabeling yield using ITLC and quantified as mentioned previously at 1 and 48 h post-radiolabeling.

Two-Dimensional lysates and Western Blot Analyses

To evaluate potential onalespib effect on the CEA expression on CEA-positive cell lines, a defined number of cells were seeded in T25 flasks (1×10^6 SNU1544 cells/flask, 0.7×10^6 LS174T cells/flask, and HT55 cells/flask), incubated in an atmosphere containing 5% CO_2 at 37°C and treated at 70% confluency. SNU1544 cells were treated with 50, 150, 350, and 700 nM of onalespib. HT55 cells were treated with 25, 50, 75, 100, and 150 nM of onalespib, and LS174T cells were treated with 600, 800, 1,000, and 2,000 nM of onalespib. Equal amounts of DMSO in the highest concentrations were used as control. Cell lysates were prepared 24 h posttreatment. Cells were washed with 1× cold PBS followed by incubating with Pierce™ IP lysis buffer (Thermo Fisher Scientific, Sweden) containing Halt™ Protease and Phosphatase inhibitor cocktail (Thermo Fisher Scientific, Sweden) for 10 min on ice. The lysates were centrifuged at 15,000 rpm for 15 min at 4°C, and supernatants were collected and stored at -20°C. Protein concentration of lysates was assessed by Pierce BCA Protein Assay Kit (Thermo Scientific, Sweden). Samples were run on 10% Bis-Tris gels in 3-(N-morpholino)propanesulfonic acid (MOPS) running buffer (Novex™, NuPAGE®, Invitrogen, Thermo Fisher Scientific, Sweden). Thereafter, the separated proteins were transferred to a Polyvinylidene Difluoride (PVDF) membrane (Merck Millipore, Darmstadt, Germany) for 2 h with the constant voltage of 100 V at 4°C. The membranes were blocked in 5% bovine serum albumin (BSA) in PBS-Tween (0.1%) for 1 h and were then incubated with primary antibodies in 1% BSA in PBS-Tween (0.1%) at 4°C overnight. Primary antibodies targeted CEA (CD66e, 14-0669-82 Mouse monoclonal antibody, eBioscience, Invitrogen, Sweden), EGFR (ab52894, Rabbit monoclonal antibody, Abcam, UK), and AKT1,2,3 (ab179463, Rabbit monoclonal antibody, Abcam, UK). Glyceraldehyde-3-Phosphate Dehydrogenase (GAPDH) (ab8245, Mouse monoclonal antibody, Abcam, UK) or β-actin (ab8227, Rabbit polyclonal antibody, Abcam, UK) was used as a loading control. Membranes were washed and incubated with secondary antibodies (Invitrogen, Sweden) in PBS-Tween (0.1%) for 1 h on the following day. Thereafter, membranes were developed using SuperSignal™ West Pico PLUS Chemiluminescent Substrate (Thermo Scientific, Sweden) and Amersham™ Imagequant™ 800 (Thermo Fisher Scientific, Sweden). The experiments were repeated at least three times.

XTT Cell Proliferation Assay

A defined number of cells were seeded in flat-bottom 96-well plates (8×10^3 SNU1544 cells/well, 1×10^4 HT55 cells/well, and 6×10^3 LS174T cells/well) and incubated in an atmosphere containing 5% CO_2 at 37°C for 48 h. For treatment, the medium was switched with onalespib-containing media (onalespib concentration range of 5–1×10^4 nM) and incubated in an atmosphere containing 5% CO_2 at 37°C for an additional 72 h. Equal amount of DMSO in the highest concentration was used as a DMSO control. The XTT cocktail (XTT activation reagent, XTT reagent, and the corresponding media) was prepared according to manufacturer's instructions (ATCC protocol 30–1011 K, Manassas, VA, USA). Cells were incubated with XTT cocktail for 4 h in an atmosphere containing 5% CO_2 at 37°C.

The dual absorbance was then measured using a BioMark Microplate Reader (Bio-Rad Laboratories AB, Sweden). Significance was determined using one-way ANOVA followed by Tukey multiple comparison test.

Binding Specificity Assay

In this study, 2.5×10^4 cells were seeded in 48-well plates and incubated for 48 h at an atmosphere containing 5% CO_2 at 37°C. After 24 h for HT55 cells, LS174T cells, and HT29 cells and 48 h for MKN45 and SNU1544 cells, 1 nM of ^{177}Lu-DOTA-M5A with 100-fold blocking solution of unlabeled antibody (DOTA-M5A, 100 nM) was added to ≥3 wells each. After 24 h, the radioactive medium was removed, cells were washed 2–3 times with the basal corresponding media, and cells were trypsinized and counted using a cell counter (TC20™ Automated Cell Counter, BioRad, Sweden). Cell-associated radioactivity was counted in a gamma counter (1480 Wizard 3′, Wallace, Finland). Significance was determined using Student's t-test.

Real-Time Binding Measurement *via* Ligand Tracer

For binding measurements, 0.7×10^6 MKN45 cells, 0.6×10^6 SNU1544 cells, or 0.5×10^6 LS174T cells were seeded in non-treated Petri dishes (Cat. No. 263991, Thermo Fisher Scientific) coated with polydopamine according to Ridgeview Instruments AB instructions. Polydopamine was used to enhance attachment of semi-adherent cells for real-time binding measurement experiments. In brief, dopamine hydrochloride (Sigma, Germany) dissolved in 10 mM Tris buffer (pH 8) to a final concentration of 2 mg/ml was added as droplets (500 µl) near the edge of dishes. The dishes were incubated for 3 h at room temperature before the remnant solution was removed, and dishes were rinsed with MQ water twice. The coated dishes were stored at 4°C until used. The abovementioned number of cells was suspended in 0.5 ml of the corresponding basal media and seeded on polydopamine followed by 1 h incubation at room temperature. Then, the basal medium was removed, and 10 ml of the corresponding complete medium was added to the dish. For HT55, 1.5×10^6 cells were seeded on tilted cell culture-treated Nunc dishes (Cat. No. 150350, Thermo Fisher Scientific). All cells were incubated in an atmosphere containing 5% CO_2 at 37°C. After 48 h incubation for MKN45 and SNU1544 cells and 24 h incubation for HT55 and LS174T cells, the real-time binding measurement was performed as previously described (53). In brief, the cell medium was switched to 3 ml of fresh medium prior to the start of the binding measurement. The binding of ^{177}Lu-DOTA-M5A to cells was measured with LigandTracer Yellow (Ridgeview Instruments AB, Uppsala, Sweden) at room temperature. A baseline signal was collected for around 15 min before stepwise adding ^{177}Lu-DOTA-M5A to final concentrations of 3 and 9 nM. Dissociation was initiated when the binding curve got sufficient curvature at least in one concentration by replacing the media with 3 ml fresh media. Polydopamine or plastic surface of an area with no cells on the same dish was used as the reference background area to investigate off-target binding of radiolabeled antibody. The reference background signal was automatically subtracted from the decay-corrected target area signal that resulted in a specific real-time binding curve of ^{177}Lu-DOTA-M5A to the target cells. Kinetic interaction evaluation was performed with TraceDrawer 1.9.2 (Ridgeview Instruments AB, Uppsala, Sweden).

Three-Dimensional Spheroid Models

The 96-well flat bottom plate (Sarstedt, Germany) was coated with 50 µl of 0.15% agarose (Sigma Aldrich, MO, USA) as previously described (54). Cells that form a 3D structure were then seeded (3,000 cells/well for HT55 and LS174T and 2,000 cells/well for SNU1544). MKN45 did not form a 3D structure and was therefore excluded for 3D model experiments. When the 3D structure (spheroids) reached 0.4 mm in diameter (3–4 days), they were treated with ^{177}Lu-DOTA-M5A (5–80 kBq) and/or onalespib (25–1,000 nM). Onalespib concentrations and ^{177}Lu-DOTA-M5A activities for the combination therapies were chosen based on the effect of monotreatments where either tumor growth or viability decreased significantly. DMSO, sodium/ammonium acetate buffer, ^{177}Lu-DOTA, and unlabeled DOTA-M5A were chosen as control groups. After treatment, the spheroid growth was assessed using Canon EOS 700D photographing (Canon Inc., Japan) mounted on a Nikon Diaphot-TMD microscope (Nikon, Japan) every 3 days. Media were added once on the third day after treatment and exchanged once on the seventh day after treatment. Spheroids were followed individually for 12 days. The cross-section area and spheroid sizes were measured and analyzed using ImageJ 1.52p software (NIH, Bethesda, MD, USA) and normalized to the size at the start of treatment (size ratio). Significance was determined using one-way ANOVA followed by Tukey multiple comparison test.

Viability of Three-Dimensional Spheroid Models

To assess the viability of the 3D models metabolically, the High-sensitivity (HS) alamarBlue® assay (Invitrogen, MA, USA) was used (55) to evaluate the treatment effects. The viabilities of the HT55 and SNU1544 spheroid models were evaluated at three time points (Day 0; treatment start, Day 6; at the half-time of the treatment period and Day 12 at the assay endpoint). Due to the fact that the LS174T spheroid model behaved differently from the other models, the viability was assessed at five time points (Day 0, Day 3, Day 6, Day 9, and Day 12). In each well of the 96-well plate, 100 µl of medium was kept and 100 µl of 20% alamarBlue-containing media (v/v) were added in order to reach the final concentration of 10% (v/v). Plates were protected from light and incubated in an atmosphere containing 5% CO_2 at 37°C (55). After 24 h of incubation, dual fluorescence absorbance was read using an ELISA reader (210 Infinite series, TECAN, Switzerland) at gain 90 constantly during the experiment. Significance was determined using one-way ANOVA followed by Tukey multiple comparison test.

Spheroid Lysates and Western Blot Analyses

To assess the molecular mechanisms of onalespib and/or ^{177}Lu-DOTA-M5A treatments and the combinations thereof, defined numbers of SNU1544 (1.5×10^5/well) and LS174T cells (3.6×10^5/

well) were seeded on AggreWell™ 800 plates (Stemcell Technologies, Canada) according to the manufacturer's instruction. Briefly, each well was covered with 500 µl of anti-adherent solution and centrifuged at 1,300×g for 5 min. Thereafter, each well was washed with 2 ml of basal media followed by adding 1 ml of complete media. Cells were harvested by trypsin, and a single-cell suspension was prepared. Cells were counted, and the aforementioned number of cells was then seeded with complete media to a total volume of 2 ml/well. The plate was immediately centrifuged at 100×g for 3 min to capture cells in the microwells. The plate was observed under microscope to verify that cells were distributed evenly among microwells. The plates were then incubated in an atmosphere containing 5% CO_2 at 37°C for 4–5 days (pretreatment incubation). For treatment, 1 ml of media in each well were switched with media containing onalespib or ^{177}Lu-DOTA-M5A and the combinations thereof. Spheroids were collected 24 h posttreatment, and lysates were prepared with Radioimmunoprecipitation Assay Buffer (RIPA) lysis buffer (Thermo Fisher Scientific, Sweden) supplemented with Halt™ Protease and Phosphatase inhibitor cocktail (Thermo Fisher Scientific, Sweden) followed by vortex/spin down cycles (30 s of vortexing followed by 30 s of spinning down, 30 s rest on ice) for 10–20 min. The lysates were centrifuged at 15,000 rpm for 15 min at 4°C, and supernatants were collected and stored at -20°C. Protein quantification of lysates was assessed by Pierce BCA Protein Assay Kit (Thermo Scientific, Sweden). The samples were separated on Sodium Dodecyl-Sulfate Polyacrylamide Gel Electrophoresis (SDS-PAGE), transferred to PVDF membrane, and blocked as described earlier. The membranes were incubated with primary antibodies targeting CEA (CD66e, 14-0669-82 Mouse monoclonal antibody, eBioscience, Invitrogen, Sweden), EGFR (ab52894, Rabbit monoclonal antibody, Abcam, UK), HSP90 (ab13492, Mouse monoclonal antibody, Abcam, UK), HSP70 (ADI-SPA-812, Rabbit polyclonal antibody, Enzo Life Science, USA), ERK1+ERK2 (ab115799, Rabbit polyclonal antibody, Abcam, UK), SMAD3 (51-1500, Rabbit polyclonal antibody, Invitrogen, Sweden), and Cleaved Poly [ADP-Ribose] Polymerase 1 (PARP1) (ab32064, Rabbit monoclonal antibody, Abcam, UK). GAPDH (ab8245, Mouse monoclonal antibody, Abcam, UK) was used as a loading control. The membranes were incubated with the secondary antibodies and developed as described previously.

Synergy Calculations and Statistical Analysis

Synergy calculations and analyses were done using SynergyFinder 2.0 (56) on spheroid size ratios (12 days after treatment) and the spheroid viabilities at the experiment end point (12 days posttreatment) for the SNU1544 and HT55 spheroid models and at day 6 posttreatment for the LS174T spheroid model. Highest single agent (HSA) (57), Bliss (58), and Zero interaction potency (ZIP) (59) models were used in the current study for synergy calculation. These models are slightly different; Bliss and ZIP models are mostly used in drug combination effects and HSA is used for the maximal single-drug effect. Bliss model is suitable when two drugs act independently and ZIP suits when it is not expected that one drug potentiates the other one (60). All experiments included in this study were performed in a minimum of two independent replicates, and data are presented as pooled data from all replicates or from one representative experiment. Statistical data analysis for other experiments was performed using GraphPad Prism Version 9.1.0 (GraphPad Software Inc., La Jolla, CA, USA). Data are presented as the means ± standard deviation (SD) if not otherwise stated.

RESULTS

^{177}Lu-Radiolabeling Characterization and Stability Assays

The optimal ^{177}Lu-labeling condition was determined for DOTA-M5A labeling (**Supplementary Figures S3, S4**). Both 1 and 2 h of incubation for labeling of DOTA-M5A (50 µg) with 15 MBq of ^{177}Lu at 42°C resulted in more than 97% of radiolabeling yield (**Supplementary Figure S4**). The stability of ^{177}Lu-DOTA-M5A was above 90% in all tested conditions (**Figure 1A**), indicating high stability and intact radioconjugation of ^{177}Lu-DOTA-M5A under physiological conditions.

^{177}Lu-DOTA-M5A Binds Specifically to Carcinoembryonic Antigen on Gastrointestinal Cancer Cell Lines

A binding specificity assay was first performed on a panel of GI cancer cell lines in order to assess the ^{177}Lu-DOTA-M5A binding specificity and to validate the individual CEA levels. All cell lines demonstrated detectable binding of ^{177}Lu-DOTA-M5A, blockable with unlabeled DOTA-M5A. This confirmed the antigen-specific binding of the conjugate and further supported that the radiolabeling did not interfere with antigen binding. Binding levels of unblocked ^{177}Lu-DOTA-M5A were in line with literature data (61), with the MKN45 and SNU1544 cell lines demonstrating the highest signal, followed by HT55 and LS174T cells, and HT29 cells demonstrating the lowest signals (**Figure 1B**).

Real-Time Binding Measurement

Real-time binding measurements of ^{177}Lu-DOTA-M5A were performed on the cell line panel in order to assess the antibody–antigen interactions in terms of on-rate, off-rate, affinity, and type of interaction (**Figure 1C** and **Supplementary Figure S5**).

Measurements of ^{177}Lu-DOTA-M5A on CEA-positive cells demonstrated high affinity binding and very slow dissociation (off-rate). Binding of ^{177}Lu-DOTA-M5A to cell lines MKN45, SNU1544, HT55, and LS174T was well described by a one-to-one or Langmuir binding model. A representative example of ^{177}Lu-DOTA-M5A interaction with CEA on MKN45 cells is shown in **Figure 1C**. Binding and interaction curves for SNU1544, HT55, and LS174T cell lines are shown in **Supplementary Figure S5**. The measured affinity of ^{177}Lu-DOTA-M5A was quite similar in all cell lines, ranging between 11 and 94 pM (**Table 1**). This further validated the antigen-specific binding of ^{177}Lu-DOTA-M5A demonstrated in the specificity assay (**Figure 1B**). The slow

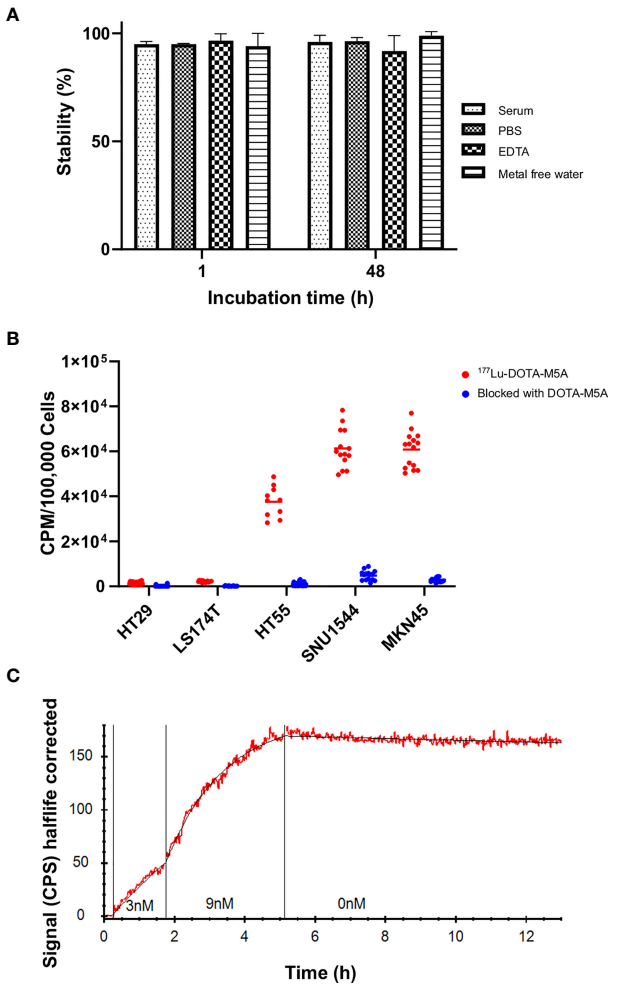

FIGURE 1 | The ^{177}Lu-DOTA-M5A stability, binding specificity assessment, and real-time binding measurement of ^{177}Lu-DOTA-M5A to the target antigen on a panel of gastrointestinal cancer cell lines. **(A)** Stability assessment of ^{177}Lu-DOTA-M5A at different conditions (PBS, mixture of mouse serum and PBS, EDTA condition, and metal-free water) 1 and 48 h after labeling. Graph displays stable ^{177}Lu-DOTA-M5A (%) on the y axis and incubation time on the x axis. **(B)** Binding specificity of ^{177}Lu-DOTA-M5A to the target antigen CEA on HT29, LS174T, HT55, SNU1544 (colorectal cancer cell lines) and MKN45 cell line (gastric cancer cell line). Graph displays signal [counts per minute (CPM)] per 100,000 cells on the y axis and tested cell lines on the x axis. **(C)** Representative binding curve of ^{177}Lu-DOTA-M5A binding to MKN45 cells (CEA-positive gastric cancer cell line, red) as measured with LigandTracer Yellow. Black curve resulting from kinetic evaluation with a one-to-one binding model. Graph displays signal [counts per second (CPS)] half-life corrected on the y axis and time on the x axis. Binding curves for LS174T, HT55, and SNU1544 (CEA-positive colorectal cancer cell lines) are shown in **Supplementary Figure S5**. PBS, Phosphate-buffered saline; EDTA, Ethylenediamine tetraacetic acid.

off-rate detected on CEA-positive cell lines indicated a stable interaction between ^{177}Lu-DOTA-M5A and the cellular target. To assess the variation in kinetic parameters, for a typical cell line, the relative standard deviation for k_a was below 5%, while the k_d was less well-defined and could vary up to 40%.

TABLE 1 | Binding characterization of ^{177}Lu-DOTA-M5A interaction with CEA on MKN45, SNU1544, HT55, and LS174T cells as estimated from LigandTracer experiments by kinetic evaluation.

Cell line	k_a (× 10^4 M^{-1} s^{-1})	k_d (× 10^{-6} s^{-1})	K_D (pM)
MKN45	1.9	1.4	74
SNU1544	0.9	0.9	94
HT55	1.5	0.9	63
LS174T	3.2	0.4	11

Summary of the association rate constant (k_a), the dissociation rate constant (k_d), and the equilibrium dissociation constant or affinity (K_D), N = 2. Kinetic evaluation was performed with a two-step approach. First the k_d of the two replicates was estimated globally with the DissociationRate model. The acquired k_d was then used as a constant in a global one-to-one binding model to assess k_a and the affinity K_D.
pM, pico molar.

Dose-Dependent and Antigen-Specific Therapeutic Effect of ^{177}Lu-DOTA-M5A in Three-Dimensional Colorectal Spheroid Models

The effects of ^{177}Lu-DOTA-M5A as a monotherapy was then assessed in three 3D colorectal spheroid models, assessing both spheroid size over time and cellular viability (**Figure 2** and **Table 2**). In general, both spheroid size and viability measurements demonstrated antigen-specific and dose-dependent therapeutic effects of ^{177}Lu-DOTA-M5A (**Figure 2** and **Table 2**).

In the high CEA-expressing model SNU1544, treatment with, e.g., 10 and 40 kBq ^{177}Lu-DOTA-M5A reduced spheroid cell viability to 54% ± 13% and 21% ± 1%, respectively, compared to untreated controls (100%) at the assay endpoint (day 12), with the corresponding spheroid size ratios of 3.6 ± 0.5 and 2.3 ± 0.6 compared to 9.5 ± 1.3 for the untreated controls at the same time point (**Figures 2A–C** and **Table 2**). Likewise, in the high CEA-expressing HT55 model, the clear dose-dependent effects of ^{177}Lu-DOTA-M5A reflected on both spheroid size and viability (**Figures 2D–F** and **Table 2**). At day 12, 10 and 20 kBq ^{177}Lu-DOTA-M5A reduced spheroid cell viability to 72% ± 5% and 27% ± 10%, respectively, compared to untreated controls (100%) at the assay endpoint (day 12), and the corresponding spheroid size ratios were 1.6 ± 0.4 and 1 ± 0.2 compared to 5.2 ± 0.5 for the untreated control. In the low CEA-expressing model LS174T, no significant reducing effects of ^{177}Lu-DOTA-M5A treatment were observed in spheroid size evaluation. At treatment with lower activities of ^{177}Lu-DOTA-M5A, a trend of reduced spheroid density could be noted at the experimental endpoint, reflected in increased spheroid diameter but not increased viability. Viability assessments demonstrated minor changes over time in the treatment groups, with some marked changes for 10 and 80 kBq ^{177}Lu-DOTA-M5A at the end point (**Figures 2G–I** and **Table 2**). None of the control groups (sodium acetate, ^{177}Lu-DOTA, and unlabeled DOTA-M5A) significantly impacted the spheroid size and viability (**Supplementary Figure S6**).

Effects of Onalespib Monotherapy in Colorectal Cancer Models

In order to assess the possibility to potentiate the effect of ^{177}Lu-DOTA-M5A with the HSP90 inhibitor onalespib, the effect of

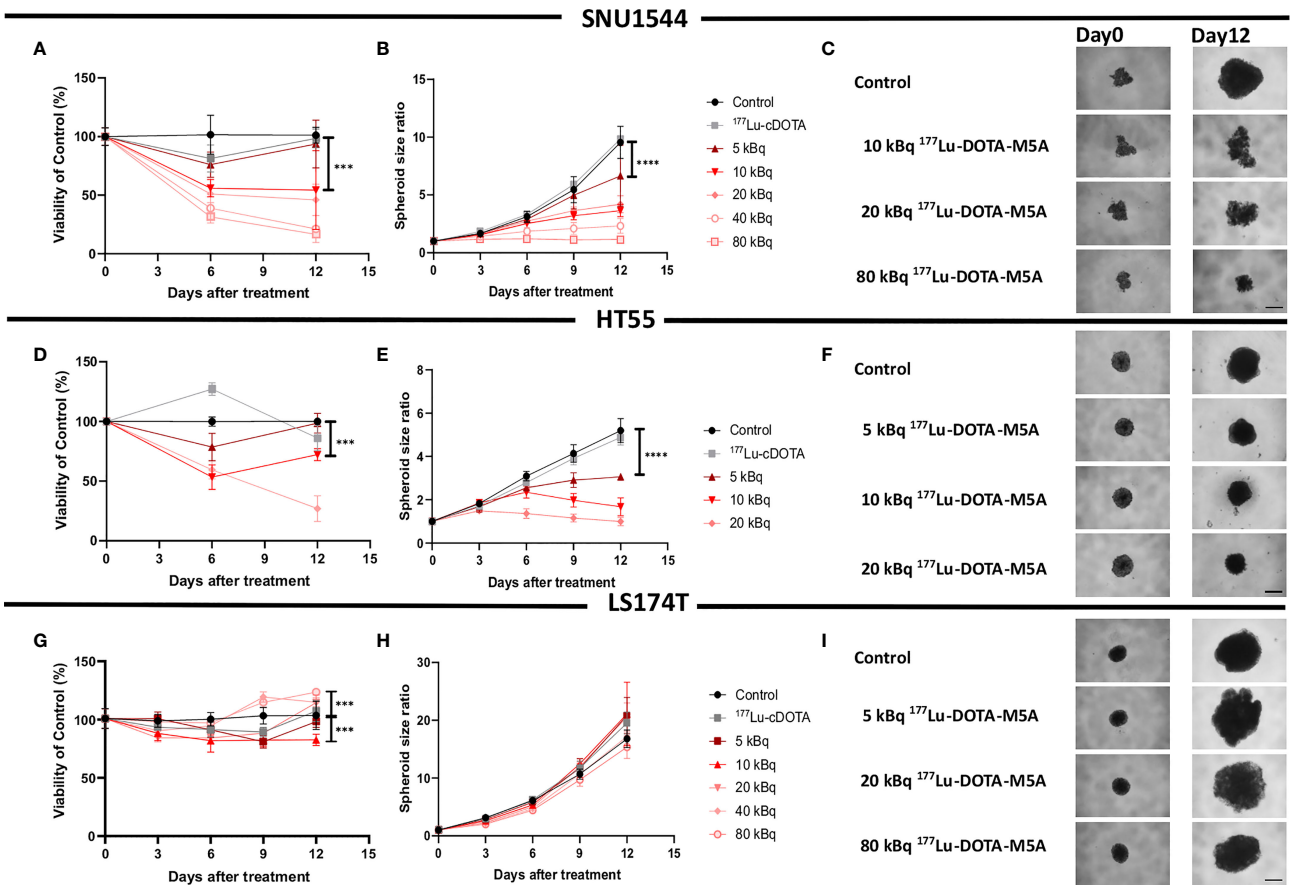

FIGURE 2 | Monotherapy with ^{177}Lu-DOTA-M5A in 3D spheroid models. Viability **(A)** and spheroid growth assessment **(B, C)** of the SNU1544 spheroid model treated with ^{177}Lu-DOTA-M5A. Viability **(D)** and spheroid growth **(E, F)** assessment of the HT55 spheroid model treated with ^{177}Lu-DOTA-M5A. Viability **(G)** and spheroid growth **(H, I)** assessment of the LS174T spheroid model treated with ^{177}Lu-DOTA-M5A. The treatment activities are indicated in graphs and images. Graphs display either spheroid size ratio or viability (% of control) on the y axis and time after treatment on the x axis (mean ± standard deviation, n ≥ 4). *P ≤ 0.05, ***P ≤ 0.001, and ****P ≤ 0.0001. For treatments, the lowest concentration that caused a significant decrease in spheroid size/viability compared to untreated control was shown. Representative images of spheroids at first time point and at the endpoint are shown in panels **(C, F, I)**; scale bar: 400 µm.

onalespib monotherapy on CEA expression levels was first evaluated. Western blot analysis displayed that CEA expression was not affected by onalespib treatment in any of the assessed colorectal cancer cell lines, while known HSP90-related markers, such as EGFR and AKT1,2,3, displayed alterations. Moreover, the assessed 3D spheroid lysates of SNU1544 and LS174T displayed higher CEA expression compared to their 2D lysates (**Supplementary Figure S7**).

Furthermore, to evaluate the half-maximal inhibitory concentration (IC50), the growth-inhibitory effect of onalespib was assessed by XTT cell proliferation assays on three different colorectal cancer cell lines. All cell lines responded to onalespib monotherapy, albeit with different sensitivities (**Figure 3**). HT55 cells were the most sensitive cells with IC50 = 67 nM (95% CI, 50–88 nM). SNU1544 cells were less sensitive with IC50 = 197 nM (95% CI, 148–260 nM), and LS174T was the least sensitive cell line with IC50 = 362 nM (95% CI, 262–498 nM).

Inhibitory growth effects of onalespib as a single drug were then assessed in 3D spheroid models by both spheroid size and viability measurements, demonstrating that all three assessed cell lines were sensitive to onalespib also in a 3D setting. Onalespib concentrations above 250 nM caused marked reduction of SNU1544 spheroid size and viability (**Figures 4A–C** and **Table 2**). Treatment with 250 and 450 nM of onalespib resulted in viability reduction to 68% ± 7% and 39% ± 7% of untreated controls (100%), respectively, at the assay endpoint, and the corresponding spheroid size ratios were 4.6 ± 0.5 and 2.6 ± 0.2 compared to 9.5 ± 1.3 for the untreated controls. The HT55 spheroid model demonstrated a higher sensitivity to onalespib compared to the SNU1544 model, with concentrations above 50 nM leading to significantly smaller spheroids and demonstrating markedly reduced viability at 25 nM at the assay endpoint (**Figures 4D–F** and **Table 2**). The LS174T spheroid model demonstrated the lowest sensitivity to onalespib, with at least 600 nM required to achieve significant

TABLE 2 | The spheroid size ratio and viability [mean ± standard deviation (SD)] of the SNU1544, HT55, and LS174T 3D spheroid models treated with monotreatment of either ^{177}Lu-DOTA-M5A or onalespib at day 12 posttreatment (n ≥ 4).

Spheroid model	Treatment		Viability (% of control) ± SD	Spheroid size ratio ± SD
SNU1544 (high CEA expression)	Untreated control	0	100	9.5 ± 1.3
	^{177}Lu-DOTA-M5A (kBq)	10	54 ± 13	3.6 ± 0.5
		20	46 ± 6	4.1 ± 0.7
		40	21 ± 1	2.3 ± 0.6
	Onalespib (nM)	250	68 ± 15	6.8 ± 1.1
		350	66 ± 27	4.6 ± 0.5
		450	39 ± 17	2.6 ± 0.2
HT55 (high CEA expression)	Untreated control	0	100	5.2 ± 0.5
	^{177}Lu-DOTA-M5A (kBq)	5	94 ± 20	3 ± 0.1
		10	54 ± 30	1.6 ± 0.4
		20	27 ± 10	1 ± 0.2
	Onalespib (nM)	25	75 ± 11	5 ± 0.6
		50	69 ± 5	3.5 ± 0.3
		75	33 ± 6	2.5 ± 0.3
LS174T (low CEA expression)	Untreated control	0	100	16.8 ± 1.5
	^{177}Lu-DOTA-M5A (kBq)	10	82 ± 5	21 ± 5.5
		40	114 ± 3	17.2 ± 0.4
		80	123 ± 2	15.3 ± 2
	Onalespib (nM)	600	90 ± 3	12.4 ± 1
		800	82 ± 4	4.4 ± 0.4
		1,000	55 ± 2	1.6 ± 0.1

SD, standard deviation.

therapeutic effects (**Figures 4G–I** and **Table 2**). Moreover, at 200–400 nM, a trend of increased spheroid diameter could be noticed at the experimental endpoint, likely reflecting reduced spheroid density.

The dose-dependent effects of onalespib on the SNU1544 spheroid model were clearly observed at early time points and persisted until the end of the experiment. The HT55 spheroid model demonstrated therapeutic effects mainly at later time points. In the LS174T spheroid model, the therapeutic effects were apparent at day 6 posttreatment, but only the highest concentration of onalespib was able to cause a lasting viability reduction and unchanged spheroid size until the end of experiments. DMSO did not demonstrate any marked effect in any of the experiments (**Supplementary Figure S6**).

Thus, both 2D and 3D experiments demonstrated that all three cell lines were sensitive to onalespib treatment, and the 3D spheroid model results were in line with 2D data regarding sensitivity levels, identifying HT55 as the most sensitive cell line and LS174T as the least sensitive to onalespib treatment.

Combination Therapy of ^{177}Lu-DOTA-M5A and Onalespib Potentiates Therapeutic Effects in Three-Dimensional Colorectal Cancer Spheroids

While both ^{177}Lu-DOTA-M5A and onalespib demonstrated therapeutic effects as monotherapies, the combination therapies demonstrated the strongest therapeutic effects for numerous combinations. Two selected combinations for each spheroid model are shown in **Figure 5** (the rest are shown in **Supplementary Figures S8–S10**). All assessed combinations are summarized in **Table 3** and accounted for the synergy calculations illustrated in **Figure 6**. In the high CEA-expressing models SNU1544 and HT55, both viability and spheroid growth in the combination treatments were reduced to lower levels than the monotreatments, with clear combination benefits visible already at study midway for the selected combinations (**Figures 5A–J**).

In the LS174T spheroid model, the least sensitive to onalespib therapy and with the lowest CEA expression, the combination treatments clearly inhibited spheroid growth more efficiently compared to monotreatments already at day 6 posttreatment, lasting until the end of the experiments. The viability also decreased until day 6 posttreatment; however, the cells recovered at later time points (**Figures 5K–O**).

Consequently, the growth inhibition results demonstrated that the combination treatments could mediate stronger therapeutic effects compared to monotreatments in all three spheroid models, also supported by the viability assays. Negative control groups did not display any significant alteration in spheroid size and viability (**Supplementary Figure S6**).

Synergistic effects were assessed with ZIP, Bliss, and HSA synergy models and were in line with spheroid growth and viability results (**Figure 6**). Synergistic evaluation on SNU1544 spheroid size ratios demonstrated that both the lowest (5 kBq) and the highest (20 kBq) assessed amounts of ^{177}Lu-DOTA-M5A combined with onalespib resulted in synergistic effects (**Figures 6A–C**). Synergy calculations of SNU1544 viability illustrated that at least seven out of nine assessed combinations displayed synergistic effects (**Figures 6D–F**). In the HT55 spheroid model, the combinations of all ^{177}Lu-DOTA-M5A activities with 25 and 50 nM of onalespib resulted in synergistic effects when spheroid size ratios were assessed (**Figures 6G–I**), and three of these also demonstrated synergistic effects in viability reduction (**Figures 6J–L**). In the LS174T spheroid model, synergistic effects were demonstrated in

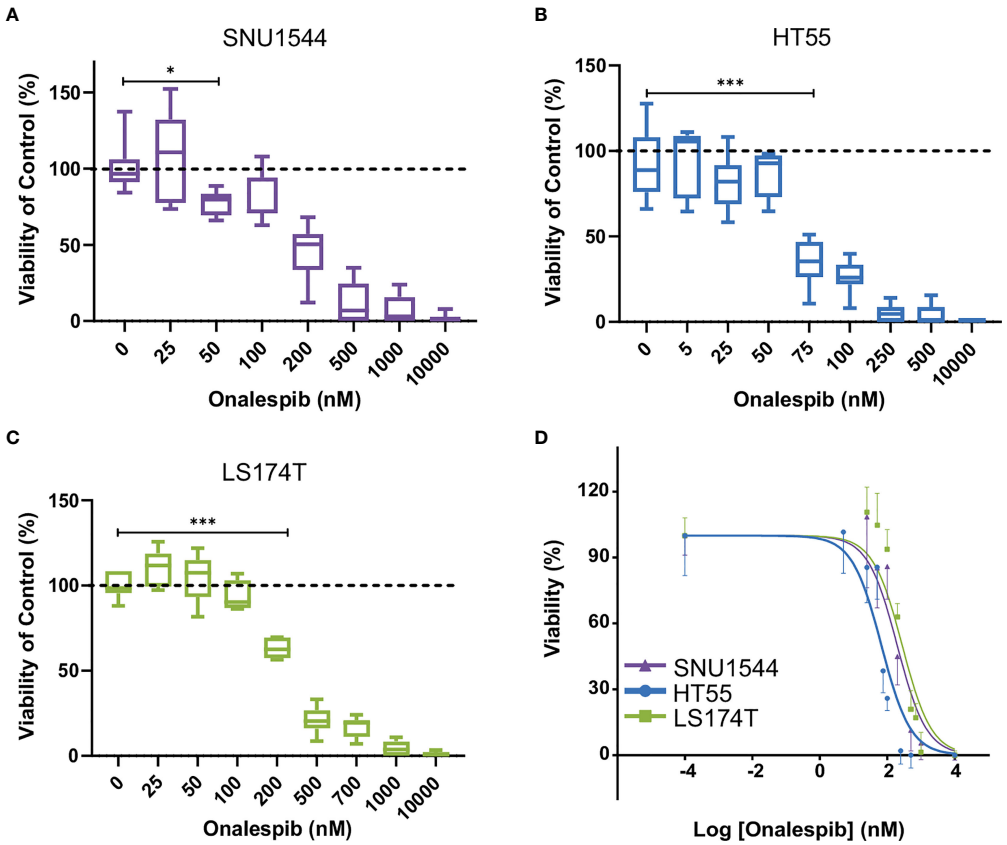

FIGURE 3 | Characterization of colorectal cancer cell lines. Effect of onalespib treatments on viability of SNU1544 cells **(A)**, HT55 cells **(B)**, and LS174T cells **(C)**. Graphs display viability (% of control) on the y axis and onalespib concentration (nM) on the x axis. For treatments, the lowest concentration that caused a significant decrease of viability compared to the untreated control was shown. *P ≤ 0.05 and ***P ≤ 0.001. **(D)** XTT proliferation assay of 2D cultures. Graph displays viability (%) on the y axis [mean and 95% confidence interval (CI), n ≥ 4] and logarithmic concentrations of onalespib on the x axis. CI, confidence interval.

all nine combinations at day 6 posttreatment assessing spheroid size ratios (**Figures 6M–O**) and for viability in seven of the combinations (**Figures 6P–R**).

Overall, the synergistic evaluations indicated that for high CEA-expressing tumor models, such as the SNU1544 and HT55, combining 177Lu-DOTA-M5A and onalespib eventually lead to synergistic therapeutic effects in some combinations regarding both spheroid size ratio and viability at the end of the experiments. In the fast-growing tumor model LS174T, synergistic effects were mainly demonstrated at earlier time points regarding both spheroid size ratio and viability. The synergy scores are summarized in **Table 4**.

Combination Therapy of ^{177}Lu-DOTA-M5A and Onalespib Downregulates HSP90 Client Proteins and Potential Carcinoembryonic Antigen-Involved Pathways

HSP90 client proteins and downstream signaling markers, a related co-chaperone, as well as potentially relevant markers to CEA, and an apoptosis marker, were assessed in the present study on lysates of 3D spheroids (SNU1544 and LS174T) 24 h after treatment with ^{177}Lu-DOTA-M5A or onalespib and the combination thereof (**Figure 7**). No marked differences of CEA or HSP90 expression levels were observed in the treatment groups compared to the control group regardless of cell line. While EGFR was downregulated in the onalespib monotreatment group in a dose-dependent manner in both cell lines, effects were even stronger in the combination group for the SNU1544 cell line. Assessing HSP70, a related co-chaperone to HSP90 revealed that ^{177}Lu-DOTA-M5A treatment did not influence HSP70 expression compared to the control; however, both onalespib and the combination treatments induced HSP70 upregulation in both assessed cell lines. Moreover, since other studies previously demonstrated that CEA interacts with the TGF-β receptor and induces proliferation in colorectal cancer cells (16, 62), SMAD family member 3 (SMAD3) expression was evaluated as a downstream marker of the TGF-β receptor. For both cell lines, SMAD3 was upregulated in all treatment groups compared to the control. To investigate whether the ^{177}Lu-DOTA-M5A and/or onalespib treatment induced apoptosis, cleaved PARP1 expression was examined. In line with the viability assessment, marked cleaved PARP1 upregulation in the combination treatments compared to monotreatments and control was displayed in the LS174T spheroid model. The

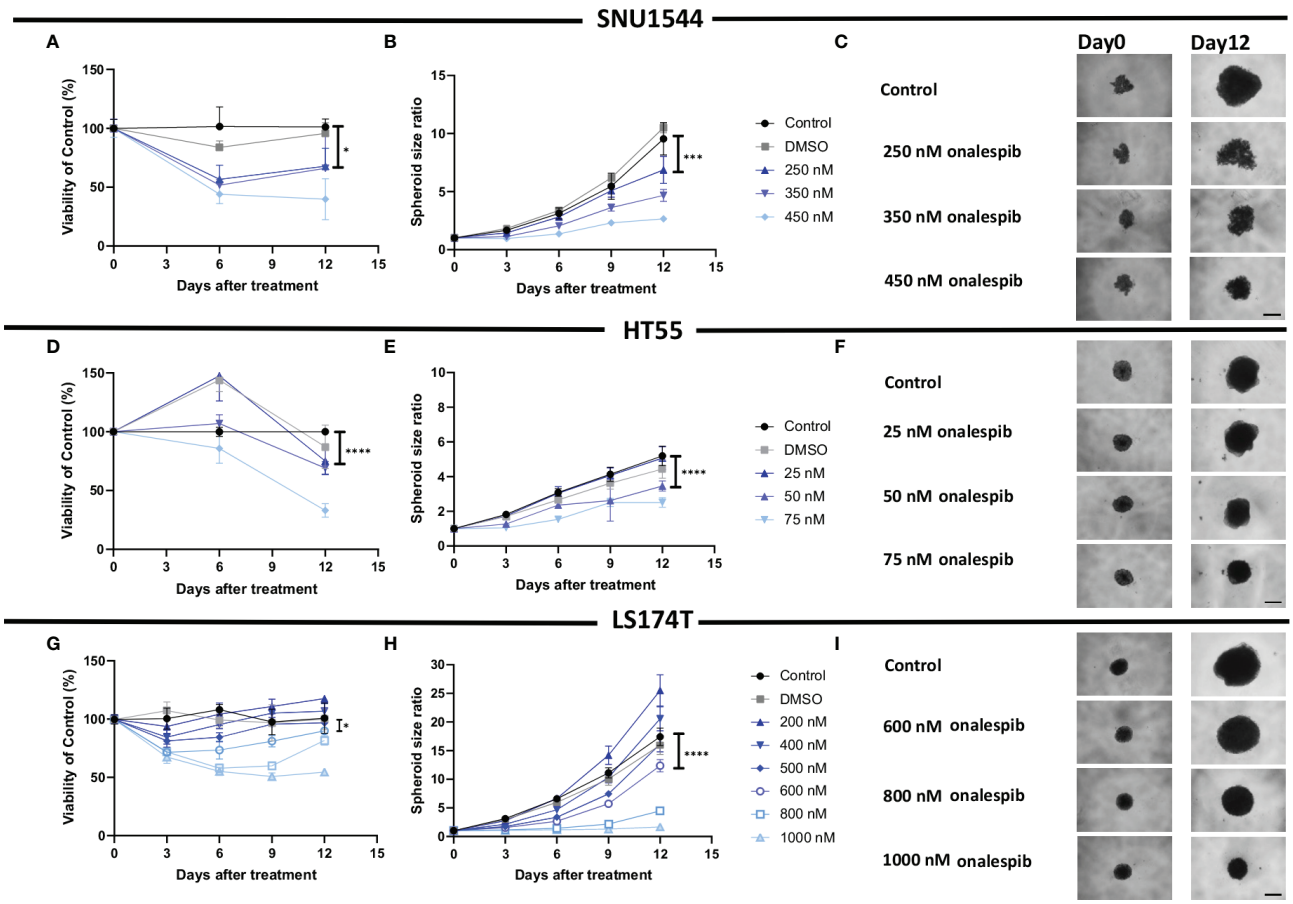

FIGURE 4 | Monotherapy with onalespib in 3D spheroid models. Viability **(A)** and spheroid growth assessment **(B)** of the SNU1544 spheroid model treated with onalespib. Viability **(D)** and spheroid growth **(E)** assessment of the HT55 spheroid model treated with onalespib. Viability **(G)** and spheroid growth **(H)** assessment of the LS174T spheroid model treated with onalespib. The treatment concentrations are indicated in the graphs and images. Graphs display either spheroid size ratio or viability (% of control) on the y axis and time after treatment on the x axis (mean ± standard deviation, n ≥ 4). For treatments, the lowest concentration that caused a significant decrease in spheroid size/viability compared to the untreated control was shown. *P ≤ 0.05, ***P ≤ 0.001, and ****P ≤ 0.0001. Representative images of spheroids at first time point and at the endpoint are shown in panels **(C, F, I)**; scale bar: 400 µm.

SNU1544 spheroid model displayed cleaved PARP1 upregulation in all treatment groups.

DISCUSSION

RIT is a promising approach for cancer therapy. For colorectal cancer, CEA has been demonstrated to be a suitable cancer-associated target for this application (7, 11). CEA targeting using hT84.66 M5A mAb has previously been assessed for RIT potential using ^{90}Y as a therapeutic radionuclide, with promising results in a Phase I clinical study (11). However, labeling with ^{177}Lu, a well-established and suitable radionuclide for cancer therapy, has not previously been assessed for RIT with an anti-CEA human mAb as a potential candidate for colorectal cancer therapy.

Although promising, there are however also potential limitations of RIT using full-sized antibodies, including restricted tumor penetration and dose-limiting bone marrow exposure (63). These limitations have encouraged exploration of combination therapies to potentiate therapeutic effects, including combining CEA-targeted therapy with chemotherapy drugs or immunocytokines with promising results (6, 8, 12, 29, 64). HSP90 inhibitors have previously demonstrated preclinical and clinical potential both as a single drug and in combination with external radiation and/or chemotherapy for GI tumors (65–69). The HSP90 inhibitor onalespib was recently demonstrated to have radiosensitizing properties when combined with either external beam radiation (45) or molecular radiotherapy through ^{177}Lu-DOTATATE in tumor xenografts (70).

In the present study, the anti-CEA M5A mAb was successfully radiolabeled with ^{177}Lu for the first time and combined with the HSP90 inhibitor onalespib. Both 2D cell experiments and 3D multicellular spheroid models were then used to further characterize the binding of ^{177}Lu-DOTA-M5A to cells and to assess potential therapeutic effects for both monotherapies and combination approaches.

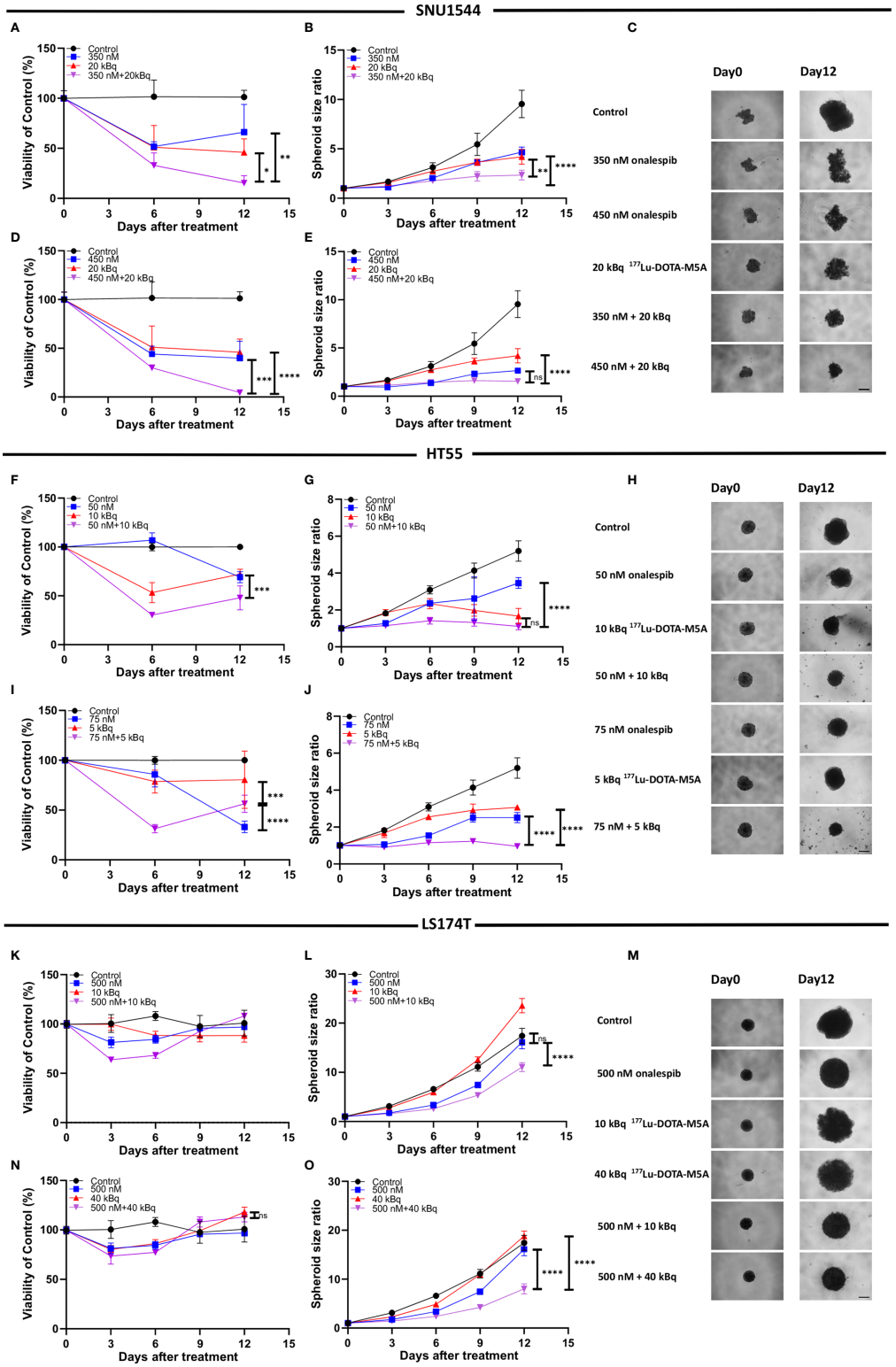

FIGURE 5 | Combination therapy with ^{177}Lu-DOTA-M5A and onalespib in 3D spheroid model SNU1544 **(A–E)**, HT55 **(F–J)**, and LS174T **(K–O)**. Treatments with ^{177}Lu-DOTA-M5A, onalespib, and combination treatments compared to the corresponding monotreatments. Graphs display either spheroid size ratio or viability (% of control) on the y axis (means ± standard deviation, n ≥ 4) and time after treatment on the x axis. ***P ≤ 0.001 and ****P ≤ 0.0001 and ns, not significant. Representative images of spheroids at first time point and endpoint are shown in panels **(C, H, M)**; scale bar: 400 µm. *P ≤ 0.05 and **P ≤ 0.01.

TABLE 3 | The spheroid size and viability [mean ± standard error of mean (SEM)] of the SNU1544 and HT55 spheroid models treated with the combination treatment of ^{177}Lu-DOTA-M5A and onalespib at day 12 posttreatment (n ≥ 4).

Spheroid model	Treatment		Viability (% of control) ± SEM	Spheroid size ratio ± SEM
			Day 12	Day 12
SNU1544 (high CEA expression)	^{177}Lu-DOTA-M5A (kBq) + Onalespib (nM)	250 + 5	44 ± 7	5.6 ± 0.7
		250 + 10	58 ± 10	5.4 ± 0.2
		250 + 20	42 ± 9	2.9 ± 0.3
		350 + 5	18 ± 3	3 ± 0.1
		350 + 10	17 ± 1	2.3 ± 0.2
		350 + 20	15 ± 3	2.3 ± 0.1
		450 + 5	11 ± 1	2.3 ± 0.2
		450 + 10	11 ± 1	2.3 ± 0.2
		450 + 20	5 ± 0.2	1.5 ± 0.1
HT55 (high CEA expression)	^{177}Lu-DOTA-M5A (kBq) + Onalespib (nM)	25 + 5	109	2.5 ± 0.1
		25 + 10	104 ± 3	1.4 ± 0.2
		25 + 20	48 ± 4	1
		50 + 5	95 ± 5	1.5 ± 0.1
		50 + 10	48 ± 5	1.1 ± 0.1
		50 + 20	37 ± 2	0.8
		75 + 5	56 ± 4	0.9 ± 0.1
		75 + 10	30 ± 3	1.1
		75 + 20	19 ± 1	1 ± 0.1
			Day 6 **Day 12**	**Day 6** **Day 12**
LS174T (low CEA expression)	^{177}Lu-DOTA-M5A (kBq) + Onalespib (nM)	400 + 10	78 ± 1 106 ± 2	3.6 ± 0.1 16.3 ± 0.3
		400 + 20	81 ± 2 125 ± 2	3.8 ± 0.1 16.4 ± 0.1
		400 + 40	84 ± 1 131 ± 2	3.3 13.1 ± 0.2
		500 + 10	68 ± 1 108 ± 1	2.6 ± 0.1 11.1 ± 0.4
		500 + 20	73 ± 2 121 ± 1	2.8 ± 0.1 11.6 ± 0.3
		500 + 40	77 ± 1 113 ± 2	2.4 8 ± 0.4
		600 + 10	68 ± 2 109 ± 2	2 ± 0.1 7.3 ± 0.2
		600 + 20	73 ± 2 110 ± 1	2 ± 0.1 6.8 ± 0.2
		600 + 40	72 ± 2 113 ± 2	2 6.6 ± 0.3

The spheroid size and viability [mean ± standard error of mean (SEM)] of the LS174T spheroid model treated with the combination treatment of ^{177}Lu-DOTA-M5A and onalespib at both days 6 and 12 posttreatment (n ≥ 4). Monotreatment and untreated control data are summarized in ***Table 2****.*
SEM, standard error of mean.

The radiolabeling of the DOTA-M5A antibody was first optimized and characterized for labeling yield, purity, and stability. Results demonstrated high yields and purity, and stability was retained for at least 48 h post-radiolabeling (**Figure 1A**). Real-time binding measurements on a panel of cell lines demonstrated picomolar binding affinity of the conjugate, with retained binding over 12 h (**Figure 1C** and **Supplementary Figure S5**). This indicated stable binding of ^{177}Lu-DOTA-M5A on all tested CEA-positive cell lines with a very slow off-rate. The one-to-one interaction model described the ^{177}Lu-DOTA-M5A and CEA interaction well. In specificity assays, the binding of ^{177}Lu-DOTA-M5A could be blocked by an excess of unlabeled DOTA-M5A on all CEA-positive cells, demonstrating specific binding of the conjugate (**Figure 1B**). The binding levels reflected the antigen density of the cells and were in line with previous data (61). These results demonstrate that DOTA-M5A can be successfully labeled with ^{177}Lu with retained antigen binding and also validated the CEA expression on assessed cell lines.

The potential therapeutic effects of ^{177}Lu-DOTA-M5A were then assessed in 3D spheroid models with varying CEA expressions. Results demonstrated CEA-specific and dose-dependent effects of the conjugate (**Figure 2**). Monotherapy with ^{177}Lu-DOTA-M5A reduced both spheroid size and viability in the high CEA-expressing SNU1544 and HT55 spheroid models, whereas the low CEA-expressing LS174T spheroid model did not display any significant spheroid size or viability reduction at the study endpoint. These results demonstrate that ^{177}Lu-DOTA-M5A mediates dose-dependent and CEA-specific therapeutic effects in CEA-positive colorectal cancer models and may potentially lead to a promising conjugate to pursue for RIT of CEA-positive colorectal cancer. Moreover, the results emphasize the need to potentiate RIT effects in order to reach also the tumors with a lower antigen expression.

The growth-inhibitory effects of the HSP90 inhibitor onalespib were then assessed on the CEA-positive colorectal cancer cell lines (SNU1544, HT55, and LS174T), as they were considered most relevant for subsequent combination studies. Effects of onalespib treatment were studied in both monolayer cultures with XTT proliferation assays, as well as in 3D spheroid models by longitudinal spheroid growth measurements and cell viability assays (**Figures 3**, **4**). Onalespib inhibited all assessed cell lines, albeit in varying degrees. In monolayer viability assays, the HT55 was the most sensitive cell line with IC50 of 66.9 nM (95% CI, 50–88 nM), and LS174T was the least sensitive one with IC50 of 361.7 nM (95% CI, 262–498 nM) (**Figure 3**). These results were further validated in 3D spheroid models, which demonstrated that onalespib mediated dose-dependent growth

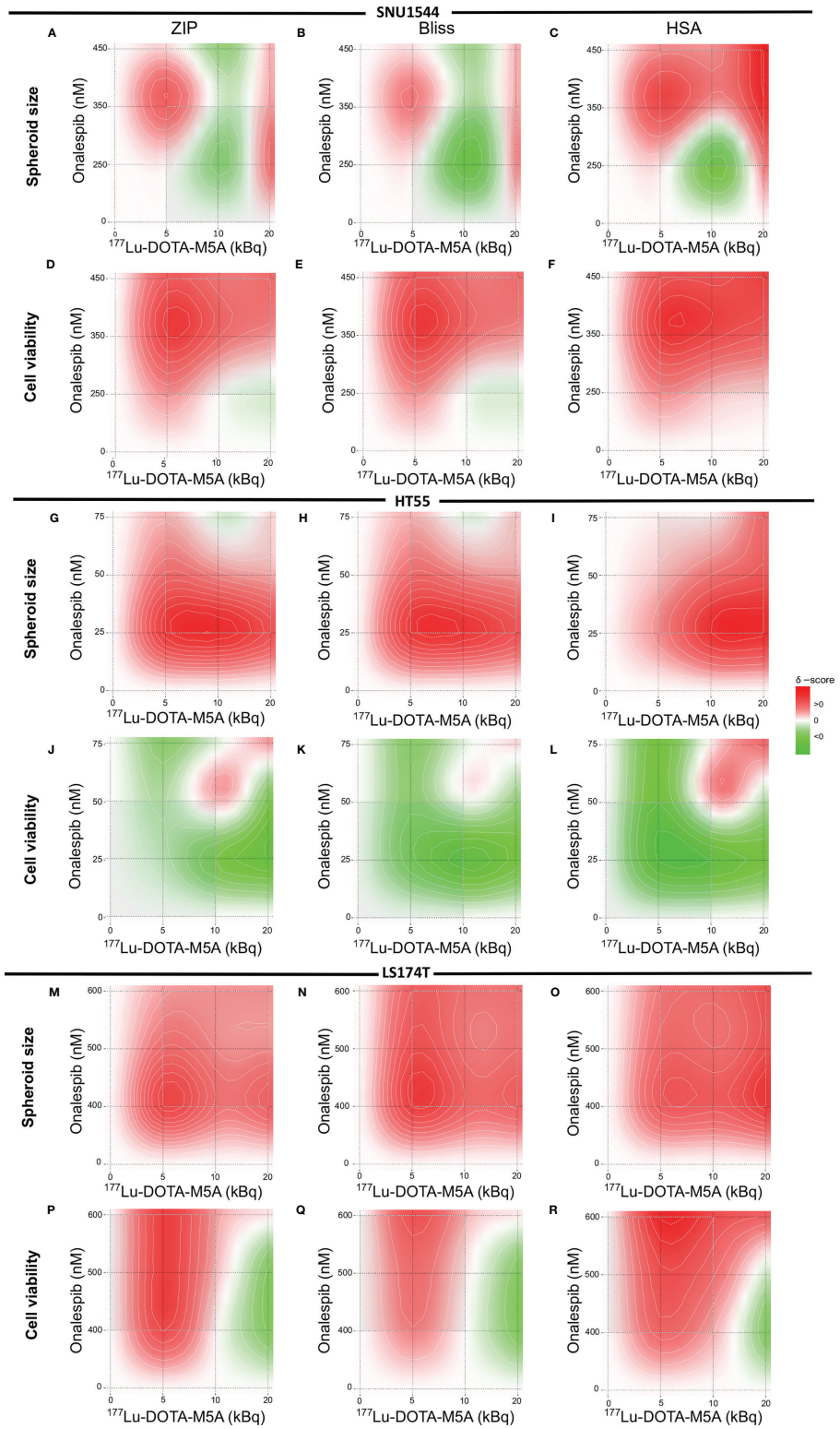

FIGURE 6 | Heat map of synergistic effects. The SNU1544 spheroid size ratio **(A–C)** and viability **(D–F)**, the HT55 spheroid size ratio **(G–I)** and viability **(J–L)** at day 12 posttreatment, and the LS174T spheroid size ratio **(M–O)** and viability **(P–R)** at day 6 posttreatment. Graphs display onalespib concentration (nM) on the y axis and activity of ^{177}Lu-DOTA-M5A (kBq) on the x axis. Values equal to zero (white area) are counted as additive effect. Values above zero (white to red area) are counted as synergistic effect, and values below zero (white to green area) are counted as antagonistic effect.

TABLE 4 | The synergy scores of ZIP, Bliss, and HSA synergy models on both viability and spheroid size ratio of the SNU1544 and HT55 spheroid models (at day 12 posttreatment) and the LS174T spheroid model (at day 6 posttreatment).

3D model	Evaluation Day	Feature	Synergy model		
			ZIP	Bliss	HSA
SNU1544	12	Viability	19.2	19.2	27.8
		Spheroid size	1.4	-0.1	8.9
HT55	12	Viability	-6.7	-19.8	-17.1
		Spheroid size	11.6	11.7	15.8
LS174T	6	Viability	3.7	2.4	6.5
		Spheroid size	15.9	15.2	15.8

Positive values indicate a synergistic effect, and negative values indicate an antagonistic effect.

inhibition and reduced cell viability, with the highest observed sensitivity for HT55 spheroid model followed by SNU1544 and LS174T spheroid models, demonstrating the lowest sensitivity. These results support HSP90 inhibition as a potential therapy for colorectal cancer, in line with recent clinical studies where inhibitors such as onalespib have demonstrated efficacy in solid tumors including colorectal cancers alone and in combination with other therapies (43, 71).

Interestingly, higher doses of onalespib were required to achieve therapeutic effects in the 3D spheroid models compared to the monolayer XTT assays. This is in agreement with previous studies comparing the effects of anticancer drugs in monolayer and 3D spheroid models, in which the latter illustrated more similarity to *in vivo* models in terms of drug penetration, cell-to-cell communication, and simulating essential tumor microenvironment factors, such as oxygen and nutrient gradients (72, 73). This emphasizes the important role of 3D models in the assessment of anticancer drugs. Moreover, the large span in onalespib sensitivity in the spheroid models also illustrates the heterogeneity within colorectal cancers and the need for combination treatments in order to widen the therapeutic window.

In the present work, ^{177}Lu-DOTA-M5A RIT was combined with onalespib to assess potential therapeutic effects on spheroid growth and viability (**Figures 5**, **6**). As expected, the high CEA-expressing and onalespib-sensitive models SNU1544 and HT55 demonstrated clear combination effects of ^{177}Lu-DOTA-M5A with onalespib, where both viability and spheroid growth were reduced to a higher extent than those with the monotherapies. For the SNU1544 spheroid model, the effect of 450 nM of onalespib on spheroid sizes was too strong to clearly demonstrate any combination benefits (**Figure 5E**), while the viability assessment displayed benefit of the combination treatment with significantly less cell viability (**Figure 5D**). Moreover, for the HT55 model, the effect of 10 kBq ^{177}Lu-DOTA-M5A was too strong to clearly demonstrate any combination benefits on spheroid sizes (**Figure 5G**), whereas the viability assessment illustrated that the combination treatment resulted in lower spheroid viability compared to the corresponding monotreatments (**Figure 5F**). These results suggest a need for evaluating 3D spheroid models both by spheroid sizes and viability to gain a better grasp of the therapeutic effects. These 3D spheroid model experiments as a whole demonstrated that the therapeutic effects of combination treatment were mediated by both cellular CEA expression levels and the sensitivity to onalespib.

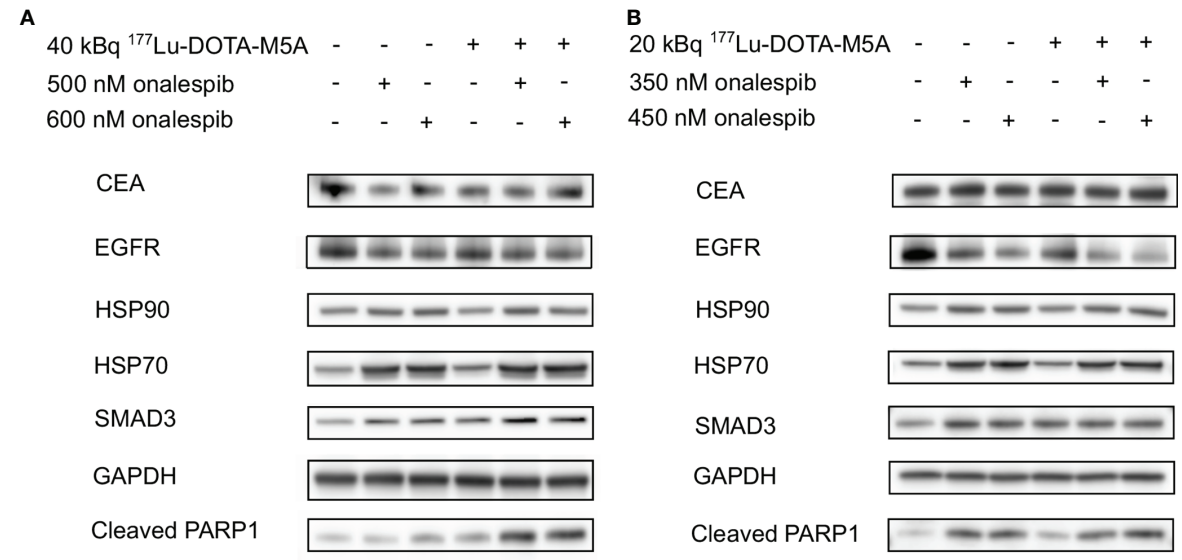

FIGURE 7 | Western blot analysis of the treated 3D spheroid models. Western blot analysis of the LS174T-treated spheroids **(A)** and the SNU1544-treated spheroids **(B)** targeting CEA, EGFR, HSP90, HSP70, SMAD3, and Cleaved PARP1 24 h after treatment. GAPDH was used as a loading control. Representative blots are shown. CEA, carcinoembryonic antigen; EGFR, epidermal growth factor receptor; HSP90, heat shock protein 90; HSP70, heat shock protein 70; Cleaved PARP1, poly adenosine diphosphate-ribose polymerase; GAPDH, glyceraldehyde 3-phosphate dehydrogenase.

Surprisingly, clear combination effects were also found for the low CEA-expressing and the least onalespib-sensitive spheroid model LS174T. It should be noted that an increase of CEA expression was observed for the LS174T 3D spheroids compared to 2D models, in line with previous observations (74). Nevertheless, whereas 10 kBq of ^{177}Lu-DOTA-M5A mediated no significant therapeutic effects as a monotherapy in this model, a combination of 10 kBq ^{177}Lu-DOTA-M5A with 500 nM of onalespib resulted in reduced viability up to 6 days posttreatment (**Figure 5K**), followed by clear spheroid growth inhibition until the study endpoint at day 12 (**Figure 5L**). Consequently, the results indicated that combination therapy with ^{177}Lu-DOTA-M5A and onalespib could potentiate the therapeutic effects in all studied 3D models at selected doses, albeit to different degrees. This reflects the potential of combination treatments as a way to overcome treatment resistance and widen the patient population eligible for RIT. Synergy calculations (**Figure 6**) further validated the effects of the combination treatments, although with varying optimal dose combinations for the different 3D spheroid models, reflecting the heterogeneity of colorectal cancers and the need to further individualize patient treatments.

To further evaluate the mechanisms and molecular effects of selected combination treatments, western blot analysis was performed on 3D tumor lysates 24 h posttreatment (**Figure 7**). The results validated previously known onalespib-mediated effects, such as downregulation of EGFR and upregulation of HSP70 (70, 71), demonstrating clear effects of HSP90 inhibition on a molecular level. Interestingly, in the high CEA-expressing spheroid model SNU1544, a combination with ^{177}Lu-DOTA-M5A reduced EGFR levels even more than onalespib alone, indicating an even more efficient block of the EGFR pathway in this group, which is in line with a previous study (46).

The role of the TGF-β family proteins in carcinogenesis is complicated; however, it was previously found that CEA expression is closely correlated with the TGF-β pathway intermediate proteins such as SMAD3 (75). It has previously been shown that there is cross talk between CEA and the TGF-β pathway, where CEA targeting restored the TGF-β signaling and its ability to inhibit proliferation in colorectal cancer cells (16, 76). Consequently, SMAD3 expression was evaluated as a downstream marker of the TGF-β receptor in the present study. Our results demonstrated SMAD3 upregulation in all treatment groups, indicating a stimulation of the TGF-β pathway. Previous reports have indicated that both onalespib treatment and RIT can mediate apoptosis in cancer cells (42, 46, 77). In the present study, cleaved PARP1 was used as an apoptosis marker. PARP1 plays a critical role in DNA repair and genome stability and is cleaved in apoptosis (mainly by caspases 3 and 7), forming two fragments of 24 and 89 kDa (78–81). Results demonstrated a clear and dose-dependent increase in all onalespib-treated groups. The ^{177}Lu-DOTA-M5A treatment also mediated apoptosis in both spheroid models, being most distinct in the LS174T spheroid model. Notably, it is likely that radiotherapy-induced apoptosis might have been even more apparent at later time points than assessed in the present study (82). Nevertheless, even at 24 h posttreatment, the combination therapies exhibited more pronounced cleaved PARP1 expression compared to the corresponding monotreatments and untreated controls in the LS174T spheroid model, indicating a higher level of apoptosis. This is also in line with previous studies, demonstrating that stimulating the TGF-β pathway and MAPK/ERK pathway leads to apoptosis marker overexpression, including X-linked Inhibitor of Apoptosis Protein (XIAP) and caspases, of which all partially end up to cleaved PARP1 (62). To conclude, the molecular assessment of SNU1544 and LS174T 3D tumor lysates indicated that treatments with ^{177}Lu-DOTA-M5A and/or onalespib could possibly restore SMAD3 expression in the TGF-β pathway. Moreover, EGFR and HSP70 alterations confirmed HPS90 inhibition in the onalespib-treated samples, and PARP1 analyses confirmed increased apoptosis, with enhanced effects in some combination treatments.

CONCLUSION

The ^{177}Lu-DOTA-M5A is a promising novel radioconjugate with potential for RIT of CEA-expressing colorectal cancers. Moreover, the combination with onalespib further potentiates the therapeutic effects of ^{177}Lu-DOTA-M5A potentially owing to the cooperative effects on the cellular tumor-suppressive pathways RTK and MAPK and increased apoptosis. In the future, combining RIT using ^{177}Lu-DOTA-M5A with HSP90 inhibitors may be a feasible therapy approach for metastatic colorectal cancers and for overcoming antitumor treatment resistance, and may have the potential to widen the targetable cancer patient population and increase the remission rates.

DATA AVAILABILITY STATEMENT

The raw data supporting the conclusions of this article will be made available by the authors without undue reservation.

AUTHOR CONTRIBUTIONS

TMS contributed to experimental studies with the focus on stability assays, XTT proliferation assays, binding specificity assays, real-time binding assays, 3D tumor spheroid-related assays, and western blotting, analyzing and interpreting the data and drafting and revising the article. PJ contributed to experimental studies with a focus on optimizing radiolabeling, radiolabeling, analyzing and interpreting the data, and drafting and revising the article. AB contributed to the analysis of real-time binding measurement *via* Ligand Tracer and drafting and revision of the article. FYF contributed to the design of the study and data interpretation and revision of the article. PJY contributed to the experimental studies with the focus on the development of the anti-CEA hT84.66 mAb, DOTA conjugation and purification, and drafting and revision of the article. MN

initiated and designed the study, contributed to data analysis and interpretation, and drafted and revised the article. All authors have read and approved the final article.

FUNDING

The study was supported by Swedish Cancer Society (CAN 21/1534, CAN 20 0191), the Swedish Research Council (2020-01377), the Swedish Childhood Cancer Fund (PR2020-0023, TJ2021-0072), and Stiftelsen Ulf Lundahls minnesfond.

SUPPLEMENTARY MATERIAL

The Supplementary Material for this article can be found online at: https://www.frontiersin.org/articles/10.3389/fonc.2022.849338/full#supplementary-material

REFERENCES

1. Arnold M, Abnet CC, Neale RE, Vignat J, Giovannucci EL, McGlynn KA, et al. Global Burden of 5 Major Types Of Gastrointestinal Cancer. *Gastroenterology* (2020) 159(1):335–349.e15. doi: 10.1053/j.gastro.2020.02.068
2. Sung H, Ferlay J, Siegel RL, Laversanne M, Soerjomataram I, Jemal A, et al. Global Cancer Statistics 2020: GLOBOCAN Estimates of Incidence and Mortality Worldwide for 36 Cancers in 185 Countries. *CA: A Cancer J Clin* (2021) 71(3):209–49. doi: 10.3322/caac.21660
3. Duffy MJ. Carcinoembryonic Antigen as a Marker for Colorectal Cancer: Is It Clinically Useful? *Clin Chem* (2001) 47(4):624–30. doi: 10.1093/clinchem/47.4.624
4. Shao Y, Sun X, He Y, Liu C, Liu H. Elevated Levels of Serum Tumor Markers CEA and CA15-3 Are Prognostic Parameters for Different Molecular Subtypes of Breast Cancer. *PloS One* (2015) 10(7):e0133830. doi: 10.1371/journal.pone.0133830
5. Deng K, Yang L, Hu B, Wu H, Zhu H, Tang C. The Prognostic Significance of Pretreatment Serum CEA Levels in Gastric Cancer: A Meta-Analysis Including 14651 Patients. *PloS One* (2015) 10(4):e0124151. doi: 10.1371/journal.pone.0124151
6. Kujawski M, Sherman M, Hui S, Zuro D, Lee W-H, Yazaki P, et al. Potent Immunomodulatory Effects of an Anti-CEA-IL-2 Immunocytokine on Tumor Therapy and Effects of Stereotactic Radiation. *OncoImmunology* (2020) 9(1):1724052. doi: 10.1080/2162402X.2020.1724052
7. Wong JYC, Chu DZ, Williams LE, Liu A, Zhan J, Yamauchi DM, et al. A Phase I Trial of 90Y-DOTA-Anti-CEA Chimeric T84.66 (Ct84.66) Radioimmunotherapy in Patients With Metastatic CEA-Producing Malignancies. *Cancer Biother Radiopharm* (2006) 21(2):88–100. doi: 10.1089/cbr.2006.21.88
8. Cahan B, Leong L, Wagman L, Yamauchi D, Shibata S, Wilzcynski S, et al. Phase I/II Trial of Anticarcinoembryonic Antigen Radioimmunotherapy, Gemcitabine, and Hepatic Arterial Infusion of Fluorodeoxyuridine Postresection of Liver Metastasis for Colorectal Carcinoma. *Cancer Biother Radiopharm* (2017) 32(7):258–65. doi: 10.1089/cbr.2017.2223
9. Cha SE, Kujawski M, Yazaki PJ, Brown C, Shively JE. Tumor Regression and Immunity in Combination Therapy With Anti-CEA Chimeric Antigen Receptor T Cells and Anti-CEA-IL2 Immunocytokine. *OncoImmunology* (2021) 10(1):1899469. doi: 10.1080/2162402X.2021.1899469
10. Schoffelen R, van der GWTA, Franssen G, Sharkey RM, Goldenberg DM, McBride WJ, et al. Pretargeted 177lu Radioimmunotherapy of Carcinoembryonic Antigen–Expressing Human Colonic Tumors in Mice. *J Nucl Med* (2010) 51(11):1780–7. doi: 10.2967/jnumed.110.079376
11. Akhavan D, Yazaki P, Yamauchi D, Simpson J, Frankel PH, Bading J, et al. Phase I Study of Yttrium-90 Radiolabeled M5A Anti-Carcinoembryonic Antigen Humanized Antibody in Patients With Advanced Carcinoembryonic Antigen Producing Malignancies. *Cancer Biother Radiopharm* (2020) 35(1):10–5. doi: 10.1089/cbr.2019.2992
12. Xu X, Clarke P, Szalai G, Shively JE, Williams LE, Shyr Y, et al. Targeting and Therapy of Carcinoembryonic Antigen-Expressing Tumors in Transgenic Mice With an Antibody-Interleukin 2 Fusion Protein. *Cancer Res* (2000) 60(16):4475–84.
13. Heskamp S, Hernandez R, Molkenboer-Kuenen JDM, Essler M, Bruchertseifer F, Morgenstern A, et al. α- Versus β-Emitting Radionuclides for Pretargeted Radioimmunotherapy of Carcinoembryonic Antigen–Expressing Human Colon Cancer Xenografts. *J Nucl Med* (2017) 58(6):926–33. doi: 10.2967/jnumed.116.187021
14. Behr TM, Becker WS, Bair H-J, Klein MW, Stühler CM, Cidlinsky KP, et al. Comparison of Complete Versus Fragmented Technetium-99m-Labeled Anti-CEA Monoclonal Antibodies for Immunoscintigraphy in Colorectal Cancer. *J Nucl Med* (1995) 36(3):430–41.
15. Schmidt MM, Thurber GM, Wittrup KD. Kinetics of Anti-Carcinoembryonic Antigen Antibody Internalization: Effects of Affinity, Bivalency, and Stability. *Cancer Immunol Immunother* (2008) 57(12):1879–90. doi: 10.1007/s00262-008-0518-1
16. Li Y, Cao H, Jiao Z, Pakala SB, Sirigiri DNR, Li W, et al. Carcinoembryonic Antigen Interacts With TGF-β Receptor and Inhibits TGF-β Signaling in Colorectal Cancers. *Cancer Res* (2010) 70(20):8159–68. doi: 10.1158/0008-5472.CAN-10-1073
17. Bertagnolli MM. Radioimmunotherapy for Colorectal Cancer. *Clin Cancer Res* (2005) 11(13):4637–8. doi: 10.1158/1078-0432.CCR-05-0485
18. Liu Z, Jin C, Yu Z, Zhang J, Liu Y, Zhao H, et al. Radioimmunotherapy of Human Colon Cancer Xenografts With 131I-Labeled Anti-CEA Monoclonal Antibody. *Bioconjug Chem* (2010) 21(2):314–8. doi: 10.1021/bc9003603
19. Song H, Sgouros G. Radioimmunotherapy of Solid Tumors: Searching for the Right Target. *Curr Drug Deliv* (2011) 8(1):26–44. doi: 10.2174/156720111793663651
20. Sahlmann C-O, Homayounfar K, Niessner M, Dyczkowski J, Conradi L-C, Braulke F, et al. Repeated Adjuvant Anti-CEA Radioimmunotherapy After Resection of Colorectal Liver Metastases: Safety, Feasibility, and Long-Term Efficacy Results of a Prospective Phase 2 Study. *Cancer* (2017) 123(4):638–49. doi: 10.1002/cncr.30390
21. Garambois V, Glaussel F, Foulquier E, Ychou M, Pugnière M, Luo RX, et al. Fully Human IgG and IgM Antibodies Directed Against the Carcinoembryonic Antigen (CEA) Gold 4 Epitope and Designed for Radioimmunotherapy (RIT) of Colorectal Cancers. *BMC Cancer* (2004) 4:75. doi: 10.1186/1471-2407-4-75
22. Beatty JD, Philben VJ, Beatty BG, Williams LE, Paxton RJ, Shively JE, et al. Imaging of Colon Carcinoma With 111-Indium-Labeled Anti-CEA Monoclonal Antibodies (Indacea) Prior to Surgery. *J Surg Oncol* (1987) 36(2):98–104. doi: 10.1002/jso.2930360205
23. Duda RB, Beatty JD, Sheibani K, Williams LE, Paxton RJ, Beatty BG, et al. Imaging of Human Colorectal Adenocarcinoma With Indium-Labeled Anticarcinoembryonic Antigen Monoclonal Antibody. *Arch Surg* (1986) 121(11):1315–9. doi: 10.1001/archsurg.121.11.1315
24. Wong JY, Thomas GE, Yamauchi D, Williams LE, Odom-Maryon TL, Liu A, et al. Clinical Evaluation of Indium-111-Labeled Chimeric Anti-CEA Monoclonal Antibody. *J Nucl Med* (1997) 38(12):1951–9.
25. Wong JYC, Shibata S, Williams LE, Kwok CS, Liu A, Chu DZ, et al. A Phase I Trial of 90Y-Anti-Carcinoembryonic Antigen Chimeric T84.66 Radioimmunotherapy With 5-Fluorouracil in Patients With Metastatic Colorectal Cancer. *Clin Cancer Res* (2003) 9(16):5842–52.
26. Wong JY, Williams LE, Yamauchi DM, Odom-Maryon T, Esteban JM, Neumaier M, et al. Initial Experience Evaluating 90yttrium-Radiolabeled Anti-Carcinoembryonic Antigen Chimeric T84.66 in a Phase I Radioimmunotherapy Trial. *Cancer Res* (1995) 55(23 Suppl):5929s–34s.
27. Wong JY, Chu DZ, Yamauchi D, Odom-Maryon TL, Williams LE, Liu A, et al. Dose Escalation Trial of Indium-111-Labeled Anti-Carcinoembryonic Antigen Chimeric Monoclonal Antibody (Chimeric T84.66) in Presurgical

Colorectal Cancer Patients. *J Nucl Med* (1998) 39(12):2097–104. doi: 10.1016/S0360-3016(97)80698-0
28. Wong JY, Somlo G, Odom-Maryon T, Williams LE, Liu A, Yamauchi D, et al. Initial Clinical Experience Evaluating Yttrium-90-Chimeric T84.66 Anticarcinoembryonic Antigen Antibody and Autologous Hematopoietic Stem Cell Support in Patients With Carcinoembryonic Antigen-Producing Metastatic Breast Cancer. *Clin Cancer Res* (1999) 5(10 Suppl):3224s–31s.
29. Shibata S, Raubitschek A, Leong L, Koczywas M, Williams L, Zhan J, et al. A Phase I Study of a Combination of Yttrium-90–Labeled Anti–Carcinoembryonic Antigen (CEA) Antibody and Gemcitabine in Patients With CEA-Producing Advanced Malignancies. *Clin Cancer Res* (2009) 15(8):2935–41. doi: 10.1158/1078-0432.CCR-08-2213
30. Yazaki PJ, Sherman MA, Shively JE, Ikle D, Williams LE, Wong JYC, et al. Humanization of the Anti-CEA T84.66 Antibody Based on Crystal Structure Data. *Protein Eng Des Sel* (2004) 17(5):481–9. doi: 10.1093/protein/gzh056
31. Dash A, Pillai MRA, Knapp FF. Production of 177Lu for Targeted Radionuclide Therapy: Available Options. *Nucl Med Mol Imaging* (2015) 49(2):85–107. doi: 10.1007/s13139-014-0315-z
32. Georgopoulos C, Welch WJ. Role of the Major Heat Shock Proteins as Molecular Chaperones. *Annu Rev Cell Biol* (1993) 9:601–34. doi: 10.1146/annurev.cb.09.110193.003125
33. Pratt WB, Toft DO. Regulation of Signaling Protein Function and Trafficking by the Hsp90/Hsp70-Based Chaperone Machinery. *Exp Biol Med (Maywood)* (2003) 228(2):111–33. doi: 10.1177/153537020322800201
34. Kuipers EJ, Grady WM, Lieberman D, Seufferlein T, Sung JJ, Boelens PG, et al. Colorectal Cancer. *Nat Rev Dis Primers* (2015) 1(1):15065. doi: 10.1038/nrdp.2015.65
35. Dienstmann R, Vermeulen L, Guinney J, Kopetz S, Tejpar S, Tabernero J. Consensus Molecular Subtypes and the Evolution of Precision Medicine in Colorectal Cancer. *Nat Rev Cancer* (2017) 17(2):79–92. doi: 10.1038/nrc.2016.126
36. Boroumand N, Saghi H, Avan A, Bahreyni A, Ryzhikov M, Khazaei M, et al. Therapeutic Potency of Heat-Shock Protein-90 Pharmacological Inhibitors in the Treatment of Gastrointestinal Cancer, Current Status and Perspectives. *J Pharm Pharmacol* (2018) 70(2):151–8. doi: 10.1111/jphp.12824
37. Zhang S, Guo S, Li Z, Li D, Zhan Q. High Expression of HSP90 Is Associated With Poor Prognosis in Patients With Colorectal Cancer. *PeerJ* (2019) 7:e7946. doi: 10.7717/peerj.7946
38. Wang J, Cui S, Zhang X, Wu Y, Tang H. High Expression of Heat Shock Protein 90 Is Associated With Tumor Aggressiveness and Poor Prognosis in Patients With Advanced Gastric Cancer. *PloS One* (2013) 8(4):e62876. doi: 10.1371/journal.pone.0062876
39. Park H-K, Yoon NG, Lee J-E, Hu S, Yoon S, Kim SY, et al. Unleashing the Full Potential of Hsp90 Inhibitors as Cancer Therapeutics Through Simultaneous Inactivation of Hsp90, Grp94, and TRAP1. *Exp Mol Med* (2020) 52(1):79–91. doi: 10.1038/s12276-019-0360-x
40. Sanchez J, Carter TR, Cohen MS, Blagg BSJ. Old and New Approaches to Target the Hsp90 Chaperone. *Curr Cancer Drug Targets* (2020) 20(4):253–70. doi: 10.2174/1568009619666191202101330
41. Jhaveri K, Taldone T, Modi S, Chiosis G. Advances in the Clinical Development of Heat Shock Protein 90 (Hsp90) Inhibitors in Cancers. *Biochim Biophys Acta (BBA) - Mol Cell Res* (2012) 1823(3):742–55. doi: 10.1016/j.bbamcr.2011.10.008
42. Spiegelberg D, Abramenkovs A, Mortensen ACL, Lundsten S, Nestor M, Stenerlöw B. The HSP90 Inhibitor Onalespib Exerts Synergistic Anti-Cancer Effects When Combined With Radiotherapy: An *In Vitro* and *In Vivo* Approach. *Sci Rep* (2020) 10(1):1–11. doi: 10.1038/s41598-020-62293-4
43. Do KT, O'Sullivan Coyne G, Hays JL, Supko JG, Liu SV, Beebe K, et al. Phase 1 Study of the HSP90 Inhibitor Onalespib in Combination With AT7519, a Pan-CDK Inhibitor, in Patients With Advanced Solid Tumors. *Cancer Chemother Pharmacol* (2020) 86(6):815–27. doi: 10.1007/s00280-020-04176-z
44. Slovin S, Hussain S, Saad F, Garcia J, Picus J, Ferraldeschi R, et al. Pharmacodynamic and Clinical Results From a Phase I/II Study of the HSP90 Inhibitor Onalespib in Combination With Abiraterone Acetate in Prostate Cancer. *Clin Cancer Res* (2019) 25(15):4624–33. doi: 10.1158/1078-0432.CCR-18-3212
45. Spiegelberg D, Dascalu A, Mortensen AC, Abramenkovs A, Kuku G, Nestor M, et al. The Novel HSP90 Inhibitor AT13387 Potentiates Radiation Effects in Squamous Cell Carcinoma and Adenocarcinoma Cells. *Oncotarget* (2015) 6(34):35652–66. doi: 10.18632/oncotarget.5363
46. Lundsten S, Spiegelberg D, Stenerlöw B, Nestor M. The HSP90 Inhibitor Onalespib Potentiates 177Lu–DOTATATE Therapy in Neuroendocrine Tumor Cells. *Int J Oncol* (2019) 55(6):1287–95. doi: 10.3892/ijo.2019.4888
47. Ku J-L, Shin Y-K, Kim D-W, Kim K-H, Choi J-S, Hong S-H, et al. Establishment and Characterization of 13 Human Colorectal Carcinoma Cell Lines: Mutations of Genes and Expressions of Drug-Sensitivity Genes and Cancer Stem Cell Markers. *Carcinogenesis* (2010) 31(6):1003–9. doi: 10.1093/carcin/bgq043
48. Watson SA, Durrant LG, Morris DL. The Effect of the E2 Prostaglandin Enprostil, and the Somatostatin Analogue SMS 201 995, on the Growth of a Human Gastric Cell Line, MKN45G. *Int J Cancer* (1990) 45(1):90–4. doi: 10.1002/ijc.2910450117
49. Cowley GS, Weir BA, Vazquez F, Tamayo P, Scott JA, Rusin S, et al. Parallel Genome-Scale Loss of Function Screens in 216 Cancer Cell Lines for the Identification of Context-Specific Genetic Dependencies. *Sci Data* (2014) 1:140035. doi: 10.1038/sdata.2014.35
50. Tom BH, Rutzky LP, Jakstys MM, Oyasu R, Kaye CI, Kahan BD. Human Colonic Adenocarcinoma Cells. I. Establishment and Description of a New Line. *In Vitro* (1976) 12(3):180–91. doi: 10.1007/BF02796440
51. Petitprez A, Poindessous V, Ouaret D, Regairaz M, Bastian G, Guérin E, et al. Acquired Irinotecan Resistance is Accompanied by Stable Modifications of Cell Cycle Dynamics Independent of MSI Status. *Int J Oncol* (2013) 42(5):1644–53. doi: 10.3892/ijo.2013.1868
52. Lewis MR, Raubitschek A, Shively JE. A Facile, Water-Soluble Method for Modification of Proteins With DOTA. Use of Elevated Temperature and Optimized pH to Achieve High Specific Activity and High Chelate Stability in Radiolabeled Immunoconjugates. *Bioconjug Chem* (1994) 5(6):565–76. doi: 10.1021/bc00030a012
53. Bondza S, Foy E, Brooks J, Andersson K, Robinson J, Richalet P, et al. Real-Time Characterization of Antibody Binding to Receptors on Living Immune Cells. *Front Immunol* (2017) 8:455. doi: 10.3389/fimmu.2017.00455
54. Friedrich J, Seidel C, Ebner R, Kunz-Schughart LA. Spheroid-Based Drug Screen: Considerations and Practical Approach. *Nat Protoc* (2009) 4(3):309–24. doi: 10.1038/nprot.2008.226
55. Eilenberger C, Kratz SRA, Rothbauer M, Ehmoser E-K, Ertl P, Küpcü S. Optimized Alamarblue Assay Protocol for Drug Dose-Response Determination of 3D Tumor Spheroids. *MethodsX* (2018) 5:781–7. doi: 10.1016/j.mex.2018.07.011
56. Ianevski A, Giri AK, Aittokallio T. SynergyFinder 2.0: Visual Analytics of Multi-Drug Combination Synergies. *Nucleic Acids Res* (2020) 48(W1):W488–93. doi: 10.1093/nar/gkaa216
57. Berenbaum MC. What Is Synergy? *Pharmacol Rev* (1989) 41(2):93–141.
58. Bliss CI. The Toxicity of Poisons Applied Jointly1. *Ann Appl Biol* (1939) 26(3):585–615. doi: 10.1111/j.1744-7348.1939.tb06990.x
59. Yadav B, Wennerberg K, Aittokallio T, Tang J. Searching for Drug Synergy in Complex Dose-Response Landscapes Using an Interaction Potency Model. *Comput Struct Biotechnol J* (2015) 13:504–13. doi: 10.1016/j.csbj.2015.09.001
60. Malyutina A, Majumder MM, Wang W, Pessia A, Heckman CA, Tang J. Drug Combination Sensitivity Scoring Facilitates the Discovery of Synergistic and Efficacious Drug Combinations in Cancer. *PloS Comput Biol* (2019) 15(5):e1006752. doi: 10.1371/journal.pcbi.1006752
61. Bacac M, Fauti T, Sam J, Colombetti S, Weinzierl T, Ouaret D, et al. A Novel Carcinoembryonic Antigen T-Cell Bispecific Antibody (CEA TCB) for the Treatment of Solid Tumors. *Clin Cancer Res* (2016) 22(13):3286–97. doi: 10.1158/1078-0432.CCR-15-1696
62. Bailey KL, Agarwal E, Chowdhury S, Luo J, Brattain MG, Black JD, et al. Tgfβ/Smad3 Regulates Proliferation and Apoptosis Through IRS-1 Inhibition in Colon Cancer Cells. *PloS One* (2017) 12(4):e0176096. doi: 10.1371/journal.pone.0176096
63. Thurber GM, Schmidt MM, Wittrup KD. Antibody Tumor Penetration. *Adv Drug Delivery Rev* (2008) 60(12):1421. doi: 10.1016/j.addr.2008.04.012
64. Klein C, Waldhauer I, Nicolini VG, Freimoser-Grundschober A, Nayak T, Vugts DJ, et al. Cergutuzumab Amunaleukin (CEA-IL2v), a CEA-Targeted IL-2 Variant-Based Immunocytokine for Combination Cancer Immunotherapy: Overcoming Limitations of Aldesleukin and Conventional

IL-2-Based Immunocytokines. *OncoImmunology* (2017) 6(3):e1277306. doi: 10.1080/2162402X.2016.1277306
65. Moser C, Lang SA, Stoeltzing O. Heat-Shock Protein 90 (Hsp90) as a Molecular Target for Therapy of Gastrointestinal Cancer. *Anticancer Res* (2009) 29(6):2031–42.
66. Saturno G, Valenti M, De Haven Brandon A, Thomas GV, Eccles S, Clarke PA, et al. Combining Trail With PI3 Kinase or HSP90 Inhibitors Enhances Apoptosis in Colorectal Cancer Cells *via* Suppression of Survival Signaling. *Oncotarget* (2013) 4(8):1185–98. doi: 10.18632/oncotarget.1162
67. Kryeziu K, Bruun J, Guren TK, Sveen A, Lothe RA. Combination Therapies With HSP90 Inhibitors Against Colorectal Cancer. *Biochim Biophys Acta (BBA) - Rev Cancer* (2019) 1871(2):240–7. doi: 10.1016/j.bbcan.2019.01.002
68. He S, Smith DL, Sequeira M, Sang J, Bates RC, Proia DA. The HSP90 Inhibitor Ganetespib has Chemosensitizer and Radiosensitizer Activity in Colorectal Cancer. *Invest New Drugs* (2014) 32(4):577–86. doi: 10.1007/s10637-014-0095-4
69. Moser C, Lang SA, Kainz S, Gaumann A, Fichtner-Feigl S, Koehl GE, et al. Blocking Heat Shock Protein-90 Inhibits the Invasive Properties and Hepatic Growth of Human Colon Cancer Cells and Improves the Efficacy of Oxaliplatin in P53-Deficient Colon Cancer Tumors In Vivo. *Mol Cancer Ther* (2007) 6(11):2868–78. doi: 10.1158/1535-7163.MCT-07-0410
70. Lundsten S, Spiegelberg D, Raval NR, Nestor M. The Radiosensitizer Onalespib Increases Complete Remission in 177Lu-DOTATATE-Treated Mice Bearing Neuroendocrine Tumor Xenografts. *Eur J Nucl Med Mol Imaging* (2020) 47(4):980–90. doi: 10.1007/s00259-019-04673-1
71. Do K, Speranza G, Chang L-C, Polley EC, Bishop R, Zhu W, et al. Phase I Study of the Heat Shock Protein 90 (Hsp90) Inhibitor Onalespib (AT13387) Administered on a Daily for 2 Consecutive Days Per Week Dosing Schedule in Patients With Advanced Solid Tumors. *Invest New Drugs* (2015) 33(4):921–30. doi: 10.1007/s10637-015-0255-1
72. Souza AG, Silva IBB, Campos-Fernandez E, Barcelos LS, Souza JB, Marangoni K, et al. Comparative Assay of 2D and 3D Cell Culture Models: Proliferation, Gene Expression and Anticancer Drug Response. *Curr Pharm Des* (2018) 24 (15):1689–94. doi: 10.2174/1381612824666180404152304
73. Lindell Jonsson E, Erngren I, Engskog M, Haglöf J, Arvidsson T, Hedeland M, et al. Exploring Radiation Response in Two Head and Neck Squamous Carcinoma Cell Lines Through Metabolic Profiling. *Front Oncol* (2019) 9:825. doi: 10.3389/fonc.2019.00825
74. Jessup JM, Brown D, Fitzgerald W, Ford RD, Nachman A, Goodwin TJ, et al. Induction of Carcinoembryonic Antigen Expression in a Three-Dimensional Culture System. *In Vitro Cell Dev Biol Anim* (1997) 33(5):352–7. doi: 10.1007/s11626-997-0005-6
75. Han S-U, Kwak T-H, Her KH, Cho Y-H, Choi C, Lee H-J, et al. CEACAM5 and CEACAM6 are Major Target Genes for Smad3-Mediated TGF- β Signaling. *Oncogene* (2008) 27(5):675–83. doi: 10.1038/sj.onc.1210686
76. Bajenova O, Gorbunova A, Evsyukov I, Rayko M, Gapon S, Bozhokina E, et al. The Genome-Wide Analysis of Carcinoembryonic Antigen Signaling by Colorectal Cancer Cells Using RNA Sequencing. *PloS One* (2016) 11(9): e0161256. doi: 10.1371/journal.pone.0161256
77. Mortensen ACL, Mohajershojai T, Hariri M, Pettersson M, Spiegelberg D. Overcoming Limitations of Cisplatin Therapy by Additional Treatment With the HSP90 Inhibitor Onalespib. *Front Oncol* (2020) 10:532285. doi: 10.3389/fonc.2020.532285
78. Herceg Z, Wang Z-Q. Functions of Poly(ADP-Ribose) Polymerase (PARP) in DNA Repair, Genomic Integrity and Cell Death. *Mutat Res Fundam Mol Mech Mutagenesis* (2001) 477(1):97–110. doi: 10.1016/S0027-5107(01)00111-7
79. Engbrecht M, Mangerich A. The Nucleolus and PARP1 in Cancer Biology. *Cancers* (2020) 12(7):1813. doi: 10.3390/cancers12071813
80. Qvarnström OF, Simonsson M, Eriksson V, Turesson I, Carlsson J. Gammah2ax and Cleaved PARP-1 as Apoptotic Markers in Irradiated Breast Cancer BT474 Cellular Spheroids. *Int J Oncol* (2009) 35(1):41–7. doi: 10.3892/ijo_00000311
81. Rahmanian N, Hosseinimehr SJ, Khalaj A. The Paradox Role of Caspase Cascade in Ionizing Radiation Therapy. *J Biomed Sci* (2016) 23(1):88. doi: 10.1186/s12929-016-0306-8
82. Feijtel D, Doeswijk GN, Verkaik NS, Haeck JC, Chicco D, Angotti C, et al. Inter and Intra-Tumor Somatostatin Receptor 2 Heterogeneity Influences Peptide Receptor Radionuclide Therapy Response. *Theranostics* (2021) 11 (2):491–505. doi: 10.7150/thno.51215

Conflict of Interest: Author AB is employed by Ridgeview Instruments AB.

The remaining authors declare that the research was conducted in the absence of any commercial or financial relationships that could be construed as a potential conflict of interest.

Publisher's Note: All claims expressed in this article are solely those of the authors and do not necessarily represent those of their affiliated organizations, or those of the publisher, the editors and the reviewers. Any product that may be evaluated in this article, or claim that may be made by its manufacturer, is not guaranteed or endorsed by the publisher.

frontiers | Frontiers in Oncology

REVIEW
published: 06 April 2022
doi: 10.3389/fonc.2022.852927

Molecular Network of Colorectal Cancer and Current Therapeutic Options

Zhe Huang[1] *and Mingli Yang*[2*]

[1] *The Department of 11th General Surgery, Minimally Invasive Colorectal Hernia Unit, Shengjing Hospital of China Medical University, Shenyang, China,* [2] *The Department of 3Oncology, Gastrointestinal Cancer Unit, Shengjing Hospital of China Medical University, Shenyang, China*

Colorectal cancer (CRC), a leading cause of cancer-related mortalities globally, results from the accumulation of multiple genetic and epigenetic alterations in the normal colonic and rectum epithelium, leading to the progression from colorectal adenomas to invasive carcinomas. Almost half of CRC patients will develop metastases in the course of the disease and most patients with metastatic CRC are incurable. Particularly, the 5-year survival rate of patients with stage 4 CRC at diagnosis is less than 10%. Although genetic understanding of these CRC tumors and paired metastases has led to major advances in elucidating early driver genes responsible for carcinogenesis and metastasis, the pathophysiological contribution of transcriptional and epigenetic aberrations in this malignancy which influence many central signaling pathways have attracted attention recently. Therefore, treatments that could affect several different molecular pathways may have pivotal implications for their efficacy. In this review, we summarize our current knowledge on the molecular network of CRC, including cellular signaling pathways, CRC microenvironment modulation, epigenetic changes, and CRC biomarkers for diagnosis and predictive/prognostic use. We also provide an overview of opportunities for the treatment and prevention strategies in this field.

Keywords: colorectal cancer, cellular signaling, microenvironment modulation, epigenetic changes, biomarkers

OPEN ACCESS

Edited by:
Shilpa S. Dhar,
University of Texas MD Anderson Cancer Center, United States

Reviewed by:
Mihai Stefan Muresan,
Iuliu Haţieganu University of Medicine and Pharmacy, Romania
Timo Gaiser,
University of Heidelberg, Germany

****Correspondence:***
Mingli Yang
mingli_1999@163.com

Specialty section:
This article was submitted to Molecular and Cellular Oncology, a section of the journal Frontiers in Oncology

Received: *11 January 2022*
Accepted: *11 March 2022*
Published: *06 April 2022*

Citation:
Huang Z and Yang M (2022) Molecular Network of Colorectal Cancer and Current Therapeutic Options. Front. Oncol. 12:852927. doi: 10.3389/fonc.2022.852927

INTRODUCTION

Colorectal cancer (CRC) is the third diagnosed malignant tumor worldwide, accounting for approximately 9% of annual cancer death (1). More than 90% of CRCs are adenocarcinoma, resulting from normal glandular colonic and rectum epithelium. Other rare types include carcinoid tumors, gastrointestinal stromal tumors, colorectal lymphoma, squamous cell carcinomas, leiomyosarcomas, and melanomas (2). Approximately 65% of CRC cases developed sporadically, without a family history or inherited genetic mutations predisposition, through multiple acquired somatic genomic and epigenetic alterations (3, 4). Other cases are associated with heritable components such as family history (25%), hereditary cancer syndrome (5%), some known CRCs low-penetrance genetic variations (<1%), and other unknown inherited genomic alterations (4, 5).

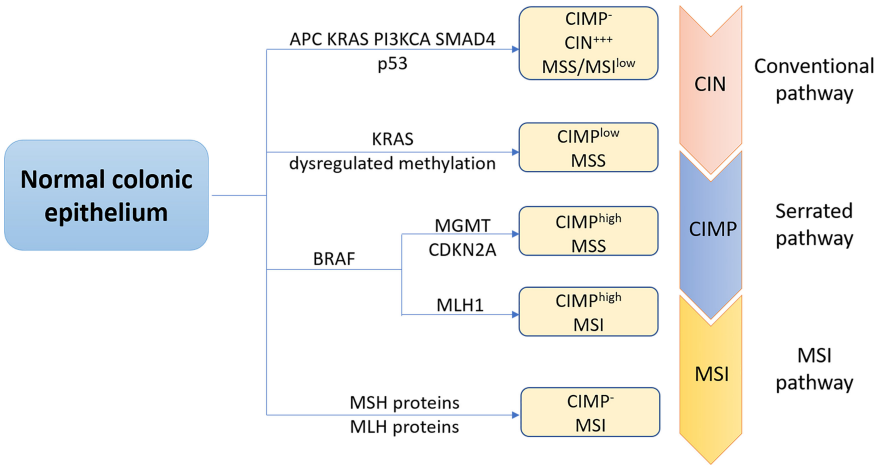

FIGURE 1 | The three major molecular pathways of colorectal cancer. The conventional chromosomal instability (CIN) pathway, initiated by APC mutation, then followed by mutations in KRAS, PIK3CA and SMAD4, loss of heterozygosity of p53 mutation was observed in most CRC cases. CRC progress and development via this pathway is often associated with no or low levels of the CpG island methylation pathway (CIMP-), high levels of CIN (CIW^{+++}), and microsatellite stability (MSS). Approximately one third CRC cases is regulated through the serrated pathway, which can be subdivided into $CIMP^{low}$ MSS tumors with KRAS mutations, BRAF mutant $CIMP^{high}$ MSS tumors or BRAF mutant $CIMP^{high}$ microsatellite instability (MSI) tumors. Serrated pathway is commonly associated with silencing of 0-6-methylguanine-DNA methyltransferase (MGMT), cyclin-dependent kinase inhibitor 2A (CDKN2A) or MLHI. MSI pathway is a third important pathway of CRC caused by dysfunction of DNA mismatch repair genes, encoding MutI homolog (MLH) or MutS homolog (MSH) proteins.

At the molecular level, CRC, like other solid tumors, is a heterogeneous disease. This can be attributed to at least three major molecular pathways (**Figure 1**). The most common pathway is the chromosomal instability (CIN), occurring in 85% of sporadic CRC (sCRC), characterized by chromosome structure and number abnormalities, frequent loss of heterozygosity (LOH) at tumor suppressor gene loci, gain or loss of chromosomal segments and chromosomal rearrangements, further resulting in gene copy number variations (6). These alterations typically are associated with mutations in specific oncogenes or tumor suppressors genes such as adenomatous polyposis coli (*APC*), Kirsten rat sarcoma virus (*KRAS*), phosphatidylinositol 4,5-bisphosphate 3-kinase catalytic subunit-α (*PIK3CA*), b-raf proto-oncogene (*BRAF*), SMAD family member 4 (*SMAD4*) or *p53* (7), which regulate cell proliferation and cell cycle and play pivotal roles in CRC initiation and progression pathways. Another important pathway to CRC is the microsatellite instability (MSI), caused by dysfunction of DNA mismatch repair (MMR) genes during DNA recombination, DNA replication and DNA damage, which encodes MutL Homolog (MLH) proteins or MutS homolog (MSH) proteins. Therefore, it is often associated with genetic hypermutability (8). CpG island methylator phenotype (CIMP) comprises the third major pathway to CRC. CIMP positive tumors can be divided into $CIMP^{high}$ tumors, with BRAF mutations, MLH1 methylation, and silencing of O-6-methylguanine-DNA methyltransferase (MGMT) or cyclin-dependent kinase inhibitor 2A (CDKN2A) and $CIMP^{low}$ tumors, with KRAS mutations. In fact, CRC pathogenesis is normally associated with multiple pathways. Specifically, approximately one third CRC cases develop *via* a serrated pathway that is associated with either KRAS or BRAF mutations in addition to CIMP mutations ($CIMP^{low}$ or $CIMP^{high}$).

Generally, CRC tumorigenesis initiates with the transformation of normal colorectal epithelial cells by a spontaneous mutation, environmental mutagens, genetic or epigenetic alterations. Then, these initiated cells rapidly expanded to form aberrant crypt foci and early adenoma, driven by mutations that cause hyperproliferation, such as APC mutations, or other signaling pathways such as WNT-β-catenin, cytokines, chemokines, and growth factors from the tumor microenvironment (TME) (9). Thus, mutations such as SMAD4, cell division control protein 4 (CDC4) and transforming growth beta factor 2 (TGFBR2) as well as chromosomal aberration such as LOH 18q further lead to the outgrowth of these clones into late adenoma and malignant tumors, known as tumor promotion. Further mutations (p53 and Bcl-2 Associated X-protein (BAX)), pro-angiogenic factors, extracellular matrix-degrading factors and other factors which promote CRC cells invasive motility facilitate these tumors efficiently to metastasize to distant organs and tissues, known as tumor progression.

Although genetic understanding of these CRC tumors and paired metastases has led to major advances in elucidating early driver genes responsible for carcinogenesis and metastasis, the pathophysiological contribution of transcriptional and epigenetic alterations in this malignancy influences many central signaling pathways have attracted attention recently. Therefore, the present review summarized the current knowledge on the molecular network of CRC, including cellular signaling pathways, CRC

microenvironment modulation, epigenetic changes, CRC and inflammatory bowel disease (IBD), and CRC biomarkers for early diagnosis and prognostic/predictive use and provide an overview of opportunities for CRC treatment.

MOLECULAR NETWORK OF CRC

Cellular Signaling Pathways

As mentioned, CRC development is a complicated multistage process with sequential mutations involved. Several cellular signaling pathways that regulate cell proliferation, differentiation, apoptosis, and survival are involved in CRC onsets, such as epidermal growth factor receptor (EGFR)/mitogen-activated protein kinase (MAPK), Wingless-related integration site (Wnt)/β-catenin, phosphoinositide 3-kinase (PI3K), transforming growth factor-β (TGF)-β, Neurogenic locus notch homolog protein (Notch), and nuclear factor (NF)-κB (10).

EGFR/MAPK Signaling Pathway

EGFR, a catalytic receptor tyrosine kinase (RTK), is a transmembrane protein containing an extracellular ligand-binding domain. After ligand binding, EGFR is activated and dimerized, resulting in the autophosphorylation of several tyrosine residues in the intercellular domain. Furthermore, the EGFR adaptor protein complex comprising the growth factor receptor-bound protein 2 (Grb2) and the son of sevenless (SOS) activates rat sarcoma virus (RAS) by conversion of guanosine diphosphate (GDP) to guanosine triphosphate (GTP) through its binding to phosphorylated tyrosine residues. Once RAS is activated, a kinase cascade includes mitogen-activated protein kinase kinase kinase-Raf (MAPKKK), mitogen-activated protein kinase kinase-MEK (MAPKK), MAPK and extracellular signal −regulated kinase (ERK) are initiated through phosphorylation (11). It has been reported that ERK signaling pathway regulates cell proliferation, differentiation, and survival. Dysregulated EGFR/MAPK signaling pathway has been reported in a variety of human cancers mainly because it can lead to malignant transformation and tumor progression through increased cell proliferation, prolonged survival, angiogenesis, anti-apoptosis, invasion, and metastasis (12). Previous studies have found that EGFR/MAPK signaling pathway was directly related to the CRC oncogenic processes and played crucial roles in CRC tumor growth and disease progression (13). Therefore, this pathway and its downstream signaling cascades have been reported as targets for CRC therapeutic intervention (14, 15).

Wnt/β-Catenin Pathway

It is known that all 19 glycoproteins from the Wnt family play regulatory roles in many developmental and carcinogenesis processes such as cell proliferation, migration, and division. In addition, Wnt/β-catenin signaling plays important role in tissue maintenance and hair, skin, and intestine regeneration. Mutations of this signaling pathway are frequently observed in sCRC. When the Wnt ligand is secreted and accumulated, it binds to its Frizzled (Fz) receptors. Then, the multifunctional glycogen synthase kinase (GSK)-3β is inactivated and β-catenin, that acts as the E-cadherin cell-cell adhesion protein and as a transcriptional activator, is stabilized, accumulated, and translocated into the nucleus where it couples with the lymphoid enhancer factor (LEF) or T-cell transcription factor (TCF) and activates specific target genes involved in proliferation and transmission. In the absence of the Wnt signal, β-catenin is targeted by casein kinase 1 (CK1) and the APC-core proteins Axin-GSK-3β complex for ubiquitination and proteasomal degradation through its phosphorylation. Wnt signaling hyperactivation contributes to tumor cell proliferation and its activation is required for tumor growth in the advanced cancer stage, especially in CRC (10, 16).

PI3K Signaling Pathway

PI3K is an important intracellular lipid kinase that regulates a variety of cellular activities such as cell growth, proliferation, differentiation, migration and survival (17). PI3K is a heterodimeric molecule containing two subunits, p85 (a regulatory subunit) and p110 (a catalytic subunit). Protein kinase B (AKT/PKB), a serine/threonine-protein kinase (Ser/Thr kinase) and a downstream effector of PI3K, regulates the PI3K effects on tumor growth and progression (18). AKT phosphorylation was reported to be involved in cell proliferation and apoptosis inhibition from human CRC. Therefore, inhibition of PI3K/Akt pathway was used for treatment in many cancers (19). PI3K is activated upon ligand binding to receptor tyrosine kinases (RTK). Then, activated PI3K phosphorylates phosphatidylinositol 4,5-bisphosphate (PIP2) to phosphatidylinositol 3,4,5-trisphosphate (PIP3). Next, PIP3 activates AKT upon its serine and threonine residues, resulting in cell proliferation and cell survival. AKT regulates downstream proteins such as the mammalian target of rapamycin (mTOR), which mediates cell cycle, proliferation, angiogenesis, protein translation, and growth and survival. Phosphatase and tensin homolog (PTEN), a tumor suppressor and a PI3K pathway downregulatory protein, dephosphorylates PIP3. This altered expression of the pathway is often observed in CRC which results in the continuous growth of cells and leads to cancer. Overall, PI3K signaling pathway was reported to play an oncogenic role in the initiation and development of CRC.

TGF-β Signaling Pathway

TGF-β signaling pathway is known to be involved in cell proliferation, growth, differentiation, division, migration and adhesion. TGF-β signaling is initiated upon its ligand binding to its receptors where these 2 heterodimer receptors group together to form a complex through receptor dimerization. Next, the kinase domain of these receptors is activated by phosphorylation and the downstream transcription factors, SMAD proteins, are further activated. Specifically, SMAD2 and SMAD3 are activated by forming phosphorylated heterodimers and this heterodimer complex binds to SMAD4 to form a heterotrimer. Then, the heterotrimers translocate into the nucleus to bind to TGF-β target genes and to regulate the transcription. Recent studies have

reported that TGF-β, as a tumor suppressor, mediates cell division, proliferation, apoptosis and differentiation in colon epithelial cells (20). TGF−β is lost in CRC cells from early stages, thereby growth inhibition resistance is often observed. Whereas, in CRC late stages, the expression of TGF-β expression is increased leading to epithelia-to-mesenchymal transition (EMT). As a result, the normal cellular immune response was decreased due to the increased invasion and cell migration. TGF-β can also induce EMT *via* a SMAD4 independent pathway, through the Ras homolog family member A (RhoA) signaling pathway (21).

Notch Signaling Pathway

The Notch signaling pathway is a highly conserved intercellular pathway that regulates cell development, differentiation, proliferation, growth and apoptosis (22). The notch signaling pathway possesses 4 types of notch receptors (Notch 1-4) and 2 types of ligands (the Jagged protein family, JAG 1 and 2, and the Delta-like protein family, DLL 1, 3, and 4). The Notch receptors are transmembrane proteins containing both extracellular and intracellular domains, and Notch ligands are the single-pass transmembrane proteins containing EGF-like repeats (23). Notch signaling is initiated when Notch ligands are activated through ubiquitination by a mind bomb protein (MIB). Then, the activated ligand binds to the extracellular component of the Notch receptor and the extracellular domain of the notch receptor is cleaved by a disintegrin and metalloproteinase (ADAM protease). Subsequently, Notch intracellular domain (NICD) is cleaved by γ-secretase, causing it to dissociate from the transmembrane domain of its receptor. Next, the free NICD translocates into the nucleus and binds to the CSL (CBF-1/suppressor hairless/LAG1) transcription factor, forming a complex with co-activators MAML (mastermind-like proteins) and a histone acetylase, p300. The p300 and the histone acetyltransferase (HAT) cause the activation of transcription factors and the transcription of notch-target genes (24, 25). Previous studies have found that the Notch receptors, Notch ligands and some downstream Notch signaling targets are overexpressed in CRC (26). A recent study has reported that Notch signaling enhanced CRC severity by regulating the cell cycle and apoptosis of p21 and p53 upregulated modulator of apoptosis (PUMA) genes (27). Therefore, inhibition of Notch signaling could be one potential treatment for CRC patients.

NF-κB Signaling Pathway

NF-κB is a heterodimer protein, containing 2 subunits p65 and p50 which are indispensable for NF-κB activation and nuclear translocation. NF-κB family consists of five transcription factors including Rel proto-oncogene (Rel)A/p65, RelB, c-Rel, NF-κB1 (p50/p105) and NF-κB2 (p52/p100), which are involved in several biological processes such as cell development, differentiation, cell cycle, and migration. These members function as heterodimers with interrelated arms of the NF-κB pathway (28, 29). Extracellular factors such as growth factors, virus, cytokines, lipopolysaccharides (LPS), Toll-like receptor (TLR), and T/B cell receptor bind to their specific ligands resulting in an upregulation of the IκB kinase (IKK) complex. The IKK complex phosphorylates IκB which binds to p65/p50 dimers. The phosphorylated IκB is subsequently degraded by the ubiquitin-proteasome, allowing for the activation of NF-κB. Activated NF-κB is translocated to the nucleus, triggering downstream genes expression to promote CRC initiation and progression (29). On the other hand, the NF-κB pathway is also activated by ligands such as the cluster of differentiation 40 ligand (CD40L), B-cell activating factor (BAFF), receptor activator of NF-κB ligand (RANKL), lymphotoxin-β receptor (LTBR) and RelB/p100 subunits. IKKα homodimers and NF-κB-inducing kinase (NIK) are also included (30). Upon NIK activation, IKKα is further phosphorylated and induces the phosphorylation of p100, triggering the conversion of p100 to p52. The RelB/p52 dimer translocates to the nucleus to promote gene transcription. Previous studies found that NF-κB signaling is extensively implicated in CRC progression and plays important role in malignancy development in multiple stages of CRC (29). It was reported that NF-κB contributes to CRC cell growth, anchorage-independent growth and cell migration (31). Collectively, the role of NF-κB plays in CRC progression makes it's a viable target for CRC treatment.

CRC Microenvironment Modulation

Increasing evidence suggests that tumor progression and recurrence are not only regulated by genetic changes of tumor cells but also by tumor microenvironment (TME). TME, composed of tumor cells, stromal cells, immune cells, and extracellular matrix which surround tumor cells, is a complex system that is involved with tumor growth and development. Metastasis formation is a multistep process that promotes transformed cells to get into the bloodstream, deposited to the target organs through microvasculature circulation, and ultimately survive and grow in a foreign tissue. The immune system, as the immunosurveillance, is responsible for destroying most of the metastatic cells. With the communication of tumor cells and the cellular compartment, new cells such as inflammatory cells and immune cells are recruited into the TME, resulting in altered metabolism of surrounding stroma, and interrupted anti-tumor effect of the immune systems (32). It is known that tumor cells and TME cells can also program immune cells into tumor−tolerant or tumor−promoting phenotypes. Interleukin-6 (IL-6) is a common cytokine involved in TME and its expression is significantly elevated during CRC progression from occurrence to development. Various cells, such as tumor-associated macrophages, fibroblasts, granulocytes, dendritic cells, lymphocytes, and CRC cells are all sources of IL-6 in the TME. One study showed that tumor-associated macrophage-derived IL-6 activates the Janus kinase (JAK) 2/signal transducer and activator of transcription (STAT) 3 axis to modulate cell migration and invasion in CRC (33). Studies have also shown that IL-6 activates autophagy through the IL-6/JAK2/Beclin-1 pathway and promotes chemotherapy resistance in CRC (34).

Metastatic CRC tumors with MSI, often associated with genetic hypermutability, produce many neoantigens on the major histocompatibility complex (MHC) of antigen-presenting cells

and serve as a foreigner recognized by T cells (35). Thus, the TME of CRC tumors with MSI is abundant with tumor-infiltrating lymphocytes (TILs) and the adaptive immune system plays a significant role in tumor progression suppression. Then, the strongly activated immune cells provoke the expression of immune-checkpoint receptors and ligands, such as cell surface protein programmed death-1 (PD-1) and cytotoxic T-lymphocyte-associated protein 4 (CTLA4), and transmembrane protein programmed death-ligand 1(PD-L1) on tumor cells, TILs, regulatory T (Treg) cells and tumor-associated macrophages. Therefore, as reported, patients diagnosed with metastatic CRC tumors with MSI are responsive to PD-1 blockade therapy. However, the frequency of MSI-CRC in stage IV is ~5% (36) and the majority of metastatic CRC tumors with microsatellite stable (MSS) were found to be a lower response to PD-1/PD-L1 or CTLA4 therapy (37, 38). This could be explained that CRC tumors with MSS have fewer tumor mutations and neoantigens and are lack infiltrating immune effector cells. All these factors promote tumor evasion from adaptive immunity to immune resistance against immune checkpoint therapy. Recent studies reported that in metastatic CRC tumors, a higher immune score, quantification of T cells (CD3) and cytotoxic T cells (CD8), positively correlates with a decreased metastasis (39) and can also predict the overall prolonged survival rate in patients with metastatic CRC (40).

Most recently, Osman et al. have found that T cell factor-1 (TCF-1) could control distinct clusters of Treg functions by regulating gene expression in Treg, inflammation and severity in CRC. TCF-1-deficient Treg cells strongly suppress T cell proliferation and CD8 T-cell cytotoxicity, leading to more severe and aggressive CRC (41). Although multiple transcription factors have already been well studied before this study, this is the first time that the link between TCF-1 and CRC was explored, and this pathway could help future drug development for CRC prevention or improve response to therapy.

Moreover, Cancer-associated fibroblasts (CAFs) or macrophages (CAMs) synergize the production of reactive oxygen species (ROS) which helps the tumor cells escape from the immune surveillance system (42). It is known that cancer cells can transform fibroblasts located at metastatic sites into CAFs, thus promoting tumor growth and metastasis by producing growth factors and ECM degrading proteases. Interestingly, in CRC, the release of TGF−β is correlated to redox control of TME by the activation of MAPK or ERK-mediated SMAD 2 phosphorylation, which further stimulates CAFs to secrete IL−11 and strengthen the survival ability of metastatic cells (43). CAFs have been identified as an important source of IL-6 recently and IL-6 mediated STAT3 activation in CAFs facilitates CRC tumor development (44).

What's more, SHP2, an oncogenic tyrosine phosphatase and a major downstream signaling molecule required for the PD-1 immune checkpoint pathway, was defined to play essential roles in all cell types of TME from mouse CRC models by single-cell sequencing technology. SHP2 modulates tumor immunosuppression by negatively regulating type I interferon signaling and allosteric inhibition of SHP2 remolds the anti-tumor TME in CRC patients, indicating SHP2 is a promising target for CRC immunotherapy (45).

In summary, understanding the relationship between CRC tumors progression and microenvironment modulation could be fundamental in developing novel therapeutic strategies for a better response on CRC patients.

CRC Epigenetic Changes

CRC progression from adenoma to adenocarcinoma is both affected by genetic and epigenetic alternations. Epigenetics is defined as heritable alterations in gene expression without DNA sequence changes, including DNA methylation, histone modification, chromatin remodeling, noncoding RNA, and microRNAs. Epigenetic disruption is a common hallmark of CRC (46). Among the above epigenetic mechanisms, DNA promoter methylation and histone modifications have gained particular interest in CRC studies because gene promoter hypermethylation transcriptionally silences the tumor suppressor genes (47) and histone modification regulates gene expression directly or by interacting with DNA methylation (48). During CRC carcinogenesis, DNA methylation typically occurs in CpG islands, characterized as the covalent modification of DNA with a methyl group (CH3) at the C5 position of the cytosine ring by DNA methyltransferases (DNMTs), generating 5-methylcytosine and this represents the most extensively studied epigenetic marks. For example, silencing of E−cadherin caused by hypermethylation results in decreased cell-cell adhesion, tumor progression and increased invasion in CRC (49).

As mentioned above, in addition to DNA methylation regulating gene expression levels, posttranslational covalent modification of histone tails is another fundamental epigenetic modification in regulating chromatin state and gene expression in human tumors. Most of the studies have focused on histone (de) acetylation, catalyzed by histone acetyltransferases (HATs) or histone deacetylases (HDACs), and methylation of lysine and arginine residues within histone tails in CRC. Histones are composed of core histones and linker histones. Specifically, the core histones consist of histones H2A, H2B, H3, and H4, and a pair of each four core histones are formed into an octamer called nucleosomes, which are interacted with other nuclear proteins to form chromatin. And the linker histones, the H1 family, localized on the entry and exit sites of the DNA to maintain its correct wrapping with core histones. Several researchers reported that global hypoacetylation in H3 and H4 lysine is often associated with decreased expression of tumor suppressors and metastasis suppressors in cell lines and primary tumors from CRC (50). It has been found that increased HDACs expression is associated with a shorter survival time of CRC patients (51). Recent studies suggested that epigenetic regulators induced transcriptional plasticity is associated with chemoresistance in CRC and these epigenetic alterations are reversible, thus providing novel opportunities for CRC treatment (52–55).

In addition, long non-coding RNAs (lncRNAs) and microRNAs (miRNAs) also play important roles in regulating signaling pathways relevant to colorectal cancer (CRC). MiRNAs function at the posttranscriptional level by regulating specific individual target mRNAs, or serve as general regulators of gene

expression, simultaneously mediating hundreds of genes expression. Many studies have identified different miRNAs expression levels between neoplastic tissues and tumor-adjacent normal tissues in CRC (56, 57). MiRNAs can act both as oncogenes or tumor suppressors, depending not only on their altered pathways but also on the primary location, such as colon or rectal cancer. Specifically, miRNA-9 (58) and miRNA-101 (59) serve as tumor suppressors in CRC by suppressing colon cancer cell migration. miRNA-200 (60), miRNA-17 (61) and miR-141 (62) are all well-known oncogenes in CRC acting by inhibiting different tumor suppressor genes or promoting cancer cells proliferation. Moreover, it was reported that overexpression of miRNA-21 was correlated with the 5-Fluorouracil chemotherapeutic drug resistance in CRC and miRNA-21 reduces G2/M arrest and apoptosis by downregulating the MSH proteins. Thus, miRNA-21 could be a potential therapeutic marker in CRC (63). Despite several miRNAs having shown great value as biomarkers for disease detection (64), progression (65), and prognosis (66) in CRC, there still are several practical problems for miRNA acting as biomarkers. For example, more sensitive detection methods and lower detection costs are required (67). Moreover, miRNAs are usually not specific to one type of cancer. For example, miRNA-155 decelerates CRC metastasis and progression (68), while it serves as a potential biomarker for cervical cancer and breast cancer (69, 70). LncRNAs are involved in many CRC-related signaling pathways such as the Wnt/β-catenin, EGFR, and TGF-β, thus affecting all pathophysiological steps in CRC carcinogenesis, progression, and metastasis (71).

Overall, epigenetic changes of CRC are of great significance to early diagnosis and prognosis evaluation, providing a new thought for the CRC treatment.

CRC and Inflammatory Bowel Disease (IBD)

Emerging evidence indicates that IBD is associated with an increased incidence of CRC development. Unlike common sCRC, IBD-CRC initiates and drives tumorigenesis from a different mechanism (72). The tumor tissues of IBD-CRC patients present less frequent somatic mutations of APC and KRAS, while p53 genomic alterations are more frequent and detected earlier during tumor progression, compared to sCRC (73–75). It has been reported that chronic inflammation in IBD promotes aberrant DNA methylation, which in turn facilitates tumor development (76). Progressively increased percentage of methylated genes in the Wnt/β-catenin pathway was observed from normal colon samples to IBD to IBD-CRC, suggesting their potential role during CRC development (75).

As previously described, tumor-associated macrophages are important immune cells in TME, and they might also play critical roles in IBD-CRC progression. It has been found that Wnt5a, a protein from the Wnt family, stimulates M2 polarization of tumor-associated macrophages *via* IL-10 to promote CRC progression (77). Thus, the Wnt/β-catenin signaling pathway can significantly impact inflammation and the IBD-CRC onset. In addition, altered M2 macrophage polarization resulting in delayed tumor progression was reported in a mouse IBD-CRC model recently (78). It is known that the two most well studies proinflammatory pathways in IBD-CRC, NF-κB and IL-6/STAT3 signaling pathways, are dysregulated and thus promote IBD-CRC progression (79). Hence, therapies against specific inflammatory cytokines involved in tumorigenesis of IBD-CRC could provide a novel approach to prevent CRC tumor initiation or progression.

CRC Biomarkers

CRC Biomarkers, derived from a patients' tissue, blood or stool samples, play crucial roles in the early diagnosis and prognostic stratification of the disease under targeted CRC treatment (30). Based on clinical criteria, CRC biomarkers can be divided into two groups: diagnostic biomarkers (for detection or confirmation of the presence of a disease) and clinical biomarkers (for prediction of patients' response to a specific treatment or their prognosis).

CRC Diagnostic Biomarkers

It has been reported that CRC cells consistently express cytokeratin 20 and CDX-2 (an intestinal epithelia-specific nuclear transcription factor), but cytokeratin 7 expression is generally negative, therefore, these three markers can serve as the diagnostic biomarkers for CRC (80–82). Several blood-based biomarkers, such as cancer antigen 19-9, serum tissue polypeptide-specific antigen (TPS) and tissue polypeptide antigen (TPA), cytokeratin 8, 18 and 19, as well as Kininogen-1 (KNG1) were all identified as potentially useful biomarkers for both early detection and prognostic purposes in CRC (83, 84). Besides peripheral blood, cell-free DNA (cfDNA) is also used to determine cellular apoptosis in patients from CRC (85). Stool-based testing, for example, hemoglobin testing, DNA and RNA-based testing and miRNA testing have also been determined as feasible biomarkers for CRC (86–88). Researchers also reported that gene expression and metabolomic profiles of urine and tissue samples from CRC-bearing mice and CRC patients revealed metabolites associated with specific metabolic changes can indicate CRC development in early-stage and these urine and tissue biomarkers could be used in the early detection of CRC (89). Recently, a single protein marker, tissue inhibitor of metalloproteinase-1 (TIMP-1) was found to be a useful non-invasive screening marker for clinical CRC as it exhibits a potential diagnostic value with around 65% sensitivity and 95% specificity for CRC (90). What's more, increased levels of insulin-like growth factor-binding protein 2 (IGFBP2) and pyruvate kinase (PKM2) have been revealed in CRC, appearing as diagnostic tools for early detection and screening of CRC (91).

CRC Prognostic Biomarkers

A CRC prognostic biomarker is defined as a marker that can be used to provide information about the outcome in CRC. Currently, the CRC staging is guided by the tumor (tumor invasion depth), node (nodal involvement) and metastasis (TNM) system. However, the prognosis outcome can be different among patients in the same disease stage. Sometimes, patients at early stages may exhibit poorer outcomes compared to patients at latter stages since CRC is a complex process with a

combination of clinical and pathological variables (92). Carcinoembryonic antigen (CEA), a glycoprotein highly expressed in colorectal malignancies, is the main prognostic blood-based biomarker widely used in clinical. The elevated level of CEA positively correlates with cancer progression and indicates CRC recurrence after surgical resection. However, CEA is not specific to CRC as increased CEA levels were also observed in other complications, such as inflammatory bowel disease, hepatic metastasis, and pancreatitis (93–95). Therefore, additional prognostic biomarkers are urgently needed for CRC patients' management and follow-up. A recent study has demonstrated that collagen proteins could be promising biomarkers for CRC metastasis through a mass spectrum-based proteomic approach, as 19 of 22 collagen alpha chains were found to be upregulated in CRC liver metastasis tissue compared to healthy adjacent liver. The upregulation of collagen type XII in the metastatic tissue was confirmed by immunohistochemistry (96). Interestingly, some studies reported that a urinary prostaglandin metabolite PGE-M might be an interesting CRC biomarker because PGE-M plays an important role in the regulation of cyclooxygenase-2 effects in CRC and elevated levels of PGE-M is associated with advanced adenomas and increased risk of CRC (97). Lymph node involvement results in poor prognosis, therefore, non-invasive protein prognostic biomarkers used for nodal status determination are urgently needed. Recently, three tissue-based protein biomarkers, FXYD3, S100A11 and GSTM3 were identified as useful markers of regional lymph node metastasis in CRC *via* a proteomic approach (98). Similarly, MX1 from CRC tissue of lymph node was also identified as a protein biomarker for predicting regional lymph node metastasis (99). Recurrence detection is most concerned for CRC patients after surgery. After surgery, around 30-40% of patients showed distant metastasis or locoregional recurrence (100). The expression of Maspin has been recently identified as a marker for early recurrence in stage IV CRC and late recurrence after surgery for CRC liver metastasis (101).

CRC Predictive Biomarkers

A CRC predictive biomarker is used to indicate the response of a specific treatment and is crucial for the management of CRC patients. Numerous numbers of immunotherapy, chemotherapy and targeted therapies make it necessary to discover important biomarkers for treatment response and monitoring (102, 103). Researchers found that poly(C)-binding protein 1 (PCBP1) expression was significantly elevated in oxaliplatin resistance patients than in responsive patients, suggesting that PCBP1 is a protein predictive marker of oxaliplatin resistance in CRCs (104). Katsila et al. evaluated the response to EGFR targeted therapies in plasma from patients with metastatic CRC. It was observed that plasma level of phosphorylated-EGFR (pEGFR) was correlated with sensitivity to cetuximab therapy, suggesting that circulating pEGFR is a potential predictive treatment-response biomarker (105). The response to tyrosine kinase-targeted therapies was also evaluated by McKinley et al. through a global phosphotyrosine proteomics analysis of patients with metastatic CRC treated with dasatinib, an effective inhibitor of the Src family of tyrosine kinases with significant anti-tumor effects (106). It was found that PKCdelta is a marker of responsiveness of Src inhibition in CRC cells lines, indicating that PKCdelta could be a useful biomarker for evaluation response to dasatinib in CRC. In general, the predictive biomarkers have the same problem of poor translation to clinical use as diagnostic biomarkers and further validation of clinical studies are needed before it can be translated into useful routine practice.

Liquid Biopsy in CRC

Recent research has focused on diverse biomarkers including circulating tumor cells (CTCs), circulating tumor DNAs (ctDNAs), circulating tumor exosomes, and circulating tumor RNAs (such as miRNAs) (107). Therefore, the concept of liquid biopsy by using these circulating biomarkers to detect tumors released from primary to metastatic sites is generated (108). Liquid biopsy has multiple advantages in terms of noninvasiveness, fast, and easy to be sampling, compared to solid biopsy. The use of CTCs in gastrointestinal cancers showed promising results in prognostic stratification, therapeutic implications, and early diagnosis (109, 110). Recently, ExoScreen technique was used for profiling exosomes such as CD147 and CD 9 in serum from CRC patients but not in healthy individuals (110). The amount of ctDNAs was also reported to be increased progressively from early stage to metastatic CRC (111). In addition to CTCs, ctDNAs, and exosomes, ctRNAs, specifically, miRNAs, are also used as CRC markers (108, 110). The application of liquid biopsy in early diagnosis, screening, and prognosis for CRC patients in clinical practice provides a new strategy for treatment guidance and post-treatment surveillance.

Thus, early diagnosis of the disease, early surgical resection and effective response of a specific treatment always offer the best chance of cure. However, accurate, and consistent protein biomarkers for CRC use are still lacking. Therefore, identification, validation, and translation of new diagnostic, prognostic, and predictive biomarkers are important to fill the presented gaps in our knowledge.

OPPORTUNITIES FOR CRC TREATMENT

Treatments of CRC include surgical resection, chemotherapy, targeted therapy, immunotherapy, gene therapy and combination therapies.

Chemotherapeutic intervention coupled with surgery is the traditional treatment for survival rate enhancement of metastatic CRC. For decades, commonly used CRC chemotherapeutic agents include 5-Fluorouracil, Irinotecan, Oxaliplatin, Calcium folinate, Capecitabine, S-1 (Tegafur/gimeracil/oteracil), and TAS-102 (Trifluridine/Tipiracil). CRC chemotherapies are usually combinations of several of those chemotherapeutic agents, such as FOLFOX (5-Fluorouracil, Calcium folinate, Oxaliplatin); FOLFIRI (5-Fluorouracil, Calcium folinate, Irinotecan); CAPEOX (Capecitabine, Oxaliplatin); FOLFOXIRI

(5-Fluorouracil, Calcium folinate, Irinotecan, Oxaliplatin) (112).

Targeted therapies can be divided into two major categories: small molecule signal transduction inhibitors and monoclonal antibodies. Small molecule inhibitors can eliminate cancer cells by specifically blocking the signaling pathways necessary for tumor growth and proliferation and they can be administered orally, with high specificity and short half-life. Monoclonal antibodies, with high specificity and long half-life, recognize tumor cells through the specific antigen and antibody interaction, which are mostly administered intravenously, without hepatic metabolism. Genomic profiling for somatic mutations detection is very important because it identifies which treatments may be effective for CRC patients. Several molecular biomarkers such as KRAS mutations, BRAF mutations, and deficient MMR/MSI are commonly observed in CRC.

KRAS, a downstream pathway of EGFR, is the most observed mutation in CRC. Therefore, inhibition of EGFR can suppress the activation of KRAS and its downstream pathways. Cetuximab (Epitol), a monoclonal antibody specifically used for blocking EGFR, is one of the most representative drugs of targeted therapy and is currently approved for first-line monotherapy in CRC patients (113). However, CRC patients with KRAS mutation are very unlikely to benefit from anti-EGFR therapy. Eventually, its downstream pathways such as BRAF, MEK and ERK were continuously activated by KRAS, resulting in tumor cells proliferation and metastasis. Thus, CRC patients with KRAS mutations need to be treated with other effective therapies. Cetuximab can also be used in combination with Irinotecan, 5-Fluorouracil, and calcium folinate in the first-line treatment regimen for CRC. It was reported that the overall survival (OS) of CRC patients with wild type KRAS under Cetuximab and FOLFIRI combination treatment was improved 8.2 months compared with patients treated with FOLFIRI alone in the CRYSTAL study (114, 115). EGFR can initiate cell proliferation downstream pathway in addition to activation of KRAS. Particularly, most patients with advanced CRC are accompanied by EGFR overexpression and metastasis in the liver and lung, resulting in poor prognosis outcomes with first- and second-line therapies. Currently, clinical studies have confirmed the beneficial effects of third-line treatment of metastatic CRC with Cetuximab in Australia and Europe (116, 117).

Angiogenesis plays an important role in CRC progression and vascular endothelial growth factor (VEGF) is a major angiogenic factor in CRC (118). Increased VEGF levels were significantly correlated with CRC progression and metastasis (119). Bevacizumab, a humanized IgG monoclonal antibody, was approved by FDA as the first VEGF-targeted agent for metastatic CRC (120) and it is still the only FDA-approved VEGF-targeted agent used as a first- and second-line for CRC treatment (121). What's more, various approved novel anti-VEGF receptor (VEGFR) agents such as Aflibercept (a VEGFR-1 and VEGFR-2 extracellular domain recombinant fusion protein) and Ramucirumab (a fully humanized monoclonal VEGFR-2-targeted IgG antibody) remained as second-line treatment of metastatic CRC. This is mainly because the combination of Aflibercept or Ramucirumab with FOLFOX regimen did not show beneficial results in progression-free survival (PFS) or response rate (122, 123). Other agents, such as various tyrosine kinase inhibitors, including Regorafenib (124) and Fruquintinib (125) are recommended for chemotherapy against refractory metastatic CRC.

Growing evidence indicates that the hepatocyte growth factor (HGF) and its tyrosine kinase receptor, mesenchymal-epithelial transition factor (c-MET) pathway plays a crucial role in tumor invasive growth and metastasis of CRC (126, 127). MET amplification and HGF/c-MET overexpression have been reported as causing factors for CRC carcinogenesis. This aberrant signaling axis triggers a series of signaling cascades activation, including EGFR/MAPK, PI3K/AKT, and JAK/STAT pathways, and is associated with dysregulated cell proliferation, apoptosis, and poor prognosis (121). Thus, various newly developed monoclonal antibodies, small molecules or miRNAs targeting HGF/c-MET have emerged. Recently, a few monoclonal HGF neutralizing antibodies have been investigated under clinical trials. Rilotumumab, a fully humanized monoclonal antibody, has demonstrated median prolonged PFS and OS in patients with MET overexpression using Rilotumumab in combination with ECX (epirubicin, cisplatin, and capecitabine) compared with those in the placebo plus ECX arm (128). There are also several novel MET antibodies, like ABT-700 and Emibetuzumab, that have been used in clinical trials (121). Small molecule c-Met kinase inhibitors target activation sites of the receptor inside the cells *via* inhibiting phosphorylation and its downstream signaling pathway. PHA-665752, c-Met inhibitor, with the combination of cetuximab suppressed more efficiently the CRC cell growth *in vitro* and *in vivo* compared with either single agent treatment (129). In addition, miRNA, such as miR-206, has been identified to be able to affect the c-MET/HGF signaling pathway *via* inhibiting CRC cells proliferation and invasion (130).

In CRC, in addition to common mutations in KRAS and BRAF, mutations in human epidermal growth factor receptor (HER) 2 are also present. Indeed, HER2 amplification has been detected in approximately 2-3% of CRC patients. However, there was no approved targeted therapy in HER2-positive metastatic CRC patients. Most recently, an open-label, multicenter, phase 2 study confirms the role of Enhertu (DS-8201, an antibody-drug conjugate targeting HER2) in HER2 overexpressing CRC. It has demonstrated that Enhertu showed promising activity in terms of objective response rate, disease control rate, PFS and OS with long-term follow-up in CRC patients with HER2 expressing which brings new hope to the majority of these patients (DS8201-A-J203, NCT03384940).

Immunotherapy, as an innovative type of cancer treatment, fights tumors by activating the body's immune system without direct attacking tumor cells. Immune checkpoint inhibitors exhibit an immense breakthrough in cancer therapeutics and the most representative ones are PD-1/PD-L1 inhibitors and CTLA-4 inhibitors. Some of these immune checkpoint inhibitors have been approved for CRC treatment. For example, nivolumab and pembrolizumab, the two most promising PD-1 inhibitors,

have been approved by FDA for the second-line treatment of metastatic CRC patients with high levels of MSI and deficient MMR in 2017 (131). However, a recent clinical study reported limited response with antibodies blocking PD1 and CTLA4 in CRC patients with MMR-MSI mutations (132). Therefore, other alternative approaches of immune modulations are required to enhance the recruitment of immune cells to the tumor, such as combination therapy. In addition to pro-proliferative effects on tumors, activation of the RAS/MAPK/MEK pathway has been associated with decreased T cell infiltration into CRC tumors and MEK is a transducer of this signaling cascade and plays a crucial role in CRC development and progression. Thus, several clinical trials with the combination of MEK inhibitors with PD-1/PD-L1 and chemotherapies are ongoing.

Gene therapy has shown remarkable efficacy in recent clinical studies (133). Lack of efficient and reliable delivery methods is the most common challenge for gene therapy, although retrovirus delivery systems are the most used. Recently, nanotechnology-based gene therapy has been approved in the clinic because it can be well-controlled (134). A group found that cancer-targeted gene therapy pigment epithelium-derived factor DNA liposomes (R-LP/PEDF) demonstrated enhanced inhibitory effects on migration, invasion, and pro-apoptosis of CRC cells and without any toxic pathological changes in the vital organs of mice that received the R-LP/PEDF treatment (135). What's more, a nano vector made from ginger-derived lipids was reported that can serve as a delivery platform for the therapeutic agent doxorubicin to treat CRC (136). This study expands our current understanding of drug-delivery systems and could be used as a foundation for a less toxic drug-delivery approach.

In recent years, proteolysis targeting chimeric (PROTAC) technology that degrades endogenous disease-related proteins through the ubiquitin-proteasome system has achieved remarkable efficacy in tumor growth inhibition and is also a promising strategy for the drug-resistant target. As discussed previously, KRAS is a well-known "undruggable" target in CRC due to its lack of deep pockets and is associated with poor prognosis and drug resistance. It has been reported that potent KRAS-specific degraders can target tumors with mutant KRAS (137). A research group led by Professor Craig M. Crews, a pioneer of PROTACs technology, firstly reported the development of endogenous KRASG12C degrader LC-2, where over half of KRAS mutant lung cancer and 3% of CRC express KRASG12C. It was demonstrated that LC-2 rapidly and consistently degraded KRASG12C, leading to inhibition of MAPK signaling. Suggesting that PROTACs-mediated degradation is a feasible strategy to attenuate oncogenic KRAS levels and downstream signaling in cancer cells (138). Therefore, PROTAC approaches can broaden drug target scope, overcome drug resistance, enhance target selectivity and this technology could be a key therapeutic modality that provides innovative treatment options for cancer patients.

It should be noted that patients with colon and rectal cancer are managed differently, and their epidemiology and clinical outcomes also exhibit different patterns (139). Zhang et al. recently reported that several genes can be used as biomarkers to identify colon cancer from rectal cancer based on the prediction of vector machine method algorithm and RNA-sequencing data, while additional research is required to support this finding (140). However, a study conducted by The Cancer Genome Atlas (TCGA) showed similar patterns of genetic alterations in the colon and rectal tissues from non-hypermutated tumors. There were almost indistinguishable differences in copy number, CIMP, mRNA and miRNA between the colon and rectal cancers from the above samples (141). A follow-up proteomics study of colon and rectal tumors analyzed previously by TCGA identified that CRC subtypes are similar to those detected by transcriptome analysis (142). The main difference between colon cancer and rectal cancer is the anatomical location, which determines the differences in their treatments modalities such as differences in surgical approaches, and preoperative and postoperative adjuvant therapies (radiotherapies). Drugs approved for colon and rectal cancer are identical according to their identical biology. Nevertheless, chemotherapies were used differently for different purposes and indications caused by their different anatomical location (143–145).

CONCLUSION

In summary, as discussed in this review, CRC represents a complex and heterogeneous group of disorders at molecular levels and signaling pathways, in which different patterns of genetic mutations and epigenetic alterations contribute to the onset and progression and are responsible for responding to the specific therapy. CRC results from the activation of multiple signaling pathways and cannot be targeted with a single treatment. Thus, a combination of conventional therapeutics with innovative inhibitors targeting different dysregulated pathways is urgently needed. A deeper understanding of CRC is required, and the efficiency of targeted therapies and the development of more efficient biomarkers provides an encouraging prospect for the future management of CRC. We believed that with the discovery of more novel targeted therapeutics, the disease burden of CRC can be decreased in the future.

AUTHOR CONTRIBUTIONS

ZH and MY wrote different sections of the manuscript. MY revised, wrote, and prepared the manuscript. All authors contributed to the article and approved the submitted version.

FUNDING

This work was supported by Natural Science Foundation of Liaoning Province (20170541001).

REFERENCES

1. Bray F, Ferlay J, Soerjomataram I, Siegel RL, Torre LA, Jemal A. Global Cancer Statistics 2018: GLOBOCAN Estimates of Incidence and Mortality Worldwide for 36 Cancers in 185 Countries. *CA: Cancer J Clin* (2018) 68(6):394–424. doi: 10.3322/caac.21492
2. Fleming M, Ravula S, Tatishchev SF, Wang HL. Colorectal Carcinoma: Pathologic Aspects. *J Gastrointestinal Oncol* (2012) 3(3):153–73. doi: 10.3978/j.issn.2078-6891.2012.030
3. Jasperson KW, Tuohy TM, Neklason DW, Burt RW. Hereditary and Familial Colon Cancer. *Gastroenterology* (2010) 138(6):2044–58. doi: 10.1053/j.gastro.2010.01.054
4. Keum N, Giovannucci E. Global Burden of Colorectal Cancer: Emerging Trends, Risk Factors and Prevention Strategies. *Nat Rev Gastroenterol Hepatol* (2019) 16(12):713–32. doi: 10.1038/s41575-019-0189-8
5. Olkinuora AP, Peltomäki PT, Aaltonen LA, Rajamäki K. From APC to the Genetics of Hereditary and Familial Colon Cancer Syndromes. *Hum Mol Genet* (2021) 30(R2):R206–24. doi: 10.1093/hmg/ddab208
6. Nguyen HT, Duong HQ. The Molecular Characteristics of Colorectal Cancer: Implications for Diagnosis and Therapy. *Oncol Lett* (2018) 16(1):9–18. doi: 10.3892/ol.2018.8679
7. Fearon ER. Molecular Genetics of Colorectal Cancer. *Annu Rev Pathol* (2011) 6:479–507. doi: 10.1146/annurev-pathol-011110-130235
8. Schmitt M, Greten FR. The Inflammatory Pathogenesis of Colorectal Cancer. *Nat Rev Immunol* (2021) 21(10):653–67. doi: 10.1038/s41577-021-00534-x
9. Papanikolaou A, Wang QS, Papanikolaou D, Whiteley HE, Rosenberg DW. Sequential and Morphological Analyses of Aberrant Crypt Foci Formation in Mice of Differing Susceptibility to Azoxymethane-Induced Colon Carcinogenesis. *Carcinogenesis* (2000) 21(8):1567–72. doi: 10.1093/carcin/21.8.1567
10. Koveitypour Z, Panahi F, Vakilian M, Peymani M, Seyed Forootan F, Nasr Esfahani MH, et al. Signaling Pathways Involved in Colorectal Cancer Progression. *Cell Biosci* (2019) 9:97. doi: 10.1186/s13578-019-0361-4
11. Ahmad R, Singh JK, Wunnava A, Al-Obeed O, Abdulla M, Srivastava SK. Emerging Trends in Colorectal Cancer: Dysregulated Signaling Pathways (Review). *Int J Mol Med* (2021) 47(3):1414. doi: 10.3892/ijmm.2021.4847
12. Barbosa R, Acevedo LA, Marmorstein R. The MEK/ERK Network as a Therapeutic Target in Human Cancer. *Mol Cancer Res MCR* (2021) 19 (3):361–74. doi: 10.1158/1541-7786.MCR-20-0687
13. Jeong WJ, Ro EJ, Choi KY. Interaction Between Wnt/β-Catenin and RAS-ERK Pathways and an Anti-Cancer Strategy *Via* Degradations of β-Catenin and RAS by Targeting the Wnt/β-Catenin Pathway. *NPJ Precis Oncol* (2018) 2 (1):5. doi: 10.1038/s41698-018-0049-y
14. Saletti P, Molinari F, De Dosso S, Frattini M. EGFR Signaling in Colorectal Cancer: A Clinical Perspective. *Gastrointestinal Cancer: Targets Ther* (2015) 5:21–38. doi: 10.2147/GICTT.S49002
15. Malki A, ElRuz RA, Gupta I, Allouch A, Vranic S, Al Moustafa AE. Molecular Mechanisms of Colon Cancer Progression and Metastasis: Recent Insights and Advancements. *Int J Mol Sci* (2020) 22(1):130. doi: 10.3390/ijms22010130
16. Świerczyński M, Szymaszkiewicz A, Fichna J, Zielińska M. New Insights Into Molecular Pathways in Colorectal Cancer: Adiponectin, Interleukin-6 and Opioid Signaling. *Biochim Biophys Acta Rev Cancer* (2021) 1875(1):188460. doi: 10.1016/j.bbcan.2020.188460
17. Narayanankutty A. PI3K/ Akt/ mTOR Pathway as a Therapeutic Target for Colorectal Cancer: A Review of Preclinical and Clinical Evidence. *Curr Drug Targets* (2019) 20(12):1217–26. doi: 10.2174/1389450120666190618123846
18. Kaya Temiz T, Altun A, Turgut N, Balcı E. Investigation of the Effects of Drugs Effective on PI3K-AKT Signaling Pathway in Colorectal Cancer Alone and in Combination. *Cumhuriyet Med J* (2014) 36(2):167–77. doi: 10.7197/1305-0028.33144
19. Castel P, Toska E, Engelman JA, Scaltriti M. The Present and Future of PI3K Inhibitors for Cancer Therapy. *Nat Cancer* (2021) 2(6):587–97. doi: 10.1038/s43018-021-00218-4
20. Jung B, Staudacher JJ, Beauchamp D. Transforming Growth Factor β Superfamily Signaling in Development of Colorectal Cancer. *Gastroenterology* (2017) 152(1):36–52. doi: 10.1053/j.gastro.2016.10.015
21. Levy L, Hill CS. Smad4 Dependency Defines Two Classes of Transforming Growth Factor {Beta} (TGF-{Beta}) Target Genes and Distinguishes TGF-{Beta}-Induced Epithelial-Mesenchymal Transition From Its Antiproliferative and Migratory Responses. *Mol Cell Biol* (2005) 25(18):8108–25. doi: 10.1128/MCB.25.18.8108-8125.2005
22. Previs RA, Coleman RL, Harris AL, Sood AK. Molecular Pathways: Translational and Therapeutic Implications of the Notch Signaling Pathway in Cancer. *Clin Cancer Res* (2015) 21(5):955–61. doi: 10.1158/1078-0432.CCR-14-0809
23. Vinson KE, George DC, Fender AW, Bertrand FE, Sigounas G. The Notch Pathway in Colorectal Cancer. *Int J Cancer* (2016) 138(8):1835–42. doi: 10.1002/ijc.29800
24. Borggrefe T, Oswald F. Setting the Stage for Notch: The Drosophila Su(H)-Hairless Repressor Complex. *PloS Biol* (2016) 14(7):e1002524. doi: 10.1371/journal.pbio.1002524
25. Carulli AJ, Keeley TM, Demitrack ES, Chung J, Maillard I, Samuelson LC. Notch Receptor Regulation of Intestinal Stem Cell Homeostasis and Crypt Regeneration. *Dev Biol* (2015) 402(1):98–108. doi: 10.1016/j.ydbio.2015.03.012
26. Tiwari A, Saraf S, Verma A, Panda PK, Jain SK. Novel Targeting Approaches and Signaling Pathways of Colorectal Cancer: An Insight. *World J Gastroenterol* (2018) 24(39):4428–35. doi: 10.3748/wjg.v24.i39.4428
27. Liao W, Li G, You Y, Wan H, Wu Q, Wang C, et al. Antitumor Activity of Notch–1 Inhibition in Human Colorectal Carcinoma Cells. *Oncol Rep* (2018) 39(3):1063–71. doi: 10.3892/or.2017.6176
28. Wong D, Teixeira A, Oikonomopoulos S, Humburg P, Lone IN, Saliba D, et al. Extensive Characterization of NF-κb Binding Uncovers Non-Canonical Motifs and Advances the Interpretation of Genetic Functional Traits. *Genome Biol* (2011) 12(7):R70. doi: 10.1186/gb-2011-12-7-r70
29. Soleimani A, Rahmani F, Ferns GA, Ryzhikov M, Avan A, Hassanian SM. Role of the NF-κb Signaling Pathway in the Pathogenesis of Colorectal Cancer. *Gene* (2020) 726:144132. doi: 10.1016/j.gene.2019.144132
30. Martin M, Sun M, Motolani A, Lu T. The Pivotal Player: Components of NF-κb Pathway as Promising Biomarkers in Colorectal Cancer. *Int J Mol Sci* (2021) 22(14):7429. doi: 10.3390/ijms22147429
31. Hartley AV, Wang B, Jiang G, Wei H, Sun M, Prabhu L, et al. Regulation of a PRMT5/NF-κb Axis by Phosphorylation of PRMT5 at Serine 15 in Colorectal Cancer. *Int J Mol Sci* (2020) 21(10):3684. doi: 10.3390/ijms21103684
32. Welch DR, Hurst DR. Defining the Hallmarks of Metastasis. *Cancer Res* (2019) 79(12):3011–27. doi: 10.1158/0008-5472.CAN-19-0458
33. Wei C, Yang C, Wang S, Shi D, Zhang C, Lin X, et al. Crosstalk Between Cancer Cells and Tumor Associated Macrophages Is Required for Mesenchymal Circulating Tumor Cell-Mediated Colorectal Cancer Metastasis. *Mol Cancer* (2019) 18(1):64. doi: 10.1186/s12943-019-0976-4
34. Hu F, Song D, Yan Y, Huang C, Shen C, Lan J, et al. IL-6 Regulates Autophagy and Chemotherapy Resistance by Promoting BECN1 Phosphorylation. *Nat Commun* (2021) 12(1):3651. doi: 10.1038/s41467-021-23923-1
35. Llosa NJ, Cruise M, Tam A, Wicks EC, Hechenbleikner EM, Taube JM, et al. The Vigorous Immune Microenvironment of Microsatellite Instable Colon Cancer Is Balanced by Multiple Counter-Inhibitory Checkpoints. *Cancer Discov* (2015) 5(1):43–51. doi: 10.1158/2159-8290.CD-14-0863
36. Ooki A, Shinozaki E, Yamaguchi K. Immunotherapy in Colorectal Cancer: Current and Future Strategies. *J Anus Rectum Colon* (2021) 5(1):11–24. doi: 10.23922/jarc.2020-064
37. Breakstone R. Colon Cancer and Immunotherapy-can We Go Beyond Microsatellite Instability? *Trans Gastroenterol Hepatol* (2021) 6:12. doi: 10.21037/tgh.2020.03.08
38. Kreidieh M, Mukherji D, Temraz S, Shamseddine A. Expanding the Scope of Immunotherapy in Colorectal Cancer: Current Clinical Approaches and Future Directions. *BioMed Res Int* (2020) 2020:9037217. doi: 10.1155/2020/9037217
39. Mlecnik B, Bindea G, Kirilovsky A, Angell HK, Obenauf AC, Tosolini M, et al. The Tumor Microenvironment and Immunoscore Are Critical Determinants of Dissemination to Distant Metastasis. *Sci Trans Med* (2016) 8 (327):327ra326. doi: 10.1126/scitranslmed.aad6352
40. Mlecnik B, Van den Eynde M, Bindea G, Church SE, Vasaturo A, Fredriksen T, et al. Comprehensive Intrametastatic Immune Quantification and Major Impact of Immunoscore on Survival. *J Natl Cancer Institute* (2018) 110(1):97–108. doi: 10.1093/jnci/djx123
41. Osman A, Yan B, Li Y, Pavelko KD, Quandt J, Saadalla A, et al. TCF-1 Controls T(reg) Cell Functions That Regulate Inflammation, CD8(+) T Cell

Cytotoxicity and Severity of Colon Cancer. *Nat Immunol* (2021) 22(9):1152–62. doi: 10.1038/s41590-021-00987-1
42. Giannoni E, Parri M, Chiarugi P. EMT and Oxidative Stress: A Bidirectional Interplay Affecting Tumor Malignancy. *Antioxid Redox Signaling* (2012) 16 (11):1248–63. doi: 10.1089/ars.2011.4280
43. Calon A, Espinet E, Palomo-Ponce S, Tauriello DV, Iglesias M, Céspedes MV, et al. Dependency of Colorectal Cancer on a TGF-β-Driven Program in Stromal Cells for Metastasis Initiation. *Cancer Cell* (2012) 22(5):571–84. doi: 10.1016/j.ccr.2012.08.013
44. Lin Y, He Z, Ye J, Liu Z, She X, Gao X, et al. Progress in Understanding the IL-6/STAT3 Pathway in Colorectal Cancer. *OncoTarg Ther* (2020) 13:13023–32. doi: 10.2147/OTT.S278013
45. Gao J, Wu Z, Zhao M, Zhang R, Li M, Sun D, et al. Allosteric Inhibition Reveals SHP2-Mediated Tumor Immunosuppression in Colon Cancer by Single-Cell Transcriptomics. *Acta Pharm Sin B* (2022) 12(1):149–66. doi: 10.1016/j.apsb.2021.08.006
46. Coppedè F. The Role of Epigenetics in Colorectal Cancer. *Expert Rev Gastroenterol Hepatol* (2014) 8(8):935–48. doi: 10.1586/17474124.2014.924397
47. Markowitz SD, Bertagnolli MM. Molecular Origins of Cancer: Molecular Basis of Colorectal Cancer. *N Engl J Med* (2009) 361(25):2449–60. doi: 10.1056/NEJMra0804588
48. Fraga MF, Ballestar E, Villar-Garea A, Boix-Chornet M, Espada J, Schotta G, et al. Loss of Acetylation at Lys16 and Trimethylation at Lys20 of Histone H4 Is a Common Hallmark of Human Cancer. *Nat Genet* (2005) 37(4):391–400. doi: 10.1038/ng1531
49. Garinis GA, Menounos PG, Spanakis NE, Papadopoulos K, Karavitis G, Parassi I, et al. Hypermethylation-Associated Transcriptional Silencing of E-Cadherin in Primary Sporadic Colorectal Carcinomas. *J Pathol* (2002) 198 (4):442–9. doi: 10.1002/path.1237
50. Gargalionis AN, Piperi C, Adamopoulos C, Papavassiliou AG. Histone Modifications as a Pathogenic Mechanism of Colorectal Tumorigenesis. *Int J Biochem Cell Biol* (2012) 44(8):1276–89. doi: 10.1016/j.biocel.2012.05.002
51. Weichert W, Röske A, Niesporek S, Noske A, Buckendahl AC, Dietel M, et al. Class I Histone Deacetylase Expression has Independent Prognostic Impact in Human Colorectal Cancer: Specific Role of Class I Histone Deacetylases *In Vitro* and *In Vivo*. *Clin Cancer Res* (2008) 14(6):1669–77. doi: 10.1158/1078-0432.CCR-07-0990
52. Esteller M. Epigenetics in Cancer. *N Engl J Med* (2008) 358(11):1148–59. doi: 10.1056/NEJMra072067
53. Shen H, Laird PW. Interplay Between the Cancer Genome and Epigenome. *Cell* (2013) 153(1):38–55. doi: 10.1016/j.cell.2013.03.008
54. Suvà ML, Riggi N, Bernstein BE. Epigenetic Reprogramming in Cancer. *Science (New York NY)* (2013) 339(6127):1567–70. doi: 10.1126/science.1230184
55. Dawson MA, Kouzarides T. Cancer Epigenetics: From Mechanism to Therapy. *Cell* (2012) 150(1):12–27. doi: 10.1016/j.cell.2012.06.013
56. Ma Y, Zhang P, Yang J, Liu Z, Yang Z, Qin H. Candidate microRNA Biomarkers in Human Colorectal Cancer: Systematic Review Profiling Studies and Experimental Validation. *Int J Cancer* (2012) 130(9):2077–87. doi: 10.1002/ijc.26232
57. Sampath SS, Venkatabalasubramanian S, Ramalingam S. Role of MicroRNAs in the Progression and Metastasis of Colon Cancer. *Endocrine Metab Immune Disord Drug Targets* (2021) 21(1):35–46. doi: 10.2174/1871530320666200825184924
58. Kim H, Kim T, Jaygal G, Woo J, Kim CJ, Baek MJ, et al. Downregulation of miR-9 Correlates With Poor Prognosis in Colorectal Cancer. *Pathol Res Pract* (2020) 216(8):153044. doi: 10.1016/j.prp.2020.153044
59. Huang Z, Wu X, Li J. miR-101 Suppresses Colon Cancer Cell Migration Through the Regulation of EZH2. *Rev Espanola Enfermedades Digestivas Organo Oficial La Sociedad Espanola Patol Digest* (2021) 113(4):255–60. doi: 10.17235/reed.2020.6800/2019
60. Carter JV, O'Brien SJ, Burton JF, Oxford BG, Stephen V, Hallion J, et al. The microRNA-200 Family Acts as an Oncogene in Colorectal Cancer by Inhibiting the Tumor Suppressor RASSF2. *Oncol Lett* (2019) 18(4):3994–4007. doi: 10.3892/ol.2019.10753
61. Knudsen KN, Nielsen BS, Lindebjerg J, Hansen TF, Holst R, Sørensen FB. microRNA-17 Is the Most Up-Regulated Member of the miR-17-92 Cluster During Early Colon Cancer Evolution. *PloS One* (2015) 10(10):e0140503. doi: 10.1371/journal.pone.0140503
62. Ding L, Yu LL, Han N, Zhang BT. miR-141 Promotes Colon Cancer Cell Proliferation by Inhibiting MAP2K4. *Oncol Lett* (2017) 13(3):1665–71. doi: 10.3892/ol.2017.5653
63. Valeri N, Gasparini P, Braconi C, Paone A, Lovat F, Fabbri M, et al. MicroRNA-21 Induces Resistance to 5-Fluorouracil by Down-Regulating Human DNA MutS Homolog 2 (Hmsh2). *Proc Natl Acad Sci USA* (2010) 107(49):21098–103. doi: 10.1073/pnas.1015541107
64. Wang S, Xiang J, Li Z, Lu S, Hu J, Gao X, et al. A Plasma microRNA Panel for Early Detection of Colorectal Cancer. *Int J Cancer* (2015) 136(1):152–61. doi: 10.1002/ijc.28136
65. Yue C, Chen J, Li Z, Li L, Chen J, Guo Y. microRNA-96 Promotes Occurrence and Progression of Colorectal Cancer *Via* Regulation of the Ampkα2-FTO-M6a/MYC Axis. *J Exp Clin Cancer Res CR* (2020) 39(1):240. doi: 10.1186/s13046-020-01731-7
66. Yuan Z, Baker K, Redman MW, Wang L, Adams SV, Yu M, et al. Dynamic Plasma microRNAs Are Biomarkers for Prognosis and Early Detection of Recurrence in Colorectal Cancer. *Br J Cancer* (2017) 117(8):1202–10. doi: 10.1038/bjc.2017.266
67. Liu HN, Liu TT, Wu H, Chen YJ, Tseng YJ, Yao C, et al. Serum microRNA Signatures and Metabolomics Have High Diagnostic Value in Colorectal Cancer Using Two Novel Methods. *Cancer Sci* (2018) 109(4):1185–94. doi: 10.1111/cas.13514
68. Liu J, Chen Z, Xiang J, Gu X. MicroRNA-155 Acts as a Tumor Suppressor in Colorectal Cancer by Targeting CTHRC1 *In Vitro*. *Oncol Lett* (2018) 15 (4):5561–8. doi: 10.3892/ol.2018.8069
69. Park S, Eom K, Kim J, Bang H, Wang HY, Ahn S, et al. MiR-9, miR-21, and miR-155 as Potential Biomarkers for HPV Positive and Negative Cervical Cancer. *BMC Cancer* (2017) 17(1):658. doi: 10.1186/s12885-017-3642-5
70. Zuo J, Yu Y, Zhu M, Jing W, Yu M, Chai H, et al. Inhibition of miR-155, a Therapeutic Target for Breast Cancer, Prevented in Cancer Stem Cell Formation. *Cancer Biomarkers Section A Dis Markers* (2018) 21(2):383–92. doi: 10.3233/CBM-170642
71. Luo J, Qu J, Wu DK, Lu ZL, Sun YS, Qu Q. Long Non-Coding RNAs: A Rising Biotarget in Colorectal Cancer. *Oncotarget* (2017) 8(13):22187–202. doi: 10.18632/oncotarget.14728
72. Baker AM, Cross W, Curtius K, Al Bakir I, Choi CR, Davis HL, et al. Evolutionary History of Human Colitis-Associated Colorectal Cancer. *Gut* (2019) 68(6):985–95. doi: 10.1136/gutjnl-2018-316191
73. Yaeger R, Shah MA, Miller VA, Kelsen JR, Wang K, Heins ZJ, et al. Genomic Alterations Observed in Colitis-Associated Cancers Are Distinct From Those Found in Sporadic Colorectal Cancers and Vary by Type of Inflammatory Bowel Disease. *Gastroenterology* (2016) 151(2):278–87.e276. doi: 10.1053/j.gastro.2016.04.001
74. Hirsch D, Wangsa D, Zhu YJ, Hu Y, Edelman DC, Meltzer PS, et al. Dynamics of Genome Alterations in Crohn's Disease-Associated Colorectal Carcinogenesis. *Clin Cancer Res* (2018) 24(20):4997–5011. doi: 10.1158/1078-0432.CCR-18-0630
75. Lucafò M, Curci D, Franzin M, Decorti G, Stocco G. Inflammatory Bowel Disease and Risk of Colorectal Cancer: An Overview From Pathophysiology to Pharmacological Prevention. *Front Pharmacol* (2021) 12:772101. doi: 10.3389/fphar.2021.772101
76. Somineni HK, Venkateswaran S, Kilaru V, Marigorta UM, Mo A, Okou DT, et al. Blood-Derived DNA Methylation Signatures of Crohn's Disease and Severity of Intestinal Inflammation. *Gastroenterology* (2019) 156(8):2254–2265.e2253. doi: 10.1053/j.gastro.2019.01.270
77. Liu Q, Yang C, Wang S, Shi D, Wei C, Song J, et al. Wnt5a-Induced M2 Polarization of Tumor-Associated Macrophages *Via* IL-10 Promotes Colorectal Cancer Progression. *Cell Commun Signaling CCS* (2020) 18 (1):51. doi: 10.1186/s12964-020-00557-2
78. Suarez-Lopez L, Kong YW, Sriram G, Patterson JC, Rosenberg S, Morandell S, et al. MAPKAP Kinase-2 Drives Expression of Angiogenic Factors by Tumor-Associated Macrophages in a Model of Inflammation-Induced Colon Cancer. *Front Immunol* (2020) 11:607891. doi: 10.3389/fimmu.2020.607891
79. Porter RJ, Arends MJ, Churchhouse AMD, Din S. Inflammatory Bowel Disease-Associated Colorectal Cancer: Translational Risks From Mechanisms to Medicines. *J Crohn's Colitis* (2021) 15(12):2131–41. doi: 10.1093/ecco-jcc/jjab102

80. Coghlin C, Murray GI. Following the Protein Biomarker Trail to Colorectal Cancer. *Colorectal Cancer* (2012) 1(2):93–6. doi: 10.2217/crc.12.7
81. Werling RW, Yaziji H, Bacchi CE, Gown AM. CDX2, a Highly Sensitive and Specific Marker of Adenocarcinomas of Intestinal Origin: An Immunohistochemical Survey of 476 Primary and Metastatic Carcinomas. *Am J Surg Pathol* (2003) 27(3):303–10. doi: 10.1097/00000478-200303000-00003
82. de Wit M, Fijneman RJ, Verheul HM, Meijer GA, Jimenez CR. Proteomics in Colorectal Cancer Translational Research: Biomarker Discovery for Clinical Applications. *Clin Biochem* (2013) 46(6):466–79. doi: 10.1016/j.clinbiochem.2012.10.039
83. Luo H, Shen K, Li B, Li R, Wang Z, Xie Z. Clinical Significance and Diagnostic Value of Serum NSE, CEA, CA19-9, CA125 and CA242 Levels in Colorectal Cancer. *Oncol Lett* (2020) 20(1):742–50. doi: 10.3892/ol.2020.11633
84. Coghlin C, Murray GI. Biomarkers of Colorectal Cancer: Recent Advances and Future Challenges. *Proteomics Clin Appl* (2015) 9(1-2):64–71. doi: 10.1002/prca.201400082
85. Bronkhorst AJ, Ungerer V, Holdenrieder S. The Emerging Role of Cell-Free DNA as a Molecular Marker for Cancer Management. *Biomol Detection Quantification* (2019) 17:100087. doi: 10.1016/j.bdq.2019.100087
86. Doubeni CA, Jensen CD, Fedewa SA, Quinn VP, Zauber AG, Schottinger JE, et al. Fecal Immunochemical Test (FIT) for Colon Cancer Screening: Variable Performance With Ambient Temperature. *J Am Board Family Med JABFM* (2016) 29(6):672–81. doi: 10.3122/jabfm.2016.06.160060
87. Carethers JM. Fecal DNA Testing for Colorectal Cancer Screening. *Annu Rev Med* (2020) 71:59–69. doi: 10.1146/annurev-med-103018-123125
88. Koga Y, Yamazaki N, Yamamoto Y, Yamamoto S, Saito N, Kakugawa Y, et al. Fecal miR-106a Is a Useful Marker for Colorectal Cancer Patients With False-Negative Results in Immunochemical Fecal Occult Blood Test. *Cancer Epidemiol Biomarkers Prev* (2013) 22(10):1844–52. doi: 10.1158/1055-9965.EPI-13-0512
89. Manna SK, Tanaka N, Krausz KW, Haznadar M, Xue X, Matsubara T, et al. Biomarkers of Coordinate Metabolic Reprogramming in Colorectal Tumors in Mice and Humans. *Gastroenterology* (2014) 146(5):1313–24. doi: 10.1053/j.gastro.2014.01.017
90. Meng C, Yin X, Liu J, Tang K, Tang H, Liao J. TIMP-1 Is a Novel Serum Biomarker for the Diagnosis of Colorectal Cancer: A Meta-Analysis. *PloS One* (2018) 13(11):e0207039. doi: 10.1371/journal.pone.0207039
91. Das V, Kalita J, Pal M. Predictive and Prognostic Biomarkers in Colorectal Cancer: A Systematic Review of Recent Advances and Challenges. *Biomed Pharmacother Biomed Pharmacother* (2017) 87:8–19. doi: 10.1016/j.biopha.2016.12.064
92. Alves Martins BA, de Bulhões GF, Cavalcanti IN, Martins MM, de Oliveira PG, Martins AMA. Biomarkers in Colorectal Cancer: The Role of Translational Proteomics Research. *Front Oncol* (2019) 9:1284. doi: 10.3389/fonc.2019.01284
93. Kelleher M, Singh R, O'Driscoll CM, Melgar S. Carcinoembryonic Antigen (CEACAM) Family Members and Inflammatory Bowel Disease. *Cytokine Growth Factor Rev* (2019) 47:21–31. doi: 10.1016/j.cytogfr.2019.05.008
94. Lee JH, Lee SW. The Roles of Carcinoembryonic Antigen in Liver Metastasis and Therapeutic Approaches. *Gastroenterol Res Pract* (2017) 2017:7521987. doi: 10.1155/2017/7521987
95. Beauchemin N, Arabzadeh A. Carcinoembryonic Antigen-Related Cell Adhesion Molecules (CEACAMs) in Cancer Progression and Metastasis. *Cancer Metastasis Rev* (2013) 32(3-4):643–71. doi: 10.1007/s10555-013-9444-6
96. van Huizen NA, Coebergh Van Den Braak RRJ, Doukas M, Dekker LJM, IJzermans JNM, Luider TM. Up-Regulation of Collagen Proteins in Colorectal Liver Metastasis Compared With Normal Liver Tissue. *J Biol Chem* (2019) 294 (1):281–9. doi: 10.1074/jbc.RA118.005087
97. Colbert Maresso K, Vilar E, Hawk ET. Urinary PGE-M in Colorectal Cancer: Predicting More Than Risk? *Cancer Prev Res (Philadelphia Pa)* (2014) 7 (10):969–72. doi: 10.1158/1940-6207.CAPR-14-0215
98. Meding S, Balluff B, Elsner M, Schöne C, Rauser S, Nitsche U, et al. Tissue-Based Proteomics Reveals FXYD3, S100A11 and GSTM3 as Novel Markers for Regional Lymph Node Metastasis in Colon Cancer. *J Pathol* (2012) 228 (4):459–70. doi: 10.1002/path.4021
99. Croner RS, Stürzl M, Rau TT, Metodieva G, Geppert CI, Naschberger E, et al. Quantitative Proteome Profiling of Lymph Node-Positive vs. -Negative Colorectal Carcinomas Pinpoints MX1 as a Marker for Lymph Node Metastasis. *Int J Cancer* (2014) 135(12):2878–86. doi: 10.1002/ijc.28929
100. Duineveld LA, van Asselt KM, Bemelman WA, Smits AB, Tanis PJ, van Weert HC, et al. Symptomatic and Asymptomatic Colon Cancer Recurrence: A Multicenter Cohort Study. *Ann Family Med* (2016) 14(3):215–20. doi: 10.1370/afm.1919
101. Snoeren N, Emmink BL, Koerkamp MJ, van Hooff SR, Goos JA, van Houdt WJ, et al. Maspin Is a Marker for Early Recurrence in Primary Stage III and IV Colorectal Cancer. *Br J Cancer* (2013) 109(6):1636–47. doi: 10.1038/bjc.2013.489
102. Alnabulsi A, Murray GI. Integrative Analysis of the Colorectal Cancer Proteome: Potential Clinical Impact. *Expert Rev Proteomics* (2016) 13 (10):917–27. doi: 10.1080/14789450.2016.1233062
103. Chauvin A, Boisvert FM. Clinical Proteomics in Colorectal Cancer, a Promising Tool for Improving Personalised Medicine. *Proteomes* (2018) 6 (4):49. doi: 10.3390/proteomes6040049
104. Guo J, Zhu C, Yang K, Li J, Du N, Zong M, et al. Poly(C)-Binding Protein 1 Mediates Drug Resistance in Colorectal Cancer. *Oncotarget* (2017) 8 (8):13312–9. doi: 10.18632/oncotarget.14516
105. Katsila T, Juliachs M, Gregori J, Macarulla T, Villarreal L, Bardelli A, et al. Circulating pEGFR Is a Candidate Response Biomarker of Cetuximab Therapy in Colorectal Cancer. *Clin Cancer Res* (2014) 20(24):6346–56. doi: 10.1158/1078-0432.CCR-14-0361
106. McKinley ET, Liu H, McDonald WH, Luo W, Zhao P, Coffey RJ, et al. Global Phosphotyrosine Proteomics Identifies Pkcδ as a Marker of Responsiveness to Src Inhibition in Colorectal Cancer. *PloS One* (2013) 8(11):e80207. doi: 10.1371/journal.pone.0080207
107. Mazouji O, Ouhajjou A, Incitti R, Mansour H. Updates on Clinical Use of Liquid Biopsy in Colorectal Cancer Screening, Diagnosis, Follow-Up, and Treatment Guidance. *Front Cell Dev Biol* (2021) 9:660924. doi: 10.3389/fcell.2021.660924
108. Fernández-Lázaro D, Hernández JLG, García AC, Castillo ACD, Hueso MV, Cruz-Hernández JJ. Clinical Perspective and Translational Oncology of Liquid Biopsy. *Diagnostics (Basel Switzerland)* (2020) 10(7):443. doi: 10.3390/diagnostics10070443
109. Yang C, Chen F, Wang S, Xiong B. Circulating Tumor Cells in Gastrointestinal Cancers: Current Status and Future Perspectives. *Front Oncol* (2019) 9:1427. doi: 10.3389/fonc.2019.01427
110. Fernández-Lázaro D, García Hernández JL, García AC, Córdova Martínez A, Mielgo-Ayuso J, Cruz-Hernández JJ. Liquid Biopsy as Novel Tool in Precision Medicine: Origins, Properties, Identification and Clinical Perspective of Cancer's Biomarkers. *Diagnostics (Basel Switzerland)* (2020) 10(4):215. doi: 10.3390/diagnostics10040215
111. Shen Z, Wu A, Chen X. Current Detection Technologies for Circulating Tumor Cells. *Chem Soc Rev* (2017) 46(8):2038–56. doi: 10.1039/C6CS00803H
112. McQuade RM, Stojanovska V, Bornstein JC, Nurgali K. Colorectal Cancer Chemotherapy: The Evolution of Treatment and New Approaches. *Curr Med Chem* (2017) 24(15):1537–57. doi: 10.2174/0929867324666170111152436
113. Moiseyenko VM, Moiseyenko FV, Yanus GA, Kuligina ES, Sokolenko AP, Bizin IV, et al. First-Line Cetuximab Monotherapy in KRAS/NRAS/BRAF Mutation-Negative Colorectal Cancer Patients. *Clin Drug Invest* (2018) 38 (6):553–62. doi: 10.1007/s40261-018-0629-1
114. Van Cutsem E, Köhne CH, Hitre E, Zaluski J, Chang Chien CR, Makhson A, et al. Cetuximab and Chemotherapy as Initial Treatment for Metastatic Colorectal Cancer. *N Engl J Med* (2009) 360(14):1408–17. doi: 10.1056/NEJMoa0805019
115. Heinemann V, Weikersthal LFV, Vehling-Kaiser U, Stauch M, Oruzio DV, Schulze M, et al. Randomized Trial Comparing Cetuximab Plus XELIRI Versus Cetuximab Plus XELOX as First Line Treatment of Patients With Metastatic Colorectal Cancer (mCRC): A Study of the German AIO CRC Study Group. *J Clin Oncol* (2008) 26:4033–3. doi: 10.1200/jco.2008.26.15_suppl.4033
116. Jonker DJ, O'Callaghan CJ, Karapetis CS, Zalcberg JR, Tu D, Au HJ, et al. Cetuximab for the Treatment of Colorectal Cancer. *N Engl J Med* (2007) 357 (20):2040–8. doi: 10.1056/NEJMoa071834
117. Arnold D, Prager GW, Quintela A, Stein A, Moreno Vera S, Mounedji N, et al. Beyond Second-Line Therapy in Patients With Metastatic Colorectal

Cancer: A Systematic Review. *Ann Oncol* (2018) 29(4):835–56. doi: 10.1093/annonc/mdy038
118. Seeber A, Gunsilius E, Gastl G, Pircher A. Anti-Angiogenics: Their Value in Colorectal Cancer Therapy. *Oncol Res Treat* (2018) 41(4):188–93. doi: 10.1159/000488301
119. Guba M, Seeliger H, Kleespies A, Jauch KW, Bruns C. Vascular Endothelial Growth Factor in Colorectal Cancer. *Int J Colorectal Dis* (2004) 19(6):510–7. doi: 10.1007/s00384-003-0576-y
120. Hurwitz H, Fehrenbacher L, Novotny W, Cartwright T, Hainsworth J, Heim W, et al. Bevacizumab Plus Irinotecan, Fluorouracil, and Leucovorin for Metastatic Colorectal Cancer. *N Engl J Med* (2004) 350(23):2335–42. doi: 10.1056/NEJMoa032691
121. Xie YH, Chen YX, Fang JY. Comprehensive Review of Targeted Therapy for Colorectal Cancer. *Signal Transduct Targeted Ther* (2020) 5(1):22. doi: 10.1038/s41392-020-0116-z
122. Folprecht G, Pericay C, Saunders MP, Thomas A, Lopez Lopez R, Roh JK, et al. Oxaliplatin and 5-FU/folinic Acid (Modified FOLFOX6) With or Without Aflibercept in First-Line Treatment of Patients With Metastatic Colorectal Cancer: The AFFIRM Study. *Ann Oncol* (2016) 27(7):1273–9. doi: 10.1093/annonc/mdw176
123. Moore M, Gill S, Asmis T, Berry S, Burkes R, Zbuk K, et al. Randomized Phase II Study of Modified FOLFOX-6 in Combination With Ramucirumab or Icrucumab as Second-Line Therapy in Patients With Metastatic Colorectal Cancer After Disease Progression on First-Line Irinotecan-Based Therapy. *Ann Oncol* (2016) 27(12):2216–24. doi: 10.1093/annonc/mdw412
124. Grothey A, Van Cutsem E, Sobrero A, Siena S, Falcone A, Ychou M, et al. Regorafenib Monotherapy for Previously Treated Metastatic Colorectal Cancer (CORRECT): An International, Multicentre, Randomised, Placebo-Controlled, Phase 3 Trial. *Lancet (London England)* (2013) 381(9863):303–12. doi: 10.1016/S0140-6736(12)61900-X
125. Li J, Qin S, Xu RH, Shen L, Xu J, Bai Y, et al. Effect of Fruquintinib vs Placebo on Overall Survival in Patients With Previously Treated Metastatic Colorectal Cancer: The FRESCO Randomized Clinical Trial. *Jama* (2018) 319(24):2486–96. doi: 10.1001/jama.2018.7855
126. Yao JF, Li XJ, Yan LK, He S, Zheng JB, Wang XR, et al. Role of HGF/c-Met in the Treatment of Colorectal Cancer With Liver Metastasis. *J Biochem Mol Toxicol* (2019) 33(6):e22316. doi: 10.1002/jbt.22316
127. Fu J, Su X, Li Z, Deng L, Liu X, Feng X, et al. HGF/c-MET Pathway in Cancer: From Molecular Characterization to Clinical Evidence. *Oncogene* (2021) 40(28):4625–51. doi: 10.1038/s41388-021-01863-w
128. Iveson T, Donehower RC, Davidenko I, Tjulandin S, Deptala A, Harrison M, et al. Rilotumumab in Combination With Epirubicin, Cisplatin, and Capecitabine as First-Line Treatment for Gastric or Oesophagogastric Junction Adenocarcinoma: An Open-Label, Dose De-Escalation Phase 1b Study and a Double-Blind, Randomised Phase 2 Study. *Lancet Oncol* (2014) 15(9):1007–18. doi: 10.1016/S1470-2045(14)70023-3
129. Jia YT, Yang DH, Zhao Z, Bi XH, Han WH, Feng B, et al. Effects of PHA-665752 and Cetuximab Combination Treatment on *In Vitro* and Murine Xenograft Growth of Human Colorectal Cancer Cells With KRAS or BRAF Mutations. *Curr Cancer Drug Targets* (2018) 18(3):278–86. doi: 10.2174/1568009617666170330112841
130. Parizadeh SM, Jafarzadeh-Esfehani R, Fazilat-Panah D, Hassanian SM, Shahidsales S, Khazaei M, et al. The Potential Therapeutic and Prognostic Impacts of the C-MET/HGF Signaling Pathway in Colorectal Cancer. *IUBMB Life* (2019) 71(7):802–11. doi: 10.1002/iub.2063
131. Ganesh K, Stadler ZK, Cercek A, Mendelsohn RB, Shia J, Segal NH, et al. Immunotherapy in Colorectal Cancer: Rationale, Challenges and Potential. *Nat Rev Gastroenterol Hepatol* (2019) 16(6):361–75. doi: 10.1038/s41575-019-0126-x
132. Overman MJ, Lonardi S, Wong KYM, Lenz HJ, Gelsomino F, Aglietta M, et al. Durable Clinical Benefit With Nivolumab Plus Ipilimumab in DNA Mismatch Repair-Deficient/Microsatellite Instability-High Metastatic Colorectal Cancer. *J Clin Oncol* (2018) 36(8):773–9. doi: 10.1200/JCO.2017.76.9901
133. Naldini L. Gene Therapy Returns to Centre Stage. *Nature* (2015) 526(7573):351–60. doi: 10.1038/nature15818
134. Wang K, Kievit FM, Zhang M. Nanoparticles for Cancer Gene Therapy: Recent Advances, Challenges, and Strategies. *Pharmacol Res* (2016) 114:56–66. doi: 10.1016/j.phrs.2016.10.016
135. Bao X, Zeng J, Huang H, Ma C, Wang L, Wang F, et al. Cancer-Targeted PEDF-DNA Therapy for Metastatic Colorectal Cancer. *Int J Pharmaceut* (2020) 576:118999. doi: 10.1016/j.ijpharm.2019.118999
136. Zhang M, Xiao B, Wang H, Han MK, Zhang Z, Viennois E, et al. Edible Ginger-Derived Nano-Lipids Loaded With Doxorubicin as a Novel Drug-Delivery Approach for Colon Cancer Therapy. *Mol Ther* (2016) 24(10):1783–96. doi: 10.1038/mt.2016.159
137. Bery N, Miller A, Rabbitts T. A Potent KRAS Macromolecule Degrader Specifically Targeting Tumours With Mutant KRAS. *Nat Commun* (2020) 11(1):3233. doi: 10.1038/s41467-020-17022-w
138. Bond MJ, Chu L, Nalawansha DA, Li K, Crews CM. Targeted Degradation of Oncogenic KRAS(G12C) by VHL-Recruiting PROTACs. *ACS Cent Sci* (2020) 6(8):1367–75. doi: 10.1021/acscentsci.0c00411
139. Hong TS, Clark JW, Haigis KM. Cancers of the Colon and Rectum: Identical or Fraternal Twins? *Cancer Discov* (2012) 2(2):117–21. doi: 10.1158/2159-8290.CD-11-0315
140. Zhang Y, Wu Y, Gong ZY, Ye HD, Zhao XK, Li JY, et al. Distinguishing Rectal Cancer From Colon Cancer Based on the Support Vector Machine Method and RNA-Sequencing Data. *Curr Med Sci* (2021) 41(2):368–74. doi: 10.1007/s11596-021-2356-8
141. Network CGA. Comprehensive Molecular Characterization of Human Colon and Rectal Cancer. *Nature* (2012) 487(7407):330–7. doi: 10.1038/nature11252
142. Zhang B, Wang J, Wang X, Zhu J, Liu Q, Shi Z, et al. Proteogenomic Characterization of Human Colon and Rectal Cancer. *Nature* (2014) 513(7518):382–7. doi: 10.1038/nature13438
143. Akgun E, Ozkok S, Tekin M, Yoldas T, Caliskan C, Kose T, et al. The Effects of Chemoradiotherapy on Recurrence and Survival in Locally Advanced Rectal Cancers With Curative Total Mesorectal Excision: A Prospective, Nonrandomized Study. *World J Surg Oncol* (2017) 15(1):205. doi: 10.1186/s12957-017-1275-4
144. Godhi S, Godhi A, Bhat R, Saluja S. Colorectal Cancer: Postoperative Follow-Up and Surveillance. *Indian J Surg* (2017) 79(3):234–7. doi: 10.1007/s12262-017-1610-6
145. Brown KGM, Koh CE. Surgical Management of Recurrent Colon Cancer. *J Gastrointestinal Oncol* (2020) 11(3):513–25. doi: 10.21037/jgo-2019-ccm-09

Conflict of Interest: The authors declare that the research was conducted in the absence of any commercial or financial relationships that could be construed as a potential conflict of interest.

frontiers | Frontiers in Oncology

ORIGINAL RESEARCH
published: 12 April 2022
doi: 10.3389/fonc.2022.844477

The CK1δ/ϵ-Tip60 Axis Enhances Wnt/β-Catenin Signaling *via* Regulating β-Catenin Acetylation in Colon Cancer

Jiong Ning[1,2†], Qi Sun[1†], Zijie Su[1,3], Lifeng Tan[1], Yun Tang[1], Sapna Sayed[1], Huan Li[1], Vivian Weiwen Xue[1], Shanshan Liu[1], Xianxiong Chen[1] and Desheng Lu[1,2]*

[1] Guangdong Provincial Key Laboratory of Regional Immunity and Diseases, International Cancer Center, Department of Pharmacology, Shenzhen University Health Science Center, Shenzhen, China, [2] Shenzhen University-Friedrich Schiller Universität Jena Joint PhD Program in Biomedical Sciences, Shenzhen University School of Medicine, Shenzhen, China, [3] Department of Research, The Affiliated Tumor Hospital of Guangxi Medical University, Nanning, China

OPEN ACCESS

Edited by:
Shilpa S. Dhar,
University of Texas MD Anderson Cancer Center, United States

Reviewed by:
Michael Choi,
University of California, San Diego, United States
Hui Dong,
University of California, San Diego, United States
Fang Guo,
Shanghai Jiao Tong University, China

***Correspondence:**
Desheng Lu
delu@szu.edu.cn

[†]These authors have contributed equally to this work

Specialty section:
This article was submitted to Molecular and Cellular Oncology, a section of the journal Frontiers in Oncology

Received: 28 December 2021
Accepted: 22 March 2022
Published: 12 April 2022

Citation:
Ning J, Sun Q, Su Z, Tan L, Tang Y, Sayed S, Li H, Xue VW, Liu S, Chen X and Lu D (2022) The CK1δ/ϵ-Tip60 Axis Enhances Wnt/β-Catenin Signaling via Regulating β-Catenin Acetylation in Colon Cancer. Front. Oncol. 12:844477. doi: 10.3389/fonc.2022.844477

Casein kinase 1δ/ϵ (CK1δ/ϵ) are well-established positive modulators of the Wnt/β-catenin signaling pathway. However, the molecular mechanisms involved in the regulation of β-catenin transcriptional activity by CK1δ/ϵ remain unclear. In this study, we found that CK1δ/ϵ could enhance β-catenin-mediated transcription through regulating β-catenin acetylation. CK1δ/ϵ interacted with Tip60 and facilitated the recruitment of Tip60 to β-catenin complex, resulting in increasing β-catenin acetylation at K49. Importantly, Tip60 significantly enhanced the SuperTopFlash reporter activity induced by CK1δ/ϵ or/and β-catenin. Furthermore, a CK1δ/CK1ϵ/β-catenin/Tip60 complex was detected in colon cancer cells. Simultaneous knockdown of CK1δ and CK1ϵ significantly attenuated the interaction between β-catenin and Tip60. Notably, inhibition of CK1δ/ϵ or Tip60, with shRNA or small molecular inhibitors downregulated the level of β-catenin acetylation at K49 in colon cancer cells. Finally, combined treatment with CK1 inhibitor SR3029 and Tip60 inhibitor MG149 had more potent inhibitory effect on β-catenin acetylation, the transcription of Wnt target genes and the viability and proliferation in colon cancer cells. Taken together, our results revealed that the transcriptional activity of β-catenin could be modulated by the CK1δ/ϵ-β-catenin-Tip60 axis, which may be a potential therapeutic target for colon cancer.

Keywords: CK1δ/ϵ, Tip60, β-catenin acetylation, Wnt/β-catenin signaling, colon cancer

INTRODUCTION

The Wnt/β-catenin signaling pathway plays crucial roles in embryonic development, tissue homeostasis, stem cell renewal and tumorigenesis (1, 2). In this pathway, β-catenin is a central component in Wnt signal transduction, acting as a transcriptional co-activator to mediate the expression of Wnt target genes (1). The stability and activity of β-catenin is regulated by post-translational modifications, such as phosphorylation, ubiquitination and acetylation (3). In the absence of Wnt stimulation, β-catenin exists in a complex, which is consisted of the adenomatosis

polyposis coli protein (APC), the scaffolding protein axin, the casein kinase 1 (CK1) and the glycogen synthetase kinase-3β enzyme (GSK-3β). GSK-3β phosphorylates β-catenin and triggers its ubiquitination-mediated degradation. Upon stimulation with Wnt, GSK-3β dissociates from the destruction complex and unphosphorylated β-catenin accumulates in the cytosol and nucleus (4). As acetyltransferases, cAMP response element binding (CREB) binding protein (CBP), p300 and p300/CBP-associated factor (PCAF) could catalyze the acetylation of β-catenin at different residues (K19, K49 and K345), thereby promoting the stability of β-catenin, enhancing the interaction between β-catenin and TCF4, ultimately stimulating the transcription of target genes (5–8).

TAT-interactive protein 60 kDa (Tip60), a member of the Moz, Ybf2/Sas3, Sas2 and Tip60 (MYST) family of histone acetyltransferases (HATs), is a crucial regulator of the DNA damage response and transcriptional co-activator (9–11). This protein has been involved in a wide variety of cellular activities, including transcriptional regulation, DNA repair, checkpoint activation, apoptosis and autophagy (11, 12). Tip60 has been shown to acetylate histone and non-histone proteins, such as histones H2A, H3, H4, p53 and ataxia telangiectasia mutant (ATM) (13–15). Previous studies showed that reduced Tip60 expression was detected in colon, lung, breast, melanoma, prostate and gastric cancers (16–20). Interestingly, it was observed that lower levels of Tip60 may correlate with a worse prognosis. Tip60 has been found to drive prostate cancer proliferation by increasing the levels of c-Myc and androgen receptor (21). Stacy et al. reported that Tip60 could promote cellular proliferation by stabilizing ΔNp63α protein levels in squamous cell carcinoma (22). Moreover, several specific inhibitors of Tip60, including NU9056 and TH1834, have been developed and demonstrated to reduce proliferation of cancer cells (23, 24). However, the molecular mechanisms by which Tip60 influence cancer progression are not fully understood.

CK1 belongs to a family of serine/threonine protein kinases, composed of seven family members α, β, γ1, γ2, γ3, δ and ϵ in human. Among them, CK1δ and CK1ϵ share the highest homology, with 98% amino acid sequence identity in their kinase domain (25, 26). CK1 kinases are important regulators in diverse signaling pathways, including the Wnt signaling pathway (26). CK1 phosphorylates several key components in the Wnt signal cascade and exhibits both positive and negative roles (26). As a component of the β-catenin destruction complex, CK1α phosphorylates β-catenin at S45 and primes β-catenin for further phosphorylation of T41, S37, and S33 by GSK3β, resulting in the ubiquitin-proteasome-mediated degradation of β-catenin (26–28). Phosphorylation of low-density lipoprotein receptor-related protein 6 (LRP6) at T1479 and T1493 by CK1γ is required for the activation of Wnt/β-catenin signaling (29). CK1δ and CK1ϵ are well-known positive regulators of Wnt/β-catenin signaling (26, 30). In response to Wnt, CK1δ/ϵ binds to dishevelled (DVL) and phosphorylates DVL at multiple sites (31). CK1ϵ also phosphorylates LRP6 at T1493 and regulates initial steps in LRP6 signalosome formation (32, 33). A recent study showed that CK1δ/ϵ could regulate the stability of amino-terminal enhancer of split (AES), a member of the Groucho/transducin-like enhancer of split/Groucho-related gene (Gro/TLE/Grg) family (34). CK1δ/ϵ promoted S phase kinase-associated protein 2 (SKP2)-mediated ubiquitination and degradation of AES through phosphorylating AES at S121, resulting in the activation of Wnt/β-catenin signaling (34). However, very little is known about how CK1δ/ϵ is implicated in β-catenin-mediated transcriptional activity.

In this study, we explored the effect of CK1 on β-catenin-mediated Wnt signaling. We found that CK1δ/ϵ could increase β-catenin-mediated transcription through regulating β-catenin acetylation. We further investigated the molecular mechanism by which CK1δ/ϵ modulated the acetylation of β-catenin. Our results revealed that a novel CK1δ/ϵ-Tip60-β-catenin axis is involved in regulation of Wnt/β-catenin signaling.

METHODS AND MATERIALS

Cell Culture

The human embryonic kidney 293T (HEK293T) cells, and colon cancer SW480 and HCT116 cells were obtained from American Type Culture Collection (ATCC, Manassas, VA, USA). These cells were maintained in DMEM (Thermo Fisher Scientific, Waltham, MA, USA) supplemented with 10% fetal bovine serum (FBS, Thermo Fisher Scientific, Waltham, MA, USA) and 1% penicillin-streptomycin (Thermo Fisher Scientific, Waltham, MA, USA) in a humidified incubator at 37°C with 5% CO_2. Cells in the logarithmic phase of growth were used for the subsequent experiments.

Chemical Regents, Antibodies and Plasmids

SR3029, D4476, MG149, NU9056, MG132 and cycloheximide (CHX) were purchased from MedChemExpress (MCE, Monmouth Junction, NJ, USA). The following primary antibodies were used: anti-CK1δ, anti-β-catenin, anti-p300, anti-acetyl-lysine, IgG (Santa Cruz Biotechnology, Heidelberg, Germany), anti-CBP, anti-acetyl-β-catenin (K49), anti-phospho-β-catenin (S45), anti-Flag, anti-V5, anti-CK1ϵ, anti-GFP, anti-mouse IgG (Cell Signaling Technology, Danvers, MA), anti-Tip60 (Abcam, Cambridge, MA, USA), and anti-GAPDH antibody (Proteintech, Chicago, IL, USA). The Tip60-Flag, PCAF-Flag, p300-Flag and pEGFP-N1 plasmids were purchased from Vigenebio (Weizhen, Shandong, China). The SuperTopFlash reporter plasmid was provided by Karl Willert (University of California at San Diego, La Jolla, CA, USA). The expression plasmids encoding β-catenin, pCMXβgal (β galactosidase, β-gal), CK1α-V5, CK1δ-V5, CK1ϵ-V5, CK1α-Flag, CK1δ-Flag, CK1ϵ-Flag, CK1γ-Flag have been described previously (35, 36). For the construction of GFP-tagged CK1δ, the cDNAs encoding human CK1δ was amplified by PCR and subcloned into the BamHI/EcoRI site of pEGFP-N1 vector using ClonExpress Ultra One Step Cloning Kit (Vazyme, Nanjing, China). The primer sequences used are as follows: CK1δ-GFP-sense, 5'-CTCGAGCTCAAGCTTCATGGAGCTGAGAGTCGGGAAC-3';

CK1δ-GFP-antisense, 5'-CTCACCATAAGGTGGC GACCGGTGTAGGTGCGTCGTG.

Lentiviral Production and Infection

The CK1 shRNA oligos were cloned into pLKO.1-GFP vector, and the Tip60 shRNA oligos were inserted into pLKO.1-TRC vector. The resulting constructs were validated by sequencing. The shRNA oligos used have been previously described (37, 38). For lentiviral production and infection, HEK293T cells were transfected with a shRNA-expressing plasmid (10 μg), an envelope plasmid (pMD2.G, 2.5 μg) and a packaging plasmid (psPAX2, 7.5 μg) using Lipofectamine 2000 regent according to manufacturer's instruction. At 48 h after transfection, viral supernatants were collected and filtered through a 0.45 μm filter. Virus was immediately added to SW480 and HCT116 cells with 8 μg/mL polybrene. After a week of infection, the GFP-positive cells were sorted by FACS AriaIII, and the knockdown of CK1δ or CK1ϵ was verified by Western blotting. For Tip60 deficient cells, cells were selected for stable expression in the presence of 3 μg/mL puromycin (Thermo Fisher Scientific, Waltham, MA, USA) after 72 h of infection. The puromycin-resistant stable clones were pooled, and Tip60 deficiency was confirmed by Western blotting.

Luciferase Reporter Gene Assays

HEK293T cells were transfected with the SuperTopFlash reporter, control vector, and the indicated expression plasmids in 24-well plates using Lipofectamine 2000 (Thermo Fisher, San Jose, California, USA). After 48 h, the cells were harvested and lysates were used to examine the expression of luciferase by a luciferase assay kit (Promega, Shanghai, China), according to the manufacturer's instructions. The luciferase values were normalized using the β-gal internal control to determine the variation in transfection efficiency. The results are presented as means ± SD of at least three independent experiments. The values for luciferase activity were presented as fold induction over control.

Immunoblotting and Immunoprecipitation

The cells were lysed in RIPA buffer containing 50 mM Tris-HCl at pH 7.4, 150 mM NaCl, 1% Nonidet P-40, 0.1% SDS, 0.5% sodium deoxycholate, 1 mM EDTA, 1 mM PMSF, protease inhibitors (Bimake, Beijing, China), and phosphatase inhibitors (Topscience, Shanghai, China). After quantifying the concentration of protein using the BCA protein assay kit (Vazyme, Nanjing, China), 30 μg of protein was loaded and separated by SDS-PAGE, followed by transferring to poly-vinylidenefluoride (PVDF) membranes (Millipore, Massachusetts, USA). Immunoblotting was performed with the indicated primary antibodies at 4°C overnight. The membranes were then incubated with horseradish peroxidase (HRP)-conjugated secondary antibody (ImmunoWay, Plano, USA) at room temperature for 2 h. After incubating the membranes with ECL Plus Western Blotting Substrate (Thermo Fisher Scientific, Shanghai, China), immunolabeled proteins were detected using X-ray film or Chemiluminescent Imaging System (Tanon 5200, Shanghai, China).

For immunoprecipitation assay, cell lysates were harvested in 500 μL RIPA buffer supplemented with protease inhibitor, phosphatase inhibitor cocktails and 1 mM PMSF, followed by centrifugation at 15000 rpm for 15 min at 4°C. Protein concentration in the supernatant was quantified by the BCA Protein Assay Kit. The supernatant was incubated with specific primary antibody or control IgG at 4°C overnight, then further incubated with protein A/G magnetic beads (Biomake, Beijing, China) for 6 h. The immunoprecipitated pellet was washed with RIPA buffer at least three times, and proteins were eluted by boiling in SDS loading buffer. The eluted proteins (30 μg) were analyzed by SDS-PAGE and immunoblotting.

Real-Time PCR Analyses

Total RNA was extracted using RNAiso Plus (TaKaRa, Kusatsu, Shiga, Japan) and then reverse-transcribed into cDNA using the PrimeScript RT reagent kit (TaKaRa, Kusatsu, Shiga, Japan) according to the manufacturer's instructions. Prepared cDNA was then subjected to quantitative PCR analysis using 2×SYBR Green qPCR Master Mix (Promega, Shanghai, China). Real-time PCR assays were performed to quantify mRNA levels of human Survivin, Cyclin D1 and Prominin 1 (PROM1) genes. The comparative Ct method was used to analyze relative expression of genes. The data was presented as the fold change. The fold change was calculated as $2^{-\Delta\Delta Ct}$, where $\Delta\Delta Ct = \Delta Ct_{treated} - \Delta Ct_{control}$. Ct is the cycle number at which fluorescence first exceeds the threshold. The ΔCt values from each target gene were obtained by subtracting the values for GAPDH Ct from the sample Ct. The primer pairs used for quantitative PCR amplification were as follows: Survivin sense, 5'-AGGACCACCGCATCTCTACAT-3' and antisense, 5'-AAG TCTGGCTCGTTCTCAGTG-3'; Cyclin D1 sense, 5'-AATGACC CCGCACGATTTC-3' and antisense, 5'-TCAGGTTCAGG CCTTGCAC-3'; PROM1 sense, 5'-AGGCTACTTTGAACATT ATCTGC-3' and antisense, 5'-GGCTTGTCATAACAGGATTGT-3'; GAPDH sense, 5'-CCAGAACATCATCCCTGCCTCTACT-3' and antisense, 5'-GGTTTTTCTAGACGGCAGGTCAGGT.

Chromatin Immunoprecipitation (ChIP) Assays

SW480 cells were treated with 240 nM SR3029 for 24 h, and ChIP assay was performed with ChIP-IT Express Enzymatic Chromatin Immunoprecipitation Kit (Sigma-Aldrich, Merck, USA) according to the manufacturer's protocols. The eluted DNA was amplified by quantitative PCR analysis using an ABI Prism 7500 Real-Time PCR System (Applied Biosystems, Foster city, CA, USA). Primer sequences were shown as follows: Survivin sense, 5'-GCGTTCTTTGAAAGCAGT-3' and antisense, 5'-ATCTGGCGGTTAATGGCG-3'; Axin2 sense, 5'-TCTGGTAGCATTATGGCCATCGCA-3' and antisense, 5'-AAAGTCCTCCAAGCCCAAATTCCC-3'; The antibodies used were anti-β-catenin and anti-mouse IgG.

Cell Viability Assays

SW480 and HCT116 cells were seeded in 96-well plates at a density of 5000 cells per well and cultured for 24 h. The cells were treated with SR3029 and MG149, alone or combined, at indicated concentrations for 48 h. Subsequently, 10 μL of MTT solution (5 mg/mL) was added into each well. The plate was further incubated for 4 h at 37°C and 100 μL of dimethyl

sulfoxide (DMSO) was added to dissolve the insoluble formazan. The absorbance of the formazan solution was measured at 570 nm. Each treatment was performed in three replicates.

BrdU Cell Proliferation Assays

SW480 and HCT116 cells were plated on 96-well plates at a density of 5000 cells per well and cultured for 24 h. The cells were treated with SR3029 and MG149, alone or combined, at indicated concentrations for 48 h. The BrdU incorporation assay was performed using the Cell Proliferation ELISA BrdU Colorimetric Kit (Roche, Basel, Switzerland) according to the manufacturer's instructions. BrdU incorporation was detected by measuring the absorbance at 450 nm. Each treatment was performed in three replicates.

Statistical Analyses

Statistical analyses were conducted using GraphPad Prism 7 software (La Jolla, CA, USA). The experiments were repeated three times, and data were exhibited as mean ± standard deviation (SD). The Student's *t*-test was applied to determine the significance of difference between the two groups. One-way analysis of variance (ANOVA) with Dunn's multiple comparisons test were utilized to compare the means of several groups. $P<0.05$ was defined as statistically significant.

RESULTS

CK1δ/ϵ Increase β-Catenin-Mediated Transcription Through Regulating β-Catenin Acetylation

To examine the effect of CK1 family members on β-catenin-mediated Wnt signaling, the Wnt-responsive reporter SuperTopFlash was transfected into HEK293T cells with expression vector encoding β-catenin, together with CK1α, CK1δ, CK1ϵ and CK1γ expression plasmids, respectively. As shown in **Figure 1A**, CK1δ or CK1ϵ dramatically enhanced β-catenin-mediated transcription in a dose-dependent manner, while CK1δ or CK1ϵ alone had a moderate effect on the SuperTopFlash reporter activity. Comparatively, CK1α or CK1γ exerted little effect on β-catenin-mediated activity (**Figure 1A**). Since β-catenin can be acetylated at lysine 49 (K49), which is required for the activation of Wnt/β-catenin signaling (3, 5, 39, 40), we tested whether CK1 family members

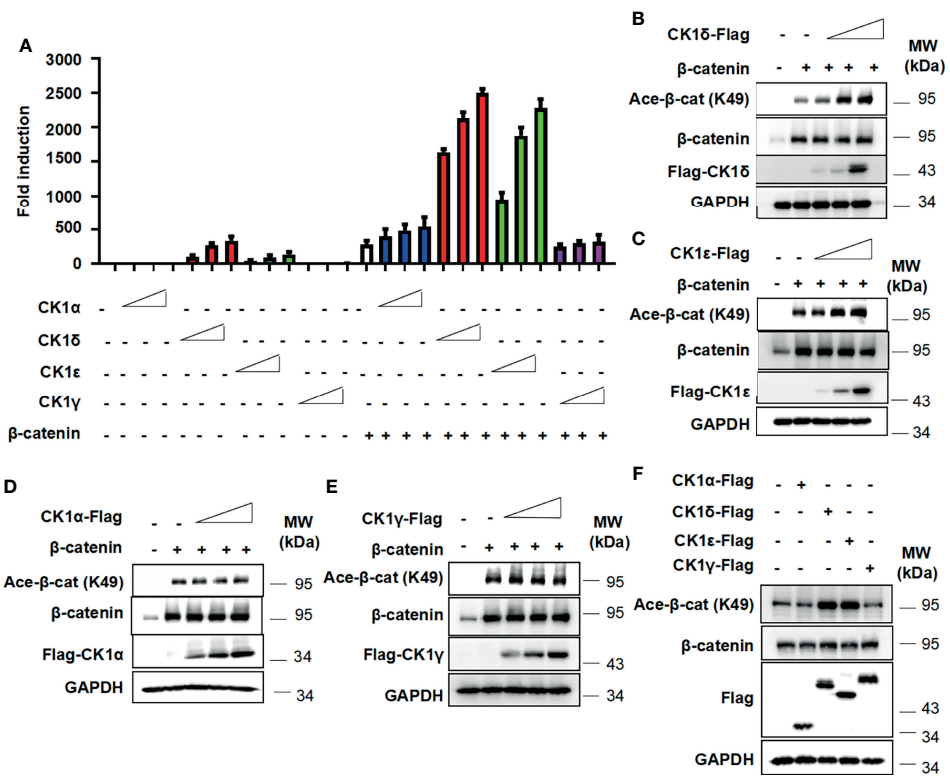

FIGURE 1 | CK1δ/ϵ enhances β-catenin-mediated Wnt signaling and increases β-catenin acetylation at K49. **(A)** The SuperTopFlash reporter was transfected into HEK293T cells with β-catenin expression plasmid together with control vector or increasing amounts (10, 25, 50 ng) of expression plasmids encoding CK1α, CK1δ, CK1ϵ, and CK1γ, respectively. The luciferase values were normalized to β-gal activities. Each treatment was performed in four replicates. **(B–E)** HEK293T cells were transfected with empty vector or β-catenin along with increasing amounts (10, 25, 50 ng) of expression plasmids encoding CK1α, CK1δ, CK1ϵ and CK1γ, respectively. **(F)** HEK293T cells were transfected with 100 ng of control vector or expression plasmids encoding CK1α, CK1δ, CK1ϵ and CK1γ, respectively. Protein expression of total β-catenin, acetylated β-catenin at K49, Flag and GAPDH was measured by Western blotting.

have any effect on the acetylation of β-catenin using an antibody against acetyl-K49 β-catenin. Our results showed that CK1δ or CK1ϵ significantly increased the K49 acetylation of exogenous β-catenin (**Figures 1B, C**). In contrast, CK1α or CK1γ had little effect on the acetyl-K49 β-catenin level (**Figures 1D, E**). Furthermore, we detected enhanced level of the K49 acetylation of endogenous β-catenin in HEK293T cells transfected with CK1δ or CK1ϵ, but not CK1α or CK1γ (**Figure 1F**). These results revealed that CK1δ and CK1ϵ may increase β-catenin-mediated transcriptional activity through regulating β-catenin acetylation.

CK1δ/ϵ Promote β-Catenin Acetylation *via* Recruiting Tip60

Multiple histone acetyltransferases, including p300, CBP and PCAF, have been shown to acetylate β-catenin at different lysine residues, resulting in enhancing its transcriptional activity and up-regulating the expression of Wnt target genes (5–8). We then assessed whether CK1δ/ϵ could promote the interaction between β-catenin and some histone acetyltransferases. A coimmunoprecipitation assay was performed using an anti-β-catenin antibody in HEK293T cells that were transiently transfected with GFP-tagged CK1δ, Flag-tagged CK1ϵ or CK1α. The results showed that the expression of CK1δ or CK1ϵ did not affect the interaction between β-catenin and p300 or CBP or PCAF. Surprisingly, CK1δ or CK1ϵ could dramatically enhance the binding of β-catenin to Tip60 (**Figures 2A, B**), while CK1α had little effect on the interaction between β-catenin and Tip60 (**Figure 2C**). To further confirm the effect of CK1δ/ϵ and Tip60 on β-catenin acetylation, HEK293T cells were transfected with Tip60-Flag expression vector along with expression plasmids for GFP-CK1δ or Flag-CK1ϵ. Cell lysates were extracted from the transfected cells and immunoprecipitated with an anti-β-catenin antibody. Western blotting analysis showed that simultaneous expression of Tip60 and CK1δ or CK1ϵ markedly increased the acetylation of β-catenin at K49 compared to cells expressing Tip60 or CK1δ or CK1ϵ alone (**Figures 2D, E**). To test whether CK1δ or CK1ϵ could phosphorylate Tip60, HEK293T cells were transfected with Tip60-Flag expression plasmid along with expression vectors for CK1δ or CK1ϵ or CK1α, respectively. Total cell extracts were used for affinity purification by anti-Flag M2 agarose. We observed that anti-Flag M2 agarose could pull down Tip60-Flag, and the presence of CK1δ or CK1ϵ elevated the level of phosphorylated Tip60, detected by a pan phospho-serine antibody, while the expression of CK1α did not affect Tip60 phosphorylation (**Figures 2F–H**). These results suggest that the binding of CK1δ/ϵ to Tip60 induced Tip60 phosphorylation and facilitated the recruitment of Tip60 to β-catenin complex, resulting in the acetylation of β-catenin.

Tip60 Significantly Enhances the Transcriptional Activity Induced by CK1δ/ϵ or/and β-Catenin

We next evaluated the effect of CK1δ/ϵ, β-catenin and Tip60, alone or combined, on the Wnt signaling pathway. The SuperTopFlash reporter was transfected into HEK293T cells together with CK1δ/ϵ, β-catenin and Tip60 expression plasmids, alone or combined, as indicated in **Figure 3**. Overexpression of Tip60 significantly enhanced the SuperTopFlash reporter activity induced by CK1δ or CK1ϵ or β-catenin or CK1δ/β-catenin or CK1ϵ/β-catenin, while Tip60 alone had no any effect on the transcription of SuperTopFlash reporter (**Figures 3A, B**). Notably, p300 or PCAF had little effect on CK1δ/ϵ-mediated transcriptional activity (**Figures 3A, B**). These results indicated that Tip60 could positively modulate Wnt signaling in the presence of CK1δ/ϵ or/and β-catenin.

The CK1δ/CK1ϵ/β-Catenin/Tip60 Complex Exists in Colon Cancer Cells and β-Catenin Interacts With Tip60 in a CK1δ/CK1ϵ-Dependent Manner

Considering that CK1δ and CK1ϵ are highly expressed in colon cancer, which is involved in advanced progression and poor prognosis (34, 41, 42), two colon cancer cell lines SW480 and HCT116 were employed to examine the interaction among CK1δ/ϵ, β-catenin and Tip60. These two cell lines have different types of mutations, SW480 cells harboring truncated mutation of APC and HCT116 cells with S45 mutation of β-catenin. The APC and β-catenin mutations are the most frequently occurred mutation types in components of the Wnt signaling pathway in colon cancer (43–45). The result of immunoprecipitation assay showed that the endogenous CK1δ, CK1ϵ, β-catenin and Tip60 proteins were immunoprecipitated with an anti-β-catenin antibody in SW480 and HCT116 cells (**Figures 4A, B**), suggesting that the CK1δ/CK1ϵ/β-catenin/Tip60 complex existed in colon cancer cells. To explore the effect of CK1δ/ϵ on the interaction between β-catenin and Tip60, lentivirus-mediated shRNAs were used to knockdown the expression of CK1δ and CK1ϵ, either alone or in combination, in colon cancer cells. Simultaneous knockdown of CK1δ and CK1ϵ dramatically attenuated the association of β-catenin with Tip60 in SW480 and HCT116 cells (**Figures 4C, D**). These results suggest that β-catenin may interact with Tip60 in a CK1δ/CK1ϵ-dependent manner.

Knockdown of CK1δ/ϵ or Treatment With CK1 Inhibitors Downregulate the Level of β-Catenin Acetylation at K49 and Inhibit the Viability and Proliferation in Colon Cancer Cells

We next check the effect of CK1δ/ϵ on β-catenin acetylation at K49 in colon cancer cells. As shown in **Figures 5A, B**, the level of the acetylation of β-catenin at K49 was dramatically reduced in two colon cancer cell lines (SW480 and HCT116) with knockdown of CK1δ and CK1ϵ simultaneously (**Figures 5A, B**). Moreover, treatment with small molecular CK1 inhibitors (SR3029, D4476 and longdaysin) markedly decreased the K49 acetylation of β-catenin in SW480 and HCT116 cells, while depletion of CK1δ/ϵ or treatment with small molecular CK1 inhibitors had little effect on the expression of Tip60 and β-catenin (**Figures 5C–H** and **Figures S1A–H**). In contrast, proteasome inhibitor MG132 increased the expression of acetylated β-catenin and total β-catenin in SW480 and HCT116

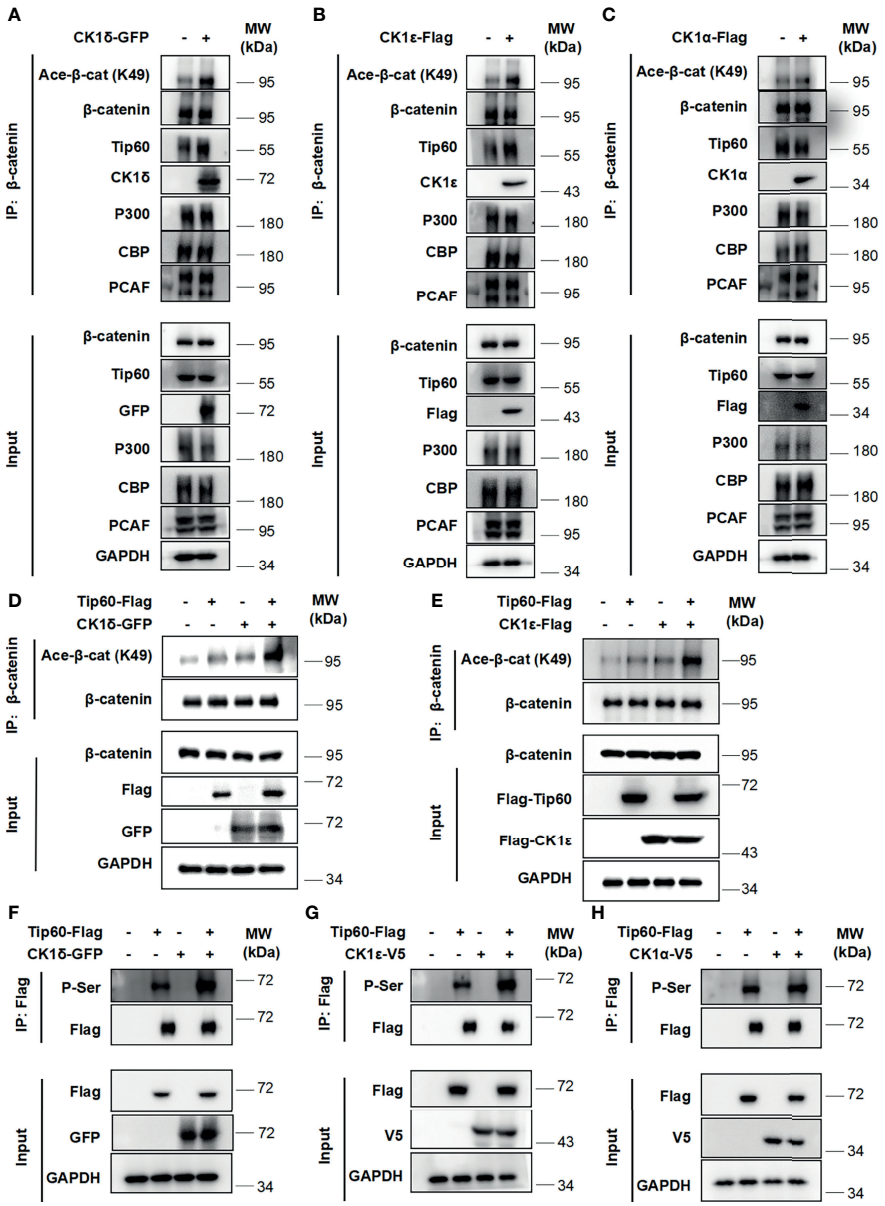

FIGURE 2 | CK1δ/ϵ promotes β-catenin acetylation through enhancing the association of β-catenin with Tip60. **(A–C)** HEK293T cells were transfected with CK1δ-GFP, CK1ϵ-Flag and CK1α-Flag expression plasmids, and cell lysates were immunoprecipitated with anti-β-catenin agarose beads. The interaction between β-catenin and some histone acetyltransferases (Tip60, PCAF, p300, and CBP) was detected by immunoblotting. **(D, E)** HEK293T cells were transfected with control vector or Tip60-Flag expression plasmid in the presence or the absence of either CK1δ-Flag **(D)** or CK1ϵ-Flag **(E)** expression vector. The β-catenin protein was pulled down with anti-β-catenin agarose beads. The expression of β-catenin, acetylated β-catenin at K49, Flag-tagged proteins and GAPDH was detected by Western blotting. **(F–H)** HEK293T cells were transfected with control vector or Tip60-Flag expression plasmid in the presence or absence of either CK1δ-GFP **(F)** or CK1ϵ-V5 **(G)** or CK1α-V5 **(H)** expression plasmids. Whole cell lysates were immunoprecipitated with anti-Flag agarose beads. The expression of serine-phosphorylated Tip60, Tip60-Flag, CK1δ-GFP, CK1ϵ-V5, CK1α-V5 and GAPDH was measured by Western blotting. The expression of serine-phosphorylated Tip60 was detected by an anti-phospho-serine antibody.

cells (**Figures S2A, B**). Consistently, treatment with the protein synthesis inhibitor CHX did not alter the kinetics of β-catenin degradation in CK1δ/ϵ-knockdown SW480 cells (**Figure S2C**). However, we detected significantly decreased level of β-catenin acetylation at K49 in CK1δ/ϵ-knockdown cells (**Figure S2C**). These results indicated that CK1δ and CK1ϵ could enhance the acetylation of β-catenin, but had little effect on its stability in colon cancer cells.

We further assessed whether the inhibition of CK1δ/ϵ activity by SR3029 had any effect on β-catenin binding to the Wnt target gene promoter. The ChIP assay was performed to detect β-catenin binding to the promoters of two known Wnt target

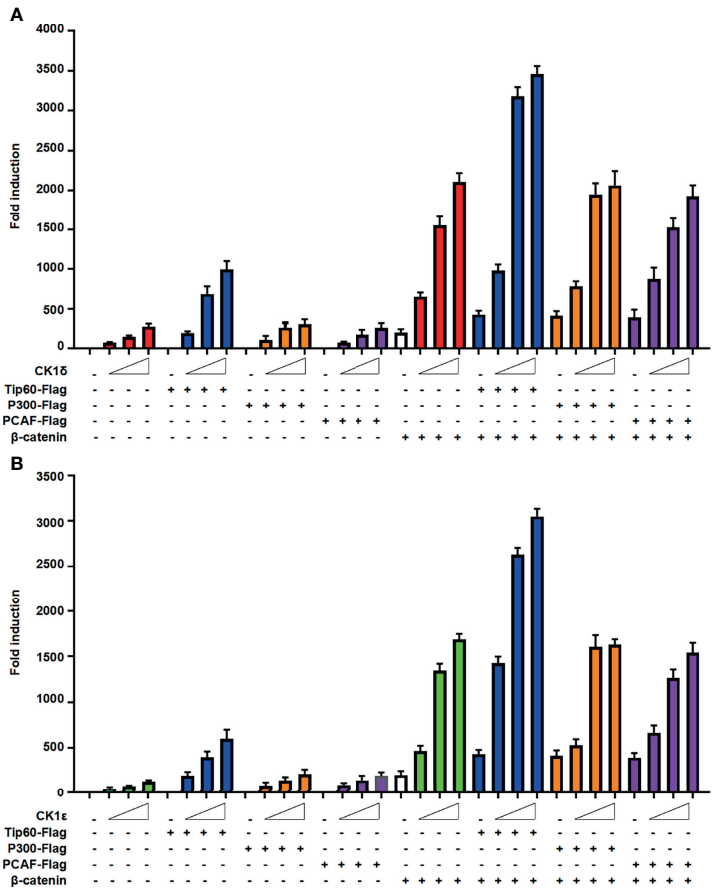

FIGURE 3 | Tip60 enhances the transcriptional activity induced by CK1δ/ϵ or/and β-catenin. **(A, B)** The SuperTopFlash reporter was transfected into HEK293T cells with control vector or increasing amounts of CK1δ **(A)** or CK1ϵ **(B)** expression plasmids together with expression vectors encoding Tip60-Flag, p300-Flag and PCAF-Flag with or without β-catenin expression vector. The luciferase values were normalized to β-gal activities. Each treatment was performed in four replicates.

genes, Survivin and Axin2, in SW480 cells. Our results showed that SR3029 treatment significantly reduced β-catenin binding to the promoters of Survivin and Axin2 (**Figures S3A, B**). We also examined the effect of CK1δ and CK1ϵ on colon cancer cell viability and proliferation. Knockdown of either CK1δ or CK1ϵ decreased the viability and proliferation in SW480 and HCT116 cells. Simultaneous knockdown of CK1δ and CK1ϵ exerted greater inhibition of viability and proliferation in both cells (**Figures S4A–D**). Taken together, these results illustrated that silencing of CK1δ/1ϵ or treatment with CK1 inhibitor could reduce the β-catenin acetylation and suppress β-catenin binding to the promoters of Wnt target genes, resulting in the inhibition of colon cancer cell viability and proliferation.

Silencing Tip60 or Treatment With Tip60 Inhibitors Downregulate the Level of β-Catenin Acetylation at K49 in Colon Cancer Cells

To determine whether Tip60 is able to regulate the acetylation of β-catenin, we silenced the expression of Tip60 using lentivirus-mediated shRNAs in colon cancer cells. Depletion of Tip60 downregulated the level of β-catenin acetylation at K49 without influencing total β-catenin expression in SW480 and HCT116 cells (**Figures 6A, B**). Two small molecular Tip60 inhibitors MG149 and NU9056 were used to block the activity of Tip60 in SW480 and HCT116 cells. The K49 acetylation of β-catenin was significantly reduced upon treatment with either MG149 or NU9056 (**Figures 6C–F**). Collectively, our results illustrated that Tip60 could regulate β-catenin acetylation in colon cancer cells.

Combined Treatment With SR3029 and MG149 Has More Potent Effect on β-Catenin Acetylation, the Transcription of Wnt Target Genes, Cell Viability and Proliferation in Colon Cancer Cells

To assess the potential consequence of combined inhibition of CK1δ/ϵ and Tip60 activities, we tested the effect of combined treatment with CK1δ/ϵ inhibitor SR3029 and Tip60 inhibitor MG149 on β-catenin acetylation, the transcription of Wnt target

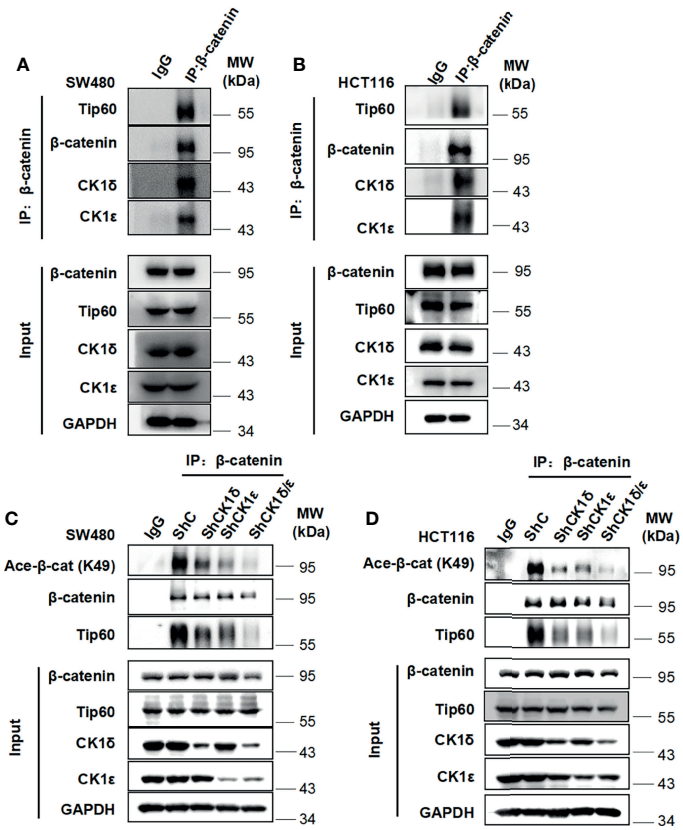

FIGURE 4 | The CK1δ/CK1ε/β-catenin/Tip60 complex is detected in colon cancer cells and β-catenin interacts with Tip60 in a CK1δ/CK1ε-dependent manner. **(A, B)** Cell lysates from SW480 **(A)** or HCT116 **(B)** cells were immunoprecipitated with normal IgG control or anti-β-catenin agarose beads, Immunoblot analysis was performed to detect the interaction among β-catenin, Tip60 and CK1δ/ε using the indicated antibodies. **(C, D)** SW480 **(C)** or HCT116 **(D)** cells were infected with shNC, shCK1δ-2, shCK1ε-2, shCK1δ/ε-2 lentivirus, then cells were lysed and subjected to immunoprecipitation with anti-β-catenin agarose beads. Immunoblotting was performed using the indicated antibodies.

genes, cell viability and proliferation in colon cancer cells. SW480 and HCT116 cells were treated with SR3029 (240 nM) and MG149 (5 and 10 μM), alone or combined. Our results showed that combined treatment markedly downregulated the level of β-catenin acetylation at K49 (**Figures 7A, B**) and the transcription of Wnt target genes Survivin, Cyclin D1 and PROM1 (**Figures S5A–F**) compared with either drug alone. Furthermore, combined treatment of SR3029 and MG149 was more effective than either drug alone in inhibiting viability and proliferation in SW480 and HCT116 cells (**Figures 7C–F**). These results revealed that combined inhibition of CK1δ/ε and Tip60 activities exert a more profound inhibitory effect on β-catenin acetylation, the transcription of Wnt target genes, the viability and proliferation in colon cancer cells.

DISCUSSION

Aberrant activation of canonical Wnt/β-catenin signaling plays a crucial role in proliferation, cellular stemness and chemoresistance in colon cancer (43). Mutations in the APC, β-catenin and RNF43 genes result in the abnormal accumulation of β-catenin and upregulation of Wnt target genes (43–46). Moreover, CK1δ and CK1ε have been shown to be highly expressed in colon cancer tissues. The upregulation of CK1δ and CK1ε were closely associated with advanced progression and poorer prognosis of colon cancer (34, 41, 42). So far, the molecular mechanism underlying CK1δ/ε-mediated downstream events in the Wnt/β-catenin signaling cascade remain unclear. In the present study, we demonstrated that CK1δ/ε increased β-catenin-mediated transcription *via* modulating the acetylation of β-catenin at K49. The interaction of CK1δ/ε with Tip60 recruited Tip60 to β-catenin complex, leading to β-catenin acetylation and the activation of Wnt signaling. Our results revealed a novel molecular mechanism by which CK1δ/ε enhances β-catenin-mediated transcription in colon cancer.

Previous studies have reported that different CK1 family members could exert a coordinated action in the activation of Wnt signaling (26). CK1α has been shown to phosphorylate β-catenin at S45, which is required for subsequent GSK-3β

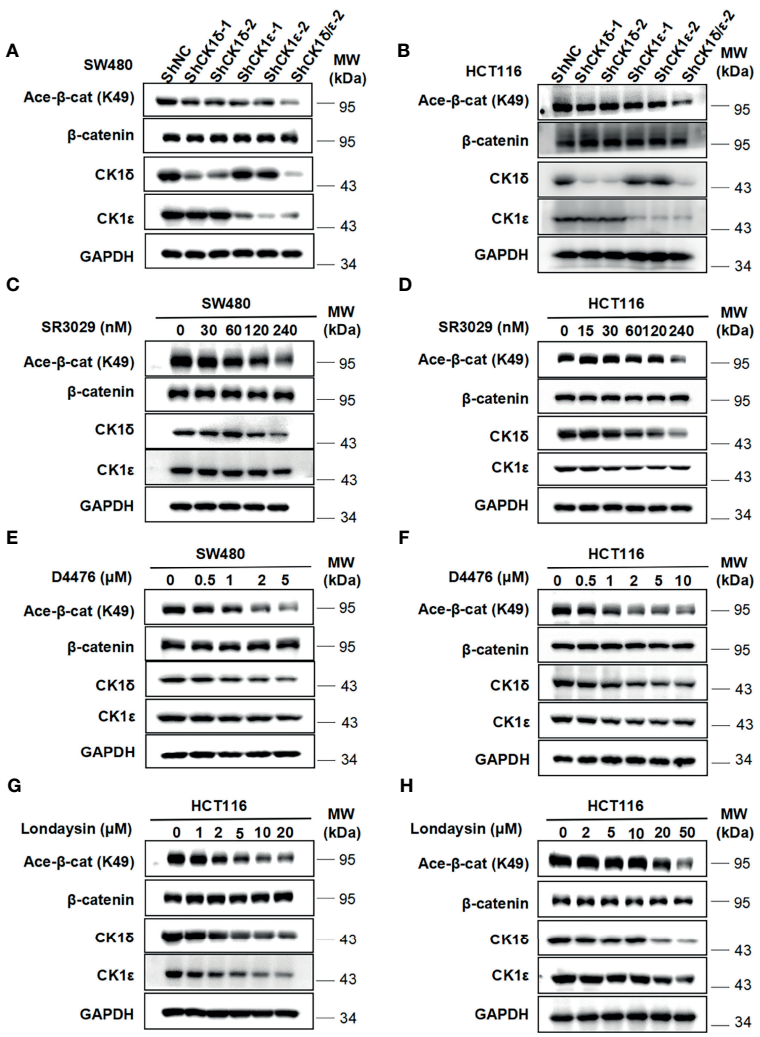

FIGURE 5 | Depletion of CK1δ/ϵ or treatment with CK1 inhibitors downregulate the level of β-catenin acetylation at K49 in colon cancer cells. **(A, B)** The expression of endogenous CK1δ and CK1ϵ was knocked down by infecting SW480 **(A)** and HCT116 **(B)** cells with shNC, shCK1δ-1, shCK1δ-2, shCK1ϵ-1, shCK1ϵ-2 and shCK1δ/ϵ-2 lentivirus. The levels of β-catenin, acetylated β-catenin at K49, CK1δ, CK1ϵ and GAPDH were detected by immunoblotting. **(C, D)** SW480 **(C)** and HCT116 **(D)** cells were serum-starved for 12 h and subsequently treated with the indicated amounts of SR3029 for 12 h Cell lysates were subjected to immunoblotting with the indicated antibodies. **(E, F)** Similar to panel C and D except that the indicated concentrations of D4476 were used. **(G, H)** Similar to panel **(C, D)** except that the indicated concentrations of longdaysin were used.

phosphorylation and degradation of β-catenin (26–28). CK1δ and CK1ϵ could positively regulate the Wnt/β-catenin pathway by acting on multiple targets, such as DVL, LRP6 and AES (32–34, 47, 48). In this study, our results demonstrated that CK1δ/ϵ could interact with and phosphorylate Tip60, promote the association of β-catenin with Tip60, and lead to the acetylation of β-catenin at K49. Simultaneous knockdown of CK1δ and CK1ϵ, or treatment with chemical CK1 inhibitors caused the downregulation of β-catenin acetylation at K49 in colon cancer cells. As expected, we observed that the expression of CK1α or CK1δ or CK1ϵ increased the phosphorylation of endogenous or exogenous β-catenin at S45 (**Figures S6A, B**). However, CK1α had little effect on Tip60 phosphorylation and the interaction between β-catenin with Tip60. These results suggest that CK1δ/ϵ-mediated phosphorylation of β-catenin at S45 may not be related to the positive regulatory function of CK1δ/ϵ in the Wnt pathway.

Increasing evidence shows that the acetylation of β-catenin has been implicated in regulating its stability, subcellular location, specific interactions, and transactivational activity (5, 6, 8, 49). The β-catenin protein has been reported to be acetylated by CBP at K49, which is frequently found mutated in multiple cancers (5). Levy et al. showed that the acetylation of β-catenin at K345 by p300 increased the affinity of β-catenin for TCF4 (6). PCAF has been shown to acetylate β-catenin at K19 and 49, improving the stability and transcriptional activity of β-catenin

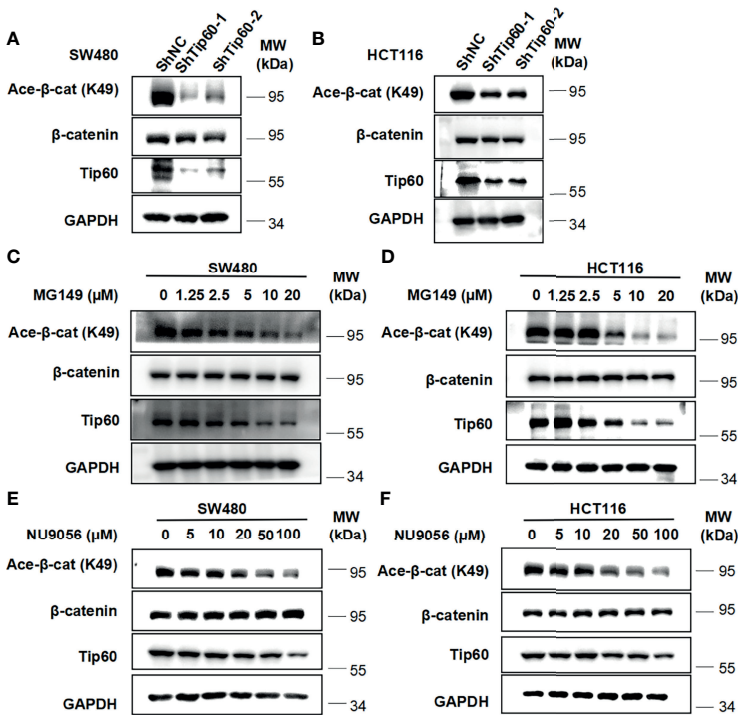

FIGURE 6 | Silencing Tip60 or treatment with Tip60 inhibitors downregulate the level of β-catenin acetylation at K49 in colon cancer cells. **(A, B)** SW480 **(A)** and HCT116 **(B)** cells were infected with shNC, shTip60-1 and shTip60-2 lentivirus, respectively. The expression of β-catenin, acetylated β-catenin at K49, CK1δ, CK1ε and GAPDH was measured by immunoblotting. **(C, D)** SW480 **(C)** and HCT116 **(D)** cells were serum-starved for 12 h and subsequently treated with the indicated amounts of MG149 for 12 h Cell lysates were subjected to immunoblotting with the indicated antibodies. **(E, F)** Similar to panel **(C, D)** except that the indicated concentrations of NU9056 were used.

(7). Recently, cell-cycle related and expression-elevated protein (CREPT) was identified as a potential oncogene in colorectal cancer. CREPT could enhance the association of p300 with β-catenin, thus promoting p300-mediated β-catenin acetylation and stabilization (50). Li et al. reported that block of proliferation 1 (BOP1) could increase Wnt/β-catenin signaling by enhancing CBP recruitment to β-catenin, thus promoting β-catenin acetylation and activation (51). A recent study showed that Bcl-3 could enhance the Wnt signaling cascade by maintaining the acetylation of β-catenin at K 49 in colorectal cancer (40). In our study, we provided several lines of evidence to demonstrate that Tip60 could acetylate β-catenin at K49 in a CK1δ/ε-dependent manner. First, CK1δ or CK1ε significantly enhanced the association of β-catenin with Tip60, but not p300 or CBP or PCAF; Second, CK1δ/ε could bind to Tip60 and increased the phosphorylation of Tip60. Future studies are needed to identify specific phosphorylation sites of Tip60 by CK1δ/ε; Third, the CK1δ/CK1ε/β-catenin/Tip60 complex was observed in colon cancer cells, and simultaneous knockdown of CK1δ and CK1ε markedly attenuated the association of β-catenin with Tip60; Fourth, knockdown of CK1δ/ε or treatment with CK1 inhibitors downregulated the level of β-catenin acetylation at K49 in colon cancer cells. Silencing Tip60 or treatment with Tip60 inhibitors also decrease the level of β-catenin acetylation at K49; Fifth, combined treatment with CK1 inhibitor SR3029 and Tip60 inhibitor MG149 had more potent effect on downregulation of β-catenin acetylation and Wnt target genes. Finally, Tip60 significantly enhanced the SuperTopFlash reporter activity induced by CK1δ/ε or/and β-catenin. Taken together, our results showed that CK1δ/ε could increase the interaction between β-catenin and Tip60, facilitating the recruitment of Tip60 to β-catenin complex, resulting in the acetylation of β-catenin at K49 and promoting of β-catenin-mediated transcriptional activity. However, we could not check the acetylation status of other lysine residues of β-catenin due to the lack of suitable antibodies. Future studies are needed to examine whether Tip60 also acetylates other lysine residues of β-catenin in a CK1δ/ε-dependent fashion.

In conclusion, our study demonstrated that CK1δ/ε could increase the transcriptional activity of β-catenin through regulating β-catenin acetylation at K49. CK1δ/ε potentiated the association of β-catenin with Tip60, and facilitated the recruitment of Tip60 to β-catenin complex, thereby leading to the acetylation of β-catenin at K49. Blockade of CK1δ/ε or/and Tip60 downregulated β-catenin acetylation and the

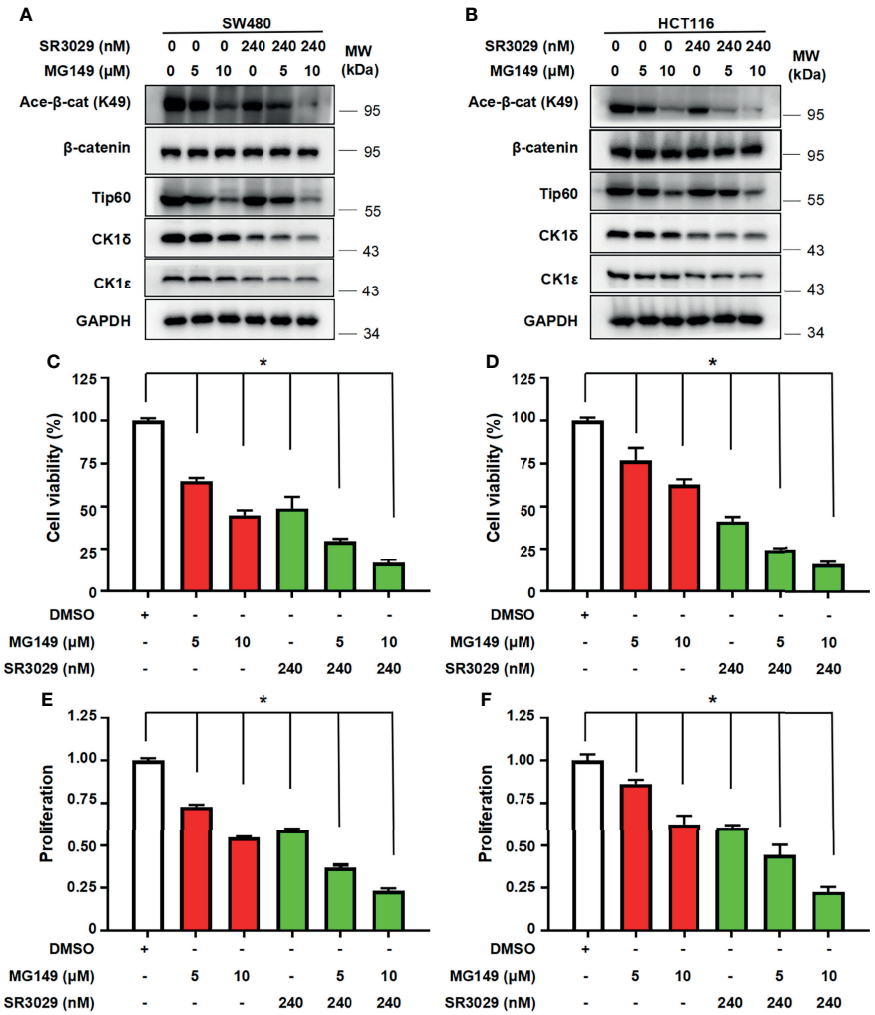

FIGURE 7 | Combined treatment with SR3029 and MG149 exhibits more potent effect on β-catenin acetylation, cell viability and proliferation in colon cancer cells. **(A, B)** SW480 **(A)** and HCT116 **(B)** cells were serum-starved for 12 h and subsequently treated with MG149 (5 and 10 μM) alone or combined with 240 nM SR3029 for 12 h The protein levels of β-catenin, acetylated β-catenin at K49, Tip60, CK1δ, CK1ε and GAPDH were detected by immunoblotting. **(C–F)** SW480 **(C, E)** and HCT116 **(D, F)** cells were serum-starved for 12 h and subsequently treated with MG149 (5 and 10 μM) alone or combined with 240 nM SR3029. After 48 h of treatment, MTT assay was used to detect cell viability **(C, D)**. Cell proliferation was detected using BrdU incorporation assay **(E, F)**. The data from three independent experiments are presented (n=3). Values shown are means ± SD. *P<0.05, significantly different from the vehicle control; one-way ANOVA followed by Dunnett's test **(C–F)**.

transcription of Wnt target genes, resulting in growth inhibition of colon cancer cells. Our study define a novel CK1δ/ε-β-catenin-Tip60 axis which is implicated in modulation of β-catenin-mediated transcription.

DATA AVAILABILITY STATEMENT

The original contributions presented in the study are included in the article/**Supplementary Material**. Further inquiries can be directed to the corresponding author.

AUTHOR CONTRIBUTIONS

JN and DL developed the concept and designed this work. JN, QS, ZS, LT, YT, SS, and HL performed the experiments, carried out the data acquisition. JN, QS, ZS, VX, SL, XC, and DL performed data analysis. JN, QS, and DL edited and revised the manuscript. DL supervised this study. All authors read and approved this manuscript.

FUNDING

This work was supported by the National Natural Science Foundation of China (31970739 and 81802662), the Natural

Science Foundation of Guangdong Province (2020A1515010340 and 2020A1515010543), the Shenzhen Key Basic Research Program (JCYJ20200109105001821), the Shenzhen Natural Science Fund (the Stable Support Plan Program) (20200826134656001).

ACKNOWLEDGMENTS

We would like to acknowledge the support provided by International Science and Technology Cooperation: Carson Cancer Stem Cell Vaccines R&D Center, Shenzhen University, and Instrument Analysis Center of Shenzhen University for the assistance with immunofluorescence analysis.

SUPPLEMENTARY MATERIAL

The Supplementary Material for this article can be found online at: https://www.frontiersin.org/articles/10.3389/fonc.2022.844477/full#supplementary-material

REFERENCES

1. Nusse R, Clevers H. Wnt/β-Catenin Signaling, Disease, and Emerging Therapeutic Modalities. *Cell* (2017) 169(6):985–99. doi: 10.1016/j.cell.2017.05.016
2. Ring A, Kim Y-M, Kahn M. Wnt/catenin Signaling in Adult Stem Cell Physiology and Disease. *Stem Cell Rev Rep* (2014) 10(4):512–25. doi: 10.1007/s12015-014-9515-2
3. Gao C, Xiao G, Hu J. Regulation of Wnt/β-Catenin Signaling by Posttranslational Modifications. *Cell Biosci* (2014) 4(13):1–20. doi: 10.1186/2045-3701-4-13
4. Grainger S, Willert K. Mechanisms of Wnt Signaling and Control. *Wiley Interdiscip Rev Syst Biol Med* (2018) 10(5):e1422. doi: 10.1002/wsbm.1422
5. Wolf D, Rodova M, Miska EA, Calvet JP, Kouzarides T. Acetylation of β-Catenin by CREB-Binding Protein (CBP). *J Biol Chem* (2002) 277(28):25562–7. doi: 10.1074/jbc.M201196200
6. Lévy L, Wei Y, Labalette C, Wu Y, Renard C-A, Buendia MA, et al. Acetylation of β-Catenin by P300 Regulates β-Catenin-Tcf4 Interaction. *Cell Mol Biol* (2004) 24(8):3404–14. doi: 10.1128/mcb.24.8.3404-3414.2004
7. Ge X, Jin Q, Zhang F, Yan T, Zhai Q, Ginsberg MH. PCAF Acetylates {Beta}-Catenin and Improves its Stability. *Mol Biol Cell* (2009) 20(1):419–27. doi: 10.1091/mbc.e08-08-0792
8. Ma H, Nguyen C, Lee K-S, Kahn M. Differential Roles for the Coactivators CBP and P300 on TCF/β-Catenin-Mediated Survivin Gene Expression. *Oncogene* (2005) 24(22):3619–31. doi: 10.1038/sj.onc.1208433
9. Sapountzi V, Logan IR, Robson CN. Cellular Functions of Tip60. *Int J Biochem Cell B* (2006) 38(9):1496–509. doi: 10.1016/j.biocel.2006.03.003
10. Sun Y, Jiang X, Price BD. Tip60: Connecting Chromatin to DNA Damage Signaling. *Cell Cycle* (2010) 9(5):930–6. doi: 10.4161/cc.9.5.10931
11. Ikura T, Ogryzko VV, Grigoriev M, Groisman R, Wang J, Horikoshi M, et al. Involvement of the Tip60 Histone Acetylase Complex in DNA Repair and Apoptosis. *Cell* (2000) 102:463–73. doi: 10.1016/s0092-8674(00)00051-9
12. Lin S-Y, Yang Li T, Liu Q, Zhang C, Li X, Chen Y, et al. GSK3-Tip60-ULK1 Signaling Pathway Links Growth Factor Deprivation to Autophagy. *Science* (2012) 336(27):477–81. doi: 10.1126/science.1217032
13. Sun Y, Jiang X, Xu Y, Ayrapetov MK, Moreau LA, Whetstine JR, et al. Histone H3 Methylation Links DNA Damage Detection to Activation of the Tumour Suppressor Tip60. *Nat Cell Biol* (2009) 11(11):1376–82. doi: 10.1038/ncb1982
14. Tang Y, Luo J, Zhang W, Gu W. Tip60-Dependent Acetylation of P53 Modulates the Decision Between Cell-Cycle Arrest and Apoptosis. *Mol Cell* (2006) 24(6):827–39. doi: 10.1016/j.molcel.2006.11.021
15. Sun Y, Jiang X, Chen S, Fernandes N, Price BD. A Role for the Tip60 Histone Acetyltransferase in the Acetylation and Activation of ATM. *Proc Natl Acad Sci USA* (2005) 102(37):13182–7. doi: 10.1073/pnas.0504211102
16. Halkidou K, Gnanapragasam VJ, Mehta PB, Logan IR, Brady ME, Cook S, et al. Expression of Tip60, an Androgen Receptor Coactivator, and its Role in Prostate Cancer Development. *Oncogene* (2003) 22(16):2466–77. doi: 10.1038/sj.onc.1206342
17. Sakuraba K, Yasuda T, Sakata M, Kitamura Y-H, Shirahata A, Goto T, et al. Down-Regulation of Tip60 Gene as a Potential Marker for the Malignancy of Colorectal Cancer. *Anticancer Res* (2009) 29:3953–6.
18. Pandey AK, Zhang Y, Zhang S, Li Y, Tucker-Kellogg G, Yang H, et al. Tip60-miR-22 Axis as a Prognostic Marker of Breast Cancer Progression. *Oncotarget* (2015) 6(38):41290–306. doi: 10.18632/oncotarget.5636
19. Chen G, Cheng Y, Tang Y, Martinka M, Li G. Role of Tip60 in Human Melanoma Cell Migration, Metastasis, and Patient Survival. *J Invest Dermatol* (2012) 132(11):2632–41. doi: 10.1038/jid.2012.193
20. Sakuraba K, Yokomizo K, Shirahata A, Goto T, Saito M, Ishibashi K, et al. Tip60 as a Potential Marker for the Malignancy of Gastric Cancer. *Anticancer Res* (2011) 31(1):77–9.
21. Tan KN, Avery VM, Carrasco-Pozo C. Metabolic Roles of Androgen Receptor and Tip60 in Androgen-Dependent Prostate Cancer. *Int J Mol Sci* (2020) 21(18):6622. doi: 10.3390/ijms21186622
22. Stacy AJ, Zhang J, Craig MP, Hira A, Dole N, Kadakia MP. TIP60 Up-Regulates Δnp63α to Promote Cellular Proliferation. *J Biol Chem* (2019) 294(45):17007–16. doi: 10.1074/jbc.RA119.010388
23. Culig Z, Coffey K, Blackburn TJ, Cook S, Golding BT, Griffin RJ, et al. Characterisation of a Tip60 Specific Inhibitor, NU9056, in Prostate Cancer. *PloS One* (2012) 7(10):e45539. doi: 10.1371/journal.pone.0045539
24. Gao C, Bourke E, Scobie M, Famme MA, Koolmeister T, Helleday T, et al. Rational Design and Validation of a Tip60 Histone Acetyltransferase Inhibitor. *Sci Rep* (2014) 4(5372):1–10. doi: 10.1038/srep05372
25. Cheong JK, Virshup DM. Casein Kinase 1: Complexity in the Family. *Int J Biochem Cell B* (2011) 43(4):465–9. doi: 10.1016/j.biocel.2010.12.004
26. Cruciat C-M. Casein Kinase 1 and Wnt/β-Catenin Signaling. *Curr Opin Cell Biol* (2014) 31:46–55. doi: 10.1016/j.ceb.2014.08.003
27. Stamos JL, Weis WI. The β-Catenin Destruction Complex. *Cold Spring Harb Perspect Biol* (2012) 5(1):a007898–a. doi: 10.1101/cshperspect.a007898
28. Liu C, Li Y, Semenov M, Han C, Tan Y, Zhang Z, et al. Control of β-Catenin Phosphorylation/Degradation by a Dual-Kinase Mechanism. *Cell* (2002) 108:837–47. doi: 10.1016/S0092-8674(02)00685-2
29. Davidson G, Wu W, Shen J, Bilic J, Fenger U, Stannek P, et al. Casein Kinase 1 γ Couples Wnt Receptor Activation to Cytoplasmic Signal Transduction. *Nature* (2005) 438(7069):867–72. doi: 10.1038/nature04170
30. del Valle-Perez B, Arques O, Vinyoles M, de Herreros AG, Dunach M. Coordinated Action of CK1 Isoforms in Canonical Wnt Signaling. *Mol Cell Biol* (2011) 31(14):2877–88. doi: 10.1128/mcb.01466-10
31. González-Sancho JM, Greer YE, Abrahams CL, Takigawa Y, Baljinnyam B, Lee KH, et al. Functional Consequences of Wnt-Induced Dishevelled 2 Phosphorylation in Canonical and Noncanonical Wnt Signaling. *J Biol Chem* (2013) 288(13):9428–37. doi: 10.1074/jbc.M112.448480
32. Niehrs C, Shen J. Regulation of Lrp6 Phosphorylation. *Cell Mol Life Sci* (2010) 67(15):2551–62. doi: 10.1007/s00018-010-0329-3
33. Zeng X, Tamai K, Doble B, Li S, Huang H, Habas R, et al. A Dual-Kinase Mechanism for Wnt Coreceptor Phosphorylation and Activation. *Nature* (2005) 438(7069):873–7. doi: 10.1038/nature04185
34. Wang Z, Zhou L, Wang Y, Peng Q, Li H, Zhang X, et al. The Ck1δ/ε-AES Axis Regulates Tumorigenesis and Metastasis in Colorectal Cancer. *Theranostics* (2021) 11(9):4421–35. doi: 10.7150/thno.53901
35. Su Z, Song J, Wang Z, Zhou L, Xia Y, Yu S, et al. Tumor Promoter TPA Activates Wnt/β-Catenin Signaling in a Casein Kinase 1-Dependent Manner. *Proc Natl Acad Sci USA* (2018) 115(32):E7522–E31. doi: 10.1073/pnas.1802422115

36. Wang L, Deng K, Gong L, Zhou L, Sayed S, Li H, et al. Chlorquinaldol Targets the β-Catenin and T-Cell Factor 4 Complex and Exerts Anti-Colorectal Cancer Activity. *Pharmacol Res* (2020) 159:104955. doi: 10.1016/j.phrs.2020.104955
37. Xiong Y, Zhou L, Su Z, Song J, Sun Q, Liu S-S, et al. Longdaysin Inhibits Wnt/β-Catenin Signaling and Exhibits Antitumor Activity Against Breast Cancer. *OncoTargets Ther* (2019) 12:993–1005. doi: 10.2147/ott.s193024
38. Chen H, Shan J, Liu J, Feng Y, Ke Y, Qi W, et al. RNF8 Promotes Efficient DSB Repair by Inhibiting the Pro-Apoptotic Activity of P53 Through Regulating the Function of Tip60. *Cell Proliferat* (2020) 53(3):1–15. doi: 10.1111/cpr.12780
39. Hoffmeyer K, Junghans D, Kanzler B, Kemler R. Trimethylation and Acetylation of β-Catenin at Lysine 49 Represent Key Elements in ESC Pluripotency. *Cell Rep* (2017) 18 (12):2815–24. doi: 10.1016/j.celrep.2017.02.076
40. Chen X, Wang C, Jiang Y, Wang Q, Tao Y, Zhang H, et al. Bcl-3 Promotes Wnt Signaling by Maintaining the Acetylation of β-Catenin at Lysine 49 in Colorectal Cancer. *Signal Transduct Tar* (2020) 5(52):1–12. doi: 10.1038/s41392-020-0138-6
41. Liu M, Hu Y, Lu S, Lu M, Li J, Chang H, et al. IC261, a Specific Inhibitor of CK1δ/ϵ, Promotes Aerobic Glycolysis Through P53-Dependent Mechanisms in Colon Cancer. *Int J Biol Sci* (2020) 16(5):882–92. doi: 10.7150/ijbs.40960
42. Richter J, Ullah K, Xu P, Alscher V, Blatz A, Peifer C, et al. Effects of Altered Expression and Activity Levels of CK1δ and ε on Tumor Growth and Survival of Colorectal Cancer Patients. *Int J Cancer* (2015) 136(12):2799–810. doi: 10.1002/ijc.29346
43. Sebio A, Kahn M, Lenz H-J. The Potential of Targeting Wnt/β-Catenin in Colon Cancer. *Expert Opin Ther Targets* (2014) 18(6):611–5. doi: 10.1517/14728222.2014.906580
44. Mehta A, Patel BM. Therapeutic Opportunities in Colon Cancer: Focus on Phosphodiesterase Inhibitors. *Life Sci* (2019) 230:150–61. doi: 10.1016/j.lfs.2019.05.043
45. Slattery ML, Pellatt DF, Mullany LE, Wolff RK, Herrick JS. Gene Expression in Colon Cancer: A Focus on Tumor Site and Molecular Phenotype. *Gene Chromosome Canc* (2015) 54(9):527–41. doi: 10.1002/gcc.22265
46. Giannakis M, Hodis E, Jasmine Mu X, Yamauchi M, Rosenbluh J, Cibulskis K, et al. RNF43 is Frequently Mutated in Colorectal and Endometrial Cancers. *Nat Genet* (2014) 46(12):1264–6. doi: 10.1038/ng.3127
47. Swiatek W, Tsai IC, Klimowski L, Pepler A, Barnette J, Yost HJ, et al. Regulation of Casein Kinase Iε Activity by Wnt Signaling. *J Biol Chem* (2004) 279(13):13011–7. doi: 10.1074/jbc.M304682200
48. Cong F, Schweizer L, Varmus H. Casein Kinase Iε Modulates the Signaling Specificities of Dishevelled. *Mol Cell Biol* (2004) 24(5):2000–11. doi: 10.1128/mcb.24.5.2000-2011.2004
49. Hecht A, Vleminckx K, Stemmler MP, Roy Fv, Kemler R. The P300/CBP Acetyltransferases Functions as Transcriptional Coactivators of β-Catenin in Vertebrates. *EMBO* (2000) 19(9):1839–50. doi: 10.1093/emboj/19.8.1839
50. Zhang Y, Wang S, Kang W, Liu C, Dong Y, Ren F, et al. CREPT Facilitates Colorectal Cancer Growth Through Inducing Wnt/β-Catenin Pathway by Enhancing P300-Mediated β-Catenin Acetylation. *Oncogene* (2018) 37 (26):3485–500. doi: 10.1038/s41388-018-0161-z
51. Li S, Wu H, Huang X, Jian Y, Kong L, Xu H, et al. BOP1 Confers Chemoresistance of Triple-Negative Breast Cancer by Promoting CBP-Mediated β-Catenin Acetylation. *J Pathol* (2021) 254(3):265–78. doi: 10.1002/path.5676

Conflict of Interest: The authors declare that the research was conducted in the absence of any commercial or financial relationships that could be construed as a potential conflict of interest.

frontiers | Frontiers in Cell and Developmental Biology

ORIGINAL RESEARCH
published: 03 June 2022
doi: 10.3389/fcell.2022.817509

Integrative Analysis Revealed Stemness Features and a Novel Stemness-Related Classification in Colorectal Cancer Patients

Meng-Ling Ye†, Si-Qi Li†, Yi-Xin Yin, Ke-Zhi Li, Ji-Lin Li and Bang-Li Hu**

Department of Research, Guangxi Medical University Cancer Hospital, Nanning, China

Cancer stem cells play crucial roles in colorectal cancer (CRC) tumorigenesis and treatment response. This study aimed to determine the value of the mRNA stemness index (mRNAsi) in CRC and introduce a stemness-related classification to predict the outcome of patients. mRNAsi scores and RNA sequence data of CRC patients were analyzed. We found that high mRNAsi scores were related to early-stage CRC and a better patient prognosis. Two stemness-based subtypes (subtype I and II) were identified. Patients in subtype I presented a significantly better prognosis than those in subtype II. Patients in these two subtype groups presented significantly different tumor immunity scores and immune cell infiltration patterns. Genomic variations revealed that patients in subtype I had a lower tumor mutation burden than those in subtype II. A three-gene stemness subtype predictor was established, showing good diagnostic value in discriminating patients in different subtypes. A prognostic signature based on five stemness-related genes was established and validated in two independent cohorts and clinical samples, showing a better predictive performance than other clinical parameters. We concluded that mRNAsi scores were associated with the clinical outcome in CRC patients. The stemness-related classification was a promising prognostic predictor for CRC patients.

Keywords: colorectal cancer, cancer stemness, tumor microenvironment, immunotherapy, prognosis

OPEN ACCESS

Edited by:
Shilpa S. Dhar, University of Texas MD Anderson Cancer Center, United States

Reviewed by:
Marco A. Velasco-Velazquez, National Autonomous University of Mexico, Mexico
Shaying Zhao, University of Georgia, United States

****Correspondence:***
Ji-Lin Li
455620024@qq.com
Bang-Li Hu
hubangli@gxmu.edu.cn

†These authors have contributed equally to this work

Specialty section:
This article was submitted to Molecular and Cellular Oncology, a section of the journal Frontiers in Cell and Developmental Biology

Received: *18 November 2021*
Accepted: *05 May 2022*
Published: *03 June 2022*

Citation:
Ye M-L, Li S-Q, Yin Y-X, Li K-Z, Li J-L and Hu B-L (2022) Integrative Analysis Revealed Stemness Features and a Novel Stemness-Related Classification in Colorectal Cancer Patients. Front. Cell Dev. Biol. 10:817509. doi: 10.3389/fcell.2022.817509

INTRODUCTION

Colorectal cancer (CRC) is the third most common cancer and the fourth most frequent cause of cancer-related death worldwide (Araghi et al., 2019). In recent years, the CRC incidence has been steadily rising worldwide, especially in developing countries (Cao et al., 2020). The pathogenesis of CRC is a complex process involving molecular alterations, gene mutations, as well as inflammatory and immune cells. These are crucial factors contributing to CRC development, treatment response, and prognosis. Although significant advancement has been made in the treatment of CRC, the prognosis of patients at later stages remains poor due to tumor metastasis, chemoresistance, and other factors (Galbraith et al., 2021; Zaborowski et al., 2021). Therefore, screening patients at a high potential risk of treatment failure or poor prognosis is critical.

Among the multiple factors involved in CRC pathogenesis, cancer stem cells are essential components of several cancer types (Friedmann-Morvinski and Verma, 2014; Shibue and Weinberg, 2017). Cancer stem cells are those with stem cell–like characteristics that could

convert into various malignant cells with different phenotypes, which are more likely to drive tumor formation, growth, and progression, ultimately affecting treatment response, tumor relapse, and prognosis (Reya et al., 2001). Therefore, finding a quantitative indicator to evaluate the degree of oncogenic dedifferentiation might help predict the outcome of cancer patients. In 2018, Malta et al. (2018) introduced the stemness index to assess the degree of oncogenic dedifferentiation through a one-class logistic regression machine learning algorithm to analyze the epigenetic and transcriptomic features derived from non-transformed stem cells and the differentiated progeny, including RNA-based stemness index (mRNAsi), DNA methylation-based stemness index, and epigenetically regulated-mRNAsi (EREG-mRNAsi). They implemented these indices to evaluate the stemness of each tumor sample in The Cancer Genome Atlas (TCGA) database, showing that these indices could precisely predict metastatic events, interpret intratumoral heterogeneity, and assess the prognosis of patients. In particular, by analyzing transcriptomic data of cancer samples, the mRNAsi yields a better prognostic value in reflecting the cancer stemness.

To date, several studies have utilized the stemness score to determine the prognosis, immunotherapy response, and clinical outcomes of various cancers, such as lung cancer (Liao et al., 2020), glioblastoma (Wang et al., 2021a), and cutaneous melanoma (Wang et al., 2020). However, little is known about the role of the stemness score in CRC, although cancer stem cells are the main culprits involved in CRC therapy resistance and disease recurrence (Zeuner et al., 2014; Das et al., 2020). Therefore, in this study, we analyzed the association of the stemness score with CRC and divided patients into two stemness-based subtype groups. Next, we examined the differences in the clinical outcomes, genomic variations, and tumor microenvironment (TME) of patients in the two stemness subtype groups and constructed a subtype predictor and prognostic signature. In our study, we aimed to explore the clinical value of stemness scores in CRC to enable clinicians to provide appropriate treatment to CRC patients on the basis of stemness subtypes.

MATERIALS AND METHODS

Data Collection and Differential Gene Expression Analysis

The CRC RNA sequence and mutation datasets (TCGA-COADREAD), including 570 colon cancer and 192 rectal cancer samples, were downloaded from TCGA database. The corresponding demographic (age, sex, histological type, and TNM stage) and survival data were extracted. The mRNA stemness index (mRNAsi) of each CRC sample from TCGA database was obtained from a previously published study (Malta et al., 2018). The mRNAsi was represented using a value ranging from 0 to 1. A high mRNAsi score indicated high tumor dedifferentiation and cancer stem cell activity. Two gene expression omnibus (GEO) datasets, GSE29621 and GSE39582, were used to validate the predictive value of the prognostic signature. Another three GEO datasets, GSE73360, GSE50421, GSE89076 and GSE62932 were used to verify the expression of stemness-related genes between tumor and normal tissues. The raw data of each dataset were preprocessed using quantile normalization and Log_2 transformation. The differentially expressed genes (DEGs) between two groups were screened using the "edgeR" package for TCGA dataset and the "limma" package for GEO datasets. An absolute value of a $\log_2$ fold change (logFC) > 0.5 and a p-value < 0.05 were used as the screening criteria for DEG selection.

Gene Functional Enrichment Analysis

The Gene Ontology (GO) and Kyoto Encyclopedia of Genes and Genomes (KEGG) functional enrichment analyses were conducted to determine the biological function of DEGs, including biological processes (BPs), cellular components (CCs), and molecular functions (MFs). Furthermore, the signaling pathways in which DEGs were enriched were determined using the "clusterProfiler" R package (Wu et al., 2021), with thresholds of $p < 0.01$ and FDR < 0.05. Moreover, Gene set variation analysis (GSVA) was applied to screen significantly enriched pathways between two groups using the Molecular Signatures Database (MSigDB) version 7.4 (Liberzon et al., 2015).

Tumor Microenvironment Pattern Analysis

The TME contains tumor cells, immune cells, stromal cells, and other cell types closely related to treatment response and patient prognosis. In this study, the Estimation of Stromal and Immune cells in Malignant Tumor tissues using Expression data (ESTIMATE) algorithm (Yoshihara et al., 2013), which generates four types of immune indexes, including immune score, stromal score, ESTIMATE score, and tumor purity, was employed to evaluate the TME in CRC. In addition, tumor-infiltrating immune cells (TIICs) were quantified using the CIBERSORT algorithm (Newman et al., 2015), generating 22 types of TIICs based on gene expression.

Classification of the Stemness-Related Gene for CRC Patients

The "ConsensusClusterPlus" package (Wilkerson and Hayes, 2010) in R, which provides quantitative stability evidence to determine a cluster count and cluster membership in an unsupervised analysis, was used to perform unsupervised consensus clustering of the samples based on the expression of stemness-related genes. The cumulative distribution function (CDF) curves were used to determine the optimal number of clusters, indexed by k value from 2 to 6. The proportion of the ambiguous clustering algorithm and the consensus Heatmap were also determined using the package.

Construction of the Diagnostic Predictor and Prognostic Signature

For the diagnostic predictor of different stemness subtypes, CRC patients were randomly classified into training and test

TABLE 1 | Comparison of clinical feature between high and low mRNAsi scores.

	High scores (*N* = 293)	Low scores (*N* = 294)	P overall
Age (years)	66.1 ± 12.7	66.5 ± 12.8	0.694
Gender			0.77
Female	135 (46.1%)	140 (47.6%)	
Male	158 (53.9%)	154 (52.4%)	
Location			0.759
Colon	215 (73.4%)	220 (74.8%)	
Rectal	78 (26.6%)	74 (25.2%)	
Histological type			0.152
Adenocarcinoma	258 (88.1%)	246 (83.7%)	
Mucinous	29 (9.90%)	44 (15.0%)	
T stage			0.065
T1	13 (4.44%)	7 (2.38%)	
T2	54 (18.4%)	47 (16.0%)	
T3	202 (68.9%)	198 (67.3%)	
T4	24 (8.19%)	42 (14.3%)	
N stage			0.002
N0	191 (65.2%)	148 (50.3%)	
N1	58 (19.8%)	79 (26.9%)	
N2	43 (14.7%)	66 (22.4%)	
NX	1 (0.34%)	1 (0.34%)	
M stage			0.286
M0	225 (76.8%)	213 (72.4%)	
M1	32 (10.9%)	48 (16.3%)	
MX	33 (11.3%)	30 (10.2%)	
Clinical stage			0.03
I	55 (18.8%)	46 (15.6%)	
II	123 (42.0%)	97 (33.0%)	
III	74 (25.3%)	93 (31.6%)	
IV	31 (10.6%)	50 (17.0%)	
NA	10 (3.41%)	8 (2.72%)	
OS	0.17 (0.37)	0.24 (0.43)	0.033
OS time (days)	886 (825)	754 (620)	0.028

OS: overall survival.

groups. The least absolute shrinkage and selection operator (LASSO) regression, extreme gradient boosting (XGBoost), and a logistic regression model were used to screen the most relevant genes by analyzing the expression of stemness-related genes. The performance of the different algorithms was assessed using receiver operating characteristic (ROC) curves, and then the areas under the curve (AUC) were compared between the two groups. The prognostic signature was constructed by multiplying the expression and the coefficients of each gene from the multiple logistic regression models to generate the risk score according to the following formula: risk score = (β $mRNA_1$ × expression of $mRNA_1$) + (β $mRNA_2$ × expression of $mRNA_2$) +. . .+ (β $mRNA_n$ × expression of $mRNA_n$). The performance of the prognostic signature from TCGA dataset was validated in two independent cohorts.

RT-PCR Assay Using CRC Clinical Samples

This experiment was approved by the ethics committee of our local hospital. Thirty fresh CRC tissues and corresponding adjacent normal tissues were collected from our hospital between January 2020 and March 2021. Total RNA from CRC tissues was isolated using the TRIzol reagent (Invitrogen; Waltham, MA, United States) according to the manufacturer's instructions. The gene primers used for RT-PCR are listed in **Supplementary Table S1**. The RT-PCR procedure was performed using the SYBR Premix Ex Taq kit following the manufacturer's instructions. The relative gene expression of each gene was calculated using the $2^{-\Delta\Delta CT}$ method.

Statistical Analysis

All statistical analyses were conducted using the R software (Version: 3.6.5). The independent Student's t-test or Mann–Whitney U test for continuous data was used to compare two groups where appropriate. Analysis of variance was used to compare differences among three groups. Kaplan–Meier analysis and the log-rank test were used to compare the overall survival (OS). Correlation analysis was performed using Pearson's correlation analysis using the "ggstatsplot" package (Patil, 2021). LASSO regression and XGBoost were performed to screen significant genes using the "glmnet" and "XGBoost" packages, respectively. Univariate and multivariate analyses were conducted using the Cox proportional regression model. A two-tailed p-value < 0.05 was considered statistically significant.

RESULTS

Stemness Scores Associated With Clinical Features in CRC Patients

The workflow of this study is presented in **Supplementary Figure S1**. Patients with CRC were divided into two groups, including 293 and 294 patients, respectively, using the median value of the mRNAsi scores, and the association between mRNAsi and clinical features was analyzed. As summarized in **Table 1**, most patients with high stemness scores were at the early N stage (N0) and clinical stage (I+II) compared with those with low mRNAsi scores ($p < 0.05$), no significant differences were observed between the high and low mRNAsi scores regarding patient age, sex, tumor location, histological type, T stage, and M stage ($p > 0.05$). Kaplan–Meier analysis indicated that patients with high mRNAsi scores or EREG-mRNAsi scores had significantly better OS (mRNAsi: HR = 1.653, log-rank $p = 0.007$; EREG-mRNAsi: HR = 2.099, log-rank $p < 0.001$) than those with low mRNAsi scores (**Figures 1A,B**).

Associations Between the Stemness Scores and Tumor Microenvironment Patterns

In TME evaluations using the ESTIMATE algorithms, we found that high mRNAsi scores were associated with lower immune and stromal ESTIMATE scores and higher tumor purity than were low mRNAsi scores (**Figure 1C**, $p < 0.05$). Correlation analysis revealed that mRNAsi scores negatively correlated with the immune, stromal, and ESTIMATE scores

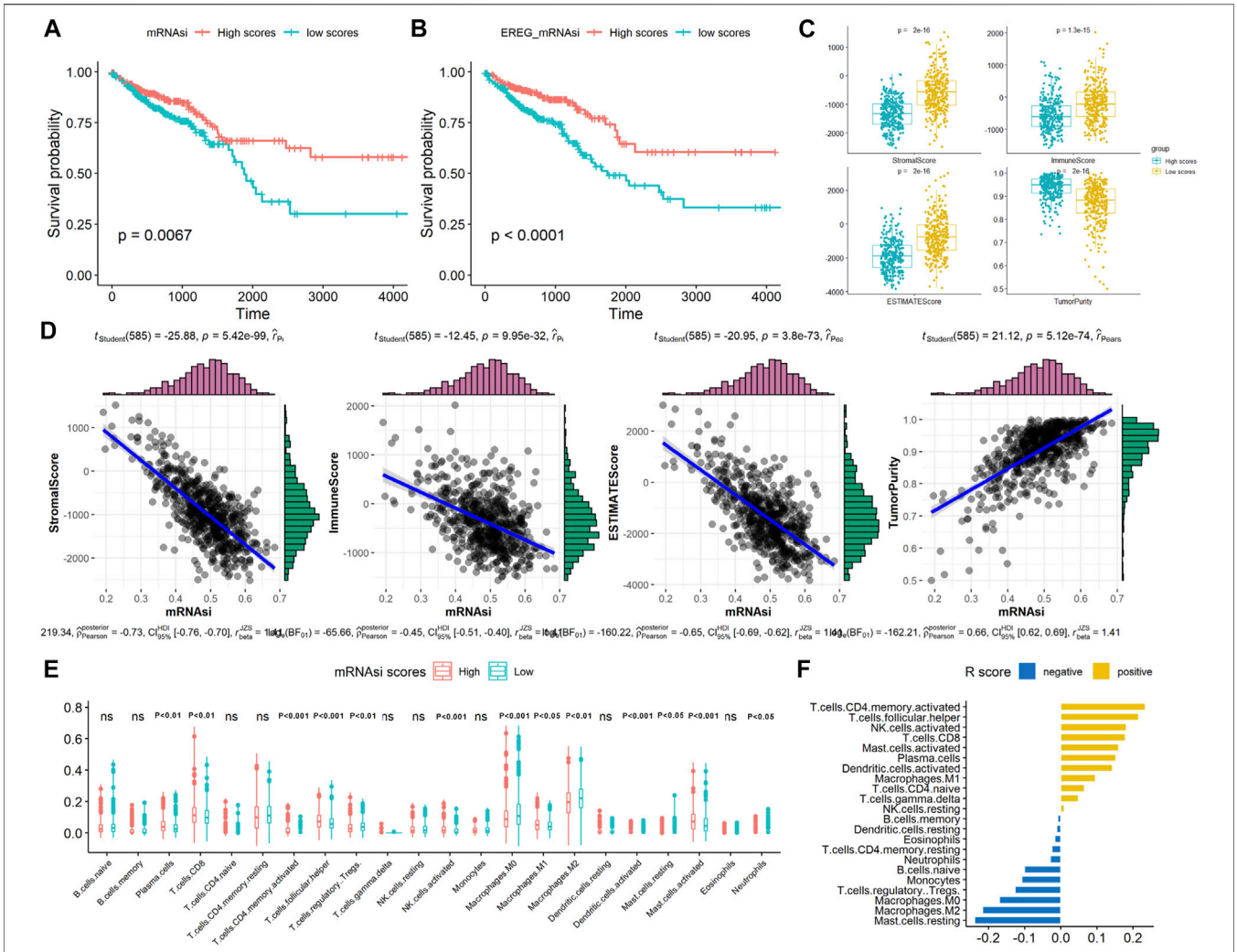

FIGURE 1 | Associations between the stemness scores and survival and TME patterns in CRC. Kaplan–Meier analyses indicated significantly better OS in the high **(A)** mRNAsi scores and **(B)** EREG mRNAsi scores; **(C)** Comparison of immune, stromal, ESTIMATE scores, and tumor purity between high and mRNAsi scores; **(D)** Correlation of mRNAsi scores with immune, stromal, ESTIMATE scores, and tumor purity; **(E)** Comparison of TIICs between high and mRNAsi scores; **(F)** Correlation of mRNAsi scores with TIICs (R value).

but positively correlated with tumor purity in CRC, indicating that the infiltration of immune and stromal cells decreased with the increased of the CRC stemness (**Figure 1D**). Next, the number of 22 types of TIICs in CRC was calculated using the CIBERSORT algorithm. As shown in **Figure 1E**, high mRNAsi scores were significantly associated with plasma cells, CD8-positive T cells, T follicular helper cells, activated mast cells, and activated natural killer cells ($p < 0.001$). In contrast, low mRNAsi scores were significantly associated with M0 and M2 macrophages. Correlation analysis revealed that high mRNAsi scores significantly positively correlated with activated memory CD4 T cells and T follicular helper cells, and negatively correlated with resting mast cells and M2 macrophages ($p < 0.001$; **Figure 1F**). Collectively, these results indicated that high stemness scores were associated with low TME scores in CRC.

Identifying Differentially Expressed Genes Related to the mRNAsi Scores and Functional Analysis

Since the different mRNAsi scores in CRC patients had prognostic value, we further utilized the differential expression analysis using the high and low mRNAsi scores. Based on the selected thresholds (logFC > 0.5 and $p < 0.05$), a total of 290 stemness-related DEGs related to mRNAsi scores were identified, including 284 upregulated and six downregulated DEGs (**Figure 2A**, **Supplementary Table S2**). Next, functional enrichment analysis of the 290 DEGs was performed using clusterProfiler algorithms. The most enriched BPs were axonogenesis, extracellular matrix organization, and extracellular structure organization; the most enriched CCs were collagen-containing extracellular matrix, distal axon, and endoplasmic reticulum lumen; the most enriched MFs were

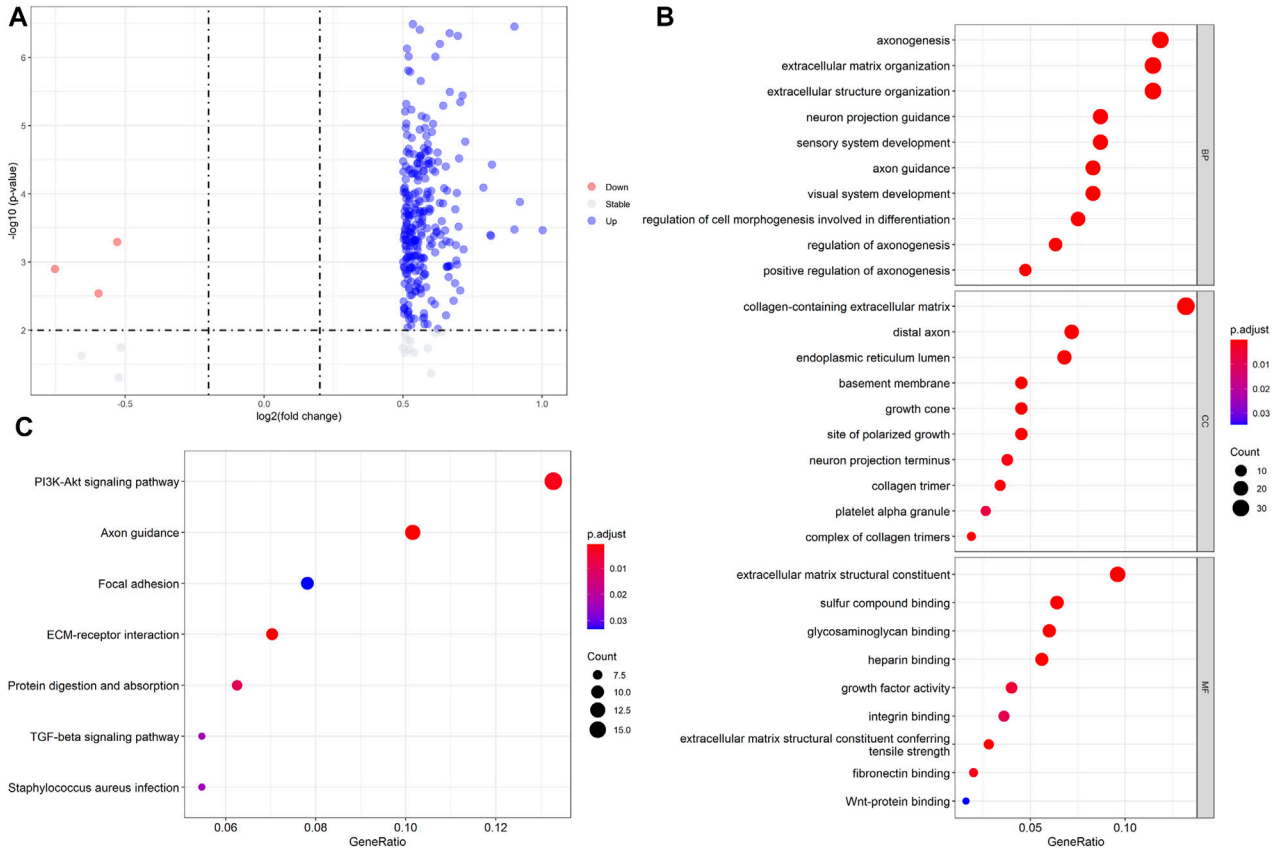

FIGURE 2 | Identifying differentially expressed genes (DEGs) related to mRNAsi scores and the functional analysis. **(A)** Volcano plot of DEGs between high and mRNAsi scores; **(B)** GO functional enrichment analysis for the DEGs; **(C)** KEGG analysis for the DEGs.

extracellular matrix constituent, sulfur compound binding, and glycosaminoglycan binding. The significantly enriched KEGG pathways were the PI3K-Akt, axon guidance, and focal adhesion pathways (**Figures 2B,C**). These results implied that these 290 stemness-related DEGs participated in these processes and pathways in CRC pathogenesis.

Identification of Two Stemness Subtypes Associated With the Clinical Outcome in CRC Patients

To classify CRC patients into different stemness-based subtypes, we used an unsupervised consensus clustering method by analyzing the expression of 290 stemness-related DEGs based on the differential expression analysis for mRNAsi scores. On the basis of the AUC of the CDF curve, we found that the optimal value of clusters for the cohort was two, implying that the k value was two (**Figures 3A–C**). Thus, the CRC patients in this cohort were divided into two subtypes, namely, stemness subtype I (284 patients, 48.4%) and stemness subtype II (303 patients, 51.6%).

Then, we explored the association of the two stemness subtypes with patient survival. The mean OS time in stemness subtype I was longer compared with that in stemness subtype II (886 vs. 754 days). Kaplan–Meier analysis also suggested that CRC patients in stemness subtype I have significantly longer OS value than did those in stemness subtype II (HR = 1.571, log-rank $p = 0.015$; **Figure 3D**).

Next, the molecular pathway and underlying mechanisms involved in the two stemness subtypes were determined using the GSVA algorithm in CRC. As shown in **Figures 3A,E** total of 185 significantly enriched pathways were identified between stemness subtypes I and II. The most significant pathways in stemness subtype I were the glycosaminoglycan biosynthesis chondroitin sulfate, ECM receptor interaction, and focal adhesion pathways, whereas those in stemness subtype II were the linoleic acid metabolism, retinol metabolism, and metabolism of xenobiotics by cytochrome p450 pathways.

Afterwards, we compared the clinical features of CRC patients between the two stemness subtypes. As summarized in **Table 2**, a higher number of patients in the stemness subtype I were at the early T stage (T1+T2), N stage (N0), and clinical stage (I+II) than were those in the stemness subtype II ($p < 0.05$). However, no significant difference between the two subtypes regarding patient age, gender, tumor location, histological type and M stage, microsatellite instability (MSI) status, and treatment strategy ($p > 0.05$). To be noted, we compared the stemness-based subtypes to the classification with different mRNAsi scores. We found a significant difference between these two

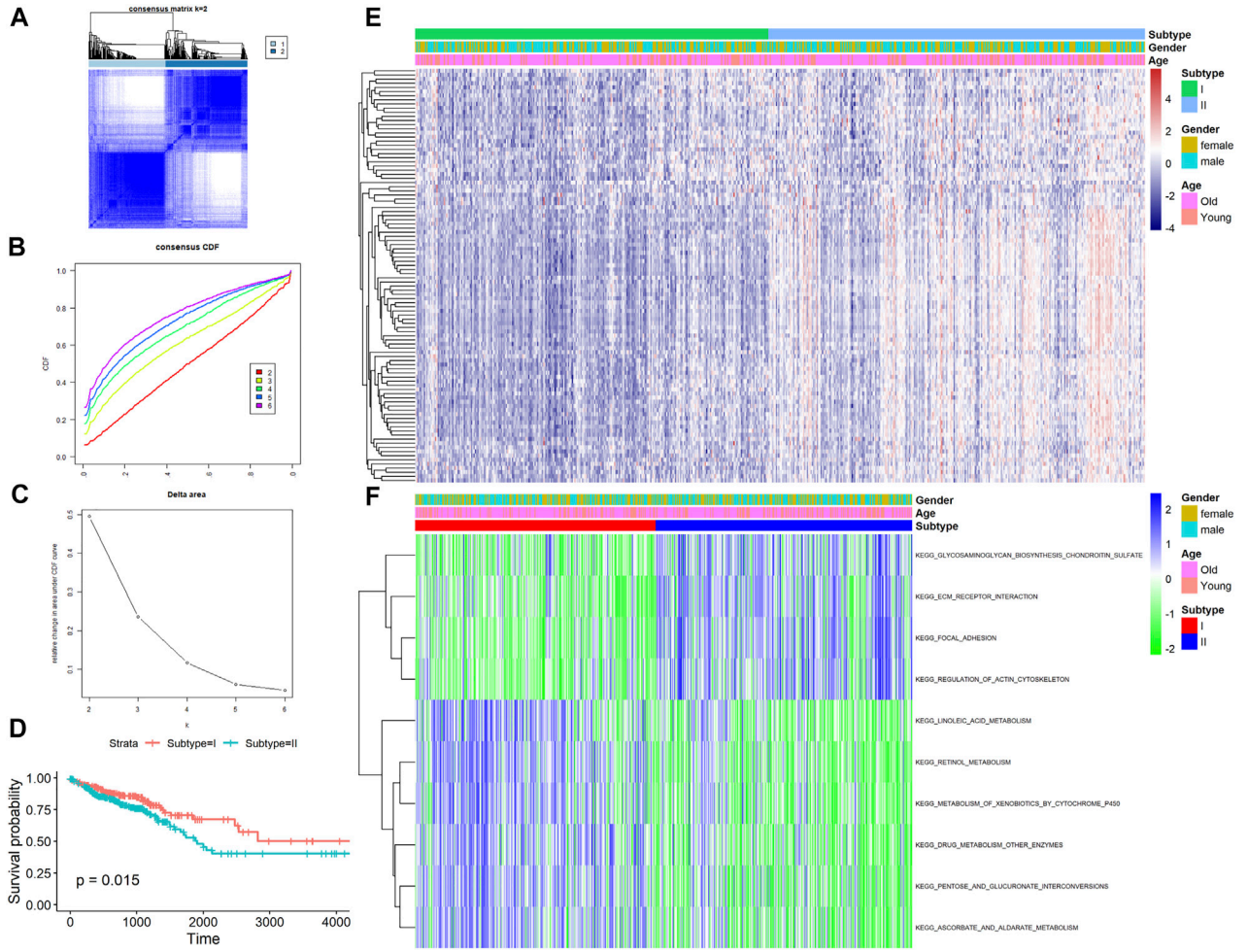

FIGURE 3 | Identification of two stemness subtypes with distinct survival outcomes and functional enrichment. **(A)** Heatmap of the consensus clustering matrix for k = 2; **(B)** CDF curves of the consensus score from k = 2 to 9. **(C)** The relative change in the area under the CDF curve from k = 2 to 9. **(D)** Kaplan–Meier analysis exhibited significantly better OS in stemness subtype I; **(E)** Heatmap of the expression patterns of top 100 DEGs between stemness subtype I and stemness subtype II. **(F)** Heatmap illustrated the enrichment scores of significantly enriched pathways evaluated by GSVA analysis between stemness subtype I and II.

classifications regarding the sample number ($p < 0.001$), with 207 samples overlapping between these two classifications. These results suggested that most patients in the stemness subtype I group were at the early stage of CRC, indicating higher levels of neoplastic stemness and better prognosis.

Previously, an international consortium study (Guinney et al., 2015) using large-scale data to show marked interconnectivity between six independent classification systems coalescing into four consensus molecular subtypes (CMSs) with distinguishing features, including: CMS1 (microsatellite instability immune), hypermutated, microsatellite unstable and strong immune activation; CMS2 (canonical), epithelial, marked WNT and MYC signaling activation; CMS3 (metabolic), epithelial and evident metabolic dysregulation; and CMS4 (mesenchymal), prominent transforming growth factor-β activation, stromal invasion and angiogenesis. We compared the previous classification with our classification, and found that the distributions of the molecular subtypes have little difference between subtype I and subtype II (Chi-square test, $p > 0.05$), suggesting that our classification is similar to their classification (**Supplementary File Figure S2**).

Stemness Subtypes Possessed Different Tumor Mutation Burdens

Genomic alterations have been reported to modulate the TME in various cancers, including the tumor immunity and immune infiltration patterns in previous studies (Huang et al., 2021; Liu et al., 2021). Hence, gene mutation analysis for the stemness-related DEGs was employed to examine the distinct genomic variation patterns in the two stemness subtypes. As shown in **Figures 4A,B**, among the top 10 mutated genes of the two stemness subtypes, APC, TTN, TP53, PIK3CA, PTEN, KRAS, SMAD4, ATM, and SYNE1 harbored the highest number of mutations in both subtypes, suggesting that these two subtypes have similar top mutated genes. These mutated genes are known

TABLE 2 | Comparison of clinical features between subtype I and subtype II.

	Subtype I (*N* = 284)	Subtype II(*N* = 303)	P overall
Age (years)	66.3 ± 12.4	66.4 ± 13.1	0.949
Gender			1.000
Female	133 (46.8%)	142 (46.9%)	
Male	151 (53.2%)	161 (53.1%)	
Location			0.577
Colon	207 (72.9%)	228 (75.2%)	
Rectal	77 (27.1%)	75 (24.8%)	
Histological type			0.053
Adenocarcinoma	250 (88.0%)	254 (83.8%)	
Mucinous	27 (9.51%)	46 (15.2%)	
T stage			<0.001
T1	13 (4.58%)	7 (2.31%)	
T2	66 (23.2%)	35 (11.6%)	
T3	186 (65.5%)	214 (70.6%)	
T4	19 (6.69%)	47 (15.5%)	
N stage			0.033
N0	180 (63.4%)	159 (52.5%)	
N1	60 (21.1%)	77 (25.4%)	
N2	43 (15.1%)	66 (21.8%)	
NX	1 (0.35%)	1 (0.33%)	
M stage			0.454
M0	220 (77.5%)	218 (71.9%)	
M1	33 (11.6%)	47 (15.5%)	
MX	28 (9.86%)	35 (11.6%)	
Clinical stage			0.005
I	66 (23.2%)	35 (11.6%)	
II	103 (36.3%)	117 (38.6%)	
III	74 (26.1%)	93 (30.7%)	
IV	33 (11.6%)	48 (15.8%)	
MSI*			0.394
Yes	4 (1.41%)	7 (2.31%)	
No	45 (15.8%)	58 (19.1%)	
Treatment*			0.136
Ancillary	5 (1.76%)	3 (0.99%)	
Chemotherapy	73 (25.7%)	96 (31.7%)	
Immunotherapy	1 (0.35%)	2 (0.66%)	
Other, specify in notes	5 (1.76%)	9 (2.97%)	
TMT	13 (4.58%)	5 (1.65%)	

*MSI: Microsatellite instability; TMT: Targeted Molecular therapy; *empty data was removed.*

to be involved in CRC pathogenesis. Next, by comparing the gene mutation frequency in stemness subtype I and subtype II, we found that BRAF, APOB, EGFR, TTN, FN1, and PKD1 had a higher mutation frequency in stemness subtype I than in stemness subtype II. However, there was no significant difference regarding the mutation status of APC, TTN, TP53, PIK3CA, PTEN, and KRAS between the two subtypes (**Figure 4C**). In addition, the results showed that patients in stemness subtype II had substantially higher TMB values than those in stemness subtype I ($p < 0.001$; **Figure 4D**). These findings suggested significantly different TMB, but the top high-frequency mutated genes showed little difference between the two stemness subtypes.

Stemness Subtypes had Distinct Tumor Microenvironment Patterns in CRC

On the basic of ESTIMATE algorithm results, the value immune, stromal, and ESTIMATE scores in stemness subtype I were significantly lower than stemness subtype II, while the tumor purity was expectedly higher in stemness subtype I than in stemness subtype II ($p < 0.001$; **Figure 5B**), suggesting a relatively low abundance of immune cells and stromal cells in the tumors of stemness subtype I. The number of TIICs was quantified using the CIBERSORT algorithm and then compared between stemness subtype I and II. As shown in **Figure 5A**, the number of plasma cells, resting CD4 memory T cells, T follicular helper cells, monocytes, and activated dendritic cells was significantly higher in stemness subtype I than in stemness subtype II ($p < 0.001$). Furthermore, the number of M0, M1, and M2 macrophages, resting mast cells, and neutrophils was remarkably high in stemness subtype II than in stemness subtype I ($p < 0.001$). Next, we explored the association of stemness subtypes with the six markers of immune checkpoint inhibitors, including PD1 (PDCD1), PD-L1 (CD274), PD-L2 (PDCD1LG2), CTLA4, CD80, and CD86. As shown in **Figure 5C**, the expression of these markers was expectedly increased in stemness subtype II compared to that in stemness subtype I. These results revealed

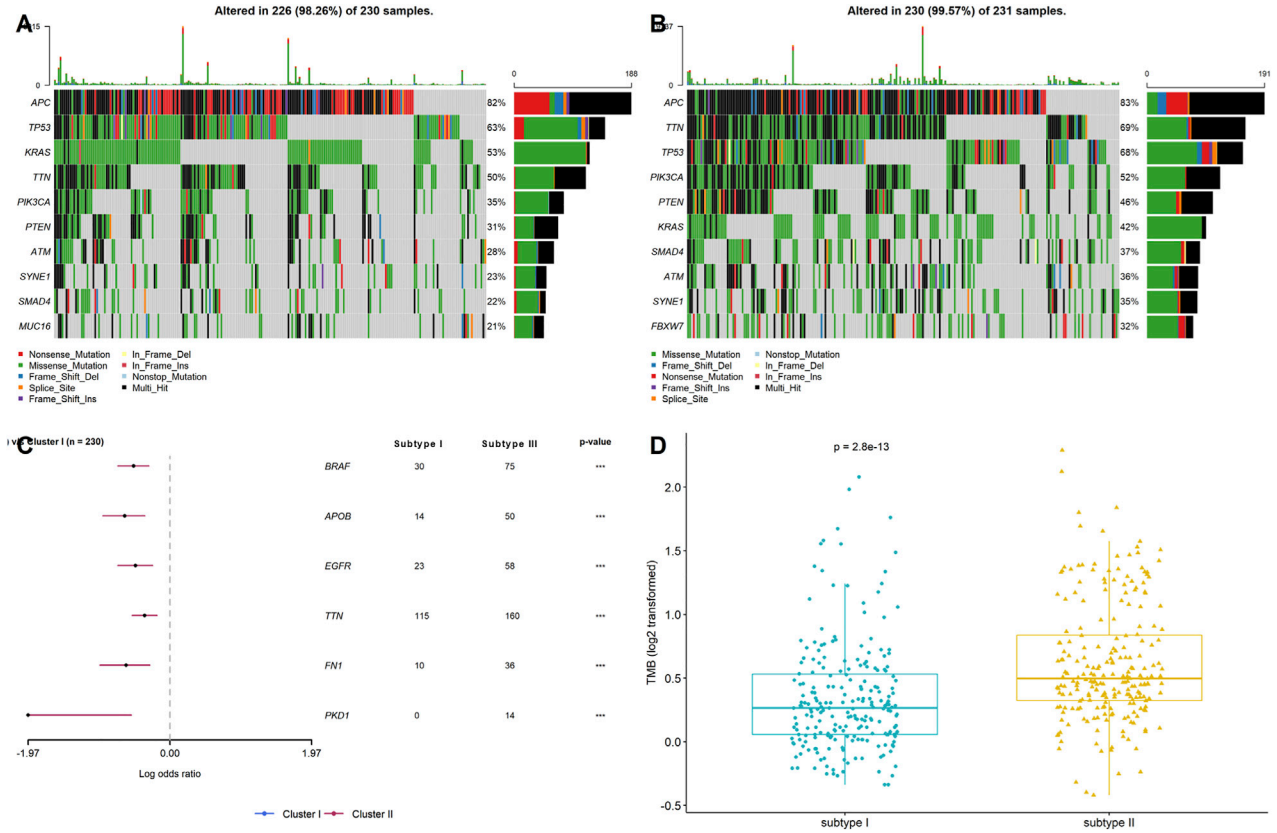

FIGURE 4 | Stemness subtypes possessed different TMB. Waterfall plots showed the top 10 mutated in **(A)** stemness subtype I and **(B)** stemness subtype II; **(C)** Forest plot exhibited the significant mutated genes between the two stemness subtypes; **(D)** The comparisons of TMB between stemness subtype I and stemness subtype II.

that tumors in stemness subtype II presented high immune cell levels and were more likely associated with a low immunotherapy response. However, these results were obtained from dataset analysis; thus, this hypothesis should be validated by an independent cohort using proper methods, such as flow cytometry or the RNA sequence.

Construction of Predictor for the Stemness Subtypes

The CRC samples were divided into two sets at a 7:3 ratio, with 410 and 177 patients in the training and testing sets, respectively. Two machine learning algorithms (LASSO and XGBoost) were applied to analyze 290 stemness-related DEGs and identified the key genes associated with the stemness subtypes. The ROC curve revealed that both LASSO and XGBoost results yielded good performances in differentiating stemness subtypes I and II (both AUC values over 0.85), with the AUC values of LASSO being higher than that of the XGBoost algorithm (**Figures 6A,B**). The LASSO and XGBoost algorithms identified 59 and six genes, respectively. The Venn diagram showed that three genes (GAS1, CHIT1, and COL10A1) overlapped between the two machine learning algorithms results (**Figure 6C**). Afterward, we conducted a multivariate logistic regression analysis to construct a diagnostic model by incorporating these three genes. As the results suggested, the optimal cutoff value of the model for discrimination was 0.412, implying that patients with scores < 0.412 were grouped in stemness subtype I and stemness subtype II if otherwise. ROC curve analysis demonstrated that the diagnostic, predictive model had an AUC of 0.928 in discriminating the two subtypes, with the sensitivity and specificity as 81.2% and 89.1% in the entire dataset (**Figure 6D**). In addition, the diagnostic model also had an excellent performance in distinguishing the two stemness subtypes in the test set, with sensitivity, specificity, and AUC of 0.837, 0.918, and 0.941, respectively (**Supplementary Table S3**).

Construction and Validation of the CRC Predictor Based on Stemness-Related Genes

We further established a prognostic signature based on stemness-related genes to screen the CRC patients with different treatment failure risks or poor prognoses. A total of 290 stemness-related DEGs were incorporated into the univariate Cox regression model and LASSO analysis, and 55

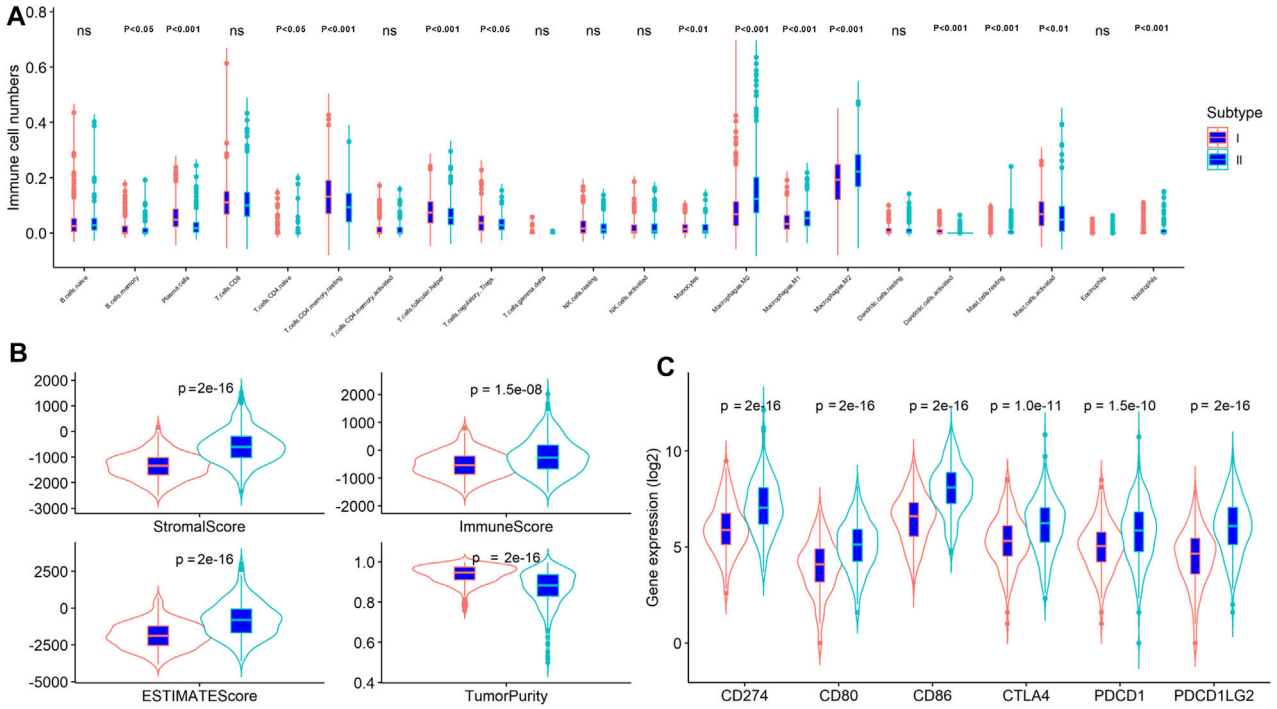

FIGURE 5 | The stemness subtypes had distinct TME patterns in CRC. Comparison of **(A)** TIICs; **(B)** immune, stromal, ESTIMATE scores and tumor purity; **(C)** Immune checkpoint inhibitors between stemness subtype I and stemness subtype II.

and 11 genes were identified by the two algorithms, respectively. Of note, five genes (FABP4, HOXC9, INHBB, NKAIN4, and PLXNB3) overlapped between these two models (**Figure 7A**). Thus, we incorporated these five genes into a multivariate Cox regression model and constructed a prognostic signature. The nomogram showed that the signature had a better prognostic value in CRC compared to that of other clinical parameters (**Figure 7B**). We categorized the CRC patients into two groups according to the median risk score value of the signature. The Kaplan–Meier analysis indicated that CRC patients with a high risk score had a poorer prognosis than those with a low risk score (log-rank $p < 0.001$; **Figure 7C**). Next, two independent cohorts, GSE29621 (65 samples) and GSE39582 (585 samples) were employed to validate the prognostic value of the signature. Similar to the results from TCGA-COADREAD dataset, the Kaplan–Meier analysis also revealed that CRC patients in the high risk score group had a poorer prognosis than those in the low risk score group (both log-rank $p < 0.001$; **Figures 7D,E**). Considering that the survival time of the three datasets varied considerably, to guarantee comparable results, we selected 3-year survival time to compare the predictive value. As shown in **Figures 7F–H**, the ROC values of the three datasets for 3-year survival were similar, all exceeding 60%, suggesting a moderate prognostic value. Taken together, these results suggested that this stemness-related gene signature has better performance in predicting the prognosis of CRC patients than other clinical parameters.

Validation of the Five Stemness-Related Genes in Independent Cohorts and CRC Clinical Samples

The expression of the five stemness-related genes related to the prognosis of CRC patients was validated in three GEO datasets: GSE73360 (92 samples), GSE50421 (49 samples), GSE89076 (80 samples), and GSE62932 (68 samples) containing normal control and tumor samples. Furthermore, 30 clinical CRC tissues (including tumor tissues and the corresponding adjacent tumor tissues as well as normal tissues) were collected, and the expression of FABP4, HOXC9, INHBB, NKAIN4, and PLXNB3 was determined using RT-PCR. The results showed that the expression of these genes was reduced in tumor tissues compared to that in normal tissues. As listed in **Figure 8**, low expression of FABP4 in tumor tissues ($p < 0.05$) was validated in five datasets, the lower expression of PLXNB3, INHBB and NKAIN4 in tumor tissues was verified in three datasets ($p < 0.05$), and the decreased expression of HOXC9 and was validated in one dataset, respectively ($p < 0.05$).

DISCUSSION

Currently, CRC remains an incurable disease because 50% of CRC patients experience tumor relapse and metastasis even if the tumor is removed prior to tumor metastasis (Conti and Thomas, 2011; Jain et al., 2011). Cancer stem cells have intrinsic chemoresistant properties, ultimately leading to chemotherapy

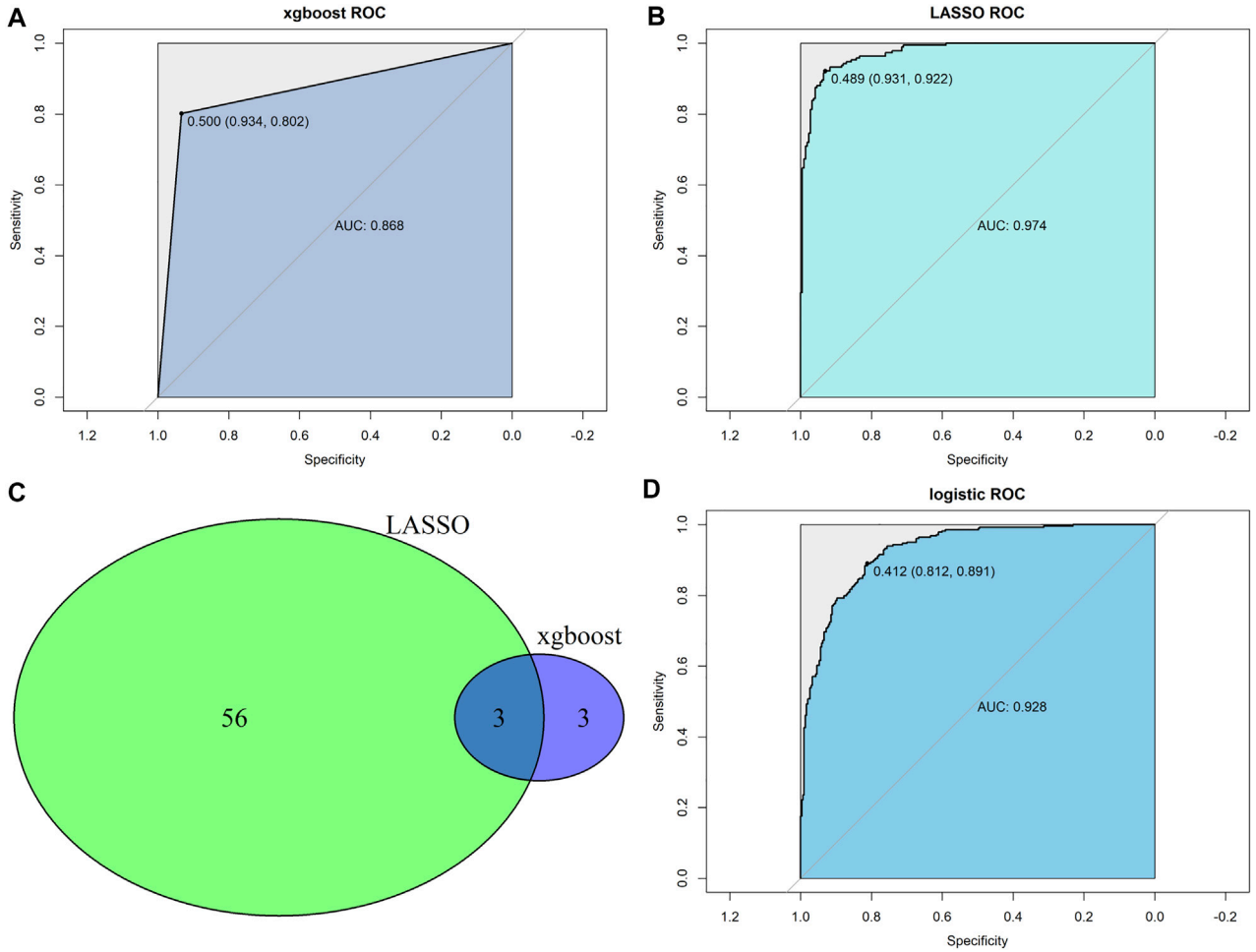

FIGURE 6 | Construction of predictor for the stemness subtypes. **(A)** XGBoost algorithms identified a model predicting the stemness subtypes; **(B)** LASSO algorithms identified a model predicting the stemness subtypes. **(C)** Venn diagram identified overlapped genes between xgboost and LASSO algorithms. **(D)** Multivariate logistic regression model revealed the diagnostic value in predicting the stemness subtypes.

failure and cancer recurrence (Zahra et al., 2021). Hence, targeting cancer stem cells or related genes might be a promising strategy for treating CRC. Previous studies indicated that molecular subtypes based on the stemness scores predict outcome in several cancers (Hong et al., 2021; Tan et al., 2021). These subtypes are reportedly associated with the TME or immune therapy in these cancers. Regarding CRC, a recent study reported that the mRNAsi score was negatively related to pathological features but positively associated with OS and recurrence-free survival in CRC patients (Wang et al., 2021b). However, this study did not conduct an in-depth analysis of the association of mRNAsi scores with the clinical outcome and TME and lacked external cohorts to validate the robustness of the results. Therefore, it is necessary to perform a detailed analysis to reveal the clinical value of stemness in CRC.

Here, we conducted a comprehensive analysis of the association of stemness scores with the clinical outcome in CRC patients, showing that the stemness scores were significantly associated with the clinical stage and survival of CRC patients. We explored the function of stemness-related genes and their association with TME. Furthermore, we identified two stemness subtypes based on the stemness scores and determined the pathways involved in the two subtypes and the association of stemness subtypes with the clinical features, survival time, gene mutation, TME, and prognostic value. Moreover, we constructed a predictor for the stemness subtypes and a prognostic signature based on stemness-related genes using machine learning algorithms. The results revealed that the stemness subtypes were significantly associated with the clinical features, TME, TMB, immunotherapy response, and prognostic value. Finally, to increase the reliability of the results, several independent cohorts and clinical samples were used to validate the diagnostic value of the predictor for stemness subtypes and the prognostic value of the prognostic signature in CRC.

At present, immunotherapy has been shown to be a promising option for CRC patients, especially for those unable to undergo radical resection or with tumor metastasis. However, many

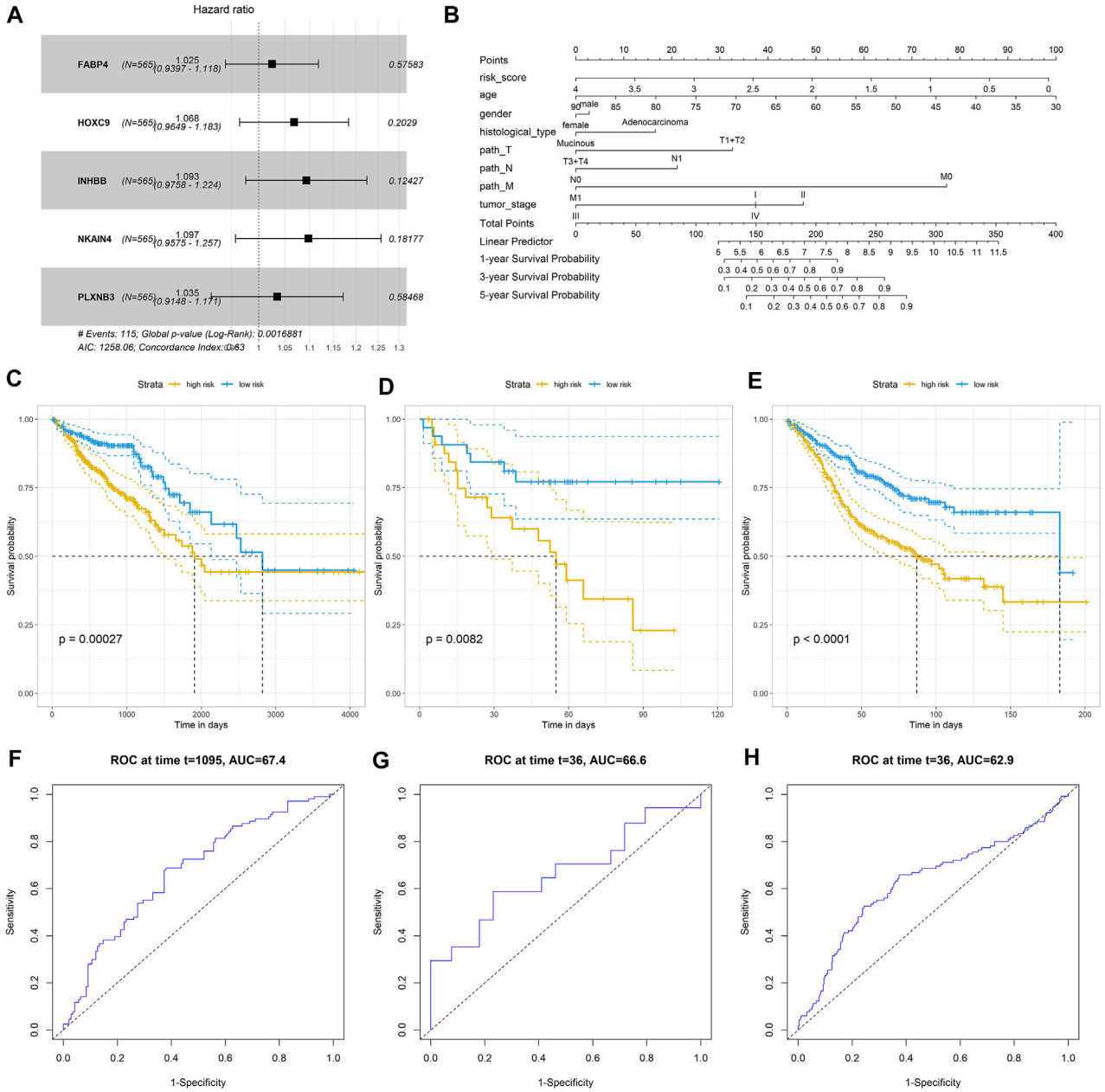

FIGURE 7 | Construction and validation of CRC predictor based on the stemness-related genes. **(A)** Forest plot showed that five stemness- related genes associated with the prognosis of patients; **(B)** Nomogram plot of showed the prognostic value of the gene signature and other clinical features in CRC; Kaplan–Meier analysis indicated the survival rated of patients with high or low risk scores in **(C)** TCGA-COADREAD dataset; **(D)** GSE29621 dataset **(E)** GSE39582 dataset; Prognostic value of the gene signature in **(F)** TCGA-COADREAD dataset; **(G)** GSE29621 dataset; **(H)** GSE36582 dataset.

factors affect CRC immunotherapy, among which cancer stem cells are a key factor that might result in immunotherapy failure. Although the association of cancer stem cells with the immune system has not been well investigated because of experimental limitations (Donini et al., 2021), evidence demonstrates that cancer stem cells have a modulatory effect on the immune system in CRC patients (Xu et al., 2018). In this study, we showed that the stemness scores were significantly associated with the TME, including the immune, stromal scores, and tumor purity, and that they greatly correlated with some TIICs. In addition, the stemness subtypes can clearly discriminate CRC patients with different TME and TMB. Furthermore, we found remarkable associations of stemness subtypes with immune checkpoint inhibitors. All these results strongly suggest that targeting the stemness scores of CRC could effectively identify patients who will benefit from immunotherapy. Interestingly, we

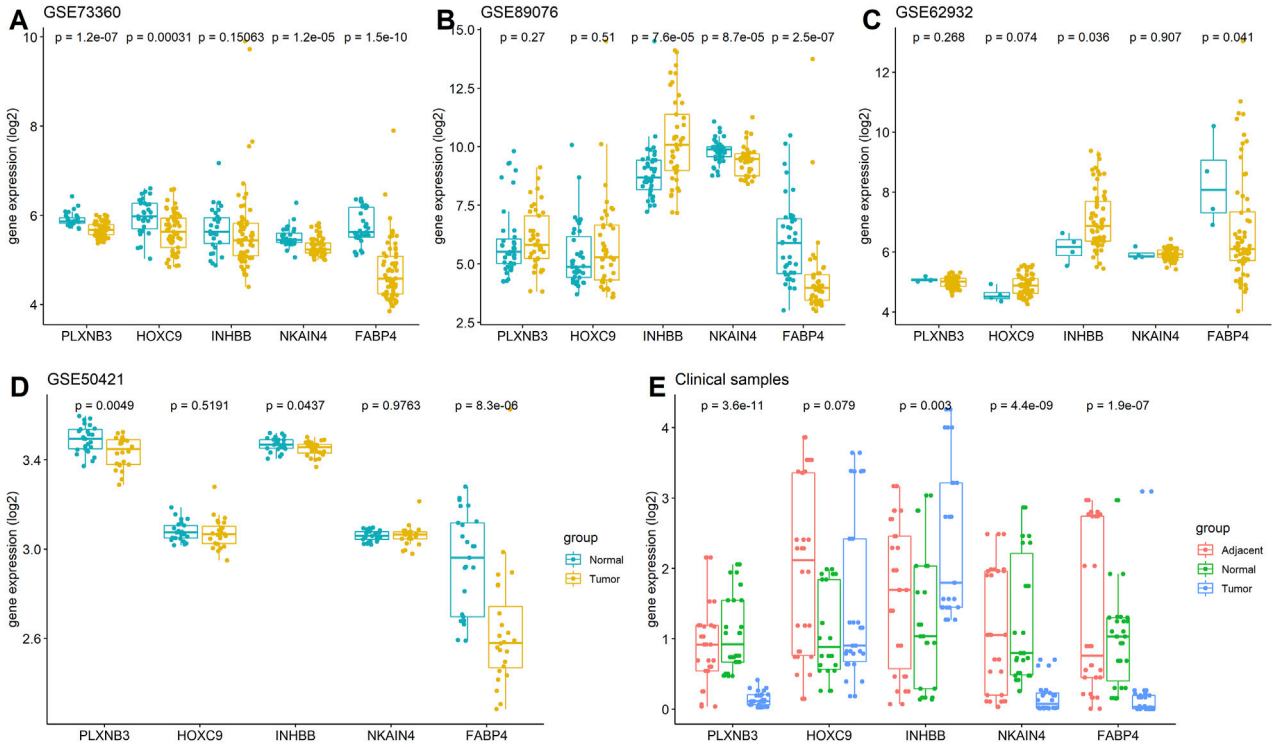

FIGURE 8 | Expressions of FABP4, HOXC9, INHBB, NKAIN4, and PLXNB3 in CRC. **(A)** GSE73360 dataset; **(B)** GSE89076 dataset; **(C)** GSE62932 dataset; **(D)** GSE50421 dataset; **(E)** Clinical tissue tested by RT-PCR assay.

found that the TMB differed between the two subtypes, which shared most of the top mutated genes, suggesting that more gene mutations need to be explored in these two stemness-based subtypes.

Since the stemness scores are calculated based on the gene expression profile, which cannot be easily used in the clinical setting, we established a stemness subtype predictor and prognostic signature based on stemness-related genes. The stemness subtype predictor established using three stemness-based genes helps to discriminate the patients of stemness subtype I from those of stemness subtype II. The prognostic signature constructed based on five genes further facilitates the screening of CRC patients at different risk levels in terms of survival. To be noted, regarding the genes used to construct the stemness subtype predictor and prognostic signature, GAS1 (Li et al., 2016a), CHIT1 (Li et al., 2016b), COL10A1 (Patra et al., 2021), FABP4 (Wang et al., 2019), HOXC9 (Hu et al., 2019), INHBB (Yuan et al., 2020), and NKAIN4 (Jin et al., 2020) have been previously found to be associated with CRC development. In contrast, the role of PLXNB3 in CRC has not been yet investigated, although it was found to be overexpressed in breast cancer (Valladares et al., 2006). This evidence suggested that each stemness-related gene is crucial to CRC development and prognosis.

In this study, we showed that patients with stemness subtype I have a better prognosis compared with those with stemness subtype II, and the TMB in stemness subtype I was lower than that in stemness subtype II, which was contrary to the current understanding, implying that high TMB may be a good prognostic factor for immune checkpoint inhibitors. We speculated that at least two reasons might explain these opposite results. First, as shown in **Table 2**, most of the patients in stemness subtype I were at an early stage of CRC; therefore, their prognosis was better than those in stemness subtype II. Although high TMB was observed in stemness subtype II, the association of TMB with the immunotherapy effect, especially the PD1 treatment, for CRC remains inconsistent in current reports. In addition, as the results showed, the mutation frequency of the most common mutated genes was similar in both stemness subtypes. Second, MSI was considered a more reliable indicator for the immunotherapy effect for CRC patients; however, our study failed to show a significant association of stemness subtypes with the MSI status; thus, the stemness subtypes might not be a good indicator to predict which CRC patients should undergo immunotherapy.

Furthermore, patients in the different subtype groups showed significantly different prognoses. Notably, the stemness subtype predictor and prognostic signature were validated using external independent cohorts and clinical samples, which confirmed the robustness of our results. However, this study also has some limitations. First, this

study only used 30 paired clinical samples to validate the results, which undermined the robustness of the conclusion. Therefore, a larger clinical cohort to further confirm the predictive value of the signature is necessary. Second, the association between stemness subtypes and immunotherapy response needs to be verified in patients who had undergone immunotherapy. Third, in the validated analysis, we found that not all gene expression was consistent with previous results; we speculated that some factors, such as different clinical characteristics, sample size, and the heterogeneity of TME might explain the inconsistent results. Therefore, additional experiments, such as flow cytometry or RNA sequencing with a larger sample size, are warranted to comprehensively analyze the TME and validate our results. Fourth, the EREG-mRNAsi is another indicator that reflects the degree of oncogenic dedifferentiation, which was generated using a set of epigenetic regulatory genes associated with stemness. The EREG-mRNAsi reflecting epigenetically regulated mRNAsi and was considered to be complementary to mRNAsi. In our study, we mainly interesting in the mRNA level, in which using mRNAsi is more appropriate, thus we used mRNAsi in our analysis. But EREG-mRNAsi is important indictor to the prognosis of patients, the similar analysis for the CRC patients by using EREG-mRNAsi should be further conduct in the future study by analyzing the epigenetically gene level and compared with the mRNA level. Therefore, our results should be accepted with caution, and studies to address these concerns should be undertaken in the future.

CONCLUSION

This study demonstrated that mRNAsi scores are closely related to the TME and survival of CRC patients. The stemness-related classification based on the mRNAsi score represents a promising predictor of the prognosis of CRC patients.

DATA AVAILABILITY STATEMENT

The original contributions presented in the study are included in the article/**Supplementary Material**, further inquiries can be directed to the corresponding authors.

AUTHOR CONTRIBUTIONS

Study concept and design: Y-XY and B-LH; Collection and assembly of data: Y-XY and S-QL; Performed the experiment: Y-XY, J-LL, and S-QL; Data analysis and interpretation: B-LH, S-QL, K-ZL, M-LY, and Y-XY; Manuscript writing and review: All authors. All authors have read and approved the manuscript in its current state.

FUNDING

This study was partially supported by the research funding from the National Natural Science Foundation of China (No. 82160446; 81860417) and the Natural Science Foundation of Guangxi (No. GUIKE-AB1850007; No. 2018JJA140136).

SUPPLEMENTARY MATERIAL

The Supplementary Material for this article can be found online at: https://www.frontiersin.org/articles/10.3389/fcell.2022.817509/full#supplementary-material

REFERENCES

Araghi, M., Soerjomataram, I., Jenkins, M., Brierley, J., Morris, E., Bray, F., et al. (2019). Global Trends in Colorectal Cancer Mortality: Projections to the Year 2035. *Int. J. Cancer.* 144 (12), 2992–3000. doi:10.1002/ijc.32055

Cao, M., Li, H., Sun, D., and Chen, W. (2020). Cancer Burden of Major Cancers in China: A Need for Sustainable Actions. *Cancer Commun. (Lond)* 40 (5), 205–210. doi:10.1002/cac2.12025

Conti, J., and Thomas, G. (2011). The Role of Tumour Stroma in Colorectal Cancer Invasion and Metastasis. *Cancers (Basel)* 3 (2), 2160–2168. doi:10.3390/cancers3022160

Das, P. K., Islam, F., and Lam, A. K. (2020), The Roles of Cancer Stem Cells and Therapy Resistance in Colorectal Carcinoma. *Cells*, 9 (6), E1392 [pii]. doi:10.3390/cells9061392

Donini, C., Rotolo, R., Proment, A., Aglietta, M., Sangiolo, D., and Leuci, V. (2021). Cellular Immunotherapy Targeting Cancer Stem Cells: Preclinical Evidence and Clinical Perspective. *Cells* 10 (3). doi:10.3390/cells10030543

Friedmann-Morvinski, D., and Verma, I. M. (2014). Dedifferentiation and Reprogramming: Origins of Cancer Stem Cells. *EMBO Rep.* 15 (3), 244–253. doi:10.1002/embr.201338254

Galbraith, N. J., Wood, C., and Steele, C. W. (2021). Targeting Metastatic Colorectal Cancer with Immune Oncological Therapies. *Cancers (Basel)* 13 (14). doi:10.3390/cancers13143566

Guinney, J., Dienstmann, R., Wang, X., de Reynies, A., Schlicker, A., Soneson, C., et al. (2015). The Consensus Molecular Subtypes of Colorectal Cancer. *Nat. Med.* 21 (11), 1350–1356. doi:10.1038/nm.3967

Hong, L., Zhou, Y., Xie, X., Wu, W., Shi, C., Lin, H., et al. (2021). A Stemness-Based Eleven-Gene Signature Correlates with the Clinical Outcome of Hepatocellular Carcinoma. *BMC Cancer.* 21 (1), 716. doi:10.1186/s12885-021-08351-0

Hu, M., Ou-Yang, W., Jing, D., and Chen, R. (2019). Clinical Prognostic Significance of HOXC9 Expression in Patients with Colorectal Cancer. *Clin. Lab.* 65 (8)190122. doi:10.7754/Clin.Lab.2019.190122

Huang, R., Li, G., Wang, K., Wang, Z., Zeng, F., Hu, H., et al. (2021). Comprehensive Analysis of the Clinical and Biological Significances of Endoplasmic Reticulum Stress in Diffuse Gliomas. *Front. Cell. Dev. Biol.* 9, 619396. doi:10.3389/fcell.2021.619396

Jain, V. K., Hawkes, E. A., and Cunningham, D. (2011). Integration of Biologic Agents with Cytotoxic Chemotherapy in Metastatic Colorectal Cancer. *Clin. Colorectal Cancer.* 10 (4), 245–257. doi:10.1016/j.clcc.2011.04.001

Jin, L. P., Liu, T., Meng, F. Q., and Tai, J. D. (2020). Prognosis Prediction Model Based on Competing Endogenous RNAs for Recurrence of Colon Adenocarcinoma. *BMC Cancer.* 20 (1), 968. doi:10.1186/s12885-020-07163-y

Li, F. F., Yan, P., Zhao, Z. X., Liu, Z., Song, D. W., Zhao, X. W., et al. (2016). Polymorphisms in the CHIT1 Gene: Associations with Colorectal Cancer. *Oncotarget* 7 (26), 39572–39581. doi:10.18632/oncotarget.9138

Li, Q., Qin, Y., Wei, P., Lian, P., Li, Y., Xu, Y., et al. (2016). Gas1 Inhibits Metastatic and Metabolic Phenotypes in Colorectal Carcinoma. *Mol. Cancer Res.* 14 (9), 830–840. doi:10.1158/1541-7786.MCR-16-0032

Liao, Y., Wang, Y., Cheng, M., Huang, C., and Fan, X. (2020). Weighted Gene Coexpression Network Analysis of Features that Control Cancer Stem Cells Reveals Prognostic Biomarkers in Lung Adenocarcinoma. *Front. Genet.* 11, 311. doi:10.3389/fgene.2020.00311

Liberzon, A., Birger, C., Thorvaldsdottir, H., Ghandi, M., Mesirov, J. P., and Tamayo, P. (2015). The Molecular Signatures Database (MSigDB) Hallmark Gene Set Collection. *Cell. Syst.* 1 (6), 417–425. doi:10.1016/j.cels.2015.12.004

Liu, Z., Lu, T., Wang, L., Liu, L., Li, L., and Han, X. (2021). Comprehensive Molecular Analyses of a Novel Mutational Signature Classification System with Regard to Prognosis, Genomic Alterations, and Immune Landscape in Glioma. *Front. Mol. Biosci.* 8, 682084. doi:10.3389/fmolb.2021.682084

Malta, T. M., Sokolov, A., Gentles, A. J., Burzykowski, T., Poisson, L., Weinstein, J. N., et al. (2018), Machine Learning Identifies Stemness Features Associated with Oncogenic Dedifferentiation. *Cell.*, 173 (2), 338–354 e15. doi:10.1016/j.cell.2018.03.034

Newman, A. M., Liu, C. L., Green, M. R., Gentles, A. J., Feng, W., Xu, Y., et al. (2015). Robust Enumeration of Cell Subsets from Tissue Expression Profiles. *Nat. Methods.* 12 (5), 453–457. doi:10.1038/nmeth.3337

Patil, I. (2021). Visualizations with Statistical Details: The 'ggstatsplot' Approach. *JOSS* 6 (61), 3167. doi:10.21105/joss.03167

Patra, R., Das, N. C., and Mukherjee, S. (2021). Exploring the Differential Expression and Prognostic Significance of the COL11A1 Gene in Human Colorectal Carcinoma: An Integrated Bioinformatics Approach. *Front. Genet.* 12, 608313. doi:10.3389/fgene.2021.608313

Reya, T., Morrison, S. J., Clarke, M. F., and Weissman, I. L. (2001). Stem Cells, Cancer, and Cancer Stem Cells. *Nature* 414 (6859), 105–111. doi:10.1038/35102167

Shibue, T., and Weinberg, R. A. (2017). EMT, CSCs, and Drug Resistance: the Mechanistic Link and Clinical Implications. *Nat. Rev. Clin. Oncol.* 14 (10), 611–629. doi:10.1038/nrclinonc.2017.44

Tan, J., Zhu, H., Tang, G., Liu, H., Wanggou, S., Cao, Y., et al. (2021). Molecular Subtypes Based on the Stemness Index Predict Prognosis in Glioma Patients. *Front. Genet.* 12, 616507. doi:10.3389/fgene.2021.616507

Valladares, A., Hernandez, N. G., Gomez, F. S., Curiel-Quezada, E., Madrigal-Bujaidar, E., Vergara, M. D., et al. (2006). Genetic Expression Profiles and Chromosomal Alterations in Sporadic Breast Cancer in Mexican Women. *Cancer Genet. Cytogenet.* 170 (2), 147–151. doi:10.1016/j.cancergencyto.2006.06.002

Wang, S., Yao, Y., Wang, X., Zheng, G., Ouyang, W., and Chen, W. (2019). 25-HC Promotes Hepatocellular Carcinoma Metastasis through Up-Regulation of TLR4 Dependent FABP4. *Am. J. Cancer Res.* 9 (10), 2140–2155.

Wang, X. C., Liu, Y., Long, F. W., Liu, L. R., and Fan, C. W. (2021). Identification of a lncRNA Prognostic Signature-Related to Stem Cell Index and its Significance in Colorectal Cancer. *Future Oncol.* 17 (23), 3087–3100. doi:10.2217/fon-2020-1163

Wang, X., Wan, Q., Jin, L., Liu, C., Cheng, Y., and Wang, Z. (2020). The Integrative Analysis Identifies Three Cancer Subtypes and Stemness Features in Cutaneous Melanoma. *Front. Mol. Biosci.* 7, 598725. doi:10.3389/fmolb.2020.598725

Wang, Z., Wang, Y., Yang, T., Xing, H., Gao, L., Guo, X., et al. (2021). Machine Learning Revealed Stemness Features and a Novel Stemness-Based Classification with Appealing Implications in Discriminating the Prognosis, Immunotherapy and Temozolomide Responses of 906 Glioblastoma Patients. *Brief. Bioinform.* 22 (5). doi:10.1093/bib/bbab032

Wilkerson, M. D., and Hayes, D. N. (2010). ConsensusClusterPlus: a Class Discovery Tool with Confidence Assessments and Item Tracking. *Bioinformatics* 26 (12), 1572–1573. doi:10.1093/bioinformatics/btq170

Wu, T., Hu, E., Xu, S., Chen, M., Guo, P., Dai, Z., et al. (2021). clusterProfiler 4.0: A Universal Enrichment Tool for Interpreting Omics Data. *Innovation* 2 (3), 100141. doi:10.1016/j.xinn.2021.100141

Xu, F., Li, S., Zhang, J., Wang, L., Wu, X., Wang, J., et al. (2018). Cancer Stemness, Immune Cells, and Epithelial-Mesenchymal Transition Cooperatively Predict Prognosis in Colorectal Carcinoma. *Clin. Colorectal Cancer.* 17 (3), e579–e592. doi:10.1016/j.clcc.2018.05.007

Yoshihara, K., Shahmoradgoli, M., Martinez, E., Vegesna, R., Kim, H., Torres-Garcia, W., et al. (2013). Inferring Tumour Purity and Stromal and Immune Cell Admixture from Expression Data. *Nat. Commun.* 4, 2612. doi:10.1038/ncomms3612

Yuan, J., Xie, A., Cao, Q., Li, X., and Chen, J. (2020). INHBB Is a Novel Prognostic Biomarker Associated with Cancer-Promoting Pathways in Colorectal Cancer. *Biomed. Res. Int.* 2020, 6909672. doi:10.1155/2020/6909672

Zaborowski, A. M., Winter, D. C., and Lynch, L. (2021). The Therapeutic and Prognostic Implications of Immunobiology in Colorectal Cancer: a Review. *Br. J. Cancer.* 125(10):1341-1349. doi:10.1038/s41416-021-01475-x

Zahra, M. H., Afify, S. M., Hassan, G., Nawara, H. M., Kumon, K., Seno, A., et al. (2021). Metformin Suppresses Self-Renewal and Stemness of Cancer Stem Cell Models Derived from Pluripotent Stem Cells. *Cell. Biochem. Funct.* 39 (7), 896–907. doi:10.1002/cbf.3661

Zeuner, A., Todaro, M., Stassi, G., and De Maria, R. (2014). Colorectal Cancer Stem Cells: from the Crypt to the Clinic. *Cell. Stem Cell.* 15 (6), 692–705. doi:10.1016/j.stem.2014.11.012

Conflict of Interest: The authors declare that the research was conducted in the absence of any commercial or financial relationships that could be construed as a potential conflict of interest.

Publisher's Note: All claims expressed in this article are solely those of the authors and do not necessarily represent those of their affiliated organizations, or those of the publisher, the editors and the reviewers. Any product that may be evaluated in this article, or claim that may be made by its manufacturer, is not guaranteed or endorsed by the publisher.

frontiers | Frontiers in Oncology

ORIGINAL RESEARCH
published: 03 June 2022
doi: 10.3389/fonc.2022.862806

Fibroblast-Induced Paradoxical PI3K Pathway Activation in PTEN-Competent Colorectal Cancer: Implications for Therapeutic PI3K/mTOR Inhibition

Fabiana Conciatori[1,2], Erica Salvati[3], Ludovica Ciuffreda[4], Senji Shirasawa[5], Italia Falcone[4], Francesco Cognetti[1], Gianluigi Ferretti[1], Massimo Zeuli[1], Donatella Del Bufalo[2], Chiara Bazzichetto[1,2†] and Michele Milella[6*†]*

[1] Medical Oncology 1, Regina Elena National Cancer Institute (IRCCS), Rome, Italy, [2] Preclinical Models and New Therapeutic Agents Unit, Regina Elena National Cancer Institute (IRCCS), Rome, Italy, [3] Institute of Molecular Biology and Pathology -National Research Council (BPM-CNR), Rome, Italy, [4] Department of Research, Advanced Diagnostics, and Technological Innovation (SAFU), Regina Elena National Cancer Institute (IRCCS), Rome, Italy, [5] Central Research Institute for Advanced Molecular Medicine, Fukuoka University, Fukuoka, Japan, [6] Section of Oncology, Department of Medicine, University of Verona School of Medicine and Verona University Hospital Trust, Verona, Italy

Purpose: Tumor-microenvironment interactions are important determinants of drug resistance in colorectal cancer (CRC). We, therefore, set out to understand how interactions between genetically characterized CRC cells and stromal fibroblasts might influence response to molecularly targeted inhibitors.

Techniques: Sensitivity to PI3K/AKT/mTOR pathway inhibitors of CRC cell lines, with known genetic background, was investigated under different culture conditions [serum-free medium, fibroblasts' conditioned medium (CM), direct co-culture]. Molecular pathway activation was monitored using Western Blot analysis. Immunoprecipitation was used to detect specific mTOR complex activation. Immunofluorescence was used to analyze cellular PTEN distribution, while different mutant PTEN plasmids were used to map the observed function to specific PTEN protein domains.

Results: Exposure to fibroblast-CM resulted in increased growth-inhibitory response to double PI3K/mTOR inhibitors in PTEN-competent CRC cell lines harboring *KRAS* and *PI3K* mutations. Such functional effect was attributable to fibroblast-CM induced paradoxical PI3K/mTORC1 pathway activation, occurring in the presence of a functional PTEN protein. At a molecular level, fibroblast-CM induced C-tail phosphorylation and cytoplasmic redistribution of the PTEN protein, thereby impairing its lipid phosphatase function and favored the formation of active, RAPTOR-containing, mTORC1 complexes. However, PTEN's lipid phosphatase function appeared to be dispensable, while complex protein-protein interactions, also involving PTEN/mTOR co-localization and subcellular distribution, were crucial for both mTORC1 activation and sensitivity to double PI3K/mTOR inhibitors.

OPEN ACCESS

Edited by:
Erika Ruiz-Garcia, National Institute of Cancerology (INCAN), Mexico

Reviewed by:
Evangelia (Litsa) Papakonstanti, University of Crete, Greece
Teresa Gagliano, University of Udine, Italy

***Correspondence:**
Chiara Bazzichetto
chiara.bazzichetto@ifo.it
Michele Milella
michele.milella@univr.it

†These authors have contributed equally to this work

Specialty section:
This article was submitted to Molecular and Cellular Oncology, a section of the journal Frontiers in Oncology

Received: *26 January 2022*
Accepted: *28 April 2022*
Published: *03 June 2022*

Citation:
Conciatori F, Salvati E, Ciuffreda L, Shirasawa S, Falcone I, Cognetti F, Ferretti G, Zeuli M, Del Bufalo D, Bazzichetto C and Milella M (2022) Fibroblast-Induced Paradoxical PI3K Pathway Activation in PTEN-Competent Colorectal Cancer: Implications for Therapeutic PI3K/mTOR Inhibition. Front. Oncol. 12:862806. doi: 10.3389/fonc.2022.862806

Data Interpretation: Microenvironmental cues, in particular soluble factors produced by stromal fibroblasts, profoundly influence PI3K pathway signaling and functional response to specific inhibitors in CRC cells, depending on their mutational background and PTEN status.

Keywords: PTEN, PI3K signaling, CRC, soluble factors, fibroblasts

INTRODUCTION

Colorectal cancer (CRC) represents the third most common malignancy worldwide (1). Despite progress in the molecular subtyping of CRC and the implementation of molecularly targeted and immunotherapy agents, metastatic disease remains largely incurable. While the epidermal growth factor (EGF) and vascular endothelial growth factor (VEGF) pathways have been successfully targeted for therapeutic purposes in advanced CRC, the prognostic and therapeutic role of other crucial signaling cascades frequently altered in CRC, such as the phosphatidylinositol 3-kinase (PI3K) pathway, remain elusive (2).

PI3K signaling regulates many oncogenic capabilities, such as protein translation, cytoskeleton remodeling, cell proliferation, and angiogenesis. PI3K phosphorylates PtdIns(4,5)P2 (PIP2) into PtdIns(3,4,5)P3 (PIP3), which acts as the second messenger for the AKT and PDK1 kinases; organization of different mTOR-containing complexes (mTORC1 and 2) signals to further effectors, such as $p70^{S6K1}$ and 4E-binding protein (4E-BP1) downstream of the mTORC1 complex, to enable activation of the translational and transcriptional machinery. The tumor suppressor phosphatase and tensin homolog (PTEN) is the major factor restraining PI3K pathway activity and counteracting its pro-tumoral function. Collectively, aberrations of the PI3K pathway, including loss of function at the PTEN locus and its epigenetic silencing, occur in a substantial proportion of CRC cases (2). Accordingly, therapeutic inhibition of PI3K and mTOR has shown antitumor activity in preclinical models (3); however, available clinical trials with dual PI3K/mTOR inhibitors (such as PF-05212384, hereafter referred to as gedatolisib - Geda) do not recapitulate these findings (4, 5), suggesting the existence of inter- or intra-pathway feedback loops mediating therapeutic resistance. Moreover, the local inflammatory cytokine milieu and other microenvironmental factors (such as composition of the gut microbiome) may crucially interact with the genetic background of CRC and modulate its sensitivity/resistance to pathway inhibition, albeit with yet poorly defined molecular mechanisms (2).

In this context, the role of PTEN as a potential prognostic and/or predictive biomarker in CRC remains debated, not only in terms of response to established therapeutic approaches, such EGF receptor (EGFR) and/or VEGF receptor blockade (6, 7), but also in reference to experimental PI3K pathway inhibition. Indeed, a recent phase I/II study combining the mTORC1 inhibitor everolimus (Eve) with a standard mFOLFOX6/bevacizumab regimen showed promising activity in metastatic CRC, particularly in patients whose tumors lacked PTEN expression (8).

In this study, we investigated whether the presence of stromal fibroblasts may modulate sensitivity of molecularly characterized CRC cell lines to PI3K signaling inhibitors. Quite surprisingly, we observed that exposure to fibroblast-derived conditioned medium (CM) increases signaling through the PI3K/mTORC1 pathway paradoxically in PTEN-competent CRC cells, thereby sensitizing them to the growth inhibitory effect of the double PI3K/mTOR inhibitor, Geda. From a molecular standpoint, fibroblast-CM induces PTEN C-tail phosphorylation and its cytoplasmic redistribution, resulting in impaired lipid phosphatase activity; however, paradoxical PI3K/mTORC1 activation and sensitization to Geda appear to be mediated by PTEN's protein-protein interaction, rather than lipid phosphatase activity and ability to co-localize with mTOR at the plasma membrane.

MATERIALS AND METHODS

Cell Cultures

X-MAN™ HCT116 Parental (RRID : CVCL_HD91) and HCT116 $PTEN^{-/-}$ (RRID : CVCL_HD92) cells were generated by Horizon from homozygous knock-out of PTEN by deleting exon 5 which encodes the active site of the protein in the CRC cell line HCT116 (Horizon Discovery www.horizondiscovery.com) (9). Isogenic cell lines HCT116, HK2–6, and HKE-3 were performed by Shirasawa's group by *KRAS* specific targeting technique (10, 11). LS180, HT29, RKO, and SW480 cell lines were kindly provided by Dr. Federica Di Nicolantonio as previously described (11). Human foreskin fibroblasts (HFF), green fluorescent protein (GFP)-labeled fibroblasts, and BJ cell lines were kindly provided by Dr. Maurizio Fanciulli. CRC cell lines were routinely maintained in RPMI 1640 medium (Euroclone, Milan, Italy) supplemented with 10% inactivated fetal bovine serum (FBS) (Gibco, Life Technologies, California, USA), whereas HFF and BJ were routinely maintained in DMEM medium supplemented with 15% inactivated FBS. All the growth media were added with 2 mM L-glutamine (Gibco, Life Technologies, California, USA) and antibiotics (Penicinillin/Streptomycin) (Gibco, Life Technologies, California, USA); cells were grown in a humidified atmosphere with 5% CO2 at 37°C.

Normal fibroblasts (NF) were isolated from normal colon tissue, derived from patients surgically treated at Regina Elena Cancer Institute. The study was reviewed and approved by the ethics committee of the Regina Elena National Cancer Institute. Normal colon tissue was digested by 0.35% Collagenase type I (Gibco, Life Technologies, California, USA); DMEM medium supplemented with 15% inactivated FBS was added with 2X Antibiotic Antimycotic Solution (Sigma Aldrich, St. Louis, USA). Isolated fibroblasts were routinely maintained in DMEM medium supplemented with 15% inactivated FBS, added with 2 mM L-glutamine (Gibco, Life Technologies, California, USA) and antibiotics (Penicinillin/Streptomycin) (Gibco, Life

Technologies, California, USA); cells were grown in a humidified atmosphere with 5% CO2 at 37°C.

Based on previous experience of our group (11), HFF-CM was obtained under standardized culture conditions: $1x10^6$ cells were seeded and after 24 h, cells were washed with PBS 1X and medium was replaced by serum-free medium (wo FBS); CM was collected after 72 h. Serum-free conditions were chosen based on the notion that production of soluble factors is tightly dependent on the type of growth media used; moreover, serum-free conditions are also necessary to characterize the pattern of expression of soluble factors released by fibroblasts (see below, paragraph 2.10), using specific ELISA and membrane-based arrays, since FBS contains basal levels of cyto/chemokines that could interfere with the detection of mediator(s) involved in the observed CM effects (12, 13).

For recombinant protein experiments, 1000 pg/mL of interleukin (IL)-8, IL-6 and monocyte chemoattractant protein (MCP)-1 were added in DMEM wo FBS. Recombinant human IL-8, IL-6, and MCP-1 were purchased from R&D Systems (R&DSystems, MN, USA).

For cell counting, Thoma chamber was used. All cell lines tested negative for mycoplasma contamination.

Drug Treatments and Cell Proliferation Assay

Trametinib (GSK1120212, Tram) was kindly provided by GlaxoSmithKline (Brentford, Middlesex, UK). Alpelisib (BYL719, Alp), dactolisib (BEZ235, Dact), and Geda (PF05212384) were purchased from Selleck Chemicals (Huston, TX, USA). MK-2206 (MK) was kindly provided by Merck and Co. (Kenilworth, NJ, USA). Alp, Geda, MK, and Tram were dissolved in DMSO as a 1 mM (Geda, MK and Tram) and 5mM (Alp) stock solution, dact was dissolved in DMF as a 1mM. All the drugs were stored at -20°C (Alp, Dact, MK, and Tram) or -80°C (Geda). Eve (RAD001) was kindly provided from Novartis Pharma (Basel, Switzerland) and was dissolved in 100% ethanol as a 10 mM stock solution and stored at -20°C.

The final concentration of drugs was obtained by dilution with culture medium.

Effects on cell growth after 72 h of different treatments were monitored by Crystal Violet assay, as previously described (10).

Direct Co-Cultures

X-MAN™ HCT116 Parental and HCT116 $PTEN^{-/-}$ cells and HFF cells were seeded alone or with a 1:1 ratio in 35 mm plates (Falcon BD, Oxford, UK) in RPMI 1640 (Euroclone, Milan, Italy) supplemented with 10% inactivated FBS (Gibco, Life Technologies, California, USA), as previously described. After 24 h, culture media were replaced with serum-free DMEM (Euroclone, Milan, Italy) containing different drug concentrations alone or in combination. After 72 h of treatment, cells were suspended in ice-cold RPMI 1640 (Euroclone, Milan, Italy) supplemented with 10% inactivated FBS (Gibco, Life Technologies, California, USA). The total amount of cells was counted using the Thoma chamber and the percentage of CRC and HFF cells were analyzed by flow cytometry analysis that allows to differentiate between HFF cellular populations, fluorescently labeled in comparison to unlabeled X-MAN™ isogenic HCT116 cells.

Plasmid and Transfection Experiments

X-MAN™ HCT116 Parental cell line was transfected with either GFP-PTEN C124S or GFP-Q399STOP plasmids, which encode for mutant PTEN C124S and PTEN Q399STOP proteins, respectively (14). Stable transfection of plasmids was performed using Lipofectamine 2000 (Invitrogen, Carlsbad, CA, USA) according to the manufacturer's instructions.

RNA Analysis

Total RNA was prepared from cells using the RNA extraction kit, RNeasy Mini Kit (Qiagen, Hilden, Germany) as per the manufacturer's instructions. Of total RNA, 1 μg was converted into single-strand cDNA using Superscript II (Invitrogen, Carlsbad, CA, USA) as per the manufacturer's instructions. Quantitative real-time PCR (RT-qPCR) was performed with Fast SYBR®Green quantitative PCR kit (Applied Biosystems, Foster City, CA, USA) for RPL19 (Forward primer sequence: 5′-CGGAAGGGCAGGCACAT-3′ and Reverse primer sequence 5′-GGCGCAAAATCCTCATTCTC-3′) and PIK3CD (Forward primer sequence: 5′-CCCACATGAAGAGGAACTGAGAT-3′ and Reverse primer sequence 3′- GGTTGGCAGGCTCA GTGACT-5′). Expression of PIK3CD was then normalized with RPL19.

Western Blot Analysis

Whole cell extracts were obtained by SDS lysis buffer, containing 20 mM TrisHCl (pH 7.4) and 2% SDS, with 1X phosphatase and protease inhibitors (Thermo Fisher Scientific, Rochester, NY, USA). Protein quantification, separation, and detection were assessed as previously described (11). Membranes were probed with the primary and secondary antibodies reported in **Supplementary Materials**.

Immunoprecipitation

Chip-Grade Protein A/G Magnetic Beads (Thermo Fisher Scientific, Rochester, NY, USA) were incubated with 2 μg of FRAP (Santa Cruz Biotechnology, Santa Cruz, CA) overnight at 4°C. Precleared beads were then incubated overnight at 4°C with 1 μg of protein. The immunoprecipitates were collected and after two washes in CHAPS buffer (containing 5 mM EDTA, 0.3% CHAPS, 50 mM Tris HCl (pH 7.4), 150 mM NaCl, 10 mM $MgCl_2$, 1mM KCl, and 1X phosphatase and protease inhibitors (ThermoFisher Scientific, Rochester, NY, USA)) re-suspended in 35 μl of the same buffer and 1X Ladder buffer. The immune complexes and 20 μg of protein total cell extract were analyzed by Western blot analysis as described above.

Immunofluorescence

$5x10^4$ cells were seeded on 22x22 mm coverslips pretreated with 2% type A from porcine skin gelatin (Sigma Aldrich, St. Louis, USA); after 24 h, culture media were replaced by wo FBS DMEM (Euroclone, Milan, Italy) or HFF CM containing the indicated concentration of drug. After 24 h from treatments, cells were fixed in 4% formaldehyde in 1X PBS for 10 min, permeabilized in

1X PBS containing 0.5% Triton X-100 for 5 min at room temperature. Coverslips were incubated with primary and secondary antibodies as previously described (11). The used antibodies are reported in **Supplementary Materials**. Images were taken using Leica DMi8 microscopy (Leica, Solms, Germany) and Zeiss LSM 880 Confocal Microscope (Carl Zeiss, Oberkochen, Germany) equipped with ×63 lenses and operated by Zen 09 black software (Carl Zeiss).

Subcellular Protein Extraction

$5x10^6$ HCT116 Parental cells were seeded into 100 mm dishes (Greiner bio-one, Kremsmünster, Austria) in RPMI 1640 (Euroclone, Milan, Italy) and after 24 h from plating cell culture media were replaced by wo FBS DMEM (Euroclone, Milan, Italy) or HFF CM containing the indicated concentration of drug. After 24 h from treatment, cells were processed according to the manufacturer's instructions of the Subcellular Protein Fractionation Kit (Thermo Fisher Scientific, Rochester, NY, USA). Membrane and cytoplasmic extract were analyzed by using Western blot assay.

Detection and Analysis of Soluble Factor Production

$3x10^5$ HFF, BJ, and NF cells were plated into 60 mm dishes (Falcon BD, Oxford, UK). After 24 h from the plating, the culture medium was replaced by wo FBS DMEM, and after 48 h from the plating media were collected and cells were counted. Cells culture media were analyzed by Human Angiogenesis Antibody Array (R&DSystems, MN, USA) according to the manufacturer's protocol. Cell culture media were also analyzed by IL-8 and IL-6 (Enzo Life Sciences, Farmingdale, NY, USA), and MCP-1 (R&DSystems, MN, USA) specific ELISA assay, according to the manufacturer's protocol. Absorbance was read at 450 nm. IL-8, IL-6, and MCP1 expression were represented as pg/mL and then related to the control assuming as to 100%.

PTEN Activity ELISA Assay

$6x10^6$ HCT116 Parental cells were seeded into 100 mm dishes (Greiner bio-one, Kremsmünster, Austria) in RPMI 1640 (Euroclone, Milan, Italy) and after 24 h from plating cell culture media were replaced by wo FBS DMEM (Euroclone, Milan, Italy) or HFF CM containing the indicated concentration of drug. After 24 h from treatment, cells were processed according to the manufacturer's instructions of the PTEN activity ELISA assay (Echelon Biosciences Inc., Salt Lake City, UT, USA). Absorbance was read at 450 nm. PTEN phosphatase activity was represented as PIP2 concentration (pmol/μL) and then related to the control assuming as to 100%.

Statistical Analysis

Results are expressed as average of three independent experiments. Results with two-tailed p values <0.05 were judged to be statistically significant. The dose of drug that causes 50% of cell growth inhibition (IC_{50}) was calculated according to the Chou-Talalay method using the Calcusyn software (Biosoft, Cambridge, United Kingdom). The same software was used for deriving combination indexes (CI): the average CI at the ED50, ED75, and ED90 <1 indicates synergism, = 1 indicates additivity, and >1 indicates antagonism, respectively. Statistical analysis for co-localization was conducted using GraphPad Prism (RRID : SCR_002798) (www.graphpad.com).

RESULTS

Exposure to Fibroblast-CM Sensitizes PTEN-Competent CRC Cells to Double PI3K/mTOR Inhibition

We evaluated the role of PTEN status and microenvironmental interactions in the modulation of CRC response to single or combined MAPK/PI3K inhibition. The X-MAN™ isogenic HCT116 cell lines [HCT116 Parental (PTEN-competent) and HCT116 $PTEN^{-/-}$ (PTEN-loss)] were treated with increasing concentrations of the MEK inhibitor Tram, the PI3K/mTOR double inhibitor Geda, or their combination (Tram+Geda, 1:1 fixed dose-ratio) for 72 h under different culture conditions: serum-free medium (wo FBS), fibroblast-CM (CM HFF), or direct CRC/fibroblast co-culture (co-co), using GFP-tagged immortalized skin fibroblast (HFF). Pathway inhibitors (alone or in combination) displayed little, if any, growth inhibitory activity on isolated HFF fibroblasts (data not shown).

In CRC cells, sensitivity to the growth-inhibitory activity of Tram significantly decreased in the absence of a functional PTEN (HCT116 $PTEN^{-/-}$ cells), regardless of cell culture conditions (**Supplementary Figure S1** and **Table 1**). Conversely, exposure to fibroblast-CM specifically sensitized PTEN-competent (HCT116 Parental), but not PTEN-loss (HCT116 $PTEN^{-/-}$) CRC cells to Geda [48% reduction in the IC_{50} in HCT116 Parental cells under CM HFF, as compared with wo FBS, conditions (**Table 1**), p-value <0.05 at all the tested doses (**Figure 1A** left panels)]; direct co-co had no effect on sensitivity to Geda, regardless of PTEN status (**Figure 1A** right panels and **Table 1**). As we previously reported (9), pharmacological interactions between Tram and Geda were highly synergistic in PTEN-loss and antagonistic in PTEN-competent cells, under isolated cell culture (wo FBS) conditions (**Figure 1B** left panels, **Supplementary Figure S2A** and **Table 1**). Exposure to HFF CM and direct co-co turned the interaction between Tram and Geda into highly synergistic in the HCT116 Parental cell line (CI: 0.01 and 0.0007, respectively), whereas only direct cell-to-cell contact influenced pharmacological interactions in HCT116 $PTEN^{-/-}$ cells, reverting synergism (CI: 0.99) and reducing (albeit not significantly) the growth inhibitory response to combined treatment (**Figure 1B** right panels, **Supplementary Figure S2B** and **Table 1**).

We focused on the observed sensitization to the growth-inhibitory effects of PI3K/mTOR inhibition under exposure to fibroblast-CM. First, the same functional sensitization effects observed with HFF CM were obtained using CM from another immortalized normal foreskin fibroblast cell line (BJ) and from primary fibroblasts isolated by normal colon tissue

TABLE 1 | Response of HCT116 Parental and HCT116 PTEN$^{-/-}$ cells to targeted inhibitors under different conditions of growth.

	Trametinib (IC_{50} nM)	Gedatolisib (IC_{50} nM)	Combo (CI)	Trametinib (IC_{50} nM)	Gedatolisib (IC_{50} nM)	Combo (CI)
		wo FBS			**CM HFF**	
HCT116 Parental	0.02	$4.2x10^3$	50	0.02	$2.2x10^3$	0.01
HCT116 PTEN$^{-/-}$	$14x10^3$	$>1x10^6$	0.006	$10x10^3$	$>1x10^6$	0.003
	Trametinib (IC_{50} nM)	**Gedatolisib (IC_{50} nM)**	**Combo (CI)**	**Trametinib (IC_{50} nM)**	**Gedatolisib (IC_{50} nM)**	**Combo (CI)**
		wo FBS			**co-co with HFF**	
HCT116 Parental	0.68	$0.4x10^3$	1.2	1.03	$0.08x10^3$	0.0007
HCT116 PTEN$^{-/-}$	24.4	$0.37x10^3$	0.07	6.35	$0.32x10^3$	0.99

IC_{50} and CI for all the drugs in absence of FBS (i.e. wo FBS) are intrinsically differ each other comparing to HFF-CM and co-co with HFF due to the different experimental setting conditions.

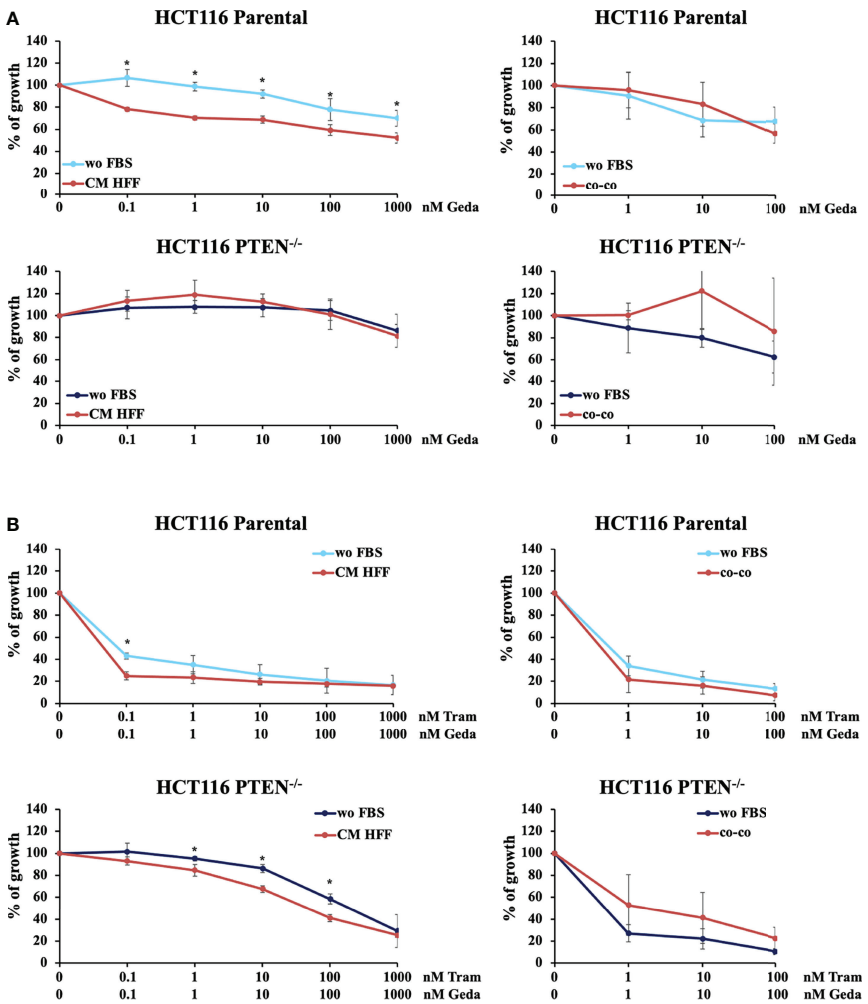

FIGURE 1 | PTEN expression and microenvironmental interactions affect the response to molecular targeted inhibition in isogenic CRC cell lines. HCT116 Parental and HCT116 PTEN$^{-/-}$ cell lines were treated with increased doses (dose range 0.1-1000 nM) of Geda or Geda and Tram combination (1:1) (**A**, **B**, respectively) in serum-free condition, fibroblast HFF derived CM (left panels) or direct CRC/GFP-tagged HFF co-culture (right panels). Cell viability for wo FBS and HFF-CM was assessed by Crystal Violet assay after 72 h of treatment. For HFF co-culture cells were counted after 72 h of treatment and the number of GFP positive and negative cells were calculated using cytofluorimetric analysis. Results are expressed as percentage of growth inhibition relative to untreated control and represent the average ± SEM of three independent experiments. Asterisks indicate statistically significant differences (p-value < 0.05 by 2-tailed Student's t test) for the comparison between treatment under wo FBS and HFF-CM or co-co conditions.

(**Supplementary Figures S3A, B**). Moreover, another double PI3K/mTOR inhibitor (Dact) exerted functional effects similar to those observed with Geda (**Supplementary Figure S4A** and **Supplementary Table S1**). Single-step inhibition along the PI3K cascade was not sufficient to obtain such functional effects: indeed, response to specific inhibitors targeting PI3K, AKT, or mTOR individually (Alp, MK, and Eve, respectively) was not modulated by exposure to fibroblast-CM in either isogenic cell line (**Supplementary Figures S4B–D** and **Supplementary Table S1**). These results confirm that exposure to normal fibroblast-CM specifically sensitizes PTEN-competent CRC cells to double PI3K/mTOR inhibition.

Additional Genetic Determinants of Fibroblast-CM Mediated Sensitization to PI3K/mTOR Inhibition in CRC

We next explored the effect of fibroblast-CM in modulating functional response to Geda in four PTEN-competent CRC cell lines (LS180, HT29, RKO, and SW480), characterized by different genetic background (*KRAS*-mut/*PIK3CA*-mut, *KRAS*-wt/*PIK3CA*-wt, *KRAS*-wt/*PIK3CA*-mut, and *KRAS*-mut/*PIK3CA*-wt, respectively) (**Figures 2A, B**). Each cell line was exposed to increasing concentrations of Geda (0.1-1000 nM) under wo FBS or HFF CM conditions for 72 h. Similar to HCT116 Parental cells, only LS180 (*PIK3CA*-mut/*KRAS*-mut/PTEN-competent) cells displayed a statistically significant difference in their response to Geda according to culture conditions (p-value < 0.05 for the lowest concentrations of Geda; **Figures 2A, B**). Conversely, in the *KRAS*-wt/*PIK3CA*-mut RKO cell line exposure to fibroblast-CM induced significant resistance to Geda at the highest concentrations. No significant differences were observed in the HT29 and SW480 cell lines (**Figure 2A**).

Since HCT116 cells are known to express high levels of the p110δ PI3K isoform (15), we also evaluated whether the pattern of p110δ PI3K expression correlated with functional response to Geda in the presence or absence of HFF-CM. As shown in **Supplementary Figure S4E**, p110δ PI3K (*PIK3CD*) expression by RT-qPCR was highest in HCT116 Parental and SW480 cells when compared in a panel of five cell lines, and did not correlate with HFF-CM induced functional sensitization to Geda-mediated growth inhibition.

We next investigated the response of isogenic *KRAS* HCT116 cell lines (parental HCT116 - heterozygous *KRAS*-mut, HK2-6 - homozygous *KRAS*-mut, and HKE-3 cell lines - homozygous *KRAS*-wt, respectively) to Geda under different culture conditions. As shown in **Figure 2C**, the most pronounced fibroblast-CM dependent functional sensitization to Geda was observed in the homozygous *KRAS*-mut isogenic cell line HK2-6. Overall, these results suggest that, in addition to the expression of a functional PTEN protein, the mutational status of both *KRAS* and *PIK3CA* plays a role in the observed functional sensitization to double PI3K/mTOR inhibition induced by fibroblast-CM in CRC cells.

Fibroblast-CM Induces Paradox PI3K Pathway Activation Which Can be Reverted by Double PI3K/mTOR Inhibition in PTEN-Competent CRC Cell Lines

We next investigated whether fibroblast-CM might influence PTEN expression and function and PI3K pathway activation. Exposure of HCT116 Parental cells (PTEN-competent) to fibroblast-CM for 24 h induced PTEN phosphorylation at Ser 380/Thr 382/383, along with relative protein accumulation, and $p70^{S6K1}$ phosphorylation at Thr 389, with relative protein accumulation; under these conditions, double PI3K/mTOR

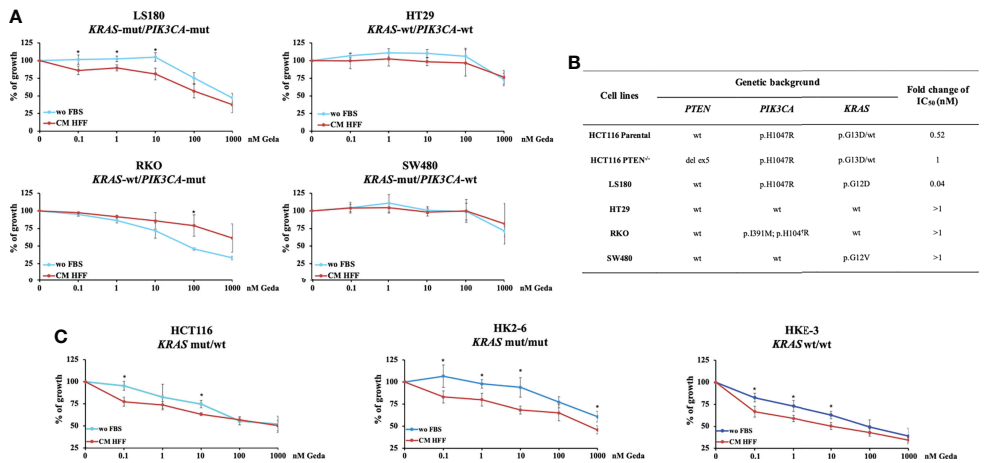

FIGURE 2 | Fibroblast-CM-dependent sensitivity to Geda occurs only in *KRAS*-mut/*PIK3CA*-mut/PTEN-competent CRC cell lines. PTEN-competent LS180, HT29, RKO and SW480 cell lines and isogenic *KRAS* HCT116 cell lines (HCT116, HK2-6 and HKE-3) were treated with increasing doses of Geda (range doses 0.1-1000 nM) in serum-free condition and fibroblast HFF-CM (**A**, **C**, respectively). Results are expressed as percentage of growth inhibition relative to untreated control and represent the average ± SEM of three independent experiments. Asterisks indicate statistically significant differences (p-value < 0.05 by 2-tailed Student's t test) for the comparison between treatment under wo FBS and HFF CM conditions. **(B)** Ratio of IC_{50} of Geda (nM) under CM HFF *vs* wo FBS condition of growth.

inhibition by Geda paradoxically induced PTEN and $p70^{S6K}$ phosphorylation under unstimulated conditions, while substantially decreasing their phosphorylation induced by fibroblast-CM (**Figure 3A** left panel). A similar modulation in p-PTEN Ser 380/Thr 382/383 and $p70^{S6K1}$ Thr 389 in response to both fibroblast-CM exposure and Geda treatment was also observed in the PTEN-competent LS180 cell line (**Supplementary Figure S5A**) and comparable results were observed using a different double PI3K/mTOR inhibitor (Dact) in HCT116 Parental cells (**Supplementary Figure S5B**). Conversely, in HCT116 $PTEN^{-/-}$ cells $p70^{S6K1}$ Thr 389 phosphorylation levels were similar under both unstimulated and fibroblast-CM stimulated conditions and were consistently decreased by Geda under either culture condition (**Figure 3A** right panel). Modulation in other pathway elements (such as reduction in p-mTOR Ser 2448, Ser 2481, and Thr 2446, and total mTOR protein; increase in p-4E-BP1 Thr 37/46 and total 4E-BP1 protein levels) upon exposure to fibroblast-CM was consistent between PTEN-competent (HCT116 Parental, left panel) and PTEN-loss (HCT116 $PTEN^{-/-}$, right panel) isogenic CRC cells (**Supplementary Figure S5C**).

Among soluble factors potentially involved in the fibroblast-CM induced PI3K pathway stimulation in PTEN-competent CRC cells, IL-8, IL-6, and MCP-1 were the most prominently produced by all three normal fibroblast cell lines tested (HFF, BJ, and NF; **Supplementary Figure S5D**); however, exogenous addition of recombinant IL-8, IL-6, or MCP-1 (alone or in combination) was not able to induce $p70^{S6K1}$ phosphorylation at Thr 389, despite upregulation of p-PTEN Ser 380/382/383 levels (**Supplementary Figure S5E**).

To further investigate the mechanisms underlying paradox PI3K pathway activation in response to fibroblast-CM stimulation in PTEN-competent cells, we examined mTOR complex formation under different culture conditions. Co-immunoprecipitation experiments shown in **Figure 3B** indicated specific binding of RAPTOR to, and dissociation of, PRAS40 from mTOR under fibroblast-CM stimulated conditions.

Overall, such evidence indicates that yet unidentified soluble factors released by normal fibroblasts paradoxically activate the PI3K axis in PTEN-competent cells, by specifically activating the mTORC1 complex.

Fibroblast-CM-Induced Paradox PI3K Pathway Activation Is Mediated by PTEN Intracellular Redistribution and Inactivation

As shown in **Figure 3A**, fibroblast-CM induced prominent phosphorylation of PTEN's C-tail (Ser 380/Thr 382/383) in PTEN-competent CRC cells. Consistent with the well-known role of PTEN phosphorylation in modulating protein localization and activity, immunofluorescence experiments conducted in HCT116 Parental cells showed predominantly membrane-bound PTEN under basal conditions (wo FBS), while its distribution became spread and predominantly cytoplasmic upon exposure to either Geda or fibroblast-CM (**Figure 4A**); under these conditions, PIP3 distribution essentially paralleled that of PTEN protein, even though the spread, cytoplasmic distribution and relative abundance of PIP3 were less evident in Geda-treated, as compared with fibroblast-CM treated, cells. Regardless, under fibroblast-CM stimulated conditions Geda treatment restored membrane-bound PTEN/PIP3 localization (**Figure 4A**). These findings were further confirmed by cell fractionation experiments (**Figure 4B**): indeed, PTEN protein decreased in the membrane-bound fraction and increased in the cytoplasmic fraction upon

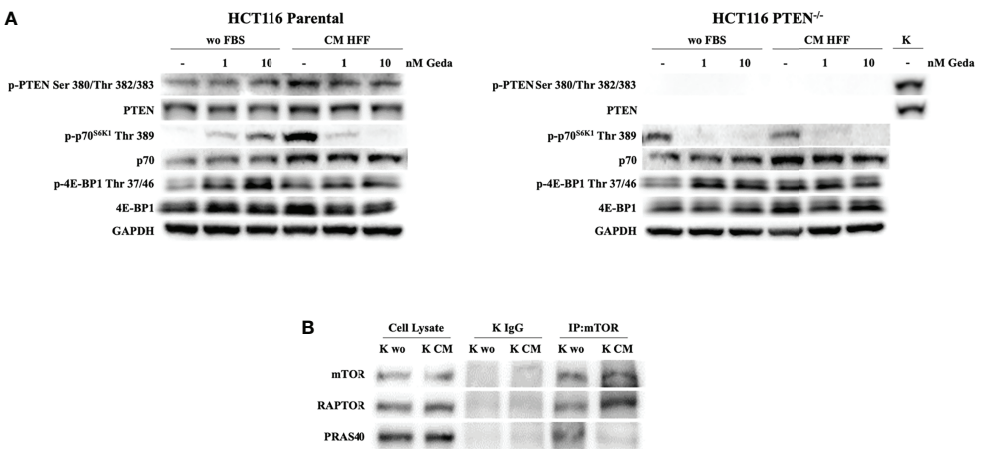

FIGURE 3 | Evaluation of PI3K pathway activation in response to Geda in the presence of fibroblast-derived CM. **(A)** HCT1116 Parental and HCT116 $PTEN^{-/-}$ cell lines were treated with 1 and 10 nM of Geda in serum-free condition and HFF-CM. Cells were lysed and analyzed by Western Blotting using specific antibodies (as indicated). GAPDH is shown as protein loading and blotting control. **(B)** HCT116 Parental cells were grown in wo FBS and HFF CM for 24 h. Endogenous mTOR was immunoprecipitated (IP:mTOR) and the immunocomplexes were blotted for RAPTOR and PRAS40. mTOR, RAPTOR and PRAS40 levels in total cell lysates are also shown. Results of a representative experiment out of three independent experiments performed are shown.

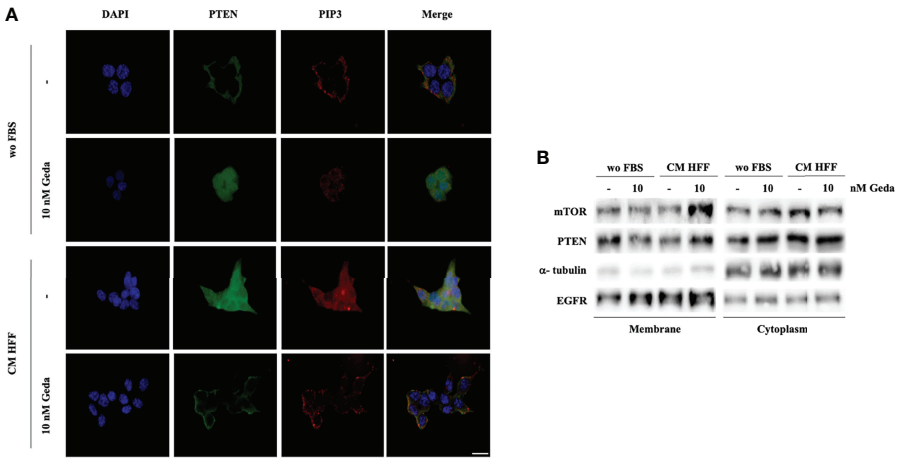

FIGURE 4 | Fibroblast-derived CM induces the reduction of PTEN activity and its re-distribution in the cell. **(A)** Direct immunofluorescence analysis of cellular localization of PTEN (green) and PIP3 (red). Nuclear staining was evaluated with DAPI in HCT116 Parental cells in both wo FBS and HFF CM, in absence or presence of 10 nM Geda. Results of a representative experiment out of three independent experiments performed are shown. Microphotographs were taken at ×63 magnification. Scale bar 50 μm. **(B)** HCT116 Parental cell line were treated with 10 nM of Geda in wo FBS and HFF-CM conditions. Membrane and cytoplasmic fractions of cell line were isolated; molecular differences were analyzed by Western Blotting using specific antibodies (EGFR and α-tubulin are shown as protein loading and blotting control for membrane and cytoplasmic extract, respectively). Results of a representative experiment out of three independent experiments performed are shown.

exposure to either Geda or fibroblast-CM and accumulated back in the membrane fraction upon combined fibroblast-CM/Geda treatment; interestingly, the mTOR protein changed its subcellular distribution in parallel to that of PTEN (**Figure 4B**). However, when PTEN enzymatic activity was measured in whole cell lysates in the presence of exogenous PIP3 by ELISA (thus not reflecting the potential role of PTEN subcellular localization), Geda treatment did not significantly affect PTEN lipid phosphatase activity under basal (wo FBS) conditions, while exposure to fibroblast-CM reduced enzymatic activity by approximately 50%; combined fibroblast CM/Geda treatment restored PTEN activity to basal levels (**Supplementary Figure 6**).

Overall, these data suggest that fibroblast-CM induced PI3K pathway activation is due, at least in part, to PTEN C-tail phosphorylation, subcellular redistribution, and impaired enzymatic activity, all of which can be restored by simultaneous PI3K/mTOR inhibition.

Protein-Protein Interaction PTEN Domain Mediates Fibroblast-CM-Dependent Paradox PI3K Activation and Sensitization to Geda

Taken together, the above-described results indicate that the presence of a functional PTEN protein is necessary for fibroblast-CM mediated paradox PI3K pathway activation and, hence, to sensitize CRC cells to the growth-inhibitory effects of double PI3K/mTOR inhibition. To dissect whether these molecular and functional effects are mediated by PTEN protein-protein interaction or lipid phosphatase domains, HCT116 Parental cells were stably transfected with two chimeric GFP-mutant PTEN genes exerting a dominant negative function: the Q399STOP construct produces a PTEN protein lacking the PDZ-domain and protein-protein interaction ability; the C124S construct produces a PTEN protein lacking enzymatic activity and the ability to dephosphorylate both proteins and lipids (14, 16, 17).

C124S transfection did not affect response to Geda under either basal (wo FBS) or fibroblast-CM stimulated conditions (**Figure 5A**, left panel). Conversely, Q399STOP transfection completely abrogated the Geda-sensitizing effect of fibroblast-CM: indeed, response to Geda was not significantly different between fibroblast-CM stimulated and unstimulated Q399STOP-transfected cells; however, Q399STOP-transfected cells were significantly more sensitive to Geda than their Parental counterpart under unstimulated conditions and less sensitive under fibroblast-CM stimulated conditions (**Figure 5A**, right panel). Molecular endpoints were modulated consistently with the observed functional effects: HFF CM-dependent stimulation of $p70^{S6K1}$ Thr 389 and 4E-BP1 Thr 37/46 phosphorylation was less pronounced in Q399STOP-transfected cells, as compared to HCT116 Parental and C124S-transfected cells (**Figure 5B**), suggesting a more prominent role for PTEN protein-protein interaction, rather than phosphatase, activity in fibroblast-CM induced paradox PI3K pathway activation. Together with evidence of fibroblast-CM mediated mTORC1 formation only in PTEN-competent cells and concomitant redistribution of both PTEN and mTOR upon treatment, this observation led us to investigate whether PTEN could physically interact with mTOR. To this purpose, we evaluated PTEN and mTOR co-localization under different culture conditions using confocal microscopy. As

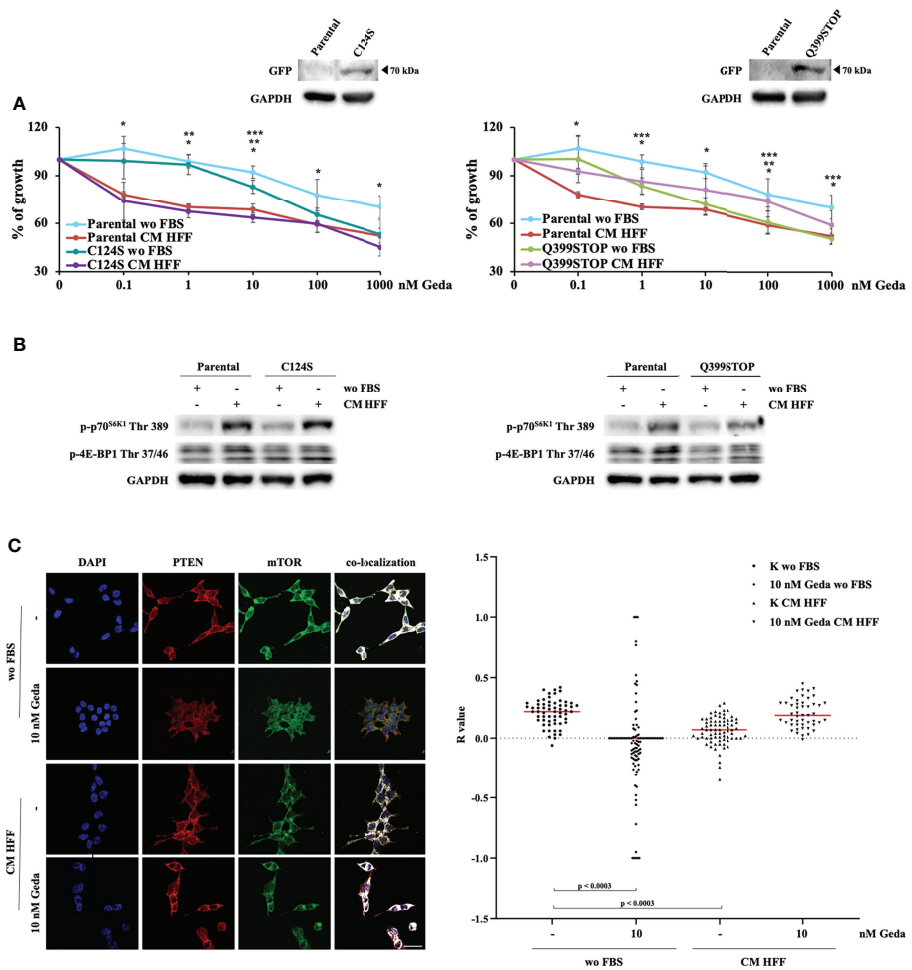

FIGURE 5 | PDZ PTEN domain mediates the effect of fibroblast-CM. **(A)** HCT116 Parental clones stably transfected with either a plasmid encoding PTEN C124S (C124S, left panel) or PTEN Q399STOP (Q399STOP, right panel) were treated with increasing doses of Geda (0.1-100 nM) in wo FBS or HFF-CM conditions. Cell viability was assessed by Crystal Violet assay after 72 h of treatment. Results are expressed as percentage of growth inhibition relative to untreated control and represent the average ± SEM of three independent experiments. Asterisks indicate statistically significant differences (p-value < 0.05 by 2-tailed Student's t test) for the comparison between different conditions (*, **, *** for Parental wo FBS *vs* HFF-CM conditions, Clones (i.e. C124S or Q399STOP) wo FBS *vs* HFF-CM, Parental wo FBS *vs* Clones wo FBS conditions, respectively). **(B)** HCT1116 Parental, C124S clone (left panel) and Q399STOP clone (right panel) cell lines were grown under wo FBS and HFF-CM conditions. Cells were lysed and analyzed by Western Blotting using specific antibodies (as indicated). GAPDH is shown as protein loading and blotting control. Results of a representative experiment out of three independent experiments performed are shown. **(C)** Colocalization analysis (representative images with white spots in left panel) confirmed a clear association in wo FBS condition and the lack of a specific association in HFF-CM and 10 nM Geda wo FBS condition. Microphotographs were taken at ×63 magnification. Scale bar: 50 µm. For the total sample (right panel), R values for control and 10 nM Geda in each condition of growth (wo FBS and HFF-CM) were analyzed by parametric unpaired *t*-test with Welch's correction. PTEN/mTOR codistribution showed a significant pattern of superimposition in wo FBS condition as compared to both HFF-CM control condition and 10 nM Geda wo FBS condition. Results of a representative experiment out of three independent experiments performed are shown.

shown in **Figure 5C**, a substantial pattern of superimposition between the two proteins was observed in unstimulated HCT116 Parental cells (wo FBS); exposure of HCT116 Parental cells to either Geda or fibroblast-CM significantly reduced the pattern of superimposition (p<0.0003 for both), which returned to basal when fibroblast-CM stimulated cells were exposed to Geda (p-value for the comparison between HCT116 Parental cells wo FBS and HCT116 Parental cells HFF-CM+Geda not significant), closely paralleling data on subcellular PTEN localization.

DISCUSSION

In this study we provide evidence that PTEN distribution and function influence the response to targeted therapies according to the presence of stromal elements. Exposure to fibroblast-CM paradoxically hyperactivates the PI3K signaling cascade in *PIK3CA*-mut/*KRAS*-mut/PTEN-competent CRC cells, resulting in increased sensitivity to the growth inhibitory effects of pharmacologic double PI3K/mTOR blockade. Such effect appears to be crucially mediated by PTEN phosphorylation

and subcellular redistribution and increased mTORC1 formation and signaling, which, in turn, appear to be related to PTEN's protein-protein interaction (rather than enzymatic) activity and, possibly, physical interaction with mTOR.

Available evidence indicates a predominant role of cancer cell's genetic background in dictating the response to MAPK signaling inhibitors (10, 18–22). In line with previous evidence from our group (9, 23), sensitivity to MEK inhibition was indeed dependent on functional PTEN expression, regardless of the condition of growth of CRC cells. Consistently, the combination of MAPK and PI3K inhibitors synergistically decreased cell viability only in PTEN-loss contexts (9). Nevertheless, the effects of PI3K pathway inhibition (alone or combined with MEK inhibition) on CRC cell growth are profoundly influenced by the presence of fibroblast-derived soluble factors or direct cell-to-cell contact, particularly in PTEN-competent cells. In HCT116 PTEN$^{-/-}$ cells direct co-culture with stromal fibroblasts only slightly modified the qualitative interaction between Tram and Geda and exposure to fibroblast-CM did not affect their relative resistance to single agent Geda. Conversely, in PTEN-competent HCT116 Parental cells both direct co-culture and exposure to fibroblast-CM changed the interaction between Tram and Geda from antagonistic/additive to strongly synergistic. Most importantly, exposure to fibroblast-CM sensitized PTEN-competent CRC cells to the growth inhibitory effects of double PI3K/mTOR inhibitors.

In a quest to understand the molecular mechanisms underlying such sensitization, we found that yet unidentified soluble factors released by normal fibroblasts induce activation of the PI3K/mTOR axis in CRC cells. Such selective activation occurs only in PTEN-competent cells, a rather paradoxical finding, since the main known function of PTEN is to negatively regulate PI3K activity, through modulation of PIP3 availability (24, 25). Indeed, PTEN inactivation (by genetic, epigenetic, or post-translational events) is usually required to elicit the activation of PI3K and its downstream effectors, such as AKT, mTOR, and p70^{S6K1} (26). mTOR, in particular, can participate in two different enzyme complexes, mTORC1 and mTORC2, with distinct signaling and functional activities (27). In our experimental model, fibroblast-CM specifically elicits mTORC1 activation, shifting the balance toward mTOR association with the RAPTOR scaffold protein and displacing the inhibitor protein PRAS40 from the complex (28, 29). The imbalance toward mTORC1 signaling induced by exposure to fibroblast-CM is supported by unequivocal phosphorylation of p70^{S6K1} (and to a lesser extent 4E-BP1), which is considered to be the main effector downstream of the mTORC1 (30, 31). On the other hand, fluctuations in p-AKT Ser 473 phosphorylation levels in cell lysates do not necessarily reflect, nor should be considered an accurate reading of, the activation status of mTOR (32) and were therefore not considered in this context.

Perhaps the most unexpected finding is that fibroblast-CM mediated PI3K/mTORC1 activation paradoxically requires an intact PTEN protein, in that it is not observed in PTEN$^{-/-}$ CRC cells. In our HCT116 Parental cells model, exposure to fibroblast-CM inactivates PTEN through its C-tail phosphorylation and consequent cellular redistribution, thereby impairing its lipid phosphatase activity (33–35). However, PTEN's phosphatase domain, which is lost in the C124S mutants (14, 36, 37), appears to be dispensable for fibroblast-CM induced p70^{S6K1} Thr 389 phosphorylation and functional sensitization to Geda. On the contrary, loss of the protein-protein interaction PDZ domain [lost in the Q399STOP mutants; (14)] reduces the ability of fibroblast-CM to activate the PI3K/mTORC1 signaling axis and completely abrogates functional sensitization to Geda's growth inhibitory effects. The observed C-terminal PTEN phosphorylation caused by fibroblast-CM stimulation affects amino acid residues (Ser 380/Thr 382/383) within the PDZ binding domain (33). Thus, in addition to subcellular redistribution and loss of lipid phosphatase activity, this may result in changes in the composition of PTEN-associated macromolecular complexes (PAC). It has indeed been shown that PI3K p85/p110β selectively associates with unphosphorylated PTEN within the PAC, raising the possibility that PTEN restrains tumor-promoting PI3K activity not only through its established lipid phosphatase activity, but also through specific protein-protein interactions (38). Co-localization experiments shown in **Figure 5** suggest mTOR itself could be part of phosphorylated PTEN-orchestrated PAC; however, the details of such putative interaction remain to be elucidated, since we could not provide direct evidence of physical interaction between PTEN and mTOR and interactomic databases do not describe such interaction (www.ebi.ac.uk/intact/interactions; www.string-db.org/cgi/input).

Interrelationships between PI3K, PTEN, AKT and mTOR subcellular localization and enzymatic activity are extremely complex. The data presented on the effects of Geda and fibroblast-CM, alone or combined, in HCT116 Parental cells expressing a functional PTEN protein support the following model (**Figure 6**) when used alone, both Geda and fibroblast-CM induce PTEN cytoplasmic redistribution, loss of PTEN/mTOR co-localization, and paradoxical pathway (re)activation; however, although the result is functionally similar (paradoxical pathway activation), the molecular mechanisms of the observed phenomena might be different between Geda and fibroblast-CM: indeed, under conditions in which pathway activation is induced by exposure to fibroblast-CM, Geda regains its ability to functionally inhibit the pathway and effectively counteract tumor cell growth. Overall, these findings suggest that under fibroblast-CM unstimulated conditions Geda induces its own resistance mechanism by, presumably, interrupting a negative feedback loop and paradoxically causing pathway (re)activation. This is reminiscent of the paradoxical MAPK activation observed BRAF-selective kinase inhibitors in *BRAF*-mut cancer models, whereby a kinase-inhibited BRAF protein is still able to form complexes with CRAF or yet unidentified interactors and paradoxically activate MEK and ERK downstream (10, 18, 19). Similar to that functional situation, which requires double MEK/ERK blockade to shut the pathway down and support clinical activity (20–22), here we show that fibroblast-CM induced paradoxical PI3K/mTORC1 specifically sensitizes PTEN-competent CRC cells to double PI3K/mTOR, but not to single PI3K, AKT, or mTOR, inhibition.

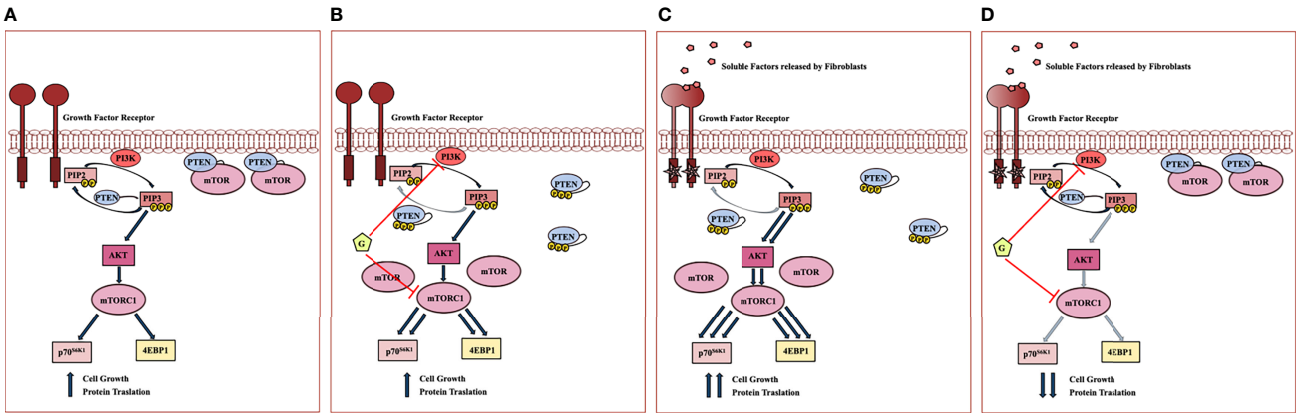

FIGURE 6 | Working model of fibroblast mediated PI3K pathway hyperactivation and response to double PI3K/mTOR inhibitors in PTEN-competent CRC cell lines. **(A)** In serum-free condition of growth, PTEN is associated to plasma membrane and co-localizes with mTOR, acting as a negative regulator of PI3K signaling at different levels. **(B)** Despite PI3K inhibition, Geda (G) causes PTEN C-terminal tail phosphorylation and cytoplasmic redistribution, accompanied by loss of co-localization with mTOR at the plasma membrane, presumably by interrupting a negative feedback loop; the net result of double PI3K/mTOR inhibition, in this context, is paradoxical pathway (re)activation, whereby Geda induces its own resistance mechanism(s). **(C)** Upon fibroblast-CM exposure, two main molecular events concurrently occur with the PTEN C-terminal tail phosphorylation and redistribution within the cells: I) PTEN loses its negative control on PIP3 phosphorylation; II) PTEN no longer co-localizes with mTOR at the plasma membrane, thus rendering mTOR more available to form functionally active complexes and causing mTORC1 and downstream pathway hyperactivation. **(D)** Under conditions in which fibroblast-CM drives PTEN-dependent PI3K/mTOR paradoxical activation, double PI3K/mTOR inhibition strongly switches off signaling through the PI3K cascade, thereby restoring Geda-mediated growth inhibition.

Overall, these results are consistent with a PTEN-centered bidirectional crosstalk between stromal and cancer cells (39). Indeed, PTEN can act as a paracrine regulator of the PI3K pathway: secreted PTEN-long, a translational variant of PTEN, can modulate PI3K activity in PTEN-loss bystander cells (40, 41). On the other hand, exosomes released by hepatocellular carcinoma cells inactivate PTEN in hepatic stellate cells, hence converting them into cancer associated fibroblasts involved in cancer progression (42). Moreover, PTEN-loss in stromal fibroblasts induces miR-320 downregulation and activates an oncogenic secretome, which in turn promotes tumor angiogenesis and tumor-cell invasion in breast cancer models (43).

The mutational status of the key genes involved in specific molecular cascades (e.g. *PIK3CA*, *KRAS*, PTEN) remains a crucial predictor of targeted drug response and it is now well established that feedback loops and pathway crosstalks are involved in conferring primary and/or acquired drug resistance, even for PI3K signaling inhibitors (44). A recent review by Brandao and coworkers critically analyzes clinical trials with PI3K inhibitors and suggests *KRAS* mutations among potential biomarkers for resistance in *PIK3CA*-mut breast cancer (45, 46). In our model, both *KRAS* and *PIK3CA* mutational status affected response to the double PI3K/mTOR inhibition in the presence of fibroblast-CM. Interestingly, mounting evidence indicates that oncogenic *KRAS* mutations in cancer cells shape tumor microenvironment composition and affect the properties and functions of its constituents (11, 47). This is of paramount importance from a clinical standpoint, since mutational status is regarded as a relatively stable characteristic in CRC and other tumors and better understanding of such relationships would provide clinicians with reliable biomarkers to select patients at the highest chance of benefit from specific targeted treatments. *KRAS* and *PIK3CA* mutations occur concomitantly in approximately 10%-12% of CRC and are significantly associated (p-value < 0.001; data retrieved from cBioportal (www.cbioportal.org); (48, 49), indicating that the findings described here might be relevant for a significant fraction of CRC patients, considered resistant to currently available treatments.

Altogether, we describe here a novel molecular circuitry, whereby soluble mediators released by microenvironmental elements (fibroblasts) modulate PTEN activity in CRC cells, causing paradoxical PI3K/mTORC1 activation and resulting in increased response to specific double PI3K/mTOR inhibitors in specific genetic contexts (*KRAS*-mut/*PIK3CA*-mut/PTEN-competent). The exact definition of the molecular mechanisms underlying such crosstalk deserves further investigation and may provide clues to the selection of CRC patients at the highest chance to benefit from PI3K pathway inhibitors and provide the rationale for novel therapeutic approaches.

DATA AVAILABILITY STATEMENT

The raw data supporting the conclusions of this article is available in "**Table 1**" in the **Supplementary Material**, further inquiries can be directed to the corresponding author/s.

AUTHOR CONTRIBUTIONS

FCon, CB, and MM contributed to conception and design of all the experiments, supervised data acquisition and analysis, and

wrote the manuscript. FCon and CB performed experiments, contributed to data acquisition, analysis and interpretation of the results. ES, LC, SS, and IF performed experiments and contributed to data acquisition and analysis. FCog, GF, MZ, and DB provided critical reagents, contributed to conception and critically revised the manuscript. All authors reviewed and gave final approval.

FUNDING

This work was supported in part by Bando Interno Ricerca Corrente IRE 2021 (Fabiana Conciatori), IFO Sperimentazioni OM1, AIRC 5 x mille Multiunit Extension (Grant #9979, Michele Milella), and Fondo Universitario per la Ricerca (FUR) University of Verona (Michele Milella). Chiara Bazzichetto was supported by an AIRC fellowship for Italy.

ACKNOWLEDGMENTS

The authors wish to thank IRCCS Scientific Director office for supporting the manuscript.

SUPPLEMENTARY MATERIAL

The Supplementary Material for this article can be found online at: https://www.frontiersin.org/articles/10.3389/fonc.2022.862806/full#supplementary-material

REFERENCES

1. Xi Y, Xu P. Global Colorectal Cancer Burden in 2020 and Projections to 2040. *Transl Oncol* (2021) 14:101174. doi: 10.1016/j.tranon.2021.101174
2. Li J, Ma X, Chakravarti D, Shalapour S, Depinho RA. Genetic and Biological Hallmarks of Colorectal Cancer. *Genes Dev* (2021) 35:787–820. doi: 10.1101/gad.348226.120
3. Foley TM, Payne SN, Pasch CA, Yueh AE, Van De Hey DR, Korkos DP, et al. Dual PI3K/mTOR Inhibition in Colorectal Cancers With APC and PIK3CA Mutations. *Mol Cancer Res* (2017) 15:317–27. doi: 10.1158/1541-7786.MCR-16-0256
4. Shapiro GI, Bell-Mcguinn KM, Molina JR, Bendell J, Spicer J, Kwak EL, et al. First-In-Human Study of PF-05212384 (PKI-587), a Small-Molecule, Intravenous, Dual Inhibitor of PI3K and mTOR in Patients With Advanced Cancer. *Clin Cancer Res* (2015) 21:1888–95. doi: 10.1158/1078-0432.CCR-14-1306
5. Wainberg ZA, Alsina M, Soares HP, Brana I, Britten CD, Del Conte G, et al. A Multi-Arm Phase I Study of the PI3K/mTOR Inhibitors PF-04691502 and Gedatolisib (PF-05212384) Plus Irinotecan or the MEK Inhibitor PD-0325901 in Advanced Cancer. *Target Oncol* (2017) 12:775–85. doi: 10.1007/s11523-017-0530-5
6. Salvatore L, Calegari MA, Loupakis F, Fassan M, Di Stefano B, Bensi M, et al. PTEN in Colorectal Cancer: Shedding Light on Its Role as Predictor and Target. *Cancers (Basel)* (2019) 11:1765. doi: 10.3390/cancers11111765
7. Xie YH, Chen YX, Fang JY. Comprehensive Review of Targeted Therapy for Colorectal Cancer. *Signal Transduct Target Ther* (2020) 5:22. doi: 10.1038/s41392-020-0116-z
8. Weldon Gilcrease G, Stenehjem DD, Wade ML, Weis J, Mcgregor K, Whisenant J, et al. Phase I/II Study of Everolimus Combined With mFOLFOX-6 and Bevacizumab for First-Line Treatment of Metastatic Colorectal Cancer. *Invest New Drugs* (2019) 37:482–9. doi: 10.1007/s10637-018-0645-2
9. Milella M, Falcone I, Conciatori F, Matteoni S, Sacconi A, De Luca T, et al. PTEN Status is a Crucial Determinant of the Functional Outcome of Combined MEK and mTOR Inhibition in Cancer. *Sci Rep* (2017) 7:43013. doi: 10.1038/srep43013
10. Del Curatolo A, Conciatori F, Cesta Incani U, Bazzichetto C, Falcone I, Corbo V, et al. Therapeutic Potential of Combined BRAF/MEK Blockade in BRAF-Wild Type Preclinical Tumor Models. *J Exp Clin Cancer Res* (2018) 37:140. doi: 10.1186/s13046-018-0820-5
11. Conciatori F, Bazzichetto C, Amoreo CA, Sperduti I, Donzelli S, Diodoro MG, et al. BRAF Status Modulates Interelukin-8 Expression Through a CHOP-Dependent Mechanism in Colorectal Cancer. *Commun Biol* (2020) 3:546. doi: 10.1038/s42003-020-01263-y
12. Beninson LA, Fleshner M. Exosomes in Fetal Bovine Serum Dampen Primary Macrophage IL-1beta Response to Lipopolysaccharide (LPS) Challenge. *Immunol Lett* (2015) 163:187–92. doi: 10.1016/j.imlet.2014.10.019
13. Tonarova P, Lochovska K, Pytlik R, Hubalek Kalbacova M. The Impact of Various Culture Conditions on Human Mesenchymal Stromal Cells Metabolism. *Stem Cells Int* (2021) 2021:6659244. doi: 10.1155/2021/6659244
14. Leslie NR, Bennett D, Gray A, Pass I, Hoang-Xuan K, Downes CP. Targeting Mutants of PTEN Reveal Distinct Subsets of Tumour Suppressor Functions. *Biochem J* (2001) 357:427–35. doi: 10.1042/bj3570427
15. Chen JS, Huang JQ, Luo B, Dong SH, Wang RC, Jiang ZK, et al. PIK3CD Induces Cell Growth and Invasion by Activating AKT/GSK-3beta/Beta-Catenin Signaling in Colorectal Cancer. *Cancer Sci* (2019) 110:997–1011. doi: 10.1111/cas.13931
16. Myers MP, Pass I, Batty IH, van der Kaay J, Stolarov JP, Hemmings BA, et al. The Lipid Phosphatase Activity of PTEN is Critical for Its Tumor Supressor Function. *Proc Natl Acad Sci USA* (1998) 95:13513–8. doi: 10.1073/pnas.95.23.13513
17. Xu W, Yang Z, Xie C, Zhu Y, Shu X, Zhang Z, et al. PTEN Lipid Phosphatase Inactivation Links the Hippo and PI3K/Akt Pathways to Induce Gastric Tumorigenesis. *J Exp Clin Cancer Res* (2018) 37:198. doi: 10.1186/s13046-018-0795-2
18. Hatzivassiliou G, Song K, Yen I, Brandhuber BJ, Anderson DJ, Alvarado R, et al. RAF Inhibitors Prime Wild-Type RAF to Activate the MAPK Pathway and Enhance Growth. *Nature* (2010) 464:431–5. doi: 10.1038/nature08833
19. Poulikakos PI, Persaud Y, Janakiraman M, Kong X, Ng C, Moriceau G, et al. RAF Inhibitor Resistance is Mediated by Dimerization of Aberrantly Spliced BRAF(V600E). *Nature* (2011) 480:387–90. doi: 10.1038/nature10662
20. Robert C, Karaszewska B, Schachter J, Rutkowski P, Mackiewicz A, Stroiakovski D, et al. Improved Overall Survival in Melanoma With Combined Dabrafenib and Trametinib. *N Engl J Med* (2015) 372:30–9. doi: 10.1056/NEJMoa1412690
21. Long GV, Flaherty KT, Stroyakovskiy D, Gogas H, Levchenko E, De Braud F, et al. Dabrafenib Plus Trametinib Versus Dabrafenib Monotherapy in Patients With Metastatic BRAF V600E/K-Mutant Melanoma: Long-Term Survival and Safety Analysis of a Phase 3 Study. *Ann Oncol* (2017) 28:1631–9. doi: 10.1093/annonc/mdx176
22. Corcoran RB, Andre T, Atreya CE, Schellens JHM, Yoshino T, Bendell JC, et al. Combined BRAF, EGFR, and MEK Inhibition in Patients With BRAF (V600E)-Mutant Colorectal Cancer. *Cancer Discov* (2018) 8:428–43. doi: 10.1158/2159-8290.CD-17-1226
23. Ciuffreda L, Falcone I, Incani UC, Del Curatolo A, Conciatori F, Matteoni S, et al. PTEN Expression and Function in Adult Cancer Stem Cells and Prospects for Therapeutic Targeting. *Adv Biol Regul* (2014) 56:66–80. doi: 10.1016/j.jbior.2014.07.002
24. Milella M, Falcone I, Conciatori F, Cesta Incani U, Del Curatolo A, Inzerilli N, et al. PTEN: Multiple Functions in Human Malignant Tumors. *Front Oncol* (2015) 5:24. doi: 10.3389/fonc.2015.00024
25. Papa A, Pandolfi PP. The PTEN(-)PI3K Axis in Cancer. *Biomolecules* (2019) 9:153. doi: 10.20944/preprints201904.0127.v1
26. Leslie NR, Downes CP. PTEN Function: How Normal Cells Control it and Tumour Cells Lose it. *Biochem J* (2004) 382:1–11. doi: 10.1042/BJ20040825

27. Conciatori F, Ciuffreda L, Bazzichetto C, Falcone I, Pilotto S, Bria E, et al. mTOR Cross-Talk in Cancer and Potential for Combination Therapy. *Cancers (Basel)* (2018) 10:23. doi: 10.3390/cancers10010023
28. Morita M, Gravel SP, Hulea L, Larsson O, Pollak M, St-Pierre J, et al. mTOR Coordinates Protein Synthesis, Mitochondrial Activity and Proliferation. *Cell Cycle* (2015) 14:473–80. doi: 10.4161/15384101.2014.991572
29. Jhanwar-Uniyal M, Wainwright JV, Mohan AL, Tobias ME, Murali R, Gandhi CD, et al. Diverse Signaling Mechanisms of mTOR Complexes: Mtorc1 and Mtorc2 in Forming a Formidable Relationship. *Adv Biol Regul* (2019) 72:51–62. doi: 10.1016/j.jbior.2019.03.003
30. Tabernero J, Rojo F, Calvo E, Burris H, Judson I, Hazell K, et al. Dose- and Schedule-Dependent Inhibition of the Mammalian Target of Rapamycin Pathway With Everolimus: A Phase I Tumor Pharmacodynamic Study in Patients With Advanced Solid Tumors. *J Clin Oncol* (2008) 26:1603–10. doi: 10.1200/JCO.2007.14.5482
31. Baselga J, Semiglazov V, Van Dam P, Manikhas A, Bellet M, Mayordomo J, et al. Phase II Randomized Study of Neoadjuvant Everolimus Plus Letrozole Compared With Placebo Plus Letrozole in Patients With Estrogen Receptor-Positive Breast Cancer. *J Clin Oncol* (2009) 27:2630–7. doi: 10.1200/JCO.2008.18.8391
32. Huang J, Manning BD. A Complex Interplay Between Akt, TSC2 and the Two mTOR Complexes. *Biochem Soc Trans* (2009) 37:217–22. doi: 10.1042/BST0370217
33. Vazquez F, Grossman SR, Takahashi Y, Rokas MV, Nakamura N, Sellers WR. Phosphorylation of the PTEN Tail Acts as an Inhibitory Switch by Preventing its Recruitment Into a Protein Complex. *J Biol Chem* (2001) 276:48627–30. doi: 10.1074/jbc.C100556200
34. Rahdar M, Inoue T, Meyer T, Zhang J, Vazquez F, Devreotes PN. A Phosphorylation-Dependent Intramolecular Interaction Regulates the Membrane Association and Activity of the Tumor Suppressor PTEN. *Proc Natl Acad Sci USA* (2009) 106:480–5. doi: 10.1073/pnas.0811212106
35. Song MS, Salmena L, Pandolfi PP. The Functions and Regulation of the PTEN Tumour Suppressor. *Nat Rev Mol Cell Biol* (2012) 13:283–96. doi: 10.1038/nrm3330
36. Leslie NR, Gray A, Pass I, Orchiston EA, Downes CP. Analysis of the Cellular Functions of PTEN Using Catalytic Domain and C-Terminal Mutations: Differential Effects of C-Terminal Deletion on Signalling Pathways Downstream of Phosphoinositide 3-Kinase. *Biochem J* (2000) 346(Pt 3):827–33. doi: 10.1042/bj3460827
37. Smith SL, Pitt AR, Spickett CM. Approaches to Investigating the Protein Interactome of PTEN. *J Proteome Res* (2021) 20:60–77. doi: 10.1021/acs.jproteome.0c00570
38. Rabinovsky R, Pochanard P, Mcnear C, Brachmann SM, Duke-Cohan JS, Garraway LA, et al. P85 Associates With Unphosphorylated PTEN and the PTEN-Associated Complex. *Mol Cell Biol* (2009) 29:5377–88. doi: 10.1128/MCB.01649-08
39. Conciatori F, Bazzichetto C, Falcone I, Ciuffreda L, Ferretti G, Vari S, et al. PTEN Function at the Interface Between Cancer and Tumor Microenvironment: Implications for Response to Immunotherapy. *Int J Mol Sci* (2020) 21:5337. doi: 10.3390/ijms21155337
40. Hopkins BD, Fine B, Steinbach N, Dendy M, Rapp Z, Shaw J, et al. A Secreted PTEN Phosphatase That Enters Cells to Alter Signaling and Survival. *Science* (2013) 341:399–402. doi: 10.1126/science.1234907
41. Fang N, Gu T, Wang Y, Wang S, Wang F, An Y, et al. Expression of PTEN-Long Mediated by CRISPR/Cas9 can Repress U87 Cell Proliferation. *J Cell Mol Med* (2017) 21:3337–46. doi: 10.1111/jcmm.13236
42. Zhou Y, Ren H, Dai B, Li J, Shang L, Huang J, et al. Hepatocellular Carcinoma-Derived Exosomal miRNA-21 Contributes to Tumor Progression by Converting Hepatocyte Stellate Cells to Cancer-Associated Fibroblasts. *J Exp Clin Cancer Res* (2018) 37:324. doi: 10.1186/s13046-018-0965-2
43. Bronisz A, Godlewski J, Wallace JA, Merchant AS, Nowicki MO, Mathsyaraja H, et al. Reprogramming of the Tumour Microenvironment by Stromal PTEN-Regulated miR-320. *Nat Cell Biol* (2011) 14:159–67. doi: 10.1038/ncb2396
44. Yang J, Nie J, Ma X, Wei Y, Peng Y, Wei X. Targeting PI3K in Cancer: Mechanisms and Advances in Clinical Trials. *Mol Cancer* (2019) 18:26. doi: 10.1186/s12943-019-0954-x
45. Mayer IA, Abramson VG, Formisano L, Balko JM, Estrada MV, Sanders ME, et al. A Phase Ib Study of Alpelisib (BYL719), a PI3Kalpha-Specific Inhibitor, With Letrozole in ER+/HER2- Metastatic Breast Cancer. *Clin Cancer Res* (2017) 23:26–34. doi: 10.1158/1078-0432.CCR-16-0134
46. Brandao M, Caparica R, Eiger D, De Azambuja E. Biomarkers of Response and Resistance to PI3K Inhibitors in Estrogen Receptor-Positive Breast Cancer Patients and Combination Therapies Involving PI3K Inhibitors. *Ann Oncol* (2019) 30 Suppl 10:x27–42. doi: 10.1093/annonc/mdz280
47. Dias Carvalho P, Guimaraes CF, Cardoso AP, Mendonca S, Costa AM, Oliveira MJ, et al. KRAS Oncogenic Signaling Extends Beyond Cancer Cells to Orchestrate the Microenvironment. *Cancer Res* (2018) 78:7–14. doi: 10.1158/0008-5472.CAN-17-2084
48. Rosty C, Young JP, Walsh MD, Clendenning M, Sanderson K, Walters RJ, et al. PIK3CA Activating Mutation in Colorectal Carcinoma: Associations With Molecular Features and Survival. *PLoS One* (2013) 8:e65479. doi: 10.1371/journal.pone.0065479
49. Haigis KM. KRAS Alleles: The Devil Is in the Detail. *Trends Cancer* (2017) 3:686–97. doi: 10.1016/j.trecan.2017.08.006

Conflict of Interest: The authors declare that the research was conducted in the absence of any commercial or financial relationships that could be construed as a potential conflict of interest.

Publisher's Note: All claims expressed in this article are solely those of the authors and do not necessarily represent those of their affiliated organizations, or those of the publisher, the editors and the reviewers. Any product that may be evaluated in this article, or claim that may be made by its manufacturer, is not guaranteed or endorsed by the publisher.

Advantages of publishing in Frontiers

OPEN ACCESS
Articles are free to read for greatest visibility and readership

FAST PUBLICATION
Around 90 days from submission to decision

HIGH QUALITY PEER-REVIEW
Rigorous, collaborative, and constructive peer-review

TRANSPARENT PEER-REVIEW
Editors and reviewers acknowledged by name on published articles

Frontiers
Avenue du Tribunal-Fédéral 34
1005 Lausanne | Switzerland

Visit us: www.frontiersin.org
Contact us: frontiersin.org/about/contact

REPRODUCIBILITY OF RESEARCH
Support open data and methods to enhance research reproducibility

DIGITAL PUBLISHING
Articles designed for optimal readership across devices

FOLLOW US
@frontiersin

IMPACT METRICS
Advanced article metrics track visibility across digital media

EXTENSIVE PROMOTION
Marketing and promotion of impactful research

LOOP RESEARCH NETWORK
Our network increases your article's readership